INTERNATIONAL DOCTORAL SCHOOL OF THE USC

Inés
Martínez Sambade

PhD Thesis

Genomics of resistance to the parasite Bonamia ostreae in the European flat oyster Ostrea edulis

Lugo, 2025

Doctoral Programme in Basic and Applied Research in Veterinary Sciences

USC
UNIVERSIDADE
DE SANTIAGO
DE COMPOSTELA

ESCOLA DE DOUTORAMENTO
INTERNACIONAL DA USC

DOCTORAL THESIS

GENOMICS OF RESISTANCE TO THE PARASITE *BONAMIA OSTREAE* IN THE EUROPEAN FLAT OYSTER *OSTREA EDULIS*

Author

Inés Martínez Sambade

Supervisor/s: Paulino Martínez Portela

Tutor: Paulino Martínez Portela

PHD PROGRAMME IN BASIC AND APPLIED RESEARCH IN VETERINARY SCIENCES

LUGO – 2025

USC
UNIVERSIDADE
DE SANTIAGO
DE COMPOSTELA

ESCOLA DE DOUTORAMENTO
INTERNACIONAL DA USC

DECLARACIÓN CONFLICTO DE INTERESE

Eu, Inés Martínez Sambade, con DNI 46093658W e con domiciliación a efectos de notificación en Ronda de Fingoi 109 2K (Lugo, Galicia), declaro que esta tese de doutoramento non presenta conflicto de interese.

En Lugo, 7 de Outubro de 2025

Fdo: Inés Martínez Sambade

USC UNIVERSIDADE DE SANTIAGO DE COMPOSTELA

FUNDING

PHD FELLOWSHIPS TO INÉS MARTÍNEZ SAMBADE

Granting organization: Campus Terra. Universidade de Santiago de Compostela

Participating entities: Universidade de Santiago de Compostela and Consellería de Cultura, Educación e Universidade

Duration: 01/08/2022 – 31/07/2025

Title: Contrato Predoutoral do Campus de especialización Campus Terra

RESEARCH PROJECTS

Granting organization: This study forms part of the Marine Science programme (ThinkInAzul) supported by Ministerio de Ciencia e Innovación and Xunta de Galicia with funding from European Union NextGenerationEU (PRTR-C17.I1) and European Maritime and Fisheries Fund. This research corresponds to the Marine Science Programme for Galicia, Work Package no 6 "*Genomic tools for sustainable management and improvement of aquaculture productivity*" and activity no. 6.3 about "*Genomic selection programmes for production improvement*" and has been funded by the Resilience and Recovery Funds.

Participating entities: Consellería do Mar-Xunta de Galicia, Universidade de Vigo, Universidade de Santiago de Compostela, Universidade da Coruña, Instituto Gallego de Formación en Acuicultura, Centro de Investigacións Mariñas (CIMA), Intecmar, IIM Sede del programa, Centro Tecnolóxico do Mar (CETMAR), Instituto Español de Oceanografía (IEO), Meteogalicia, Incipit CSIC, Centro de Supercomputación de Galicia (CESGA).

Duration: 01/01/2022 – 31/12/2025

Working Package 6 Coordinator: Paulino Martínez Portela

Project title: Programa de Ciencias Mariñas de Galicia

Reference number: 2022-CP076

USC DE SANTIAGO DE COMPOSTELA

USC
UNIVERSIDADE
DE SANTIAGO
DE COMPOSTELA

LIST OF PUBLICATIONS

The results reproduced in Chapter I of this thesis have been published in international journals. Find below the correspondence between the PhD chapters and the published articles.

CHAPTER I

Title: A single genomic region involving a putative chromosome rearrangement in flat oyster (*Ostrea edulis*) is associated with differential host resilience to the parasite *Bonamia ostreae*.

Authors: Inés Martínez Sambade[1], Adrian Casanova[1], Andrés Blanco[1], Manu K. Gundappa[2], Tim P. Bean[2], Daniel J. Macqueen[2], Ross D. Houston[2], Antonio Villalba[3,4,5], Manuel Vera[1], Pauline Kamermans [6,7] & Paulino Martínez [1]

Affiliations: [1]Department of Zoology, Genetics and Physical Anthropology, ACUIGEN Group, Faculty of Veterinary, Universidade de Santiago de Compostela, Lugo, Spain [2]The Roslin Institute and Royal (Dick) School of Veterinary Studies, Midlothian, UK [3]Centro de Investigacións Mariñas (CIMA), Vilanova de Arousa, Spain [4]Departamento de Ciencias de la Vida, Universidad de Alcalá, Alcalá de Henares, Spain [5]Research Centre for Experimental Marine Biology and Biotechnology (PIE), University of the Basque Country (UPV/EHU), Plentzia, Spain [6]Wageningen Marine Research, Yerseke, The Netherlands [7]Marine Animal Ecology Group, Wageningen University, Wageningen, The Netherlands

Published in: Evolutionary Applications (2022) 15,9 doi: 10.1111/eva.13446 (Table 1).

USC UNIVERSIDADE DE SANTIAGO DE COMPOSTELA

Contribution: Inés Martínez Sambade: Methodology, Investigation, Formal analysis, Writing – Original draft preparation. Adrian Casanova: Methodology, Investigation, Formal analysis, Writing – Original draft preparation. Andrés Blanco: Formal analysis. Manu K. Gundappa: Formal analysis. Tim P. Bean: Formal analysis. Daniel J. Macqueen: Formal analysis. Ross D. Houston: Formal analysis. Antonio Villalba: Review & Editing. Manuel Vera: Review & Editing, Pauline Kamermans: Funding acquisition, Review & Editing & Paulino Martínez: Conceptualization, Methodology, Funding acquisition, Investigation, Supervision, Formal analysis, Writing – Original draft preparation.

Conflict of interest: The authors declare no conflict of interest.

Copyright © This is an open access article under the terms of the Creative Commons Attribution License, which permits use, distribution and reproduction in any medium, provided the original work is properly cited.

Title: *Bonamia*-free flat oyster (*Ostrea edulis* L.) seed for restoration projects: non-destructive screening of broodstock, hatchery production and test for *Bonamia*-tolerance

Authors: Pauline Kamermans[1,2], Ainhoa Blanco[1], Pim van Dalen[1], Marc Engelsma[3], Nienke Bakker[4], Pascalle Jacobs[5,6], Marco Dubbeldam[7], Inés M. Sambade[8], Manuel Vera[8] and Paulino Martinez[8]

Affiliations: [1]Wageningen Marine Research, P.O. Box 77, 4400 AB Yerseke, The Netherlands [2]Marine Animal Ecology Group, Department of Animal Sciences, Wageningen University, PO Box 226, 6700 AE Wageningen, The Netherlands [3]Wageningen Bioveterinary Research, P.O. Box 65, 8200AB Lelystad, The Netherlands [4]Hatchery Roem van Yerseke, Groeninx van Zoelenstraat 35, 4401 KZ Yerseke, The Netherlands [5]Royal Netherlands Institute of Sea Research, Texel, The Netherlands [6]Aquaculture in Delta Areas, University of Applied Sciences, P.O. Box 364, 4380 AJ Vlissingen, The Netherlands [7]Stichting Zeeschelp, Oosthavendijk 7, 4493 BK Kamperland, The Netherlands [8]Department of Zoology, Genetics and Physical Anthropology, Faculty of Veterinary, University of Santiago de Compostela, 27002 Lugo, Spain

Published in: Aquatic Living Resources 36, 11 doi: 10.1051/alr/2023005 (Table 1).

Contribution: Pauline Kamermans: Conceptualization, Methodology, Funding acquisition, Investigation, Supervision, Formal analysis, Writing – Original draft preparation. Ainhoa Blanco: Methodology, Investigation, Writing – Review & Editing. Pim van Dalen: Methodology, Investigation. Nienke Bakker: Resources. Marc Engelsma: Validation, Investigation, Formal analysis, Writing − Original draft preparation. Pascalle Jacobs: Resources, Writing − Review & Editing. Marco Dubbeldam: Resources. Inés M. Sambade: Investigation, Formal analysis, Writing − Original draft preparation. Manuel Vera: Review & Editing. Paulino Martinez: Investigation, Supervision, Writing − Original draft preparation.

USC UNIVERSIDADE

Conflict of interest: The authors declare no conflict of interest.

Copyright © This is an Open Access article distributed under the terms of the Creative Commons Attribution License (https://creativecommons.org/licenses/by/4.0), which permits unrestricted use, distribution, and reproduction in any medium, provided the original work is properly cited.

Table 1. Impact factors in the year of publication, quartile and ISSN of the journals containing the results being reproduced in this thesis.

Journal	IF	Quartile	ISSN
Evolutionary Applications (Chapter I)	4.1 (2022)	Q1	1752-4571
Aquatic Living Resources	1.5 (2023)	Q2	1765-2952

CHAPTER II

Title: Disentangling the role of chromosome inversions in the structure of flat oyster (*Ostrea edulis*): origin, adaptation and phylogeography

Authors: Inés M. Sambade[1], Vivian Hlordzi[2,3], Andrés Blanco[1], Miguel Hermida[1], Manuel Vera[1], Sarah Culloty[2,3], Tim Bean[4], Sharon A. Lynch[2,3], Paulino Martínez[1].

Affiliations: [1]Department of Zoology, Genetics and Physical Anthropology, ACUIGEN Group, Faculty of Veterinary, Universidade de Santiago de Compostela, Lugo, Spain [2]School of Biological, Earth and Environmental Sciences, University College Cork, Cork, Ireland [3]Environmental Research Institute, University College Cork, Cork, Ireland [4]The Roslin Institute and Royal (Dick) School of Veterinary Studies, Midlothian, UK

Preprint in: bioRxiv (Cold Spring Harbor Laboratory) doi:10.1101/2025.06.12.659260

Contribution: Inés Martínez Sambade: Methodology, Investigation, Formal analysis, Writing – Original draft preparation. Vivian Hlordzi: Sample collection and processing. Andrés Blanco: Formal analysis. Miguel Hermida: Review & Editing, Manuel Vera: Review & Editing. Sarah Culloty: Funding acquisition, Review & Editing. Sharon A. Lynch: Funding acquisition, Review & Editing & Paulino Martínez: Conceptualization, Methodology, Funding acquisition, Investigation, Supervision, Formal analysis, Writing – Original draft preparation.

Conflict of interest: The authors declare no conflict of interest.

The copyright holder for this preprint is the author/funder, who has granted bioRxiv a license to display the preprint in perpetuity. It is made available under a CC-BY-NC-ND 4.0 International license.

USC UNIVERSIDADE DE SANTIAGO DE COMPOSTELA

USC
UNIVERSIDADE
DE SANTIAGO
DE COMPOSTELA

ACKNOWLEDGMENTS

Cando acabei de escribir a tese este verán, respirei fondo… ata que me din conta de que aínda me faltaban os agradecementos. Estes últimos meses foron de tomar moitas decisións, e de tomalas un pouco como iba cadrando. Aínda agora non sei si algunha sería na dirección correcta. O que si que teño claro, é que no momento de tomalas tiven unha batería de xente á que pedirlle opinión. Todas foron distintas, con distintos puntos de vista e distintos niveis de experiencia, pero todas desde o cariño e a sinceridade. Vinme moi apoiada no proceso de escribir esta tese, e a todos vós intentarei darvos as gracias a continuación o mellor que poida.

En primer lugar, quiero expresar mi agradecimiento a la Universidad de Santiago de Compostela y al grupo ACUIGEN por darme el espacio y los recursos necesarios para desarrollar esta tesis. También agradezco el apoyo económico a través de Campus Terra, que hizo posible que pudiera dedicarme a la investigación estos años y que fomentan la investigación en el campus de Lugo y en ámbitos a los que a veces no se le da la suficiente importancia.

Mi mayor agradecimiento es para mi director, Paulino Martínez, por su guía, paciencia y apoyo durante estos tres años; por saber encontrar el equilibrio entre exigencia y apoyo, y por saber gestionar las diferentes personalidades que tiene a su cargo, ayudándonos a cada uno como necesitamos. Gracias por confiar en mí y darme la oportunidad de embarcarme en este proyecto.

USC
UNIVERSIDADE DE SANTIAGO DE COMPOSTELA

A mis compañeros de grupo: Óscar, gracias por acompañarme desde el primer huesito esperando a defender el TFM, por escucharme las mismas preocupaciones una y otra vez, y por seguir ayudándome hasta hoy (literalmente, mientras escribo estoy esperando a que me resuelvas una duda de formato). Marina, compañera de moluscos y desde el principio, gracias por todas las pausas y los tés, que eran menos por la infusión y más por la otra acepción de la palabra.

Andrés, por enseñarme todo lo que sé de bioinformática, siempre desde el buen humor y sin importarle que le pidiéramos cincuenta veces el mismo script. Paula, gracias por abrirme los ojos en muchos aspectos, y por contagiarme (una proporción minúscula) de una pasión por la ciencia que no había visto antes en nadie, y también por sacarme de casa en Edimburgo. Dori, por la complicidad, y por dejar de ser pánico en los momentos en los que era yo la que paniqueaba. A Rocío, para la que no hay opiniones controvertidas, a Maialen, Varo, Chiclana y Hurzos, por estar ahí en el día a día.

Y a todos los que pasaron y consiguieron encajar una silla en algún hueco del despacho durante estos tres años. En especial a Raquel, de la que creo que seguiré contando anécdotas toda mi vida. En general, me gustaría desearos mucha suerte a todos los que os quedáis trabajando en el departamento, y también a los que llegan, como Fernando, que promete un montón.

Al resto del grupo, gracias por la compañía y el apoyo: Manel, Laura, Belén, Jaime, Miguel, Rafi, Nico, Susana, Lucía, Carlos, Adri, Raquel, Peke, Juan, Eduardo, Diego, Marialaura, Sara, Noe… En especial a Soni y Moni, que nos cuidan y acompañan desde el primer día, y nos hacen sentir parte del grupo desde que llegamos. Todo funciona gracias a vosotras. También a Anny y a Cris, por la paciencia infinita, y a Carmen, que siempre se preocupó por mí como si fuera también mi directora. Gracias a todos.

I would also like to thank the groups where I carried out my research stays, both at UCC and at the Roslin Institute. My gratitude goes to Vivian for her warm welcome and kindness during my stay at UCC, an enriching experience both personally and professionally, where I even regained a bit of my enthusiasm for lab work. I am equally grateful to the Aquaculture team at Roslin, especially to Clémence for her kind welcome and for sharing her time, knowledge, and enthusiasm for research. Thank you all for always including me in plans outside of work and for making me feel at home during those months.

De Lugo quédome co depar pero tamén co que non é depar, porque aínda que non sei aínda se me irei chorando (ás veces dudo si conseguirei marchar nalgún momento), aquí coñecín xente que non sei como podía vivir antes sin telos na miña vida. A Manu, non só por axudarme cas imaxes deste traballo, tamén pola túa paciencia, por animarme e por escoitarme cando me queixaba sempre do mesmo, e por recordarme que hai Inés máis alá da Inés que produce.

A miña familia: aos meus pais por quererme sempre, por apoiarme e por ensinarme que da igual de onde veñas, que podes chegar case a onde queiras. Sempre nos dixéstedes as cousas tal e como eran, e creo que polo esixentes que fóstedes, parte do mérito do que conseguimos as dúas é tamén voso.

USC
UNIVERSIDADE DE COMPOSTELA

Tamén porque papá contoume a historia dos chícharos de Mendel e dos pimpíns de Darwin desde que teño memoria, e pode que teña parte da culpa de que me acabara dedicando á xenética. A Iria, por acollerme tanto nos primeiros meses en Lugo, e non só polo colchón no chan. Teño tamén moitísima sorte de ter aínda a meus tres avós comigo: gracias por criarme, por apoiarme e presumirme tanto, ata cando non entendiades exactamente a que me dedicaba.

Ás miñas amigas de bio: Alex, Aldara, Olga, Marta, Vio, Ali, Icía e María, que estiveron en todas as etapas destes anos, celebrando xuntas logros e fracasos, e compartindo queixas sobre as poucas saídas que ten a carreira, e o puteadas que estamos na investigación (por las precarias!). Porque prometemos vernos dúas veces ao ano e vémonos case dúas veces ao mes. Estou super orgullosa de vós, de todas sen excepción, e sei que vos tamén de min. Estou desexando ver as vosas teses, aínda que non me vaia enterar de nada. Marta, eres a seguinte.

E a Capi, que a pesar de que fostes sempre de bota pura, e de que non lle vías interés ningún á investigación, tiñas a paciencia de escoitar e aconsellarme. Vou botar moito de menos as fotos de moniños que mandabas. Deixas o mundo millor, pero quedamos moi mal sin ti. Creo que non nos demos conta aínda de ata que punto.

Finalmente, gracias a todas las personas que de una forma u otra han estado presentes en este viaje. Este trabajo es también vuestro.

USC
UNIVERSIDADE DE SANTIAGO DE COMPOSTELA

USC
UNIVERSIDADE
DE SANTIAGO
DE COMPOSTELA



"Cada día aprendía algo nuevo sobre el mundo, y cada cosa que aprendía hacía que el mundo fuera más grande."



— Jacqueline Kelly, La evolución de Calpurnia Tate

USC
UNIVERSIDADE DE SANTIAGO DE COMPOSTELA

USC
UNIVERSIDADE
DE SANTIAGO
DE COMPOSTELA

INDEX

ABBREVIATIONS AND SYMBOLS 23

RESUMEN (CASTELLANO): Genómica de la resistencia al parásito *Bonamia ostreae* en la ostra europea *Ostrea edulis* 33

SUMMARY (ENGLISH): Genomics of resistance to the parasite *Bonamia ostreae* in the European flat oyster *Ostrea edulis* 35

RESUMO EXTENDIDO EN GALEGO 37

GENERAL INTRODUCTION 45

1. *OSTREA EDULIS*: BIOLOGY AND CONSERVATION 47

1.1. The European flat oyster 48

1.2. Distribution of O. edulis 48

1.3. Decline and threats to O. edulis: bonamiosis 49

1.4. European restoration efforts 52

1.5. Restoration challenges and opportunities in Ireland and the Netherlands: case studies 53

2. *OSTREA EDULIS* IMMUNE SYSTEM 56

2.1. The innate immune system of molluscs 56

2.2. Cellular components of the immune system in molluscs 56

2.3. Humoral components and effector mechanisms 58

2.4. Pattern recognition receptors (PRRs) and immune signalling 60

2.5. New insights in Immune System in Oysters 61

2.6. Immune response to *B. ostreae* 63

3. GENETIC STRUCTURE OF *O. EDULIS* AND ITS RESISTANCE TO *B. OSTREAE* 65

3.1. Genetic diversity and population structure of *O. edulis* 65

USC UNIVERSIDADE DE SANTIAGO DE COMPOSTELA

3.2. *O. edulis* response to *B. ostreae*: a population perspective 65
3.3. Genomic resources and molecular tools 69
3.4. Selective breeding and practical applications 69

4. STRUCTURAL VARIATION AND THE ROLE OF CHROMOSOMAL INVERSIONS IN *OSTREA EDULIS* 71
4.1. Evolutionary significance of chromosomal inversions 71
4.2. Chromosomal inversions in marine invertebrates and bivalves 73
4.3. Structural variation and inversion polymorphisms in *O. edulis* 74

OBJECTIVES 75

CHAPTER I: A major genomic region associated with *Bonamia* resistance in flat oyster (*Ostrea edulis*): validation using *Bonamia*-free and long-term affected populations 79
ABSTRACT 80
1. INTRODUCTION 81
2. MATERIALS AND METHODS 83
2.1. Sampling 83
2.2. DNA extraction and SNP genotyping 84
2.3. Genetic diversity and parentage 85
2.4. Genetic structure 86
2.5. Linkage disequilibrium 86
2.6. Mapping SNPs and differentially expressed genes in the flat oyster genome: functional enrichment assessment 86
3. RESULTS 87
3.1. Population genomics validation 87
3.2. Common garden experiment to check the performance of NV and LTA strains 96

CHAPTER II: Disentangling the role of chromosome inversions in the structure of flat oyster (*Ostrea edulis*): origin, adaptation and phylogeography 99

USC UNIVERSIDADE

ABSTRACT **100**

1. INTRODUCTION **101**

2. MATERIALS AND METHODS **103**

2.1. Sampling 103
2.2. DNA extraction 104
2.3. SNP genotyping 104
2.4. Genomic characterization of chromosomal inversions 105
2.5. Genetic structure at the light of inversions 108
2.6. Signals of selection 108

3. RESULTS **110**

3.1. Genomic characterization of chromosome inversions 110
3.2. Population genomics of *O. edulis* 114

CHAPTER III: Genomics and Transcriptomics Insights into Resistance to *Bonamia ostreae* in the European Flat Oyster (*Ostrea edulis*) **121**

ABSTRACT **122**

1. INTRODUCTION **123**

2. MATERIALS AND METHODS **125**

2.1. Sample collection 125
2.2. Tissue processing and infection classification 125
2.3. DNA extraction and genotyping 126
2.4. Population genomics analyses 127
2.5. RNA extraction and transcriptomic analysis 127
2.6. A multiplex SNP tool for assisting breeding programs for resistance to *B. ostreae* 128

3. RESULTS **130**

3.1. Assessment of infection level 130
3.2. SNP genotyping and inversion arrangement karyotypes 131
3.3. Validation of a targeted genotyping panel for assisted breeding 133
3.4. Transcriptomic response to *B. ostreae* in the wild 134

USC UNIVERSIDADE DE SANTIAGO DE COMPOSTELA

GENERAL DISCUSSION 147

1. General overview 149
2. Validation of resistance-associated SNPs and identification of the C8 inversion 150
3. Genomic architecture, evolutionary history, and adaptative significance of chromosomal inversions 151
4. Individual-level resistance and infection dynamics 153
5. Transcriptomic insights into infection responses 155
6. Integration across chapters: structural variation, resistance mechanisms, and adaptation 158
7. Applications for selective breeding, restoration, and conservation 160
8. Limitations and future research directions 161

CONCLUSIONS 163

REFERENCES 167

ANEX I: SUPPLEMENTARY FIGURES 203

Supplementary Figures Chapter I 205

Supplementary Figures Chapter II 207

Supplementary Figures Chapter III 214

ANEX II: SUPPLEMENTARY TABLES 217

Supplementary Tables Chapter II 219

Supplementary Tables Chapter III 266

ANEX III: PERMISSIONS FOR RE-USE OF JOURNAL CONTENT 357

USC UNIVERSIDADE DE SANTIAGO DE COMPOSTELA

ABBREVIATIONS AND SYMBOLS

Abbreviation/Symbol	Meaning / Unit
A	Adenine (nucleotide)
AIF-1	Allograft Inflammatory Factor-1
ALI	Alicante population
AMP	Adenosine monophosphate (context-dependent)
AMPK	AMP-activated protein kinase
AMPs	Antimicrobial Peptides
ANOVA	Analysis of Variance
AP-2ε	Activating enhancer-binding protein 2 epsilon
APGW-amide	Neuropeptide APGW-amide
Ar	Allelic Richness
ATP	Adenosine Triphosphate
ATP5F	ATP synthase subunit f
BAYESCAN	Bayesian software for detecting loci under selection
BER	Bergen population
BLAST	Basic Local Alignment Search Tool
BP	Biological Process
bp	Base pairs
BPIs	Bactericidal/Permeability-Increasing Proteins
BRCA2	Breast Cancer Type 2 Susceptibility Protein
BUB3	Mitotic checkpoint protein BUB3
C	Cytosine
C2	Inversion in chromosome 2
C5	Inversion in chromosome 5
C8	Inversion in chromosome 8

USC UNIVERSIDADE DE SANTIAGO DE COMPOSTELA

C1qDCs	C1q Domain-Containing Proteins
CAT	Catalase
CC	Cellular Component
CC BY	Creative Commons Attribution License
CDS	Coding sequence
CESGA	Supercomputing Center of Galicia
CgTLR3	Toll-like receptor 3 (Crassostrea gigas)
CIMA	Centro de Investigacións Mariñas
cm	Centimeter
COX15	Cytochrome c oxidase assembly protein COX15
COX5B	Cytochrome c oxidase subunit 5B
CSPL	Cell and Tissue Lysis Buffer
cvSI-1	Serine protease inhibitor 1 (Crassostrea virginica)
cvSI-2	Serine protease inhibitor 2 (Crassostrea virginica)
DAMPS	Damage-Associated Molecular Patterns
DAPC	Discriminant Analysis of Principal Components
DEGs	Differentially Expressed Genes
DESeq2	Differential Expression Sequencing (R package)
DHC	Differential Haemocyte Count
DNA	Deoxyribonucleic Acid
DNA/hAT	DNA transposon family (hAT superfamily)
EMS Y	BRCA2-interacting transcriptional repressor EMSY
ETosis	Release of extracellular traps by immune cells
ETs	Extracellular Traps
FAO	Food and Agriculture Organization
FAS	Fas cell surface death receptor
FAS ligand	Fas ligand (apoptosis-inducing protein)
FC	Fold Change
FCGR2B	Low affinity immunoglobulin gamma Fc region receptor II-b
FDR	False Discovery Rate

USC

Fig	Figure
F_{IS}	Inbreeding Coefficient
F_{ST}	Fixation Index
FREPs	Fibrinogen-Related Proteins
G	Guanine (nucleotide)
G-protein	Guanine nucleotide-binding protein
GAL	Galway population
GM2A	Ganglioside GM2 activator
GNBPs	Gram-Negative Bacteria-Binding Proteins
GO	Gene Ontology
GOfuncR	R package for GO enrichment analysis
GVR	Grevelingen population
H1	Histone 1
H2A	Histone 2A
H2B	Histone 2B
H_2O_2	Hydrogen peroxide
H3	Histone 3
H3K4	Histone 3 Lysine 4 (methylation site)
H4	Histone 4
H5	Histone 5
He	Expected Heterozygosity
Ho	Observed Heterozygosity
Hsp-16.48	Heat shock protein 16.48
Hsp-16.49	Heat shock protein 16.49
Hsp70	Heat shock protein 70
HSPs	Heat Shock Proteins
HWE	Hardy–Weinberg Equilibrium
IAP	Inhibitor of Apoptosis Protein
IFN	Interferon
IGV	Integrative Genomics Viewer

USC

IL-17	Interleukin-17
i.e.	Id est (that is)
JAK	Janus Kinase
K	Number of most probable clusters in STRUCTURE
K	Thousand (when following a number)
KAT8	Lysine acetyltransferase 8 (MYST histone acetyltransferase)
Kb	Kilobase
L1	Level 1 (infection stage)
L2	Level 2
L3	Level 3
L4	Level 4
LBPs	Lipopolysaccharide-Binding Proteins
LD	Linkage Disequilibrium
LDA	Linear Discriminant Analysis
LIM	Limerick population
LINE	Long Interspersed Nuclear Element
LR	Loch Ryan population (Thesis)
LRy	Loch Ryan population (Vera et al., 2019)
LTA	Long-Term Affected population
LW	Lough Swilly population
m	Meters
MALDI-TOF	Matrix-Assisted Laser Desorption/Ionization Time-of-Flight
MAMPs	Microbe-Associated Molecular Pattern
MAPKs	Mitogen-Activated Protein Kinases
MAS	Marker-Assisted Selection
Mb	Megabase
MF	Molecular Function
MIF	Macrophage Migration Inhibitory Factor
min	Minutes
miRNAs	MicroRNAs

USC

MS	Mali Stone Bay population
n	Number of individuals / sample size
NADPH	Nicotinamide adenine dinucleotide phosphate (reduced form)
Ne	Effective population size
NF-κB	Nuclear Factor kappa-light-chain-enhancer of activated B cells
NIOZ	Royal Netherlands Institute for Sea Research
NO	Noya population
NO	Nitric Oxide
NOD-like receptors	Nucleotide-Binding Oligomerization Domain-like Receptors
NORA	Native Oyster Restoration Alliance
NOS	Nitric Oxide Synthase
NV	Naïve population
NW	Northwest
O_2^-	Superoxide anion
OE	*Ostrea edulis* (European flat oyster)
OeFas-ligand	*O. edulis* Fas ligand gene
OeIAP	*O. edulis* Inhibitor of Apoptosis Protein gene
OR	Ortigueira population (Thesis)
ORT	Ortigueira population (Vera et al., 2019)
OS	Oosterschelde population
OSH	Oosterschelde hatchery
OsHV uvar	Ostreid Herpesvirus 1 microvariant
OSPAR	Oslo-Paris Convention for the Protection of the Marine Environment
p-value	Probability value
PacBio HiFi	Pacific Biosciences High-Fidelity sequencing
PAF	Pairwise mApping Format
PAMPs	Pathogen-Associated Molecular Patterns
PANZZER	Protein ANNotation with Z-scoRE
PBS	Phosphate-buffered saline
PCA	Principal Component Analysis
PC	Principal Component

USC DE COMPOSTELA

PCR	Polymerase Chain Reaction
PGC1α	Peroxisome proliferator-activated receptor gamma coactivator 1-alpha
PGRPs	Peptidoglycan Recognition Proteins
PIE	Plentzia Marine Station (UPV/EHU)
poly(I:C)	Polyinosinic:polycytidylic acid
POMS	Pacific Oyster Mortality Syndrome
PON	Pontevedra population
PRDX2	Peroxiredoxin-2
PRMT6	Protein arginine N-methyltransferase 6
PRRs	Pattern Recognition Receptors
psu	Practical Salinity Unit
QUI	Quiberon population
QPX	Quahog Parasite Unknown
qPCR	Quantitative Polymerase Chain Reaction
QTL	Quantitative Trait Locus
RAD-Seq	Restriction site–Associated DNA Sequencing
REs	Repetitive elements
RIG-I	Retinoic acid-inducible gene I
RLHs	RIG-I-Like Helicases
RLRs	RIG-I-like receptors
RNA	Ribonucleic Acid
RNA-seq	RNA sequencing
RNS	Reactive Nitrogen Species
ROS	Reactive Oxygen Species
RMSE	Root Mean Square Error
RSEM	RNA-Seq by Expectation Maximization
RvY	Roem van Yerseke hatchery
SNP	Single Nucleotide Polymorphism
SOD	Superoxide Dismutase
SOX2	SRY-box transcription factor 2

USC

SRs	Scavenger Receptors
STAT	Signal Transducer and Activator of Transcription pathway
t	Tonnes
T	Thymine (nucleotide)
TB	Tralee Bay population (Thesis)
TBay	Tralee Bay population (Vera et al., 2019)
TEPs	Thioester-containing proteins
TGF-β	Transforming Growth Factor Beta
THC	Total Haemocyte Count
TPM	Transcripts Per Million
TLRs	Toll-like receptors
TNF	Tumour Necrosis Factor
TPM	Transcripts Per Million
TRIM2	Tripartite motif-containing protein 2
TRIM33	Tripartite motif-containing protein 33
TRIM56	Tripartite motif-containing protein 56
TRIM71	Tripartite motif-containing protein 71
UPV/EHU	University of the Basque Country
UCC	University College Cork
USC	University of Santiago de Compostela
v	Version
vcf	Variant Call Format
WGS	Whole-Genome Sequencing
WZH	Waddenzee hatchery
Zn	Zinc
°C	Degrees Celsius (temperature)
µm	Micrometer
µL	Microliter
ΔK	Delta K (Evanno statistic for population clustering)
χ^2	Chi-square (statistical test)

USC UNIVERSIDADE DE SANTIAGO DE COMPOSTELA

USC
UNIVERSIDADE
DE SANTIAGO
DE COMPOSTELA

GENERAL SUMMARY

USC
UNIVERSIDADE
DE SANTIAGO
DE COMPOSTELA

USC
UNIVERSIDADE
DE SANTIAGO
DE COMPOSTELA

RESUMEN: Genómica de la resistencia al parásito *Bonamia ostreae* en la ostra europea *Ostrea edulis*

La ostra plana europea (*Ostrea edulis*) es una especie de gran relevancia ecológica, económica y cultural, cuyo papel como ingeniero ecosistémico la convierte en un componente clave de los ecosistemas costeros europeos. Sin embargo, las poblaciones naturales han sufrido un drástico declive en el último siglo debido a la sobreexplotación, la degradación del hábitat y, especialmente, a la aparición de la bonamiosis, enfermedad causada por el protozoo intracelular *Bonamia ostreae*. Esta enfermedad provoca elevadas mortalidades en ostras adultas y constituye uno de los principales obstáculos para la recuperación de los bancos naturales y el desarrollo de programas de repoblación. En este contexto, resulta esencial comprender la base genética de la resistencia y desarrollar herramientas de selección que permitan producir semilla tolerante o resistente.

En esta tesis se adoptó un enfoque multidisciplinar, integrando genómica de poblaciones, estudios de estructura cromosómica y transcriptómica, con el objetivo de desentrañar los mecanismos genéticos y moleculares que subyacen a la resistencia a *B. ostreae*. En el primer capítulo, se validó un conjunto de SNPs previamente asociados a resistencia a *Bonamia* mediante el genotipado de poblaciones procedentes de áreas libres de bonamiosis y de zonas con exposición prolongada al parásito. Los resultados confirmaron la existencia de un gran bloque genómico en el cromosoma 8 (C8) fuertemente asociado a la historia de exposición y a la supervivencia en ensayos de infección natural, mostrando un patrón de desequilibrio de ligamiento característico de una inversión cromosómica que suprime la recombinación.

El segundo capítulo amplió la investigación a escala genómica, caracterizando de forma detallada tres grandes inversiones en los cromosomas 2, 5 y 8. Mediante una combinación de genotipado con un nuevo SNP-array multiespecie en 13 poblaciones europeas, análisis de desequilibrio de ligamiento, y secuenciación de genoma completo con lecturas largas, se delimitaron los límites de las tres inversiones y se evaluó su frecuencia y distribución a lo largo de la distribución natural de la especie. Los resultados revelaron que las tres inversiones abarcan aproximadamente el 8 % del genoma de *O. edulis* y muestran altos niveles de diferenciación genética entre las dos orientaciones, lo que sugiere un origen antiguo mantenido por selección divergente o balanceada. El análisis funcional de los genes contenidos en las inversiones evidenció un enriquecimiento en procesos relacionados con inmunidad, metabolismo y respuesta al estrés, lo que refuerza su posible papel adaptativo.

USC DE SANTIAGO

En el tercer capítulo, se validó la asociación entre la inversión C8 y la resistencia a nivel individual, combinando el genotipado de más de 400 individuos de tres poblaciones irlandesas con el SNP-array con el diagnóstico de infección por PCR e histología. Ningún individuo homocigoto para la orientación asociada a resistencia ("naranja") resultó infectado, lo que confirma su asociacióncon la resistencia a *Bonamia*. Además, se desarrolló y validó un panel MassARRAY para genotipado rápido y económico de los alelos diagnósticos para facilitar su aplicación en programas de selección asistida por marcadores. Paralelamente, el análisis transcriptómico en corazones de individuos con distintos niveles de infección reveló una respuesta progresiva caracterizada por la activación metabólica en etapas tempranas, estimulación inmune y mitocondrial en infecciones moderadas, y supresión generalizada de genes de adhesión, apoptosis y metabolismo en infecciones severas, sugiriendo interferencia transcripcional por el parásito.

En conjunto, esta tesis proporciona una visión integral de la arquitectura genómica de la resistencia a *B. ostreae* en *O. edulis* y suministra herramientas aplicables a la restauración de sus bancos naturales. Los resultados refuerzan la hipótesis de que la inversión C8 actúa como un supergén que mantiene un conjunto coadaptado de alelos bajo presión de selección, y sientan las bases para programas de cría orientados a la recuperación de esta especie emblemática en zonas endémicas de bonamiosis.

.

USC
UNIVERSIDADE DE SANTIAGO DE COMPOSTELA

SUMMARY: Genomics of resistance to the parasite *Bonamia ostreae* in the European flat oyster *Ostrea edulis*

The European flat oyster (*Ostrea edulis*) is a species of great ecological, economic, and cultural importance, whose role as an ecosystem engineer makes it a key component of European coastal ecosystems. However, natural populations have suffered a dramatic decline over the past century due to overexploitation, habitat degradation, and, in particular, the emergence of bonamiosis, a disease caused by the intracellular protozoan *Bonamia ostreae*. This disease causes high mortality in adult oysters and constitutes one of the main obstacles to the recovery of natural oyster beds and the development of restocking programs. In this context, it is essential to understand the genetic basis of resistance and to develop selection tools to produce tolerant or resistant seed.

This thesis adopts a multidisciplinary approach, integrating population genomics, chromosomal structure analyses, and transcriptomics to unravel the genetic and molecular mechanisms underlying resistance to *B. ostreae*. In the first chapter, a set of SNPs previously associated with resistance to *Bonamia* was validated by genotyping populations from bonamiosis-free areas and from regions with long-term parasite exposure. Results confirmed the presence of a large genomic block on chromosome 8 (C8), strongly associated with exposure history and survival under natural infection, showing a linkage disequilibrium pattern characteristic of a chromosomal inversion suppressing recombination.

The second chapter expanded the investigation to the genomic scale, thoroughly characterizing three large inversions on chromosomes 2, 5, and 8. By combining genotyping with a new multi-species SNP array in 13 European populations, linkage disequilibrium analyses, and long-read whole-genome sequencing, the breakpoints of the three inversions were delimited, and their frequency and distribution were assessed across the species' native range. Results revealed that the three inversions span approximately 8% of the *O. edulis* genome and display high levels of genetic differentiation between orientations, suggesting an ancient origin maintained by divergent or balancing selection. Functional analysis of genes within the inversions revealed enrichment in processes related to immunity, metabolism, and stress response, supporting their potential adaptive role.

USC UNIVERSIDADE DE SANTIAGO DE COMPOSTELA

In the third chapter, the association between the C8 inversion and resistance was validated at the individual level by combining genotyping of more than 400 individuals from three Irish populations with SNP array data and infection diagnosis by PCR and histology. No homozygous individuals for the resistance-associated ("orange") arrangement were found to be infected, confirming its strong association with *Bonamia* resistance. In addition, a cost-effective MassARRAY panel for rapid genotyping of diagnostic alleles was developed and validated, facilitating its implementation in marker-assisted selection programs. In parallel, transcriptomic analysis of heart tissues from individuals at different infection levels revealed a progressive response characterized by metabolic activation in early stages, immune and mitochondrial stimulation in moderate infections, and generalized suppression of adhesion, apoptosis, and metabolic genes in severe infections, suggesting parasite-driven transcriptional interference.

Altogether, this thesis provides a comprehensive view of the genomic architecture of resistance to *B. ostreae* in *O. edulis* and delivers tools applicable to the restoration of natural oyster beds. The results reinforce the hypothesis that the C8 inversion acts as a supergene maintaining a coadapted set of alleles under selection pressure and lay the groundwork for breeding programs aimed at recovering this emblematic species in bonamiosis-endemic areas.

USC
UNIVERSIDADE DE SANTIAGO DE COMPOSTELA

RESUMO EXTENDIDO EN GALEGO

A ostra plana europea (*Ostrea edulis*) é unha especie mariña clave, tanto ecolóxica como economicamente, cunha distribución nativa que abrangue as costas atlánticas de Europa e o mar Mediterráneo (Yongue, 1960). A especie é un bivalvo sésil, filtrador e planctotrófico (Ezgeta-Balić et al., 2020; Peharda et al., 2012), capaz de acadar ata 20 cm de tamaño e vivir ata 20 anos, o que a fai particularmente vulnerable á sobrepesca e lenta para recuperarse de colapsos poboacionais.

Alén do seu valor comercial, *O. edulis* desempeña un papel fundamental nos ecosistemas mariños costeiros, contribuíndo á filtración da auga, ao ciclo de nutrientes e á provisión de hábitat para numerosos organismos mariños (Astrup et al., 2019; Pogoda et al., 2019a). Os seus arrecifes bioxénicos incrementan a biodiversidade ao fornecer refuxio e substrato de asentamento para unha ampla variedade de invertebrados bentónicos e peixes xuvenís (Smaal et al., 2015). É por iso, que a restauración dos bancos de *O. edulis* é cada vez máis recoñecida como unha solución baseada na natureza para promover a resiliencia costeira, mellorar a biodiversidade e mitigar os efectos do cambio climático mediante o secuestro de carbono no material calcáreo da cuncha e no sedimento (Pogoda et al., 2019a; zu Ermgassen et al., 2020). Iniciativas europeas como NORA (Native Oyster Restoration Alliance) subliñan a necesidade urxente de contar con stocks resistentes e xeneticamente diversos para repoboar hábitats historicamente importantes e recuperar funcións ecosistémicas perdidas. Os resultados desta tese contribúen directamente a estes obxectivos, ao ofrecer marcadores xenéticos e variantes estruturais que poden guiar a selección de reprodutores e o seguimento a longo prazo das poboacións restauradas.

USC DE SANTIAGO

Historicamente, *O. edulis* sustentou pesquerías extensas, mais desde mediados do século XX as poboacións sufriron declives dramáticos debido a unha combinación de sobreexplotación, degradación do hábitat e a aparición de enfermidades (Zu Ermgassen et al., 2020). A mediados de século, a especie xa se atopaba funcionalmente extinta no mar do Norte neerlandés (Pogoda et al., 2019b).

Dende entón puxéronse en marcha esforzos de restauración en toda Europa, mais o seu éxito viuse severamente limitado pola propagación de enfermidades infecciosas, en particular a bonamiose causada por *Bonamia ostreae* (Colsoul et al., 2021). *B. ostreae* é un protozoo parasito pertencente ao filo Haplosporidia (Carnegie & Cochennec-Laureau, 2004; Lopez-Flores et al., 2007), coñecido por infectar os hemocitos da ostra plana, alterando a fisioloxía do hóspede e provocando con frecuencia mortalidade (Grizel, 1985). Aínda que o seu ciclo vital fóra do hóspede segue a ser pouco coñecido, crese que a transmisión ocorre directamente entre ostras, xa sexa mediante cohabitación ou por inxección de parasitos purificados (Hervio et al., 1995), o que suxire que un hóspede intermedio podería non ser necesario. A prevalencia adoita aumentar a partir do outono, acadando o seu máximo a finais do inverno ou comezos da primavera (Culloty & Mulcahy, 1996; Engelsma et al., 2010). Ademais, *O. edulis* parece máis susceptible a *B. ostreae* despois de períodos de baixa dispoñibilidade de alimento ou de salinidade reducida (Engelsma et al., 2010).

Despois da súa aparición en Francia, *B. ostreae* espallouse rapidamente por Europa: a España e Dinamarca en 1980, a Inglaterra en 1982 e a Irlanda en 1987. Porén, o parasito xa estaba presente nas poboacións irlandesas desde comezos da década de 1980. O primeiro brote confirmado tivo lugar en Rossmore, situado no Canle Norte do Porto de Cork, onde a mortalidade comezou a incrementarse en 1984 e superou o 90 % en ostras de catro anos ou máis en 1987 (McArdle et al., 1991). Máis recentemente, o parasito foi detectado en Lough Foyle (2005) e Lough Swilly (2006). Nos Países Baixos, a introdución de *B. ostreae* en 1980 a través de importacións de ostras procedentes de Francia complicou aínda máis as perspectivas de restauración. O parasito volveuse endémico nas poboacións neerlandesas tras se espallar desde o Oosterschelde ata o lago Grevelingen (Van Banning, 1982; Van Banning, 1991).

A distribución irregular de *B. ostreae* permitiu estudos comparativos entre poboacións naïve (NV) e poboacións afectadas a longo prazo (LTA), revelando evidencias de adaptación local e selección diverxente (Pardo et al., 2016; Ronza et al., 2018; Vera et al., 2019). Observouse resistencia natural en poboacións previamente expostas, que tenden a mostrar menor susceptibilidade en comparación coas naïve (Elston et al., 1987; Lynch et al., 2014). Comprender a base xenética desta resistencia é clave para desenvolver estratexias de control e xestión eficaces. Os enfoques xenómicos identificaron QTLs e SNPs asociados a resistencia (Lallias et al., 2009; Harrang et al., 2015).

USC UNIVERSIDADE DE SANTIAGO DE COMPOSTELA

Empregando un *SNP array* (Gutiérrez et al., 2017), Vera et al. (2019) identificaron loci *outlier* baixo selección diverxente entre poboacións NV e LTA, moitos dos cales se agruparon nunha única rexión xenómica, suxerindo a existencia dun QTL maior asociado a resistencia. Estes resultados constituíron a base do primeiro capítulo desta tese, centrado na validación destes marcadores en poboacións independentes e contextos experimentais.

Esta tese doutoral adoptou un enfoque multiescala para dilucidar os mecanismos xenéticos subxacentes á resistencia a *B. ostreae* en *O. edulis*, integrando xenómica poboacional, xenómica estrutural e transcriptómica. O primeiro capítulo centrouse na validación de SNPs asociados a resistencia identificados orixinalmente por Vera et al. (2019). Mediante cribado xenómico dun grande número de ostras de bancos NV e LTA distribuídos entre as principais rexións xenéticas da especie, confirmouse que varios marcadores relacionados con maior supervivencia segregaban consistentemente entre NV e LTA. Estes marcadores localizáronse maioritariamente dentro dunha inversión cromosómica putativa, na que unha das orientacións pareceu asociarse coa resistencia, en concordancia coa información previa de Vera et al. (2019).

As análises de xenómica poboacional empregando un *SNP array* Affymetrix Axiom de densidade media (14.950 SNPs; densidade media: 1 SNP por ~63 kb ao longo do xenoma da ostra plana, 935,6 Mb; Gutiérrez et al., 2017) revelaron unha diferenciación baixa pero significativa entre poboacións silvestres do mar do Norte, cun sinal claro de illamento por distancia. Isto contrastou cos resultados de Galicia, onde Vera et al. (2016) non detectaron estrutura xenética, o que probablemente reflicte distintos patróns de conectividade oceanográfica. Como era de agardar, as mostras de criadeiro amosaron menor diversidade xenética que as poboacións silvestres debido ao tamaño efectivo reducido durante a xestión de reprodutores. Porén, as contribucións parentais equilibradas observadas suxiren que os protocolos actuais de criadeiro poden ser axeitados, sempre que se incremente o número de reprodutores e de lotes para garantir a variabilidade xenética a longo prazo nos programas de repoboación.

As análises baseadas en loci *outlier* revelaron dous grupos xenéticos distintos dentro das mostras do mar do Norte: os xenotipos “laranxa” e “azul”, sendo o clúster laranxa máis frecuente nas poboacións LTA. Este patrón confirmouse na gran mostra utilizada no experimento de ambiente común: a poboación NIOZ (NV), caracterizada por unha proporción moito menor de individuos laranxas, experimentou unha mortalidade substancialmente maior en comparación coa poboación RvY (LTA), onde a frecuencia de xenotipos laranxas foi máis alta e a mortalidade notablemente reducida. Aínda que non se detectou infección por parasito nas ostras de Lake Grevelingen mediante qPCR, os contrastes de supervivencia apoian que existe un compoñente xenético que sustenta a resistencia a *B. ostreae* máis alá dos factores ambientais. A falla de detección por qPCR no mar do Norte podería deberse ao tecido escollido (branquias), que non conteñen as células diana de *Bonamia* (hemocitos), polo que unha proba usando hemolinfa ou corazón sería máis axeitada. Ademais, como se suxeriu previamente (Ronza et al., 2018; Hoffman et al., 2021), unha fase latente no ciclo de infección do parasito tamén podería explicar esta observación.

USC

As análises de desequilibrio de ligamento (LD) revelaron fortes correlacións entre SNPs *outlier*, consistentes cunha gran inversión cromosómica subxacente que suprime a recombinación ao longo dun segmento de ~34 Mb do cromosoma 8. Este LD inusualmente alto suxire a presenza dunha variante estrutural que mantén un bloque haplotípico coadaptado baixo selección. Isto viuse apoiado por picos de F_{ST}, valores negativos de F_{IS} dentro de orientacións e a caída abrupta do LD nos límites da inversión. Mecanismos semellantes foron descritos noutras especies mariñas como impulsores de adaptación local e resistencia a patóxenos (Mérot et al., 2021).

A partir da evidencia da inversión en C8, o segundo capítulo ampliou o foco á variación estrutural xenómica en *O. edulis*, confirmando a presenza de tres inversións principais nos cromosomas 2, 5 e 8. O xenotipado denso con SNPs en 13 poboacións ao longo da distribución da especie revelou que estas inversións cobren en conxunto preto do 8 % do xenoma. As análises de LD, a secuenciación PacBio e a validación por PCR dos puntos de ruptura converxeron en coordenadas precisas da inversión, mentres que elementos repetitivos (LINEs, DNA/hAT, PLE/Naiad) e duplicacións en tándem flanqueando os puntos de ruptura suxeriron mecanismos implicando recombinación ectópica ou reparación escalonada de roturas de dobre febra na súa orixe (Evgen'ev et al., 2000; Lee et al., 2008; Araya et al., 2025). A validación exitosa dos puntos de ruptura mediante PCR fornece unha ferramenta molecular práctica para futuros xenotipados, aínda que distinguir heterocariotas de homocariotas requirirá aproximacións complementarias como SNaPshot ou ensaios MassARRAY.

É importante destacar que os puntos de ruptura coincidiron con elementos repetitivos, consistente co seu papel proposto na formación de inversións en diversos taxóns (Evgen'ev et al., 2000; Villeoutreix et al., 2021).

As tres inversións amosaron unha diferenciación xenética extraordinariamente alta entre orientacións (F_{ST} = 0,49–0,68) fronte á media xenómica (F_{ST} ≈ 0,04), o que suxire unha forte selección diverxente actuando sobre ambos arranxos. A diversidade elevada dentro das orientacións, particularmente no arranxo "laranxa" do sur (C8) e no "verde" (C2), suxire unha orixe antiga. Diversas liñas de evidencia apuntan a un orixe ancestral destas inversións: representan eventos mutacionais únicos que tenden a ser eliminados das poboacións pola menor fertilidade dos heterocigotos, a non ser que confiran unha vantaxe selectiva substancial —xa sexa por selección positiva ou sobredominancia— que permita que se manteñan ao longo do tempo (Berdan et al., 2023). Os valores extremos de F_{ST} observados para SNPs dentro das inversións entre arranxos alternativos (≥ 0,50) apoian unha selección diverxente forte e unha orixe anterior á aparición de *B. ostreae*, seguida de contacto secundario entre liñaxes historicamente diverxentes (Monteiro et al., 2024). De acordo coas expectativas teóricas, a diversidade xenética dentro do arranxo máis recente tende a ser menor, aumentando gradualmente a través de mutación, fluxo xenético mediante dobres cruzamentos e conversión xenética (Kapun et al., 2023; Charlesworth, 2023).

USC UNIVERSIDADE DE SANTIAGO DE COMPOSTELA

Os escaneos de loci *outlier* amosaron un enriquecemento elevado de loci baixo selección diverxente dentro das inversións (76%) en comparación co xenoma ao redor (8%), apoiando o seu papel como reservorios de variación adaptativa. As análises de enriquecemento funcional dos xenes situados dentro das inversións revelaron procesos biolóxicos potencialmente ligados á adaptación a factores abióticos (temperatura, salinidade) e bióticos (exposición a patóxenos, competencia). A inversión C2 abarcou xenes implicados en sinalización de neuropéptidos, regulación epixenética, respostas inmunes e rutas metabólicas, potencialmente subxacentes á resiliencia fronte a flutuacións ambientais. Xenes relacionados coa sinalización de neuropéptidos e detección de estímulos externos, así como aqueles implicados no transporte transmembrana e actividade de canais iónicos, poderían explicar adaptacións á variabilidade de temperatura e salinidade (Clark et al., 2013, 2020; Signorini et al., 2025). Así mesmo, xenes ligados á actividade ciliar e á filtración de fitoplancto apuntan a diferenzas en estratexias de alimentación e metabolismo enerxético (Marinković et al., 2019).

Pola contra, a inversión C5 contiña xenes implicados no transporte e homeostase do zinc. O zinc é esencial para procesos celulares que inclúen actividade encimática, regulación transcripcional e respostas ao estrés oxidativo. Reportáronse expresións diferenciais de xenes relacionados co zinc en resposta á contaminación por metais en *M. gigas* (Meng et al., 2021) e *Crassostrea hongkongensis* (Li et al., 2020).

A inversión C8, previamente asociada á resistencia a *B. ostreae*, incluíu 14 dos 16 SNPs *outlier* relacionados con resistencia identificados en estudos anteriores (Vera et al., 2019; Capítulo 1). Os xenes nesta rexión estaban enriquecidos en funcións relacionadas co metabolismo de carbohidratos, produción de enerxía, remodelado tisular e rutas inmunes, incluíndo sinalización de receptores de citoquinas e de factor de necrose tumoral (Canesi et al., 2022). Estes achados suxiren que esta rexión xenómica podería modular respostas inmunes e mecanismos de reparación tisular tras infeccións por *B. ostreae*, un parasito intracelular. De xeito interesante, poboacións NV ou con baixa afectación, como Bergen e Lough Swilly, amosaron maior frecuencia do arranxo “azul” en comparación con poboacións LTA xeograficamente próximas como Oosterschelde e Galway. A predominancia do arranxo “laranxa” en poboacións meridionais, xunto coa asociación entre brotes de *Bonamia* e temperaturas máis cálidas (Audemard et al., 2008), podería explicar o patrón observado. Porén, non se pode descartar a posibilidade dunha correlación espuria impulsada por clinas norte–sur nas frecuencias das inversións e na distribución latitudinal do parasito.

Desde unha perspectiva evolutiva, a persistencia da inversión C8 e a súa alta frecuencia de heterocariotas suxiren un equilibrio entre presións selectivas e posibles custos de fertilidade. Isto é consistente con modelos teóricos nos que as inversións actúan como “superxenes” que preservan combinacións de alelos beneficiosos baixo réximes de selección heteroxénea (Faria et al., 2019). O mantemento de arranxos alternativos ao longo de escalas temporais evolutivas podería estar impulsado por selección espacial ou temporalmente variable, así como por posibles efectos de sobredominancia que confiran vantaxe aos heterocigotos.

USC UNIVERSIDADE DE COMPOSTELA

A detección de fortes sinais de selección diverxente ($F_{ST} \geq 0,50$) e de clinas latitudinais nas frecuencias dos arranxos reforza a hipótese de mantemento a longo prazo baixo selección, en lugar dunha varrida selectiva recente.

O terceiro capítulo validou a asociación da inversión C8 coa resistencia/tolerancia á bonamiose a nivel individual e combinou esta perspectiva con análises transcriptómicas no medio natural. Non se atoparon homocariotas laranxas infectados, mentres que se observaron infeccións en homocariotas azuis e heterocariotas, confirmando unha relación aditiva entre arranxos e fenotipos de resistencia. Desenvolveuse un panel dirixido MassARRAY para fornecer unha ferramenta práctica de detección de arranxos resistentes e susceptibles que permita apoiar programas de selección e o seguimento de bancos naturais. Complementando estes resultados xenómicos, as análises transcriptómicas de ostras de Lough Swilly revelaron un cambio progresivo na expresión xenética ao longo dos niveis de infección: a infección temperá asociouse a reprogramación metabólica; a infección moderada, a procesos mitocondriais e do citoesqueleto; e a infección severa, a vías de sinalización e transdución de enerxía.

En todas as etapas observouse unha represión transcriptómica xeneralizada, particularmente en xenes implicados en apoptose, adhesión e función mitocondrial, o que suxire a capacidade de *B. ostreae* para superar a resposta do hóspede e garantir a supervivencia e proliferación intracelular.

A nivel transcriptómico, a represión xeneralizada de efectores inmunes, compoñentes mitocondriais e moléculas de adhesión destaca como *B. ostreae* xenera procesos clave do hóspede para asegurar a súa supervivencia. A infraexpresión de xenes relacionados coa apoptose é especialmente relevante, xa que probablemente evita a eliminación mediada polos hemocitos de células infectadas, permitindo que o parasito prolifere intracelularmente. A represión de transcritos do citoesqueleto e da matriz extracelular suxire unha motilidade hemocitaria e unha actividade fagocítica comprometidas, críticas para a eliminación do parasito. En conxunto, estes patróns apuntan a unha estratexia sofisticada de evasión inmune por parte de *B. ostreae*, convertendo a maquinaria celular do hóspede nun ambiente permisivo. O feito de que moitos destes xenes reprimidos se localicen dentro dos límites da inversión C8 sinala esta inversión como un nodo funcional de resiliencia, cuxa integridade de expresión é clave para os fenotipos de resistencia.

Un patrón consistente e rechamante foi a predominancia de xenes infrarrepresentados á baixa en individuos infectados. A través de todos os niveis de infección, o número de transcritos reprimidos superou amplamente os inducidos, cun desequilibrio especialmente acusado en niveis de infección intermedios, o que suxire que *B. ostreae* manipula activamente a expresión xenética do hóspede para suprimir respostas inmunes e funcións celulares, garantindo a persistencia intracelular. Estratexias semellantes foron descritas para outros parasitos intracelulares, que a miúdo interfiren coa transcrición do hóspede, a apoptose e as vías de estrés oxidativo para establecer infeccións crónicas (Gómez-Díaz et al., 2012; Canesi et al., 2022).

Varios dos transcritos máis fortemente reprimidos caeron dentro dos límites de C8, incluíndo factores de transcrición (tipo Sox-2), ligasas de ubiquitina (TRIM2, TRIM56), proteínas do citoesqueleto e de adhesión (β-tubulina, α-catenina-2, coláxeno C4-like, condroaderina-like), encimas metabólicos (enolasa-fosfatasa E1, desaturasa de esfingolípidos DES1-like, MPDU1) e proteínas de tráfico vesicular (SorCS1, Shisa-5, sinaptobrevina/YKT6). O feito de que a represión inducida polo parasito se dirixa desproporcionadamente a este clúster xenético reforza a idea de que C8 funciona como unha reserva de alelos coadaptados esenciais para a resistencia.

En conxunto, estes resultados fornecen unha explicación práctica que conecta a xenómica estrutural coas respostas funcionais: en xenotipos resistentes portadores do arranxo "laranxa", o haplotipo C8 probablemente mantén a expresión coordinada de módulos citoesqueléticos, metabólicos e reguladores que sustentan a activación inmune e a integridade tisular. En contraste, os xenotipos susceptibles "azuis" son incapaces de evitar que o parasito suprima estas funcións, o que conduce a unha adhesión hemocitaria minguada, fagocitose deficiente, colapso do metabolismo enerxético e bloqueo da apoptose.

A superposición entre os patróns de xenes diferencialmente expresados e o contido xenético de C8 unifica así os achados xenómicos e transcriptómicos, conectando os marcadores de resistencia baseados en SNP (Capítulos 1 e 3) coa variante estrutural subxacente (Capítulo 2).

Os achados desta tese teñen tamén importantes implicacións aplicadas. A validación da inversión C8 como marcador xenómico fiable para a resistencia a *B. ostreae* abre a porta á selección asistida por marcadores en criadeiros e programas de restauración. Mediante o cribado de reprodutores e semente para o haplotipo protector "laranxa", os xestores de criadeiros poden aumentar a probabilidade de producir descendencia con resistencia completa, mellorando así a supervivencia en contornas endémicas de *B. ostreae*. Porén, a presenza de heterocariotas que amosan tolerancia parcial suscita cuestións epidemiolóxicas, xa que tales individuos poderían actuar como portadores asintomáticos. Aínda que contribúen á resiliencia demográfica, tamén poderían facilitar a persistencia e transmisión do parasito en ecosistemas restaurados.

Finalmente, cómpre recoñecer algunhas limitacións. Este estudo baseouse en infeccións naturais que, se ben achegan información ecoloxicamente realista, limitan a capacidade de controlar as condicións de exposición. A dose de infección, o momento e o contexto ambiental non se puideron estandarizar, deixando certa incerteza sobre se os controis non infectados representan realmente ostras resistentes ou individuos que simplemente evitaron o contacto co parasito. Polo tanto, son esenciais experimentos de desafío controlado entre xenotipos e cariotipos para diferenciar resistencia (baixa carga de infección) de tolerancia (supervivencia a pesar da infección) e para cuantificar posibles compensacións de fitness asociadas a cada estratexia. Outra limitación é a caracterización funcional incompleta de xenes localizados dentro das inversións identificadas.

USC UNIVERSIDADE DE SANTIAGO DE COMPOSTELA

Aínda que a inversión C8 se asociou consistentemente coa resistencia a *Bonamia*, moitos dos xenes situados na inversión permanecen pobremente anotados, restrinxindo as interpretacións funcionais. Enfoques como transcriptómica de lectura longa, RNA-seq de célula única e perfilaxe epixenómica poderían fornecer mapas de alta resolución de redes reguladoras e respostas específicas de tipo celular. Estas ferramentas tamén aclararían a posible contribución de procesos a nivel de cromatina —como o enriquecemento de complexos de histona acetiltransferase e a expresión diferencial de histonas observada nesta tese— á modulación de respostas inmunes innatas.

En resumo, esta tese ofrece unha exploración integral e multiescala das bases xenómicas e moleculares da resistencia a *B. ostreae* na ostra plana europea. Ao combinar xenómica de poboacións, descubrimento de variantes estruturais e transcriptómica, demóstrase que a resistencia está en gran medida capturada pola inversión do cromosoma 8, que mantén un haplotipo coadaptado enriquecido en funcións inmunes e metabólicas. Esta variante estrutural non só predí a supervivencia a nivel poboacional, senón que determina o resultado da infección a nivel individual, e o seu contido xenético correspóndese con funcións clave reprimidas durante a infección. A integración destes achados ofrece tanto coñecemento fundamental sobre coevolución hóspede–parasito como ferramentas prácticas para a acuicultura, apoiando o desenvolvemento de liñas de ostras resistentes e a restauración de poboacións naturais baixo presión parasitaria.

USC
UNIVERSIDADE DE SANTIAGO DE COMPOSTELA

GENERAL INTRODUCTION

USC
UNIVERSIDADE
DE SANTIAGO
DE COMPOSTELA

USC
UNIVERSIDADE
DE SANTIAGO
DE COMPOSTELA

1. *OSTREA EDULIS*: BIOLOGY AND CONSERVATION

1.1. The European flat oyster

The European flat oyster, *Ostrea edulis* (Linneaus, 1758), is a marine bivalve mollusc belonging to the family Ostreidae, valued for its ecological, economic, and cultural significance. With a long history of human exploitation dating back to the Mesolithic era, this species has long been a staple in the European seafood market (Haussman et al., 2019). Beyond its commercial value, *O. edulis* plays a key role in coastal marine ecosystems, contributing to water filtration, nutrient cycling, and the provision of habitat for numerous marine organisms (Astrup et al., 2019; Pogoda et al., 2019a).

O. edulis is a sessile, filter-feeding, planktotrophic species (Peharda et al., 2012; Ezgeta-Balić et al., 2020), capable of reaching up to 20 cm in size and living for up to 20 years. Morphologically, it has a rough-textured shell with irregular edges. The two valves are held together by an elastic ligament and are unequal in both shape and function: the left valve is concave and permanently attached to the substrate, while the right valve is flatter and fits over the other, acting as a lid (Bayne, 2017). It typically inhabits firm benthic substrates composed of mud, rocks, hard silt, or artificial materials such as broken shells (cultch), and can be found at depths of up to 80 m. *O. edulis* feeds by filtering seawater, which it pumps through its gills that act as natural filters. In this way, the oyster captures suspended particles such as phytoplankton or dissolved organic matter, which constitute its main food source (Grant et al., 1990).

The species is a protandrous hermaphrodite, generally changing sexes twice within a single reproductive season. This process is influenced by environmental conditions, particularly seawater temperature, which plays a key role in the species' reproduction cycle (Ruiz et al., 1992; Stechele et al., 2022). It also appears to be regulated by epigenetic factors, such as differences in DNA gill methylation in hermaphroditic individuals (Valk et al., 2025).

Fertilization is internal: ova are fertilized within the female's pallial cavity by sperm transported through the gills as part of the normal feeding process. After an incubation period of 8-10 days, the free-swimming larvae are released into the water column, where they remain planktonic for 10-30 days before setting and undergoing metamorphosis (Berghahn & Ruth, 2005; Bayne, 2017). Oyster generations often settle atop previous ones, forming vertically structured reefs that provide additional habitat complexity and biological richness (Chambers et al., 2017).

USC UNIVERSIDADE DE SANTIAGO DE COMPOSTELA

O. edulis beds, or reefs, represent hotspots of marine biodiversity and trophic complexity. These biogenic structures transform otherwise flat, microbially dominated benthic areas into dynamic ecosystems that support diverse communities of fish, crustaceans, macroalgae, and invertebrates (Christianen et al., 2018; Fig. 1). In doing so, they deliver vital ecosystem services such as shoreline stabilization, substrate formation, and water quality improvement.

Beyond its ecological significance, *O. edulis* has long held cultural value in European coastal regions. Historically harvested in both fisheries and aquaculture, the species remains economically relevant today. Molluscs represent one of the most diverse and productive animal groups, and within aquaculture, bivalves account for around 20% of global aquatic animal production by weight (Gatta, 2022). The species' culinary value and adaptability also make a prime candidate for restoration and aquaculture initiatives. Historical records and socio-economic data are increasingly used to support conservation policies and restoration goals (Hayden-Hughes et al., 2023).



Figure 1. Illustration of a native European flat oyster reef in Galicia (NW Spain) with the associated benthic community. The reef provides habitat and refuge for a wide range of native species and enhances local biodiversity, contributes to nutrient cycling, and improves water quality through filter feeding. Original figure.

1.2. Distribution of *O. edulis*

Historically, *O. edulis* was abundant throughout its range, forming extensive and dense reefs along Europe's coastline, playing a critical ecological role in maintaining biodiversity, stabilizing habitats, and supporting the productivity of coastal zones (Beck et al., 2011; zu Ermgassen et al., 2021).

USC DE SANTIAGO

Its distribution extended from the Atlantic coasts of Morocco to Norway, and throughout the Mediterranean and Black Seas (Yongue, 1960). Today, natural populations of *O. edulis* persist across parts of Northern Europe, including the North and Baltic Seas, and Southern Europe, notably along the Atlantic coasts of France and Spain (Pouvreaeu et al., 2023). In the Mediterranean, viable populations remain in specific areas such as the Adriatic and Aegean Seas (Acarli et al., 2011; Stagličić et al., 2020), as well as the Mar Menor in southeastern Spain (Albentosa et al., 2023).

O. edulis is native to at least 14 European countries, including Belgium, Croatia, Denmark, France, Germany, Greece, Ireland, Italy, the Netherlands, Norway, Portugal, Spain, Sweden, and the United Kingdom (Bonham & Roberts, 2022), with France, Spain, the Netherlands, and the UK currently being the largest producers (Gatta, 2022).

The species has also been introduced beyond its natural range through human-mediated transfers, primarily for aquaculture and restoration activities, including parts of the Atlantic coast of North America (Vercaemer et al., 2006) and Western Australia (Morton et al., 2003). In the eastern United States, naturalized populations remain along the coast from Maine to Rhode Island, originating from international introductions in the mid-20th century.

1.3. Decline and threats to *O. edulis*: bonamiosis

Despite its ecological value and historical prominence, *O. edulis* populations have suffered a dramatic population decline over the past century. Overharvesting, coastal development, water pollution, and destructive fishing practices such as dredging have all contributed to the widespread degradation of oyster habitats.

To counterbalance decline, restocking programs were launched in many European countries, often involving translocations of oysters between regions. While well-intentioned, these efforts inadvertently accelerated the spread of infectious diseases, particularly the protozoan parasite *Bonamia ostreae*, one of the causative agents of bonamiosis (Colsoul et al., 2021).

As filter-feeding organisms constantly exposed to diverse microorganisms, oysters rely on innate immune defences to protect themselves against infections. These defences, mediated by circulating haemocytes and diverse humoral effectors, provide rapid but non-specific responses that determine the outcome of host–pathogen interactions. Understanding the components and mechanisms of this immune system is therefore essential to interpret the impact of *B. ostreae* on oyster populations (See section 2).

Bonamia ostreae is a protozoan parasite belonging to the phylum Haplosporidia (Carnegie & Cochennec-Laureau, 2004; Lopez-Flores et al., 2007), known to infect haemocytes of the flat oyster, disrupting host physiology and often resulting in mortality (Grizel, 1985).

UNIVERSIDADE

Although its life cycle outside the host remains poorly understood, transmission is thought to occur directly between oysters, either through cohabitation or via injection of purified parasites (Hervio et al., 1995), suggesting that an intermediate host may not be necessary. Nevertheless, the potential involvement of benthic macroinvertebrates and zooplankton in the parasite's transmission has been explored, with *Ophiothrix fragilis* identified as a possible vector (Lynch et al., 2007).

The detection of the parasite in both adults and larvae indicates that vertical transmission may occur during the brooding period, when *O. edulis* retains its larvae within the pallial cavity for 8–10 days prior to release (Marteil, 1960). This incubation period could favour parasite transfer from the adult to its progeny, and infection has indeed been confirmed in larvae by PCR and *in situ* hybridisation (da Silva et al., 2008; Arzul et al., 2011). Although prevalence in larvae appears generally low, their planktonic stage could nonetheless contribute to parasite dispersal over larger spatial scales via water currents. Moreover, *B. ostreae* has been shown to survive in seawater for at least one week (Arzul et al., 2011), providing additional opportunities for transmission through the water column. However, the patchiness distribution of the parasite across flat oyster shellfish beds suggests limitations to its spreading through larval advection (Vera et al., 2019).

In addition to *O. edulis*, *B. ostreae* can infect *Magallana gigas* and *Ostrea chilensis*, although the severity of infection varies. In areas where *M. gigas* coexists with native flat oysters, it is often considered a carrier or reservoir species (Lynch et al., 2010). Despite the occasional detection of parasite DNA in other aquatic organisms (Lynch et al., 2007), the correlation between oyster density and bonamiosis prevalence suggests that flat oysters remain the principal hosts and drivers of parasite persistence and spread (Grizel, 1985; Van Banning, 1987; Hudson & Hill, 1991).

The parasite primarily targets the host's haemocytes—the key components of the oyster's immune system—causing chronic infections that undermine immune competence and can lead to death, particularly in densely populated environments (Comps et al., 1980). However, *B. ostreae* can also be found extracellularly, between epithelial or interstitial cells in the gills and stomach, and within necrotic connective tissue (Fig. 2). Intraepithelial infections have also been observed in the gills (Montes et al., 1994) and in ovarian tissue (Van Banning, 1990). In these cases, since the target cells are the haemocytes, the presence of *Bonamia* among tissue cells in the gills does not necessarily indicate an active infection. *Bonamia* cells may enter through the gills in the same way that food particles are taken in during filter feeding (Fig. 3A).

Prevalence of infection is highly variable, ranging from 0% to 80%, and tends to be higher in individuals older than two years. The disease can occur and be transmitted throughout the year but displays marked seasonal patterns. Prevalence generally increases from autumn, peaking in late winter or early spring (Grizel, 1985; Culloty & Mulcahy, 1996; Arzul et al., 2006; Engelsma et al., 2010). Laboratory studies suggest that purified parasites survive better in seawater at 4°C or 15°C than at higher temperatures such as 25°C (Arzul et al., 2009).

USC UNIVERSIDADE

Likewise, high salinities (35–45 psu) appear to favour parasite survival (Arzul et al., 2009). Although annual prevalence patterns vary geographically, two main peaks are typically observed: one in winter–spring and another in autumn (Culloty & Mulcahy, 1996; Arzul et al., 2006). Environmental factors seem to modulate these dynamics, as lower summer temperatures combined with higher salinities have been associated with increased prevalence during the subsequent winter (Arzul et al., 2006). In addition, *O. edulis* appears to be more susceptible to *B. ostreae* after periods of reduced food availability or decreased salinity (Engelsma et al., 2010), and coinfections with other pathogens, including neoplasms and apicomplexans, further increase vulnerability to bonamiosis (da Silva et al., 2011).

B. ostreae was first detected in Europe in 1979 in France and is thought to have been introduced via oyster imports from the United States (Carnegie & Cochennec-Laureaeu, 2004). Following its appearance in France, *B. ostreae* rapidly spread across Europe: to Spain and Denmark in 1980, England in 1982, and Ireland in 1987. It has since been detected in Wales (2006), Northern Ireland (2006), and Morocco (2005), demonstrating the difficulty of containing its spread once established (van Banning, 1987; Culloty & Mulcahy, 2007; Colsoul et al., 2021).

Bonamiosis typically causes mortality rates between 50% and 80% in susceptible oyster populations, particularly among individuals that have reached reproductive age and they are close to commercialization (da Silva et al., 2005; Lallias et al., 2008). These losses have not only undermined aquaculture profitability but also severely impacted natural oyster beds, contributing to reef collapse and loss of ecosystem functions. With declining oyster populations, the structural complexity and ecological benefits of reefs—including sediment stabilization and water filtration—have also diminished (Pogoda et al., 2019a).

The distribution of *B. ostreae* vary across European coastal regions and is influenced by environmental factors such as water temperature and salinity. Thus, parasite's viability and host susceptibility (Arzul et al., 2009) leads to the formation of disease "hotspots" that complicate management and restoration. Consequently, *O. edulis* has been largely replaced in commercial aquaculture by the Pacific oyster (*M. gigas*), which is more resilient to this parasite and grows faster (Colsoul et al., 2021).

The long-term presence of *B. ostreae* in European waters continues to pose major challenges for the recovery of *O. edulis*. While some oyster populations have developed partial resistance or tolerance, complete immunity remains elusive. Integrated approaches that combine habitat restoration, disease monitoring, selective breeding, and genetic management are needed to support the long-term viability of native oyster populations.

USC
UNIVERSIDADE DE SANTIAGO DE COMPOSTELA

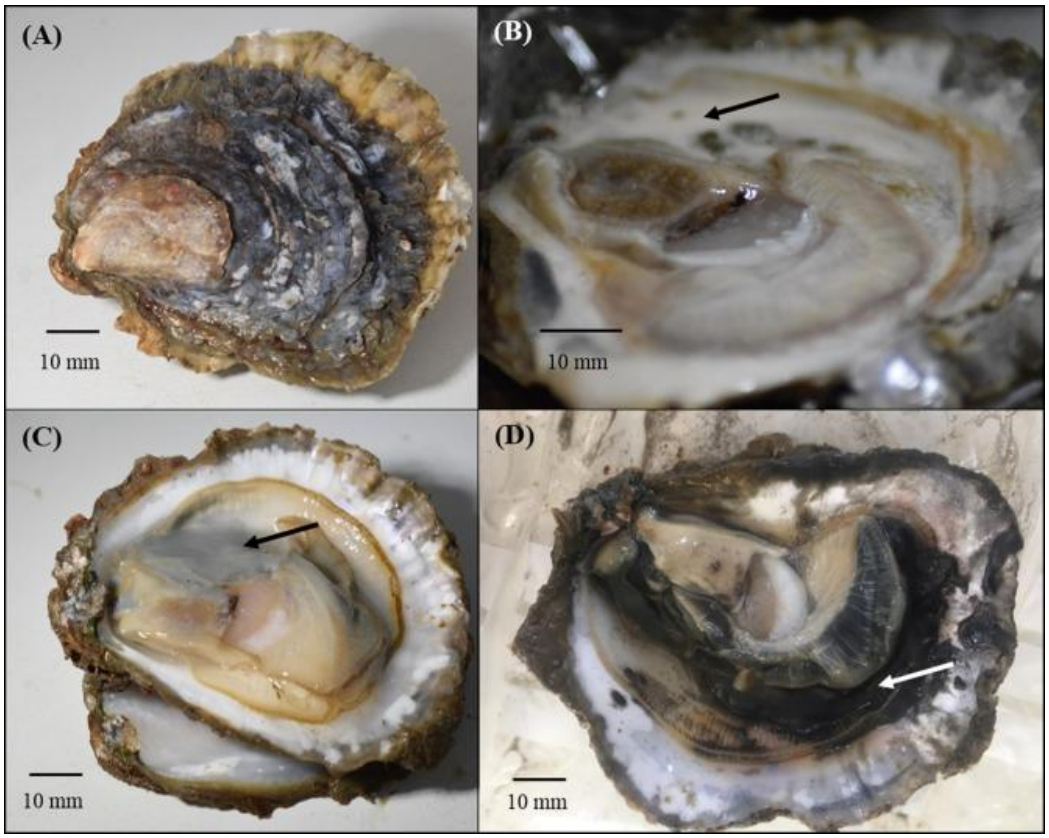


Figure 2. A) Brooding oyster prior to shucking; brooding oysters containing larvae referred to as (B) white "sick", (C) grey "sick" and (D) black "sick" stages of development. Larvae within the pallial cavity in and around the gill and mantle structures are indicated by arrows. Reproduced from Helmer et al., (2020) under Creative Commons Attribution (CC BY).

1.4. European restoration efforts

The combined effects of overexploitation, habitat degradation, and diseases outbreaks have prompted numerous scientific, political, and civil society efforts aimed at restoring *O. edulis* across its native range. In recent years, oyster restoration has gained renewed attention as part of broader marine conservation strategies, supported by a growing recognition of the species' ecological and socio-economic value.

Several European countries – including Germany, the Netherlands, and Belgium – have drawn on historical records to reconstruct the former distribution of *O. edulis* and guide site selection for pilot restoration projects (De Mesel et al., 2018; Kamermans et al., 2018; Pogoda et al., 2019b). These efforts revealed not only the extent of historical losses but also the potential for targeted reintroduction in areas with suitable environmental conditions.

USC UNIVERSIDADE DE SANTIAGO DE COMPOSTELA

Organizations such as the OSPAR Commission and Native Oyster Restoration Alliance (NORA) have coordinated restoration actions across Europe, including the reintroduction of oysters to historic habitats, the establishment of protected zones, and research into disease-resistant genotypes (Pogoda et al., 2019a; Thorngren et al., 2019; Vera et al., 2019). A basic mass breeding program has been developed in Rossmore along more than 30 years with encouraging results (Lynch et al et al., 2014).

Research into disease-resistant or tolerant genotypes has also become a priority, particularly in regions where *B. ostreae* remains endemic. These efforts highlight the urgent need for integrated approaches that combine ecological restoration, genetic conservation, breeding programs and disease management to ensure the long-term survival of the species.

1.5. Restoration challenges and opportunities in Ireland and the Netherlands: case studies

The complex interplay between historical exploitation, disease dynamics, and conservation policy is clearly illustrated in the cases of Ireland and the Netherlands, two countries where *O. edulis* once flourished but later declined dramatically. Both countries now serve as active fronts in the effort to restore native oyster populations, and their contrasting ecological and management context offer valuable insights for broader European initiatives.

In Ireland, *O. edulis* has a long-standing history, where, until the early nineteenth century, almost every bay and harbour along the coast supported abundant natural oyster beds. However, increasing demand from British markets led to intense exploitation, driven by the expansion of dredging technologies and improved transport networks—by the 1830s, millions of oysters were being exported annually from Irish ports (Kirkpatrick et al., 2024). Concerns about overfishing emerged soon thereafter. The Irish Fisheries Reports from the mid-nineteenth century frequently documented declining stocks and overexploitation continued into the twentieth century, culminating in the widespread collapse of natural beds (Culloty & Mulcahy, 2007). By the early 2000s production of *M. gigas* vastly exceeded that of *O. edulis*, with annual outputs above 270 and 590 tonnes in Strangford and Belfast Loughs, respectively, compared to only 50 tonnes of native oysters—equivalent to a difference of over 2 and 6 million oysters (Ferreira et al., 2008). The situation further deteriorated in the late 1990s following the detection of the parasite *B. ostreae* in *O. edulis* aquaculture stocks, leading to high mortality and diminished interest in native oyster farming (Kennedy & Roberts, 1999). However, *B. ostreae* had in fact been present in Irish oyster populations since the 1980s. The first confirmed outbreak occurred in Rossmore, located in the North Channel of Cork Harbour, where mortality began increasing from 1984 and exceeded 90% in oysters aged four years or older by 1987 (McArdle et al., 1991).

USC UNIVERSIDADE DE SANTIAGO DE COMPOSTELA

Interestingly, oysters from Rossmore later exhibited reduced susceptibility to the parasite in controlled experiments, suggesting the development of partial resistance through natural selection (Culloty et al., 2004*)*. Despite the widespread presence of *B. ostreae*, genetic studies did not find sound evidence of population bottlenecks or significant loss of genetic diversity in Irish oyster populations (Flannery et al., 2014).

This suggests that certain stocks may have either recolonised affected areas or possess inherent resilience to the parasite, making them valuable candidates for restoration programmes. Moreover, persistent but low-intensity infections in some sites hint at potential tolerance mechanisms that warrant further investigation.

Retrospective analyses suggest the parasite had been present several years prior to its official detection, as evidenced by its presence in oysters frozen in 1986 (Rogan et al., 1991). In 1989, *B. ostreae* was also diagnosed in oysters from Galway Bay that had been relayed to more sheltered inlets, with localized mortalities of up to 80%. By 1991, the disease had spread to five additional sites in the bay, though with low prevalence and minimal mortality. Controlled infection trials later revealed interpopulation variation in susceptibility among Irish oyster beds, with some populations from the west coast showing consistently lower prevalence or infection intensities (Culloty et al., 2004). More recently, the parasite was detected in Lough Swilly in 2006, following its discovery in Lough Foyle in 2005. Until then, the entire Northern Ireland coastline had held approved zone status for both *B. ostreae* and *Marteilia refringens*. The loss of disease-free status has had significant implications for the management and restoration of native oyster populations. Although small wild populations persisted in some regions, others like the Belfast region were considered locally extinct by the 2010s (Smyth et al., 2023). The existence of putatively resistant oyster populations in historically affected areas has since gained attention as a valuable resource for restoration and breeding programmes.

A similar trajectory of historical abundance, collapse, and modern restoration can be observed in the Netherlands. Historically, *O. edulis* covered approximately 6.2% of the North Sea seafloor (Bennema et al., 2020). However, intensive bottom fishing practices, particularly dredging and trawling, caused widespread population declines (Reise, 2005; Callaway et al., 2007). By the mid-twentieth century the species had become functionally extinct in the Dutch North Sea (Pogoda et al., 2019b). The introduction of *B. ostreae* in 1980 via oyster imports from France further complicated restoration prospects. The parasite became endemic in Dutch oyster populations after spreading from the Oosterschelde to Lake Grevelingen (Van Banning, 1987; 1991). Nevertheless, long-term exposure has led to the development of local tolerance to *Bonamia* in some Dutch stocks (Culloty et al., 2004). Oysters from Lake Grevelingen, for example, have demonstrated high survival and growth despite persistent infections and have been identified as genetic markers associated with *Bonamia* tolerance in Dutch populations (Vera et al., 2019).

USC
UNIVERSIDADE DE SANTIAGO DE COMPOSTELA

Restoration initiatives in the Netherlands were initiated in 2014 with feasibility assessments, followed by the launch of nearshore and offshore pilot projects beginning in 2016 (Smaal et al., 2015; Sas et al., 2016). These projects aimed to evaluate environmental suitability and re-establish reproductive populations that could serve as larval sources. However, while locally adapted stocks exhibit *Bonamia* tolerance, they are not disease-free. Conversely, hatchery-produced, disease-free seed remains vulnerable upon exposure. This trade-off underscores the importance of careful source population selection and highlights the need for integrated disease management in the design and implementation of restoration strategies.

Altogether, the restoration efforts in Ireland and the Netherlands illustrate the complex interplay between historical exploitation, disease dynamics, and modern conservation planning. They also demonstrate the critical role of long-term ecological monitoring, selective breeding, and cross-sector collaboration in the recovery of *O. edulis* populations across Europe.

USC
UNIVERSIDADE DE SANTIAGO DE COMPOSTELA

2. *OSTREA EDULIS* IMMUNE SYSTEM

2.1. The innate immune system of molluscs

Molluscs, as invertebrates, lack a classical acquired immune system (Escoubas et al., 2016). Instead, they rely entirely on a highly conserved and complex innate immune system composed of cellular and humoral components to interact with microorganisms and defend against pathogens (Song et al., 2010). Despite being considered evolutionary more ancient, this system offers surprisingly effective defence, allowing molluscs to successfully colonize a wide range of aquatic and terrestrial habitats (Sokolova, 2009).

In bivalves, the defence system includes multiple physical and chemical defence lines, such as shell, mucus, and epithelial tissues (Allam & Raftos, 2015). The first barrier is the shell, which provides mechanical protection and structural support. The second barrier formed by the external epithelium and the mucosal layers covering the body and pallial organs. These mucosal secretions not only trap invading microorganisms but also aid in their removal through ciliary movement. Furthermore, they contain various antimicrobial molecules, including hydrolytic enzymes (lysozymes and peptidases), agglutinins (lectins) and other bioactive molecules (Allam & Pales Espinosa, 2016; Fernández-Boo et al., 2019).

Once these internal barriers are breached, internal defence mechanisms are activated. These rely on both humoral and cellular components circulating in the haemolymph, a multifunctional fluid responsible not only for defence but also for nutrient transport, osmoregulation, gas exchange, waste removal, and hydrostatic balance (Gosling, 2015). The main cellular component are haemocytes, circulating immune-component cells, which act in coordination with humoral factors to detect pathogens, initiate immune signalling, and restore homeostasis (Cheng, 1975; Bachère et al., 2004; Schmitt et al., 2011).

The innate response in molluscs unfolds in three main steps: (i) recognition of microbial or damage-associated molecular patterns (MAMPs/DAMPs) by pattern recognition receptors (PRRs); (ii) activation of intracellular signalling cascades; and (iii) production of antimicrobial effectors such as reactive oxygen species (ROS) or antimicrobial peptides (AMPs) (Janeway, 1994).

2.2. Cellular components of the immune system in molluscs

Haemocytes are the central effectors of molluscan immunity, orchestrating most cellular defence responses. They mediate phagocytosis, encapsulation, and the release of extracellular traps (ETs), while also participating in would healing, shell calcification, and tissue homeostasis (Cheng, 1996; Allam & Raftos, 2015). Haemocytes circulate in the haemolymph and infiltrate soft tissues and mucosal epithelia, reflecting their wide distribution and functional versatility (Escoubas et al., 2016).

USC DE SANTIAGO

Functionally and morphologically, haemocytes are commonly classified into granulocytes and agranulocytes (or hyalinocytes). Granulocytes (10–20 μm) are larger, contain numerous cytoplasmic granules, and represent the main phagocytic population. Subclasses of granulocytes have been described based on staining affinity, lysosomal content, and vacuolar morphology (Allam et al., 2002; Cavalcanti et al., 2012). They share structural and physiological features with vertebrate monocytes and macrophages, using intracellular digestion and oxidative mechanisms, including the release of reactive oxygen species (ROS) and nitric oxide (NO), to kill pathogens (Canesi et al., 2002; Davidson et al., 2004). In contrast, agranulocytes (4–6 μm) lack granules and appear more involved in tissue repair and cell aggregation than in direct antimicrobial activity (Castellanos-Martínez et al., 2014).

Upon recognition of pathogen-associated molecular patterns (PAMPs), haemocytes migrate towards infection sites following chemotactic signals (Cheng & Howland, 1979). Pathogen recognition can lead to aggregation, ETosis, encapsulation, or phagocytosis/endocytosis.

During phagocytosis, haemocytes adhere to and internalize pathogens using conserved receptors such as integrins, scavenger receptors (SRs), and C-type lectins (Humphries & Yoshino, 2003; Liu et al., 2011). Pathogens are then destroyed by lysosomal enzymes, antimicrobial peptides (AMPs), cytotoxic molecules, and oxidative burst reactions (Allam & Raftos, 2015). Granulocytes constitute the main phagocytic cell type, with phagosomes containing AMPs, ROS, NO, and hydrolytic enzymes that mediate pathogen destruction (Loker, 2010; Song et al., 2010; Castellanos-Martínez et al., 2014).

The production of ROS and reactive nitrogen species (RNS) is a hallmark of haemocyte immunity. These molecules are generated during the respiratory burst, mediated by transmembrane NADPH oxidases that produce superoxide anions (O_2^-), later converted into hydrogen peroxide (H_2O_2) by superoxide dismutase (SOD; Donaghy et al., 2015). H_2O_2 can then react from hydroxyl radicals, singlet oxygen, and other microbicidal compounds, myeloperoxidases may further convert H_2O_2 into hypochlorous acid or chloramines (Fang, 2004). In parallel, nitric oxide synthase (NOS) catalyses NO production, and derived RNS synergize with ROS to enhance antimicrobial toxicity (Anderson,1994; Romero et al., 2011).

Studies in *M. gigas* have shown that semigranular and granular haemocytes display strong phagocytic activity, producing ROS, NO, lysozymes, and AMPs in response to *Vibrio splendidus* infection (Bachère et al., 2015). Because excessive ROS/RNS can damage host tissues, antioxidant enzymes such as SOD, catalase, and glutathione peroxidase regulate oxidative stress (Morga et al., 2011).

When pathogens are too large or resistant to intracellular killing, haemocytes form multicellular capsules that may lead to granuloma formation (Loker et al., 1982; Dove et al., 2004).

USC UNIVERSIDADE DE SANTIAGO DE COMPOSTELA

In addition, haemocytes can release ETs, web-like structures of DNA and proteins that immobilize and kill pathogens. ETosis is strongly dependent on ROS production and appears to be an evolutionarily conserved defence mechanism in marine invertebrates (Poirier et al., 2014; Romero et al., 2020).

Other immune-related processes mediated by haemocytes include autophagy and apoptosis, that contribute to immune regulation and homeostasis. The movement of haemocytes toward infection sites may be triggered by pathogen-derived products or by host cytokines released from infected cells (Allam & Raftos, 2015).

Autophagy, the lysosomal degradation of damaged organelles or intracellular pathogens, is triggered by stressors such as hypoxia, malnutrition, or toxins and has been observed in haemocytes of *M. gigas* (Mizushima et al., 2008; Deretic & Levine, 2009; Picot et al., 2019). The autophagic process includes the formation of autophagosomes, which then fuse with lysosomes to form autolysosomes where degradation occurs (Eskelinen et al., 2004; Eskelinen,2008). Apoptosis removes infected or damaged cells without causing inflammation, involving caspase activation via intrinsic (mitochondrial) or extrinsic (death receptor) pathways (Kiss, 2010; Estévez-Calvar et al., 2013). In molluscs, these pathways are conserved but may display species-specific adaptations to environmental stressors such as temperature, pollutants, and heavy metals, often mediated by p38-MAPKs and Hsp70 signalling (Coles et al., 1995; Sokolova et al., 2004; Raftos et al., 2014).

2.3. Humoral components and effector mechanisms

Alongside cellular defences, molluscs rely on numerous humoral factors circulating in the haemolymph or secreted into mucosal surfaces. These soluble molecules contribute to pathogen recognition, immune signalling, and direct antimicrobial activity, acting synergistically with haemocytes to ensure effective defence.

Among the most important humoral components are AMPs, which are small, cationic molecules that act as ancient host defence effectors present in most animal phyla, with broad-spectrum activity against bacteria, fungi, and viruses (Lehrer & Ganz, 2003; Travers et al., 2010; Wang et al., 2018). They disrupt microbial membranes or interfere with intracellular processes, and their expression typically increases upon pathogen challenge (Adhya et al., 2012; Allam et al., 2014).

However, AMP upregulation does not always correlate with antiparasitic activity: for example, histone H4 expression increased in *M. gigas* infected with *Perkinsus marinus*, but recombinant H4 showed no direct effect on the parasite (Nikapitiya et al., 2013). Similarly, defensins were upregulated in *Mercenaria mercenaria* infected by QPX without demonstrated antiparasitic activity (Perrigault et al., 2009). These findings suggest that AMPs in bivalves may primarily maintain microbial homeostasis and protect against secondary bacterial infections rather than directly targeting eukaryotic parasites (Allam & Raftos, 2015).

USC DE SANTIAGO

Enzymes, such as lysozymes and proteases also play a crucial role in innate defence, particularly against bacteria (Anderson & Beaven, 2001). Lysozymes hydrolyse β-1,4-glycosidic bonds in peptidoglycan, compromising bacterial cell wall integrity (Anderson & Beaven, 2001). Multiple isoforms have evolved via gene duplication and diversification, expanding substrate specificity (Allam et al., 2014). Lysozyme activity has been detected in mucosal secretions such as mantle mucus, constituting a first line of defence against microbial invasion (McDade & Tripp, 1967; Allam & Paillard, 1998), and in tissues such as the digestive gland epithelium in *M. gigas* and *Crassostrea virginica*, where they act against Gram-positive and Gram-negative bacteria (Haug et al., 2004; Itoh & Takahashi, 2009; Xue et al., 2007). Some lysozymes also potentiate AMP activity and can affect eukaryotic parasites such as *P. marinus* (La Peyre et al., 2004).

In addition to lysozymes, bivalve tissues and secretions contain a broad range of protease inhibitors, including those targeting serine, cysteine, and metalloproteases (Moreira et al., 2012a; McDowell et al., 2014). These molecules are thought to neutralize proteolytic enzymes secreted by invading pathogens, thereby preventing tissue degradation and facilitating immune defence. For example, two serine protease inhibitors (cvSI-1 and cvSI-2) from *C. virginica* plasma inhibited *P. marinus* proliferation *in vitro* (Xue et al., 2006; La Peyre et al., 2010), and resistance to *P. marinus* has been linked to mutations in the *cvSI-1* promoter region (Yu et al., 2011). Interestingly, their regulation appears tissue-specific: in clams with brown ring disease, serine protease inhibitor transcripts increased in extrapallial fluid and mantle tissue but decreased in haemolymph (Allam et al., 2014).

Finally, additional humoral factors include lectins, which bind to carbohydrate motifs on microbial surfaces and facilitate agglutination or opsonisation; complement-like proteins, which promote lysis or phagocytosis of pathogens; and heat shock proteins (HSPs), which act as molecular chaperones and modulate immune signalling (Encomio & Chu, 2007; Anyanful et al., 2009; Roberts et al., 2010).

C1q domain-containing proteins (C1qDCs) and fibrinogen-related proteins (FREPs) are particularly diverse, suggesting rapid evolution under pathogen-driven selection (Zhang S. et al., 2004). In *Mytilus galloprovincialis*, 168 different C1qDC transcripts were reported, many upregulated after bacterial challenge (Gerdol et al., 2011; Moreira et al., 2012a).

Similar patterns occur in *Ruditapes decussatus* infected with *Perkinsus olseni* (Leite et al., 2013) and *Ruditapes philippinarum* infected with *Vibrio tapetis* (Allam et al., 2014). Functional studies in *Argopecten irradians* revealed that recombinant C1qDCs bind diverse microbial ligands and enhance haemocyte phagocytosis, supporting their role as broad-spectrum pattern recognition receptors (Kong et al., 2010).

Together, humoral effectors from AMPs and lysozymes to lectins, complement-like proteins, and C1qDCs, form a versatile molecular arsenal that complements haemocyte-mediated defences, providing molluscs with a multi-layered immune system despite the absence of adaptive immunity.

2.4. Pattern recognition receptors (PRRs) and immune signalling

The rapid detection of invading pathogens or damaged host tissues constitutes the first step of the innate immune response in molluscs. This process relies on pattern recognition receptors (PRRs), which recognize conserved structural motifs on microbial surfaces—microbe-associated molecular patterns (MAMPs) or pathogen-associated molecular patterns (PAMPs)—as well as danger-associated molecular patterns (DAMPs) released by host cells (Escoubas et al., 2016).

Upon ligand binding, PRRs trigger intracellular signalling cascades that recruit haemocytes to infection sites, stimulate phagocytosis, and induce the production of humoral immune effectors. Oxidative mechanisms such as the respiratory burst, which generates ROS, often mediate pathogen killing and highlight the evolutionary pressure imposed by pathogens on innate immunity in the absence of adaptive defences (Escoubas et al., 2016). Based on their cellular location, PRRs in molluscs can be broadly classified into three groups: secreted receptors, membrane-bound receptors, and cytoplasmic sensors (Escoubas et al., 2016).

Secreted PRRs include peptidoglycan recognition proteins (PGRPs), gram-negative bacteria-binding proteins (GNBPs), bactericidal/permeability-increasing proteins (BPIs), lipopolysaccharide-binding proteins (LBPs), and fibrinogen-related proteins (FREPs) (Allam & Raftos, 2015). These molecules often initiate proteolytic cascades that promote opsonisation via thioester-containing proteins (TEPs), enhancing phagocytosis. Secreted PRRs show remarkable diversification within and across molluscan species, suggesting rapid evolution under pathogen-driven selection (Zhang H. et al., 2007; Prado-Alvarez et al., 2009; Zhang H. et al., 2009).

Membrane-bound PRRs include scavenger receptors (SRs) and Toll-like receptors (TLRs). SRs participate in clearing apoptotic or altered host cells and mediating pathogen internalization, whereas TLRs, localized at epithelial barriers and in intracellular compartments such as endosomes and lysosomes, activate signalling cascades culminating in the nuclear translocation of transcription factors like NF-κB, which drive immune gene expression (Peiser et al., 2002; Sarrias et al., 2004).

Numerous NF-κB pathway components have been described in molluscs, underlining its central role in innate immunity (Escoubas et al., 2016). Although most studies rely on transcriptomic or genomic data rather than functional assays, the consistent upregulation of TLR pathway genes during viral, bacterial, and protozoan infections strongly supports their role in immune activation (Tanguy et al., 2004; Perrigault et al., 2009; Renault et al., 2011; Green & Montagnani, 2013).

Cytoplasmic sensors include RIG-I-like helicases (RLHs), which recognize viral RNA, as well as nucleotide-binding oligomerization domain (NOD)-like receptors and cytoplasmic DNA sensors (Sirard et al., 2007; Yoneyama & Fujita, 2007; Kawai & Akira, 2010; Barber, 2011). Homologues of these sensors have been recently identified in bivalves, suggesting that these recognition mechanisms have an ancestral origin (Venier et al., 2011; Mukherjee et al., 2014; Zhang Y. et al., 2014).

USC UNIVERSIDADE

Activation of PRRs leads to the production of signalling molecules such as cytokines, which orchestrate immune responses in molluscs. Several cytokines have been identified, including homologues of transforming growth factor-beta (TGF-β), tumour necrosis factor (TNF), interleukin-17 (IL-17), macrophage migration inhibitory factor (MIF), interferon-like proteins, and allograft inflammatory factor-1 (AIF-1). Notably, AIF-1 appears to play a central role by inducing proinflammatory cytokines such as TNF, IL-17, and MIF upon pathogen detection (Wang et al., 2008; Zhang Y. et al., 2013; Sun et al., 2014; Xu et al., 2014).

In summary, PRRs provide the molecular interface between pathogen recognition and immune activation in molluscs. Their diversification and rapid evolution reflect strong selective pressures imposed by pathogens, while downstream signalling cascades and cytokines coordinate cellular and humoral responses to infection.

2.5. New insights on mollusc and oyster immune system: "priming"

Recent advances in molluscan immunology have revealed that the immune system of oysters exhibits unexpected levels of plasticity, challenging the traditional view that invertebrate immunity is strictly short-lived and non-specific. Studies in *M. gigas* have revealed a surprisingly complex immune capacity despite the absence of adaptive immunity. Like other bivalves, oysters possess a highly diverse repertoire of immune-related genes showing extensive polymorphism and gene family expansion (Zhang L. et al., 2014).

Transcriptomic analyses indicate that oysters mount pathogen-specific immune responses, with distinct gene expression patterns depending on whether the challenge involves bacteria, viruses, or protozoan parasites (Green et al., 2016). This specificity is particularly evident in experiments demonstrating that priming with heat- or formalin-inactivated *V. splendidus* enhances phagocytic activity and immune reactivity during subsequent exposure to the same live pathogen, whereas no such enhancement occurs when oysters are later challenged with other *Vibrio* species (Zhang X. et al., 2014; Li et al., 2017; Montagnani et al., 2024). These results point towards a form of immune "memory" or long-term modulation of innate responses, a phenomenon sometimes referred to as immune priming or training in invertebrates.

The molecular mechanisms underlying this immune training appear to involve epigenetic reprogramming. In *M. gigas*, for instance, immune-primed oysters exhibit increased trimethylation of histone H3K4 at the *CgTLR3* promoter region, a modification typically associated with transcriptional activation (Lian et al., 2024). Transcriptomic analyses have also revealed persistent or recall-like expression of immune and metabolic genes following secondary challenges, particularly in components of the Toll/NF-κB signalling pathway (Lian et al., 2024). However, most studies have focused on relatively short priming intervals of less than one week, and survival outcomes have not always been quantified, leaving open questions about the duration and functional relevance of these responses under natural conditions (Montagnani et al., 2024).

Beyond antibacterial immunity, evidence for immune training has also been reported in antiviral responses. In *M. gigas*, administration of poly(I:C), a synthetic analogue of viral double-stranded RNA, by injection or immersion induces long-term protection against *Ostreid herpesvirus 1* (OsHV-1 µVar), the main causative agent of Pacific Oyster Mortality Syndrome (POMS) (Lafont et al., 2017). This protection appears pathogen-specific: poly(I:C)-primed oysters resist subsequent OsHV-1 µVar infections but remain susceptible to *Vibrio* challenges, and conversely, bacterial priming does not protect against viral disease (Lafont et al., 2017). Mechanistically, poly(I:C) exposure induces sustained upregulation of immune genes involved in interferon-like responses, Toll/NF-κB signalling, and apoptosis regulation (Lafont et al., 2020). Remarkably, transgenerational effects have been observed: offspring of poly(I:C)-primed females show increased resistance to OsHV-1 µVar despite no major baseline differences in gene expression, suggesting maternal transfer of immune factors or epigenetic inheritance as potential mechanisms (Lafont et al., 2019).

Comparable processes may also occur in *O. edulis*. Following *B. ostreae* infection, haemocyte transcriptomes from *O. edulis* revealed unique sequences homologous to histone genes (H1, H2A, H2B, H3, H4, and H5), suggesting a possible link between chromatin dynamics and immune modulation in this species as well (Pardo et al., 2016). Furthermore, integrative transcriptomic and genomic approaches have identified at least 24 candidate genes potentially involved in resistance or susceptibility to bonamiosis, spanning diverse functional categories such as G-protein and integrin-mediated signalling, ubiquitin pathways, apoptosis regulation, protease inhibition, complement activation, and cell–matrix interactions (Ronza et al., 2018). These findings provide a valuable framework for exploring genetic markers of resistance and the molecular basis of host–parasite interactions in *O. edulis*.

Environmental factors further modulate oyster immunity, sometimes producing effects reminiscent of immune training. For example, exposing oyster larvae to non-pathogenic environmental microbiota under controlled conditions has been shown to confer resistance to POMS both within and across generations. This protection correlates with long-term transcriptional reprogramming and epigenetic changes affecting pattern recognition receptors (e.g., lectins, TLRs, RLRs), signalling cascades (e.g., IFN, JAK/STAT, Toll), and effector molecules such as TNF, antimicrobial peptides, and antioxidant enzymes (Fallet et al., 2022; Montagnani et al., 2024). Similarly, natural populations of oysters surviving recurrent POMS outbreaks exhibit progressively increased resistance, suggesting that repeated pathogen exposure in the wild may select for or induce tolerant phenotypes over time (Liu et al., 2023). Abiotic stressors such as elevated temperature have also been linked to enhanced survival following pathogen exposure, likely through transcriptional and physiological adjustments that prime the immune system to withstand infection more effectively (Delisle et al., 2018; 2020).

USC
UNIVERSIDADE DE SANTIAGO DE COMPOSTELA

Altogether, these studies portray oyster immunity as a dynamic and plastic system shaped not only by immediate pathogen recognition but also by long-term environmental, epigenetic, and possibly transgenerational influences. The convergence of evidence from *C. gigas* and *O. edulis* highlights a conserved capacity for immune modulation across oyster species, opening new perspectives on disease resistance, host–pathogen coevolution, and the potential for selective breeding programs targeting immune resilience.

2.6. Immune response to *B. ostreae*

Infections caused by *B. ostreae* elicit systemic immune responses in *O. edulis*, typically characterised by haemocyte mobilisation, haematopoiesis, degranulation, and haemocyte lysis (Ford et al., 1993; Cochennec-Laureau et al., 2003; Villalba et al., 2004). However, despite the generally high phagocytic activity and cytotoxic capacity displayed by haemocytes, the parasite can persist and multiply within these cells, illustrating its ability to subvert or evade host immune mechanisms (Morga et al., 2012).

A central aspect of this interaction involves the regulation of apoptosis. Experimental studies have shown that apoptosis-related genes such as *Fas ligand*, *inhibitor of apoptosis protein* (*IAP*), and *cathepsin B* are differentially expressed following infection, and this regulation appears to be linked to the infection outcome.

In resistant oyster populations, overexpression of *OeFas-ligand* has been associated with the induction of apoptosis as a host strategy to limit parasite proliferation, whereas *B. ostreae* upregulates the anti-apoptotic gene *OeIAP* to prevent programmed cell death and favour its intracellular survival (Morga et al., 2012). This dynamic suggests a molecular arms race in which host and parasite manipulate cell death pathways to their advantage.

Beyond apoptosis, *B. ostreae* also modulates haemocyte effector functions after internalisation. *In vitro* assays have demonstrated that parasite infection rapidly suppresses esterase activity and ROS production in haemocytes, effects that are more pronounced when cells interact with live rather than dead parasites, indicating an active interference mechanism (Morga et al., 2009). Parasite-derived enzymes such as acid phosphatases are thought to inactivate NADPH oxidase, thereby impairing ROS production—a strategy reminiscent of immune evasion mechanisms employed by intracellular protozoan parasites including *Leishmania* and *Toxoplasma* spp. (Murray, 1981; Shrestha et al., 2006; Morga et al., 2009).

Comparable immune evasion mechanisms have been described in other host–pathogen systems. For instance, in *C. virginica*, *Haplosporidium nelsoni* avoids phagocytosis altogether, a process linked to parasite surface antigens that mask recognition sites; chemical modification of these epitopes restores haemocyte-mediated engulfment, underlining the importance of surface molecules in determining immune evasion or clearance (Ford et al., 1993).

USC DE COMPOSTELA

Similarly, bacterial pathogens such as *Vibrio vulnificus*, *V. parahaemolyticus*, and *Escherichia coli* alter their surface properties to prevent haemocyte adhesion and killing (Harris-Young et al., 1995; Genthner et al., 1999).

Comparative studies between *O. edulis* and the Pacific oyster *M. gigas*, which is not susceptible to bonamiosis, have revealed that while *B. ostreae* is phagocytosed in both species, it is only effectively eliminated in *M. gigas* (Chagot et al., 1992; Xue & Renault, 2000). Further research has shown that the parasite can inhibit the respiratory burst in *O. edulis* haemocytes but not in *M. gigas*, suggesting that the inability to suppress oxidative defences in the latter species may explain its resistance. Nevertheless, other immune parameters, such as total haemocyte counts (THC), differential haemocyte counts (DHC), or phagocytic indices, have produced inconsistent results when correlated with susceptibility in *O. edulis* populations. For example, phagocytic activity against zymosan particles appears similar in resistant and susceptible oyster stocks, implying that differences in pathogen recognition or in the downstream activation of cytotoxic mechanisms, rather than in phagocytosis itself, may be more critical in determining disease outcomes.

The lack of consistent associations between conventional haemocyte parameters and resistance suggests that other molecular or physiological processes could modulate infection success. Potential candidates include lysosomal enzyme activity, protease inhibitors, and stress-response proteins such as heat shock proteins, which have been linked to immune regulation in bivalves (Comesaña et al., 2012).

Moreover, environmental factors such as temperature and salinity, known to influence both parasite viability and host physiology, may further shape the outcome of infection by modulating haemocyte function or immune gene expression.

Altogether, these findings indicate that *B. ostreae* employs a multifaceted immune evasion strategy involving suppression of oxidative defences, modulation of apoptosis, and possibly interference with signalling pathways, enabling its persistence within haemocytes and the establishment of chronic infections. At the same time, resistant oyster populations and refractory species such as *M. gigas* point towards additional, yet incompletely characterised, defence mechanisms beyond classical haemocyte responses. Understanding these mechanisms at cellular and molecular levels remains essential for developing effective strategies for disease management and selective breeding in *O. edulis*.

USC
UNIVERSIDADE DE SANTIAGO DE COMPOSTELA

3. GENETIC STRUCTURE OF *O. EDULIS* AND ITS RESISTANCE TO *B. OSTREAE*

3.1. Genetic diversity and population structure of *O. edulis*

Numerous studies have explored the genetic diversity and population structure of the native European flat oyster (*O. edulis*), revealing spatial patterns shaped by historical events and contemporary forces. Early analyses based on allozymes (Saavedra et al., 1993) and mitochondrial DNA (Diaz-Almela et al., 2004) suggested low overall geographic differentiation but indicated clines in allele frequencies at specific loci and the presence of distinct haplogroups, potentially shaped by glacial refugia and postglacial colonization (Hayer et al., 2021). Nuclear markers, including microsatellites and Single Nucleotide Polymorphisms (SNPs), have confirmed a general pattern of isolation by distance (Vera et al., 2016; Lapègue et al., 2022), but also revealed unexpected genetic affinities between geographically distant regions, such as the North Sea and Eastern Mediterranean.

Across the Northeast Atlantic, three main genetic clusters have been consistently identified: (i) southern populations around the Iberian Peninsula, (ii) central populations from Ireland, Britain and France, and (iii) northern populations from the Netherlands and Denmark (Vera et al., 2016). This pattern, however, has been increasingly blurred by human-mediated translocations of oysters and seed stocks, which have led to admixture, loss of genetic diversity, and the erosion of rare alleles (Launey et al., 2001).

Despite this homogenizing effect, recent studies using high-resolution SNP datasets (Vera et al., 2019) and genome resequencing approaches (Robert et al., 2025) have uncovered evidence of fine-scale structure and local adaptation. Notably, population differentiation was observed at local scales along the Scandinavian coasts, suggesting that population dynamics, local environmental conditions, and restricted gene flow may all contribute to shaping the genetic landscape of *O. edulis*. Conversely a great homogeneity and intergeneration stability was observed in Galicia (NW Spain; Vera et al., 2016).

3.2. *O. edulis* response to *B. ostreae*: a population perspective

Understanding the genetic basis of host response to *B. ostreae* is key to developing effective control and management strategies. Both experimental inoculations and *in vitro* assays have shown that contact with the parasite triggers immune responses in the host, including the activation haemocytes, modulation of cellular parameters, and upregulation of immune-related genes (Pardo et al., 2016; Ronza et al., 2018).

USC UNIVERSIDADE DE SANTIAGO DE COMPOSTELA

Natural resistance has been observed in oyster populations previously exposed to *B. ostreae*, which tend to exhibit lower susceptibility compared to naïve populations (Elston et al., 1987; Lynch et al., 2014; Ronza et al., 2018). Differential expression of immune-related genes, proteins, and microRNAs involved in phagocytosis, respiratory burst, and apoptosis has been reported between tolerant and naïve individuals (Morga et al., 2011; Martín-Gómez et al., 2014; Vera et al., 2019). Ronza et al. (2018) identified differential expressed genes related to extracellular matrix and apoptosis when comparing long-term affected (LTA) and naïve (NV) oysters, suggestive of the two main mechanisms of defence against an intracellular parasite, using a flat oyster microarray (Pardo et al., 2016). Similarly, selected individuals showed lower parasite load, inhibition of phagocytosis (limiting parasite spread), and upregulation of apoptosis-related genes (Morga et al., 2017). However, distinguishing resistance, tolerance, susceptibility and resilience remain conceptually challenging. Resistance implies an ability to prevent infection or reduce parasite replication and load (Råberg et al., 2007), whereas tolerance refers to the host's capacity to survive or being less affected in production traits despite carrying the infection. Resilience involves recovery after infection, often at population or ecosystem level (Råberg et al., 2007). On the contrary, susceptible individuals are infected and die by disease. *O. edulis* individuals from *Bonamia*-exposed populations have demonstrated a reduced susceptibility to the parasite (Morga et al., 2017; Ronza et al., 2018), however, these traits are difficult to disentangle experimentally, and especially in the wild, as host-parasite interactions are dynamic and highly context-dependent (Fig. 3A). As for *B. ostreae* infection, in non-resistant oysters the parasite can invade the gills and reach haemolymph and heart, where it infects haemocytes and proliferates. In resistant oysters, parasite entry through the gills as part as the normal feeding process, but it does not get haemolymph (Fig. 3B). In this Thesis, the combined term "resistance/tolerance" will be used to broadly refer to the ability of oysters to overcome or limit the impact of parasite infection.

The interpretation of immune response is further complicated by the fact that cellular processes such as phagocytosis, apoptosis, or respiratory burst may play dual roles. For example, while phagocytosis is a key defence mechanism, it also allows *B. ostreae* to enter haemocytes, which are both effectors and targets of infection (Holbrook et al., 2021). On the other hand, the parasite can suppress host immune responses by inhibiting phagocytosis and oxidative burst, potentially as a virulence mechanism or a host tolerance strategy (Holbrook et al., 2021). Also, the extracellular matrix surrounding the haemocytes can be critical to avoid parasite entrance (Ronza et al., 2018). Consequently, relying solely on cellular assays is insufficient to distinguish between resistance and tolerance, and complementary molecular, ecological and population genomic approaches are needed.

Infection progression is also unpredictable. While *B. ostreae* can invade haemocytes within an hour, the onset and severity of disease (bonamiosis) vary widely, with some infections leading up to 80% mortality (da Silva et al., 2005, Lallias et al., 2010). Grading systems based on histology, cardiac smears, and haemocyte parasite counts have been developed to describe different infection levels (Holbrook et al., 2021).

Interestingly, some tolerant populations, such as those in Ireland, maintain low parasite loads with no associated mortality even after decades of coexistence, suggesting mechanisms that limit disease progression. It has been hypothesised that *B. ostreae* may enter a latent state within haemocytes, like other intracellular pathogens such as *Plasmodium* or *Toxoplasma*, thereby avoiding detection and conserving energy (Ronza et al., 2018; Holbrook et al., 2021).

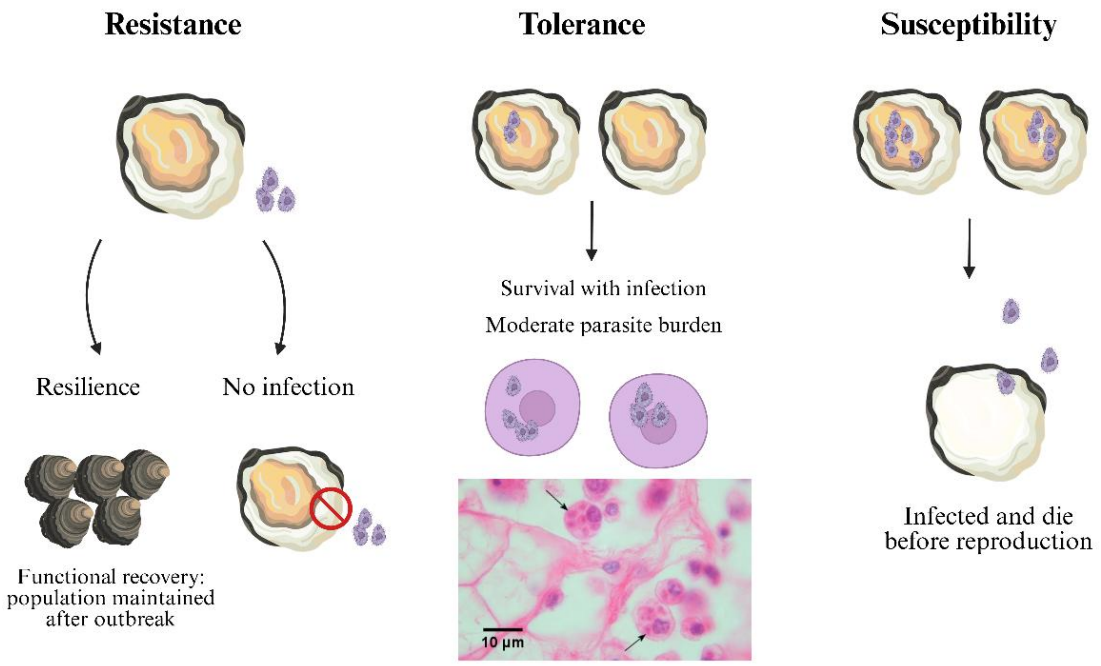
Heritability of survival traits to pathogen infections has been demonstrated oyster species (Dégremont et al., 2015), to say survivors of outbreaks may transmit resistance, tolerance, or resilience to their progeny. Substantial gains have been reported after just one generation of selective breeding. However, most studies do not differentiate between resistance and tolerance as distinct traits. Genome-wide population scans have suggested selective sweeps in exposed vs naïve populations (e.g., Vera et al., 2019), but the underlying biological mechanisms remain unclear. Furthermore, gene flow via larval dispersal or oyster translocations may dilute resistance alleles in wild populations, posing a challenge to the long-term maintenance of resistance (Holbrook et al., 2021).

As outlined before, comparative transcriptomic analyses between NV and LTA oyster populations have identified candidate genes associated with resistance, including antimicrobial peptides and components of the extracellular matrix (Ronza et al., 2018). These studies suggest that host resistance / tolerance involves both constitutive and induced immune mechanisms, and that selective pressure by the parasite has likely shaped the genomic architecture of resistance.

Efforts to map genetic variation associated with resistance traits have identified multiple QTLs that co-localize with differentially expressed immune genes (Lallias et al., 2009; Harrang et al., 2015). Further, signals of divergent selection between NV and LTA populations based on a medium-density SNP array have suggested the presence of a major genomic region under selection (Vera et al., 2019). This region shows strong linkage disequilibrium between markers and may correspond to a big QTL associated with resistance / tolerance. In this regard, studying haplotypes, defined as combinations of alleles at adjacent loci that are inherited together, represent an interesting approach for large genetic regions associated with traits of interest. Prior research has identified several SNPs linked to bonamiosis resistance or tolerance in *O. edulis* (Vera et al., 2019). Haplotype-based approaches align with current conservation genomics studies, which emphasizes the importance of linkage disequilibrium for estimating effective population size, migration rates, and understanding local adaptation (Snyder et al., 2015; McKinney et al., 2017; Leitwein et al., 2020).

USC UNIVERSIDADE DE SANTIAGO DE COMPOSTELA

A)



B)

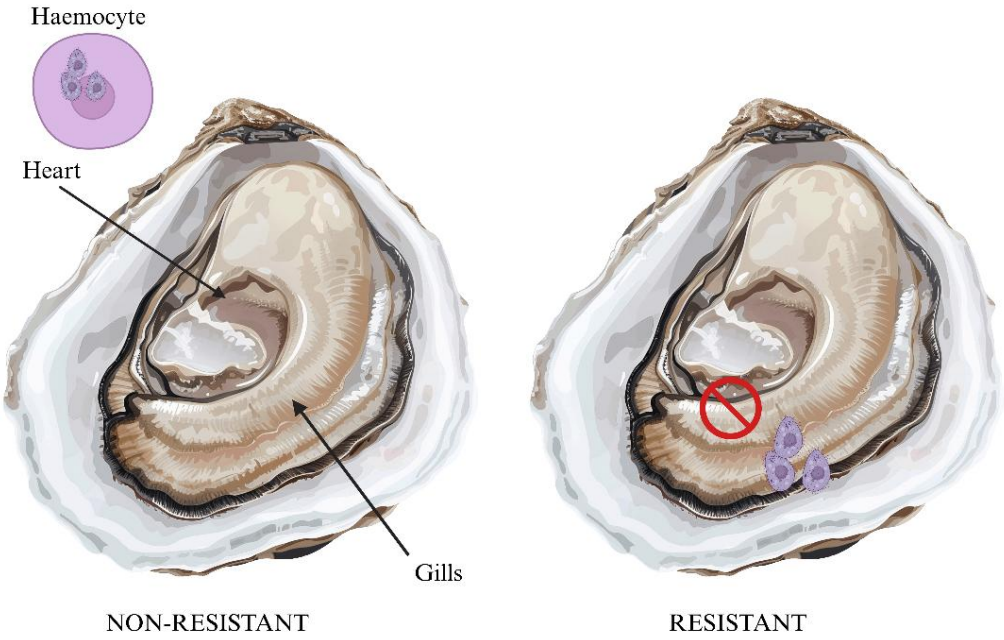


Figure 3. A) Conceptual framework of resistance, tolerance, and susceptibility to *Bonamia ostreae* in *Ostrea edulis*. Image from of *B. ostreae* cells (arrows) within haemocytes in haemal spaces from Fisheries and Oceans Canada 2015 (https://www.dfo-mpo.gc.ca/science/aah-saa/diseases-maladies/bonostoy-eng.html) B) Schematic representation of parasite localization in resistant and non-resistant *Ostrea edulis* individuals.

USC
DE SANTIAGO
DE COMPOSTELA

3.3. Genomic resources of flat oyster

In recent years, significant progress has been made in developing genomic resources and tools for *O. edulis*, paving the way for more comprehensive studies of host-parasite interactions and selective breeding. An immune-enriched oligo-microarray has been developed in *O. edulis* (Pardo et al. 2016) and a reference transcriptome constructed in *B. ostreae* (Chevignon et al., 2022), which have aid for deepening in functional understanding of host-parasite interaction across the infection process. Also, a 14K SNP array was developed using RAD-seq genotyping by Gutiérrez et al. (2017) has enabled high-throughput genotyping and facilitated discovery of marker associated resistance traits (Vera et al., 2019). Additional markers associated to differentially expressed genes (Ronza et al., 2018) are candidates to be incorporated into genotyping platforms.

More recently, several chromosome-level reference genomes have been assembled in *O. edulis* (Boutet et al., 2022; Gundappa et al., 2022; Li et al., 2022; Adkins & Mrowicki, 2023), which has opened new avenues for the identification of QTL, deepening into the study of structural variation and providing an essential resource for identification of candidate genes and functional genomics. Notably, a structural variant located at the end of pseudo-chromosome 8 has been suggested to play a role in resistance to *B. ostreae*, potentially affecting both wild and farmed populations (Holbrook et al., 2021).

Despite these advances, genome-wide analyses covering the full geographic range of the species remain limited. There is a need for integrative studies combining high-resolution genotyping, whole-genome sequencing, and environmental data to fully understand the evolutionary dynamics of resistance and the adaptive potential of flat oyster populations.

3.4. Selective breeding and practical applications

Selective breeding programmes aimed at enhancing resistance to bonamiosis have been implemented in various regions and have yielded promising results. These programmes have typically relied on mass selection of survivors from heavily affected areas, assuming the heritability of resistance traits. In Ireland, the Rossmore line represents the success of a long-term selective breeding program, with significantly reduced mortality observed after decades of exposure to *B. ostreae* (Lynch et al., 2014). Similar initiatives have been carried out in Spain (da Silva et al., 2005; Albentosa et al., 2023) and the Netherlands (Smaal et al., 2015), where resistance breeding has supported restoration efforts in the Mar Menor lagoon and Wadden Sea respectively.

The integration of genomic tools into breeding strategies offers new opportunities for accelerating selection through marker-assisted or genomic selection. However, challenges remain, including the maintenance of genetic diversity in breeding lines, the validation of resistance loci across populations, and the interaction of genetic and environmental factors in determining resistance.

USC DE COMPOSTELA

Altogether, current evidence points to a dynamic interplay between genetic diversity, environmental adaptation, and host–parasite interactions in *O. edulis*. Yet, recent discoveries of large chromosomal inversions across the oyster genome suggest that structural variants may represent key drivers of both adaptation and resistance. By preserving advantageous allele combinations and reducing recombination, these inversions offer a plausible explanation for some of the genomic patterns described above. Importantly, advances in whole-genome sequencing and long-read technologies now enable high-resolution characterization of these structural variants, providing unprecedented opportunities to explore their evolutionary role and functional significance in shaping *O. edulis* populations.

USC
UNIVERSIDADE DE SANTIAGO DE COMPOSTELA

4. STRUCTURAL VARIATION AND ROLE OF CHROMOSOMAL INVERSIONS IN *OSTREA EDULIS*

4.1. Evolutionary significance of chromosomal inversions

Low-recombination regions, such as chromosomal inversions, play a key role in evolution and speciation by suppressing recombination between locally co-adapted haplotypes (Berdan et al., 2023). Alleles in such regions are inherited as large units, amplifying the effects of evolutionary forces that create genomic islands across extensive genomic regions. This promotes the maintenance of co-adapted gene complexes, facilitating adaptation to specific environments and reinforcing reproductive isolation between diverging populations (Lowry & Willis, 2010). Additionally, low recombination favours the accumulation of genetic incompatibilities, which can reduce hybrid viability or fertility, thereby promoting divergence (Zhang W. et al., 2023). These regions protect adaptive allele combinations by preventing the breakdown of linkage between key loci, which is especially relevant under scenarios of secondary contact between differentiating populations (Lowry & Willis, 2010).

Chromosomal inversions—first discovered in *Drosophila* over a century ago (Sturtevant, 1920)—are structural variants in which a segment of DNA changes its orientation within the chromosome. They have long been implicated in adaptation due to their ability to ensure the co-transmission of favourable allele sets as haplotypes by suppressing recombination (i.e., supergenes; Dobzhansky, 1970; Reeve et al., 2024). Their origin may also be driven by lower genetic load associated with specific haplotypes or by fitness effects at the inversion breakpoints (Berdan et al., 2023). The persistence of inversion polymorphisms can be explained by divergent selection, balancing selection, or a combination of evolutionary processes (Kirkpatrick & Barton, 2006; Faria et al., 2019).

They may be pericentric (including the centromere) or paracentric (excluding it), with the latter more commonly reported. These inversions can persist for thousands or even millions of generations—for example, a 900 kb inversion in humans originated approximately three million years ago (Stefansson et al., 2005). But evolutionary dynamics of inversions are best described using a two-type framework (Faria et al., 2019) (Fig. 4). Type I inversions are associated with divergent selection between environments and may fix in one population while being absent in another, leading to reproductive isolation (*Littorina fabalis*; Le Moan et al., 2022). In contrast, Type II inversions are maintained by balancing selection and remain polymorphic within populations, often involving complex fitness trade-offs (Schneller et al., 2025). These mechanisms are not mutually exclusive and can coexist in a species, shifting over time due to ecological or demographic changes.

USC UNIVERSIDADE DE SANTIAGO DE COMPOSTELA

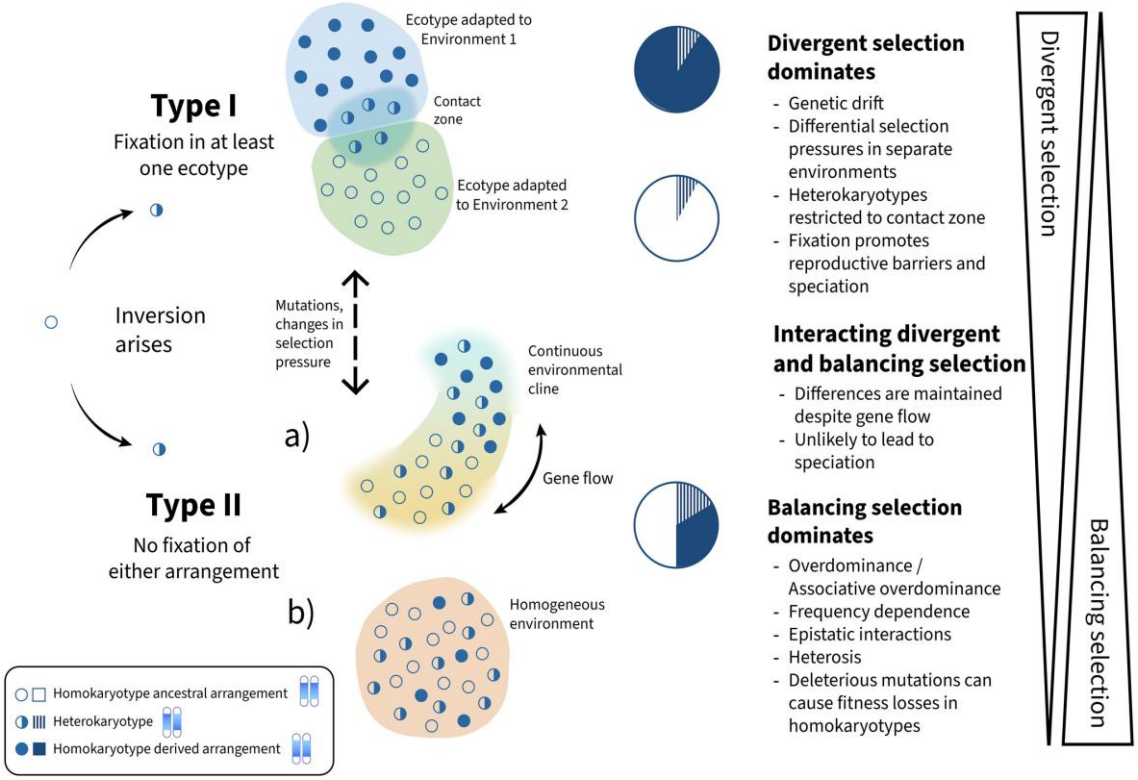


Figure 4. Overview of the Type I / Type II framework for classifying an inversion polymorphism and understanding the role of inversions in adaptation. Reproduced from Hoff et al. (2024), Evolutionary Applications under Creative Commons Attribution (CC BY).

In Type I, divergent selection drives fixation of alternative arrangements in different environments, and heterokaryotypes are rare and mostly restricted to contact zones. In Type II, balancing selection maintains both arrangements across the entire population, resulting in frequent heterokaryotypes and clinal distribution patterns. Recognizing this typology can help predict the evolutionary consequences of different management actions. For instance, the introduction of Type I heterokaryotypes into non-native backgrounds may lead to strong fitness reductions, while in Type II systems, maintaining genetic diversity may require monitoring the frequency of both arrangements to avoid homozygous deleterious effects.

Although research on inversions declined with the rise of molecular genetics in the 1970s (Kirkpatrick, 2010), recent genomic tools have reignited interest. High-throughput sequencing, long-read assemblies, and local Principal Component Analysis (PCA) have enabled the detection and fine-scale characterization of inversion breakpoints, genetic content, and population frequencies (De Coster & Van Broekhoven, 2019; Schneller et al., 2025). Inversions often span tens of megabases (Mb) and may cover over 50% of the genome (Wellenreuther & Bernatchez, 2018), including adaptive loci involved in key traits such as temperature tolerance, reproduction, and immune response (Petterson et al., 2019; Han et al., 2020).

USC DE SANTIAGO

Beyond their adaptive potential, inversions may also have deleterious effects. Because recombination is suppressed in heterokaryotypes, inversions can accumulate recessive deleterious mutations that reduce fitness in homokaryotypes, leading to associative overdominance or even outbreeding depression (Jay et al., 2021; Berdan et al., 2022). This effect is especially pronounced in Type II inversions, where both arrangements are maintained across the population and heterozygotes are frequent, thereby masking deleterious variants and allowing them to persist (Berdan et al., 2021; Schneller et al., 2025).

A practical implication of this duality is that inversions may simultaneously contribute to adaptive potential and increase the risk of inbreeding or outbreeding depression. For example, in Type I systems—where alternate arrangements are fixed in different populations—hybrids in the contact zone may suffer from reduced fitness due to disrupted co-adapted gene complexes. Conversely, in Type II systems, excessive accumulation of hidden deleterious load may reduce the fitness of homokaryotypes. Therefore, the success of genetic management actions—such as translocations, selective breeding, or assisted gene flow—may depend on properly accounting for inversion structure and karyotypic variation within and between populations (Schneller et al., 2025). Understanding the dual role of inversions in harbouring both adaptive and deleterious variation is thus critical not only for evolutionary biology, but also for conservation genomics and sustainable resource management.

4.2. Chromosomal inversions in marine invertebrates and bivalves

Chromosomal inversions are widespread among aquatic organisms and have been associated with adaptive variation even in the absence of clear barriers to gene flow (Berg et al., 2016; Catanach et al., 2019; Pearse et al., 2019; Hollenbeck et al., 2022; Thorstensen et al., 2022). In molluscs, inversion polymorphisms have been linked to distinct ecotypes across the range of *Littorina saxatilis* (Reeve et al., 2024), a seawater temperature cline in *Pecten maximus* (Hollenbeck et al., 2022), or an *arginine kinase* (*ark*) polymorphism potentially involved in shell size in *L. fabalis* (Le Moan et al., 2024).

Bivalves represent a particularly promising model to explore relationship between genome architecture and adaptation, given strong evidence for local adaptation across heterogeneous environments (Hollenbeck et al., 2018) and the increasing number of studies documenting exceptional structural variation in their genomes (Calcino et al., 2021). However, the role of chromosomal inversions in the evolution and population structure of bivalves remains understudied, and most evidence comes from indirect signals such as patterns of LD, heterozygosity, and outlier loci clustering. Climate change is imposing unprecedented pressures on marine ecosystems, intensifying the need to understand and preserve the genetic basis of adaptive potential. Chromosomal inversions are emerging as critical elements in this context, as they can maintain co-adapted gene complexes that confer resilience to environmental stressors such as temperature anomalies, acidification, and altered nutrient regimes (Schneller et al., 2025).

USC UNIVERSIDADE

By reducing recombination between beneficial alleles, inversions facilitate local adaptation in species with high gene flow and wide geographic distributions. This is especially relevant in marine taxa, where dispersal can obscure population boundaries, but selective pressures remain spatially heterogeneity. For instance, seascape genomic studies in reef-building corals have shown that genetic divergence is often better explained by environmental gradients—such as depth, salinity, and nutrient levels—than by temperature alone (Black et al., 2025), suggesting that adaptive variants, potentially housed within inversions, may underlie fine-scale local adaptation. In Artic codfish, chromosomal fusions and large-scale inversions were shown to play key roles in adaptation for freezing temperatures. Structural variants often exhibit high conservation at their breakpoint regions and have been linked to ecological differentiation between lineages (Hoff et al., 2024). Evidence from molluscan studies indicates that chromosomal rearrangements could play a role in promoting ecological specialisation and early stages of speciation in marine bivalves, especially when subjected to intense selective forces like diseases or harsh environmental gradients.

As such, incorporating structural variants into conservation planning is crucial not only for identifying resilient genotypes, but also for avoiding maladaptive crosses that disrupt inversion-linked adaptations. In the face of rapid climate shifts, understanding the role of inversions in shaping species' responses may prove to be essential for designing effective genetic interventions and supporting long-term ecosystem stability.

4.3. Structural variation and inversion polymorphisms in *Ostrea edulis*

High structural variation has been reported in the flat oyster (*O. edulis*), including long inversions on three chromosomes (Lapègue et al., 2022; Monteiro et al., 2024) of its karyotype (n = 10; Thiriot-Quiévreux, 1984). These inversions span several Mb and have been consistently detected using independent datasets and approaches (e.g., whole-genome resequencing, RAD-seq, long-read assemblies, and linkage maps), confirming their conservation across populations.

The distribution of inversion arrangements in *O. edulis* has revealed significant population differentiation across its native range and their frequencies correlate with geographic gradients and historical processes, including glacial refugia and postglacial recolonization, suggesting an interaction between inversion dynamics and species' demographic history (Lapègue et al., 2022; Monteiro et al., 2024). Furthermore, one inversion has been involved in resistance to the parasite *B. ostreae* (Vera et al., 2019), indicating a potential role in host–pathogen coevolution.

These findings highlight the relevance of structural genomic variation when assessing adaptive potential and disease resistance in *O. edulis*, particularly in the context of ongoing restoration efforts and selective breeding programs.

USC UNIVERSIDADE DE SANTIAGO DE COMPOSTELA

OBJECTIVES

USC
UNIVERSIDADE
DE SANTIAGO
DE COMPOSTELA

USC
UNIVERSIDADE
DE SANTIAGO
DE COMPOSTELA

The main objective of this doctoral thesis was to provide a comprehensive understanding of the genomic structure and adaptive variation of European flat oyster (*Ostrea edulis*), a species of high ecological and economic value, with a particular focus on the genetic mechanisms underlying resistance to the intracellular parasite *Bonamia ostreae*, the main responsible of population decline throughout its distribution range. This was addressed through an integrative approach combining population genomics, association studies, genome characterization of structural variants, and comparative transcriptomics.

Specifically, we aimed to:

1. **Identify and validate previously reported genetic markers of resistance / tolerance to *B. ostreae*** in an independent scenario by evaluating their predictive association power at both population and individual levels.

2. **Characterize large-scale genomic chromosome inversions**, to determine their distribution, evolutionary history, and role on adaptation to environmental factors—particularly the inversion on chromosome 8 (C8) previously associated with resistance to *B. ostreae*.

3. **Elucidate transcriptional response to *Bonamia* infection in the wild** by characterizing differentially expressed genes across progressive infection stages, identifying key biological pathways involved in immune activation, metabolic reprogramming, and parasite-driven immunosuppression.

4. **Integrate genomic, structural, and transcriptomic evidence** into a unified framework to clarify the mechanistic link between genomic architecture and functional resistance, providing insights into the evolutionary dynamics of host–parasite interactions.

5. **Generate actionable knowledge for management and restoration of flat oyster**, designing molecular tools and conceptual guidelines that can inform selective breeding, enhance the resilience of hatchery stocks, and support the recovery of natural oyster beds in *B. ostreae*-endemic areas.

Overall, this thesis combines population genomics, genome structural analysis, and transcriptomics to deepen our understanding of *O. edulis* biology and to deliver practical guidelines for its conservation and selective breeding under persistent parasite pressure.

USC UNIVERSIDADE DE SANTIAGO DE COMPOSTELA

USC
UNIVERSIDADE
DE SANTIAGO
DE COMPOSTELA

CHAPTER I

A major genomic region associated with *Bonamia* resistance in flat oyster (*Ostrea edulis*): validation using *Bonamia*-free and long-term affected populations

The results from this chapter have already been published as:

Sambade, I. M.[1], Casanova, A.[1], Blanco, A.[1], Gundappa, M. K.[2], Bean, T. P.[2], Macqueen, D. J.[1], Houston, R. D.[2], Villalba, A.[3,4,5], Vera, M.[1], Kamermans, P.[6,7], & Martínez, P.[1] (2022). A single genomic region involving a putative chromosome rearrangement in flat oyster (*Ostrea edulis*) is associated with differential host resilience to the parasite *Bonamia ostreae*. *Evolutionary Applications*, *15*(9), 1408-1422. https://doi.org/10.1111/eva.13446 ISSN: 1752-4571.

and:

Kamermans, P. [6,7], Blanco, A. [6], Van Dalen, P. [6], Engelsma, M. [8], Bakker, N. [9], Jacobs, P. [10,11], Dubbeldam, M. [12], Sambade, I. M. [1], Vera, M. [1], & Martínez, P.[1] (2023). *Bonamia*-free flat oyster (*Ostrea edulis* L.) seed for restoration projects: non-destructive screening of broodstock, hatchery production and test for *Bonamia*-tolerance. *Aquatic Living Resources*, *36*, 11. https://doi.org/10.1051/alr/2023005 ISSN: 1765-2952

[1] Department of Zoology, Genetics and Physical Anthropology, ACUIGEN Group, Faculty of Veterinary, Universidade de Santiago de Compostela, Lugo, Spain
[2] The Roslin Institute and Royal (Dick)School of Veterinary Studies, Midlothian, UK
[3] Centro de Investigacións Mariñas (CIMA), Vilanova de Arousa, Spain
[4] Departamento de Ciencias de la Vida, Universidad de Alcalá, Alcalá de Henares, Spain
[5] Research Centre for Experimental Marine Biology and Biotechnology (PIE), University of the Basque Country (UPV/EHU), Plentzia, Spain
[6] Wageningen Marine Research, P.O. Box 77, 4400 AB Yerseke, The Netherlands
[7] Marine Animal Ecology Group, Wageningen University, Wageningen, The Netherlands
[8] Wageningen Bioveterinary Research, P.O. Box 65, 8200AB Lelystad, The Netherlands
[9] Hatchery Roem van Yerseke, Groeninx van Zoelenstraat 35, 4401 KZ Yerseke, The Netherlands
[10] Royal Netherlands Institute of Sea Research, Texel, The Netherlands
[11] Aquaculture in Delta Areas, University of Applied Sciences, P.O. Box 364, 4380 AJ Vlissingen, The Netherlands
[12] Stichting Zeeschelp, Oosthavendijk 7, 4493 BK Kamperland, The Netherlands

ABSTRACT

The European flat oyster (*Ostrea edulis*) is a key ecological and cultivated species in the North Sea that has experienced dramatic population declines due to the intracellular parasite *Bonamia ostreae*. Genomic tools have been employed to understand the mechanisms of resistance to bonamiosis and to support restoration and breeding programs. In this chapter, we integrate two complementary studies to understand the response of flat oyster to this parasite. Firstly, using a SNP array comprising ~14,000 markers, genome-wide patterns of genetic diversity were compared across wild and hatchery populations from bonamiosis-free (naïve) and long-term affected areas. Outlier loci previously associated with divergent selection strongly differentiated populations by their bonamiosis exposure history, with major signals concentrated on chromosome 8, supporting the presence of a large genomic region contributing to resistance. This region showed strong linkage disequilibrium over a long region suggesting the presence of an inversion preventing recombination. Secondly, a field-based experimental approach compared the survival of naïve and exposed seed oysters exposed to *B. ostreae* and their association with candidate markers. Seed derived from affected areas showed higher survival rates and resistance-associated genotypes, highlighting the potential for marker-assisted selection for flat oyster restoration. Together, these results validate a panel of SNPs previously associated with *B. ostreae* resistance and provide practical applications for the recovery of *O. edulis* populations in bonamiosis-endemic areas.

Keywords: bonamiosis, chromosome rearrangement, disease resistance, *Ostrea edulis*, SNP-array.

USC
UNIVERSIDADE DE SANTIAGO DE COMPOSTELA

1. INTRODUCTION

The European flat oyster (*Ostrea edulis* L.) is a marine bivalve of great ecological and economic importance, historically widespread from the Atlantic coast of Morocco to the Norwegian Sea and throughout the Mediterranean and Black Seas (Perry et al., 2017). Due to its high commercial value, populations have also been introduced beyond their natural range (Colsoul et al., 2021). This sessile, filter-feeding species can live up to 20 years and reproduce as protandrous hermaphrodites via internal fertilization and larval incubation (Bayne, 2017), with dispersal distances exceeding 10 km (Berghahn & Ruth, 2005). Oysters are considered ecosystem engineers due to their reef-building activity, providing habitat and enhancing benthic biodiversity (Smaal et al., 2018).

Beyond its ecological role, *O. edulis* has been a key aquaculture species, but global production has dropped from nearly 30,000 t in 1961 to 2,000 t in 2012 (FAO, 2020). This decline results from overexploitation, habitat degradation, and diseases—particularly bonamiosis, caused by the intracellular parasite *Bonamia ostreae* (Sas et al., 2020). The parasite infects haemocytes and epithelia, often causing adult mortalities and potentially affecting younger stages (Arzul et al., 2011). Since its first detection in France in 1979, *B. ostreae* has spread across Europe, reaching the Netherlands in the early 1980s (Van Banning, 1987; Engelsma et al., 2010), though some regions remain free of infection (Mortensen et al., 2016). Restoration efforts are ongoing across Europe (Pogoda et al., 2019b), but the presence of *B. ostreae* poses major challenges. *Bonamia*-free sites require uninfected seed, while naïve stocks are highly susceptible (Culloty et al., 2004). Conversely, oysters from long-term affected areas like Lake Grevelingen (NL) show higher survival, suggesting evolved tolerance (Culloty et al., 2004; OYSTERECOVER, 2013), making them potential candidates for selective breeding.

Understanding the genetic basis of resistance to *B. ostreae* remains a central objective in flat oyster research. Genomic studies have already uncovered QTLs and SNPs associated with differential responses to the parasite (Lallias et al., 2009; Harrang et al., 2015). More recently, analyses based on the SNP array developed by Gutiérrez et al. (2017) allowed Vera et al. (2019) to detect several outlier loci under divergent selection between naïve and long-term affected populations, with a significant concentration in one genomic region, consistent with the presence of a major resistance-related QTL.

The objective of this chapter was to validate the previously reported association between a panel of SNP markers and *B. ostreae* resistance in flat oysters within a geographically smaller area, minimizing potential genetic differentiation related to local environmental adaptation. We also aimed to evaluate these markers at the individual level in the same region, examining both population-level mortality and individual resistance (i.e. whether oysters became infected or not).

USC UNIVERSIDADE DE SANTIAGO DE COMPOSTELA

To achieve this, we used a flat oyster SNP array to validate genetic markers linked to *B. ostreae* resistance (Vera et al., 2019) in a North Sea region with variable disease pressure and subsequently positioned the validated markers on the newly assembled chromosome-level *O. edulis* genome (Gundappa et al., 2022) to delineate the genomic region associated with resistance. To further validate this association, a common garden trial was performed in a naturally infected estuary, where parasite-free juveniles from both a naïve and a long-term affected population were cohabited and monitored. This design would made it possible to compare survival across origins and to test the relationship between genetic markers and parasite load at the individual level.

This integrative approach aimed to confirm the relevance of the markers, explore their potential colocalization with immune genes, and assess the breeding potential of resistant or tolerant stocks.

USC
UNIVERSIDADE DE SANTIAGO DE COMPOSTELA

2. MATERIALS AND METHODS

2.1. Sampling

This study combined two complementary approaches to ascertain the genetic basis of *B. ostreae* resistance in O. *edulis*: i) a population genomics validation based on field-collected and hatchery-produced individuals from the North Sea, and ii) a common garden experiment to test survival and marker association under natural parasite exposure.

For the population genomics validation, 134 oysters collected in 2019 from locations with different bonamiosis prevalence: (i) three oyster wild beds from the North Sea (OS, GVR, BER); (ii) two hatchery batches (OSH, WZH) from the same area (FAO subarea 27.4, https://www.fao.org/fishery/en/area/27/en) (Fig. 1; Table 1). Hatchery samples were produced from local wild broodstock and conditioned for spawning. These batches were included due to their relevance to develop marker-assisted breeding and restoration programs but were also used to test parental contribution and to evaluate genetic diversity for future restoration plans.

Sampling sites were classified according to bonamiosis status: (i) naïve (NV), with no known history of infection, and (ii) long-term affected (LTA), where the parasite has been present and monitored for over 30 years (Engelsma et al., 2010; Table 1).

Table 1. Summary of *O. edulis* samples analysed included in the genomic and field-based analyses.

Sample code	Location	Country	Origin	N	Bonamiosis status
OS[1]	Oosterschelde	The Netherlands	Wild	28	LTA
OSH[1]	Oosterschelde	The Netherlands	Hatchery	28	LTA
GVR[1]	Grevelingen	The Netherlands	Wild	21	LTA
WZH[1]	Waddenze	The Netherlands	Hatchery	27	NV
BER[1]	Bergen	Norway	Wild	30	NV
NIOZ[2]	Waddenze	The Netherlands	Hatchery	189	NV
RvY[2]	Oosterschelde	The Netherlands	Hatchery	192	LTA

[1]Individuals used for SNP validation through a population genomics approach. [2] Individuals monitored in the common garden experiment (common garden) conducted in Lake Grevelingen.

For the common garden experiment, flat oyster seed was produced in 2018 by the Royal Netherlands Institute for Sea Research from the NV Wadden Sea (NIOZ, Jacobs et al., 2020) and by Roem van Yerseke from the LTA Oosterschelde (RvY) broodstock.

USC UNIVERSIDADE DE SANTIAGO DE COMPOSTELA

A second set of oysters from NIOZ was introduced in February 2021. Survival was checked every six weeks, at which point 60 individuals from each group were sampled and stored at −20 °C for subsequent parasite diagnosis and SNP genotyping. In total, 381 oysters were genotyped: 192 from RvY and 189 from NIOZ. Both Lake Grevelingen and the Oosterschelde are known as *Bonamia*-endemic sites (Van Banning, 1987; Haenen & Engelsma, 2020). Survival comparisons between groups were carried out using *t*-tests at each sampling date.

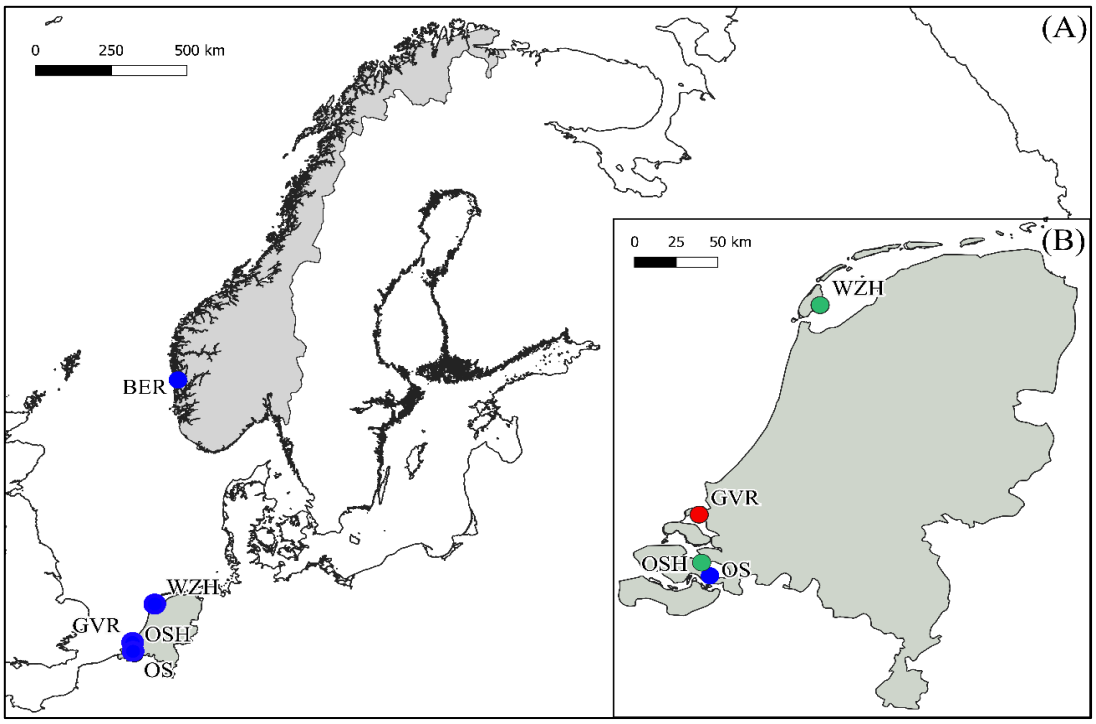


Figure 1. Sampling locations of *Ostrea edulis* used in this study: (A) overview of collection sites across the North Sea; (B) detail of the Dutch region, highlighting populations used for the population genomic analysis (blue) and the broodstock origins for the common garden experiment (green) carried out in Lake Grevelingen (red).

2.2. DNA extraction and SNP genotyping

Gill tissue served as the source for genomic DNA extraction. Approximately 30–50 mg of tissue was digested overnight with proteinase K in lysis buffer, followed by RNase A treatment and successive purification steps according to the E.Z.N.A. Mollusc DNA Kit (OMEGA Bio-Tek). DNA concentration and purity were assessed with a Nanodrop spectrophotometer, and samples were subsequently normalized prior to SNP genotyping.

For the population genomics validation, oysters were genotyped using a medium-density Affymetrix Axiom SNP array comprising 14,950 markers (average density of approximately one SNP every 63 Kb across the 935.6 Mb flat oyster genome; Gutiérrez et al., 2017).

USC UNIVERSIDADE DE SANTIAGO

After quality control, which excluded loci with call rates <90%, 11,641 SNPs remained. Monomorphic sites (n = 611) were further removed prior to population structure analyses. Based on previous findings (Vera et al., 2019), three subsets of SNPs were defined: (i) the full dataset, (ii) outlier datasets associated with bonamiosis resistance (consistent and suggestive), and (iii) a neutral SNP set.

In the common garden experiment, the 22 consistent SNPs previously associated with *Bonamia* resistance (Vera et al., 2019) were genotyped using a MassARRAY platform (Sequenom, San Diego, CA). This method involves locus-specific PCR amplification followed by single-base extension using mass-modified dideoxynucleotides (Oeth et al., 2009; Ellis & Ong, 2017). Primer sequences from the SNP chip were mapped in the chromosome-level assembled flat oyster genome ('OEROSLIN'; NCBI Bioproject: PRJNA772111; Assembly accession: JAJSPN000000000; Gundappa et al., 2022), and ±100 bp flanking regions were used for primer design (Supplementary Table 1). Among the 22 SNPs, 18 were successfully included in a single multiplex. MALDI-TOF mass spectrometry genotyping was conducted at the UCIM Genomics Platform (University of Valencia).

Gill tissue of approximately 4 mm^2, was collected also collected for *Bonamia* detection in DNA using a real-time PCR following the protocol of Marty et al. (2006). Amplifications were carried out on an ABI 7500 Fast Thermocycler (Applied Biosystems) using TaqMan chemistry in a final reaction volume of 20 µl, including forward and reverse primers, a Minor Groove Binding probe, Uracil-DNA Glycolase (UDG), and template DNA. Each run included positive, negative, and non-template controls, as well as an endogenous 18S rRNA control to verify DNA integrity.

2.3. Genetic diversity and parentage

Genetic diversity within samples was described using expected (H_e) and observed (H_o) heterozygosity, together with allelic richness (A_r), the latter standardized by rarefaction to correct for unequal sample sizes. These estimates were obtained with the *basicStats* function in the R package DiveRsity v1.9 (Keenan et al., 2013). Departure from Hardy–Weinberg equilibrium (HWE) was tested using the exact procedure implemented in Genepop v4.7.5 (Rousset, 2008). The intrapopulation fixation index (F_{IS}) was also calculated in Genepop to evaluate the magnitude and direction of deviations from random mating.

To investigate pedigree structure, parentage was reconstructed with the program Colony v2.0.6.6 (Jones & Wang, 2010). Given the computational constraints of the software when handling very large marker sets, we selected a subset of 1,000 highly polymorphic SNPs (MAF > 0.35), evenly distributed across the genome, from the 11,641 retained loci. Colony was then used to estimate both the number of contributing parents per sample and their proportional contributions. The same framework was also employed under a maximum-likelihood approach to estimate effective population sizes, assuming random mating.

USC UNIVERSIDADE DE SANTIAGO DE COMPOSTELA

2.4. Genetic structure

Genetic differentiation between populations was assessed through pairwise F_{ST} estimates, following the method of Weir and Cockerham (1984), as implemented in the F_{ST} function of Genepop.

Bayesian clustering of genotypes was performed with STRUCTURE using the admixture model. Each dataset was analysed in ten replicate runs with a burn-in of 100,000 followed by 200,000 MCMC iterations. Values of K between 1–6 were explored for the population genomic dataset, while for the common garden data K was limited to 1–3. The most likely number of clusters was identified using both the ΔK method (Evanno et al., 2005) and the log-likelihood criterion (Pritchard et al., 2000), as implemented in StructureSelector (Li & Liu, 2018) and CLUMPAK (Kopelman et al., 2015).

In addition, an analysis with prior population information (POPINFO = 1) was run with K = 2, incorporating reference naïve (LIM, LRy, TBay) and long-term affected (ORT, ROS, QUI) populations described in Vera et al. (2019). Associations between infection status (NV vs. LTA) and cluster assignment were tested using Fisher's exact tests. To complement STRUCTURE, Discriminant Analysis of Principal Components (DAPC) was carried out in the Adegenet R package (Jombart & Ahmed, 2011). The number of PCs retained was optimized by cross-validation, retaining those explaining at least 90% of cumulative variance.

2.5. Linkage disequilibrium

Pairwise linkage disequilibrium (LD) between outliers mapping in the same chromosome was estimated using the square of the correlation coefficient r^2 as implemented in using PLINK 1.9b5 (Chang et al., 2015), calculating pairwise LD values for all SNPs without imposing a distance threshold. The results were represented in a LD heatmap plot using the same R package. These values were then visualised as heatmaps using the LDheatmap package in R (Shin et al., 2006).

2.6. Mapping SNPs and differentially expressed genes in the flat oyster genome: functional enrichment assessment

The chromosome-level flat oyster genome assembly (935.6 Mb, 1365 scaffolds; N50: 94.05 Mb) (Gundappa et al., 2022) was used to map all SNPs and the 715 DEGs previously reported by Ronza et al. (2018). The 10 biggest scaffolds (875.78 Mb; 93.6% of total genome assembly) corresponded to the haploid chromosome number of flat oyster ($2n$ = 20; Thiriot-Quiévreux, 1984). For functional mapping, all SNPs-including both consistent and putative outliers linked to resistance-as well as differentially expressed genes (DEGs), were aligned to the reference genome to examine potential co-localization.

USC UNIVERSIDADE DE SANTIAGO DE COMPOSTELA

3. RESULTS

This study integrated two complementary strategies to assess the genetic basis for resistance to *B. ostreae* in *O. edulis*: i) a population genomics validation of previous *Bonamia*-resistant markers; ii) a common garden experiment in the wild to test the performance of NV and LTA strains exposed to the parasite. Distinct SNP panels were applied depending on the specific aim of each strategy (Table 2). The complete SNP data set—including both polymorphic and monomorphic loci—was used to estimate genetic diversity and compare it with previous studies in *O. edulis*, while the neutral and outlier SNP subsets were employed to explore patterns of genetic structure depending on bonamiosis pressure over samples (i.e., NV vs. LTA). Because the sampling covered a relatively narrow geographic range, the number of polymorphic outliers identified here was smaller than in the broader survey of Vera et al. (2019). Specifically, the total number of suggestive and consistent outliers decreased from 87 to 71 and from 21 to 16, respectively. The subset of the most consistent outlier SNPs was used for the common garden experiment using a massARRAY genotyping protocol (Table 2).

Table 2. SNP panels used for the different analyses performed in *O. edulis* from the North Sea

SNP number	SNP panels used	Genetic diversity	Population differentiation/structure
11,641	Initial panel	✓	
10,591	Neutral panel[a]		✓
71 and 16	Outlier panel[b]	✓	✓
18	Outlier panel[c]		✓

[a]Only polymorphic loci; [b]Suggestive and consistent outliers according to Vera et al. (2019); [c]Consistent outliers genotyped via MassARRAY in the common garden experiment

3.1. Population genomics validation

3.1.1 Genetic diversity

Across the 11,641 filtered SNPs, genetic diversity was quantified according to sampling origin. Genetic diversity across wild populations showed low but consistent variability: observed heterozygosity (H_o) ranged between 0.264 (BER) and 0.275 (OS), averaging 0.269 ± 0.003; expected heterozygosity (H_e) varied between 0.265 and 0.271 (mean = 0.268 ± 0.002); and allelic richness (A_r) ranged from 1.893 (WZH) to 1.908 (OS and GVR), with an overall mean of 1.903 ± 0.005 (Table 3A). Hatchery groups displayed lower values for all metrics compared with wild populations (e.g., A_r = 1.833 vs. 1.903; He = 0.257 vs. 0.268; Kruskal–Wallis, $p < 0.001$).

USC UNIVERSIDADE DE SANTIAGO DE COMPOSTELA

All populations conformed to Hardy–Weinberg equilibrium ($p > 0.05$ after Bonferroni correction), but hatchery samples displayed significantly negative F_{IS} values, indicating heterozygote excess. Similar results were obtained when only neutral loci were considered (data not shown).

Table 3. Summary of genetic diversity metrics in *O. edulis* samples from the North Sea, based on: (A) the complete SNP dataset; (B) the 16 consistent outliers; and (C) the 71 suggestive outliers

(A)

Sample	Bonam. status	Polym. SNPs	A_r	H_o	H_e	F_{IS}
OS	LTA	10,371	1.908	0.275	0.271	−0.013
OSH	LTA	9,471	1.839	0.271	0.259	**−0.048**
GVR	LTA	9,905	1.908	0.267	0.268	0.003
WZH	NV	9,050	1.827	0.273	0.254	**−0.076**
BER	NV	10,132	1.893	0.264	0 .265	0.002

(B)

Sample	Bonam. status	A_r	H_o	H_e	F_{IS}
OS	LTA	2.000	0.266	0.273	0.024
OSH	LTA	1.934	0.205	0.252	0.090
GVR	LTA	2.000	0.206	0.252	0.184
WZH	NV	1.435	0.110	0.114	0.039
BER	NV	1.880	0.169	0.158	−0.076

(C)

Sample	Bonam. status	A_r	H_o	H_e	F_{IS}
OS	LTA	1.972	0.301	0.301	-0.001
OSH	LTA	1.903	0.265	0.267	0.006
GVR	LTA	1.986	0.283	0.300	0.056
WZH	NV	1.700	0.250	0.224	**−0.115**
BER	NV	1.906	0.256	0.263	0.027

Bold type indicates significant F_{IS} values

USC UNIVERSIDADE DE SANTIAGO DE COMPOSTELA

Parental contribution analysis performed with *Colony* estimated that the OSH hatchery sample originated from 16 breeders—six males and ten females—with an effective population size (Ne) of 11. Similarly, the WZH hatchery group also derived from 16 breeders—seven males and nine females—and Ne = 10, indicating relatively balanced sex ratios and contributions. The average number of individuals per family was 1.47 ± 0.21 (19 full-sib families, range: 1–4) for OSH and 2.08 ± 0.38 (13 families, range: 1–7) for WZH. In contrast, no parental relationships were detected among individuals from the wild populations GVR and BER, yielding Ne estimates of 2,147,483,647, and only two half-sibs were identified among the 28 individuals analysed from OS (Ne = 1,512). These results agree with the higher genetic diversity observed in wild populations.

Interestingly, when genetic diversity was assessed using the outlier SNP panels, the trend was related to bonamiosis status. NV samples (BER and WZH) exhibited lower genetic diversity values than LTA samples (GVR, OS, OSH), particularly when considering the 16 consistent outliers. In this case, allelic richness was significantly lower in NV samples (A_r = 1.658) than in LTA ones (A_r = 1.978, p = 0.004), and the same held for expected heterozygosity (H_e = 0.136 vs. 0.259, p = 0.004) (Table 3B, 3C).

3.1.2. Genetic structure and differentiation

Population structure was evaluated using both neutral and outlier SNPs linked to resistance to *B. ostreae*. In the population genomics validation, moderate yet statistically significant genetic differentiation was observed across most pairwise comparisons among the five sampling locations in the North Sea when using neutral markers (mean F_{ST} = 0.0283; Table 4A). Among the wild populations, the Dutch samples OS and GVR showed no differentiation (F_{ST} = 0.0003), whereas BER from Norway showed the highest divergence (mean F_{ST} = 0.0169). The greatest pairwise differentiation with the neutral dataset was detected between the hatchery populations (F_{ST} = 0.0540), which also presented higher average F_{ST} values compared to wild samples (0.0356).

Using the outlier SNP subsets, average pairwise F_{ST} values were slightly lower across all comparisons: 0.0253 for the 16 consistent outliers and 0.0159 for the 71 suggestive outliers. However, greater divergence was detected between NV (BER and WZH) and long-term LTA (GVR, OS, OSH) populations when using these outlier markers (F_{ST} = 0.0348 and 0.0289 for the consistent and the suggestive ones, respectively), though not significant (p > 0.05; Tables 4B and 4C).

USC UNIVERSIDADE DE SANTIAGO DE COMPOSTELA

Table 4. Pairwise F_{ST} values among North Sea *O. edulis* populations using: (A) 10,591 neutral SNPs; (B) 16 consistent outliers; and (C) 71 suggestive outliers

(A)

	OS	OSH	GVR	WZH	BER
OS	-	0.0000	0.1848	0.0000	0.0000
OSH	**0.0228**	-	0.0000	0.0000	0.0000
GVR	0.0003	**0.0269**	-	0.0000	0.0000
WZH	**0.0282**	**0.0540**	**0.0299**	-	0.0000
BER	**0.0165**	**0.0409**	**0.0172**	**0.0463**	-

(B)

	OS	OSH	GVR	WZH	BER
OS	-	0.9992	1.0000	0.0001	0.0000
OSH	-0.0111	-	0.9963	0.0000	0.0515
GVR	-0.0182	-0.0138	-	0.0000	0.2311
WZH	**0.0491**	**0.0439**	**0.0401**	-	0.0002
BER	**0.0219**	0.0112	0.0073	**0.0286**	-

(C)

	OS	OSH	GVR	WZH	BER
OS	-	0.9992	1.0000	0.0001	0.0000
OSH	-0.0111	-	0.9963	0.0000	0.0515
GVR	−0.0182	−0.0138	-	0.0001	0.2311
WZH	**0.0491**	**0.0439**	**0.0401**	-	0.0002
BER	**0.0219**	0.0112	0.0073	**0.0286**	-

Pairwise F_{ST} and their *p*-values below and above the diagonal, respectively. Bold type indicates significant F_{ST}.

Bayesian clustering with STRUCTURE without prior population information showed K = 3 and K = 2 the most likely number of clusters for the neutral and outlier SNP panels, respectively. Using the neutral markers, a clear genetic distinction was detected between hatchery (WZH and OSH) and wild (BER, GVR, OS) samples, with the latter grouping into a single cluster across all K values (Fig. 2A). In contrast, when using the outlier SNPs two genetic clusters, labelled "orange" and "blue", were consistently identified with both outlier SNP datasets in all samples (Fig. 2B, 2C). Individuals from both clusters were found at all sampling sites, but their frequencies varied according to bonamiosis status: the lowest proportion of “orange” individuals was detected in WZH (3.7%), while the highest was found in OS (32.1%).

USC UNIVERSIDADE DE SANTIAGO DE COMPOSTELA

A marginally significant association between bonamiosis status and the proportion of "orange" individuals was detected (LTA: OS, GVR, OSH = 21; NV: BER, WZH = 6; Fisher's exact test, $p = 0.054$).

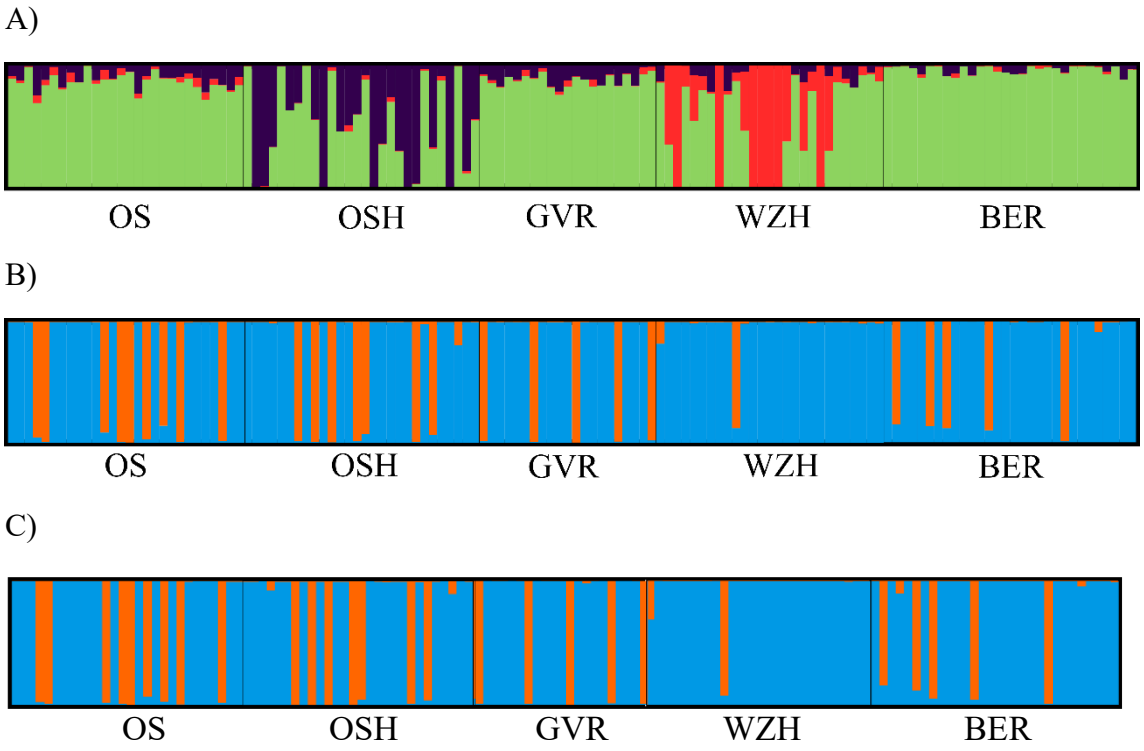


Figure 2. Genetic clustering of *O. edulis* individuals from the North Sea inferred with STRUCTURE using: A) neutral SNPs (K = 3); B) 16 consistent outliers; and C) 71 suggestive outliers (both K = 2). Each bar represents one individual, and the colour proportions indicate assignment probabilities to the inferred clusters.

To confirm the biological relevance of the "orange" and "blue" clusters detected, STRUCTURE analyses were repeated using prior information from Vera et al. (2019), with reference allele frequencies derived from their NV and LTA samples. The clusters obtained with prior assignment were found to correspond exactly to the NV (blue) and LTA (orange) reference groups without prior information in both the 16 (Fig. 3) and 71-outlier datasets (similar results; data not shown).

USC UNIVERSIDADE DE SANTIAGO DE COMPOSTELA

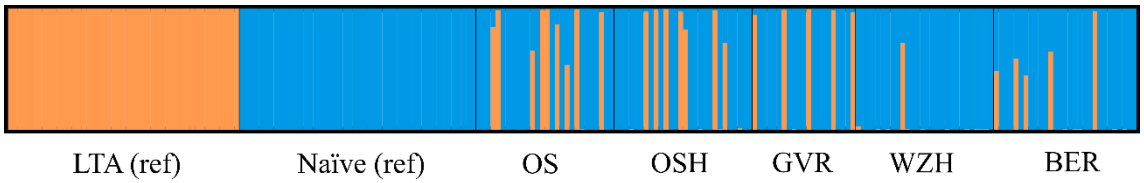


Figure 3. STRUCTURE results for *O. edulis* individuals (N = 134) using the 16 consistent outliers, incorporating prior information from Vera et al. (2019) for long-term affected (LTA, orange, N = 47) and naïve (NV, blue, N = 48) reference samples. Each bar represents the ancestry proportions of a single individual.

Further examination of genetic structure was conducted using Discriminant Analysis of Principal Components (DAPC), yielding consistent results with STRUCTURE. For the neutral panel, 101 principal components were retained, explaining 90.4% of the variance.

Genetic differentiation was primarily associated with geographic distance for wild samples (BER vs OS/GRV) and with origin (hatchery vs wild) using neutral SNPs (Fig. 4A). For the 16 outlier SNP panel, six principal components were retained (90.5% variance explained), with less separation observed among locations, but increased dispersion within sites (Fig. 4B). Individuals most distant from their sample centroids corresponded to the "orange" cluster identified with STRUCTURE. The same distribution pattern was observed with the 71-SNP panel (data not shown).

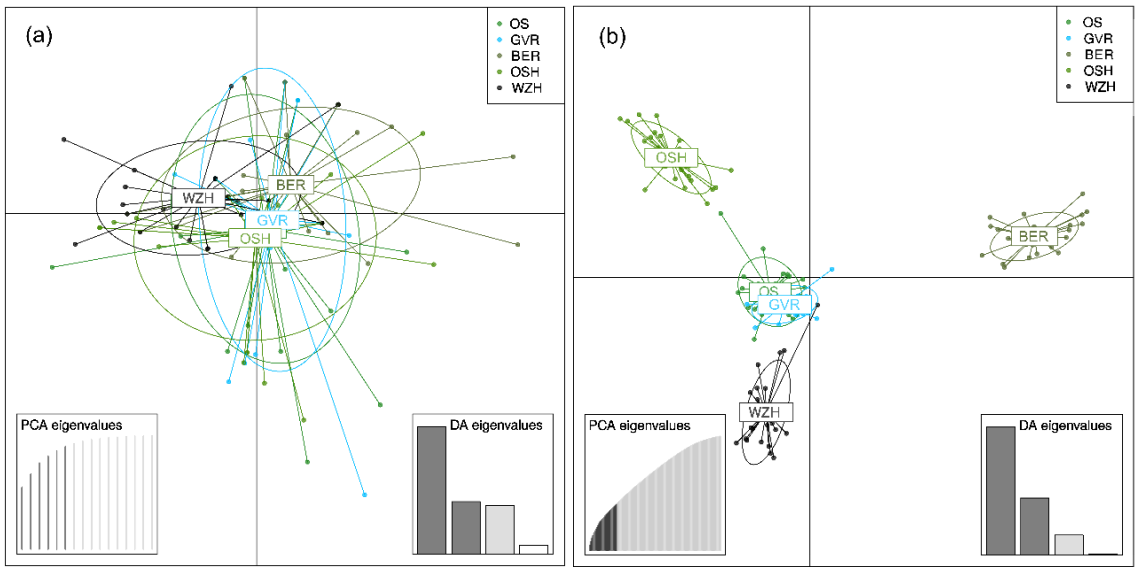


Figure 4. Discriminant Analysis of Principal Components (DAPC) plots for *O. edulis* from the North Sea based on: A) the neutral SNP panel (101 PCs, 90.4% variance); B) the 16 consistent outliers (6 PCs, 90.5% variance); Axes represent the first two principal components.

USC
UNIVERSIDADE DE SANTIAGO DE COMPOSTELA

Based on the STRUCTURE membership coefficients, individuals were assigned to either the “orange” (n = 27) or “blue” (n = 107) clusters using a threshold q-value > 0.5. Individuals with admixed ancestry were assigned to the cluster for which the q-value was the highest. Expected heterozygosity (H_e) was found to be nearly double in the “orange” group compared to the “blue” group across both outlier panels. The inbreeding coefficient (F_{IS}) was significantly negative in the “orange” group, suggesting an excess of heterozygotes, whereas values in the “blue” group conformed to Hardy–Weinberg expectations (Table 5). This heterozygote excess was more pronounced for the consistent outlier panel (F_{IS} = -0.376) than for the suggestive panel (F_{IS} = -0.196).

Table 5. Genetic diversity in the STRUCTURE-inferred "orange" and "blue" groups from North Sea *O. edulis* samples using: (A) 16 consistent and (B) 71 suggestive outliers.

(A)

Population	A_r	H_o	H_e	F_{IS}
Orange	2.000	0.590	0.430	**−0.376**
“blue”	1.910	0.270	0.270	−0.064

(B)

Population	A_r	H_o	H_e	F_{IS}
Orange	1.970	0.430	0.360	**−0.196**
“blue”	1.720	0.230	0.230	−0.009

Bold type indicates significant F_{IS} values

A DAPC conducted on the “orange” and “blue” clusters indicated no divergence (K = 1) when using the neutral markers, but clear clustering (K = 2) with both outlier panels. Pairwise F_{ST} between clusters was highly significant: 0.5118 for the consistent panel and 0.2274 for the suggestive panel ($p < 0.001$), while no significant with neutral markers (F_{ST} = 0.008, $p > 0.05$).

Distributions of F_{ST} values across loci revealed that neutral SNPs were largely confined to the lowest interval (0–0.1), whereas outlier loci showed broader distributions, with consistent outliers exhibiting modal peaks between 0.7 and 0.8 (Fig. S1). F_{IS} values showed similar patterns: neutral SNPs were around zero, while outlier SNPs showed a strong bias toward negative values (Fig. S2). The mean F_{IS} was -0.110 (range: -0.919 to 0.784) for the 71 outliers and -0.288 (range: -0.919 to 0.076) for the 16 consistent outliers.

USC UNIVERSIDADE DE SANTIAGO DE COMPOSTELA

3.1.3. Mapping of outliers and linkage disequilibrium

Validated outlier SNPs were mapped using the flat oyster genome (Gundappa et al., 2022). A large proportion of the 71 suggestive outliers (37) and nearly all of the 16 consistent outliers (14 SNPs) were mapped to chromosome OE-C8 (Table 6).

To assess whether these markers were in linkage disequilibrium (LD), LD analysis was conducted on the 37 SNPs located on OE-C8. These markers spanned a genomic segment of approximately 29.44 Mb (between AX-169174678 and AX-169187911), encompassing the 14 consistent outliers. A strong LD pattern across this region. All consistent outliers, with the exception of AX-189186592 (which showed the lowest F_{ST} between "orange" and "blue" clusters, $F_{ST} = 0.182$), were found to be in significant LD following Bonferroni correction (mean $r^2 = 0.554$; range: 0.20–0.92; $p < 0.00064$; Fig. 5 and Fig. S3).

Table 6. Chromosome-level distribution of resistance-associated outlier SNPs from Vera et al. (2019) in the *O. edulis* genome.

Chromosome	Length (pb)	Total	71 outliers	16 outliers
1	117,440,623	4,750	10	-
2	101,867,661	3,960	4	**1**
3	101,833,125	3,720	2	-
4	99,930,069	4,022	7	-
5	95,564,955	3,720	1	-
6	94,056,450	3,743	3 (1)	-
7	84,932,467	3,167	1	1
8	70,328,625	2,714	37	14
9	65,180,066	2,512	1 (1)	-
10	44,655,554	1,520	2	-
No match			3	-

In parentheses two outliers with the same matching score in two different chromosomes counted twice

Moreover, most SNPs within this genomic region displayed significantly elevated F_{ST} values between "orange" and "blue" genetic clusters, as well as highly negative F_{IS} values within groups when compared to genome-wide averages. This was assessed through sliding window analyses using 50-SNP intervals (Fig. 6), allowing the identification of a candidate divergent region extending up to 33.83 Mb. The presence of multiple additional SNPs with similar characteristics within this interval suggests the existence of other potential resistance-associated loci.

USC UNIVERSIDADE DE SANTIAGO DE COMPOSTELA

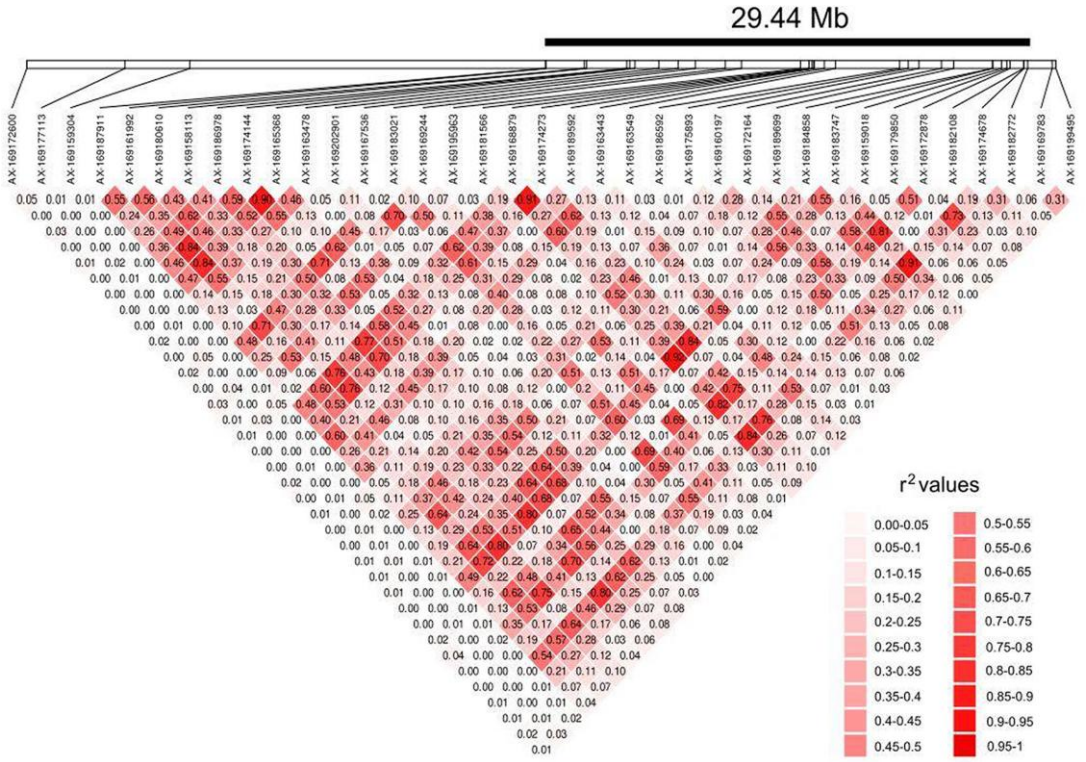


Figure 5. Heatmap illustrating pairwise linkage disequilibrium (r^2) among 37 outlier SNPs located on chromosome OE-C8 in *O. edulis*. Colour intensity ranges from white (low LD) to red (high LD), as indicated by the legend.

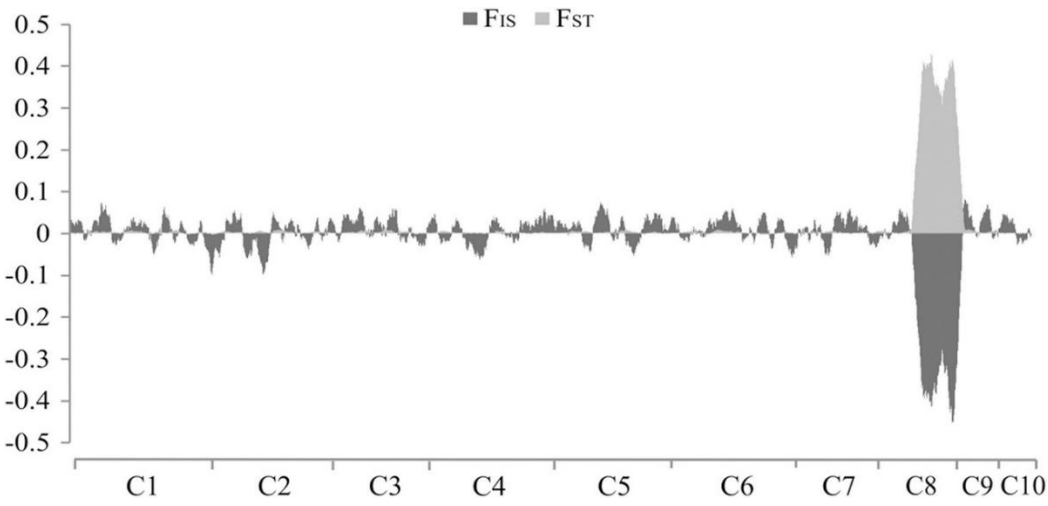


Figure 6. Genome-wide patterns of F_{ST} between the "orange" and "blue" genetic clusters and F_{IS} within each group, based on 9,277 SNPs mapped across the 10 *O. edulis* chromosomes. Average values were calculated using sliding windows of 50 SNPs.

USC UNIVERSIDADE DE SANTIAGO DE COMPOSTELA

3.2. Common garden experiment to check the performance of NV and LTA strains

The LTA strain (RvY group) showed a significant survival rate than the NV one (NIOZ group) at the end of the common garden experiments performed in 2020 and 2021 ($p < 0.05$), differences being detected around the fifth month onwards. Final survival rates ranged from 73–92% for RvY and 25–54% for NIOZ, with mortality peaking in midsummer, likely reflecting increased disease pressure (Fig. 7). This data aligned with the genetic clustering patterns observed in the two strains.

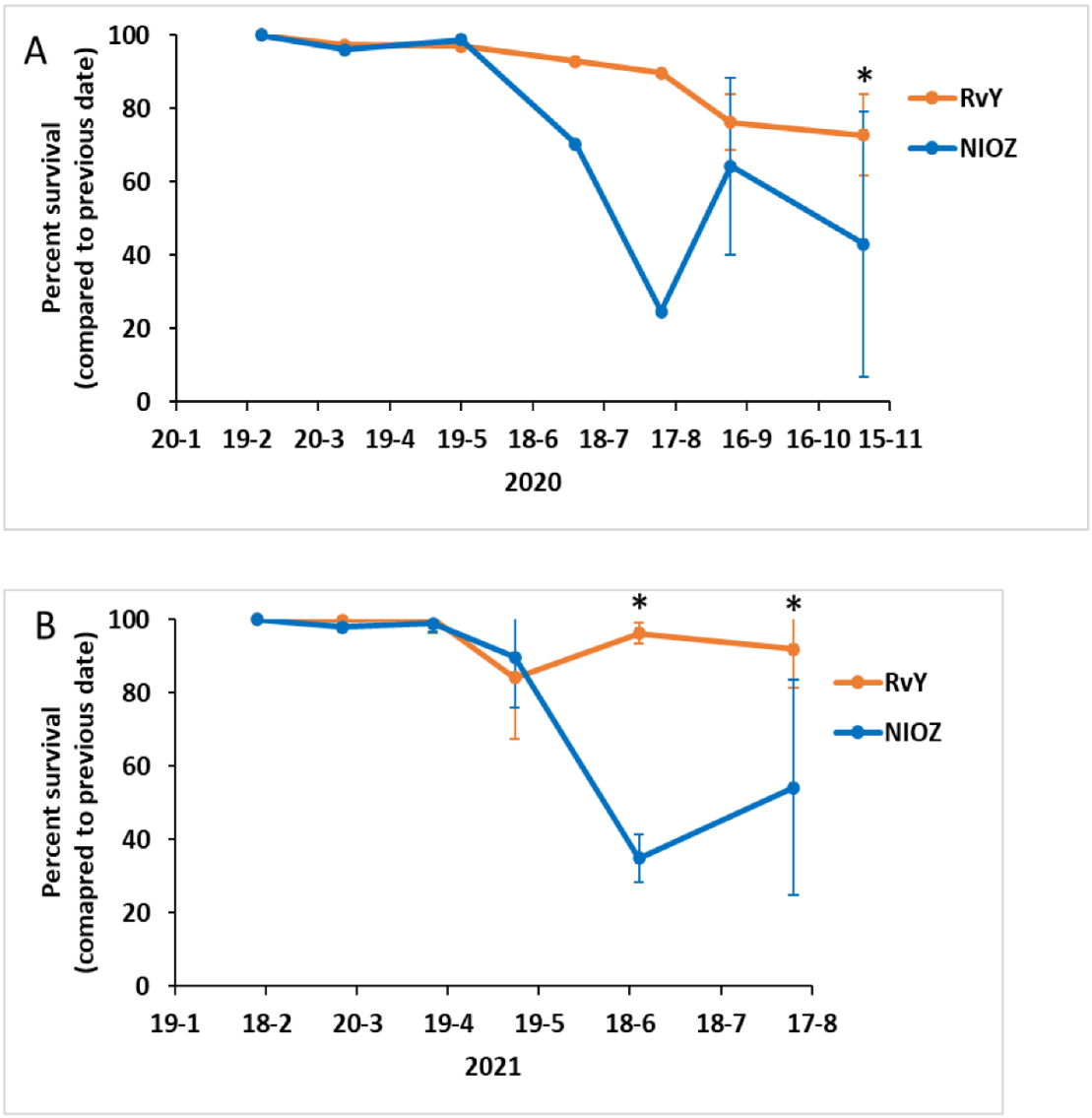


Figure 7. Survival rates of hatchery-produced *O. edulis* from different broodstock origins: RvY (long-term affected; LTA) and NIOZ (naïve; NV), in 2020 (A) and 2021 (B), measured as percentage survival since the previous sampling point.

USC
UNIVERSIDADE DE SANTIAGO DE COMPOSTELA

STRUCTURE analysis using the 18 high-confidence SNP outliers, rendered a two-cluster solution (K = 2). A significantly higher proportion of RvY individuals from LTA broodstock were assigned to the "orange" cluster (48 out of 187) compared to NIOZ individuals from NV broodstock (7 out of 185), reinforcing the relationship between the genetic background and bonamiosis exposure ($p < 0.00001$; Fig. 8). We also aimed to assess the association between parasite infection and oyster genotype (orange/blue) at the individual level; however, no parasite presence was detected in the gill tissue of any individual analysed using qPCR.

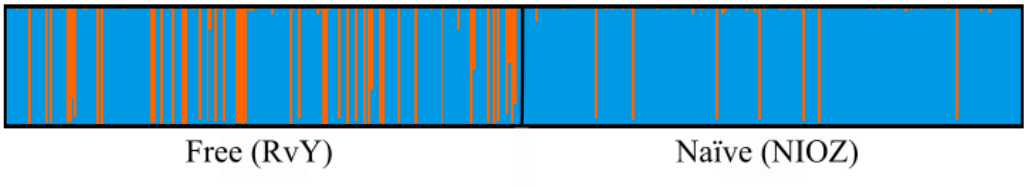


Figure 8. STRUCTURE barplot based on the 18 consistent SNP outliers associated with bonamiosis resistance for seed oysters from RvY (LTA origin) and NIOZ (NV origin) sampled during the April challenge.

USC UNIVERSIDADE DE SANTIAGO DE COMPOSTELA

USC
UNIVERSIDADE
DE SANTIAGO
DE COMPOSTELA

CHAPTER II

Disentangling the role of chromosome inversions in the structure of flat oyster (*Ostrea edulis*): origin, adaptation and phylogeography

The results presented in this chapter are based on the following preprint:

Sambade, I. M.[1], Hlordzi, V.[2], Blanco, A.[1], Hermida, M.[1], Vera, M. [1], Culloty, S.[2,3,4], Bean, T.[5], Lynch, S. A.[2,3], and Martínez, P.[1] (2025). Disentangling the role of chromosome inversions in the structure of flat oyster (*Ostrea edulis*): origin, adaptation and phylogeography. bioRxiv. https://doi.org/10.1101/2025.06.12.659260

[1] Department of Zoology, Genetics and Physical Anthropology, ACUIGEN Group, Faculty of Veterinary, Universidade de Santiago de Compostela, Lugo, Spain
[2] School of Biological, Earth and Environmental Sciences and Aquaculture and Fisheries Development Centre, University College Cork, Cork, Ireland
[3] Environmental Research Institute, University College Cork, Cork, Ireland
[4] MaREI Centre, Environmetal Reseach Institute, University College Cork, Cork, Ireland
[5] The Roslin Institute and Royal (Dick)School of Veterinary Studies, Midlothian, UK

USC UNIVERSIDADE DE SANTIAGO DE COMPOSTELA

ABSTRACT

Chromosomal inversions are large-scale structural variants that disrupt recombination and contribute to population differentiation and local adaptation. In this study, we characterized the genomic features, frequency, and evolutionary significance of chromosomal inversions in the European flat oyster (*Ostrea edulis*), a species of ecological and commercial relevance. Using a new low-density SNP array (~5K), we screened the genome across the native European distribution of the species. We confirmed the presence of inversions at chromosome (C) 2, C5 and C8 and refined their breakpoints by combining linkage disequilibrium in a large sample and whole genome long-read sequencing. This enabled us to identify the SNPs and genes mapping within the three inversions, spanning 27, 7 and 35 Mb, respectively, for comparative population genomics and functional evaluation. A north to south cline was observed for the three inversions, although with low-moderate correlation between them. Strong signals for divergent selection were detected for the three inversions, although with specific profiles suggestive of adaptive peaks around highly divergent SNPs across the inversion length. The three inversions seem to be old considering genetic diversity and differentiation between arrangements. Phylogeographic events and adaptation to the current environment seem to underlie the structural pattern observed. Gene content and enrichment analyses within inversions suggest that these polymorphisms may play a role in the immune system and response to different stressors including parasite resistance. Our results provide new insights into the genomic architecture of adaptation in *O. edulis* and highlight the potential of structural variants as targets for conservation and selective breeding.

Keywords: Chromosomal inversions, structural variants, native distribution, adaptation, *Ostrea edulis*

USC
UNIVERSIDADE DE SANTIAGO DE COMPOSTELA

1. INTRODUCTION

Chromosomal inversions, first described in *Drosophila* (Sturtevant, 1920), are structural variants involving the reorientation of DNA segments within a chromosome. These variants can reduce recombination by preserving sets of adaptive alleles (supergenes), thus playing a key role in local adaptation and speciation (Dobzhansky, 1970; Kirkpatrick & Barton, 2006; Reeve et al., 2024). Inversions can persist through evolutionary time due to divergent or balancing selection and are often associated with environmental gradients and genetic incompatibilities that contribute to reproductive isolation (Lowry & Willis, 2010; Wellenreuther & Bernatchez, 2018; Faria et al., 2019).

Inversions may span large genomic regions—up to 100 Mb—and account for significant portions of some genomes (Walkowiak et al., 2020). Technological advances, including high-throughput sequencing and bioinformatic tools, have revived the interest on inversions by allowing precise identification of their boundaries and distribution (De Coster & Van Broekhoven, 2019). These tools have confirmed that inverted regions often show high genetic differentiation and can represent hotspots for adaptive variation (Wellenreuther & Bernatchez, 2018).

In aquatic organisms, including molluscs, chromosomal inversions are increasingly recognized as important drivers of adaptation (Berg et al., 2016; Hollenbeck et al., 2022). For example, inversions have been linked to ecotype differentiation in *Littorina saxatilis* and *Pecten maximus* (Hollenbeck et al., 2022; Reeve et al., 2024). In bivalves, the presence of extensive structural variation and local adaptation across heterogeneous environments makes them ideal systems to study genome evolution (Calcino et al., 2021).

The European flat oyster, *Ostrea edulis*, is a key marine species, both ecologically and economically. It contributes to ecosystem functioning through water filtration and habitat formation and is cultivated for food and conservation purposes (Albentosa et al., 2023; Pogoda et al., 2023; Zu Ermgassen et al., 2023). Distributed from Northern to Southern Europe, including parts of the Mediterranean (FAO, 2022; Pouvreau et al., 2023), *O. edulis* shows complex population structure influenced by phylogeographic events, historical translocations, oceanographic barriers, and local adaptation (Vera et al., 2016; Hayer et al., 2021; Lapègue et al., 2022).

Recent studies have identified large inversions in three chromosomes of *O. edulis* (Lapégue et al., 2022; Monteiro et al., 2024), including one in chromosome (C)8 associated with resistance to *Bonamia ostreae* (Chapter I). These inversions show geographic variation suggestive of adaptive or historical significance.

USC
UNIVERSIDADE DE SANTIAGO DE COMPOSTELA

The objective of this chapter was to investigate genome structural variation in *O. edulis*, with a particular focus on chromosomal inversions and their potential link to *B. ostreae* resistance. Specifically, we sought to identify and characterize chromosomal inversions using population-scale and long-read genomic data, to examine their frequency and distribution throughout the species' native range, and to assess the overlap between inversion regions and genomic loci previously associated with resistance (Chapter I). In addition, we aimed to explore the potential functional roles of two newly characterized inversions. Understanding the boundaries, distribution, and evolutionary significance of these structural variants is essential for elucidating their role in population structure, local adaptation, and the sustainable management of this threatened species.

USC
UNIVERSIDADE DE SANTIAGO DE COMPOSTELA

2. MATERIALS AND METHODS

2.1. Sampling

A total of 343 wild *O. edulis* individuals were sampled across 13 natural shellfish beds to conduct population genomics analyses (Fig. 1; Table 1). The sampling strategy aimed to encompass the natural range of the species, integrating both newly collected individuals and samples analysed in earlier studies. This comprehensive collection design facilitated a refined assessment of population structure, particularly in relation to the main chromosomal inversions recently reported in the species (Lapègue et al., 2022; Monteiro et al., 2024). Additionally, 384 oysters from two geographically close Irish locations—Lough Swilly (LW) and Galway (GAL), separated by approximately 125 nautical miles—were included for specific analyses on Hardy-Weinberg equilibrium (HWE) and for delineating inversion boundaries based on linkage disequilibrium (LD).

Table 1. Main features of the *O. edulis* shellfish beds

Location	Code	Country	N	Sample collection
Bergen	BER	Norway	30	this study
Grevelingen	GVR	The Netherlands	21	this study
Oosterschelde	OS	The Netherlands	28	this study
Loch Ryan	LR	Scotland	16	1
Lough Swilly	LW	Ireland	33 (192)	this study
Tralee Bay	TB	Ireland	16	1
Galway	GAL	Ireland	37 (192)	this study
Quiberon	QUI	France	15	1
Ortigueira	OR	Spain	16	1
Noia	NO	Spain	33	2
Pontevedra	PON	Spain	33	2
Alicante	ALI	Spain	30	this study
Mali Ston Bay	MS	Croatia	35	3

1. Vera et al. (2019), 2. Vera et al. (2016), 3. Šegvić-Bubić et al. (2020); in parentheses the samples used to test HW and LD for the three inversions in LW and GAL.

USC UNIVERSIDADE DE SANTIAGO DE COMPOSTELA

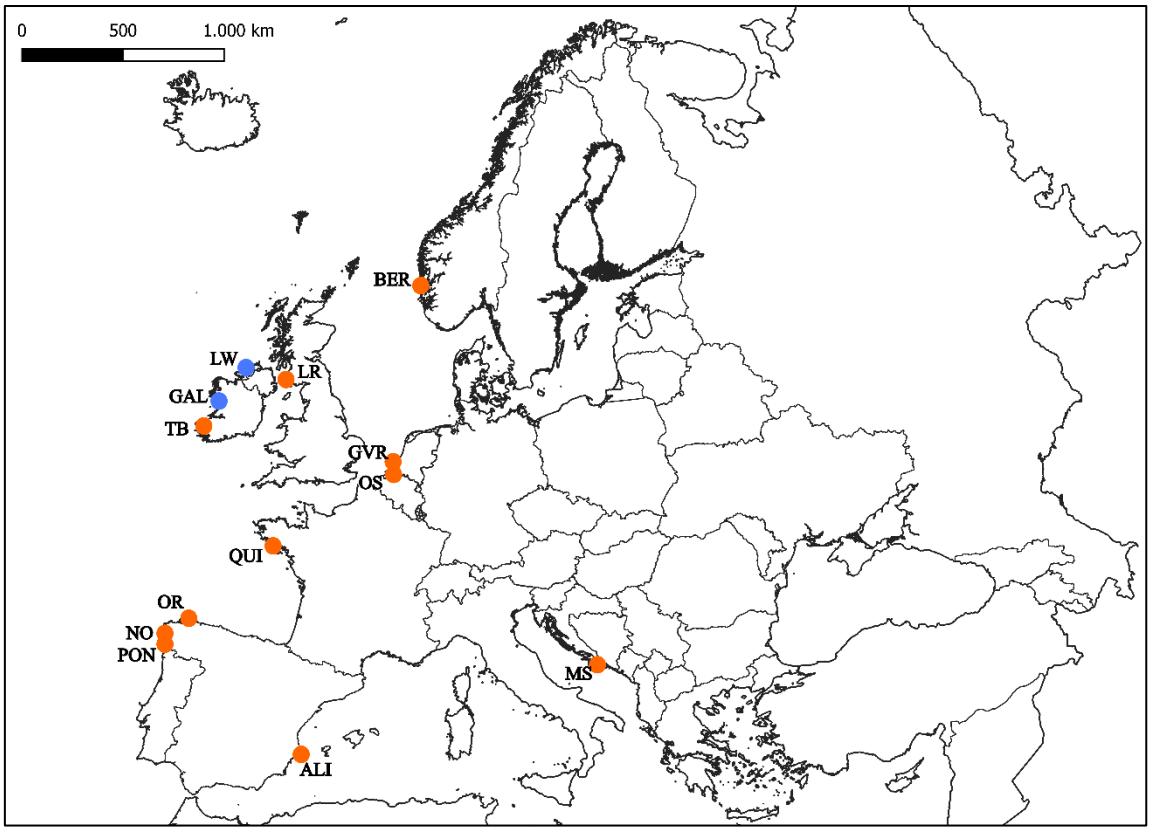


Figure 1. Sampling locations of *O. edulis* in this study. Sampling codes from Table 1. The two populations with the largest sampling effort, Lough Swilly and Galway, are represented in blue.

2.2. DNA extraction

Genomic DNA was extracted from gill tissue using the E.Z.N.A.® Mollusc DNA Kit (OMEGA Bio-Tek), following the manufacturer's guidelines. Approximately 30–50 mg of tissue, either freshly collected or preserved in absolute ethanol, were digested in a lysis solution containing 700 µL of CSPL buffer and 20 µL of proteinase K and incubated overnight at 65°C with continuous agitation. After enzymatic digestion, RNA was removed via RNase A treatment, and DNA was purified through several wash and centrifugation steps. The concentration and purity of the resulting DNA extracts were measured with a Nanodrop spectrophotometer, and DNA concentrations were adjusted for SNP genotyping.

2.3. SNP genotyping

Genotyping was conducted using a multispecies Affymetrix Axiom Custom SNP Array. Samples that were already analysed in Vera et al. (2019) and in Chapter I of this Thesis were genotyped using the full panel of ~15,000 SNPs developed for *O. edulis* (Gutiérrez et al., 2017; Table 1).

USC UNIVERSIDADE DE SANTIAGO DE COMPOSTELA

The remaining individuals were genotyped with a new array panel including 4,741 SNPs from that original Gutierrez et al. (2017), selected from previous population genomics data based on the following criteria: minor allele frequency (MAF) > 0.05, missing data < 20%, and even distribution across the genome (Gundappa et al., 2022). This reduced set was integrated into a custom multispecies Axiom SNP array designed by the University of Santiago de Compostela in collaboration with Thermo-Fisher Scientific and Xenética Fontao S.A. SNP data of this reduced panel were retrieved from the original genotyping for those samples analysed with the 15K array, so all samples were analysed with the same SNP dataset. The average SNP density of the reduced panel was 4.9 markers per megabase, with chromosome-specific densities ranging from 2.8 to 6.9 SNPs/Mb (Fig. 2).



Figure 2. Frequency distribution of SNPs of the multi-species Axiom array across the 10 chromosomes (C) of *O. edulis*

2.4. Genomic characterization of chromosome inversions

To define the boundaries of the reported C2, C5 and C8 chromosomal inversions (see Results) (Lapègue et al., 2022: LG1, LG6 and LG4, respectively; Monteiro et al., 2024: scaffold5, scaffold4, scaffold8; see Results), two complementary approaches were followed.

USC UNIVERSIDADE DE SANTIAGO DE COMPOSTELA

2.4.1. Linkage disequilibrium analysis

A rough location of the boundaries of chromosomal inversions was performed using linkage disequilibrium (LD) in a large dataset of 384 oysters. SNP density (4.9 SNPs/Mb) precluded a precise identification of the three inversion breakpoints. Samples were collected between May and September 2023 from two Irish populations (LW and GAL; see Fig. 1 and Table 1), a region previously reported to harbour a high polymorphism for these inversions (Vera et al., 2019; Lapègue et al., 2022; Monteiro et al., 2024).

Initial LD decay patterns were examined by computing r^2 values with PopLDdecay (Zhang C. et al., 2019) and visualised as scatterplots generated with the R package ggplot2 (Wickham, 2009), where r^2 values were plotted against physical distance between SNPs. Chromosomes that exhibited atypical LD decay profiles were further analysed using PLINK 1.9b5 (Chang et al., 2015), calculating pairwise LD values for all SNPs without imposing a distance threshold. These values were then visualised as heatmaps using the LDheatmap package in R (Shin et al., 2006), which enabled delineation of high-LD regions consistent with putative inversions on chromosomes C2, C5, and C8 (see Results). All these analyses were carried out taking as reference the flat oyster genome released by Gundappa et al. (2022).

LD profile along C2, C5, and C8 lengths was further explored using a sliding window approach. Mean r^2 values were computed over windows of ten consecutive SNPs, shifting one SNP per step, using PLINK 1.9b5. These profiles were later used to investigate the correspondence between LD patterns and genetic differentiation across the inversion spans.

Since the inversion lengths identified in this study diverged from those reported in earlier studies (Lapègue et al., 2022; Monteiro et al., 2024), two comparative analyses were performed: (i) the microsatellite markers used by Lapègue et al. (2022) were aligned against the *O. edulis* reference genome (Gundappa et al., 2022) using BLAST (Altschul et al., 1990); and (ii) the genome assembly published by Boutet et al. (2022) was aligned to that of Gundappa et al. (2022) using Minimap2 (Li, 2018). The resulting PAF files were visualised using ggplot2 and the pafr package in R (Winter, 2020).

2.4.2. Long-read high-fidelity (Hi-Fi) PacBio sequencing

To define the exact breakpoints of inversions, whole-genome sequencing (WGS) with PacBio HiFi technology was carried out on six individuals selected from the Irish populations LW and GAL based on their inferred inversion genotypes (see Results). Sequencing was performed at Novogene using a target coverage of 20X, according to the estimated flat oyster genome size of 935 Mb (Gundappa et al., 2022).

USC UNIVERSIDADE DE SANTIAGO DE COMPOSTELA

Raw reads were quality-filtered with Chopper (De Coster & Rademakers, 2023), applying the following parameters: a minimum read quality of 20, minimum length of 5,000 bp, and 10 bp trimmed from both ends. For each sample, read quality metrics were computed (number of reads, minimum and maximum lengths, average length, and total read size) to ensure data integrity.

To detect inversion breakpoints, the first and last 1,000 bp of each long read were extracted and aligned to the *O. edulis* genome using Bowtie2 (Langmead & Salzberg, 2012; Langmead et al., 2018). Reads overlapping an inversion breakpoint were expected to split between two distant loci, depending on the arrangement orientation in the reference genome. Reads where the start and end fragments mapped at least 1 Mb apart were retained for downstream inspection. These reads were aligned to candidate regions defined by the LD analyses using a custom script and manually inspected in the Integrative Genomics Viewer (IGV; Robinson et al., 2011). Reads that consistently ended at the same positions were considered as candidate breakpoint-containing fragments.

2.4.3. PCR validation of inversion breakpoints

Primers flanking the putative inversion boundaries were designed with Primer3 (Untergasser et al., 2012) using the reference genome and taking care to avoid repetitive regions. Amplifications were tested on individuals with inferred homokaryotypes and heterokaryotype genotypes, based on population genomics data (see Results). PCR conditions included an initial denaturation at 95°C for 10 minutes; 35 cycles of denaturation at 94°C for 45 s, annealing at 58°C (C2 and C5) or 60°C (C8) for 50 s, and extension at 72°C for 50 seconds; followed by a final extension step at 72°C for 10 min.

2.4.4. Origin of inversions

To investigate potential mechanisms responsible for inversion formation, flanking regions were analysed for the presence of repetitive sequences. Structural variation in the vicinity of breakpoints can offer insights into the origin and evolutionary history of inversions (Orengo et al., 2019). RepeatMasker 2.0 was used to detect general repetitive elements, and a custom script was employed to identify tandem repeats. For this, 100 bp windows across the flanking regions were aligned to the genome using Bowtie2 to detect local duplications. Repetitive elements are frequently implicated in the generation of inversions via mechanisms such as ectopic recombination or breakage-and-rejoining events (Delprat et al., 2009; Villoutreix et al., 2021; Pascarella et al., 2022; Huang et al., 2025).

USC UNIVERSIDADE DE SANTIAGO DE COMPOSTELA

2.5. Genetic structure at the light of inversions

Once the boundaries of the inversions were defined, patterns of genetic diversity and population structure were analysed across the natural range of *O. edulis*, incorporating the structural rearrangements and using different subsets of SNPs. Specifically, the following SNP datasets were considered: (i) the full set of 4,741 SNPs; (ii) a filtered set excluding all SNPs located within the inversion regions (4,186 SNPs); and (iii) inversion-specific subsets, including 151 SNPs on C2, 65 on C5, and 209 on C8 (see Results).

Genetic diversity (expected heterozygosity, H_e), HWE, and the sense of deviations from random mating (F_{IS}) were analysed using the R package Genepop v4.7.5. Population structure pairwise genetic differentiation between populations (F_{ST}) were calculated following the method of Weir and Cockerham (1984), also using Genepop v4.7.5 and the built-in 'Fst' function. Bayesian clustering analysis was conducted using the STRUCTURE software (Pritchard et al., 2000). The number of genetic clusters (K) was explored across a predefined range (K = 1 to 15), using 100,000 iterations for each run and a burn-in period of 200,000 iterations. The optimal K was determined using StructureSelector (Li & Liu, 2018), which applies multiple estimators (ΔK; Evanno et al., 2005) and generates CLUMPAK-compatible outputs (Kopelman et al., 2015).

As a complementary multivariate approach, Discriminant Analysis of Principal Components (DAPC) was performed to uncover the number of genetic clusters. This method was implemented in R using the 'dapc' function the Adegenet package (Jombart & Ahmed, 2011). Genotypic matrices were first transformed through Principal Component Analysis (PCA), and the resulting principal components (PCs) were then subjected to Linear Discriminant Analysis (LDA). The optimal number of PCs retained for LDA was determined by a cross-validation procedure, selecting the configuration that minimized the Root Mean Square Error (RMSE).

2.6. Signals of selection

To investigate potential mechanisms maintaining inversion polymorphisms in *O. edulis*, deviations from HWE were assessed for the structural variants within the large Irish sample set (combined GAL + LW populations). These analyses aimed to explore whether patterns such as heterozygote excess or deficiency might reflect selective forces like overdominance or divergent selection acting on the inversions.

Genetic diversity and differentiation profiles were also evaluated across the full span of each inversion. Both single-locus values and averages calculated across sliding windows of 5 or 10 consecutive SNPs (with one SNP per shift) were considered. These profiles were examined to identify peaks of genetic differentiation or diversity potentially indicative of adaptive regions within the inversions.

USC UNIVERSIDADE DE SANTIAGO DE COMPOSTELA

Genes located near these putative adaptive peaks or close to the inversion breakpoints were analysed to identify functional candidates that could help explain the evolutionary relevance of rearrangements.

To detect SNPs with unusual patterns of differentiation that may reflect divergent selection, genome-wide outlier analyses were conducted using BAYESCAN v2.01 (Foll & Gaggiotti, 2008). This method is based on a Bayesian framework that estimates the posterior probability that a given SNP is under selection, relying on F_{ST}-based differentiation across populations. BAYESCAN was executed using default settings, which included 20 pilot runs, a prior odds value of 10, a burn-in of 50,000 iterations, and a total of 100,000 iterations, from which 5,000 samples were collected.

All coding genes located within the inversion regions were retrieved from the *O. edulis* reference genome (Gundappa et al., 2022). These genes were then functionally annotated using the PANNZER annotation pipeline (Törönen & Holm, 2022), which provides gene ontology (GO) terms and biological function predictions. Enrichment analysis of GO terms within each inversion was conducted using the R package *GOfuncR* v1.14.0 (Grote, 2021), to identify overrepresented biological processes and molecular functions compared to the whole transcriptome.

USC
UNIVERSIDADE DE SANTIAGO DE COMPOSTELA

3. RESULTS

3.1. Genomic characterization of chromosome inversions

Due to no genetic differentiation (F_{ST} = 0.0074; p = 0.093), the two large Irish populations (GAL and LW) were merged (n = 384) to enhance the statistical power of LD-based analyses. Across the genome, LD exhibited the expected L-shaped decay pattern in most chromosomes, with r^2 values falling below 0.2 at around 100 kb (Fig. S1A). However, chromosomes C2, C5, and C8 displayed atypical patterns, with high r^2 values remaining significant over ~27.5 Mb, ~7 Mb, and ~40 Mb, respectively (Figs. S1B, S1C, S1D).

Pairwise LD confirmed high correlation between SNPs within specific genomic regions at C2, C5, and C8 (Fig. S3), suggesting the presence of large structural variants suppressing recombination. The abrupt LD drop at both ends of these blocks allowed us to delimit their chromosomic distribution. Specifically, the C2 block extended from the start of the chromosome (between 1 bp and 779,719 bp) to approximately 27.5 Mb (between 27,544,809 bp and 27,592,275 bp); for C5, from ~86.4 Mb (86,428,703–86,508,092 bp) to ~93.1 Mb (93,012,400–93,108,624 bp); and for C8, from ~33.9 Mb (33,908,317–35,041,583 bp) to ~69.6 Mb (68,632,940–69,558,118 bp) (Fig. 3; Fig. S2).

We further analysed the LD variation pattern across the length of these regions by computing average pairwise r^2 values in sliding windows of 5 or 10 SNPs, shifting one SNP by step. This was done both for the full oyster distribution dataset and for the Irish sample alone (Figs. S3A–F). In both cases, LD showed consistent sawtooth profiles across the inversion spans, with the background LD remaining substantially lower. As expected under the inversion hypotheses, LD heatmaps generated separately for homokaryotypes of each arrangement within each inversion revealed no LD, supporting the presence of long inversions (Fig. S4). Considering that the largest chromosomes in *O. edulis* are primarily biarmed (Thiriot-Quiévreux, 1984), the rearrangements on C2 and C5 are likely paracentric. Although C8 could correspond to a submetacentric chromosome, its LD profile suggests that a paracentric inversion is also plausible (Fig. S3C and S3F).

USC UNIVERSIDADE DE SANTIAGO DE COMPOSTELA

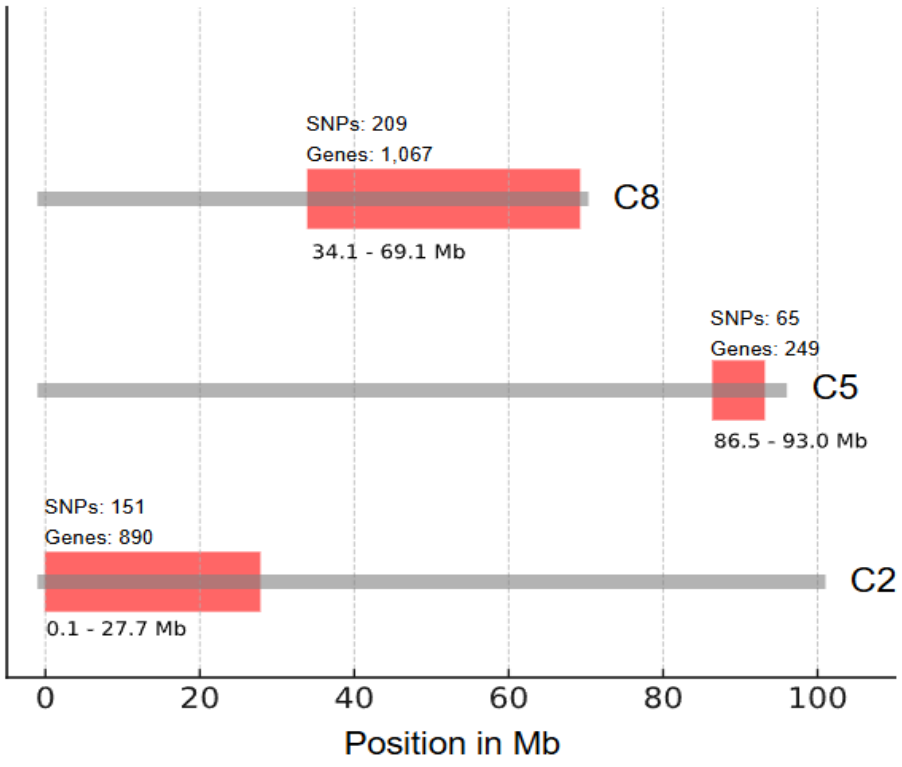


Figure 3. Main genomic features of the three chromosomic inversions in *O. edulis*.

By aligning the microsatellite flanking sequences from the linkage map of Harrang et al. (2015) to the *O. edulis* reference genome (Gundappa et al., 2022), we confirmed that inversions on C2, C5 and C8 corresponded to the LG1, LG6 and LG4 regions identified by Lapègue et al. (2022). Alignments using Minimap2 between the genomes from Gundappa et al. (2022) and Boutet et al. (2022) further validated the correspondence with scaffold5 (C2), scaffold4 (C5), and scaffold8 (C8) described in Monteiro et al. (2024). While Lapègue's inversion sizes roughly aligned with our estimates, notable discrepancies emerged with Monteiro et al.'s study, particularly for C2 (11.2 Mb vs. 27.5 Mb) and C8 (24.5 Mb vs. 34.8 Mb), likely explained by missing segments in their assembly and fragmented alignments between genomes (Fig. S5).

We sequenced six selected oysters from GAL and LW with suitable genotypes (homokaryotypes or heterokaryotypes) for the three inversions using PacBio HiFi technology. STRUCTURE analyses of SNPs within inversion enabled accurate assignment of these individuals to specific genotypes (Fig. S6). Sequencing outputs ranged from 876,960 to 1,393,841 reads, with average read lengths between 6,675–11,635 bp; one sample (GAL_173) was discarded due to low read quality (Table S1). After filtering, retained reads represented 57.7–87.4% of the initial dataset. We identified reads with 1 kb ends mapping >1 Mb apart and aligned them against the inversion LD windows. These "split" reads were manually inspected in IGV to determine inversion breakpoints. Based on this approach, the inferred inversion spans were: C2 – 80,922 to 27,676,307 bp; C5 – 86,546,053 to 93,001,597 bp; and C8 – 34,069,607 to 69,085,710 bp.

To confirm these limits and design simple genotyping tools, we analysed flanking regions to develop PCR primers to be tested in a large sample (~100 individuals; Fig.4). Sequencing of PCR amplicons validated and identified the breakpoint coordinates at both ends of C8 and at one end of C2 (5') and C5 (3'). Therefore, the 3' end of C2 and 5' of C5 breakpoint intervals defined via LD were used instead (Figs. 4A–B).

Table 2. Genomic features of the inversions at C2, C5 and C8 of *O. edulis* and PCR settings for their genotyping.

Chromosome	Start (bp)	End (bp)	Amplicon length	Primer pairs
C2	80,922	*27,676,307*	485	F-AGGTCTTGGAAAATCACAGTGC
				R-GTGCAACGCTTTCTTTCATTTCT
			584	*F-TCCCCTGCTAATGGAACTCC*
				R- TGGGGTGTCAATGGATGGAA
C5	*86,546,053*	93,001,597	390	*F-ATATTAGTCCCACTCCCGCG*
				R-TGTACTCACCCCTGACCTCA
			457	F- AAGATGGCGGCGTGGTATA
				R- GTACGGCATGGAACTTTCT
C8	34,069,607	69,085,710	277	F-TACCCTGACACCTATCGGCT
				R-ACTGCCGTGATTAGAAATGGC
			389	F-CATCTGGTCCCAGGGTTCAC
				R-GAGTCCACTGTTGCTGCTGA

In italics the inversion ends and primers that failed PCR amplification

To investigate the potential mechanisms underlying the occurrence of these rearrangements, repetitive elements (REs) at their breakpoints were analysed. In all four validated breakpoints (5′ end of C2, 3′ end of C5, and both ends of C8), distinct transposable elements were observed in proximity. Specifically, LINE elements were detected flanking one side of the identified breakpoint in all inversions, while either DNA/hAT (at 5′ C2 and 3′ C8) or PLE/Naiad elements (at 3′ C5 and 5′ C8) were present on the opposite side. These elements were located at short distances—9.4 kb at the 5′ end of C2, 1.4 kb at the 3′ end of C5 (with a 173 bp overlap with the PLE/Naiad), 1.3 kb at the 5′ end of C8, and 2.5 kb at its 3′ end—suggesting a possible role for ectopic recombination or breakage-and-repair events in the origin of these inversions.

In addition to transposable elements, large duplicated genomic regions of short motifs were identified at the inversion flanks using 100 bp sliding windows. These duplications did not match to known RE families. On chromosome C2, duplicated regions spanned from 71,500 to 74,400 bp and from 27,788,100 to 27,792,500 bp. Similarly, on chromosome C5, duplicated segments were found between 86,497,300 and 86,503,200 bp, and between 93,004,200 and 93,006,100 bp. These tandem duplications may have facilitated structural rearrangements through mispairing during meiosis.

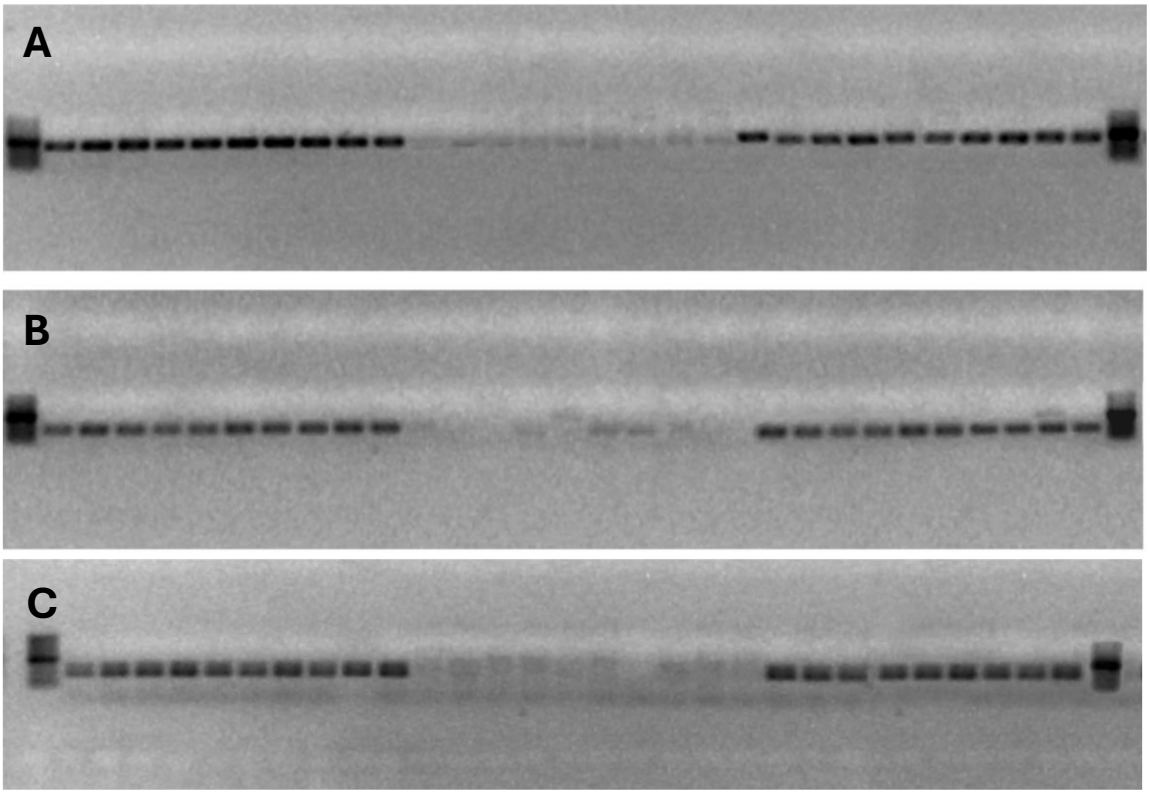


Figure 4. Agarose gels of representative *O. edulis* heterokaryotype and homokaryotype individuals for both arrangements at: A) C2 5'end, B) C5 3' end, and C) C8 5' end using a PCR tool; 100bp ladder at both ends; lanes 1-10: homokaryotype for one arrangement; lanes 11-20: homokaryotype for the opposite arrangement; lanes 21-30: heterokaryotypes.

To explore the potential functional significance of these genomic rearrangements, Gene Ontology (GO) annotations of genes located within the three inversions were examined (FDR < 5%; Table S2). Within the C2 inversion, which contains 890 annotated genes, biological process enrichment was related to detection and processing of environmental stimuli, such as epidermal cell proliferation. Correspondingly, cellular component terms associated with membranes, intracellular transport, and organelles were enriched, alongside molecular functions linked to neuropeptide receptor and G protein-coupled peptide receptor activity. Regarding C5, which harbours 249 genes, only one molecular function category showed significant enrichment—zinc ion transmembrane transporter activity. For the largest inversion, C8, encompassing 1,067 annotated genes, functional enrichment was detected in pathways related to carbohydrate metabolism, energy processing, and tissue remodelling. These included monocarboxylic acid transport, glucokinase and hexokinase activity, and glucose binding. Additionally, several immune-related functions were enriched, such as cytokine receptor binding and tumour necrosis factor receptor signalling, suggesting that genes within this inversion may play a role in host defence mechanisms (Table S3).

USC
DE SANTIAGO
DE COMPOSTELA

3.2. Population genomics of *O. edulis*

3.2.1. Chromosomal inversion arrangement distribution across the species range

In order to assess the distribution of chromosomal inversion arrangements across the geographical range of *O. edulis*, samples from thirteen shellfish beds were inspected (Fig. 1; Table 1). STRUCTURE analyses using SNPs located within each of the three inversions consistently supported K = 2 as the most likely number of clusters across all sampling sites. Individuals could be readily assigned to either homokaryotype or heterokaryotype genotypes for both arrangements, as indicated by clear or intermediate genomic ancestry coefficients, respectively (Fig. 5).

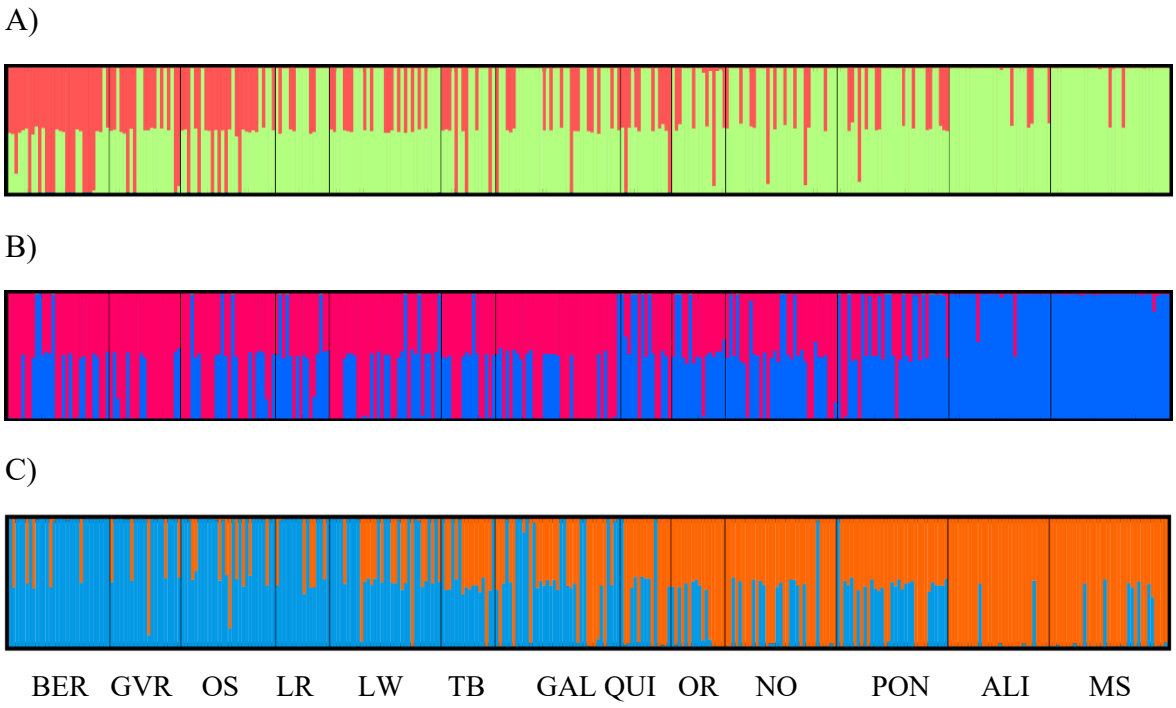


Figure 5. STRUCTURE analysis (K = 2) using SNPs within each of the inversions at C2 (A), C5 (B) and C8 (C) in *O. edulis* across the distribution range.

The frequencies of alternative arrangements for each inversion followed a latitudinal gradient from north to south across the species' distribution (Fig. 5; Table S4). For the inversions on chromosomes C5 and C8, both arrangements were detected at similar frequencies (approximately 0.500), while the "green" arrangement was more frequent in the C2 inversion (0.732). Genotypic frequencies for each inversion were consistent with Hardy-Weinberg equilibrium in all shellfish beds ($p > 0.05$; Table S5). Overall genetic differentiation (global F_{ST}) among beds based on inversion arrangements was 0.294, with higher values for C8 (0.376) and C5 (0.311) than for C2 (0.170), all statistically significant ($p < 0.001$).

Pairwise F_{ST} comparisons revealed an isolation-by-distance pattern from north to south ($p < 0.001$), although distinct deviations from this trend were apparent, especially between C2 and the other two inversions (Table S6). For example, LW and LR exhibited virtually no differentiation from other Atlantic beds for C2 (mean $F_{ST} = –0.006$), whereas significant differentiation was observed for C5 (mean $F_{ST} = 0.107$; $p < 0.001$) and C8 (mean $F_{ST} = 0.268$; $p < 0.001$). Correlations between pairwise F_{ST} values across inversions were moderate but statistically significant (Spearman's rho: C2 vs. C5 = 0.399; C2 vs. C8 = 0.358; C5 vs. C8 = 0.551; $p < 0.001$ in all comparisons).

Deviation from Hardy-Weinberg equilibrium was further examined in the large Irish population (GAL + LW; n = 384) to assess the potential effects of divergent selection (indicated by heterozygote deficiency) or overdominance (heterozygote excess). A significant heterozygote excess was detected only for the C5 inversion ($F_{IS} = –0.130$; $p = 0.012$), whereas C2 and C8 conformed to expectations. No significant linkage disequilibrium between pairs of inversions was found based on exact tests for genotypic equilibrium ($p > 0.05$ in all three pairwise comparisons) discarding some kind of epistatic selection between inversions.

3.2.2. Genetic diversity and population structure of O. edulis considering chromosomal inversions

Most shellfish beds exhibited relatively high and comparable genetic diversity when using the complete 4,741 SNPs panel (expected heterozygosity, $H_e \approx 0.4$), with the exception of the two Mediterranean populations (MS and ALI), which displayed lower diversity likely attributable to increased isolation ($H_e = 0.360$ and 0.334). When focusing on SNPs located within the chromosomal inversions, genetic diversity was slightly reduced compared to the genome-wide average (mean H_e within inversions = 0.362; outside inversions = 0.398; Wilcoxon paired test, $p = 0.022$).

Overall genetic differentiation (F_{ST}) between populations using the full SNP dataset was moderate (global $F_{ST} = 0.055$; $p < 0.001$), with pairwise values ranging from negligible (GRV vs. OS < 0.001) to substantial (BER vs. MS = 0.149). As expected, Mediterranean populations displayed greater differentiation. When inversion-linked SNPs were excluded, global genetic differentiation decreased significantly ($F_{ST} = 0.040$; $p < 0.001$), highlighting the elevated divergence observed for SNPs within the three inversions (F_{ST} across all inversions = 0.158; C2 = 0.106; C5 = 0.189; C8 = 0.166; all $p < 0.001$).

Analysis with the complete SNP dataset supported the presence of three main genetic clusters (K = 3), roughly corresponding to: (i) the North Sea region (BER, OS, GRV), (ii) the Atlantic coast from Ireland and Scotland down to France and Spain (GAL, LW, LRY, QUI, OR, NO, PO), and (iii) the Mediterranean Sea (ALI, MS).

USC UNIVERSIDADE DE SANTIAGO DE COMPOSTELA

Despite this structure, chromosomal inversions appeared to have a considerable influence, as many individuals exhibited mixed ancestry profiles across the entire distribution (Fig. 6A). Excluding SNPs from the three identified inversions revealed a clearer latitudinal cline and supported the presence of four distinct genetic groups (K = 4) (Fig. 6B).

At the range ends, Norway (BER) and Croatia (MS) formed discrete, highly divergent clusters, while intermediate clusters were identified in the Iberian Peninsula and France (ALI to QUI), the British Isles (GAL to LR), and the central North Sea (OS and GRV). Additional STRUCTURE analyses with higher K values (Fig. S7) revealed further substructuring, such as a genetic connection between the North Sea, TB, and the Cantabrian region for K = 5. Results from DAPC analysis closely matched those from STRUCTURE, especially at the geographic ends (Fig. S8A). However, excluding inversion-associated SNPs resulted in more distinct separation among Spanish, British, and North Sea populations (Fig. S8B).

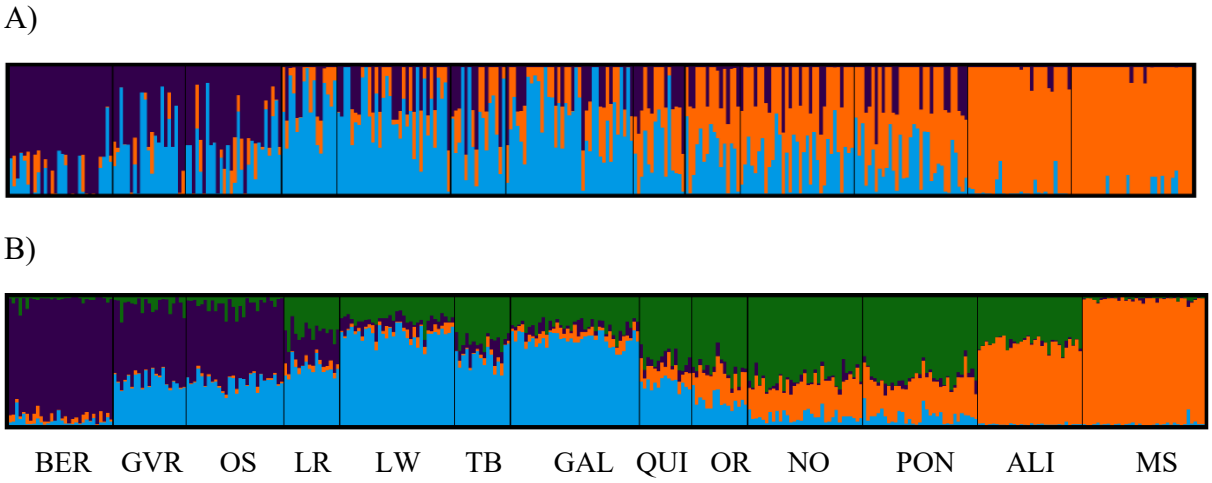


Figure 6. STRUCTURE analysis for *O. edulis* from 13 European beds using different SNP datasets: A) full SNP panel of 4,741 SNPs (K = 3); B) dataset excluding SNPs within chromosomal inversions (4,316 SNPs; K = 4).

Analysis using BAYESCAN revealed a strong enrichment of outlier loci within inversions compared to the rest of the genome (Table 3). Across all SNPs located within the inversions, 76.1% were classified as outliers under divergent selection (C2: 67.4%; C5: 81.0%; C8: 80.8%), whereas only 7.8% of non-inversion SNPs showed similar signatures. The C5 and C8 inversions exhibited particularly strong signals of divergent selection relative to C2.

USC UNIVERSIDADE DE SANTIAGO DE COMPOSTELA

Table 3. Outliers for divergent selection and neutral SNPs within the inversions in C2, C5 and C8 and for the rest of the genome across the 13 samples of *O. edulis*

	C2		**C5**		**C8**		**all inversions**		**rest genome**	
	N	ratio	N	ratio	N	ratio	N	ratio	N	ratio
outliers	97	1.820	47	7.231	168	4.800	312	13.851	338	0.553
neutral	47	0.882	11	1.692	40	1.000	98	3.574	4332	7.087

N: number of SNPs; ratio: number of SNPs / Mb

3.2.3 Genetic diversity and differentiation throughout the inversions

Patterns of genetic diversity (H_e) for each chromosomal arrangement and of genetic differentiation (F_{ST}) between arrangements were analysed across the full span of the three identified inversions using homokaryotype individuals. This analysis was conducted using both the full dataset of 13 populations covering the species' range and the large Irish sample (GAL + LW), applying both single-SNP estimates and sliding window averages of He and F_{ST} (Table S7 and S8).

In the dataset including all 13 populations, within-arrangement genetic diversity for each inversion was markedly lower than that observed across the rest of the genome (C2: H_e_green = 0.160, H_e_red = 0.065; C5: H_e_pink = 0.108, H_e_darkblue = 0.103; C8: H_e_orange = 0.204, H_e_blue = 0.159; genome-wide $H_e \sim 0.400$). In contrast, the differentiation between arrangements was strikingly elevated (F_{ST}_C2 = 0.681; F_{ST}_C5 = 0.609; F_{ST}_C8 = 0.494; all $p < 0.001$), far exceeding the average differentiation across the rest of the genome after removing inversion SNPs ($F_{ST} = 0.040$). These observations were supported by the high proportion of SNPs fixed or nearly fixed for alternative alleles between arrangements ($F_{ST} > 0.9$: C2 = 34.4%; C5 = 34.8%; C8 = 16.2%).

Evidence from all analyses indicates that these genomic regions are subject to strong divergent selection. However, the patterns observed differed among the three inversions, not only in terms of the lower genetic differentiation between alternative arrangements in C8, but also in the specific F_{ST} distributions along each inversion (Fig. 7). For example, C5 exhibited a pronounced peak of differentiation near the 5′ breakpoint and, to a lesser extent, close to the 3′ breakpoint, following an overall valley-shaped profile. In contrast, C2 and C8 showed a saw-tooth profile with multiple peaks corresponding to highly differentiated subregions. As anticipated, these F_{ST} patterns closely mirrored the LD profiles (Fig. S4), suggesting the occurrence of selective sweeps in discrete genomic intervals within all three inversions. Similar trends were obtained when analyses were performed using the larger Irish dataset

USC UNIVERSIDADE DE SANTIAGO DE COMPOSTELA

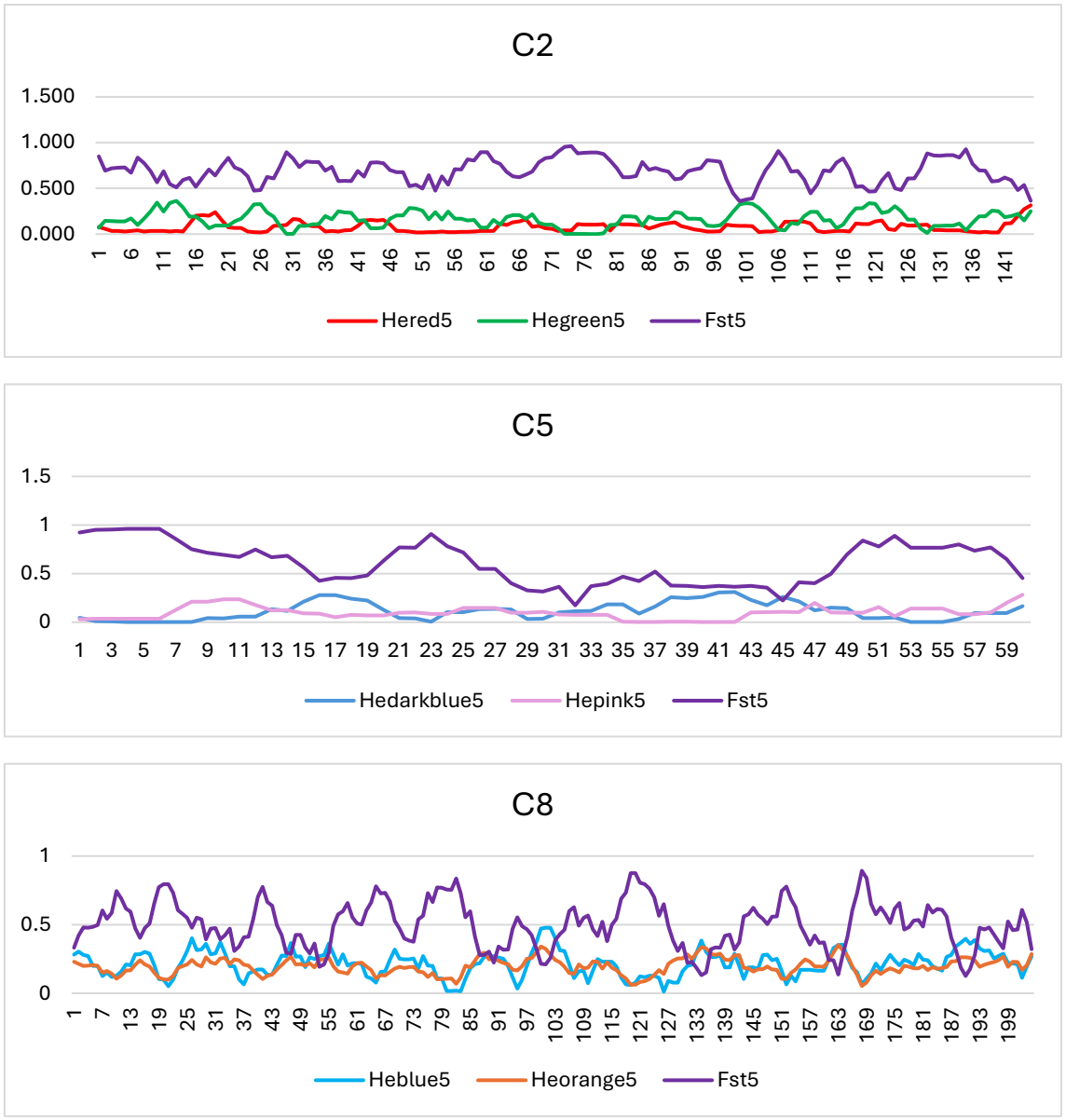


Figure 7. Genetic diversity (H_e) and genetic differentiation (F_{ST}) profiles across the full length of inversions at C2, C5 and C8 using average values across sliding windows of 5 SNPs with one SNP shift per step.

To identify potential candidate genes or biological functions underlying the high differentiation signals, gene content was examined within 100 kb of the inversion breakpoints and around the putative adaptive peaks detected inside each inversion. Approximately 40 % of the annotated genes in these regions correspond to low-quality or uncharacterized proteins, which hindered functional interpretation and highlight the need for improved annotation in molluscan genomes. Clusters of genes located within adaptive peaks were found at the breakpoints of C2 and C5, as well as internally within all three inversions.

USC UNIVERSIDADE DE SANTIAGO DE COMPOSTELA

In C2, a notable internal block between positions 14,851,830 and 18,175,022 bp was strongly enriched in functions related to neural communication and sensory perception, including *synaptonemal complex protein 2*, *pikachurin*, *cerebral cavernous malformations protein 2*, *eyes absent homolog 2*, *otoferlin*, *substance-P receptor*, and *multiple G-protein coupled receptors*, among other genes (Boyd et al., 1986; Baxter & Morse, 1987; Duncan et al., 1997; Herpin et al., 2004; Lek et al., 2010; Grishaeva & Bogdanov, 2014; Kumar et al., 2014; Roy et al., 2021). These findings are consistent with the GO enrichment results for the entire inversion, which indicated over-representation of neural detection and transmission of external and abiotic stimuli. Another internal region in C2, spanning from 24,540,917 to 25,925,072 bp, harboured genes implicated in immune function (*toll-like receptor 4*, *zinc metalloproteinase nas-6*, *calreticulin*, *Ig-like V-type domain-containing protein FAM187A*; Gordy et al., 2015; Wang et al., 2019; Ishita et al., 2023), digestion (*elastase-1*, *gastrin/cholecystokinin type B receptor*; Cui et al., 2021; Nie et al., 2025), and lipid metabolism (l*ow-density lipoprotein receptor*, *very low-density lipoprotein receptor*, *palmitoyl transferase ZDHHC6*; Timmins-Schiffman & Roberts, 2012; Liu et al., 2013).

Near the 3′ breakpoint of C5, between positions 93,721,388 and 94,446,371 bp, several genes were identified that participate in ion transport (including multiple zinc transporters, in agreement with the GO enrichment for the inversion as a whole), shell mineralization (*dentin sialo phosphoprotein*, *nacrein*; Shi et al., 2018a), immune defence (*killer cell lectin receptor*, *tripartite motif-containing protein 2*; Humphries & Yoshino, 2003; Bowden et al., 2020), and growth (*growth hormone secretagogue receptor*, *multiple epidermal growth factor*; Hermann et al., 2000).

In C8, two noteworthy regions were detected: (i) from 47,837,933 to 48,692,737 bp, containing numerous immune-related genes (*cytochrome P450 26A1*, *E3 ubiquitin-protein ligase hrd-like protein 1*, *coiled-coil domain-containing protein 125*, *protein fem-1 homolog C*, *BRCA2-interacting transcriptional repressor EMSY*, *cytochrome c oxidase assembly protein COX15*, *ubiquitin thioesterase zranb1-B*, *autophagy-related protein 16-1*, *E3 ubiquitin-protein ligase TRIM33*), as well as genes involved in transcriptional regulation (*transcription factor AP-2-epsilon*, *KAT8 regulatory NSL complex subunit 3*, *zinc finger protein 227*); and (ii) from 62,520,325 to 63,035,988 bp, which included genes associated with reproduction (*spermatogenesis-associated protein 24*, *sex peptide receptor*), immune response (*E3 ubiquitin-protein ligase TRIM71*, *serine/threonine-protein kinase 26*, *mitotic checkpoint protein BUB3*, *ubiquitin domain-containing protein 2*, *transient receptor potential cation channel subfamily M member-like 2*), growth (*growth hormone-regulated TBC protein 1-A*, *sarcoplasmic calcium-binding protein*; Hermann & Cox, 1995), and neurogenesis (*slit homolog 1 protein*).

USC UNIVERSIDADE DE SANTIAGO DE COMPOSTELA

USC
UNIVERSIDADE
DE SANTIAGO
DE COMPOSTELA

CHAPTER III

Genomics and transcriptomics insights into resistance to *Bonamia ostreae* in the European flat oyster (*Ostrea edulis*)

USC
UNIVERSIDADE
DE SANTIAGO
DE COMPOSTELA

ABSTRACT

The European flat oyster (*Ostrea edulis*) faces critical threats from *Bonamia ostreae*, a protozoan parasite responsible for mass mortality events and the collapse of traditional oyster beds. This study investigates the resistance to *B. ostreae* at the individual level using three Irish populations with contrasting bonamiosis histories. A total of 436 oysters were genotyped with a medium-density SNP array including previously identified resistance-associated markers. Infection status was determined by PCR and histological examination of heart and gill tissues. Population structure analyses revealed a strong association between resistance and a chromosomal inversion on chromosome 8 (C8). Further, the association of C8 inversion with resistance was also checked at individual level and "orange" homokaryotype oysters showed to be non-infected. No significant associations were found for the other two inversions (C2 and C5).

Gene expression of individuals representing different infection levels was explored through RNA-seq in the Lough Swilly shellfish bed. A total of 3,711 genes were differentially expressed across all comparisons. Early infection was associated with metabolic activation, moderate infection with immune and mitochondrial responses, and severe infection with stress-related pathways and reduced transcriptional diversity. Functional enrichment analyses supported a progression from innate immune response to cellular disruption under parasite pressure.

These results confirm the role of the C8 inversion in host resistance and provide novel insights into the transcriptional interaction between host and parasite along the infection process, providing essential information for selective breeding and flat oyster restoration strategies. A MassARRAY tool including diagnostic alleles for resistant ("orange") and sensitive ("blue") arrangements was designed and validated using previous genotyping information to be used in marker-assisted selection programs.

Keywords: *Ostrea edulis*, bonamiosis, host-parasite interaction, immunity, MassARRAY genotyping, selective breeding

USC UNIVERSIDADE DE SANTIAGO DE COMPOSTELA

1. INTRODUCTION

The European flat oyster (*Ostrea edulis*) is a bivalve of significant ecological and economic importance throughout European coastal ecosystems. However, natural populations have suffered a marked decline due to overfishing, habitat degradation, and disease outbreaks (Sas et al., 2020). Among the most impactful diseases, bonamiosis, caused by the intracellular protozoan *Bonamia ostreae*, has led to mass mortality events and the collapse of traditional oyster fisheries across Europe (Perry et al., 2017; Colsoul et al., 2021). First detected in France in the 1970s (Carnegie & Cochennec-Laureaeu, 2004) and in Ireland during the 1980s, *B. ostreae* continues to expand, exacerbated by bad aquaculture practices and the spread of non-native oysters for alternative production like *Magallana gigas* (Classen, 2020).

B. ostreae primarily infects haemocytes, the key immune oyster cells, triggering a first host defence involving reactive oxygen species (ROS) (Montagnani et al., 2024). However, the parasite can evade immune response and survive intracellularly by inhibiting lysosome-phagosome fusion, suppressing ROS production, and modulating apoptosis (Hine & Wesney, 1995; Ahmed et al., 2003). These strategies enable systemic replication within the host leading to death close to oyster commercialization. While *O. edulis* lacks an adaptive immune system, evidence is growing that innate immune response and putative priming mechanisms following repeated pathogen exposure, such as epigenetic regulation of immune genes, can enhance resistance (Gourbal et al., 2018; Zhao et al., 2023; Montagnani et al., 2024).

Recent studies suggest that populations with prolonged exposure to *B. ostreae* display increased survival and faster immune responses than naïve populations, suggesting selection or priming for enhancing resistance (Ronza et al., 2018; Chapter I). Genome-wide population analyses revealed associations between resistance and specific SNPs, mostly located within a chromosomal inversion on chromosome (C)8 (Vera et al., 2019; Chapter I). This region includes genes linked to apoptosis and extracellular matrix remodelling—processes relevant for host defence (Ronza et al., 2018). Nonetheless, population-level association requires validation at the individual level to assess their potential for marker-assisted selection (MAS) programs aimed at restoring oyster beds using resistant strains.

Irish oyster beds offer a suitable scenario to understand the mechanisms related to resistance, as they show diverse bonamiosis histories. The disease was first reported in Rossmore in 1984 and later in Galway Bay and Lough Swilly (McArdle et al., 1991; Culloty & Mulcahy, 2007). Notably, Rossmore Oyster Ltd has implemented a long-term selection program using non-infected individuals as breeders, which has demonstrated a higher resistance to *Bonamia* (Lynch et al., 2014).

USC UNIVERSIDADE DE SANTIAGO DE COMPOSTELA

The objective of this chapter was to investigate resistance / tolerance to *B. ostreae* in three Irish oyster populations with contrasting disease histories by combining genomic and transcriptomic approaches. Specifically, we aimed to analyze the association between individual genotypes at the C8 inversion and both infection status and intensity, and to characterize immune-related pathways involved in host response by integrating transcriptomic and genotypic information. In addition, we sought to develop and validate a simple MassARRAY genotyping assay to reliably identify homozygous individuals for the arrangement associated with resistance, providing a practical tool for marker-assisted selection programs.

USC
UNIVERSIDADE DE SANTIAGO DE COMPOSTELA

2. MATERIALS AND METHODS

2.1. Sample collection

Between May and October 2023, flat oyster specimens were collected monthly from three shellfish beds: Lough Swilly (LW), Galway (GAL), and Rossmore (ROS) (Fig. 1). Approximately 60 individuals per bed were sampled each month and transported alive to the Aquaculture & Fisheries Development Centre in the University College Cork for tissue processing and analyses.

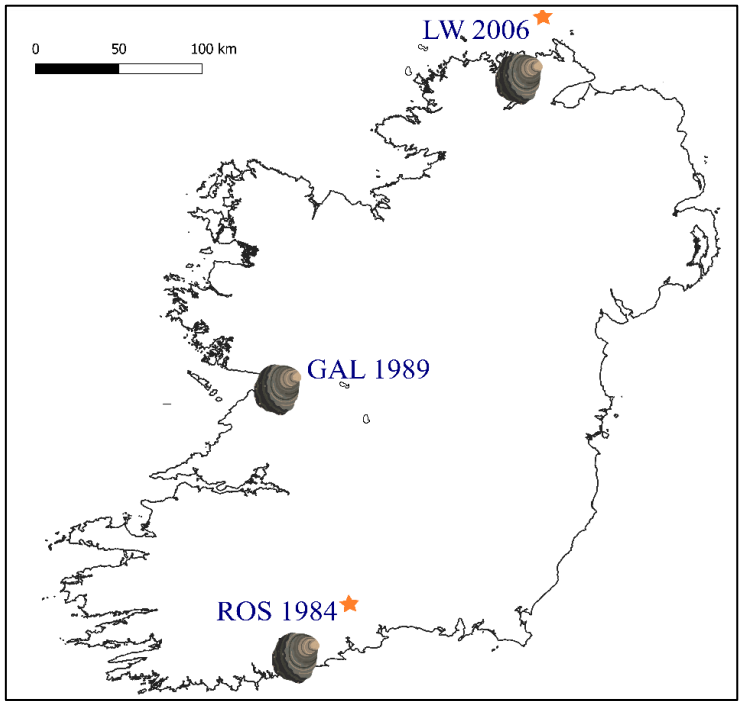


Figure 1. Location of the three Irish *O. edulis* beds sampled (LW, GAL, ROS), showing the year when *B. ostreae* was first detected at each site. At all sites, infection diagnostics were performed on gill and heart tissues, and gill tissue was preserved in ethanol for DNA extraction. Stars denote sites where heart tissue was also preserved in RNAlater for RNA extraction (LW and ROS); only LW heart samples were used.

2.2. Tissue processing and infection classification

Upon arrival at the UCC laboratory, oysters were opened, and several tissues were collected and preserved for different downstream analyses: i) ~1 cm² gill fragment was preserved in absolute ethanol for DNA extraction; ii) the whole cardiac tissue was preserved in RNAlater® (Thermo Fisher Scientific) for RNA extraction, in individuals from LW and ROS; iii) heart smears were prepared to estimate the infection level in each individual based on microscopic quantification of *B. ostreae*; iv) a qualitative PCR assay was performed to assess the presence of *B. ostreae* both in gill and heart tissues to confirm microscopic evaluation (Fig. 2).

USC UNIVERSIDADE DE SANTIAGO

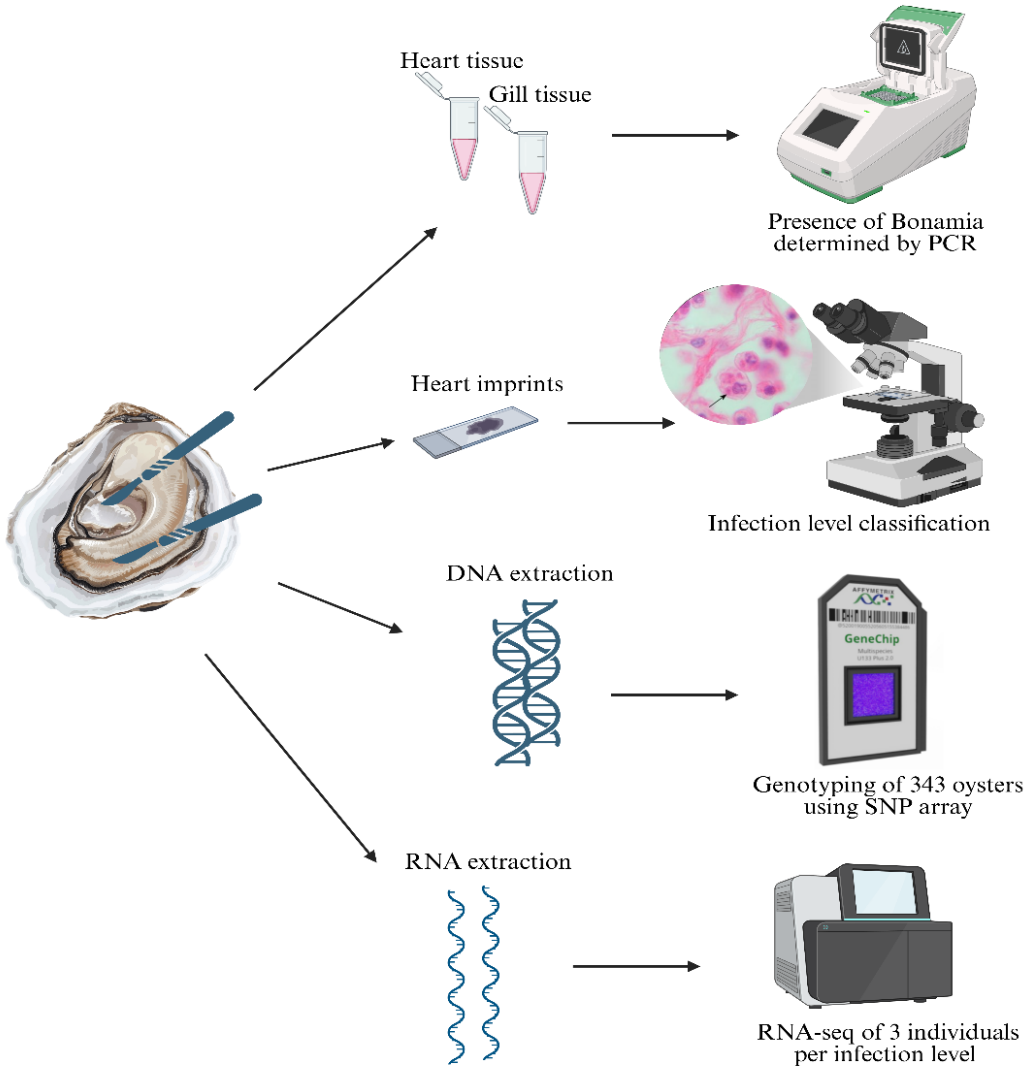


Figure 2. Scheme of the field/laboratory-sampling procedure.

2.3. DNA extraction and genotyping

DNA was extracted in gill tissue to check for association with genetic markers, using the EZNA® Mollusc DNA Kit (Omega Bio-Tek) according to the manufacturer's protocol. Genotyping was performed using a multi-species Affymetrix Axiom® Custom SNP Array, which included 4,986 SNPs previously described in Chapter II. The array was developed through a collaboration between the University of Santiago de Compostela (USC), Thermo Fisher Scientific, and Xenética Fontao S.A., and it was derived from the earlier panel developed by Gutierrez et al. (2017).

In total, 436 gill samples out of ~840 oysters collected (60 per population from May to September, except June in GAL) were selected for SNP array genotyping and infection-level classification (Table S1).

2.4. Population genomics analyses

STRUCTURE (Pritchard et al., 2000) was run using 100,000 iterations per run and a burn-in period of 200,000 iterations using SNPs genotyped for the C2, C5 and C8 inversions in the three populations, an information that enabled genotyping individuals for the alternative arrangements of the three inversions (Chapter II). Hardy-Weinberg equilibrium (HWE) was assessed using the R package Genepop v4.7.5 (Rousset, 2008) both at SNP and arrangement levels for the three inversions.

The association between chromosomal inversion arrangement genotypes (homo- and heterokaryotypes) and bonamiosis infection status (infected *vs*. non-infected) was assessed using contingency tables and chi-square tests. Following the same approach, the relationship between inversion genotypes and infection intensity (ordinal scale 0–4) was evaluated to determine whether infection levels differed significantly across genotypic classes. Furthermore, we used the R package SNPassoc (González et al., 2007) to study the association at SNP level and testing for allelic interaction models for significant SNP markers within inversions. Infection status (infected vs. non-infected) was considered the binary response phenotype, and SNP genotypes were used as predictors. We tested three inheritance models for each SNP: codominant, dominant, and additive. Association tests were performed using the WGassociation function, and significance was evaluated using likelihood ratio tests. A Bonferroni correction was applied to account for multiple testing, setting the significance threshold at $\alpha = 0.05$ / number of SNPs tested for each inversion. Analyses were conducted separately for SNPs located within the three inversions (C2, C5, and C8; Chapter II), as well as for the outliers previously related to *Bonamia*-resistance (Vera et al., 2019; Chapter I).

2.5. RNA extraction and transcriptomic analysis

RNA extraction was performed exclusively from heart tissue, as the parasite enters through the gills but ultimately targets haemocytes. Therefore, detection in this tissue was considered indicative of the level of infection. A total of 12 heart samples were selected for transcriptomic analysis trying to cover all infection stages as determined by microscopy. Cardiac tissue was only collected for LW and ROS populations, but the latter samples did not include all infection levels (Table S2).

RNA was extracted using TRIzol® reagent following manufacturer instructions. RNA quality and concentration were assessed using a Bioanalyzer device (Bonsai Technologies, Madrid, Spain) and a NanoDrop® ND-1000 spectrophotometer (NanoDrop Technologies Inc., Wilmington, DE, USA). Samples were submitted to Novogene (Germany) for high-throughput sequencing.

Infection intensity in heart tissue was obtained from heart smears collected for all oysters sampled. Individuals were classified on a semiquantitative scale from 0 to 4 based on the number of parasitic cells observed by adapting the protocol by Culloty et al. (2004).

USC
UNIVERSIDADE DE COMPOSTELA

In our study, however, we did not detect any samples corresponding to Class 4 (heavy parasite burden in all host cells). Instead, an additional category was introduced: samples that were positive by PCR but showed no microscopically detectable parasites were assigned to a new Level 1. As a result, the original Classes 1 to 3 were renumbered as Levels 2 to 4, respectively, for this study. All the 12 individuals analysed were selected from the LW population, as heart tissue samples were not available from GAL, and no individuals with infection levels above Level 2 were found in ROS.

Raw RNA-seq data were processed using the nf-core/rnaseq v3.14.0 pipeline with default parameters (Ewels et al., 2020) in the Centro de Supercomputación de Galicia (CESGA) using as reference the flat oyster genome (GCA_023158985; Ensembl; Gundappa et al., 2022). The pipeline included quality control (FastQC; Andrews, 2010), adapter and quality trimming of reads (Trim Galore!; Martin, 2011); then filtered reads were aligned to the host genome using STAR (Dobin et al., 2013), and finally all transcripts were normalized and quantified with RSEM (Li & Dewey, 2011). All analyses were performed in singularity containers which provide isolated computational environments that bundle software, dependencies, and libraries, thereby ensuring full reproducibility across systems (Kurtzer et al., 2017).

Count matrices were filtered to remove transcripts with expression below a threshold < 5 TPM (reads per million and kb of gene) and detected in less than two samples per infection condition. Differentially expressed genes (DEGs) between the different infection levels and uninfected samples used as reference were identified using the R package DESeq v1.38.1 (Love et al., 2014). The fold change (FC: $-\log_2$ (infection level normalized counts / uninfected normalized counts) was calculated for each gene and comparison performed. Genes with a false discovery rate (FDR)-adjusted *p*-value ≤ 0.05 were considered differentially expressed. Functional enrichment of DEGs was performed using gofuncR v.1.26.0 (Grote, 2024). All genes expressed in heart tissue were used as background set for Gene Ontology (GO) analyses.

2.6. A multiplex SNP tool for assisting breeding programs for resistance to *B. ostreae*

Five SNPs fixed or nearly fixed for alternative variants in both arrangements of the C8 inversion (frequency of the common allele ≥ 0.95) across the flat oyster distribution range were selected from the SNP-array dataset to design a tool for a cost-effective C8 inversion genotyping tool (Table 1; Chapter II).

For each SNP, the two alternative alleles together with the flanking sequences (± 75bp) were delivered to the Genotyping Platform of the Universitat de Valencia to design a multiplex MassARRAY panel for the selected SNPs.

USC UNIVERSIDADE DE SANTIAGO DE COMPOSTELA

Genotyping was performed using the Agena Bioscience MassARRAY system, following the manufacturer's iPLEX® Gold protocol. Briefly, PCR amplification of the target regions using flanking primers was followed by a single base extension reaction from an internal primer (Rodi et al., 2002). The resulting products were desalted and analysed by MALDI-TOF mass spectrometry, and allele calling was carried out with MassARRAY Typer Analyzer software (Agena Bioscience; Stanssens et al., 2004).

Table 1. SNPs used in the MassARRAY panel for inversion arrangement C8 genotyping. Freq1 and Freq2 indicate allele frequencies of each SNP from "orange" arrangement, as inferred from homokaryotypes of the SNP-array data in the whole distribution range of *O. edulis*.

SNP	Chromosome	Position	Alelle1	Freq1	Allele2	Freq2
AX-169174144	8	42,412,919	A	0.95	G	0.05
AX-169194812	8	48,537,302	C	0	T	1
AX-169172626	8	55,034,318	A	0.027	G	0.973
AX-169189135	8	60,302,802	C	0.988	T	0.013
AX-169203361	8	66,964,430	A	0	G	1

USC UNIVERSIDADE DE SANTIAGO DE COMPOSTELA

3. RESULTS

3.1. Assessment of infection level

Individuals were classified based on the number of *B. ostreae* cells both in gill and heart, and their infection level was assessed using heart tissue following Culloty et al. (2004; see Material and Methods). A total of 72 oysters were found to be infected in gill and 71 in heart (Fig. 3; Table S1). Most gill infections were detected in ROS, particularly in June (46 cases out of 51), while only 13 were detected in GAL and 5 in LW. Heart infections were more frequent in GAL (37) and even in LW (19) than in ROS (11). These results suggest a higher bonamiosis prevalence in ROS and GAL (39.5% and 34.3%, respectively) than in LW (16.6%), as suggested by records. However, infections in heart, which involve the presence of the parasite within haemocytes (true infections), over *Bonamia* detection (heart + gill) were much higher in LW (79.2%), then in GAL (74%), and finally in ROS (21.6%), which suggest higher resistance of ROS to infection. Notably, no data were available from GAL in July, which weaken the comparison with this population. Based on the infection dynamics observed in ROS and LW during that month, it is likely that the percentage of true infections in GAL would be lower the 74% observed.

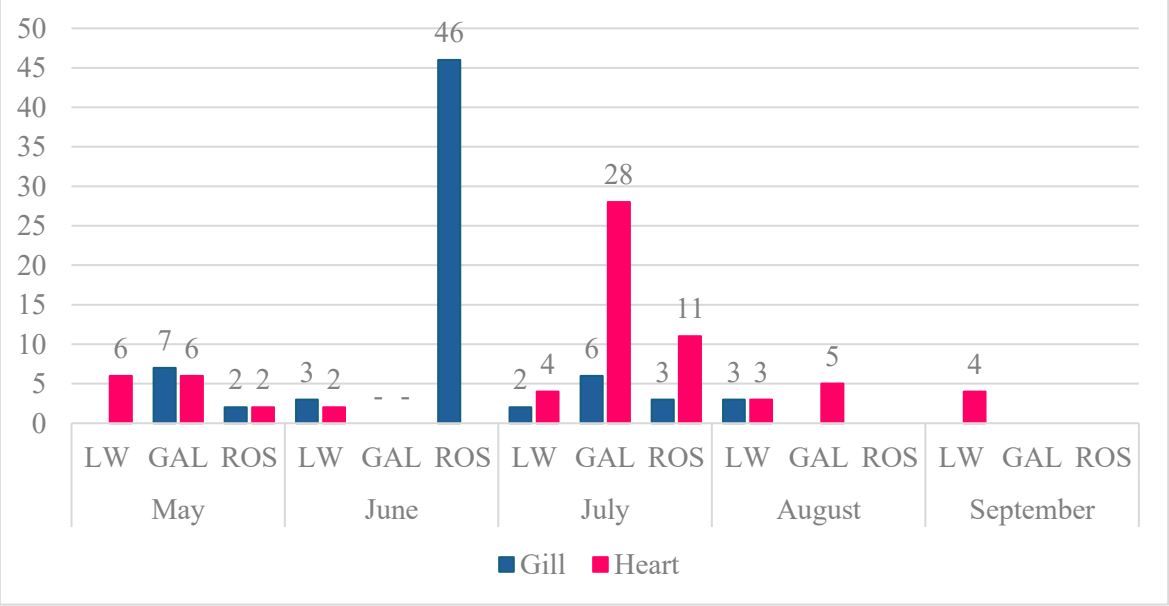


Figure 3. Bar plot showing the number of *O. edulis* individuals with parasites in gill and heart for each shellfish bed along sampling months

USC UNIVERSIDADE DE SANTIAGO DE COMPOSTELA

3.2. SNP genotyping and inversion arrangement karyotypes

DNA was extracted from a subset of 436 individuals sampled from three Irish flat oyster (*O. edulis*) shellfish beds: LW, n = 145; GAL, n = 134; and ROS, n = 157. Individuals were genotyped using the medium-density SNP array previously described in Chapter II, which included several resistance-associated SNPs reported by Vera et al. (2019) and validated in Chapter I.

To determine the ancestry of individuals related to "blue" and "orange" C8 arrangements, as well as the heterokaryotype, we performed a STRUCTURE analysis with the SNPs mapping in the inversion (Fig. 4A). In GAL, 31 individuals were homokaryotypes for the "orange" arrangement (23%), 48 homokaryotypes for "blue" (36%), and 55 were heterokaryotypes (41%); similar distributions were obtained for LW (12% "orange", 48% "blue", 41% heterokaryotypes) and ROS (20% "orange", 31% "blue", 49% heterokaryotype). Frequency for the "orange" arrangement ranged from 32% (LW) to 44% (ROS). No significant deviation from HWE was detected in any of the three populations ($p > 0.05$).

As expected, STRUCTURE analysis using the consistent SNP outliers previously associated with *Bonamia*-resistance (Vera et al., 2019; Chapter I) yielded very similar results. Of the 16 consistent markers identified previously, 11 were included in the SNP chip used in this study (Chapter II), and 10 of them were located within the boundaries of the C8 inversion (Fig. 4B). Similar analyses were conducted with the other two inversions, with results consistent with those already described in Chapter I for GAL and LW populations (Table S2; Fig. S2).

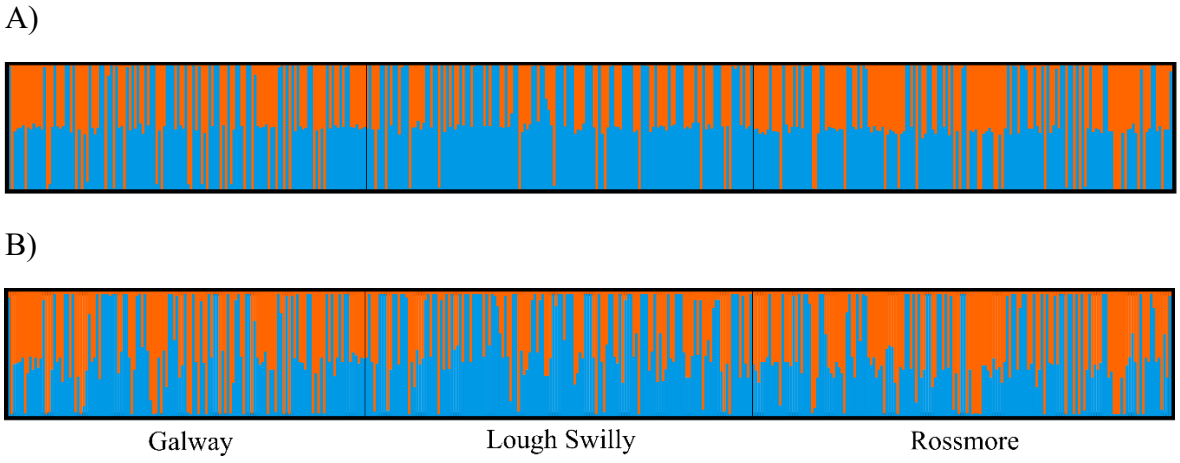


Figure 4. STRUCTURE analysis (K = 2) using the (A) 208 SNPs mapping in the C8 inversion and (B) the 11 consistent SNP outliers from Vera et al., 2019 available in the SNP array (Chapter II).

USC UNIVERSIDADE DE SANTIAGO DE COMPOSTELA

We evaluated the association between C8 inversion genotyping and the presence/absence of *B. ostreae* in gill and heart by pooling the data from the three populations. No association was found in gill between the C8 inversion genotypes and infection phenotypes (infected vs non-infected) ($\chi^2 = 0.007$, $p = 0.9333$), suggesting that gill prevalence occurs similarly in the three inversion genotypes. In contrast, a highly significant association was detected when using heart samples (true infection; $\chi^2 = 17.49$, $p = 1.595e^{-04}$), no "orange" individuals being infected, while 32 (17%) heterokaryotypes and 39 (23.5%) "blue" homokaryontypes were infected.

Association was also explored using the infection level phenotypes, results being also highly significant ($\chi^2 = 28.69$, $p = 3.583e^{-04}$), the "blue" homokaryotypes showing the most extreme cases (level 4).

Table 2. Distribution of *B. ostreae* infection levels across C8 inversion genotypes. Number of individuals per infection level (from 0 to 4) within each genotypic group: homokaryotype "orange", heterokaryotype, and homokaryotype "blue".

	Uninfected	Level 1	Level 2	Level 3	Level 4
Orange	79	0	0	0	0
Heterokaryotype	159	19	9	3	0
Blue	127	16	18	2	3

To further investigate the genetic basis of resistance, we tested the association between infection status and SNPs located within the C8 inversion using SNPassoc. Among the 208 SNPs analysed, 45 showed significant association under a codominant model (Fig. 5) and 4 under a dominant model. The predominance of significant results in the codominant model suggests an additive genetic effect; the greater the number of 'orange' arrangements in the genotype, the greater the resistance. Notably, no SNPs showed evidence of overdominance, consistent with the HWE observed across all analyses.

USC UNIVERSIDADE DE SANTIAGO DE COMPOSTELA

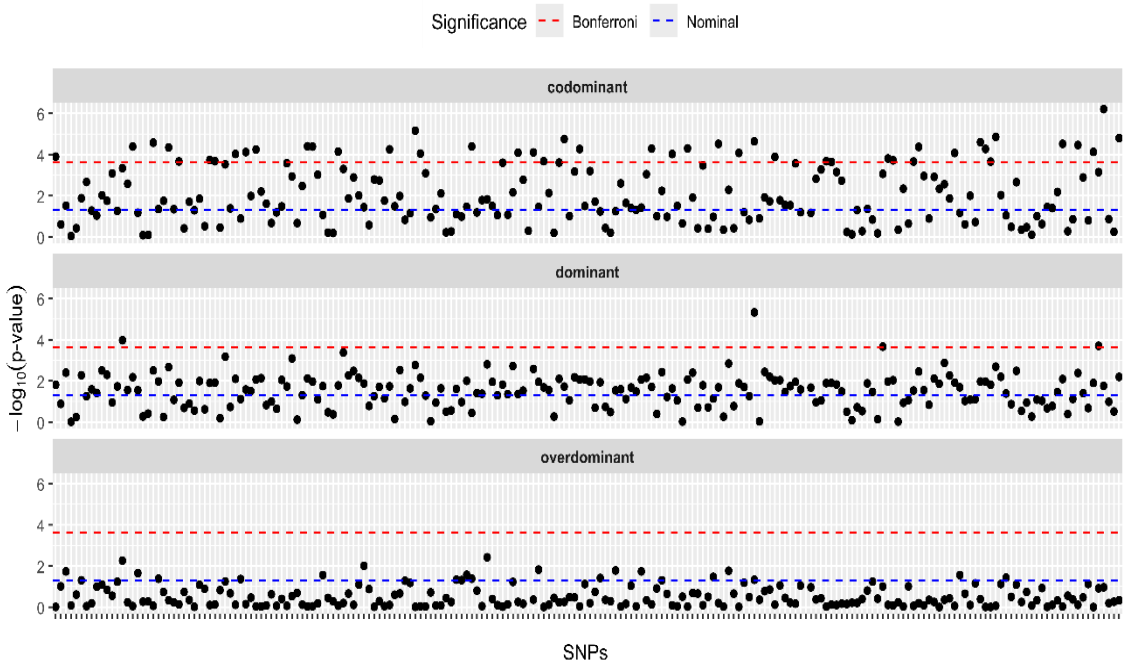


Figure 5. Association analysis between SNPs and infection phenotype under three genetic models (codominant, dominant, and overdominant) using the SNPassoc package in R. Each point represents the –log10(p-value) for a given SNP under the corresponding model. The dashed blue line indicates nominal significance (α = 0.05) and the dashed red line represents the Bonferroni-corrected threshold (208 SNPs).

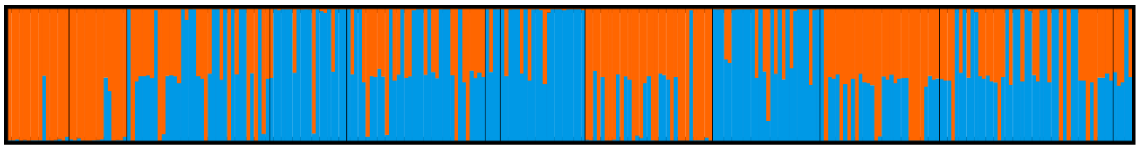
To assess whether the other two genomic inversions (C2 and C5; Chapter II) could be involved in resistance, we analysed SNPs located within the boundaries of these two inversions. In C2, only one SNP showed a significant association with infection under a codiminant model; in C5, no SNP showed significant association with infection under any model. Moreover, no significant association was found between infection status (infected/non-infected) and inferred arrangement genotypes for either C2 (χ^2 =1.94, p = 0.378) or C5 (χ^2 =0.364, p = 0.834) (Fig. S1).

3.3. Validation of a targeted genotyping panel for assisted breeding

The five-SNP MassARRAY panel designed for a cost-effective tool successfully genotyped the 320 individuals included in the assay representative of the flat oyster distribution range and validated the allelic variants and genotypes obtained with the Axyom SNP array. Further, it precisely recapitulated the inversion genotypes inferred with the 208-SNP panel using STRUCTURE even with a clearer pattern (Fig. 6).

USC UNIVERSIDADE DE SANTIAGO DE COMPOSTELA

A)



B)

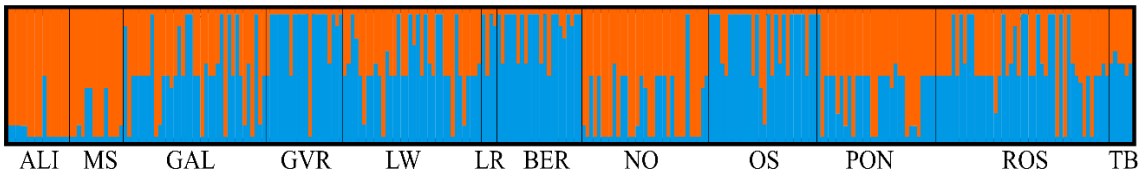


Figure 6. STRUCTURE analysis (K = 2) comparing SNP array and MassARRAY genotyping for the orange arrangement associated with immune resistance to *B. ostreae* based on: A) 5 nearly diagnostic SNPs, and B) the whole inversion 208 SNP dataset. Populations included in this study: ALI – Alicante (Spain), MS – Mali Ston (Croatia), GVR – Grevelingen (The Netherlands), BER – Bergen (Norway), NO – Noia (Spain), OS – Oosterschelde (The Netherlands), PON – Pontevedra (Spain), and TB – Tralee Bay (UK).

3.4. Transcriptomic response to *B. ostreae* in the wild

Twelve *O. edulis* individuals from the LW population corresponding to uninfected oysters and three infection levels were selected for transcriptomic analysis including three replicates per condition. ROS population was not considered because, as outlined before, only low infection levels were detected in this population. Pairwise comparisons were performed using heart samples between uninfected and the histologically defined infection levels:

- Reference group: 3 individuals
- Infection Level 1: 3 individuals
- Infection Level 2: 3 individuals
- Infection Levels 3 and 4: 1 and 2 individuals, respectively, pooled together as "Level 3" due to limited sample size.

RNA-seq generated on average 25,673,412 raw reads per sample, with high read quality (mean Phred score > 39). After quality control and trimming, approximately 85% of the reads mapped to the *O. edulis* genome on average, indicating high-quality sequencing and alignment metrics (Table S3). To reduce noise, count matrices were filtered by removing transcripts with expression < 5 TPM and detected in fewer than two samples per condition (Uninfected, Level 1, Level 2 and Level 3). After this step, 7,916 genes expressed in heart samples were retained for subsequent PCA and enrichment analyses.

USC
DE SANTIAGO
DE COMPOSTELA

Principal Component Analysis (PCA) of normalized expression data revealed separation between infected and uninfected oysters, especially for two of them (Fig. 7A). PC1 accounted for 66% of the total variance and discriminated infected from uninfected individuals, while PC2 (8%) further separated individuals with high infection loads (Level 3) from those with lower infection levels (Level 1/2). One uninfected sample clustered within the low-level infected individuals, potentially reflecting early or subclinical infection (Fig. 7B). When the extreme infection levels, Uninfected and Level 3, were excluded, the Uninfected sample appeared rather separated from infection levels 1 and 2, so we maintained this sample within the Uninfected group.

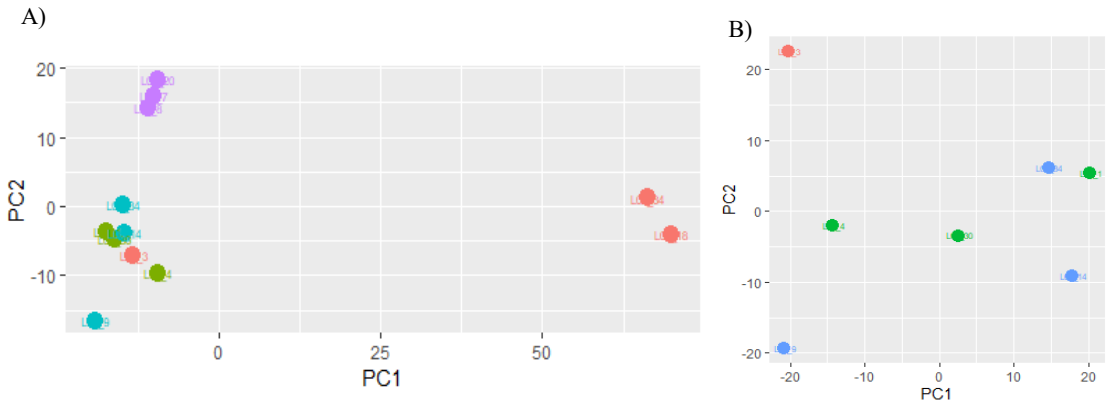


Figure 7. Principal component analysis (PCA) of gene expression profiles across infection levels in *O. edulis*: (A) including all 12 individuals; (B) using infection levels 1 and 2. Uninfected = red, Level 1 = green, Level 2 = blue, Level 3 = purple.

3.4.1. Functional characterization of differentially expressed genes

Pairwise differential expression analyses between each infection level and the uninfected group revealed a total of 3,711 differentially expressed genes (DEGs; FDR ≤ 0.05; Table 2). The strongest transcriptomic response was observed in oysters with moderate infection (Level 2), with 1,453 DEGs, followed by Level 1 (1,225 DEGs) and Level 3 (1,033 DEGs).

Table 2. Number of differentially expressed genes (DEGs) for each *Bonamia* infection level compared to the uninfected group.

	Upregulated	Downregulated	Total
Level 1	259	966	1,225
Level 2	310	1,143	1,453
Level 3	205	828	1,033

USC UNIVERSIDADE DE SANTIAGO DE COMPOSTELA

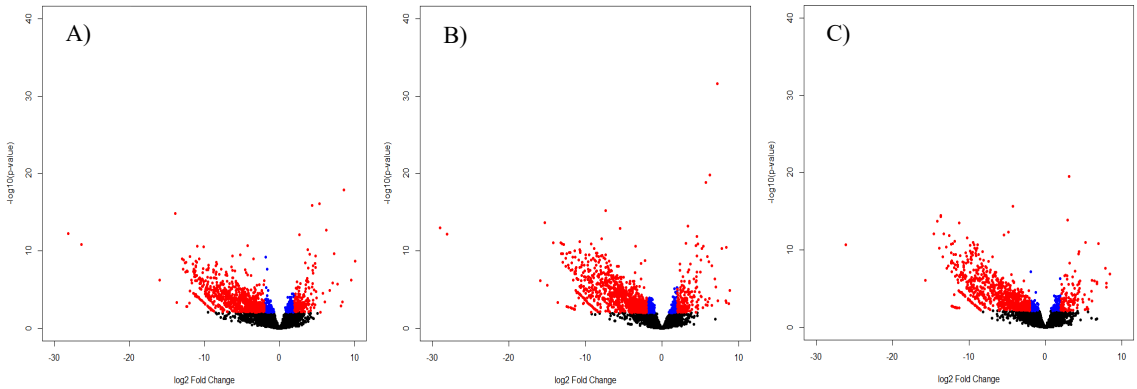


Figure 8. Volcano plots showing differentially expressed genes (DEGs) between uninfected and infected oysters at L1 (A), L2 (B), and L3 (C). Red dots represent significantly upregulated (right, FC > 2) and downregulated (left, FC < -2).

The comparative analysis of DEGs revealed contrasting patterns between those upregulated in infected oysters and those downregulated (i.e., more expressed in the Uninfected group). A higher number of downregulated than upregulated DEGs were observed at the three infection levels (Table 2, Fig. 8), which suggests an important transcriptional repression in response to infection.

Upregulated genes in infected oysters showed a high overlap across infection stages: 90 shared genes, compared with 75, 90, and 55 specific to L1, L2, and L3, respectively. This shared set included genes with basic cellular and regulatory functions, such as *ribosomal proteins*, *peroxiredoxin prdx-2-like*, and *protein arginine N-methyltransferase 6-like*, which likely reflects a general activation of housekeeping pathways under infection conditions. Stage-specific upregulated genes also highlighted distinct processes: in L1, several were related to growth signaling (*fibroblast growth factor receptor 3-like*); in L2, genes involved in lipid metabolism and transport, such as *caveolin-1-like* and *ganglioside GM2 activator-like*; and in L3, genes linked to immune regulation and stress responses, such as *heat shock protein Hsp-16.48/Hsp-16.49-like*.

In the case of downregulated genes in infected individuals (Fig. 9B), a substantial overlap was also observed across infection levels, with 563 genes shared, although a considerable number of genes were stage-specific (134 exclusive to L1, 207 to L2, and 87 to L3). Among the shared genes, several were associated with mitochondrial and energy metabolism processes, such as *cytochrome c oxidase subunit 5B*, *succinate-CoA ligase*, and *ATP synthase subunit f*, as well as innate immunity-related genes including *dual oxidase maturation factor 1-like* and *toll-like receptor 4*. Conversely, stage-specific genes reflected differential functions linked to infection progression; for instance, in L1 there was repression of immune receptors such as *RIG-I-like* and *interferon alpha-inducible protein 27-like*, whereas in L2 signaling receptors like *prostaglandin E2 receptor EP4* and membrane-remodeling proteins (*caveolin-like*) were downregulated. In L3, genes associated with tissue damage and cellular signaling, such as *matrix metalloproteinase-19-like* and *sex peptide receptor-like*, were particularly prominent.

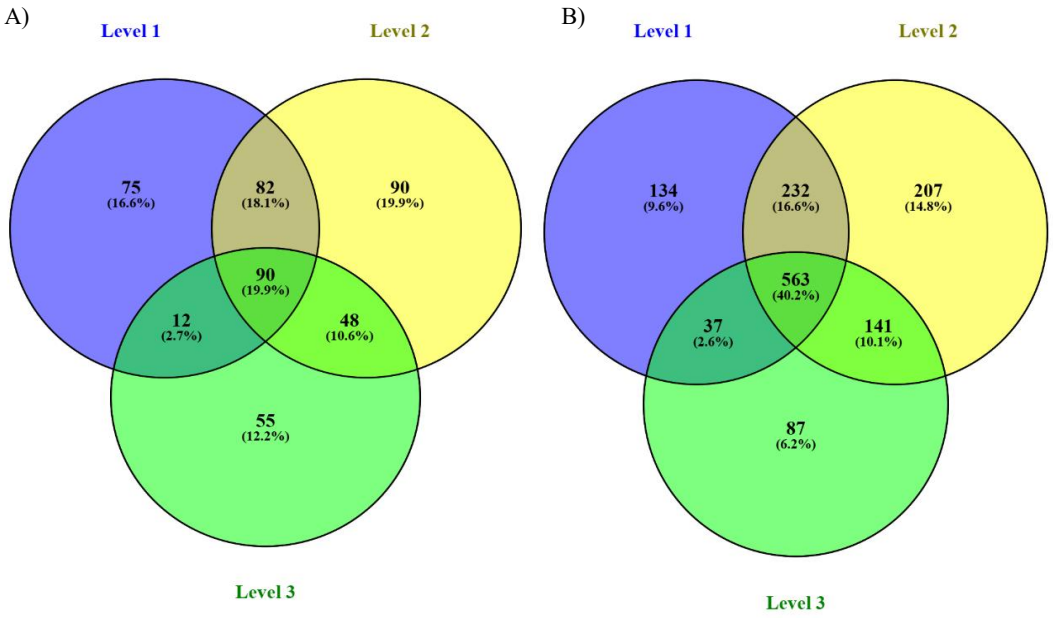


Figure 9. Venn diagrams of differently expressed genes across infection levels with respect to the uninfected reference. (A) upregulated genes in infected oysters. (B) Downregulated genes in infected oysters

Moving into a more detailed analysis, upregulated genes in infected oyster revealed different processes related to immune activation, apoptosis regulation, oxidative stress, and cellular remodelling (Fig. 9A). At the initial infection stage (L1), the most strongly induced transcripts included *fibrinogen-like protein A*, *procathepsin L-like, tripartite motif-containing protein 2-like* (*trim2*), and *acetylcholine receptor subunit delta-like*. These genes have been associated with innate immune recognition, lysosomal degradation, and neuroimmune signaling (Niu et al., 2013; Moreira et al., 2018; Prokhorova & Ataev, 2023). Several metabolic and stress-related transcripts, such as *retinoid-inducible serine carboxypeptidase-like*, *retinol dehydrogenase 12-like*, and *apolipoprotein D-like*, were also upregulated, pointing to early activation of oxidative stress responses and lipid transport mechanisms during pathogen challenge (Odoemelam, 2009; Ronza et al., 2018; Song et al., 2022). Finally, *orexin receptor type 2-like* and *neutral amino acid transport A-like* suggested infection-associated changes in cellular signaling and nutrient transport.

At intermediate stage (L2), several immune-related transcripts remained consistently induced, including *trim2*, *procathepsin L-like*, *low-affinity immunoglobulin epsilon Fc receptor-like*, and *ganglioside GM2 activator-like*, indicating a sustained activation of innate immune pathways and antigen processing mechanisms (Abdallah, 2021). Notably, *FAS-associated death domain protein-like* and *testis-specific serine/threonine-protein kinase 1-like* were upregulated at this level, suggesting enhanced apoptotic signaling and kinase-mediated signal transduction as infection progresses (Morga et al., 2017; Kron, 2022).

At the highest infection levels (L3 and L4), expression profiles largely overlapped with previous stages, including persistent upregulation of *trim2*, *procathepsin L-like*, *retinol dehydrogenase 12-like*, and *apolipoprotein D-like*. However, additional transcripts emerged, such as *bone morphogenetic protein 10-like*, associated with tissue remodeling, and *cytochrome P450 2U1-like*, further indicating increased xenobiotic metabolism in heavily infected individuals (Odoemelam, 2009; Vizzini et al., 2021; Zhang et al., 2024). The repeated induction of *low-affinity immunoglobulin epsilon Fc receptor-like* and *prion-like domain-bearing proteins* across all infection levels suggested a consistent role for immune recognition and protein homeostasis mechanisms throughout infection progression.

In contrast, the most strongly downregulated genes in infected oysters were those related to cell membrane organization and signaling, including caveolins (*caveolin-1-like* and *caveolin-3-like*), repeatedly detected across comparisons, as well as *integrin alpha-PS3 and calcium-* and *integrin-binding proteins*. These results are consistent with the repression of integrin-mediated signaling and cell-matrix adhesion pathways during infection. Similarly, several genes encoding extracellular matrix (ECM) components, such as *collagen alpha-1(I) chain-like*, *tenascin-R*, *hemicentin-1*, and *metalloproteinase inhibitor*s, were downregulated. This agrees with the increased expression of collagens and pregnancy zone protein in uninfected oysters, both linked to tissue integrity and negative regulation of proteases, potentially limiting parasite entry or tissue degradation, as shown in LTA oysters to *B. ostreae* by Ronza et al. (2018).

Multiple cytoskeletal and motor proteins, including *kinesin-like* and *rho GTPase-activating proteins*, displayed higher expression in uninfected oysters, consistent with their role in microtubule-based transport and parasite clearance or confinement (Doma et al., 2010; Venier et al., 2016). Likewise, *G protein-coupled receptors* (*gpcr*) were more active in uninfected individuals (Reboul & Ewbank, 2016), reflecting the likely importance of immune sensing and chemotaxis pathways on resistance (Hanlon & Andrew, 2015; Venier et al., 2016).

Downregulation was also evident among mitochondrial components (e.g., *cytochrome c oxidase* subunits, *NADH dehydrogenase-related proteins*) and metabolic enzymes, suggesting a global suppression of energy metabolism in infected oysters. Similarly, *vinculin*, *fermitin* family-like proteins, and *catenin beta*, associated with cellular adhesion and cytoskeletal anchoring, were repressed, pointing to a loss of structural integrity and immune signaling capacity to hamper infection (Moreira et al., 2012a; McDowell et al., 2014; Pardo et al., 2016).

Genes associated with apoptotic regulation, including *endonuclease G* and *salvador-like protein 1*, were also downregulated, in agreement with the ability of *B. ostreae* to inhibit haemocyte apoptosis to ensure intracellular persistence (Morga et al., 2012). Their higher expression in the uninfected oysters suggests that apoptosis activation could represent a host defense strategy to limit parasite proliferation (Romero et al., 2015; Morga et al., 2017).

USC UNIVERSIDADE

Similarly, genes involved in oxidative stress and detoxification, such as *cytochrome P450 monooxygenases* and *peroxidases*, were activated in uninfected oysters, consistent with earlier reports of antioxidant enzyme modulation during *Bonamia* infection (Pardo et al., 2016). Finally, although no GO terms related to chromatin or histone organization reached statistical significance, several histone genes (*h2a*, *h2b*, *h4*) showed higher expression in the uninfected group, consistent with previous findings in LTA oysters (Poirier et al., 2014; Lian et al., 2024).

By positioning differentially expressed genes within the C8 inversion, we identified more than 40 transcripts located inside this large structural variant. The vast majority were strongly downregulated in infected oysters, highlighting a consistent suppression of functions that overlap with functional processes enriched in the inversion (Chapter II). Among the most repressed genes were those encoding regulatory factors, such as *sox-2-like* (FC ≈ –12), components of the extracellular matrix, including *short-chain collagen C4-like* and *chondroadherin-like*, and immune-related ligases such as *trim2-like* and *trim56-like*. Several genes encoding signaling and structural proteins, including *APGW-amide neuropeptide-like*, *sorCS1-like receptor*, *tubulin beta chain*, and *catenin alpha-2-like*, also showed significant repression, suggesting impaired cell adhesion, motility, and signaling. In parallel, genes involved in metabolic and homeostatic functions were consistently silenced, such as *enolase-phosphatase E1-like*, *sphingolipid delta(4)-desaturase DES1-like*, *methyltransferase-like protein 27*, and *PGC1α-like*, pointing to a collapse of glycolytic and lipid-related processes in infected oysters. Taken together, these results suggest that the C8 inversion harbors a cluster of immune, apoptotic, structural, and metabolic genes, many of which are transcriptionally repressed in *Bonamia* infected oysters but activated in uninfected ones. This functional overlapping supports the interpretation of C8 may act as a resistance-associated "supergene," where the resistant "orange" arrangement may maintain allelic variants associated with immune and metabolic activity, while the "blue" susceptible arrangement would experience parasite-induced transcript shutdown alleles.

Across all infection levels, a substantial proportion (30–50%) of the most strongly induced transcripts remained unannotated, underscoring the limited functional annotation of the *O. edulis* genome and the potential presence of novel immune-related genes responding to *B. ostreae* infection.

3.4.2. Enriched functional categories across infection levels

The functional enrichment analysis of differentially upregulated genes revealed both common and infection-level-specific biological processes, molecular functions, and cellular components associated with *B. ostreae* infection in *O. edulis* (Table 3). At Level 1, significantly overrepresented GO categories were mainly related to primary metabolic pathways, including hexose biosynthetic process, nucleoside diphosphate metabolic process, and glycolytic process, together with monosaccharide biosynthetic process and nucleoside diphosphate phosphorylation.

USC DE COMPOSTELA

These results suggest that energy metabolism and carbohydrate processing were among the first biological processes to be altered upon infection, possibly reflecting the initial metabolic costs of immune activation and cellular stress responses (Table 3A). At Level 2 the enrichment landscape expanded towards energy production and cytoskeletal organization, with categories such as ATP metabolic process, generation of precursor metabolites and energy, and pyruvate metabolic process being significantly overrepresented. Moreover, the actin cytoskeleton category appeared at this level, highlighting the importance of cytoskeletal remodeling during infection progression. The enrichment of purine ribonucleotide metabolic process and related pathways further indicated changes in nucleotide metabolism that may reflect increased transcriptional and translational demands at this intermediate stage (Table 3B). At Level 3 GO terms shifted towards membrane signaling and energy transduction, including transmembrane signaling receptor activity, signaling receptor activity, and molecular transducer activity. Additionally, the proton-transporting ATP synthase complex (both coupled and uncoupled) was upregulated, suggesting profound alterations in mitochondrial activity and cellular energy homeostasis in heavily infected oysters. These findings are consistent with the transcriptional repression of mitochondrial genes observed in infected individuals and point to a late-stage disruption of bioenergetic and signaling processes (Table 3C).

In uninfected oysters, the enrichment landscape was dominated by a consistent set of biological processes related to ciliary function and microtubule-driven motility, which were significantly overrepresented across all comparisons with infected groups. Core categories included cilium movement, cilium organization, microtubule-based process, microtubule-based movement, and cilium- or flagellum-dependent cell motility, indicating that healthy individuals maintain a transcriptional profile strongly committed to sustaining ciliary assembly, axonemal structure, and motile function (Table 3A–C). This conserved enrichment pattern suggests that ciliary activity represents a key physiological state in uninfected oysters, supporting effective water flow, particle clearance, and epithelial homeostasis at the gill surface. Beyond this common core, each infection level comparison revealed additional processes specifically enriched in uninfected oysters. At L1, the enrichment was particularly focused on microtubule-dependent movement and axoneme assembly, consistent with active maintenance and turnover of motile cilia in healthy tissues. At L2, the signal extended to include processes involved in the regulation of cell projections and plasma membrane-bounded projection cytoplasm, suggesting that intermediate infection levels are associated with transcriptional changes in cell morphology and structural remodelling, which are absent or less pronounced in uninfected individuals. Finally, at L3, uninfected oysters uniquely showed enrichment of categories related to cilium-dependent cell motility and organization of the cytoskeleton, highlighting that the most heavily infected oysters exhibit a marked loss of these functions.

USC
UNIVERSIDADE DE SANTIAGO DE COMPOSTELA

Altogether, these results indicate that uninfected oysters maintain a transcriptional program that supports robust ciliary motility and microtubule-based cytoskeletal dynamics, a signature that is progressively attenuated as infection intensifies. The loss of these processes with increasing infection levels suggests that *B. ostreae* compromises not only ciliary activity but also the broader structural integrity and motility of epithelial cells, which may have important consequences for mucosal defence and pathogen clearance.

Table 3. Gene Ontology (GO) enrichment for differentially expressed genes across infection levels. (A) uninfected *vs* L1; (B) uninfected *vs* L2; (C) uninfected *vs* L3. BP = Biological Process.

A)

Ontology	GO term	Function	Expression in L1
BP	GO:0019319	hexose biosynthetic process	UP
BP	GO:0009132	nucleoside diphosphate metabolic process	UP
BP	GO:0046364	monosaccharide biosynthetic process	UP
BP	GO:0006096	glycolytic process	UP
BP	GO:0006165	nucleoside diphosphate phosphorylation	UP
BP	GO:0006757	ATP generation from ADP	UP
BP	GO:0046939	nucleotide phosphorylation	UP
BP	GO:0006094	gluconeogenesis	UP
BP	GO:0009135	purine nucleoside diphosphate metabolic process	UP
BP	GO:0009179	purine ribonucleoside diphosphate metabolic process	UP
BP	GO:0009185	ribonucleoside diphosphate metabolic process	UP
BP	GO:0046031	ADP metabolic process	UP
BP	GO:0016051	carbohydrate biosynthetic process	UP
BP	GO:0006006	glucose metabolic process	UP
BP	GO:0006090	pyruvate metabolic process	UP
BP	GO:0006091	generation of precursor metabolites and energy	UP
BP	GO:0016310	phosphorylation	UP
BP	GO:0019318	hexose metabolic process	UP
BP	GO:0005996	monosaccharide metabolic process	UP
BP	GO:0046034	ATP metabolic process	UP
BP	GO:1901575	organic substance catabolic process	UP
BP	GO:0003341	cilium movement	DOWN
BP	GO:0007017	microtubule-based process	DOWN
BP	GO:0007018	microtubule-based movement	DOWN
BP	GO:0001539	cilium or flagellum-dependent cell motility	DOWN
BP	GO:0060285	cilium-dependent cell motility	DOWN
BP	GO:0044782	cilium organization	DOWN
BP	GO:0060294	cilium movement involved in cell motility	DOWN
BP	GO:0060271	cilium assembly	DOWN
BP	GO:0006928	movement of cell or subcellular component	DOWN
BP	GO:0001578	microtubule bundle formation	DOWN
BP	GO:0030030	cell projection organization	DOWN
BP	GO:0120031	plasma membrane bounded cell projection assembly	DOWN
BP	GO:0030031	cell projection assembly	DOWN

USC UNIVERSIDADE DE SANTIAGO DE COMPOSTELA

BP	GO:0120036	plasma membrane bounded cell projection organization	DOWN
BP	GO:0097722	sperm motility	DOWN
BP	GO:0035082	axoneme assembly	DOWN
BP	GO:0007283	spermatogenesis	DOWN
BP	GO:0048232	male gamete generation	DOWN
BP	GO:0000003	reproduction	DOWN
BP	GO:0022414	reproductive process	DOWN
BP	GO:0040011	locomotion	DOWN
BP	GO:0098609	cell-cell adhesion	DOWN
BP	GO:0048515	spermatid differentiation	DOWN
BP	GO:0007155	cell adhesion	DOWN
BP	GO:0022610	biological adhesion	DOWN
BP	GO:0048870	cell motility	DOWN
BP	GO:0051674	localization of cell	DOWN
BP	GO:0070925	organelle assembly	DOWN
BP	GO:0007286	spermatid development	DOWN
BP	GO:0030317	flagellated sperm motility	DOWN
BP	GO:0000226	microtubule cytoskeleton organization	DOWN
BP	GO:0003006	developmental process involved in reproduction	DOWN
BP	GO:0007276	gamete generation	DOWN
BP	GO:0019953	sexual reproduction	DOWN
BP	GO:0048609	multicellular organismal reproductive process	DOWN
BP	GO:0044458	motile cilium assembly	DOWN
BP	GO:0044703	multi-organism reproductive process	DOWN
BP	GO:0032502	developmental process	DOWN
BP	GO:0051704	multi-organism process	DOWN
BP	GO:0098742	cell-cell adhesion via plasma-membrane adhesion molecules	DOWN
BP	GO:0007156	homophilic cell adhesion via plasma membrane adhesion molecules	DOWN
BP	GO:0032504	multicellular organism reproduction	DOWN

B)

Ontology	GO term	Function	Expression in L2
BP	GO:0046034	ATP metabolic process	UP
BP	GO:0006091	generation of precursor metabolites and energy	UP
BP	GO:0006090	pyruvate metabolic process	UP
BP	GO:0009150	purine ribonucleotide metabolic process	UP
BP	GO:0009132	nucleoside diphosphate metabolic process	UP
BP	GO:0072521	purine-containing compound metabolic process	UP
BP	GO:0009259	ribonucleotide metabolic process	UP
BP	GO:0019319	hexose biosynthetic process	UP
BP	GO:0006163	purine nucleotide metabolic process	UP
BP	GO:0046364	monosaccharide biosynthetic process	UP
BP	GO:0019693	ribose phosphate metabolic process	UP

USC UNIVERSIDADE DE SANTIAGO DE COMPOSTELA

BP	GO:0055086	nucleobase-containing small molecule metabolic process	UP
BP	GO:0006096	glycolytic process	UP
BP	GO:0006165	nucleoside diphosphate phosphorylation	UP
BP	GO:0006757	ATP generation from ADP	UP
BP	GO:0046939	nucleotide phosphorylation	UP
BP	GO:0006753	nucleoside phosphate metabolic process	UP
BP	GO:0009135	purine nucleoside diphosphate metabolic process	UP
BP	GO:0009179	purine ribonucleoside diphosphate metabolic process	UP
BP	GO:0009185	ribonucleoside diphosphate metabolic process	UP
BP	GO:0046031	ADP metabolic process	UP
BP	GO:0006094	gluconeogenesis	UP
BP	GO:0003341	cilium movement	DOWN
BP	GO:0007017	microtubule-based process	DOWN
BP	GO:0007018	microtubule-based movement	DOWN
BP	GO:0006928	movement of cell or subcellular component	DOWN
BP	GO:0044782	cilium organization	DOWN
BP	GO:0001539	cilium or flagellum-dependent cell motility	DOWN
BP	GO:0060285	cilium-dependent cell motility	DOWN
BP	GO:0060271	cilium assembly	DOWN
BP	GO:0001578	microtubule bundle formation	DOWN
BP	GO:0035082	axoneme assembly	DOWN
BP	GO:0060294	cilium movement involved in cell motility	DOWN
BP	GO:0120031	plasma membrane bounded cell projection assembly	DOWN
BP	GO:0030031	cell projection assembly	DOWN
BP	GO:0120036	plasma membrane bounded cell projection organization	DOWN
BP	GO:0030030	cell projection organization	DOWN
BP	GO:0097722	sperm motility	DOWN
BP	GO:0040011	locomotion	DOWN
BP	GO:0048870	cell motility	DOWN
BP	GO:0051674	localization of cell	DOWN
BP	GO:0098609	cell-cell adhesion	DOWN
BP	GO:0000003	reproduction	DOWN
BP	GO:0022414	reproductive process	DOWN
BP	GO:0000226	microtubule cytoskeleton organization	DOWN
BP	GO:0007155	cell adhesion	DOWN
BP	GO:0022610	biological adhesion	DOWN
BP	GO:0030317	flagellated sperm motility	DOWN
BP	GO:0048232	male gamete generation	DOWN
BP	GO:0007283	spermatogenesis	DOWN
BP	GO:0070925	organelle assembly	DOWN
BP	GO:0070286	axonemal dynein complex assembly	DOWN
BP	GO:0048515	spermatid differentiation	DOWN
BP	GO:0098742	cell-cell adhesion via plasma-membrane adhesion molecules	DOWN
BP	GO:0007010	cytoskeleton organization	DOWN

USC UNIVERSIDADE DE SANTIAGO DE COMPOSTELA

BP	GO:0036158	outer dynein arm assembly	DOWN
BP	GO:0044458	motile cilium assembly	DOWN
BP	GO:0007156	homophilic cell adhesion via plasma membrane adhesion molecules	DOWN
BP	GO:0008610	lipid biosynthetic process	DOWN
BP	GO:0050878	regulation of body fluid levels	DOWN

C)

Ontology	GO term	Function	Expression in L3
BP	GO:0004888	transmembrane signaling receptor activity	UP
BP	GO:0045263	proton-transporting ATP synthase complex, coupling factor F(o)	UP
BP	GO:0045259	proton-transporting ATP synthase complex	UP
BP	GO:0038023	signaling receptor activity	UP
BP	GO:0060089	molecular transducer activity	UP
BP	GO:0033177	proton-transporting two-sector ATPase complex, proton-transporting domain	UP
BP	GO:0004930	G protein-coupled receptor activity	UP
BP	GO:0004508	steroid 17-alpha-monooxygenase activity	UP
BP	GO:0005576	extracellular region	UP
BP	GO:0006754	ATP biosynthetic process	UP
BP	GO:0042448	progesterone metabolic process	UP
BP	GO:0003341	cilium movement	DOWN
BP	GO:0007017	microtubule-based process	DOWN
BP	GO:0007018	microtubule-based movement	DOWN
BP	GO:0001539	cilium or flagellum-dependent cell motility	DOWN
BP	GO:0060285	cilium-dependent cell motility	DOWN
BP	GO:0044782	cilium organization	DOWN
BP	GO:0001578	microtubule bundle formation	DOWN
BP	GO:0060294	cilium movement involved in cell motility	DOWN
BP	GO:0060271	cilium assembly	DOWN
BP	GO:0035082	axoneme assembly	DOWN
BP	GO:0120031	plasma membrane bounded cell projection assembly	DOWN
BP	GO:0006928	movement of cell or subcellular component	DOWN
BP	GO:0030030	cell projection organization	DOWN
BP	GO:0030031	cell projection assembly	DOWN
BP	GO:0097722	sperm motility	DOWN
BP	GO:0120036	plasma membrane bounded cell projection organization	DOWN
BP	GO:0000003	reproduction	DOWN
BP	GO:0022414	reproductive process	DOWN
BP	GO:0000226	microtubule cytoskeleton organization	DOWN
BP	GO:0048870	cell motility	DOWN
BP	GO:0051674	localization of cell	DOWN
BP	GO:0030317	flagellated sperm motility	DOWN
BP	GO:0070925	organelle assembly	DOWN

USC UNIVERSIDADE DE SANTIAGO DE COMPOSTELA

BP	GO:0040011	locomotion	DOWN
BP	GO:0007283	spermatogenesis	DOWN
BP	GO:0048232	male gamete generation	DOWN
BP	GO:0048515	spermatid differentiation	DOWN
BP	GO:0007010	cytoskeleton organization	DOWN
BP	GO:0007286	spermatid development	DOWN
BP	GO:0070286	axonemal dynein complex assembly	DOWN
BP	GO:0003006	developmental process involved in reproduction	DOWN
BP	GO:0007276	gamete generation	DOWN
BP	GO:0019953	sexual reproduction	DOWN
BP	GO:0048609	multicellular organismal reproductive process	DOWN
BP	GO:0044703	multi-organism reproductive process	DOWN
BP	GO:0051704	multi-organism process	DOWN
BP	GO:0098742	cell-cell adhesion via plasma-membrane adhesion molecules	DOWN
BP	GO:0036158	outer dynein arm assembly	DOWN
BP	GO:0032504	multicellular organism reproduction	DOWN
BP	GO:0007156	homophilic cell adhesion via plasma membrane adhesion molecules	DOWN
BP	GO:0098609	cell-cell adhesion	DOWN
BP	GO:0022607	cellular component assembly	DOWN
BP	GO:0007155	cell adhesion	DOWN
BP	GO:0007281	germ cell development	DOWN
BP	GO:0022610	biological adhesion	DOWN

USC UNIVERSIDADE DE SANTIAGO DE COMPOSTELA

USC
UNIVERSIDADE
DE SANTIAGO
DE COMPOSTELA

GENERAL DISCUSSION

USC
UNIVERSIDADE
DE SANTIAGO
DE COMPOSTELA

USC
UNIVERSIDADE
DE SANTIAGO
DE COMPOSTELA

1. General overview

The European flat oyster (*Ostrea edulis*) has undergone a dramatic decline over recent decades due to habitat degradation, overexploitation, and, most critically, the emergence of the protozoan parasite *Bonamia ostreae* (Engelsma et al., 2014). This haplosporidian organism, first reported in France in the 1970s (Comps et al., 1980; Pichot et al., 1980), has since become a persistent threat to flat oyster stocks across Europe, particularly in the Northeast Atlantic and North Sea.

Unlike many marine parasites with broad dispersal capacity, *B. ostreae* exhibits a patchy distribution despite its potential transmission via oyster larvae (Arzul et al., 2011). This discontinuous occurrence has enabled comparative studies between naïve (NV) and long-term affected (LTA) populations, which have revealed patterns of local adaptation and divergent selection linked to the parasite's presence (Pardo et al., 2016; Vera et al., 2019). The resilience of certain flat oyster populations in highly affected areas has raised key questions regarding the genetic and functional basis of resistance and tolerance, and whether these traits can be exploited for sustainable restoration and management.

Understanding the genomic basis of resistance to *B. ostreae* is therefore essential for both conservation and aquaculture, as natural populations continue to collapse and restoration programs increasingly rely on resistant broodstock (Hollenbeck & Johnston, 2018). In this thesis, a multi-layered approach was employed to explore resistance at different biological scales: (i) the validation of candidate SNPs associated with resistance across populations and individuals, (ii) the characterization of large chromosomal inversions shaping population structure and adaptive variation, and (iii) the investigation of transcriptional responses to *B. ostreae* in naturally infected oysters. Together, these approaches provide a comprehensive view of the genetic and molecular mechanisms underlying resistance in *O. edulis* and provide tools for selection and restoration of natural beds (De Mesel et al., 2018; Kamermans et al., 2018; Pogoda et al., 2019b).

The first chapter focused on the validation of resistance-associated SNPs originally identified in Vera et al. (2019). By genotyping large numbers of oysters from multiple beds, several markers were confirmed to consistently segregate between NV and LTA populations and to be related to higher survival at the population level, supporting their use as candidate markers for selective breeding and population monitoring.

The second chapter expanded the population genomics view by characterizing large chromosomal inversions shaping population structure and adaptive architecture. Among three major inversions identified, the inversion on chromosome 8 (C8) emerged as the most relevant in the context of resistance. This region harbours multiple loci linked to apoptosis, immune processes, and extracellular matrix remodelling, suggesting that it may act as a reservoir of co-adapted alleles under parasite pressure. By contrast, inversions on chromosomes 2 and 5 did not show significant associations with resistance, although they may be involved in other important functions in oysters.

USC UNIVERSIDADE DE SANTIAGO DE COMPOSTELA

The third chapter validated the role of the C8 inversion at the individual level and combined this genomic perspective with transcriptomic analyses. No "orange" homokaryotypes (resistant arrangement) were found to be infected, whereas infections occurred in "blue" homokaryotypes and heterokaryotypes, confirming the strong association between the inversion and resistance phenotypes. In addition, a cost-effective MassARRAY panel was developed to provide a practical tool for karyotyping resistant and susceptible individuals. Complementing these results, transcriptomic analyses of oysters with different infection levels from Lough Swilly revealed a progressive shift in gene expression through disease progression: early infection was associated with metabolic reprogramming, moderate infection with mitochondrial and cytoskeletal processes, and severe infection with signalling and energy transduction pathways. Across all stages, widespread transcriptional repression was observed, particularly in genes involved in apoptosis, adhesion, and mitochondrial function, suggesting that *B. ostreae* may affect host transcription to ensure intracellular survival.

2. Validation of resistance-associated SNPs and identification of the C8 inversion

One of the primary objectives of this thesis was to validate whether previously identified SNPs associated with resistance to *B. ostreae* could be confirmed in independent samples and populations. Earlier studies exploiting the patchy distribution of *B. ostreae* across Europe identified outlier SNPs with signatures of divergent selection between LTA and NV oyster populations (Vera et al., 2019). These markers were hypothesized to tag a quantitative trait locus (QTL) underlying resistance, but their genomic organization, stability across populations, and predictive power remained unresolved. Additionally, we studied the performance of hatchery batches from different sources to be potentially used for restoration.

Our validation efforts using a population genomics approach in the North Sea and a common garden experiment confirmed the low but significant genetic differentiation among wild populations across the Northeast Atlantic, with a clear signal of isolation by distance. As expected, hatchery samples displayed lower genetic diversity than wild populations, likely due to the reduced effective population size during broodstock management (Liu et al., 2017). Nevertheless, the even parental contributions observed suggest that current hatchery protocols may be adequate, provided that the number of breeders and batches is increased to secure long-term genetic variability in restocking programs.

Analyses based on outlier loci revealed two distinct genetic clusters within the North Sea samples: "orange" and "blue", with the "orange" cluster occurring more frequently in LTA populations. This pattern was further confirmed in the large sample used in the common garden experiment: the NIOZ (NV) population, characterized by a much lower proportion of "orange" individuals, experienced substantially higher mortality compared to the RvY (LTA) population, where the frequency of "orange" genotypes was higher and mortality was markedly reduced.

USC DE COMPOSTELA

Although none of the oysters seemed to be infected with the parasite during exposure in Lake Grevelingen according to qPCR, the contrasting survival patterns support that genetic differences underlie resistance rather than environmental factors alone (Holbrook et al., 2021). The failure of the qPCR test in the North Sea could be related to the chosen tissue (gill) that does not contain the haemocyte target *Bonamia* cells, so a test using haemolymph or heart should be more appropriate for this analysis (Comps et al., 1980; Hine, 1991). Additionally, as suggested previously (Ronza et al., 2018), a latent phase in the parasite's infection cycle may be also involved in this observation.

Linkage disequilibrium (LD) analyses revealed strong correlation between resistance-associated SNPs, consistent with a large underlying chromosomal inversion suppressing recombination across a ~34 Mb segment of chromosome 8. This unusually high LD suggests the presence of a structural variant, such as a chromosomal inversion, maintaining a haplotype coadapted allele block of under selection. This was further supported by F_{ST} peaks between clusters, negative F_{IS} values within orientations, and the abrupt LD decay at inversion boundaries. Similar mechanisms have been described in other marine species as drivers of local adaptation and pathogen resistance (Mérot et al., 2021).

3. Genomic architecture, evolutionary history, and adaptative significance of chromosomal inversions

Chromosomal inversions are structural variants that suppress recombination within large genomic regions, thereby maintaining co-adapted gene complexes (Berdan et al., 2023). They have increasingly been recognized as key drivers of adaptation in many taxa, including marine invertebrates (Kirkpatrick & Barton, 2006; Wellenreuther & Bernatchez, 2018). By reducing recombination in heterokaryotypes, inversions can preserve sets of favourable alleles, acting as "supergenes" that facilitate adaptation to heterogeneous environments or complex selective pressures (Hoffmann & Rieseberg, 2008; Faria et al., 2019).

Building on the evidence of an inversion in chromosome 8, Chapter II expanded the focus to genome-wide structural variation in *O. edulis*, confirming the presence of three major inversions on chromosomes 2, 5, and 8. Dense SNP genotyping across 13 populations spanning the species' range revealed that these inversions collectively span ~8% of the genome. LD analyses, PacBio sequencing, and PCR-based breakpoint validation converged on precise inversion coordinates, while repetitive elements (LINEs, DNA/hAT, PLE/Naiad) and tandem duplications flanking breakpoints suggested mechanisms involving ectopic recombination or staggered double-strand break repair in their origin (Evgen'ev et al., 2000; Lee et al., 2008; Araya et al., 2025).

USC UNIVERSIDADE DE SANTIAGO DE COMPOSTELA

The successful PCR-based validation of inversion breakpoints provides a practical molecular tool for future genotyping, although distinguishing heterokaryotypes from homokaryotypes will require complementary approaches such as SNaPshot or MassARRAY assays. Importantly, inversion breakpoints coincided with repetitive elements, consistent with their proposed role in inversion formation across taxa (Evgen'ev et al., 2000; Villeoutreix et al., 2021).

SNPs within the three inversions exhibited striking high genetic differentiation between orientations (F_{ST} = 0.49–0.68) compared to genome-wide SNPs ($F_{ST} \approx 0.04$), suggesting long-term maintenance of alternative arrangements. The elevated diversity within orientations, particularly for the southern "orange" (C8) and "green" (C2) arrangements, suggest an ancient origin of inversions. Although the clinal variation for the three inversions may reflect historical phylogeographic divergence (Monteiro et al., 2024), the overlap with parasite distribution and environmental gradients raises the possibility of contemporary selection shaping these polymorphisms.

The lack of Hardy–Weinberg deviation for most inversions implies limited fertility costs for heterokaryotypes, contrasting with classical models where crossovers within paracentric inversions generate unbalanced gametes (Sturtevant & Beadle, 1936). A notable exception was the C5 inversion in Irish populations, where heterokaryotype excess could indicate overdominance or local selective advantages.

Outlier scans revealed strong enrichment of loci under divergent selection within inversions (76%) compared to the collinear genome (8%), supporting their role as reservoirs of locally adaptive variation. Functional enrichment analyses of genes located within inversions revealed biological processes potentially linked to adaptation to both abiotic (temperature, salinity) and biotic (pathogen exposure, competition) factors. The C2 inversion encompassed genes involved in neuropeptide signalling, epigenetic regulation, immune responses, and metabolic pathways, potentially underlying resilience to environmental fluctuations. Genes related to neuropeptide signalling and external stimulus detection, as well as those involved in transmembrane transport and ion channel activity, may underlie adaptation to temperature and salinity variation (Clark et al., 2021; Signorini et al., 2025; Oliveira et al., 2025). Likewise, genes linked to ciliary activity and phytoplankton filtration point to differences in feeding strategies and energy metabolism (Marinković et al., 2019). Conversely, the C5 inversion contained genes involved in zinc transport and homeostasis. Zinc is essential for cellular processes including enzymatic activity, transcriptional regulation, and oxidative stress responses (Marreiro et al., 2017). Differential expression of zinc-related genes has been reported in response to metal pollution in *M. gigas* (Meng et al., 2021) and *Crassostrea hongkongensis* (Chan & Wang, 2019).

The C8 inversion, previously associated with *B. ostreae* resistance, encompassed 14 of the 16 resistance-related SNP outliers identified in earlier studies (Vera et al., 2019; Chapter I). Genes within this region were enriched for functions related to carbohydrate metabolism, energy production, tissue remodelling, and immune pathways, including cytokine receptor signalling and tumour necrosis factor signalling (Canesi et al., 2022).

These findings suggest that this genomic region could modulate immune responses and tissue repair mechanisms following infections by *B. ostreae*, an intracellular parasite. Interestingly, naïve or low-affected populations, such as Bergen and Lough Swilly, exhibited a higher frequency of the "blue" arrangement compared with geographically close but long-term affected populations such as Oosterschelde and Galway. The predominance of the "orange" arrangement in southern populations, together with the association between *Bonamia* outbreaks and warmer temperatures (Audemard et al., 2008), could explain the observed pattern. However, the possibility of a spurious correlation driven by north–south clines in inversion frequencies and the latitudinal distribution of the parasite cannot be excluded.

Overall, Chapter II positioned chromosomal inversions as key genomic regions maintaining co-adapted gene complexes involved in environmental stressor and pathogen responses. Their characterization provides not only evolutionary insights into *O. edulis* history but also valuable tools for conservation genomics and the potential development of disease-resilient oyster stocks. However, their validation at the individual level indoor or in the wild would be critical for its confirmation and application in breeding programs for obtaining resilient strains to recover flat oyster shellfish beds.

4. Individual-level resistance and infection dynamics

A central contribution of this thesis is the demonstration that the association between the C8 inversion and resistance to *B. ostreae* extends beyond population-level patterns and holds true at the individual level. Earlier analyses suggested that the "orange" arrangement was more frequent in long-term affected populations and associated with survival in common garden experiments (Chapter I), but these observations may potentially be confounded by population structure or environmental variation. By directly comparing individual infection status with inferred inversion karyotypes, this study provides compelling evidence of a causal relationship between them.

Pooling data from three Irish beds with contrasting disease histories revealed a strong association between inversion karyotypes and true infection in heart tissue. No "orange" homokaryotypes were infected, while a significant proportion of "blue" homokaryotypes carried infections. Heterokaryotypes—carrying one "orange" and one "blue" orientation—consistently showed lower infection prevalence and intensity than "blue" homokaryotypes but were not completely protected. This intermediate outcome suggests partial resistance or tolerance, a distinction with both evolutionary and epidemiological consequences (RåBerg et al., 2007; Holbrook et al., 2021).

No genotype effect was detected for gill prevalence. This dichotomy is biologically coherent: detection in gills reflects exposure and initial contact, since the parasite can enter during normal filtration (Grant et al., 1990), whereas infection in heart tissue indicates established intracellular proliferation within haemocytes (Hine & Wesney, 1995).

UVG UNIVERSIDAD

The predominance of a codominant association pattern within C8 further supports an additive contribution of the "orange" arrangement to resistance, consistent with suppressed recombination across inversion behaving like a supergene or block of adaptive allelic variants.

Resistance is typically defined as the ability to reduce pathogen load through immune control, whereas tolerance refers to the capacity to limit the fitness costs of infection without necessarily affecting pathogen burden (Råberg et al., 2007; Holbrook et al., 2021). Our results align with this conceptual framework: heterokaryotypes may not fully prevent parasite entry into haemocytes, but they appear to limit proliferation or mitigate associated damage. Indeed, none of the heterokaryotypes reached the highest histological infection level (L4), and most exhibited only mild to moderate parasitic loads. This pattern points to a dose-dependent effect of the resistance-associated inversion, where a single copy of the "orange" arrangement provides partial protection, but two copies are required for complete resistance.

This intermediate tolerance phenotype is biologically meaningful and practically relevant. In restoration or breeding programs, tolerant individuals may survive and reproduce under parasite pressure, thereby contributing to population resilience. However, by surviving as asymptomatic carriers, tolerant oysters might also facilitate parasite persistence and transmission within restored ecosystems (Hanley et al., 2023). This duality underscores the need for careful management strategies that weigh the benefits of survival against the epidemiological risks of maintaining *B. ostreae* reservoirs.

Although the protective role of the "orange" arrangement is strongly supported, the evolutionary maintenance of inversion polymorphisms often reflects trade-offs (Faria et al., 2019). The persistence of the "blue" arrangement across populations suggests it may confer advantages in parasite-free environments where other stressors could be operating, or that balancing selection maintains both orientations (Wellenreuther & Bernatchez, 2018). These hypotheses need to be tested but highlight the importance of considering both the benefits and potential costs of selectively propagating resistant genotypes.

No associations with *Bonamia* infection were detected for inversions C2 or C5, indicating that resistance to *B. ostreae* is largely specific to C8 rather than a polygenic trait distributed across multiple structural variants. This specificity reinforces the central role of C8 in shaping host–parasite interactions.

From an applied perspective, the MassARRAY panel targeting five near-diagnostic SNPs distributed across the C8 inversion successfully replicated the karyotypes inferred from the denser SNP-array data and offers a scalable tool for hatcheries and restoration programs. Its implementation would enable (i) marker-assisted broodstock selection to increase the frequency of the resistance-associated arrangement, and (ii) traceability of karyotype composition in translocations.

USC UNIVERSIDADE DE SANTIAGO DE COMPOSTELA

Given that gill exposure does not differ by genotype whereas heart infection does, marker-assisted selection should prioritize genotypes conferring within-host resistance better than focusing on avoidance of exposure, since the parasite biology remains largely unknown yet.

Finally, the potential contribution of epigenetic priming cannot be excluded. Previous studies (Ronza et al., 2018; Yang et al., 2021; Montagnani et al., 2024; Wang et al., 2025) suggested that long-term exposed populations may mount faster and stronger immune responses, potentially mediated by selection of specific variants or through transgenerational epigenetic inheritance. The presence of methylation-related genes within the C8 inversion supports this hypothesis and warrants deeper investigation into the interplay between genetic and epigenetic mechanisms of resilience in *O. edulis*.

5. Transcriptomic insights into infection responses

Complementing the genomic perspective, the transcriptomic analyses performed in naturally infected oysters from Lough Swilly provide a dynamic view of how host gene expression changes along the progression of infection. By comparing uninfected individuals with oysters representing three histologically defined infection levels, this study identified 3,711 differentially expressed genes (DEGs), revealing widespread transcriptional reprogramming in response to *B. ostreae*.

A consistent and striking pattern was the predominance of downregulated genes in infected individuals. Across all infection levels, the number of repressed transcripts greatly exceeded those that were activated, suggesting that *B. ostreae* actively interferes in host gene expression to suppress humoral and cellular responses, ensuring their intracellular persistence (Morga et al., 2012). Similar strategies have been described for other intracellular parasites, which often interfere with host transcription, apoptosis, and oxidative stress pathways to establish chronic infections (Carballeira et al., 2012; Canesi et al., 2022).

At the early stage of infection (L1), upregulated genes were enriched for metabolic and stress-related functions. Transcripts such as *fibrinogen-like protein A*, *procathepsin L-like*, and *trim2-like* indicate the activation of innate immune recognition, lysosomal degradation, and antiviral-like signalling (Niu et al., 2013; Moreira et al., 2018). At the same time, metabolic enzymes such as *retinol dehydrogenase 12-like* and *apolipoprotein D-like* were induced, pointing to oxidative stress responses and lipid mobilization. The activation of *orexin receptor type 2-like* and amino acid transporter transcripts further suggests changes in nutrient uptake and signalling cascades. Together, these responses depict an oyster mobilizing some metabolic resources and initiating immune defences in the earliest stages of infection (Song et al., 2022).

USC UNIVERSIDADE DE SANTIAGO DE COMPOSTELA

At intermediate infection (L2), more than 1,400 DEGs were identified. Immune-related transcripts such as *trim2*, *procathepsin L-like*, *Fc receptor-like*, and *ganglioside GM2 activator-like* were consistently upregulated, reflecting sustained immune activation. The induction of *FAS-associated death domain protein-like* and *serine/threonine-protein kinase 1-like* highlights the engagement of apoptotic and kinase-mediated signalling pathways (Morga et al., 2017; Kron, 2022). GO enrichment revealed an expansion of pathways related to ATP metabolism, purine nucleotide turnover, and actin cytoskeleton organization, indicating high energetic demands and structural remodelling of haemocytes during active infection.

At advanced infection (L3), expression profiles overlapped with earlier stages but also revealed novel signatures. *Bone morphogenetic protein 10-like* and *cytochrome P450 2U1-like* emerged as strongly upregulated, suggesting activation of tissue remodelling and xenobiotic detoxification pathways (Odoemelam, 2009; Vizzini et al., 2021). Persistent induction of *trim2*, *procathepsin L-like*, and *Fc receptor-like* transcripts underscores their importance throughout infection. Moreover, GO categories pointed to metabolic reprogramming and enhanced mitochondrial activity with enrichment of proton-transporting ATP synthase complexes, ATP biosynthetic process, and diverse signalling receptor pathways.

The most downregulated genes in infected oysters were associated with membrane organization and signalling: *caveolins* (*caveolin-1/-3*), *integrin α-PS3*, and *calcium- and integrin-binding proteins*. Several extracellular matrix (ECM) components were also downregulated (e.g., *collagen α-1(I)-like*, *tenascin-R, hemicentin-1*, *metalloproteinase inhibitors*), consistent with reduced integrin-mediated signalling and cell–matrix adhesion. Together with the decreased expression of cytoskeletal and motor proteins (*kinesins*, *Rho-GTPase regulators*), results point to impaired haemocyte motility, phagocytosis, and physical confinement of the parasite (Doma et al., 2010; Venier et al., 2016).

Mitochondrial components (*cytochrome-c oxidase* and *NADH-dehydrogenase subunits*) and multiple metabolic enzymes were also repressed, suggesting a broad collapse of oxidative metabolism. Adhesion/anchoring proteins (*vinculin*, *fermitin-family-like*, *β-catenin*) were more expressed in uninfected oysters, indicating their greater structural integrity and signalling capacity (Moreira et al., 2012b; McDowell et al., 2014; Pardo et al., 2016). Pro-apoptotic genes (*endonuclease G*, *savI*) were downregulated in infected oysters, consistent with *B. ostreae*'s ability to inhibit haemocyte apoptosis to ensure intracellular survival (Morga et al., 2012). Finally, reduced expression of *cytochrome P450 monooxygenases* and *peroxidases* indicates compromised oxidative-stress responses, likely facilitating parasite persistence by limiting reactive oxygen species (Pardo et al., 2016).

USC UNIVERSIDADE DE SANTIAGO DE COMPOSTELA

These observations are congruent with Ronza et al. (2018), who, soon after challenge, reported enrichment of ECM functions and over-expression of protease inhibitors (e.g., *pregnancy zone protein*, *ITI heavy chains*, *AMBP*, *murinoglobulin*), together with *collagens*, *tenascin*, and *hemicentin* in the long-term exposed (AS) stock—interpreted as a "ready-to-respond" state that strengthens tissue barriers and limits parasite proteolysis. The same study observed early activation of *integrin α-PS3* and *cIbl* (supporting adhesion/phagocytosis), plus induction of *C1q-domain proteins* and *collectins* as humoral pattern-recognition molecules. Our data recapitulate this logic: uninfected oysters showed higher expression of *collectin-12-like* and multiple *C1q-like* genes, whereas infected individuals exhibit repression of several *C1q-like* transcripts ($\log_2$FC ≈ −7 to −11), consistent with reduced humoral recognition during established infection *vs* the reinforced recognition observed in tolerant AS oysters post-challenge (Pardo et al., 2016; Ronza et al., 2018; Zong et al., 2018).

A similar contrast appears for GPCRs: globally, we detected higher GPCR abundance in controls, echoing the early upregulation of *rhodopsin-like* GPCRs (including *orexin receptor 2*, *prostaglandin E2 receptor 4, cck-A*, *npffr2*) and *tlr1* reported by Ronza et al. (2018) in the AS stock. Together, these signals support the concept of enhanced immune sensing ("pre-activation") in resistant genotypes, mirrored in our uninfected oysters and blunted in established infections.

An important limitation, however, is that uninfected oysters cannot be unequivocally classified as resistant, since some of them may simply not have been exposed to the parasite. Nevertheless, the PCA patterns, with controls clustering separately from infected individuals, suggest that, irrespectively, transcriptomic profiles largely reflect their uninfected status.

GO terms showed a clear temporal logic: hexose/glycolytic and monosaccharide biosynthetic processes at L1, mitochondria/ATP synthase complexes (with ATP/pyruvate metabolism) at L2, and GPCR activity plus F_0/F_1-ATPase complexes at L3 (Reboul & Ewbank, 2016). Despite these functional terms being enriched, gene-level data showed broad repression of respiratory chain subunits (COX, NADH), indicating a decoupling: mitochondria and signalling reorganize under pressure, but net oxidative phosphorylation declines in infected oysters—consistent with the global transcriptional "shutdown" most evident at L2–L3.

Although no GO terms related to chromatin or histone organization were significantly enriched after multiple-testing correction, several histone genes (H2A, H2B, H4) were overexpressed in uninfected oysters, as also reported for long-term exposed oysters (Poirier et al., 2014; Lian et al., 2024). This aligns with the pattern in long exposed AS stocks (Pardo et al., 2016; Ronza et al., 2018) and supports a role for chromatin regulation in setting the pace/tonality of innate responses, although histones have been demonstrated to act as antimicrobial peptides (Shen et al., 2023; Wang et al., 2024).

USC UNIVERSIDADE DE SANTIAGO DE COMPOSTELA

Collectively, these transcriptional patterns suggest a dynamic host–parasite arms race. At early stages, oysters mobilize metabolic and immune resources to combat infection. At intermediate levels, these responses peak, but the parasite increasingly suppresses host functions, leading to widespread downregulation. At severe infection, cellular energy and signalling collapse, leaving the host vulnerable. This progression mirrors findings in other molluscs exposed to pathogens, where initial immune activation gives way to parasite-induced suppression (Zhang X. et al., 2014; Escoubas et al., 2016).

Additionally, to controls not being unequivocally classified as resistant, the restriction to a single population (Lough Swilly) and tissue (heart) means that broader patterns of resistance may not be fully captured. Despite these caveats, the results provide the most detailed description to date of the transcriptional dynamics of *O. edulis* in response to natural *Bonamia* infection.

6. Integration across chapters: structural variation, resistance mechanisms, and adaptation

Taken together, the three chapters of this thesis provide complementary perspectives that converge on a consistent picture: resistance of *O. edulis* to *B. ostreae* is underpinned by a complex interplay of genomic architecture, interindividual variation, and transcriptomic plasticity. The integration of these lines of evidence highlights the central role of the large C8 inversion and provides functional insights into the processes that differentiate resistant from susceptible genotypes.

Chapters I and III together highlight the predictive value of SNPs for resistance. In Chapter I, outlier SNPs previously reported by Vera et al. (2019) were validated in independent populations and confirmed to segregate between NV and LTA beds. These markers correlated with higher survival under common garden exposure, suggesting their utility for breeding and monitoring. Chapter III provided the complementary individual-level perspective: oysters carrying the “orange” orientation of the C8 inversion (tagged by those SNPs) were never found infected, while heterokaryotypes and “blue” homokaryotypes showed progressive susceptibility. These results demonstrate that SNPs initially associated with population-level survival differences also predict infection outcomes at the individual scale, strengthening their role as resistance markers. At the same time, linkage disequilibrium analyses in Chapter I suggested that many of these SNPs were not independent but embedded within a larger block of suppressed recombination—foreshadowing the inversion architecture later described in Chapter II.

In contrast, Chapter II broadened the perspective beyond C8, revealing two additional large inversions on chromosomes C2 and C5. Together, the three inversions span nearly 8% of the *O. edulis* genome and exhibit hallmarks of ancient origin, including high divergence between orientations, substantial internal genetic diversity, and widespread geographic distributions following latitudinal clines. The enrichment of outlier loci and adaptive functional annotations within all three inversions suggests that they collectively act as reservoirs of locally adapted haplotypes.

Still, only the C8 inversion was consistently associated with *B. ostreae* resistance, while C2 and C5 likely mediate adaptation to other selective pressures such as temperature, salinity, or pollutants. This contrast underscores the importance of distinguishing between historical processes shaping genomic architecture and contemporary selection imposed by emerging diseases.

Despite their different selective drivers, the three inversions share key evolutionary features. Their strong linkage disequilibrium, reduced recombination, and clustering of adaptive variants mirror patterns observed in other taxa where inversions maintain co-adapted gene complexes under heterogeneous selection (Peixoto & Klaczko, 1991). The high frequency of heterokaryotypes in natural populations, coupled with the absence of strong Hardy–Weinberg deviations, further suggests limited fertility costs, facilitating the long-term maintenance of these polymorphisms.

The transcriptomic analyses of Chapter III provide the functional dimension of these patterns, particularly in the context of the C8 inversion. Across all infection levels, a pervasive repression of immune, apoptotic, and metabolic genes was observed, suggesting that *B. ostreae* interfere host transcription to ensure intracellular survival and proliferation (Morga et al., 2012). When DEG coordinates were intersected with inversion boundaries, dozens of the most strongly downregulated transcripts fell within the limits of C8. These included genes encoding transcription factors (*sox-2-like*), ubiquitin ligases (*trim2*, *trim56*), cytoskeletal and adhesion proteins (*β-tubulin*, *α-catenin-2*, *collagen C4-like*, *chondroadherin-like*), metabolic enzymes (*enolase-phosphatase E1*, *sphingolipid desaturase DES1-like*, *mdpu1*), and vesicle-trafficking proteins (*SorCS1*, *Shisa-5*, *synaptobrevin/YKT6*) (Doma et al., 2010; Allam & Raftos, 2015; Bowden et al., 2020; Song et al., 2022). The fact that parasite-driven repression disproportionately targets this gene cluster reinforces the idea that C8 functions as a reservoir of co-adapted alleles essential for resistance. Moreover, the functional enrichments identified for C8 in Chapter II—cytoskeleton organization, N-glycosylation, spindle assembly, and the H4 histone acetyltransferase complex—mirror the very pathways that were transcriptionally silenced in heavily infected oysters (Morga et al., 2012).

This integration provides a mechanistic explanation: in resistant genotypes carrying the “orange” arrangement, the C8 haplotype likely maintains the coordinated expression of cytoskeletal, metabolic, and regulatory modules that support immune activation and tissue integrity. In contrast, susceptible “blue” genotypes are unable to prevent the parasite from suppressing these functions, leading to impaired haemocyte adhesion, defective phagocytosis, collapsed energy metabolism, and blocked apoptosis. The overlap between DEG patterns and C8 gene content therefore unifies the genomics and transcriptomics findings, connecting SNP-based markers of resistance (Chapters I and III) with the structural variant that underlies them (Chapter II).

USC
UNIVERSIDADE DE SANTIAGO DE COMPOSTELA

Finally, the integration with earlier studies further supports this view. Ronza et al. (2018) and Pardo et al. (2016) demonstrated that tolerant oysters (AS) mount rapid reinforcement of extracellular matrix integrity, protease inhibition, and pathogen recognition through C1q-domain proteins and collectins, whereas susceptible stocks fail to sustain these responses.

In our study, uninfected controls recapitulated this "pre-activated" profile, showing higher expression of GPCRs, collectins, and histones, while infected oysters displayed widespread suppression. Together, these results suggest that resistance in *O. edulis* arises not from a single pathway but from the preservation of a coordinated suite of functions, many of which are captured within the C8 inversion.

In summary, the three chapters collectively demonstrate how genetic markers, structural variants, and transcriptional programs converge to shape resistance to *B. ostreae*. SNPs validated across populations and individuals provide practical tools for monitoring and breeding. Large inversions, particularly C8, reveal genomic architecture maintaining adaptive haplotypes. Transcriptomic data show that parasite pressure specifically represses the very pathways enriched within C8. This multi-layered approach thus advances our understanding of host–parasite coevolution in marine invertebrates and highlights C8 as a key target for both evolutionary and applied perspectives.

7. Applications for selective breeding, restoration, and conservation

The validation of the C8 inversion as a reliable genomic marker for resistance to *B. ostreae* has direct and promising applications in flat oyster breeding and restoration programs. Selective breeding strategies that incorporate molecular tools such as SNP arrays, inversion-genotyping PCR assays or MASS-array tools, can significantly accelerate the development of resistant oyster strains, particularly in hatcheries. By screening broodstock and seed for the protective "orange" haplotype, hatchery managers can increase the likelihood of producing offspring with full resistance, thereby enhancing survival in *B. ostreae*-endemic environment (Sas et al., 2016).

Moreover, the finding that resistance is tightly linked to a non-recombining region allows for stable transmission of this trait across generations. However, as shown in this thesis, resistance is not universally fixed in all long-term affected populations, and haplotypic diversity within the "orange" group suggests that not all protective genotypes are equivalent. For this reason, selection efforts should not focus exclusively on a narrow set of markers but rather adopt a "supergene" and structurally informed approach that accounts for potential variation within the inversion (Berdan et al., 2022).

Importantly, restoration of natural oyster beds using hatchery-produced seed requires careful balancing of disease resistance with genetic diversity, local adaptation, and ecosystem function. Hatchery batches, while offering disease-resistant seed, showed lower levels of genetic variation compared to wild populations in this and previous studies (Vera et al., 2019; Chapter I).

USC

Therefore, restocking programs should maximize the number of parental lines, combine multiple seed batches, and—when possible—incorporate genetic background from local resilient populations to maintain evolutionary potential.

Another consideration relates to the epidemiological consequences of tolerance. Tolerant individuals (e.g., heterozygotes) that survive infection while harbouring low to moderate parasite loads may act as asymptomatic carriers, complicating efforts to eradicate the pathogen from restored beds. While such individuals contribute to demographic resilience, their use must be carefully weighed depending on whether the goal is containment, co-existence, or eradication of *Bonamia*. These findings advocate for a tailored strategy depending on the infection pressure of the recipient site and the functional goals of the intervention (RåBerg et al., 2007)

Finally, the discovery of structural variants like C2 and C5, although not directly linked to *Bonamia* resistance in this thesis, offers valuable insights into broader adaptive mechanisms. Their inclusion in marker panels may improve fitness under variable environmental conditions (e.g., salinity, temperature, metal exposure) and help ensure long-term success of both aquaculture and conservation initiatives (RåBerg et al., 2007).

In this sense, a combined approach that integrates disease resistance markers with loci underlying abiotic stress resilience could maximize the adaptive capacity of restored oyster populations. Such integrative breeding programs would not only secure survival under parasitic pressure but also promote population persistence under rapidly changing climatic and anthropogenic conditions (Hollenbeck & Johnston, 2018).

8. Limitations and future research directions

Despite the advances presented in this thesis, several limitations must be acknowledged. First, this study relied on natural infections, which, while providing ecologically realistic insights, limit the ability to control exposure conditions. Infection dose, timing, and environmental context could not be standardized, leaving some uncertainty about whether uninfected controls represent truly resistant oysters or individuals that simply avoided contact with the parasite. Controlled challenge experiments across genotypes and karyotypes might provide a complementary perspective to disentangle resistance (reduced infection burden) from tolerance (survival despite infection) and to quantify potential fitness trade-offs associated with each strategy (Liu et al., 2023). Second, the transcriptomic analyses were restricted to a single population (Lough Swilly) and one tissue type (heart), potentially overlooking population-specific or tissue-specific responses. Additionally, the small number of individuals at advanced infection levels (Levels 3–4) required pooling, which reduces the resolution for distinguishing late-stage responses.

USC UNIVERSIDADE DE SANTIAGO DE COMPOSTELA

Another limitation is the incomplete functional characterization of genes located within the identified inversions. Although the C8 inversion was consistently associated with *Bonamia* resistance, many candidate genes remain poorly annotated, restricting mechanistic interpretation. Functional genomics approaches such as long-read transcriptomics, single-cell RNA-seq, and epigenomic profiling (e.g., DNA methylation and histone modification analyses) could provide higher-resolution maps of regulatory networks and cell-type-specific responses.

These tools would also clarify the potential contribution of chromatin-level processes—such as the enrichment of histone acetyltransferase complexes and differential histone expression observed in this thesis—to the modulation of innate immune responses.

Finally, although this thesis identified the C8 inversion as central to *Bonamia* resistance, the additional inversions on chromosomes C2 and C5 were not associated with infection outcomes but displayed functional enrichment for processes related to abiotic tolerance, including salinity, temperature, and metal homeostasis. These results point to the broader role of inversions as reservoirs of adaptive variation. Experimental validation under multi-stressor conditions is needed to determine whether resilience to environmental challenges interacts with or trades off against parasite resistance.

Future research should expand in several directions. Integrating epigenomic data (particularly DNA methylation and histone modifications) could clarify the role of transgenerational epigenetic priming suggested by previous work (Ronza et al., 2018; Yang et al., 2021; Montagnani et al., 2024; Wang et al., 2025). Functional genomic approaches, such as ATAC-seq, EM-seq or ChIP-seq, could further reveal how chromatin accessibility within C8 influences infection responses. Multi-omics integration (proteomics, metabolomics, immunometabolomics) would provide a more comprehensive view of host–parasite interactions, particularly regarding metabolic reprogramming during infection (Männer et al., 2021)

From an applied perspective, long-term monitoring of inversion frequencies in natural populations under variable parasite prevalence and environmental stressors is essential to assess the evolutionary stability of resistance. Experimental infections using oysters of known karyotype, ideally across multiple environmental contexts (temperature, salinity, pollutants), will help disentangle the interplay between genomic architecture and ecological resilience. Finally, conservation programs must evaluate the epidemiological consequences of deploying tolerant genotypes and consider management strategies that minimize the risk of creating parasite reservoirs.

USC
UNIVERSIDADE DE SANTIAGO DE COMPOSTELA

CONCLUSIONS

USC
UNIVERSIDADE
DE SANTIAGO
DE COMPOSTELA

USC
UNIVERSIDADE
DE SANTIAGO
DE COMPOSTELA

- **Genomic markers of resistance** This thesis validated previously identified resistance-associated SNPs, demonstrating their consistent association with survival across populations and experimental settings. These markers provide a reliable genomic resource for monitoring population health and guiding selective breeding programs.

- **Structural genomic variation.** Large chromosomal inversions were revealed as major features of the *O. edulis* genome, spanning nearly 8% of its length. Among them, the C8 inversion consistently emerged as the strongest predictor of resistance to *Bonamia ostreae*, enriched in immune, apoptotic, and metabolic functions. Its structural properties—tight linkage disequilibrium and suppressed recombination—support its role as a "supergene" maintaining co-adapted haplotypes under parasite pressure.

- **Individual-level dynamics.** Analysis of infection status and inversion karyotypes demonstrated that orange homozygotes were fully resistant, heterokaryotypes displayed partial tolerance, and blue homokaryotypes remained susceptible. These findings highlight the additive contribution of C8 to resistance and reveal important epidemiological trade-offs, as tolerant individuals may survive while still transmitting the parasite.

- **Transcriptomic responses.** RNA-seq analyses uncovered widespread transcriptional reprogramming across infection levels, dominated by repression of apoptosis, oxidative metabolism, adhesion, and immune recognition pathways. Early infection triggered metabolic and immune activation, while advanced infection was marked by mitochondrial dysfunction and energy collapse. Many of the differentially expressed genes overlapped with functions enriched within the C8 inversion, linking genomic architecture to transcriptional resilience.

- **The integration of SNP validation, inversion discovery, and transcriptomic analyses** provides practical tools for the development of resistant oyster strains. Marker-assisted selection targeting C8 "orange" homokaryotypes can accelerate breeding programs, but it should be balanced with the maintenance of genetic diversity and local adaptation to ensure long-term sustainability of restoration programs.

USC
UNIVERSIDADE DE SANTIAGO DE COMPOSTELA

USC
UNIVERSIDADE
DE SANTIAGO
DE COMPOSTELA

REFERENCES

USC
UNIVERSIDADE
DE SANTIAGO
DE COMPOSTELA

USC
UNIVERSIDADE
DE SANTIAGO
DE COMPOSTELA

Abdallah, S. (2021). Transcriptomic characterization of hemocytes from different body fluids of the eastern oyster, *Crassostrea virginica* (Order No. 28541491). Available from ProQuest Dissertations & Theses Global. (2544922523). Retrieved from https://www.proquest.com/dissertations-theses/transcriptomic-characterization-hemocytes/docview/2544922523/se-2

Acarli, S., Lök, A., Küçükdermenci, A., Yildiz, H., & Serdar, S. (2011). Comparative growth, survival and condition index of flat oyster, *Ostrea edulis* (Linnaeus 1758) in Mersin Bay, aegean sea, Turkey. *Kafkas Universitesi Veteriner Fakultesi Dergisi*, *17*(2), 203–210. https://app.trdizin.gov.tr/makale/TVRFek5URTNOdz09/comparative-growth-survival-and-condition-index-of-flat-oyster-ostrea-edulis-linnaeus-1758-in-mersin-bay-aegean-sea-turkey

Adhya, M., Jeung, H., Kang, H., Choi, K., Lee, D. S., & Cho, M. (2012). Cloning and localization of MCdef, a defensin from Manila clams (*Ruditapes philippinarum*). *Comparative Biochemistry and Physiology Part B Biochemistry and Molecular Biology*, *161*(1), 25-31. https://doi.org/10.1016/j.cbpb.2011.09.003

Adkins, P., & Mrowicki, R. (2023). The genome sequence of the European flat oyster, *Ostrea edulis* (Linnaeus, 1758). *Wellcome Open Research*, *8*, 556. https://doi.org/10.12688/wellcomeopenres.19916.1

Ahmed, H., Schott, E. J., Gauthier, J. D., & Vasta, G. R. (2003). Superoxide dismutases from the oyster parasite *Perkinsus marinus*: purification, biochemical characterization, and development of a plate microassay for activity. *Analytical Biochemistry*, *318*(1), 132-141. https://doi.org/10.1016/s0003-2697(03)00192-1

Albentosa, M., Akinyemi, M. I., Vera, M., Ibarrola, I., Filgueira, R., Galimany, E., Da Costa, F., Pardo, B. G., Vázquez-Luis, M., Hernández, A., Hernandis, S., & Martínez, P. (2023). Recovery of eutrophized marine ecosystems using the European flat oyster, *Ostrea edulis*. *Aquatic Conservation Marine and Freshwater Ecosystems*, *33*(7), 645–660. https://doi.org/10.1002/aqc.3926

Allam, B., & Paillard, C. (1998). Defense factors in clam extrapallial fluids. *Diseases of Aquatic Organisms*, *33*, 123-128. https://doi.org/10.3354/dao033123

Allam, B., Ashton-Alcox, K., & Ford, S. (2002). Flow cytometric comparison of haemocytes from three species of bivalve molluscs. *Fish & Shellfish Immunology*, *13*(2), 141-158. https://doi.org/10.1006/fsim.2001.0389

Allam, B., Pales Espinosa, E., Tanguy, A., Jeffroy, F., Bris, C. L., & Paillard, C. (2014). Transcriptional changes in Manila clam (*Ruditapes philippinarum*) in response to Brown Ring Disease. *Fish & Shellfish Immunology*, *41*(1), 2-11. https://doi.org/10.1016/j.fsi.2014.05.022

Allam, B., & Raftos, D. (2015). Immune responses to infectious diseases in bivalves. *Journal of Invertebrate Pathology*, *131*, 121-136. https://doi.org/10.1016/j.jip.2015.05.005

Allam, B., & Pales Espinosa, E. (2016). Bivalve immunity and response to infections: Are we looking at the right place? *Fish & Shellfish Immunology*, *53*, 4-12. https://doi.org/10.1016/j.fsi.2016.03.037

Altschul, S. F., Gish, W., Miller, W., Myers, E. W., & Lipman, D. J. (1990). Basic local alignment search tool. *Journal of Molecular Biology*, *215*(3), 403–410. https://doi.org/10.1016/s0022-2836(05)80360-2

Anderson, R. S. (1994). Hemocyte-derived reactive oxygen intermediate production in four bivalve mollusks. *Developmental & Comparative Immunology*, *18*(2), 89-96. https://doi.org/10.1016/0145-305x(94)90237-2

Anderson, R. & Baeaven, A. (2001). Antibacterial activities of oyster (*Crassostrea virginica*) and mussel (*Mytilus edulis* and *Geukensia demissa*) plasma. *Aquatic Living Resources*, *14*(6), 343-349. https://doi.org/10.1016/s0990-7440(01)01143-3

Andrews, S. (2010). FastQC: A quality control tool for high throughput sequence data. Available online at: http://www.bioinformatics.babraham.ac.uk/projects/fastqc/

Anyanful, A., Easley, K. A., Benian, G. M., & Kalman, D. (2009). Conditioning protects *C. elegans* from lethal effects of enteropathogenic *E. coli* by activating genes that regulate lifespan and innate immunity. *Cell Host & Microbe*, *5*(5), 450–462. https://doi.org/10.1016/j.chom.2009.04.012

Arzul, I., Miossec, L., Blanchet, E., Garcia, C., Francois, C., & Joly, J. (2006). *Bonamia ostreae* and *Ostrea edulis:* a stable host-parasite system in France? *Proceedings of the 11th International Symposium on Veterinary Epidemiology and Economics, 2006* https://archimer.ifremer.fr/doc/00000/6381/

Arzul, I., Gagnaire, B., Bond, C., Chollet, B., Morga, B., Ferrand, S., Robert, M., & Renault, T. (2009). Effects of temperature and salinity on the survival of *Bonamia ostreae*, a parasite infecting flat oysters *Ostrea edulis*. *Diseases of Aquatic Organisms*, *85*, 67-75. https://doi.org/10.3354/dao02047

Arzul, I., Langlade, A., Chollet, B., Robert, M., Ferrand, S., Omnes, E., Lerond, S., Couraleau, Y., Joly, J., François, C., & Garcia, C. (2011). Can the protozoan parasite *Bonamia ostreae* infect larvae of flat oysters *Ostrea edulis*? *Veterinary Parasitology*, *179*(1–3), 69–76. https://doi.org/10.1016/j.vetpar.2011.01.060

Astrup, P. M., Skriver, C., Benjamin, J., Stankiewicz, F., Ward, I., McCarthy, J., Ross, P., Baggaley, P., Ulm, S., & Bailey, G. (2019). Underwater shell middens: excavation and remote sensing of a submerged Mesolithic site at Hjarnø, Denmark. *The Journal of Island and Coastal Archaeology*, *15*(4), 457-476. https://doi.org/10.1080/15564894.2019.1584135

Audemard, C., Carnegie, R. B., Bishop, M. J., Peterson, C. H., & Burreson, E. M. (2008). Interacting effects of temperature and salinity on *Bonamia* sp. parasitism in the Asian oyster *Crassostrea ariakensis*. *Journal of Invertebrate Pathology*, *98*(3), 344-350. https://doi.org/10.1016/j.jip.2008.03.010

Bachère, E., Gueguen, Y., Gonzalez, M., De Lorgeril, J., Garnier, J., & Romestand, B. (2004). Insights into the anti-microbial defense of marine invertebrates: the penaeid shrimps and the oyster *Crassostrea gigas*. *Immunological Reviews*, *198*(1), 149–168. https://doi.org/10.1111/j.0105-2896.2004.00115.x

Bachère, E., Rosa, R. D., Schmitt, P., Poirier, A. C., Merou, N., Charrière, G. M., & Destoumieux-Garzón, D. (2015). The new insights into the oyster antimicrobial defense: Cellular, molecular and genetic view. *Fish & Shellfish Immunology*, *46*(1), 50-64. https://doi.org/10.1016/j.fsi.2015.02.040

Barber, G. N. (2011). Innate immune DNA sensing pathways: STING, AIMII and the regulation of interferon production and inflammatory responses. *Current Opinion in Immunology*, *23*(1), 10–20. https://doi.org/10.1016/j.coi.2010.12.015

Baxter, G., & Morse, D. E. (1987). G protein and diacylglycerol regulate metamorphosis of planktonic molluscan larvae. *Proceedings of the National Academy of Sciences*, *84*(7), 1867–1870. https://doi.org/10.1073/pnas.84.7.1867

Bayne, B. L. (2017). *Biology of Oysters (ISSN Book 41) (English Edition)* (1.ª ed., Vol. 41). Academic Press.

Beck, M. W., Brumbaugh, R. D., Airoldi, L., Carranza, A., Coen, L. D., Crawford, C., Defeo, O., Edgar, G. J., Hancock, B., Kay, M. C., Lenihan, H. S., Luckenbach, M. W., Toropova, C. L., Zhang, G., & Guo, X. (2011). Oyster reefs at risk and recommendations for conservation, restoration, and management. *BioScience*, *61*(2), 107–116. https://doi.org/10.1525/bio.2011.61.2.5

Bennema, F. P., Engelhard, G. H., & Lindeboom, H. (2020). *Ostrea edulis* beds in the central North Sea: delineation, ecology, and restoration. *ICES Journal of Marine Science*, *77*(7-8), 2694-2705. https://doi.org/10.1093/icesjms/fsaa134

Berdan, E. L., Blanckaert, A., Butlin, R. K., & Bank, C. (2021). Deleterious mutation accumulation and the long-term fate of chromosomal inversions. *PLoS Genetics*, *17*(3), e1009411. https://doi.org/10.1371/journal.pgen.1009411

Berdan, E. L., Blanckaert, A., Butlin, R. K., Flatt, T., Slotte, T., & Wielstra, B. (2022). Mutation accumulation opposes polymorphism: supergenes and the curious case of balanced lethals. *Philosophical Transactions of The Royal Society B Biological Sciences*, *377*(1856), 20210199. https://doi.org/10.1098/rstb.2021.0199

Berdan, E. L., Barton, N. H., Butlin, R., Charlesworth, B., Faria, R., Fragata, I., Gilbert, K. J., Jay, P., Kapun, M., Lotterhos, K. E., Mérot, C., Mitchell, E. D., Pascual, M., Peichel, C. L., Rafajlović, M., Westram, A. M., Schaeffer, S. W., Johannesson, K., & Flatt, T. (2023). How chromosomal inversions reorient the evolutionary process. *Journal of Evolutionary Biology*, *36*(12), 1761-1782. https://doi.org/10.1111/jeb.14242

USC UNIVERSIDADE DE SANTIAGO DE COMPOSTELA

Berg, P. R., Star, B., Pampoulie, C., Sodeland, M., Barth, J. M. I., Knutsen, H., Jakobsen, K. S., & Jentoft, S. (2016). Three chromosomal rearrangements promote genomic divergence between migratory and stationary ecotypes of Atlantic cod. *Scientific Reports*, *6*(1), 23246. https://doi.org/10.1038/srep23246

Berghahn, R., & Ruth, M. (2005). The disappearance of oysters from the Wadden Sea: a cautionary tale for no-take zones. *Aquatic Conservation: Marine and Freshwater Ecosystems*, *15*(1), 91-104. https://doi.org/10.1002/aqc.635

Black, K. L., Rippe, J. P., & Matz, M. V. (2025). Environmental drivers of genetic divergence in two corals from the Florida Keys. *Evolutionary Applications*, *18*(7), e70126. https://doi.org/10.1111/eva.70126

Bonham, V., & Roberts, D. (2022). *Ostrea edulis* (European oyster). In *CABI Compendium*. https://doi.org/10.1079/cabicompendium.71177

Boutet, I., Monteiro, H. J. A., Baudry, L., Takeuchi, T., Bonnivard, E., Billoud, B., Farhat, S., Gonzales-Araya, R., Salaun, B., Andersen, A. C., Toullec, J., Lallier, F. H., Flot, J., Guiglielmoni, N., Guo, X., Li, C., Allam, B., Pales-Espinosa, E., Hemmer-Hansen, J., Moreau, P., Marbouty, M., Koszul, R., & Tanguy, A. (2022). Chromosomal assembly of the flat oyster (*Ostrea edulis* L.) genome as a new genetic resource for aquaculture. *Evolutionary Applications*, *15*(11), 1730-1748. https://doi.org/10.1111/eva.13462

Bowden, T. J., Kraev, I., & Lange, S. (2020). Extracellular Vesicles and Post-Translational Protein Deimination Signatures in Mollusca—The Blue Mussel (*Mytilus edulis*), Soft Shell Clam (*Mya arenaria*), Eastern Oyster (*Crassostrea virginica*) and Atlantic Jacknife Clam (*Ensis leei*). *Biology*, *9*(12), 416. https://doi.org/10.3390/biology9120416

Boyd, P. J., Walker, R. J., & Osborne, N. N. (1986). Actions of substance P on central neurones and peripheral tissues, and co-existence of 5-hydroxytryptamine and a substance p-like peptide in the heart of the snail *Helix aspersa*. *Neurochemistry International*, *8*(3), 345–353. https://doi.org/10.1016/0197-0186(86)90008-2

Calcino, A. D., Kenny, N. J., & Gerdol, M. (2021). Single individual structural variant detection uncovers widespread hemizygosity in molluscs. *Philosophical Transactions of The Royal Society B Biological Sciences*, *376*(1825), 20200153. https://doi.org/10.1098/rstb.2020.0153

Callaway, R., Engelhard, G., Dann, J., Cotter, J., & Rumohr, H. (2007). A century of North Sea epibenthos and trawling: comparison between 1902-1912, 1982-1985 and 2000. *Marine Ecology Progress Series*, *346*, 27-43. https://doi.org/10.3354/meps07038

Canesi, L., Gallo, G., Gavioli, M., & Pruzzo, C. (2002). Bacteria–hemocyte interactions and phagocytosis in marine bivalves. *Microscopy Research and Technique*, *57*(6), 469-476. https://doi.org/10.1002/jemt.10100

Canesi, L., Auguste, M., Balbi, T., & Prochazkova, P. (2022). Soluble mediators of innate immunity in annelids and bivalve mollusks: A mini-review. *Frontiers in Immunology*, *13,* 1051155. https://doi.org/10.3389/fimmu.2022.1051155

Carballeira, C., Ramos-Gómez, J., Martín-Díaz, L., & Del Valls, T. (2012). Identification of specific malformations of sea urchin larvae for toxicity assessment: Application to marine pisciculture effluents. *Marine Environmental Research*, *77*, 12-22. https://doi.org/10.1016/j.marenvres.2012.01.001

Carnegie, R. B., & Cochennec-Laureau, N. (2004). Microcell parasites of oysters: Recent insights and future trends. *Aquatic Living Resources*, *17*(4), 519-528. https://doi.org/10.1051/alr:2004055

Castellanos-Martínez, S., Arteta, D., Catarino, S., & Gestal, C. (2014). De novo transcriptome sequencing of the *Octopus vulgaris* hemocytes using Illumina RNA-Seq technology: response to the infection by the gastrointestinal parasite *Aggregata octopiana*. *PLoS ONE*, *9*(10), e107873. https://doi.org/10.1371/journal.pone.0107873

Catanach, A., Crowhurst, R., Deng, C., David, C., Bernatchez, L., & Wellenreuther, M. (2019). The genomic pool of standing structural variation outnumbers single nucleotide polymorphism by threefold in the marine teleost *Chrysophrys auratus*. *Molecular Ecology*, *28*(6), 1210-1223. https://doi.org/10.1111/mec.15051

Cavalcanti, M., Filho, F., Mendonça, A., Duarte, G., Barbosa, C., De Castro, C., Alves, L., & Brayner, F. (2012). Morphological characterization of hemocytes from *Biomphalaria glabrata* and *Biomphalaria straminea*. *Micron*, *43*(2-3), 285-291. https://doi.org/10.1016/j.micron.2011.09.002

Chagot, D., Boulo, V., Hervio, D., Mialhe, E., Bachere, E., Mourton, C., & Grizel, H. (1992). Interactions between *Bonamia ostreae* (Protozoa: Ascetospora) and hemocytes of *Ostrea edulis* and *Crassostrea gigas* (Mollusca: Bivalvia): Entry mechanisms. *Journal of Invertebrate Pathology*, *59*(3), 241–249. https://doi.org/10.1016/0022-2011(92)90128-q

Chambers, L. G., Gaspar, S. A., Pilato, C. J., Steinmuller, H. E., McCarthy, K. J., Sacks, P. E., & Walters, L. J. (2017). How well do restored intertidal oyster reefs support key biogeochemical properties in a Coastal Lagoon? *Estuaries And Coasts*, *41*(3), 784-799. https://doi.org/10.1007/s12237-017-0311-5

Chan, C. Y., & Wang, W. (2019). Biomarker responses in oysters *Crassostrea hongkongensis* in relation to metal contamination patterns in the Pearl River Estuary, southern China. *Environmental Pollution*, *251*, 264-276. https://doi.org/10.1016/j.envpol.2019.04.140

Chang, C. C., Chow, C. C., Tellier, L. C., Vattikuti, S., Purcell, S. M., & Lee, J. J. (2015). Second-generation PLINK: rising to the challenge of larger and richer datasets. *GigaScience*, *4*(1), 7. https://doi.org/10.1186/s13742-015-0047-8

Cheng, T. C. (1975). Functional morphology morphology and biochemistry of molluscan phagocytes*. *Annals of the New York Academy of Sciences*, *266*(1), 343–379. https://doi.org/10.1111/j.1749-6632.1975.tb35116.x

USC UNIVERSIDADE DE SANTIAGO DE COMPOSTELA

Cheng, T. C. (1996). Hemocytes: forms and functions. In: Newell, R.I.E., Kennedy, V.S., Eble, A.F. (Eds.), *The eastern oyster Crassostrea virginica*, Maryland Sea Grant College, Bethesda, Maryland, pp. 299-334.

Cheng, T. C., & Howland, K. H. (1979). Chemotactic attraction between hemocytes of the oyster, *Crassostrea virginica*, and bacteria. *Journal of Invertebrate Pathology*, *33*(2), 204-210. https://doi.org/10.1016/0022-2011(79)90154-x

Chevignon, G., Dotto-Maurel, A., Serpin, D., Chollet, B., & Arzul, I. (2022). De novo transcriptome assembly and analysis of the flat oyster pathogenic protozoa *Bonamia ostreae*. *Frontiers in Cellular and Infection Microbiology*, *12,* 921136. https://doi.org/10.3389/fcimb.2022.921136

Christianen, M. J. A., Lengkeek, W., Bergsma, J. H., Coolen, J. W. P., Didderen, K., Dorenbosch, M., Driessen, F. M. F., Kamermans, P., Reuchlin-Hugenholtz, E., Sas, H., Smaal, A., Van Den Wijngaard, K. A., & Van Der Have, T. M. (2018). Return of the native facilitated by the invasive? Population composition, substrate preferences and epibenthic species richness of a recently discovered shellfish reef with native European flat oysters (*Ostrea edulis*) in the North Sea. *Marine Biology Research*, *14*(6), 590–597. https://doi.org/10.1080/17451000.2018.1498520

Clark, D., Stephenson, F., Hewitt, J., Ellis, J., Zaiko, A., Berthelsen, A., Bulmer, R., & Pilditch, C. (2021). Influence of land-derived stressors and environmental variability on compositional turnover and diversity of estuarine benthic communities. *Marine Ecology Progress Series*, *666*, 1-18. https://doi.org/10.3354/meps13714

Classen, R (2020). Marine Protected Areas – Restoring Ireland's Ocean Wildlife II. Report on Ireland's Failure to Protect Marine Natura 2000 Sites. *Irish Wildlife Trust*.

Cochennec-Laureau, N., Auffret, M., Renault, T., & Langlade, A. (2003). Changes in circulating and tissue-infiltrating hemocyte parameters of European flat oysters, *Ostrea edulis*, naturally infected with *Bonamia ostreae*. *Journal of Invertebrate Pathology*, *83*(1), 23-30. https://doi.org/10.1016/s0022-2011(03)00015-6

Coles, J., Farley, S., & Pipe, R. (1995). Alteration of the immune response of the common marine mussel *Mytilus edulis* resulting from exposure to cadmium. *Diseases of Aquatic Organisms*, *22*, 59-65. https://doi.org/10.3354/dao022059

Colsoul, B., Boudry, P., Pérez-Parallé, M. L., Cetinić, A. B., Hugh-Jones, T., Arzul, I., Mérou, N., Wegner, K. M., Peter, C., Merk, V., & Pogoda, B. (2021). Sustainable large-scale production of European flat oyster (*Ostrea edulis*) seed for ecological restoration and aquaculture: a review. *Reviews in Aquaculture*, *13*(3), 1423–1468. https://doi.org/10.1111/raq.12529

USC UNIVERSIDADE DE SANTIAGO DE COMPOSTELA

Colsoul, B., Pouvreau, S., Di Poi, C., Pouil, S., Merk, V., Peter, C., Boersma, M., & Pogoda, B. (2021). Addressing critical limitations of oyster (*Ostrea edulis*) restoration: Identification of nature-based substrates for hatchery production and recruitment in the field. *Aquatic Conservation Marine and Freshwater Ecosystems*, *30*(11), 2101–2115. https://doi.org/10.1002/aqc.3454

Comesaña, P., Casas, S. M., Cao, A., Abollo, E., Arzul, I., Morga, B., & Villalba, A. (2012). Comparison of haemocytic parameters among flat oyster *Ostrea edulis* stocks with different susceptibility to bonamiosis and the Pacific oyster *Crassostrea gigas*. *Journal of Invertebrate Pathology*, *109*(3), 274-286. https://doi.org/10.1016/j.jip.2011.12.007

Comps, M., Tigé, G., & Grizel, H. (1980). Etude ultrastructurale d'un protiste parasite de l'huître *Ostrea edulis* L. L.C.R., Acad. Sc. Paris, Sér. D, 290, 383–385.

Culloty, S. C., & Mulcahy, M. F. (1996). Season-, age-, and sex-related variation in the prevalence of bonamiasis in flat oysters (*Ostrea edulis* L.) on the south coast of Ireland. *Aquaculture*, *144*(1-3), 53-63. https://doi.org/10.1016/s0044-8486(96)01290-2

Culloty, S., Cronin, M., & Mulcahy, M. (2004). Potential resistance of a number of populations of the oyster *Ostrea edulis* to the parasite *Bonamia ostreae*. *Aquaculture*, *237*(1-4), 41-58. https://doi.org/10.1016/j.aquaculture.2004.04.007

Culloty, S. C., & Mulcahy, M. F. (2007). *Bonamia ostreae* in the Native Oyster *Ostrea edulis*. *Marine Environment and Health Series* No. 29, Marine Institute. http://hdl.handle.net/10793/269

Da Silva, P. M., Fuentes, J., & Villalba, A. (2005). Growth, mortality and disease susceptibility of oyster *Ostrea edulis* families obtained from brood stocks of different geographical origins, through on-growing in the Ría de Arousa (Galicia, NW Spain). *Marine Biology*, *147*(4), 965–977. https://doi.org/10.1007/s00227-005-1627-4

Da Silva, P., Renault, T., Fuentes, J., & Villalba, A. (2008). Herpesvirus infection in European flat oysters *Ostrea edulis* obtained from brood stocks of various geographic origins and grown in Galicia (NW Spain). *Diseases of Aquatic Organisms*, *78*, 181-188. https://doi.org/10.3354/dao01874

Da Silva, P. M., Fuentes, J., & Villalba, A. (2011). Disseminated neoplasia in flat oysters *Ostrea edulis* from Galicia (NW Spain): Occurrence, ultrastructural aspects and relationship with bonamiosis. *Journal of Invertebrate Pathology*, *107*(1), 50-59. https://doi.org/10.1016/j.jip.2011.01.001

Davidson, S. K., Koropatnick, T. A., Kossmehl, R., Sycuro, L., & McFall-Ngai, M. J. (2004). NO means «yes» in the squid-vibrio symbiosis: nitric oxide (NO) during the initial stages of a beneficial association. *Cellular Microbiology*, *6*(12), 1139-1151. https://doi.org/10.1111/j.1462-5822.2004.00429.x

USC UNIVERSIDADE DE SANTIAGO DE COMPOSTELA

De Coster, W., & Van Broeckhoven, C. (2019). Newest methods for detecting structural variations. *Trends in Biotechnology*, *37*(9), 973-982. https://doi.org/10.1016/j.tibtech.2019.02.003

De Coster, W., & Rademakers, R. (2023). NanoPack2: population-scale evaluation of long-read sequencing data. *Bioinformatics*, *39*(5), btad311. https://doi.org/10.1093/bioinformatics/btad311

De Mesel, I., Kapasakali, D., Kerckhof, F., Vigin, L., Lacroix, G., Barbut, L., & Degraer S. (2018). *Ostrea edulis* restoration in the Belgian part of the North Sea: Feasibility study. In: *World Aquaculture Society Meeting* (Aqua 2018), 25-29 August 2018, Montpellier, France.

Dégremont, L., Garcia, C., & Allen, S. K. (2015). Genetic improvement for disease resistance in oysters: A review. *Journal of Invertebrate Pathology*, *131*, 226-241. https://doi.org/10.1016/j.jip.2015.05.010

Delisle, L., Petton, B., Burguin, J. F., Morga, B., Corporeau, C., & Pernet, F. (2018). Temperature modulate disease susceptibility of the Pacific oyster *Crassostrea gigas* and virulence of the Ostreid herpesvirus type 1. *Fish & Shellfish Immunology*, *80*, 71-79. https://doi.org/10.1016/j.fsi.2018.05.056

Delisle, L., Pauletto, M., Vidal-Dupiol, J., Petton, B., Bargelloni, L., Montagnani, C., Pernet, F., Corporeau, C., & Fleury, E. (2020). High temperature induces transcriptomic changes in *Crassostrea gigas* that hinders progress of Ostreid herpesvirus (OsHV-1) and promotes survival. *Journal of Experimental Biology, 223*(Pt 20): jeb226233. https://doi.org/10.1242/jeb.226233

Delprat, A., Negre, B., Puig, M., & Ruiz, A. (2009). The transposon galileo generates natural chromosomal inversions in drosophila by ectopic recombination. *PLoS ONE*, *4*(11), e7883. https://doi.org/10.1371/journal.pone.0007883

Deretic, V., & Levine, B. (2009). Autophagy, immunity, and microbial adaptations. *Cell Host & Microbe*, *5*(6), 527-549. https://doi.org/10.1016/j.chom.2009.05.016

Diaz-Almela, E., Boudry, P., Launey, S., Bonhomme, F., & Lapègue, S. (2004). Reduced female gene flow in the European flat oyster *Ostrea edulis*. *Journal of Heredity*, *95*(6), 510–516. https://doi.org/10.1093/jhered/esh073

Dobin, A., Davis, C. A., Schlesinger, F., Drenkow, J., Zaleski, C., Jha, S., Batut, P., Chaisson, M., & Gingeras, T. R. (2013). STAR: ultrafast universal RNA-seq aligner. *Bioinformatics*, *29*(1), 15-21. https://doi.org/10.1093/bioinformatics/bts635

Dobzhansky, T. (1970). Genetics of the evolutionary process. *Columbia University Press*, *139*.

USC UNIVERSIDADE DE SANTIAGO DE COMPOSTELA

Doma, E., Chakrabandhu, K., & Hueber, A. (2010). A novel role of microtubular cytoskeleton in the dynamics of caspase-dependent Fas/CD95 death receptor complexes during apoptosis. *FEBS Letters*, *584*(5), 1033-1040. https://doi.org/10.1016/j.febslet.2010.01.059

Donaghy, L., Hong, H., Jauzein, C., & Choi, K. (2015). The known and unknown sources of reactive oxygen and nitrogen species in haemocytes of marine bivalve molluscs. *Fish & Shellfish Immunology*, *42*(1), 91-97. https://doi.org/10.1016/j.fsi.2014.10.030

Dove, A. D. M., Bowser, P. R., & Cerrato, R. M. (2004). Histological analysis of an outbreak of QPX disease in wild hard clams *Mercenaria mercenaria* in New York. *Journal of Aquatic Animal Health*, *16*(4), 246-250. https://doi.org/10.1577/h03-052.1

Duncan, M. K., Kos, L., Jenkins, N. A., Gilbert, D. J., Copeland, N. G., & Tomarev, S. I. (1997). Eyes absent: A gene family found in several metazoan phyla. *Mammalian Genome*, *8*(7), 479–485. https://doi.org/10.1007/s003359900480

Ellis, J. A., & Ong, B. (2017). The MassARRAY® system for targeted SNP genotyping. *Methods in Molecular Biology*, *1492*, 77–94. https://doi.org/10.1007/978-1-4939-6442-0_5

Elston, R., Kent, M., & Wilkinson, M. (1987). Resistance of *Ostrea edulis* to *Bonamia ostreae* infection. *Aquaculture*, *64*(3), 237-242. https://doi.org/10.1016/0044-8486(87)90328-0

Encomio, V., & Chu, F. (2007). Heat shock protein (hsp70) expression and thermal tolerance in sublethally heat-shocked eastern oysters *Crassostrea virginica* infected with the parasite *Perkinsus marinus*. *Diseases of Aquatic Organisms*, *76*, 251-260. https://doi.org/10.3354/dao076251

Engelsma, M., Kerkhoff, S., Roozenburg, I., Haenen, O., Van Gool, A., Sistermans, W., Wijnhoven, S., & Hummel, H. (2010). Epidemiology of *Bonamia ostreae* infecting European flat oysters *Ostrea edulis* from Lake Grevelingen, The Netherlands. *Marine Ecology Progress Series*, *409*, 131-142. https://doi.org/10.3354/meps08594

Engelsma, M., Culloty, S., Lynch, S., Arzul, I., & Carnegie, R. (2014). Bonamia parasites: a rapidly changing perspective on a genus of important mollusc pathogens. *Diseases of Aquatic Organisms*, *110*(1), 5-23. https://doi.org/10.3354/dao02741

Escoubas, J., Gourbal, B., Duval, D., Green, T. J., Charrière, G. M., Destoumieux-Garzón, D., & Montagnani, C. (2016). Immunity in Molluscs. In: Ratcliffe, J. H. (ed). *Encyclopedia of Immunology*. Academic Press. pp. 417-436. https://doi.org/10.1016/b978-0-12-374279-7.12004-1

Eskelinen, E.L. (2008). Fine structure of the Autophagosome. In: Deretic, V. (ed) *Autophagosome and Phagosome. Methods in Molecular Biology*™, vol 445. Humana Press. pp: 11-28. https://doi.org/10.1007/978-1-59745-157-4_2

USC UNIVERSIDADE DE SANTIAGO DE COMPOSTELA

Eskelinen, E., Schmidt, C. K., Neu, S., Willenborg, M., Fuertes, G., Salvador, N., Tanaka, Y., Lüllmann-Rauch, R., Hartmann, D., Heeren, J., Von Figura, K., Knecht, E., & Saftig, P. (2004). Disturbed cholesterol traffic but normal proteolytic function in LAMP-1/LAMP-2 double-deficient fibroblasts. *Molecular Biology of The Cell*, *15*(7), 3132-3145. https://doi.org/10.1091/mbc.e04-02-0103

Estévez-Calvar, N., Romero, A., Figueras, A., & Novoa, B. (2013). Genes of the mitochondrial apoptotic pathway *in Mytilus galloprovincialis*. *PLoS ONE*, *8*(4), e61502. https://doi.org/10.1371/journal.pone.0061502

Evanno, G., Regnaut, S., & Goudet, J. (2005). Detecting the number of clusters of individuals using the software structure: a simulation study. *Molecular Ecology*, *14*(8), 2611–2620. https://doi.org/10.1111/j.1365-294x.2005.02553.x

Evgen'ev, M. B., Zelentsova, H., Poluectova, H., Lyozin, G. T., Veleikodvorskaja, V., Pyatkov, K. I., Zhivotovsky, L. A., & Kidwell, M. G. (2000). Mobile elements and chromosomal evolution in the virilis group of Drosophila. *Proceedings of The National Academy of Sciences*, *97*(21), 11337-11342. https://doi.org/10.1073/pnas.210386297

Ewels, P. A., Peltzer, A., Fillinger, S., Patel, H., Alneberg, J., Wilm, A., Garcia, M. U., Di Tommaso, P., & Nahnsen, S. (2020). The nf-core framework for community-curated bioinformatics pipelines. *Nature Biotechnology*, *38*(3), 276-278. https://doi.org/10.1038/s41587-020-0439-x

Ezgeta-Balić, D., Šantić, D., Šegvić-Bubić, T., Bojanić, N., Bužančić, M., Vidjak, O., Varezić, D., Stagličić, N., Kundid, P., Peharda, M., Žužul, I., Grubišić, L., & Briski, E. (2020). Competitive feeding interactions between native *Ostrea edulis* and non-native *Crassostrea gigas* with implications of introducing *C. gigas* into commercial aquaculture in the eastern Adriatic Sea. *Marine Environmental Research*, *160*, 105051. https://doi.org/10.1016/j.marenvres.2020.105051

Fallet, M., Montagnani, C., Petton, B., Dantan, L., De Lorgeril, J., Comarmond, S., Chaparro, C., Toulza, E., Boitard, S., Escoubas, J., Vergnes, A., Grand, J. L., Bulla, I., Gueguen, Y., Vidal-Dupiol, J., Grunau, C., Mitta, G., & Cosseau, C. (2022). Early life microbial exposures shape the *Crassostrea gigas* immune system for lifelong and intergenerational disease protection. *Microbiome*, *10*(1), 85. https://doi.org/10.1186/s40168-022-01280-5

Fang, F. C. (2004). Antimicrobial reactive oxygen and nitrogen species: concepts and controversies. *Nature Reviews Microbiology*, *2*(10), 820-832. https://doi.org/10.1038/nrmicro1004

FAO. (2020). *The state of world fisheries and aquaculture 2020. Sustainability in action*. FAO. https://doi.org/10.4060/ca9229en

Faria, R., Johannesson, K., Butlin, R. K., & Westram, A. M. (2019). Evolving inversions. *Trends in Ecology & Evolution*, *34*(3), 239-248. https://doi.org/10.1016/j.tree.2018.12.005

Fernández-Boo, S., Gervais, O., Prado-Alvarez, M., Chollet, B., Claverol, S., Lecadet, C., Dubreuil, C., & Arzul, I. (2019). Is pallial mucus involved in *Ostrea edulis* defenses against the parasite *Bonamia ostreae*? *Journal of Invertebrate Pathology*, *169*, 107259. https://doi.org/10.1016/j.jip.2019.107259

Ferreira, J., Hawkins, A., Monteiro, P., Moore, H., Service, M., Pascoe, P., Ramos, L., & Sequeira, A. (2008). Integrated assessment of ecosystem-scale carrying capacity in shellfish growing areas. *Aquaculture*, *275*(1-4), 138-151. https://doi.org/10.1016/j.aquaculture.2007.12.018

Flannery, G., Lynch, S. A., Carlsson, J., Cross, T. F., & Culloty, S. C. (2014). Assessment of the impact of a pathogen, *Bonamia ostreae*, on *Ostrea edulis* oyster stocks with different histories of exposure to the parasite in Ireland. *Aquaculture*, *432*, 243-251. https://doi.org/10.1016/j.aquaculture.2014.04.038

Foll, M., & Gaggiotti, O. (2008). A Genome-Scan method to identify selected loci appropriate for both dominant and codominant markers: A Bayesian perspective. *Genetics*, *180*(2), 977–993. https://doi.org/10.1534/genetics.108.092221

Ford, S. E., Kanaley, S. A., & Littlewood, D. (1993). Cellular responses of oysters infected with *Haplosporidium nelsoni*: changes in circulating and tissue-infiltrating hemocytes. *Journal of Invertebrate Pathology*, *61*(1), 49-57. https://doi.org/10.1006/jipa.1993.1009

Gatta, P. P. (2022). The State of World Fisheries and Aquaculture 2022. En *FAO eBooks*. https://doi.org/10.4060/cc0461en

Genthner, F. J., Volety, A. K., Oliver, L. M., & Fisher, W. S. (1999). Factors influencing in vitro killing of bacteria by hemocytes of the Eastern oyster (*Crassostrea virginica*). *Applied and Environmental Microbiology*, *65*(7), 3015-3020. https://doi.org/10.1128/aem.65.7.3015-3020.1999

Gerdol, M., Manfrin, C., De Moro, G., Figueras, A., Novoa, B., Venier, P., & Pallavicini, A. (2011). The C1q domain containing proteins of the Mediterranean mussel *Mytilus galloprovincialis*: A widespread and diverse family of immune-related molecules. *Developmental & Comparative Immunology*, *35*(6), 635-643. https://doi.org/10.1016/j.dci.2011.01.018

González, J. R., Armengol, L., Solé, X., Guinó, E., Mercader, J. M., Estivill, X., & Moreno, V. (2007). SNPassoc: an R package to perform whole genome association studies. *Bioinformatics*, *23*(5), 654-655. https://doi.org/10.1093/bioinformatics/btm025

Gordy, M. A., Pila, E. A., & Hanington, P. C. (2015). The role of fibrinogen-related proteins in the gastropod immune response. *Fish & Shellfish Immunology*, *46*(1), 39–49. https://doi.org/10.1016/j.fsi.2015.03.005

Gosling, E. (2015). *Marine bivalve molluscs*. 2nd Edition, Wiley-Blackwell, Hoboken, 258. http://dx.doi.org/10.1002/9781119045212

Gourbal, B., Pinaud, S., Beckers, G. J. M., Van Der Meer, J. W. M., Conrath, U., & Netea, M. G. (2018). Innate immune memory: An evolutionary perspective. *Immunological Reviews*, *283*(1), 21-40. https://doi.org/10.1111/imr.12647

Grant, J., Enright, C. T., & Griswold, A. (1990). Resuspension and growth of *Ostrea edulis*: A field experiment. *Marine Biology*, *104*(1), 51-59. https://doi.org/10.1007/bf01313157

Green, T. J., & Montagnani, C. (2013). Poly I:C induces a protective antiviral immune response in the Pacific oyster (*Crassostrea gigas*) against subsequent challenge with Ostreid herpesvirus (OsHV-1 µvar). *Fish & Shellfish Immunology*, *35*(2), 382-388. https://doi.org/10.1016/j.fsi.2013.04.051

Green, T. J., Vergnes, A., Montagnani, C., & De Lorgeril, J. (2016). Distinct immune responses of juvenile and adult oysters (*Crassostrea gigas*) to viral and bacterial infections. *Veterinary Research*, *47*(1), 72. https://doi.org/10.1186/s13567-016-0356-7

Grishaeva, T. M., & Bogdanov, Y. F. (2014). Conservation and variability of synaptonemal complex proteins in phylogenesis of eukaryotes. *International Journal of Evolutionary Biology*, *2014*, 1–16. https://doi.org/10.1155/2014/856230

Grizel H. (1985). Etude des récentes épizooties de l'huître plate Ostrea edulis L. et de leur impact sur l'ostréiculture bretonne. Thèse de doctorat, Université des Sciences et Techniques de Languedoc, Montpellier, France.

Grote, S (2024). *Grote S. GOfuncR: Gene Ontology enrichment using FUNC. R package version 1.26.0.*

Gundappa, M. K., Peñaloza, C., Regan, T., Boutet, I., Tanguy, A., Houston, R. D., Bean, T. P., & Macqueen, D. J. (2022). Chromosome-level reference genome for European flat oyster (*Ostrea edulis* L.). *Evolutionary Applications*, *15*(11), 1713-1729. https://doi.org/10.1111/eva.13460

Gutierrez, A., Turner, F., Gharbi, K., Talbot, R., Lowe, N., Peñaloza, C., McCullough, M., Prodöhl, P., Bean, T., & Houston, R. (2017). Development of a medium density combined-species SNP array for Pacific and European oysters (*Crassostrea gigas* and *Ostrea edulis*). *G3 Genes|Genomes|Genetics*, *7*(7), 2209-2218. https://doi.org/10.1534/g3.117.041780

Haenen OLM., & Engelsma MY. 2020. Jaarverslag schelpdierziekten 2019; Resultaten van het onderzoek naar ziekten in schelpdierbestanden van het Grevelingenmeer en de Oosterschelde. Wageningen Bioveterinary Research, WBVR Report 2010660.

Han, F., Jamsandekar, M., Pettersson, M. E., Su, L., Fuentes-Pardo, A. P., Davis, B. W., Bekkevold, D., Berg, F., Casini, M., Dahle, G., Farrell, E. D., Folkvord, A., & Andersson, L. (2020). Ecological adaptation in Atlantic herring is associated with large shifts in allele frequencies at hundreds of loci. *eLife*, *9, e61076*. https://doi.org/10.7554/elife.61076

USC UNIVERSIDADE DE SANTIAGO DE COMPOSTELA

Hanlon, C. D., & Andrew, D. J. (2015). Outside-in signaling – a brief review of GPCR signaling with a focus on the *Drosophila* GPCR family. *Journal of Cell Science, 128,* 3533-3542. https://doi.org/10.1242/jcs.175158

Harrang, E., Heurtebise, S., Faury, N., Robert, M., Arzul, I., & Lapègue, S. (2015). Can survival of European flat oysters following experimental infection with *Bonamia ostreae* be predicted using QTLs? *Aquaculture*, *448*, 521-530. https://doi.org/10.1016/j.aquaculture.2015.06.019

Harris-Young, L., Tamplin, M. L., Mason, J. W., Aldrich, H. C., & Jackson, J. K. (1995). Viability of *Vibrio vulnificus* in association with hemocytes of the American oyster (*Crassostrea virginica*). *Applied and Environmental Microbiology*, *61*(1), 52-57. https://doi.org/10.1128/aem.61.1.52-57.1995

Haug, T., Stensvåg, K., Olsen, Ø. M., Sandsdalen, E., & Styrvold, O. B. (2004). Antibacterial activities in various tissues of the horse mussel, *Modiolus modiolus*. *Journal of Invertebrate Pathology*, *85*(2), 112-119. https://doi.org/10.1016/j.jip.2004.02.006

Hausmann, N., Robson, H. K., & Hunt, C. (2019). Annual growth patterns and interspecimen variability in Mg/Ca records of archaeological *Ostrea edulis* (European oyster) from the Late Mesolithic site of Conors Island. *Open Quaternary*, *5*, 9 https://doi.org/10.5334/oq.59

Hayden-Hughes, M., Bayford, P., King, J., & Smyth, D. (2023). The European native oyster, *Ostrea edulis*, in Wales, a historical account of a forgotten fishery. *Aquatic Living Resources*, *36*, 7. https://doi.org/10.1051/alr/2022024

Hayer, S., Brandis, D., Immel, A., Susat, J., Torres-Oliva, M., Ewers-Saucedo, C., & Krause-Kyora, B. (2021). Phylogeography in an "oyster" shell provides first insights into the genetic structure of an extinct *Ostrea edulis* population. *Scientific Reports*, *11*(1), 2307 https://doi.org/10.1038/s41598-021-82020-x

Helmer, L., Hauton, C., Bean, T., Bass, D., Hendy, I., Harris-Scott, E., & Preston, J. (2020). Ephemeral detection of *Bonamia exitiosa* (Haplosporida) in adult and larval European flat oysters *Ostrea edulis* in the Solent, United Kingdom. *Journal of Invertebrate Pathology*, *174*, 107421. https://doi.org/10.1016/j.jip.2020.107421

Hermann, P. M., Van Kesteren, R. E., Wildering, W. C., Painter, S. D., Reno, J. M., Smith, J. S., Kumar, S. B., Geraerts, W. P. M., Ericsson, L. H., Smit, A. B., Bulloch, A. G. M., & Nagle, G. T. (2000). Neurotrophic actions of a novel molluscan epidermal growth factor. *Journal of Neuroscience*, *20*(17), 6355–6364. https://doi.org/10.1523/jneurosci.20-17-06355.2000

Herpin, A., Badariotti, F., Rodet, F., & Favrel, P. (2004). Molecular characterization of a new leucine-rich repeat-containing G protein-coupled receptor from a bivalve mollusc: evolutionary implications. *Biochimica Et Biophysica Acta (BBA) - Gene Structure and Expression*, *1680*(3), 137–144. https://doi.org/10.1016/j.bbaexp.2004.09.003

USC DE COMPOSTELA

Hervio, D., Bachère, E., Boulo, V., Cochennec, N., Vuillemin, V., Coguic, Y. L., Cailletaux, G., Mazurié, J., & Mialhe, E. (1995). Establishment of an experimental infection protocol for the flat oyster, *Ostrea edulis*, with the intrahaemocytic protozoan parasite, *Bonamia ostreae*: application in the selection of parasite-resistant oysters. *Aquaculture*, *132*(3-4), 183-194. https://doi.org/10.1016/0044-8486(94)00342-l

Hine, P., & Wesney, B. (1995). Interaction of phagocytosed *Bonamia* sp. (Haplosporidia) with haemocytes of oysters *Tiostrea chilensis*. *Diseases of Aquatic Organisms*, *20*, 219-229. https://doi.org/10.3354/dao020219

Hoff, S. N., Maurstad, M., Tørresen, O. K., Berg, P. R., Præbel, K., Jakobsen, K. S., & Jentoft, S. (2024). Chromosomal fusions and large-scale inversions are key features for adaptation in Arctic codfish species. *bioRxiv (Cold Spring Harbor Laboratory)*. https://doi.org/10.1101/2024.06.28.599280

Hoffmann, A. A., & Rieseberg, L. H. (2008). Revisiting the impact of inversions in evolution: from population genetic markers to drivers of adaptive shifts and speciation? *Annual Review of Ecology Evolution and Systematics*, *39*(1), 21-42. https://doi.org/10.1146/annurev.ecolsys.39.110707.173532

Holbrook, Z., Bean, T. P., Lynch, S. A., & Hauton, C. (2021). What do the terms resistance, tolerance, and resilience mean in the case of *Ostrea edulis* infected by the haplosporidian parasite *Bonamia ostreae*. *Journal of Invertebrate Pathology*, *182*, 107579. https://doi.org/10.1016/j.jip.2021.107579

Hollenbeck, C. M., & Johnston, I. A. (2018). Genomic tools and selective breeding in molluscs. *Frontiers in Genetics*, *9,* 253. https://doi.org/10.3389/fgene.2018.00253

Hollenbeck, C. M., Portnoy, D. S., De la Serrana, D. G., Magnesen, T., Matejusova, I., & Johnston, I. A. (2022). Temperature-associated selection linked to putative chromosomal inversions in king scallop (*Pecten maximus*). *Proceedings of The Royal Society B Biological Sciences*, *289*(1984), 20221573. https://doi.org/10.1098/rspb.2022.1573

Huang, C., Ji, B., Shi, Z., Wang, J., Yuan, J., Yang, P., Xu, X., Jing, H., Xu, L., Fu, J., Zhao, L., Ren, Y., Guo, K., & Li, G. (2025). A comparative genomic analysis at the chromosomal-level reveals evolutionary patterns of aphid chromosomes. *Communications Biology*, *8*(1), 427. https://doi.org/10.1038/s42003-025-07851-0

Hudson, E., & Hill, B. (1991). Impact and spread of bonamiasis in the UK. *Aquaculture*, *93*(3), 279-285. https://doi.org/10.1016/0044-8486(91)90240-8

Humphries, J. E., & Yoshino, T. P. (2003). Cellular receptors and signal transduction in molluscan hemocytes: connections with the innate immune system of vertebrates. *Integrative and Comparative Biology*, *43*(2), 305-312. https://doi.org/10.1093/icb/43.2.305

USC UNIVERSIDADE DE SANTIAGO DE COMPOSTELA

Ishita, Y., Onodera, A., Ekino, T., Chihara, T., & Okumura, M. (2023). Co-option of an astacin metalloprotease is associated with an evolutionarily novel feeding morphology in a predatory nematode. *Molecular Biology and Evolution*, *40*(12), msad266. https://doi.org/10.1093/molbev/msad266

Itoh, H., Ishii, Y., Watari, T., Tokuda, N., & Tsuchiya, T. (2007). 38. Recordings of shell movements and tension changes *in vivo* in adductor of bivalve. *Comparative Biochemistry and Physiology Part B Biochemistry and Molecular Biology*, *148*(3), 351–352. https://doi.org/10.1016/j.cbpb.2007.07.076

Itoh, N., & Takahashi, K. G. (2009). A novel peptidoglycan recognition protein containing a goose-type lysozyme domain from the Pacific oyster, *Crassostrea gigas*. *Molecular Immunology*, *46*(8–9), 1768–1774. https://doi.org/10.1016/j.molimm.2009.01.022

Jacobs, P., Greeve, Y., Sikkema, M., Dubbeldam, M., & Philippart, C. J. (2020). Successful rearing of *Ostrea edulis* from parents originating from the Wadden Sea, the Netherlands. *Aquaculture Reports*, *18*, 100537. https://doi.org/10.1016/j.aqrep.2020.100537

Janeway, C. A. (1994). The role of microbial pattern recognition in self: nonself discrimination in innate and adaptive immunity. *Phylogenetic Perspectives in Immunity, the Insect Host Defence*, *1*(1), 115-122.

Jay, P., Chouteau, M., Whibley, A., Bastide, H., Parrinello, H., Llaurens, V., & Joron, M. (2021). Mutation load at a mimicry supergene sheds new light on the evolution of inversion polymorphisms. *Nature Genetics*, *53*(3), 288-293. https://doi.org/10.1038/s41588-020-00771-1

Jombart, T., & Ahmed, I. (2011). adegenet 1.3-1: new tools for the analysis of genome-wide SNP data. *Bioinformatics*, *27*(21), 3070–3071. https://doi.org/10.1093/bioinformatics/btr521

Jones, O. R., & Wang, J. (2010). COLONY: a program for parentage and sibship inference from multilocus genotype data. *Molecular Ecology Resources*, *10*(3), 551-555. https://doi.org/10.1111/j.1755-0998.2009.02787.x

Kamermans, P., Walles, B., Kraan, M., Van Duren, L., Kleissen, F., Van Der Have, T., Smaal, A., & Poelman, M. (2018). Offshore Wind farms as potential locations for flat oyster (*Ostrea edulis*) restoration in the Dutch North Sea. *Sustainability*, *10*(11), 3942. https://doi.org/10.3390/su10113942

Kawai, T., & Akira, S. (2010). The role of pattern-recognition receptors in innate immunity: update on Toll-like receptors. *Nature Immunology*, *11*(5), 373-384. https://doi.org/10.1038/ni.1863

Keenan, K., McGinnity, P., Cross, T. F., Crozier, W. W., & Prodöhl, P. A. (2013). diveRsity: An R package for the estimation and exploration of population genetics parameters and their associated errors. *Methods in Ecology and Evolution*, *4*(8), 782–788. https://doi.org/10.1111/2041-210x.12067

Kennedy, R. J., & Roberts, D. (1999). A survey of the current status of the flat oyster *Ostrea edulis* in Strangford Lough, Northern Ireland, with a view to the restoration of its oyster beds. *Biology and Environment: Proceedings of The Royal Irish Academy*, *99B*, 79-88. https://www.jstor.org/stable/20500055

Kirkpatrick, M. (2010). How and why chromosome inversions evolve. *PLoS Biology*, *8*(9), e1000501. https://doi.org/10.1371/journal.pbio.1000501

Kirkpatrick, M., & Barton, N. (2005). Chromosome inversions, local adaptation and speciation. *Genetics*, *173*(1), 419-434. https://doi.org/10.1534/genetics.105.047985

Kirkpatrick, J., Millar, R., & Smyth, D. (2024). The history of the European native oyster *Ostrea edulis* in Northern Irish waters and the four phases of resource exploitation. *Aquatic Living Resources*, *37*, 14. https://doi.org/10.1051/alr/2024012

Kiss, T. (2010). Apoptosis and its functional significance in molluscs. *APOPTOSIS*, *15*(3), 313-321. https://doi.org/10.1007/s10495-009-0446-3

Kong, P., Zhang, H., Wang, L., Zhou, Z., Yang, J., Zhang, Y., Qiu, L., Wang, L., & Song, L. (2010). AiC1qDC-1, a novel gC1q-domain-containing protein from bay scallop *Argopecten irradians* with fungi agglutinating activity. *Developmental & Comparative Immunology*, *34*(8), 837-846. https://doi.org/10.1016/j.dci.2010.03.006

Kopelman, N. M., Mayzel, J., Jakobsson, M., Rosenberg, N. A., & Mayrose, I. (2015). Clumpak: a program for identifying clustering modes and packaging population structure inferences across K. *Molecular Ecology Resources*, *15*(5), 1179–1191. https://doi.org/10.1111/1755-0998.12387

Kron, N. S. (2022). In search of the Aplysia immunome: an *in silico* study. *BMC Genomics*, *23*(1), 543. https://doi.org/10.1186/s12864-022-08780-6

Kumar, A., Bhandari, A., & Goswami, C. (2014). Surveying genetic variants and molecular phylogeny of cerebral cavernous malformation gene, CCM3/PDCD10. *Biochemical and Biophysical Research Communications*, *455*(1–2), 98–106. https://doi.org/10.1016/j.bbrc.2014.10.105

Kurtzer, G. M., Sochat, V., & Bauer, M. W. (2017). Singularity: Scientific containers for mobility of compute. *PLoS ONE*, *12*(5), e0177459. https://doi.org/10.1371/journal.pone.0177459

La Peyre, M., Nickens, A., Volety, A., Tolley, G., & La Peyre, J. (2004). Environmental significance of freshets in reducing *Perkinsus marinus* infection in eastern oysters *Crassostrea virginica*: potential management applications. *Marine Ecology Progress Series*, *248*, 165-176. https://doi.org/10.3354/meps248165

La Peyre, M. K., Casas, S. M., Gayle, W., & La Peyre, J. F. (2010). The combined influence of sub-optimal temperature and salinity on the *in vitro* viability of *Perkinsus marinus*, a protistan parasite of the eastern oyster *Crassostrea virginica*. *Journal of Invertebrate Pathology*, *105*(2), 176-181. https://doi.org/10.1016/j.jip.2010.06.010

Lafont, M., Petton, B., Vergnes, A., Pauletto, M., Segarra, A., Gourbal, B., & Montagnani, C. (2017). Long-lasting antiviral innate immune priming in the Lophotrochozoan Pacific oyster, *Crassostrea gigas*. *Scientific Reports*, *7*(1). https://doi.org/10.1038/s41598-017-13564-0

Lafont, M., Goncalves, P., Guo, X., Montagnani, C., Raftos, D., & Green, T. (2019). Transgenerational plasticity and antiviral immunity in the Pacific oyster (*Crassostrea gigas*) against Ostreid herpesvirus 1 (OsHV-1). *Developmental & Comparative Immunology*, *91*, 17-25. https://doi.org/10.1016/j.dci.2018.09.022

Lafont, M., Vergnes, A., Vidal-Dupiol, J., De Lorgeril, J., Gueguen, Y., Haffner, P., Petton, B., Chaparro, C., Barrachina, C., Destoumieux-Garzon, D., Mitta, G., Gourbal, B., & Montagnani, C. (2020). A sustained immune response supports long-term antiviral immune priming in the Pacific oyster, *Crassostrea gigas*. *mBio*, *11*(2), e02777-19. https://doi.org/10.1128/mbio.02777-19

Lallias, D., Arzul, I., Heurtebise, S., Ferrand, S., Chollet, B., Robert, M., Beaumont, A. R., Boudry, P., Morga, B., & Lapègue, S. (2008). *Bonamia ostreae*-induced mortalities in one-year old European flat oysters *Ostrea edulis*: experimental infection by cohabitation challenge. *Aquatic Living Resources*, *21*(4), 423–439. https://doi.org/10.1051/alr:2008053

Lallias, D., Stockdale, R., Boudry, P., Beaumont, A. R., & Lapègue, S. (2009). Characterization of 27 microsatellite loci in the European flat oyster *Ostrea edulis*. *Molecular Ecology Resources*, *9*(3), 960-963. https://doi.org/10.1111/j.1755-0998.2009.02515.x

Lallias, D., Boudry, P., Lapègue, S., King, J. W., & Beaumont, A. R. (2010). Strategies for the retention of high genetic variability in European flat oyster (*Ostrea edulis*) restoration programmes. *Conservation Genetics*, *11*(5), 1899-1910. https://doi.org/10.1007/s10592-010-0081-0

Langmead, B., & Salzberg, S. L. (2012). Fast gapped-read alignment with Bowtie 2. *Nature Methods*, *9*(4), 357–359. https://doi.org/10.1038/nmeth.1923

Langmead, B., Wilks, C., Antonescu, V., & Charles, R. (2018). Scaling read aligners to hundreds of threads on general-purpose processors. *Bioinformatics*, *35*(3), 421–432. https://doi.org/10.1093/bioinformatics/bty648

Lapègue, S., Reisser, C., Harrang, E., Heurtebise, S., & Bierne, N. (2022). Genetic parallelism between European flat oyster populations at the edge of their natural range. *Evolutionary Applications*, *16*(2), 393-407. https://doi.org/10.1111/eva.13449

Launey, S., Barre, M., Gerard, A., & Naciri-Graven, Y. (2001). Population bottleneck and effective size in *Bonamia ostreae*-resistant populations of *Ostrea edulis* as inferred by microsatellite markers. *Genetics Research*, *78*(3), 259–270. https://doi.org/10.1017/s0016672301005353

USC
UNIVERSIDADE DE SANTIAGO DE COMPOSTELA

Le Moan, A., Panova, M., De Jode, A., Ortega-Martinez, O., Duvetorp, M., Faria, R., Butlin, R., & Johannesson, K. (2022). An allozyme polymorphism is associated with a large chromosomal inversion in the marine snail *Littorina fabalis*. *Evolutionary Applications*, *16*(2), 279-292. https://doi.org/10.1111/eva.13427

Le Moan, A. L., Stankowski, S., Rafajlović, M., Ortega-Martinez, O., Faria, R., Butlin, R. K., & Johannesson, K. (2024). Coupling of twelve putative chromosomal inversions maintains a strong barrier to gene flow between snail ecotypes. *Evolution Letters*, *8*(4), 575-586. https://doi.org/10.1093/evlett/qrae014

Lehrer, R. I., & Ganz, T. (2003). Defensins of vertebrate animals. *Current Opinion in Immunology*, *14*(1), 96-102. https://doi.org/10.1016/s0952-7915(01)00303-x

Leite, R. B., Milan, M., Coppe, A., Bortoluzzi, S., Anjos, A. D., Reinhardt, R., Saavedra, C. F., Patarnello, T., Cancela, M. L., & Bargelloni, L. (2013). mRNA-Seq and microarray development for the Grooved carpet shell clam, *Ruditapes decussatus*: a functional approach to unravel host -parasite interaction. *BMC Genomics*, *14*(1), 741. https://doi.org/10.1186/1471-2164-14-741

Leitwein, M., Duranton, M., Rougemont, Q., Gagnaire, P., & Bernatchez, L. (2020). Using haplotype information for conservation genomics. *Trends in Ecology & Evolution*, *35*(3), 245–258. https://doi.org/10.1016/j.tree.2019.10.012

Lek, A., Lek, M., North, K. N., & Cooper, S. T. (2010). Phylogenetic analysis of ferlin genes reveals ancient eukaryotic origins. *BMC Evolutionary Biology*, *10*(1), 231. https://doi.org/10.1186/1471-2148-10-231

Li, B., & Dewey, C. N. (2011). RSEM: accurate transcript quantification from RNA-Seq data with or without a reference genome. *BMC Bioinformatics*, *12*(1). https://doi.org/10.1186/1471-2105-12-323

Li, H. (2018). Minimap2: pairwise alignment for nucleotide sequences. *Bioinformatics*, *34*(18), 3094–3100. https://doi.org/10.1093/bioinformatics/bty191

Li, X., Bai, Y., Dong, Z., Xu, C., Liu, S., Yu, H., Kong, L., & Li, Q. (2022). Chromosome-level genome assembly of the European flat oyster (*Ostrea edulis*) provides insights into its evolution and adaptation. *Comparative Biochemistry and Physiology Part D Genomics and Proteomics*, *45*, 101045. https://doi.org/10.1016/j.cbd.2022.101045

Li, Y., Song, X., Wang, W., Wang, L., Yi, Q., Jiang, S., Jia, Z., Du, X., Qiu, L., & Song, L. (2017). The hematopoiesis in gill and its role in the immune response of Pacific oyster *Crassostrea gigas* against secondary challenge with *Vibrio splendidus*. *Developmental & Comparative Immunology*, *71*, 59-69. https://doi.org/10.1016/j.dci.2017.01.024

Li, Y., & Liu, J. (2018). StructureSelector: A web-based software to select and visualize the optimal number of clusters using multiple methods. *Molecular Ecology Resources*, *18*(1), 176–177. https://doi.org/10.1111/1755-0998.12719

USC UNIVERSIDADE DE SANTIAGO DE COMPOSTELA

Lian, X., Li, Y., Wang, W., Zuo, J., Yu, T., Wang, L., & Song, L. (2024). The modification of H3K4me3 enhanced the expression of CgTLR3 in hemocytes to increase CgIL17-1 production in the immune priming of *Crassostrea gigas*. *International Journal of Molecular Sciences*, *25*(2), 1036. https://doi.org/10.3390/ijms25021036

Liu, L., Yang, J., Qiu, L., Wang, L., Zhang, H., Wang, M., Vinu, S., & Song, L. (2011). A novel scavenger receptor-cysteine-rich (SRCR) domain containing scavenger receptor identified from mollusk mediated PAMP recognition and binding. *Developmental & Comparative Immunology*, *35*(2), 227-239. https://doi.org/10.1016/j.dci.2010.09.010

Liu, O. M., Hick, P. M., & Whittington, R. J. (2023). The resistance to lethal challenge with ostreid herpesvirus-1 of Pacific oysters (*Crassostrea gigas*) previously exposed to this virus. *Viruses*, *15*(8), 1706. https://doi.org/10.3390/v15081706

Loker, E. S. (2010). Gastropod immunobiology. *Advances In Experimental Medicine And Biology*, 17-43. https://doi.org/10.1007/978-1-4419-8059-5_2

Loker, E. S., Bayne, C. J., Buckley, P. M., & Kruse, K. T. (1982). Ultrastructure of encapsulation of *Schistosoma mansoni* mother sporocysts by hemocytes of juveniles of the 10-r2 strain of *Biomphalaria glabrata*. *Journal of Parasitology*, *68*(1), 84. https://doi.org/10.2307/3281328

López-Flores, I., Suárez-Santiago, V. N., Longet, D., Saulnier, D., Chollet, B., & Arzul, I. (2007). Characterization of actin genes in *Bonamia ostreae* and their application to phylogeny of the Haplosporidia. *Parasitology*, *134*(14), 1941-1948. https://doi.org/10.1017/s0031182007003307

Love, M. I., Huber, W., & Anders, S. (2014). Moderated estimation of fold change and dispersion for RNA-seq data with DESeq2. *Genome Biology*, *15*(12), 550. https://doi.org/10.1186/s13059-014-0550-8

Lowry, D. B., & Willis, J. H. (2010). A widespread chromosomal inversion polymorphism contributes to a major life-history transition, local adaptation, and reproductive isolation. *PLoS Biology*, *8*(9), e1000500. https://doi.org/10.1371/journal.pbio.1000500

Lynch, S., Armitage, D., Coughlan, J., Mulcahy, M., & Culloty, S. (2007). Investigating the possible role of benthic macroinvertebrates and zooplankton in the life cycle of the haplosporidian *Bonamia ostreae*. *Experimental Parasitology*, *115*(4), 359-368. https://doi.org/10.1016/j.exppara.2006.09.021

Lynch, S. A., Abollo, E., Ramilo, A., Cao, A., Culloty, S. C., & Villalba, A. (2010). Observations raise the question if the Pacific oyster, *Crassostrea gigas*, can act as either a carrier or a reservoir for *Bonamia ostreae* or *Bonamia exitiosa*. *Parasitology*, *137*(10), 1515-1526. https://doi.org/10.1017/s0031182010000326

Lynch, S., Flannery, G., Hugh-Jones, T., Hugh-Jones, D., & Culloty, S. (2014). Thirty-year history of Irish (Rossmore) *Ostrea edulis* selectively bred for disease resistance to *Bonamia ostreae*. *Diseases of Aquatic Organisms*, *110*(1), 113–121. https://doi.org/10.3354/dao02734

Marinković, M., Berger, J., & Jékely, G. (2019). Neuronal coordination of motile cilia in locomotion and feeding. *Philosophical Transactions of The Royal Society B Biological Sciences*, *375*(1792), 20190165. https://doi.org/10.1098/rstb.2019.0165

Marteil, L. (1960). Ecologie des huîtres du Morbihan *Ostrea edulis* Linné et *Gryphea angulata* Lamarck. Rev. Trav. Inst. Pêches marit. 24, 329-446.

Martin, M. (2011). Cutadapt removes adapter sequences from high-throughput sequencing reads. *EMBnet Journal*, *17*(1), 10. https://doi.org/10.14806/ej.17.1.200

Martín-Gómez, L., Villalba, A., Carballal, M. J., & Abollo, E. (2014). Cloning and characterization of neoplasia-related genes in flat oyster *Ostrea edulis*. *Infection Genetics and Evolution*, *23*, 138-149. https://doi.org/10.1016/j.meegid.2014.02.004

Marty, G. D., Bower, S. M., Clarke, K. R., Meyer, G., Lowe, G., Osborn, A. L., Chow, E. P., Hannah, H., Byrne, S., Sojonky, K., & Robinson, J. H. (2006). Histopathology and a real-time PCR assay for detection of *Bonamia ostreae* in *Ostrea edulis* cultured in Western Canada. *Aquaculture*, *261*(1), 33-42. https://doi.org/10.1016/j.aquaculture.2006.07.024

McArdle, J. F., McKiernan, F., Foley, H., & Jones, D. H. (1991). The current status of *Bonamia* disease in Ireland. *Aquaculture*, *93*(3), 273-278. https://doi.org/10.1016/0044-8486(91)90239-4

McDade, J. E., & Tripp, M. R. (1967). Mechanism of agglutination of red blood cells by oyster hemolymph. *Journal of Invertebrate Pathology*, *9*(4), 523-530. https://doi.org/10.1016/0022-2011(67)90133-4

McDowell, I. C., Nikapitiya, C., Aguiar, D., Lane, C. E., Istrail, S., & Gomez-Chiarri, M. (2014). Transcriptome of American oysters, *Crassostrea virginica*, in response to bacterial challenge: insights into potential mechanisms of disease resistance. *PLoS ONE*, *9*(8), e105097. https://doi.org/10.1371/journal.pone.0105097

McKinney, G. J., Seeb, J. E., & Seeb, L. W. (2017). Managing mixed-stock fisheries: genotyping multi-SNP haplotypes increases power for genetic stock identification. *Canadian Journal of Fisheries and Aquatic Sciences*, *74*(4), 429-434. https://doi.org/10.1139/cjfas-2016-0443

Meng, J., Wang, W., Li, L., & Zhang, G. (2021). Accumulation of different metals in oyster *Crassostrea gigas*: Significance and specificity of SLC39A (ZIP) and SLC30A (ZnT) gene families and polymorphism variation. *Environmental Pollution*, *276*, 116706. https://doi.org/10.1016/j.envpol.2021.116706

Mizushima, N., Levine, B., Cuervo, A. M., & Klionsky, D. J. (2008). Autophagy fights disease through cellular self-digestion. *Nature*, *451*(7182), 1069-1075. https://doi.org/10.1038/nature06639

USC UNIVERSIDADE DE SANTIAGO DE COMPOSTELA

Montagnani, C., Morga, B., Novoa, B., Gourbal, B., Saco, A., Rey-campos, M., Bourhis, M., Riera, F., Vignal, E., Corporeau, C., Charrière, G. M., Travers, M., Dégremont, L., Gueguen, Y., Cosseau, C., & Figueras, A. (2024). Trained immunity: Perspectives for disease control strategy in marine mollusc aquaculture. *Reviews in Aquaculture*, *16*(4), 1472-1498. https://doi.org/10.1111/raq.12906

Monteiro, H. J. A., Bekkevold, D., Pacheco, G., Mortensen, S., Lou, R. N., Therkildsen, N. O., Tanguy, A., Robert, C., De Wit, P., Meldrup, D., Laugen, A. T., Ermgassen, P. S. E. Z., Strand, Å., Saurel, C., & Hemmer-Hansen, J. (2024). Genome-wide population structure in a marine keystone species, the European flat oyster (*Ostrea edulis*). *Molecular Ecology, 12, e17573*. https://doi.org/10.1111/mec.17573

Montes, J., Anadón, R., & Azevedo, C. (1994). A possible life cycle for *Bonamia ostreae* on the basis of electron microscopy studies. *Journal of Invertebrate Pathology*, *63*(1), 1-6. https://doi.org/10.1006/jipa.1994.1001

Moreira, R., Balseiro, P., Planas, J. V., Fuste, B., Beltran, S., Novoa, B., & Figueras, A. (2012a). Transcriptomics of *in vitro* immune-stimulated hemocytes from the Manila clam *Ruditapes philippinarum* using high-throughput sequencing. *PLoS ONE*, *7*(4), e35009. https://doi.org/10.1371/journal.pone.0035009

Moreira, R., Balseiro, P., Romero, A., Dios, S., Posada, D., Novoa, B., & Figueras, A. (2012b). Gene expression analysis of clams *Ruditapes philippinarum* and *Ruditapes decussatus* following bacterial infection yields molecular insights into pathogen resistance and immunity. *Developmental & Comparative Immunology*, *36*(1), 140-149. https://doi.org/10.1016/j.dci.2011.06.012

Moreira, R., Balseiro, P., Forn-Cuní, G., Milan, M., Bargelloni, L., Novoa, B., & Figueras, A. (2018). Bivalve transcriptomics reveal pathogen sequences and a powerful immune response of the Mediterranean mussel (*Mytilus galloprovincialis*). *Marine Biology*, *165*(4), 61. https://doi.org/10.1007/s00227-018-3308-0

Morga, B., Renault, T., Faury, N., Chollet, B., & Arzul, I. (2011). Cellular and molecular responses of haemocytes from *Ostrea edulis* during in vitro infection by the parasite *Bonamia ostreae*. *International Journal for Parasitology*, *41*(7), 755-764. https://doi.org/10.1016/j.ijpara.2011.01.013

Morga, B., Renault, T., Faury, N., & Arzul, I. (2012). New insights in flat oyster *Ostrea edulis* resistance against the parasite *Bonamia ostreae*. *Fish & Shellfish Immunology*, *32*(6), 958-968. https://doi.org/10.1016/j.fsi.2012.01.026

Morga, B., Renault, T., Faury, N., Lerond, S., Garcia, C., Chollet, B., Joly, J., Lapègue, S., Harrang, E., & Arzul, I. (2017). Contribution of *in vivo* experimental challenges to understanding flat oyster *Ostrea edulis* resistance to *Bonamia ostreae*. *Frontiers in Cellular and Infection Microbiology*, *7*, 433 https://doi.org/10.3389/fcimb.2017.00433

USC UNIVERSIDADE DE SANTIAGO DE COMPOSTELA

Mortensen, S., Sælemyr, L., Skår, C. K., Bodvin, T., & Jelmert, A. (2016). The surveillance and control programme for bonamiosis and marteiliosis in European flat oysters, *Ostrea edulis*, and blue mussels, *Mytilus* sp. in Norway in 2015. Annual report. *11 S.* https://www.hi.no/hi/nettrapporter/rapport-fra-havforskningen-en-2024-14

Morton, B., Lam, K., & Slack-Smith, S. (2003). First report of the European flat oyster *Ostrea edulis*, identified genetically, from Oyster Harbour, Albany, south-western Western Australia. *Molluscan Research*, *23*(3), 199. https://doi.org/10.1071/mr03005

Mukherjee, K., Korithoski, B., & Kolaczkowski, B. (2014). Ancient origins of vertebrate-specific innate antiviral immunity. *Molecular Biology and Evolution*, *31*(1), 140–153. https://doi.org/10.1093/molbev/mst184

Murray, H. (1981). Susceptibility of leishmania to oxygen intermediates and killing by normal macrophages. *The Journal of Experimental Medicine*, *153*(5), 1302–1315. https://doi.org/10.1084/jem.153.5.1302

Nikapitiya, C., Dorrington, T., & Gómez-Chiarri, M. (2013). The role of histones in the immune responses of aquatic invertebrates. *DOAJ (DOAJ: Directory Of Open Access Journals)*. https://doaj.org/article/cc6c6a80d4cd43f4a54722b2f13d7382

Niu, D., Jin, K., Wang, L., Feng, B., & Li, J. (2013). Molecular characterization and expression analysis of four cathepsin L genes in the razor clam, *Sinonovacula constricta*. *Fish & Shellfish Immunology*, *35*(2), 581-588. https://doi.org/10.1016/j.fsi.2013.06.001

Odoemelam, E. C. (2009). Genomic analysis of the fresh water mollusc *Biomphalaria glabrata to understand host: Parasite interactions*. PhD Thesis. Brunel University School of Health Sciences and Social Care PhD Theses http://bura.brunel.ac.uk/handle/2438/4431

Oeth, P., Del Mistro, G., Marnellos, G., Shi, T., & Boom, D. (2009). Qualitative and quantitative genotyping using single base primer extension coupled with matrix-assisted laser desorption/ionization time-of-flight mass spectrometry (MassARRAY®). *Methods in Molecular Biology*, *578*, 307–343. https://doi.org/10.1007/978-1-60327-411-1_20

Oliveira, A. F., Marques, S. C., Pereira, J., & Azeiteiro, U. M. (2025). Salinity and temperature influence on the early development of mysid *Mesopodopsis slabberi* in a temperate estuary: implications to climate change effect. *Marine Environmental Research*, *209*, 107239. https://doi.org/10.1016/j.marenvres.2025.107239

Orengo, D. J., Puerma, E., Cereijo, U., & Aguadé, M. (2019). The molecular genealogy of sequential overlapping inversions implies both homologous chromosomes of a heterokaryotype in an inversion origin. *Scientific Reports*, *9*(1), 17009. https://doi.org/10.1038/s41598-019-53582-8

OYSTERECOVER (2013). European native oyster restoration: feasibility and knowledge. EU Interreg IVB project report. https://northsearegion.eu/oysterecover

USC UNIVERSIDADE DE SANTIAGO DE COMPOSTELA

Pardo, B., Álvarez-Dios, J., Cao, A., Ramilo, A., Gómez-Tato, A., Planas, J., Villalba, A., & Martínez, P. (2016). Construction of an *Ostrea edulis* database from genomic and expressed sequence tags (ESTs) obtained from *Bonamia ostreae* infected haemocytes: Development of an immune-enriched oligo-microarray. *Fish & Shellfish Immunology*, *59*, 331-344. https://doi.org/10.1016/j.fsi.2016.10.047

Pascarella, G., Hon, C. C., Hashimoto, K., Busch, A., Luginbühl, J., Parr, C., Yip, W. H., Abe, K., Kratz, A., Bonetti, A., Agostini, F., Severin, J., Murayama, S., Suzuki, Y., Gustincich, S., Frith, M., & Carninci, P. (2022). Recombination of repeat elements generates somatic complexity in human genomes. *Cell*, *185*(16), 3025-3040.e6. https://doi.org/10.1016/j.cell.2022.06.032

Pearse, D. E., Barson, N. J., Nome, T., Gao, G., Campbell, M. A., Abadía-Cardoso, A., Anderson, E. C., Rundio, D. E., Williams, T. H., Naish, K. A., Moen, T., Liu, S., Kent, M., Moser, M., Minkley, D. R., Rondeau, E. B., Brieuc, M. S. O., Sandve, S. R., Miller, M. R., . . . Lien, S. (2019). Sex-dependent dominance maintains migration supergene in rainbow trout. *Nature Ecology & Evolution*, *3*(12), 1731-1742. https://doi.org/10.1038/s41559-019-1044-6

Peharda, M., Ezgeta-Balić, D., Davenport, J., Bojanić, N., Vidjak, O., & Ninčević-Gladan, I. (2012). Differential ingestion of zooplankton by four species of bivalves (Mollusca) in the Mali Ston Bay, Croatia. *Marine Biology*, *159*(4), 881-895. https://doi.org/10.1007/s00227-011-1866-5

Peiser, L., Mukhopadhyay, S., & Gordon, S. (2002). Scavenger receptors in innate immunity. *Current Opinion in Immunology*, *14*(1), 123–128. https://doi.org/10.1016/s0952-7915(01)00307-7

Perrigault, M., Tanguy, A., & Allam, B. (2009). Identification and expression of differentially expressed genes in the hard clam, *Mercenaria mercenaria*, in response to quahog parasite unknown (QPX). *BMC Genomics*, *10*(1), 377. https://doi.org/10.1186/1471-2164-10-377

Perry, F., Jackson, A., & Garrad, S. L. (2017). MarLIN – The marine life information network – Native oyster (*Ostrea edulis*). MarLIN. www.marlin.ac.uk/species/detail/1146

Pettersson, M. E., Rochus, C. M., Han, F., Chen, J., Hill, J., Wallerman, O., Fan, G., Hong, X., Xu, Q., Zhang, H., Liu, S., Liu, X., Haggerty, L., Hunt, T., Martin, F. J., Flicek, P., Bunikis, I., Folkvord, A., & Andersson, L. (2019). A chromosome-level assembly of the Atlantic herring genome—detection of a supergene and other signals of selection. *Genome Research*, *29*(11), 1919-1928. https://doi.org/10.1101/gr.253435.119

Pichot, Y., Comps, M., Tige, G., Grizel, H. & Rabouin, M. A. (1980). Recherches sur *Bonamia ostreae* gen. n., sp. n., parasite nouveau de l'huitre plate *Ostrea edulis* L. Rev. Trav. Inst. Peches Marit. 43,131-140.

USC UNIVERSIDADE DE SANTIAGO DE COMPOSTELA

Picot, S., Morga, B., Faury, N., Chollet, B., Dégremont, L., Travers, M., Renault, T., & Arzul, I. (2019). A study of autophagy in hemocytes of the Pacific oyster, *Crassostrea gigas*. *Autophagy*, *15*(10), 1801-1809. https://doi.org/10.1080/15548627.2019.1596490

Pogoda, B. (2019a). Current status of European oyster decline and restoration in Germany. *Humanities*, *8*(1), 9. https://doi.org/10.3390/h8010009

Pogoda, B., Brown, J., Hancock, B., Preston, J., Pouvreau, S., Kamermans, P., Sanderson, W., & Von Nordheim, H. (2019b). The Native Oyster Restoration Alliance (NORA) and the Berlin Oyster Recommendation: bringing back a key ecosystem engineer by developing and supporting best practice in Europe. *Aquatic Living Resources*, *32*, 13. https://doi.org/10.1051/alr/2019012

Pogoda, B., Hausen, T., Rothe, M., Bakker, F., Hauser, S., Colsoul, B., Dureuil, M., Krause, J., Heinicke, K., Pusch, C., Eisenbarth, S., Kreutle, A., Peter, C., & Pesch, R. (2023). Come, tell me how you live: Habitat suitability analysis for *Ostrea edulis* restoration. *Aquatic Conservation Marine and Freshwater Ecosystems*, *33*(7), 678–695. https://doi.org/10.1002/aqc.3928

Poirier, A. C., Schmitt, P., Rosa, R. D., Vanhove, A. S., Kieffer-Jaquinod, S., Rubio, T. P., Charrière, G. M., & Destoumieux-Garzón, D. (2014). Antimicrobial histones and DNA traps in invertebrate immunity. *Journal of Biological Chemistry*, *289*(36), 24821-24831. https://doi.org/10.1074/jbc.m114.576546

Pouvreau, S., Lapègue, S., Arzul, I., & Boudry, P. (2023). Fifty years of research to counter the decline of the European flat oyster (*Ostrea edulis*): a review of French achievements and prospects for the restoration of remaining beds and revival of aquaculture production. *Aquatic Living Resources*, *36*, 13. https://doi.org/10.1051/alr/2023006

Prado-Alvarez, M., Rotllant, J., Gestal, C., Novoa, B., & Figueras, A. (2009). Characterization of a C3 and a factor B-like in the carpet-shell clam, *Ruditapes decussatus*. *Fish & Shellfish Immunology*, *26*(2), 305–315. https://doi.org/10.1016/j.fsi.2008.11.015

Pritchard, J. K., Stephens, M., & Donnelly, P. (2000). Inference of population structure using multilocus genotype data. *Genetics*, *155*(2), 945–959. https://doi.org/10.1093/genetics/155.2.945

Prokhorova, E. E., & Ataev, G. L. (2023). Fibrinogen-related proteins of gastropoda molluscs. *Biology Bulletin Reviews*, *13*(S2), S184-S198. https://doi.org/10.1134/s2079086423080091

RåBerg, L., Sim, D., & Read, A. F. (2007). Disentangling genetic variation for resistance and tolerance to infectious diseases in animals. *Science*, *318*(5851), 812-814. https://doi.org/10.1126/science.1148526

USC UNIVERSIDADE DE SANTIAGO DE COMPOSTELA

Raftos, D. A., Kuchel, R., Aladaileh, S., & Butt, D. (2014). Infectious microbial diseases and host defense responses in Sydney rock oysters. *Frontiers in Microbiology*, *5*, 135. https://doi.org/10.3389/fmicb.2014.00135

Reboul, J., & Ewbank, J. J. (2016). GPCRs in invertebrate innate immunity. *Biochemical Pharmacology*, *114*, 82-87. https://doi.org/10.1016/j.bcp.2016.05.015

Reeve, J., Butlin, R. K., Koch, E. L., Stankowski, S., & Faria, R. (2024). Chromosomal inversion polymorphisms are widespread across the species ranges of rough periwinkles (*Littorina saxatilis* and *L. arcana*). *Molecular Ecology*, *33*(24), e17160. https://doi.org/10.1111/mec.17160

Reise, K. (2005). Coast of change: habitat loss and transformations in the Wadden Sea. *Helgoland Marine Research*, *59*(1), 9-21. https://doi.org/10.1007/s10152-004-0202-6

Renault, T., Faury, N., Barbosa-Solomieu, V., & Moreau, K. (2011). Suppression substractive hybridisation (SSH) and real time PCR reveal differential gene expression in the Pacific cupped oyster, *Crassostrea gigas*, challenged with Ostreid herpesvirus 1. *Developmental & Comparative Immunology*, *35*(7), 725–735. https://doi.org/10.1016/j.dci.2011.02.004

Robert, C., Monteiro, H. J. A., Moan, A. L., Tanguy, A., Laugen, A. T., Hemmer-Hansen, J., Strand, Å., & De Wit, P. (2025). Fine scale patterns of population structure and connectivity in Scandinavian flat oysters in Scandinavia (*Ostrea edulis* L.). *Evolutionary Applications*, *18*(4), e70096. https://doi.org/10.1111/eva.70096

Roberts, R. J., Agius, C., Saliba, C., Bossier, P., & Sung, Y. Y. (2010). Heat shock proteins (chaperones) in fish and shellfish and their potential role in relation to fish health: a review. *Journal of Fish Diseases*, *33*(10), 789-801. https://doi.org/10.1111/j.1365-2761.2010.01183.x

Robinson, J. T., Thorvaldsdóttir, H., Winckler, W., Guttman, M., Lander, E. S., Getz, G., & Mesirov, J. P. (2011). Integrative genomics viewer. *Nature Biotechnology*, *29*(1), 24–26. https://doi.org/10.1038/nbt.1754

Rodi, C. P., Darnhofer-Patel, B., Stanssens, P., Zabeau, M., & Van Den Boom, D. (2002). A strategy for the rapid discovery of disease markers using the MassARRAY™ system. *BioTechniques*, *32(6)*, S62-S69. https://doi.org/10.2144/jun0204

Rogan, E., Culloty, S. C., Cross, T. F., & Mulcahy, M. F. (1991). The detection of *Bonamia ostreae* (Pichot et al. 1980) in frozen oysters (*Ostrea edulis* L.) and the effect of the parasite on condition. *Aquaculture*, *97*(4), 311-315. https://doi.org/10.1016/0044-8486(91)90323-y

Romero, A., Dios, S., Poisa-Beiro, L., Costa, M. M., Posada, D., Figueras, A., & Novoa, B. (2011). Individual sequence variability and functional activities of fibrinogen-related proteins (FREPs) in the Mediterranean mussel (*Mytilus galloprovincialis*) suggest ancient and complex immune recognition models in invertebrates. *Developmental & Comparative Immunology*, *35*(3), 334-344. https://doi.org/10.1016/j.dci.2010.10.007

Romero, A., Novoa, B., & Figueras, A. (2015). The complexity of apoptotic cell death in mollusks: An update. *Fish & Shellfish Immunology*, *46*(1), 79-87. https://doi.org/10.1016/j.fsi.2015.03.038

Romero, A., Novoa, B., & Figueras, A. (2020). Extracellular traps (ETosis) can be activated through NADPH-dependent and -independent mechanisms in bivalve mollusks. *Developmental & Comparative Immunology*, *106*, 103585. https://doi.org/10.1016/j.dci.2019.103585

Ronza, P., Cao, A., Robledo, D., Gómez-Tato, A., Álvarez-Dios, J., Hasanuzzaman, A., Quiroga, M., Villalba, A., Pardo, B., & Martínez, P. (2018). Long-term affected flat oyster (*Ostrea edulis*) haemocytes show differential gene expression profiles from naïve oysters in response to *Bonamia ostreae*. *Genomics*, *110*(6), 390-398. https://doi.org/10.1016/j.ygeno.2018.04.002

Rousset, F. (2008). genepop'007: a complete re-implementation of the genepop software for Windows and Linux. *Molecular Ecology Resources*, *8*(1), 103–106. https://doi.org/10.1111/j.1471-8286.2007.01931.x

Roy, N. L., Ganot, P., Aranda, M., Allemand, D., & Tambutté, S. (2021). The skeletome of the red coral *Corallium rubrum* indicates an independent evolution of biomineralization process in octocorals. *BMC Ecology and Evolution*, *21*(1). https://doi.org/10.1186/s12862-020-01734-0

Ruiz, C., Martinez, D., Mosquera, G., Abad, M., & Sánchez, J. L. (1992). Seasonal variations in condition, reproductive activity and biochemical composition of the flat oyster, *Ostrea edulis*, from San Cibran (Galicia, Spain). *Marine Biology*, *112*(1), 67-74. https://doi.org/10.1007/bf00349729

Saavedra, C., Zapata, C., Guerra, A., & Alvarez, G. (1993). Allozyme variation in European populations of the oyster *Ostrea edulis*. *Marine Biology*, *115*(1), 85-95. https://doi.org/10.1007/bf00349389

Sarrias, M. R., Gronlund, J., Padilla, O., Madsen, J., Holmskov, U., & Lozano, F. (2004). The scavenger receptor Cysteine-Rich (SRCR) domain: an ancient and highly conserved protein module of the innate immune system. *Critical Reviews in Immunology*, *24*(1), 1–38. https://doi.org/10.1615/critrevimmunol.v24.i1.10

Sas, H., Kamermans, P., van der Have, T. M., Lengkeek, W., & Smaal, A. C. (2016). *Shellfish reef restoration pilots: Voordelta The Netherlands*. (Annual report; No. 2016). Wageningen Marine Research. https://edepot.wur.nl/405730

Sas, H., Deden, B., Kamermans, P., Ermgassen, P. S. Z., Pogoda, B., Preston, J., Helmer, L., Holbrook, Z., Arzul, I., Van Der Have, T., Villalba, A., Colsoul, B., Lown, A., Merk, V., Zwerschke, N., & Reuchlin, E. (2020). *Bonamia* infection in native oysters (*Ostrea edulis*) in relation to European restoration projects. *Aquatic Conservation Marine and Freshwater Ecosystems*, *30*(11), 2150–2162. https://doi.org/10.1002/aqc.3430

USC DE COMPOSTELA

Schmitt, P., Duperthuy, M., Montagnani, C., Bachere, E., & Destoumieux-Garzón, D. (2011). Immune responses in the Pacific oyster *Crassostrea gigas*: An overview with focus on summer mortalities. In Qin, J.G. (ed) *Oysters*. Nova Science Publishers, Inc. Chapter 9. 48pp.

Schneller, N. M., Strugnell, J. M., Field, M. A., Johannesson, K., & Cooke, I. (2025). Putting structural variants into practice: the role of chromosomal inversions in the management of marine environments. *Molecular Ecology, 8,* e17776. https://doi.org/10.1111/mec.17776

Šegvić-Bubić, T., Žužul, I., Talijančić, I., Ugrin, N., Pleić, I. L., Žuvić, L., Stagličić, N., & Grubišić, L. (2020). Translocation and aquaculture impact on genetic diversity and composition of wild self-sustainable *Ostrea edulis* populations in the Adriatic sea. *Frontiers in Marine Science, 7,* 84. https://doi.org/10.3389/fmars.2020.00084

Shen, C., Liang, H., Guo, Z., & Zhang, M. (2023). Members of the histone-derived antimicrobial peptide family from the pearl oyster *Pinctada fucata martensii*: Inhibition of bacterial growth. *Fish and Shellfish Immunology, 132,* 108439. https://doi.org/10.1016/j.fsi.2022.11.027

Shin, J., Blay, S., Graham, J., & McNeney, B. (2006). LDheatmap: AnRFunction for graphical display of pairwise linkage disequilibria between single nucleotide polymorphisms. *Journal of Statistical Software*, *16*(3), 1-9. https://doi.org/10.18637/jss.v016.c03

Shrestha, S. P., Tomita, T., Weiss, L. M., & Orlofsky, A. (2006). Proliferation of *Toxoplasma gondii* in inflammatory macrophages *in vivo* is associated with diminished oxygen radical production in the host cell. *International Journal for Parasitology*, *36*(4), 433–441. https://doi.org/10.1016/j.ijpara.2006.01.006

Signorini, S. G., Munari, M., Crocetta, F., Moro, I., D'Aniello, I., Nigro, L., Micheli, F., & Della Torre, C. (2025). Short and long-term exposure to ocean acidification in limpets from the Castello Aragonese vent systems (Ischia Island, Italy). *Environmental Research*, *279*, 121874. https://doi.org/10.1016/j.envres.2025.121874

Sirard, J., Vignal, C., Dessein, R., & Chamaillard, M. (2007). Nod-like receptors: cytosolic watchdogs for immunity against pathogens. *PLoS Pathogens*, *3*(12), e152. https://doi.org/10.1371/journal.ppat.0030152

Smaal, A., Kamermans, P., Van Der Have, T., Engelsma, M., & Sas, H. (2015). Feasibility of flat oyster (*Ostrea edulis* L.) restoration in the Dutch part of the North Sea. *Research Output of Wageningen University & Research Staff*. 58pp. http://edepot.wur.nl/335033

Smaal, A. C., Ferreira, J. G., Grant, J., Petersen, J. K., & Strand, Ø. (2018). *Goods and services of marine bivalves (English Edition)* (1st ed.). Springer.

USC UNIVERSIDADE DE SANTIAGO DE COMPOSTELA

Smyth, D., Millar, R., Clements, A., McIvenny, H., & Hayden-Hughes, M. (2023). Population dynamics of the European native oyster in a Marine Conservation Zone exposed to unregulated harvesting. *Aquatic Living Resources*, *36*, 3. https://doi.org/10.1051/alr/2022023

Snyder, M. W., Adey, A., Kitzman, J. O., & Shendure, J. (2015). Haplotype-resolved genome sequencing: experimental methods and applications. *Nature Reviews Genetics*, *16*(6), 344-358. https://doi.org/10.1038/nrg3903

Sokolova, I. M. (2009). Apoptosis in molluscan immune defense. *DOAJ (DOAJ: Directory of Open Access Journals)*. https://doaj.org/article/38e2b2c7b6b04564a9d18cfcf7c38073

Sokolova, I. M., Evans, S., & Hughes, F. M. (2004). Cadmium-induced apoptosis in oyster hemocytes involves disturbance of cellular energy balance but no mitochondrial permeability transition. *Journal of Experimental Biology*, *207*(19), 3369-3380. https://doi.org/10.1242/jeb.01152

Song, J., Liu, B., & Wang, C. (2022). Metabolomic and transcriptomic responses of *Argopecten irradians concentricus* to thermal stresses. *Frontiers in Marine Science*, *9,* 818083. https://doi.org/10.3389/fmars.2022.818083

Song, L., Wang, L., Qiu, L., & Zhang, H. (2010). Bivalve immunity. In: Söderhäll, K. (ed). *Invertebrate Immunity. Advances in Experimental Medicine and Biology*, vol 708. Springer, Boston, MA., 44-65. https://doi.org/10.1007/978-1-4419-8059-5_3

Stagličić, N., Šegvić-Bubić, T., Ezgeta-Balić, D., Varezić, D. B., Grubišić, L., Žuvić, L., Lin, Y., & Briski, E. (2020). Distribution patterns of two co-existing oyster species in the northern Adriatic Sea: The native European flat oyster *Ostrea edulis* and the non-native Pacific oyster *Magallana gigas*. *Ecological Indicators*, *113*, 106233. https://doi.org/10.1016/j.ecolind.2020.106233

Stanssens, P., Zabeau, M., Meersseman, G., Remes, G., Gansemans, Y., Storm, N., Hartmer, R., Honisch, C., Rodi, C. P., Böcker, S., & Van Den Boom, D. (2004). High-throughput MALDI-TOF discovery of genomic sequence polymorphisms. *Genome Research*, *14*(1), 126–133. https://doi.org/10.1101/gr.1692304

Stechele, B., Maar, M., Wijsman, J., Van Der Zande, D., Degraer, S., Bossier, P., & Nevejan, N. (2022). Comparing life history traits and tolerance to changing environments of two oyster species (*Ostrea edulis* and *Crassostrea gigas*) through Dynamic Energy Budget theory. *Conservation Physiology*, *10*(1), coac034. https://doi.org/10.1093/conphys/coac034

Stefansson, H., Helgason, A., Thorleifsson, G., Steinthorsdottir, V., Masson, G., Barnard, J., Baker, A., Jonasdottir, A., Ingason, A., Gudnadottir, V. G., Desnica, N., Hicks, A., Gylfason, A., Gudbjartsson, D. F., Jonsdottir, G. M., Sainz, J., Agnarsson, K., Birgisdottir, B., Ghosh, S., . . . Stefansson, K. (2005). A common inversion under selection in Europeans. *Nature Genetics*, *37*(2), 129-137. https://doi.org/10.1038/ng1508

Sturtevant, A. H. (1920). Genetic studies on *Drosophila simulans*. I. Introduction. Hybrids with *Drosophila melanogaster*. *Genetics*, *5*(5), 488-500. https://doi.org/10.1093/genetics/5.5.488

Sturtevant, A. H., & Beadle, G. W. (1936). The relations of inversions in the X chromosome of *Drosophila melanogaster* to crossing over and disjunction. *Genetics*, *21*(5), 554-604. https://doi.org/10.1093/genetics/21.5.554

Sun, Y., Zhou, Z., Wang, L., Yang, C., Jianga, S., & Song, L. (2014). The immunomodulation of a novel tumor necrosis factor (CgTNF-1) in oyster *Crassostrea gigas*. *Developmental & Comparative Immunology*, *45*(2), 291–299. https://doi.org/10.1016/j.dci.2014.03.007

Tanguy, A., Guo, X., & Ford, S. E. (2004). Discovery of genes expressed in response to *Perkinsus marinus* challenge in Eastern (*Crassostrea virginica*) and Pacific (*C. gigas*) oysters. *Gene*, *338*(1), 121–131. https://doi.org/10.1016/j.gene.2004.05.019

Thiriot-Quiévreux, C. (1984). Analyse comparée des caryotypes d'Ostreidae (Bivalvia). *Cahiers Biologie Marine*, *25*, 407-418.

Thiriot-Quiévreux, C., & Insua, A. (1992). Nucleolar organiser region variation in the chromosomes of three oyster species. *Journal of Experimental Marine Biology and Ecology*, *157*(1), 33–40. https://doi.org/10.1016/0022-0981(92)90072-i

Thorngren, L., Bergström, P., Holthuis, T. D., & Lindegarth, M. (2019). Assessment of the population of *Ostrea edulis* in Sweden: A marginal population of significance? *Ecology and Evolution*, *9*(24), 13877-13888. https://doi.org/10.1002/ece3.5824

Thorstensen, M. J., Euclide, P. T., Jeffrey, J. D., Shi, Y., Treberg, J. R., Watkinson, D. A., Enders, E. C., Larson, W. A., Kobayashi, Y., & Jeffries, K. M. (2022). A chromosomal inversion may facilitate adaptation despite periodic gene flow in a freshwater fish. *Ecology and Evolution*, *12*(5), e8898. https://doi.org/10.1002/ece3.8898

Törönen, P., & Holm, L. (2022). PANNZER—A practical tool for protein function prediction. *Protein Science*, *31*(1), 118–128. https://doi.org/10.1002/pro.4193

Travers, M., Meistertzheim, A., Cardinaud, M., Friedman, C. S., Huchette, S., Moraga, D., & Paillard, C. (2010). Gene expression patterns of abalone, *Haliotis tuberculata*, during successive infections by the pathogen *Vibrio harveyi*. *Journal of Invertebrate Pathology*, *105*(3), 289-297. https://doi.org/10.1016/j.jip.2010.08.001

Untergasser, A., Cutcutache, I., Koressaar, T., Ye, J., Faircloth, B. C., Remm, M., & Rozen, S. G. (2012). Primer3—new capabilities and interfaces. *Nucleic Acids Research*, *40*(15), e115. https://doi.org/10.1093/nar/gks596

Valk, S., Engelsma, M., Megens, H., Kamermans, P., Murk, A. J., & Nijland, R. (2025). Oysters in transition: hermaphrodite oysters display unique DNA methylation patterns in gill tissue. *BMC Genomics*, *26*(1), 567. https://doi.org/10.1186/s12864-025-11736-1

USC DE COMPOSTELA

Van Banning, P. (1987). Further results of the *Bonamia ostreae* challenge tests in Dutch oyster culture. *Aquaculture*, *67*(1-2), 191-194. https://doi.org/10.1016/0044-8486(87)90025-1

Van Banning, P. (1990). The life cycle of the oyster pathogen *Bonamia ostreae* with a presumptive phase in the ovarian tissue of the European flat oyster, *Ostrea edulis*. *Aquaculture*, *84*(2), 189-192. https://doi.org/10.1016/0044-8486(90)90348-q

Van Banning, P. (1991). Observations on bonamiasis in the stock of the European flat oyster, *Ostrea edulis*, in the Netherlands, with special reference to the recent developments in Lake Grevelingen. *Aquaculture*, *93*(3), 205-211. https://doi.org/10.1016/0044-8486(91)90232-v

Venier, P., Varotto, L., Rosani, U., Millino, C., Celegato, B., Bernante, F., Lanfranchi, G., Novoa, B., Roch, P., Figueras, A., & Pallavicini, A. (2011). Insights into the innate immunity of the Mediterranean mussel *Mytilus galloprovincialis*. *BMC Genomics*, *12*(1), 69. https://doi.org/10.1186/1471-2164-12-69

Venier, P., Domeneghetti, S., Sharma, N., Pallavicini, A., & Gerdol, M. (2016). Immune-related signaling in mussel and bivalves. In: Ballarin, L., & Cammarata, M. (eds). *Lessons in Immunity*. Academic Press. pp. 93-105. https://doi.org/10.1016/b978-0-12-803252-7.00007-2

Vera, M., Carlsson, J., Carlsson, J. E., Cross, T., Lynch, S., Kamermans, P., Villalba, A., Culloty, S., & Martínez, P. (2016). Current genetic status, temporal stability and structure of the remnant wild European flat oyster populations: conservation and restoring implications. *Marine Biology*, *163*(12), 239. https://doi.org/10.1007/s00227-016-3012-x

Vera, M., Pardo, B., Cao, A., Vilas, R., Fernández, C., Blanco, A., Gutiérrez, A., Bean, T., Houston, R., Villalba, A., & Martínez, P. (2019). Signatures of selection for bonamiosis resistance in European flat oyster (*Ostrea edulis*): New genomic tools for breeding programs and management of natural resources. *Evolutionary Applications*, *12*(9), 1781-1796. https://doi.org/10.1111/eva.12832

Vercaemer, B., Spence, K. R., Herbinger, C. M., Lapègue, S., & Kenchington, E. L. (2006). Genetic diversity of the European oyster (*Ostrea edulis* L.) in Nova Scotia: Comparison with other parts of Canada, Maine and Europe and implications for broodstock management. *Journal of Shellfish Research*, *25*(2), 543-551. https://doi.org/10.2983/0730-8000(2006)25

Villalba, A., Reece, K. S., Ordás, M. C., Casas, S. M., & Figueras, A. (2004). Perkinsosis in molluscs: A review. *Aquatic Living Resources*, *17*(4), 411-432. https://doi.org/10.1051/alr:2004050

Villoutreix, R., Ayala, D., Joron, M., Gompert, Z., Feder, J. L., & Nosil, P. (2021). Inversion breakpoints and the evolution of supergenes. *Molecular Ecology*, *30*(12), 2738-2755. https://doi.org/10.1111/mec.15907

USC DE COMPOSTELA

Vizzini, A., Bonura, A., La Paglia, L., Fiannaca, A., La Rosa, M., Urso, A., Mauro, M., Vazzana, M., & Arizza, V. (2021). Transcriptomic analyses reveal 2 and 4 family members of cytochromes P450 (CYP) involved in LPS inflammatory response in pharynx of *Ciona robusta*. *International Journal of Molecular Sciences*, *22*(20), 11141. https://doi.org/10.3390/ijms222011141

Walkowiak, S., Gao, L., Monat, C., Haberer, G., Kassa, M. T., Brinton, J., Ramirez-Gonzalez, R. H., Kolodziej, M. C., Delorean, E., Thambugala, D., Klymiuk, V., Byrns, B., Gundlach, H., Bandi, V., Siri, J. N., Nilsen, K., Aquino, C., Himmelbach, A., Copetti, D., . . . Pozniak, C. J. (2020). Multiple wheat genomes reveal global variation in modern breeding. *Nature*, *588*(7837), 277–283. https://doi.org/10.1038/s41586-020-2961-x

Wang, H., Liao, Z., Yang, Z., Xiao, W., Yang, Z., He, J., Zhang, X., Yan, X., & Tang, C. (2024). Histone derived antimicrobial peptides identified from *Mytilus coruscus* serum by peptidomics. *Fish and Shellfish Immunology, 149,* 109546. https://doi.org/10.1016/j.fsi.2024.109546

Wang, K., Ren, H., Xu, D., Cai, L., & Yang, M. (2008). Identification of the up-regulated expression genes in hemocytes of variously colored abalone (*Haliotis diversicolor* Reeve, 1846) challenged with bacteria. *Developmental & Comparative Immunology*, *32*(11), 1326–1347. https://doi.org/10.1016/j.dci.2008.04.007

Wang, L., Zhang, H., Wang, M., Zhou, Z., Wang, W., Liu, R., Huang, M., Yang, C., Qiu, L., & Song, L. (2018). The transcriptomic expression of pattern recognition receptors: Insight into molecular recognition of various invading pathogens in Oyster C*rassostrea gigas*. *Developmental & Comparative Immunology*, *91*, 1-7. https://doi.org/10.1016/j.dci.2018.09.021

Wang, W., Wang, L., & Song, L. 2025. The immune priming in aquaculture invertebrates: inspiration from cellular perspective and future investigation. *Reviews in Aquaculture, 17,* e12977. https://doi.org/10.1111/raq.12977

Weir, B. S., & Cockerham, C. C. (1984). Estimating F-Statistics for the analysis of population structure. *Evolution*, *38*(6), 1358-1370. https://doi.org/10.1111/j.1558-5646.1984.tb05657.x

Wellenreuther, M., & Bernatchez, L. (2018). Eco-Evolutionary genomics of chromosomal inversions. *Trends in Ecology & Evolution*, *33*(6), 427-440. https://doi.org/10.1016/j.tree.2018.04.002

Wickham, H. (2009). *ggplot2: Elegant graphics for data analysis*. http://ndl.ethernet.edu.et/bitstream/123456789/60263/1/107.pdf

Winter, D. (2020). *pafr: Read, Manipulate and Visualize "Pairwise mApping Format" Data*. https://doi.org/10.32614/cran.package.pafr

Xu, T., Xie, J., Zhu, B., Liu, X., & Wu, X. (2014). Allograft inflammatory factor 1 functions as a pro-inflammatory cytokine in the oyster, *Crassostrea ariakensis*. *PLoS ONE*, *9*(4), e95859. https://doi.org/10.1371/journal.pone.0095859

Xue, Q., Waldrop, G. L., Schey, K. L., Itoh, N., Ogawa, M., Cooper, R. K., Losso, J. N., & La Peyre, J. F. (2006). A novel slow-tight binding serine protease inhibitor from eastern oyster (*Crassostrea virginica*) plasma inhibits perkinsin, the major extracellular protease of the oyster protozoan parasite *Perkinsus marinus*. *Comparative Biochemistry and Physiology Part B Biochemistry and Molecular Biology*, *145*(1), 16-26. https://doi.org/10.1016/j.cbpb.2006.05.010

Xue, Q., Renault, T., Cochennec, N., & Gerard, A. (2000). Separation of European flat oyster, *Ostrea edulis*, haemocytes by density gradient centrifugation and SDS-PAGE characterisation of separated haemocyte sub-populations. *Fish & Shellfish Immunology*, *10*(2), 155–165. https://doi.org/10.1006/fsim.1999.0234

Xue, Q., Itoh, N., Schey, K. L., Li, Y.-., Cooper, R. K., & La Peyre, J. F. (2007). A new lysozyme from the eastern oyster (*Crassostrea virginica*) indicates adaptive evolution of i-type lysozymes. *Cellular and Molecular Life Sciences*, *64*(1), 82-95. https://doi.org/10.1007/s00018-006-6386-y

Yang, W., Tran, N. T., Zhu, C.-H., Yao, D.-F., Aweya, J. J., Gong, Y., Ma, H.-Y., Zhang, Y.-L., Li, G.-L., & Li, S.-K. 2021. Immune priming in shellfish: A review and an updating mechanistic insight focused on cellular and humoral responses. *Aquaculture, 530,* 735831. https://doi.org/10.1016/j.aquaculture.2020.735831

Yoneyama, M., & Fujita, T. (2007). RIG-I family RNA helicases: Cytoplasmic sensor for antiviral innate immunity. *Cytokine & Growth Factor Reviews*, *18*(5–6), 545–551. https://doi.org/10.1016/j.cytogfr.2007.06.023

Yongue (1960). Oysters By C. M. Yonge New Naturalist Special Volume, Collins, London, 1960. Pp. xiv + 209, 17 plates and 72 text-figures. Price 21s. *Journal of the Marine Biological Association of the United Kingdom*, *41*(3), 835–835. https://doi.org/10.1017/s0025315400016350

Yu, H., He, Y., Wang, X., Zhang, Q., Bao, Z., & Guo, X. (2011). Polymorphism in a serine protease inhibitor gene and its association with disease resistance in the eastern oyster (*Crassostrea virginica* Gmelin). *Fish & Shellfish Immunology*, *30*(3), 757-762. https://doi.org/10.1016/j.fsi.2010.12.015

Zhang, C., Dong, S., Xu, J., He, W., & Yang, T. (2019). PopLDdecay: a fast and effective tool for linkage disequilibrium decay analysis based on variant call format files. *Bioinformatics*, *35*(10), 1786–1788. https://doi.org/10.1093/bioinformatics/bty875

Zhang, H., Song, L., Li, C., Zhao, J., Wang, H., Gao, Q., & Xu, W. (2007). Molecular cloning and characterization of a thioester-containing protein from Zhikong scallop *Chlamys farreri*. *Molecular Immunology*, *44*(14), 3492–3500. https://doi.org/10.1016/j.molimm.2007.03.008

USC UNIVERSIDADE DE SANTIAGO DE COMPOSTELA

Zhang, H., Wang, L., Song, L., Zhao, J., Qiu, L., Gao, Y., Song, X., Li, L., Zhang, Y., & Zhang, L. (2009). The genomic structure, alternative splicing and immune response of *Chlamys farreri* thioester-containing protein. *Developmental & Comparative Immunology*, *33*(10), 1070–1076. https://doi.org/10.1016/j.dci.2009.05.007

Zhang, L., Li, L., Zhu, Y., Zhang, G., & Guo, X. (2013). Transcriptome Analysis reveals a rich gene set related to innate immunity in the Eastern oyster (*Crassostrea virginica*). *Marine Biotechnology*, *16*(1), 17–33. https://doi.org/10.1007/s10126-013-9526-z

Zhang, L., Li, L., Guo, X., Litman, G. W., Dishaw, L. J., & Zhang, G. (2015). Massive expansion and functional divergence of innate immune genes in a protostome. *Scientific Reports*, *5*(1), 8693. https://doi.org/10.1038/srep08693

Zhang, Q., Chen, J., Wang, W., Lin, J., & Guo, J. (2024). Genome-wide investigation of the TGF-β superfamily in scallops. *BMC Genomics*, *25*(1), 24. https://doi.org/10.1186/s12864-023-09942-w

Zhang, S., Adema, C. M., Kepler, T. B., & Loker, E. S. (2004). Diversification of IG superfamily genes in an invertebrate. *Science*, *305*(5681), 251–254. https://doi.org/10.1126/science.1088069

Zhang, W., Tan, C., Hu, H., Pan, R., Xiao, Y., Ouyang, K., Zhou, G., Jia, Y., Zhang, X., Hill, C. B., Wang, P., Chapman, B., Han, Y., Xu, L., Xu, Y., Angessa, T., Luo, H., Westcott, S., Sharma, D., . . . Li, C. (2023). Genome architecture and diverged selection shaping pattern of genomic differentiation in wild barley. *Plant Biotechnology Journal*, *21*(1), 46-62. https://doi.org/10.1111/pbi.13917

Zhang, X., Bai, X., Yan, B., Bi, K., & Qin, L. (2014). *Vibrio harveyi* as a causative agent of mass mortalities of megalopa in the seed production of swimming crab *Portunus trituberculatus*. *Aquaculture International*, *22*(2), 661–672. https://doi.org/10.1007/s10499-013-9695-9

Zhang, Y., Li, J., Yu, F., He, X., & Yu, Z. (2013). Allograft inflammatory factor-1 stimulates hemocyte immune activation by enhancing phagocytosis and expression of inflammatory cytokines in *Crassostrea gigas*. *Fish & Shellfish Immunology*, *34*(5), 1071–1077. https://doi.org/10.1016/j.fsi.2013.01.014

Zhang, Y., Yu, F., Li, J., Tong, Y., Zhang, Y., & Yu, Z. (2014). The first invertebrate RIG-I-like receptor (RLR) homolog gene in the pacific oyster *Crassostrea gigas*. *Fish & Shellfish Immunology*, *40*(2), 466–471. https://doi.org/10.1016/j.fsi.2014.07.029

Zhao, M., Lin, Z., Zheng, Z., Yao, D., Yang, S., Zhao, Y., Chen, X., Aweya, J. J., & Zhang, Y. (2023). The mechanisms and factors that induce trained immunity in arthropods and mollusks. *Frontiers in Immunology*, *14,* 1241934. https://doi.org/10.3389/fimmu.2023.1241934

USC UNIVERSIDADE DE SANTIAGO DE COMPOSTELA

Zong, Y., Liu, Z., Wu, Z., Han, Z., Wang, L., & Song, L. (2018). A novel globular C1q domain containing protein (C1qDC-7) from *Crassostrea gigas* acts as pattern recognition receptor with broad recognition spectrum. *Fish & Shellfish Immunology*, *84*, 920–926. https://doi.org/10.1016/j.fsi.2018.10.079

zu Ermgassen, P., Bonačić, K., Boudry, P., Bromley, C., Cameron, T., Colsoul, B., Coolen, J., Frankić, A., Hancock, B., Have, T., Holbrook, Z., Kamermans, P., Laugen, A., Nevejan, N., Pogoda, B., Pouvreau, S., Preston, J., Ranger, C., Sanderson, W., . . . Sutherland, W. (2021). Forty questions of importance to the policy and practice of native oyster reef restoration in Europe. *Aquatic Conservation: Marine and Freshwater Ecosystems*, *30*(11), 2038-2049. https://doi.org/10.1002/aqc.3462

zu Ermgassen, P. S., Strand, Å., Bakker, N., Blanco, A., Bonačić, K., Boudry, P., Brundu, G., Cameron, T. C., Connellan, I., Da Costa, F., Debney, A., Fabra, M., Frankic, A., Gamble, C., Gray, M. W., Helmer, L., Holbrook, Z., Hugh-Jones, T., Kamermans, P., . . . Colsoul, B. (2023). Overcoming *Ostrea edulis* seed production limitations to meet ecosystem restoration demands in the UN decade on restoration. *Aquatic Living Resources*, *36*, 16. https://doi.org/10.1051/alr/2023012

USC UNIVERSIDADE DE SANTIAGO DE COMPOSTELA

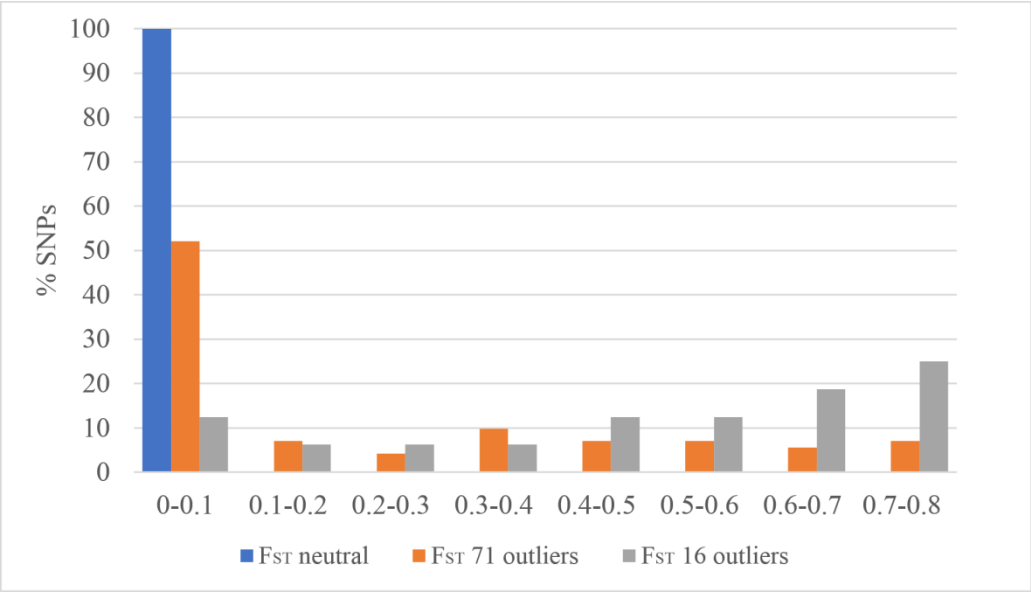
ANNEX I:

SUPPLEMENTARY FIGURES

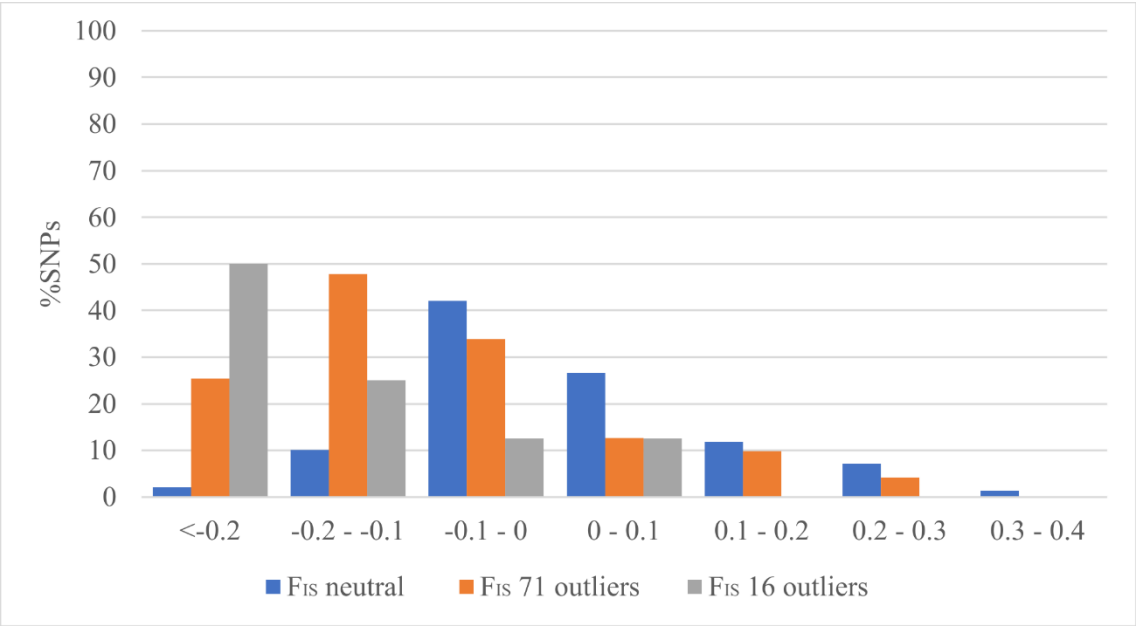
USC
UNIVERSIDADE
DE SANTIAGO
DE COMPOSTELA

USC
UNIVERSIDADE
DE SANTIAGO
DE COMPOSTELA

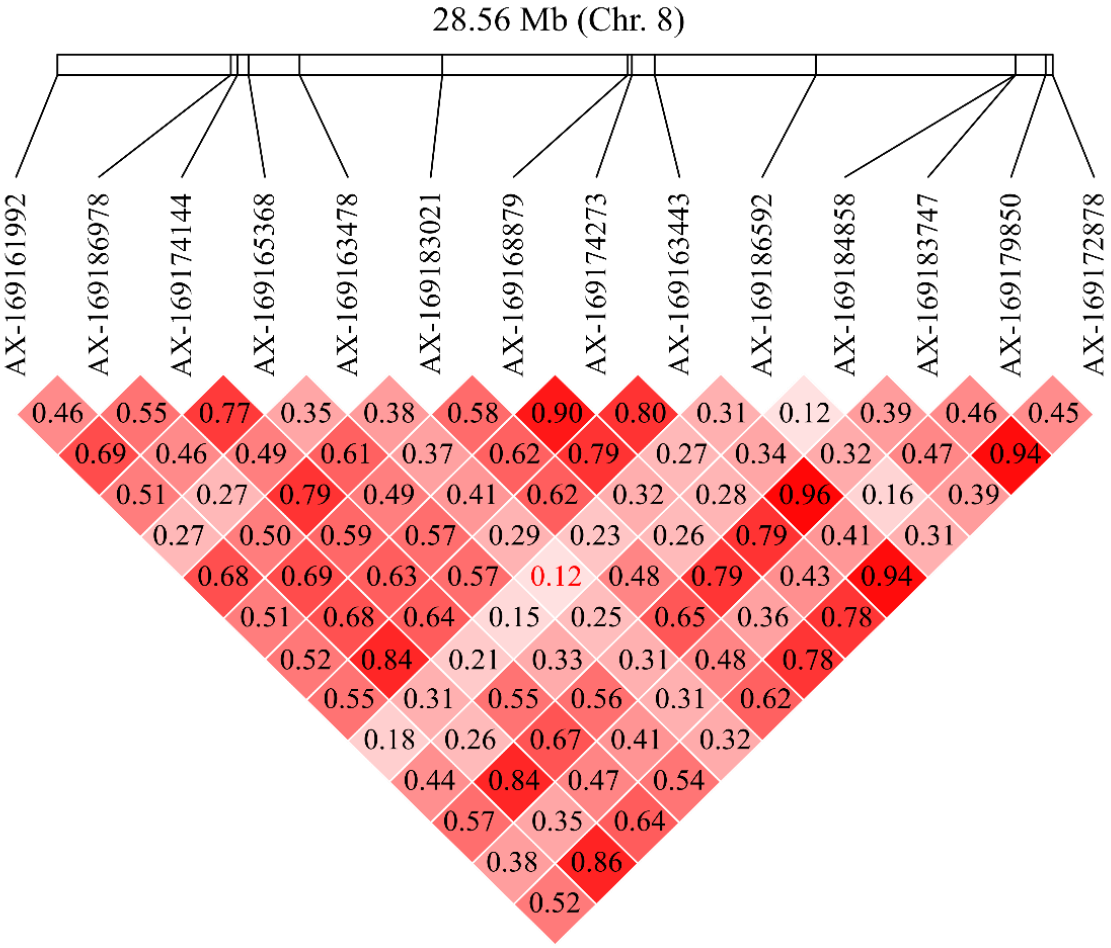
SUPPLEMENTARY FIGURES CHAPTER 1:



Supplementary Figure 1. Frequency histogram showing the number of outliers per F_{ST} interval using the neutral, the 71 suggestive and 16 consistent SNP outlier panels between NV and LTA samples of *Ostrea edulis* from the North Sea.



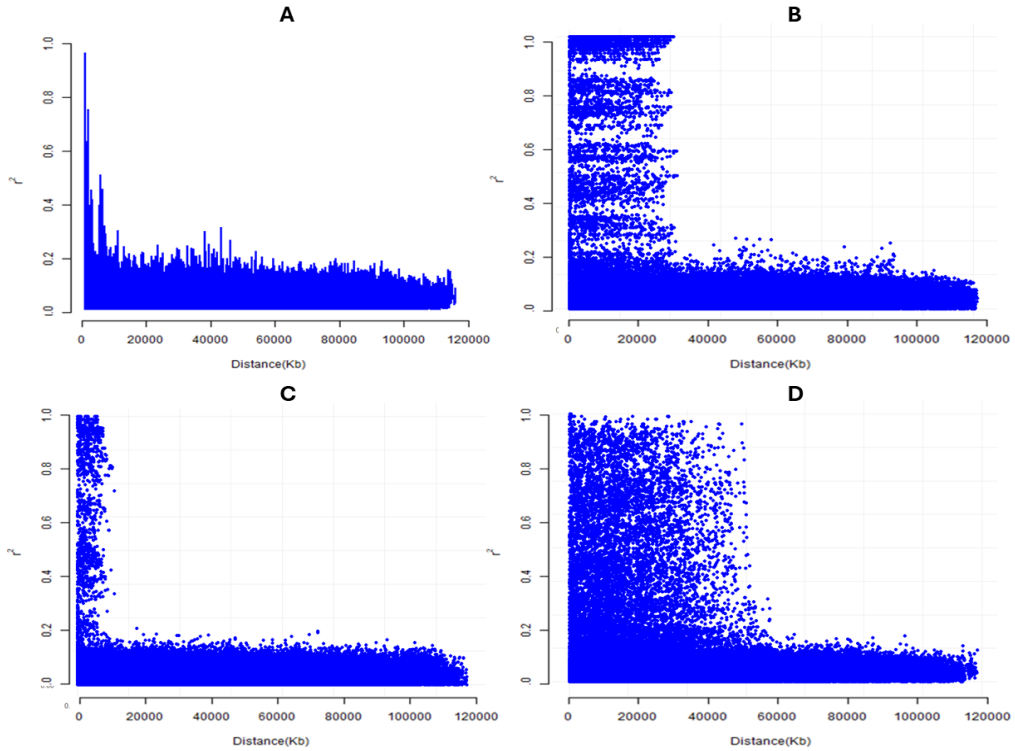
Supplementary Figure 2. Comparative frequency histogram of the number of outliers per F_{IS} interval using the neutral, the 71 suggestive and 16 consistent SNP outlier panels within NV and LTA samples of *Ostrea edulis* from the North Sea



Supplementary Figure 3. Linkage disequilibrium (r^2) between all pairs of consistent outliers at OE-C8 of *Ostrea edulis*. LD intensity ($r^2$from 0 to 1) is shown using a range from whitish to reddish colours, respectively. All r^2 values significant after Bonferroni correction ($P < 0.00005$), except that highlighted in red font.

USC
UNIVERSIDADE DE SANTIAGO DE COMPOSTELA

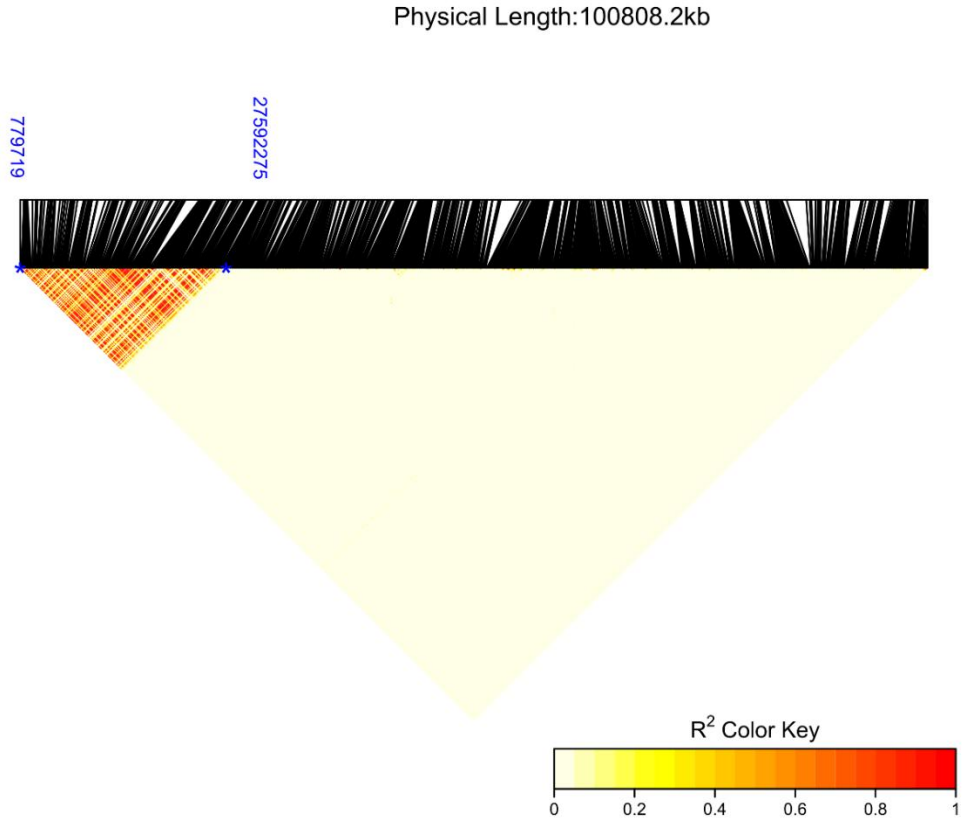
SUPPLEMENTARY FIGURES CHAPTER 2:



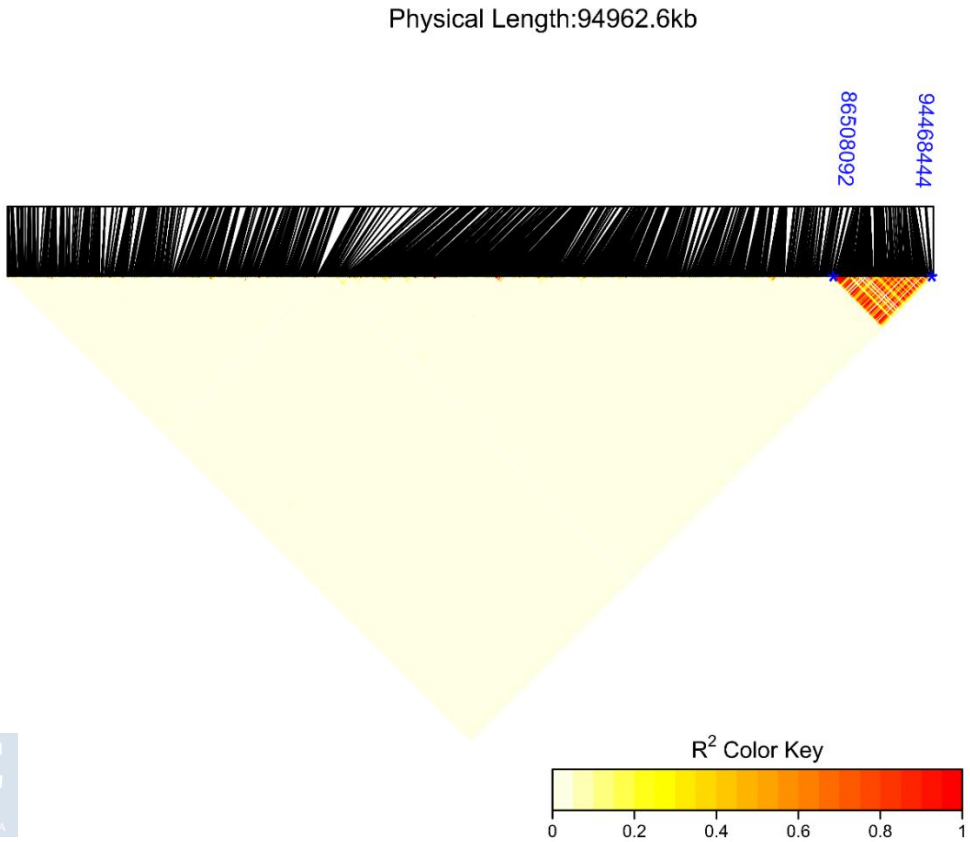
Supplementary Figure 1. Average Linkage Disequilibium (r^2) decay with physical distance in *O. edulis*: A) All chromosomes excluding chromosomes 2, 5 and 8; B) chromosome 2; C) chromosome 5; D) chromosome 8

USC
UNIVERSIDADE DE SANTIAGO DE COMPOSTELA

A)

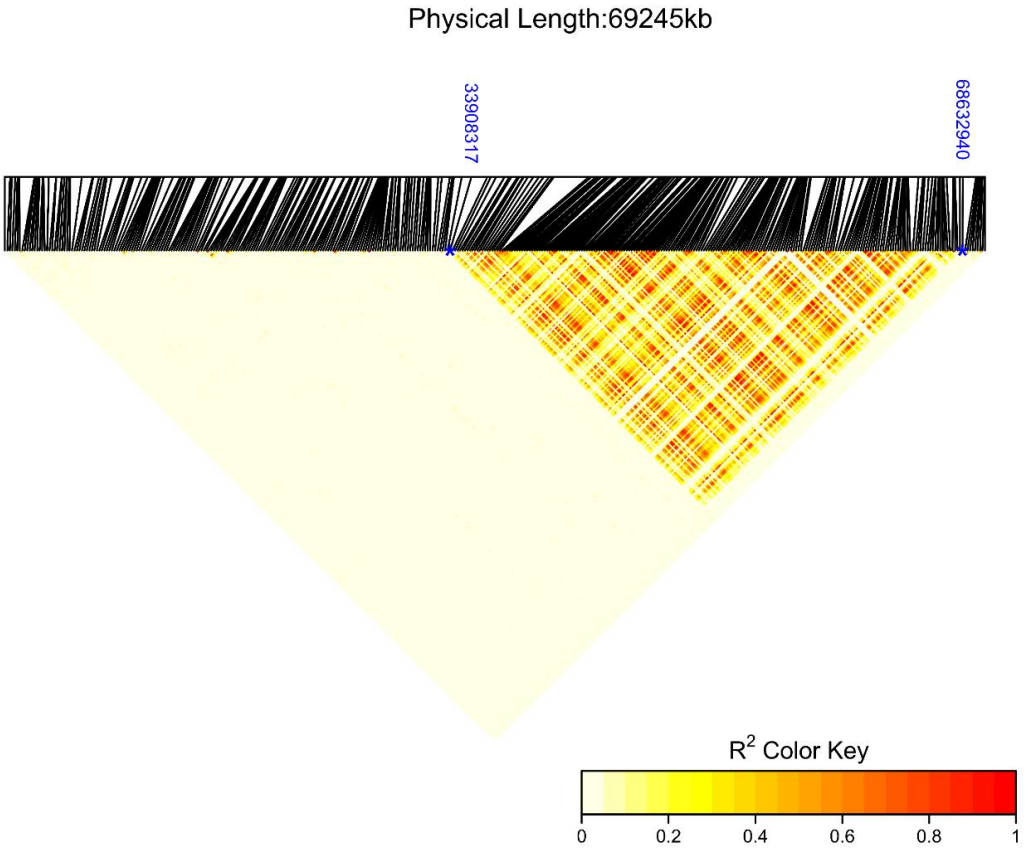


B)



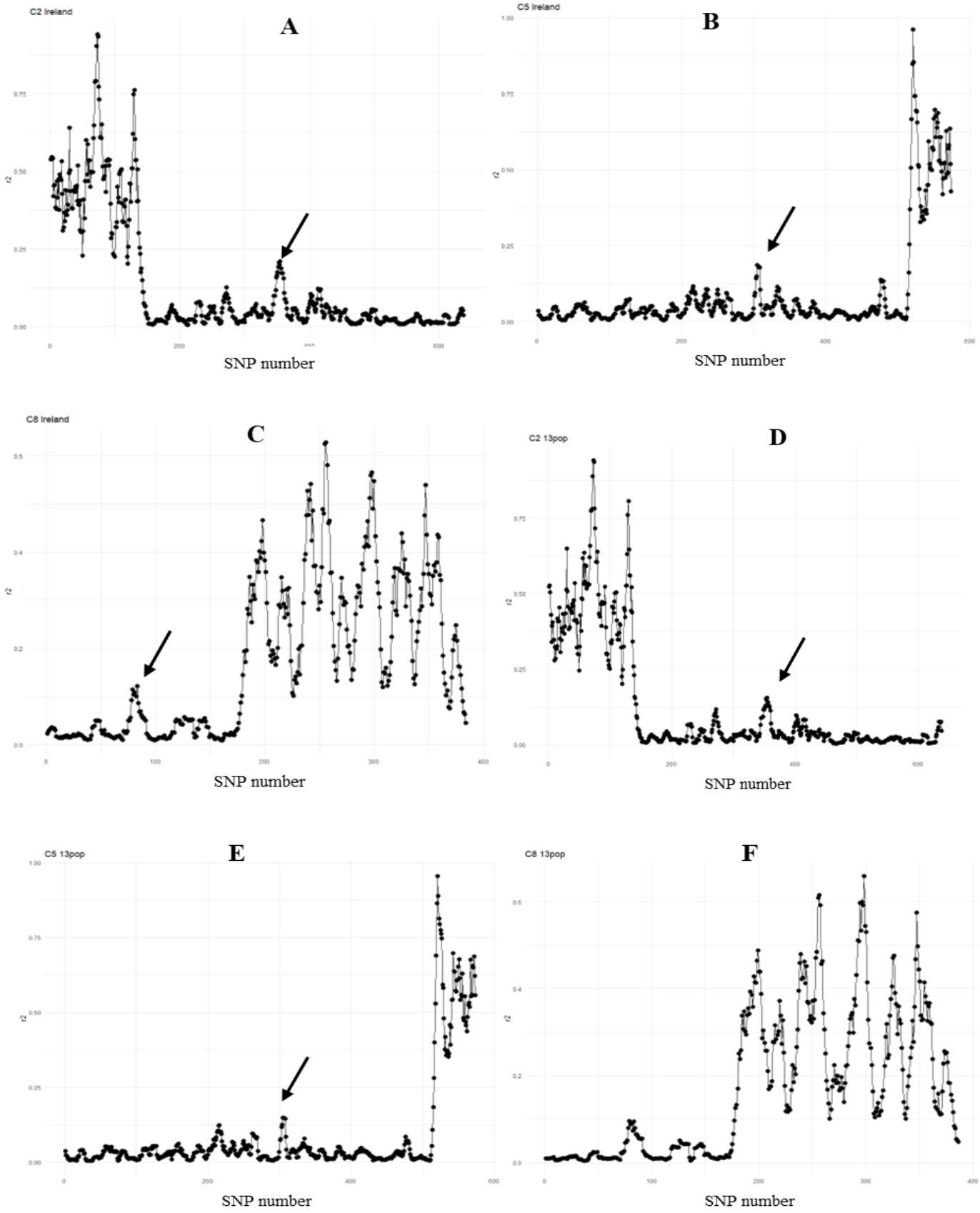
USC
UNIVERSIDADE DE SANTIAGO DE COMPOSTELA

C)

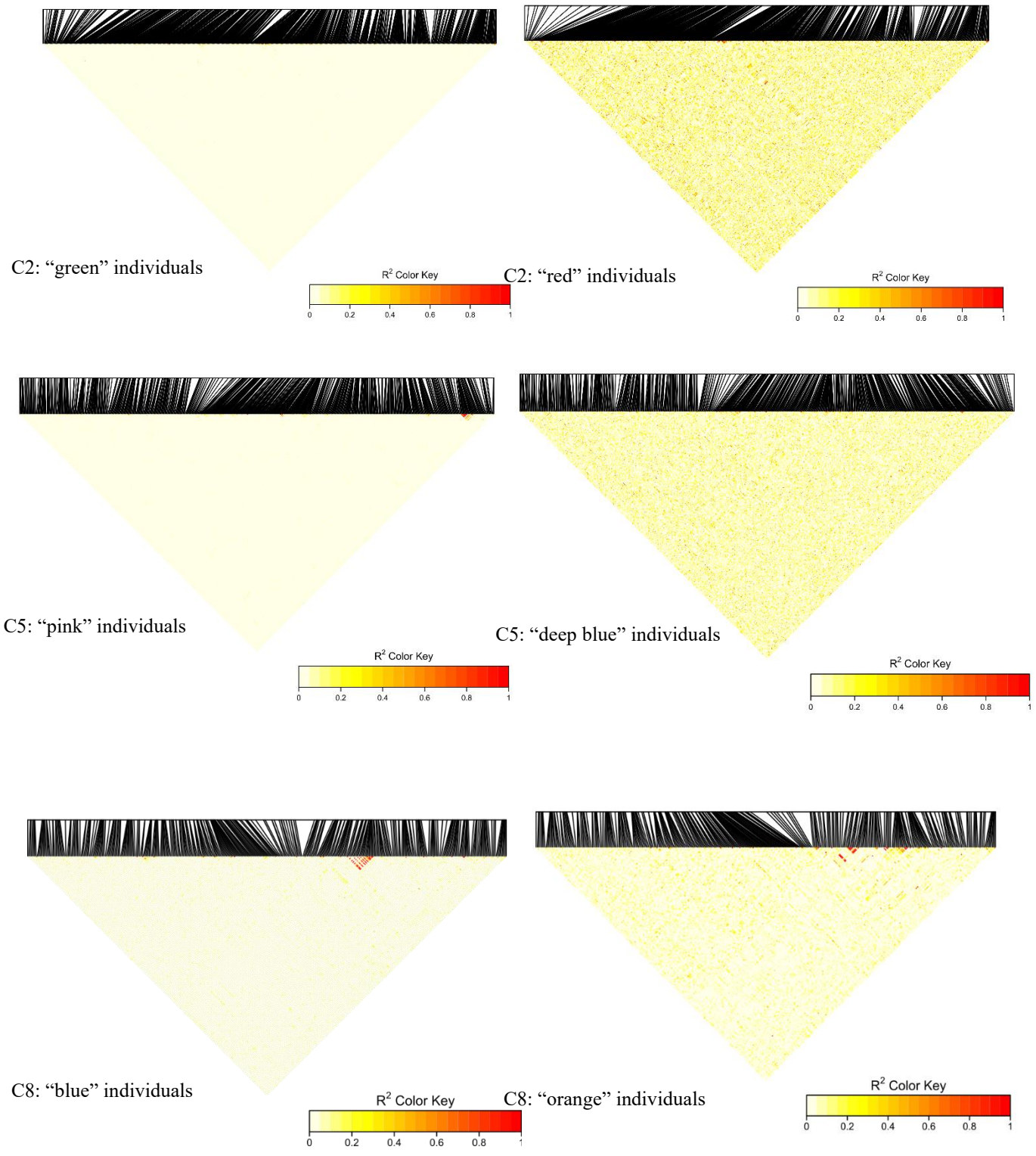


Supplementary Figure 2. Heatmap r^2 plots for chromosomes with atypical LD: A) C2, B) C5, and C) C8.

USC
UNIVERSIDADE DE SANTIAGO DE COMPOSTELA

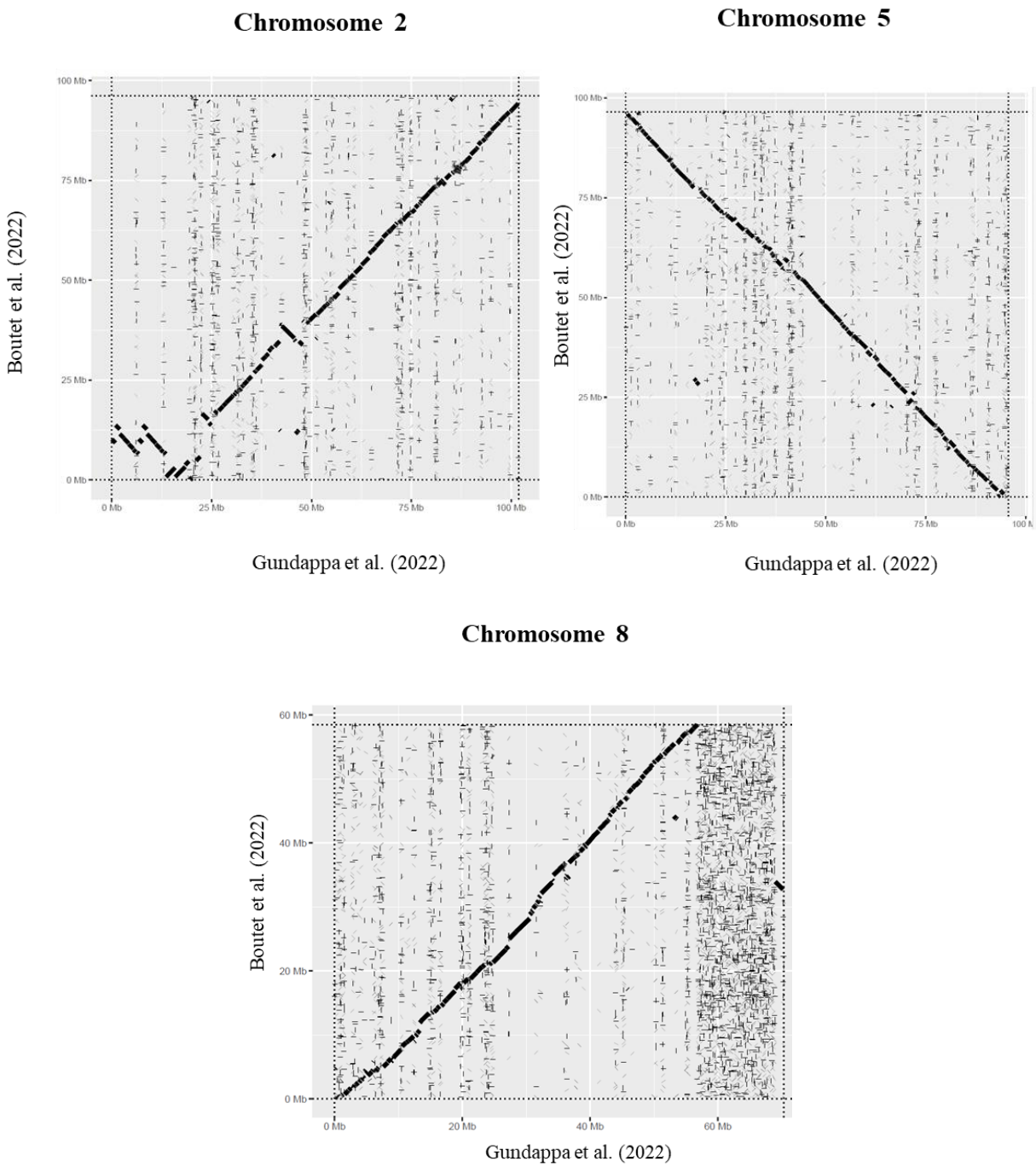


Supplementary Figure 3. Linkage disequilibrium (LD) variation across C2 (A, D), C5 (B, E) and C8 (C, F) of *O. edulis* using average LD over 10 SNP sliding windows from the two big Irish population (A, B, C) and the whole population (D, E, F) datasets. Arrows show a putative position for centromeres in the two longest metacentric C2 and C5 and submetacentric C8.



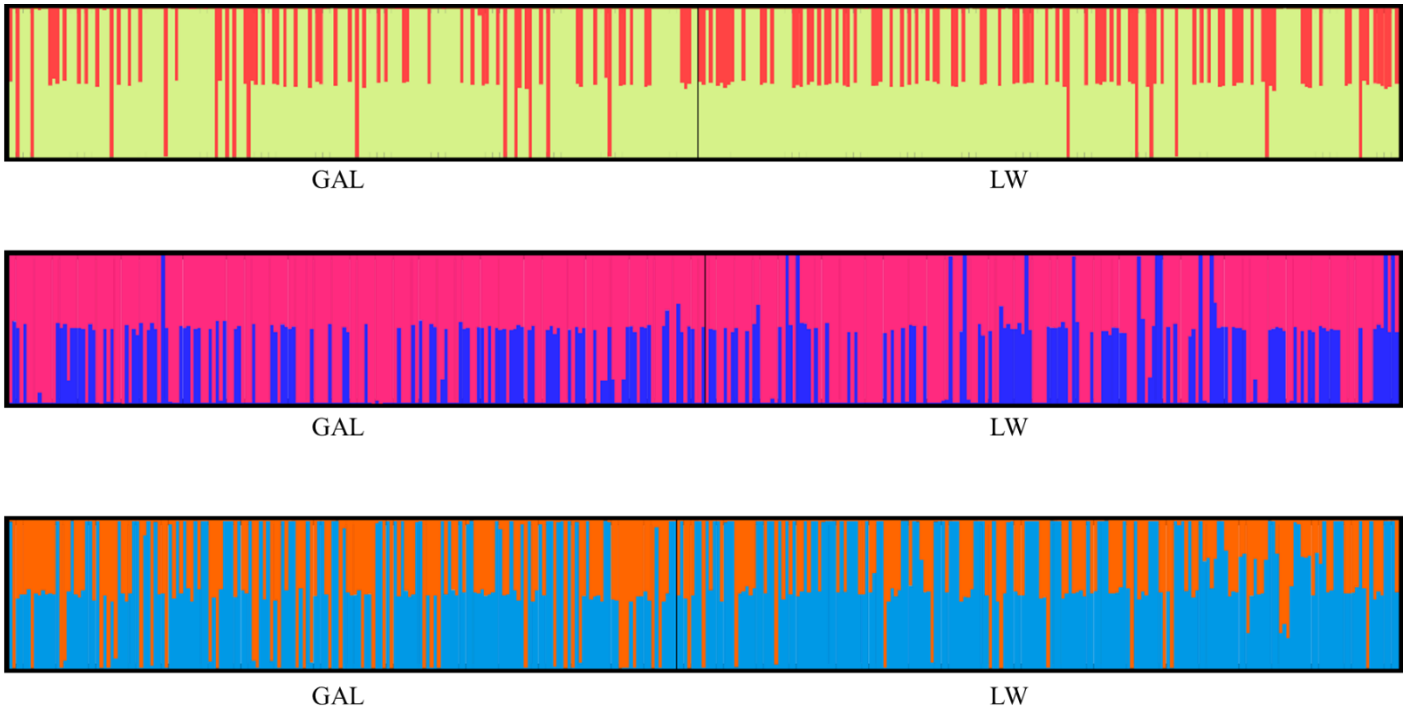
Supplementary Figure 4. LD heatmap plots for homozygotes in each arrangement within inversions: A) C2 “green”; B) C2 “red”; C) C5 “pink”; D) C5 “deep blue”; E) C8 “blue (F) C8 “orange”

USC
UNIVERSIDADE DE SANTIAGO DE COMPOSTELA

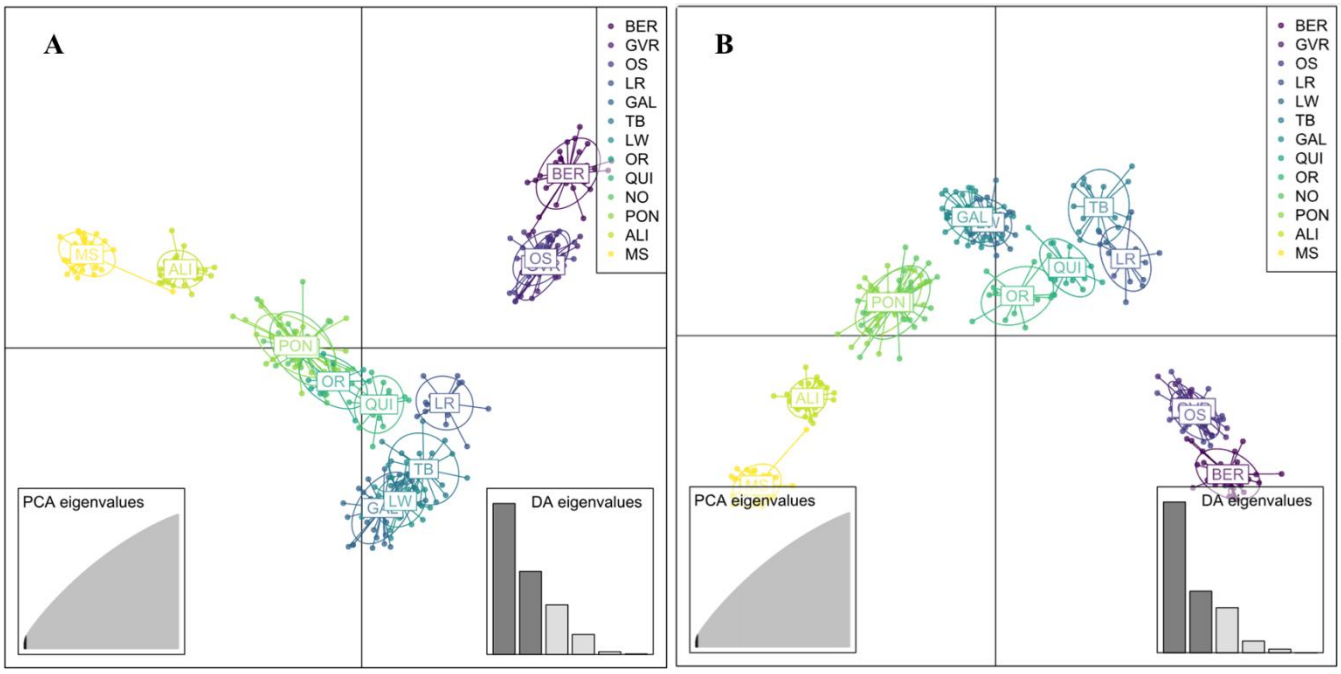


Supplementary Figure 5. Sequence alignment of chromosomes 2, 5 and 8 from Gundappa et al. (2022) and Boutet et al. (2022) using Minimap2 (Li, 2018)

USC
UNIVERSIDADE DE SANTIAGO DE COMPOSTELA



Supplementary Figure 6. STRUCTURE analysis (K = 2) in 384 individuals from the three Irish populations using SNPs within inversion at C2, C5, and C8 (from top to bottom).

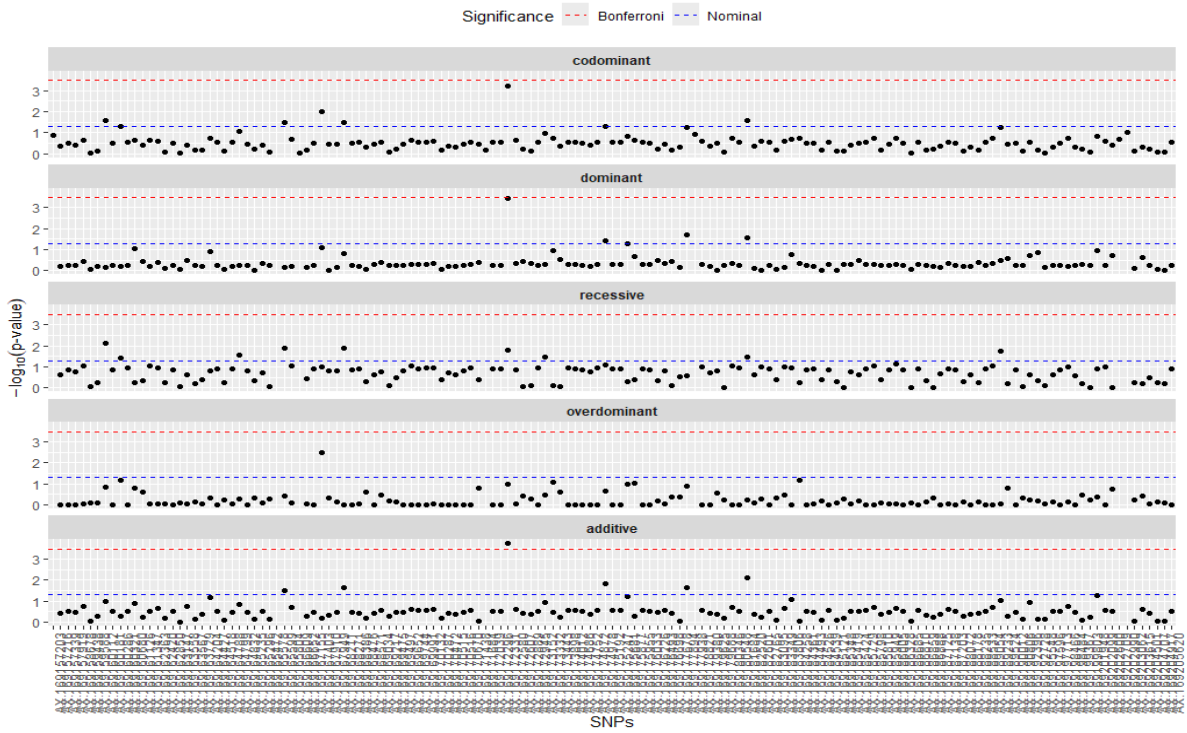


Supplementary Figure 8. DAPC plots for 13 European populations of *O. edulis* using different SNP datasets: A) whole SNP panel of 4,741 SNPs; and B) excluding SNPs within inversions (4,316 SNPs).

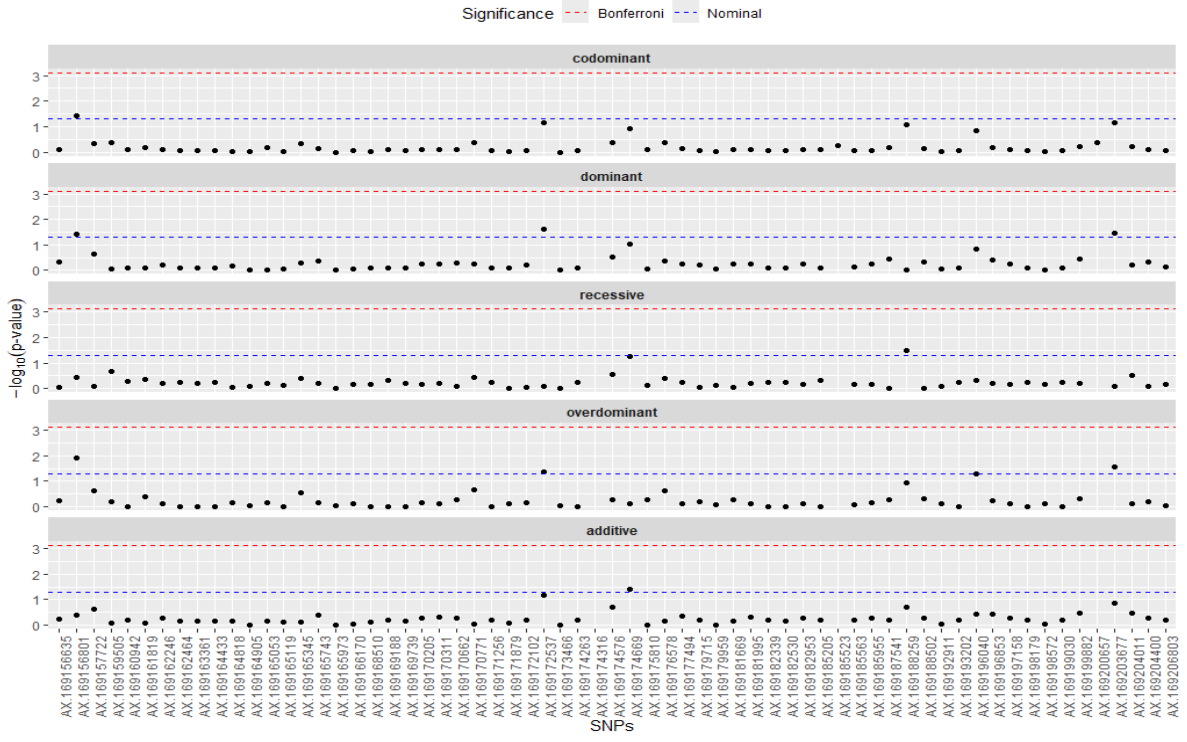
USC
UNIVERSIDADE DE SANTIAGO DE COMPOSTELA

SUPPLEMENTARY FIGURES CHAPTER 3:

A)

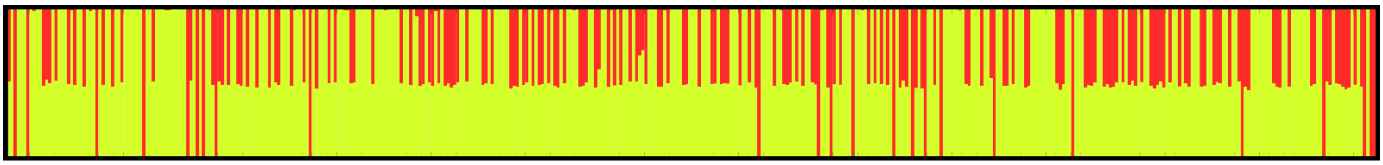


B)

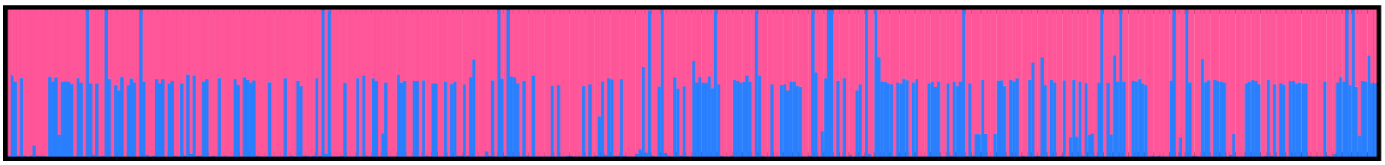


Supplementary Figure 1. Association analysis between SNPs and infection under five genetic models (codominant, dominant, recessive, overdominant, and additive) using the SNPassoc package in R. Each point represents the –log10(p-value) for a given SNP under the corresponding model. The dashed blue line indicates nominal significance (α = 0.05) and the dashed red line represents the Bonferroni-corrected threshold. (A) C2 and (B) C5.

A)



B)



Galway Lough Swilly Rossmore

Supplementary Figure 2. STRUCTURE analysis (K = 2) using the SNPs included at inversion C2 (A) and C5 (B)

USC
UNIVERSIDADE DE SANTIAGO DE COMPOSTELA

USC
UNIVERSIDADE
DE SANTIAGO
DE COMPOSTELA

ANNEX II:

SUPPLEMENTARY TABLES

USC
UNIVERSIDADE
DE SANTIAGO
DE COMPOSTELA

USC
UNIVERSIDADE
DE SANTIAGO
DE COMPOSTELA

SUPPLEMENTARY TABLES CHAPTER II:

Table S1: Statistics of raw PacBio sequencing reads.

Sample	Total Reads	Retained Reads	Retained	Min Length (bp)	Max Length (bp)	Mean Length (bp)	Total Size (bp)
LW_2	1310002	869155	0.663	138	50687	8761	11477130884
LW_15	957865	837331	0.874	192	34566	8981	8602293658
LW_33	1393841	804100	0.577	173	34471	6675	9303540320
LW_87	954020	739086	0.775	156	43235	8089	7716737688
GAL_7	876960	728839	0.831	84	44541	11635	10203687427
GAL_173	174412	19646	0.113	94	38185	3223.363	562193210

Table S2. Coding genes annotated within the inversions at A) C2, B) C5 and C) C8

Gene	Annotation	START	END
LOC125667883	STAM-binding protein-like	6353626	6371286
LOC125667884	uncharacterized protein LOC125667884	6476492	6478300
LOC125667889	WD repeat-containing protein 70-like	20877982	20891371
LOC125667890	alpha-1%2C3/1%2C6-mannosyltransferase ALG2-like isoform X4	20867523	20876358
LOC125667891	cAMP-dependent protein kinase catalytic subunit 1 isoform X1	20803683	20854647
LOC125667909	craniofacial development protein 2-like	6656036	6657424
LOC125667914	LOW QUALITY PROTEIN: uncharacterized protein LOC125667914	7038939	7225996
LOC125667921	uncharacterized protein LOC125667921	7335379	7337419
LOC125667922	helicase with zinc finger domain 2-like isoform X1	23191483	23205916
LOC125667923	LOW QUALITY PROTEIN: helicase with zinc finger domain 2-like	23230513	23244321
LOC125667924	uncharacterized protein LOC125667924	7435003	7438313
LOC125667925	uncharacterized protein LOC125667925	7527486	7528652
LOC125667927	uncharacterized protein LOC125667927	7703261	7791730
LOC125667935	uncharacterized protein LOC125667935	21820737	21827831
LOC125667936	uncharacterized protein LOC125667936 isoform X2	21768296	21775684
LOC125667937	uncharacterized protein LOC125667937	21798122	21820125
LOC125667939	uncharacterized protein LOC125667939	21800383	21808180
LOC125667940	uncharacterized protein LOC125667940	21762651	21768193
LOC125667941	uncharacterized protein LOC125667941	21828750	21830266
LOC125667942	uncharacterized protein LOC125667942	21778170	21791177
LOC125667947	LOW QUALITY PROTEIN: uncharacterized protein LOC125667947	8015403	8062503
LOC125667951	uncharacterized protein LOC125667951	8285947	8288016
LOC125667979	uncharacterized protein LOC125667979	9061450	9064010
LOC125667980	carbohydrate sulfotransferase 12-like	9078664	9079794
LOC125667981	RYamide receptor-like	9180822	9187770
LOC125667982	uncharacterized protein LOC125667982	9250446	9258925
LOC125667983	threonylcarbamoyladenosine tRNA methylthiotransferase-like	26441793	26470954
LOC125667984	uncharacterized protein LOC125667984	26507999	26517634
LOC125667991	uncharacterized protein LOC125667991	9691768	9693483
LOC125667997	uncharacterized protein LOC125667997	9940390	9943540
LOC125667999	uncharacterized protein LOC125667999	9996674	9997321
LOC125668010	uncharacterized protein LOC125668010	10250885	10437924
LOC125668011	elongator complex protein 3 isoform X3	8085311	8105172
LOC125668012	uncharacterized protein LOC125668012 isoform X1	8033049	8043411
LOC125668013	nuclear transcription factor Y subunit gamma-like	8065734	8085308
LOC125668015	uncharacterized protein LOC125668015	10536062	10544163

LOC125668016	uncharacterized protein LOC125668016	10547298	10549345
LOC125668018	uncharacterized protein LOC125668018	10646899	10650207
LOC125668027	uncharacterized protein LOC125668027	11181168	11189046
LOC125668029	uncharacterized protein LOC125668029	11267460	11268287
LOC125668045	DBH-like monooxygenase protein 1 homolog	24660784	24700869
LOC125668046	uncharacterized protein LOC125668046 isoform X2	24663255	24690292
LOC125668049	von Willebrand factor A domain-containing protein 3A-like	10030403	10046337
LOC125668050	dynein axonemal assembly factor 5-like	10051690	10058141
LOC125668051	uncharacterized protein LOC125668051	10063298	10065513
LOC125668053	uncharacterized protein LOC125668053 isoform X3	10067335	10097427
LOC125668054	uncharacterized protein LOC125668054	10004254	10015050
LOC125668055	uncharacterized protein LOC125668055	10097358	10098988
LOC125668068	uncharacterized protein LOC125668068	11779408	11780247
LOC125668081	hydroxyacyl-coenzyme A dehydrogenase%2C mitochondrial-like	12010107	12021546
LOC125668082	zinc finger protein ubi-d4-like	12222225	12234663
LOC125668083	probable endochitinase	12326426	12329234
LOC125668088	chitotriosidase-1-like	12329348	12332493
LOC125668112	methylated-DNA--protein-cysteine methyltransferase-like	12855558	12864020
LOC125668116	uncharacterized protein LOC125668116	13085138	13086288
LOC125668123	LOW QUALITY PROTEIN: STAM-binding protein-like	13190556	13209089
LOC125668124	uncharacterized protein LOC125668124	13315664	13317762
LOC125668125	ADP-ribosylation factor 4-like	13324459	13324905
LOC125668136	uncharacterized protein LOC125668136	13336521	13338712
LOC125668137	uncharacterized protein LOC125668137	13339982	13340410
LOC125668140	trypsin-like	13525060	13527308
LOC125668141	LOW QUALITY PROTEIN: uncharacterized protein LOC125668141	13576212	13664092
LOC125668144	elongator complex protein 3 isoform X1	1289997	1309821
LOC125668145	uncharacterized protein LOC125668145 isoform X2	1237750	1248091
LOC125668149	nuclear transcription factor Y subunit gamma-like	1270429	1287315
LOC125668152	uncharacterized protein LOC125668152	14088106	14113679
LOC125668212	long-chain-fatty-acid--CoA ligase 1-like isoform X1	25961271	26005766
LOC125668214	meiotic recombination protein DMC1/LIM15 homolog	25945009	25961705
LOC125668215	NHP2-like protein 1	25935830	25944632
LOC125668227	DNA-dependent protein kinase catalytic subunit-like	22133765	22155887
LOC125668228	dolichyl pyrophosphate Man9GlcNAc2 alpha-1%2C3-glucosyltransferase-like isoform X2	22067910	22102591
LOC125668230	uncharacterized protein LOC125668230	22078912	22133637
LOC125668233	coiled-coil domain-containing protein 78-like isoform X4	20671580	20688676
LOC125668234	AP-1 complex subunit mu-1-like	20655008	20671055
LOC125668235	uncharacterized protein LOC125668235	20696299	20706102
LOC125668257	receptor-type tyrosine-protein phosphatase alpha-like isoform X2	1372619	1461092
LOC125668270	receptor-type tyrosine-protein phosphatase alpha-like isoform X2	8167953	8256431
LOC125668272	pre-mRNA-splicing factor 38A-like	19067241	19073165
LOC125668301	epsin-2-like isoform X1	26010170	26034670
LOC125668303	uncharacterized protein LOC125668303	26034870	26058776
LOC125668353	ras GTPase-activating protein-binding protein 2-like	26067678	26084501
LOC125668354	uncharacterized protein LOC125668354 isoform X7	26061346	26067588
LOC125668399	LOW QUALITY PROTEIN: focal adhesion kinase 1-like	15219740	15248494
LOC125668400	membrane progestin receptor beta-like	15283667	15286356
LOC125668428	LOW QUALITY PROTEIN: (E3-independent) E2 ubiquitin-conjugating enzyme UBE2O-like	23912641	23942100
LOC125668429	multiple epidermal growth factor-like domains protein 10 isoform X1	23690004	23714837
LOC125668431	TBC1 domain family member 2B-like	23850912	23880637
LOC125668432	uncharacterized protein LOC125668432	23627005	23631519
LOC125668433	choline transporter-like protein 1 isoform X2	23717553	23742056
LOC125668434	heparan-alpha-glucosaminide N-acetyltransferase-like isoform X1	23952484	23983824
LOC125668436	protein wntless homolog	23633749	23673043
LOC125668437	uncharacterized protein LOC125668437	23903503	23906701
LOC125668438	XK-related protein 6-like	23680667	23689789
LOC125668439	uncharacterized protein LOC125668439	23785575	23789167
LOC125668440	uncharacterized protein LOC125668440	23776181	23780291
LOC125668441	inositol monophosphatase 3-like	23789241	23805225
LOC125668442	peroxisomal 2%2C4-dienoyl-CoA reductase [(3E)-enoyl-CoA-producing]-like	23942984	23952299

LOC125668445	RAB7A-interacting MON1-CCZ1 complex subunit 1-like	23867678	23902947
LOC125668446	40S ribosomal protein S7-like	23834485	23842800
LOC125668447	ubiquitin-conjugating enzyme E2 W-like	23805456	23826917
LOC125668448	uncharacterized protein LOC125668448	23644121	23677775
LOC125668454	uridine-cytidine kinase-like 1 isoform X1	23017571	23038567
LOC125668456	UDP-N-acetylglucosamine/UDP-glucose/GDP-mannose transporter-like isoform X2	23001270	23034402
LOC125668478	YTH domain-containing protein 1-like isoform X3	21848198	21874478
LOC125668518	uncharacterized protein LOC125668518	16251266	16260282
LOC125668522	LOW QUALITY PROTEIN: ubiquitin carboxyl-terminal hydrolase 43-like	6040234	6061770
LOC125668523	mismatch repair endonuclease PMS2-like isoform X1	5952865	6001532
LOC125668524	LOW QUALITY PROTEIN: hepatocyte growth factor-regulated tyrosine kinase substrate-like	6080780	6094800
LOC125668525	uncharacterized protein LOC125668525	6235440	6245791
LOC125668526	LOW QUALITY PROTEIN: calpain-9-like	6279592	6290688
LOC125668527	LOW QUALITY PROTEIN: cytochrome P450 4V2-like	6258211	6279521
LOC125668528	uncharacterized protein LOC125668528	6250060	6252969
LOC125668529	LOW QUALITY PROTEIN: serine hydroxymethyltransferase-like	6173330	6189659
LOC125668530	L-rhamnonate dehydratase-like	6306160	6307576
LOC125668531	clusterin-associated protein 1-like isoform X2	6153147	6166281
LOC125668532	LOW QUALITY PROTEIN: thioredoxin domain-containing protein 15-like	6120244	6126323
LOC125668533	L-threonine 3-dehydrogenase-like	6293194	6297169
LOC125668534	testis-specific serine/threonine-protein kinase 1-like	6149435	6150841
LOC125668535	elongation of very long chain fatty acids protein 6-like	6142115	6145547
LOC125668536	LOW QUALITY PROTEIN: methyltransferase-like 26	6094751	6098446
LOC125668537	methylated-DNA--protein-cysteine methyltransferase-like	6031942	6040215
LOC125668539	LOW QUALITY PROTEIN: MAPK regulated corepressor interacting protein 2-like	6097284	6104175
LOC125668540	ADP-ribosylation factor-like protein 16	6066453	6080532
LOC125668541	LOW QUALITY PROTEIN: ras-associating and dilute domain-containing protein-like	6110192	6120146
LOC125668542	LOW QUALITY PROTEIN: protein FAM13A-like	6308102	6348831
LOC125668602	uncharacterized protein LOC125668602 isoform X5	24722541	24748464
LOC125668610	LOW QUALITY PROTEIN: RB1-inducible coiled-coil protein 1-like	15137107	15174125
LOC125668625	germ cell-less protein-like 1	2312691	2333154
LOC125668637	germ cell-less protein-like 1	9108123	9128592
LOC125668638	uncharacterized protein LOC125668638 isoform X2	9094317	9099764
LOC125668679	transmembrane channel-like protein 7	5708011	5749612
LOC125668680	chitobiosyldiphosphodolichol beta-mannosyltransferase-like	5757434	5770325
LOC125668681	uncharacterized protein LOC125668681	5742591	5744906
LOC125668682	LOW QUALITY PROTEIN: 5'(3')-deoxyribonucleotidase%2C mitochondrial-like	5750452	5757287
LOC125668688	ras-related protein Rab-37-like isoform X2	26232062	26247554
LOC125668690	ras-related protein Rab-26-like	26250701	26263465
LOC125668719	LOW QUALITY PROTEIN: tuberin-like	16805189	16870449
LOC125668720	pancreatic triacylglycerol lipase-like	16878655	16931103
LOC125668722	uncharacterized protein LOC125668722	16874161	16878557
LOC125668723	uncharacterized protein LOC125668723 isoform X1	22473588	22515789
LOC125668725	tubulin polyglutamylase TTLL7-like	22891965	22912991
LOC125668726	uncharacterized protein LOC125668726	22448493	22466412
LOC125668727	uncharacterized protein LOC125668727	22917088	22922130
LOC125668728	metalloprotease TIKI1-like	22790923	22806731
LOC125668729	uncharacterized protein LOC125668729 isoform X1	22748574	22765993
LOC125668731	heparan sulfate glucosamine 3-O-sulfotransferase 1-like	22941084	22990772
LOC125668733	uncharacterized protein LOC125668733	22702828	22744834
LOC125668734	heparan sulfate glucosamine 3-O-sulfotransferase 5-like	22957991	22975631
LOC125668735	elongation of very long chain fatty acids protein 2-like isoform X1	22810805	22827331
LOC125668736	calcyphosin-like protein isoform X1	22868530	22886106
LOC125668737	profilin-4-like	22643221	22643952
LOC125668738	40S ribosomal protein S12-like	22932626	22941018
LOC125668739	U6 snRNA-associated Sm-like protein LSm4	22774920	22786395
LOC125668758	ornithine decarboxylase-like	20597752	20620407

LOC125668792	LOW QUALITY PROTEIN: ankyrin repeat and KH domain-containing protein 1-like	13213895	13240085
LOC125668798	protein Hook homolog 3-like isoform X1	23450492	23478068
LOC125668799	E3 ubiquitin-protein ligase RNF170-like	23429988	23450101
LOC125668807	UDP-N-acetylglucosamine transferase subunit ALG14 homolog isoform X3	14855566	14876578
LOC125668808	tetratricopeptide repeat protein 4-like	21701132	21711843
LOC125668809	probable dimethyladenosine transferase	21665552	21701139
LOC125668812	LOW QUALITY PROTEIN: regulator of G-protein signaling 22-like	15546893	15571469
LOC125668814	LOW QUALITY PROTEIN: bone morphogenetic protein 2-A-like	16456133	16469575
LOC125668815	probable G-protein coupled receptor Mth-like 3	16391412	16393210
LOC125668816	uncharacterized protein LOC125668816	16484244	16490992
LOC125668818	LOW QUALITY PROTEIN: rho GTPase-activating protein 45-like	21022702	21061118
LOC125668819	uncharacterized protein LOC125668819	14137274	14139682
LOC125668820	G-protein coupled receptor Mth-like	14221397	14223289
LOC125668821	Werner syndrome ATP-dependent helicase-like	14477068	14478838
LOC125668822	uncharacterized protein LOC125668822	14514139	14515708
LOC125668823	uncharacterized protein LOC125668823	14711933	14717988
LOC125668824	N(6)-adenine-specific methyltransferase METTL4-like	14916497	14924414
LOC125668825	transcription factor glial cells missing 2-like	14995548	15016653
LOC125668826	synaptonemal complex protein 2-like	15043495	15137487
LOC125668827	uncharacterized protein K02A2.6-like	15839168	15840877
LOC125668829	uncharacterized protein LOC125668829	15840941	15841363
LOC125668830	LOW QUALITY PROTEIN: uncharacterized protein LOC125668830	15851765	15932977
LOC125668831	uncharacterized protein LOC125668831	16420583	16422688
LOC125668833	probable G-protein coupled receptor Mth-like 3	16506383	16508792
LOC125668835	uncharacterized protein LOC125668835	16756743	16759733
LOC125668836	uncharacterized protein K02A2.6-like	16947743	16951777
LOC125668837	uncharacterized protein LOC125668837	17009353	17010996
LOC125668838	transcription factor glial cells missing 2-like	17291121	17300421
LOC125668839	LOW QUALITY PROTEIN: synaptonemal complex protein 2-like	17338858	17442472
LOC125668840	LOW QUALITY PROTEIN: uncharacterized protein LOC125668840	17609094	17649318
LOC125668841	uncharacterized protein K02A2.6-like	18140852	18142526
LOC125668842	uncharacterized protein LOC125668842	18247963	18256162
LOC125668843	LOW QUALITY PROTEIN: fatty acid synthase-like	18407123	18435995
LOC125668844	uncharacterized protein LOC125668844	18717340	18717816
LOC125668845	serine/threonine-protein phosphatase 6 regulatory ankyrin repeat subunit C-like	18726227	18727404
LOC125668846	serine/threonine-protein kinase RIO1-like	18741975	18779175
LOC125668847	uncharacterized protein LOC125668847	19024754	19116270
LOC125668848	uncharacterized protein K02A2.6-like	19123221	19126802
LOC125668852	uncharacterized protein LOC125668852	19947795	19951313
LOC125668853	uncharacterized protein LOC125668853	20286972	20512303
LOC125668854	uncharacterized protein LOC125668854	20797075	20798017
LOC125668855	major royal jelly protein 5-like	20841660	20842304
LOC125668856	major royal jelly protein 5-like	20842838	20843545
LOC125668857	putative uncharacterized protein DDB_G0286901	20851300	20852106
LOC125668858	uncharacterized protein LOC125668858	20963076	20963725
LOC125668859	uncharacterized protein K02A2.6-like	21148770	21152621
LOC125668861	tigger transposable element-derived protein 6-like	21742018	21742662
LOC125668862	uncharacterized protein LOC125668862	21754406	21757027
LOC125668863	uncharacterized protein K02A2.6-like	21827891	21828784
LOC125668864	aminopeptidase O-like	21953315	21964753
LOC125668865	PHD finger protein 24-like	22030633	22039412
LOC125668866	DNA-dependent protein kinase catalytic subunit-like	22166217	22171683
LOC125668869	uncharacterized protein LOC125668869	22194331	22195425
LOC125668870	PI-PLC X domain-containing protein 3-like	22196559	22197686
LOC125668871	tripartite motif-containing protein 2-like	22239880	22241031
LOC125668872	uncharacterized protein LOC125668872	22252649	22253908
LOC125668873	uncharacterized protein LOC125668873	22261517	22266220
LOC125668874	uncharacterized protein LOC125668874	22299645	22300352
LOC125668875	uncharacterized protein LOC125668875	22620070	22622432
LOC125668876	uncharacterized protein LOC125668876	22634476	22635757
LOC125668877	uncharacterized protein LOC125668877	22730665	22744061

LOC125668878	teratocarcinoma-derived growth factor 1-like	23397270	23414703
LOC125668879	uncharacterized protein LOC125668879	23481331	23482734
LOC125668880	relaxin receptor 1-like	24099599	24123105
LOC125668881	uncharacterized protein LOC125668881	24139645	24176091
LOC125668882	N-glycosidase YbiA-like	24708236	24708700
LOC125668883	uncharacterized protein LOC125668883	24763329	24766634
LOC125668884	uncharacterized protein LOC125668884	24861076	24923366
LOC125668885	chromosome transmission fidelity protein 18 homolog	25214518	25247346
LOC125668886	E3 ubiquitin-protein ligase TRIM33-like	25595650	25597428
LOC125668887	Ig-like V-type domain-containing protein FAM187A	25827849	25838751
LOC125668888	uncharacterized protein LOC125668888	26189900	26231181
LOC125668889	small proline-rich protein 3-like	26249633	26250292
LOC125668890	uncharacterized protein LOC125668890	26311543	26314688
LOC125668891	uncharacterized protein LOC125668891	26470961	26554382
LOC125668892	uncharacterized protein LOC125668892	26666583	26723981
LOC125668893	uncharacterized protein LOC125668893	27402572	27408179
LOC125668924	LOW QUALITY PROTEIN: eyes absent homolog 2-like	15574171	15643497
LOC125669260	LOW QUALITY PROTEIN: ankyrin repeat domain-containing protein 17-like	6376081	6402515
LOC125669261	intraflagellar transport protein 74 homolog	17161416	17209128
LOC125669268	S-adenosylmethionine synthase-like	26618468	26625710
LOC125669269	LOW QUALITY PROTEIN: UBX domain-containing protein 8-like	26587609	26618358
LOC125669271	protein FAM13A-like isoform X2	13144264	13185776
LOC125669272	L-rhamnonate dehydratase-like	13142322	13143744
LOC125669273	LOW QUALITY PROTEIN: L-threonine 3-dehydrogenase-like	13129184	13133174
LOC125669392	protein FAM149B1-like isoform X4	27068288	27119695
LOC125669400	polyadenylate-binding protein-interacting protein 1-like isoform X2	21364318	21387171
LOC125669401	ribosome biogenesis protein BRX1 homolog	21350744	21364162
LOC125669408	LOW QUALITY PROTEIN: pikachurin-like	15300517	15337245
LOC125669411	LOW QUALITY PROTEIN: unconventional myosin-XV-like	5775206	5835243
LOC125669414	uncharacterized protein LOC125669414 isoform X2	12352893	12369180
LOC125669415	LOW QUALITY PROTEIN: ribosome biogenesis protein BMS1 homolog	11951262	11997151
LOC125669416	LOW QUALITY PROTEIN: diacylglycerol lipase-beta-like	12178146	12204362
LOC125669417	uncharacterized protein LOC125669417	12389777	12401584
LOC125669418	LOW QUALITY PROTEIN: TOM1-like protein 2	12271265	12304720
LOC125669419	LOW QUALITY PROTEIN: dynein regulatory complex subunit 3-like	12265283	12270012
LOC125669420	UPF0489 protein C5orf22 homolog	12001110	12009995
LOC125669422	LOW QUALITY PROTEIN: tachykinin-like peptides receptor 99D	12048801	12088614
LOC125669423	uncharacterized protein LOC125669423	12421902	12428428
LOC125669424	ATP synthase mitochondrial F1 complex assembly factor 2-like	12253192	12260050
LOC125669425	voltage-dependent calcium channel gamma-5 subunit-like isoform X1	12417677	12451219
LOC125669427	uncharacterized protein LOC125669427	12455402	12497884
LOC125669428	uncharacterized protein LOC125669428	12488586	12490728
LOC125669429	uncharacterized protein LOC125669429	12174256	12177057
LOC125669430	uncharacterized protein LOC125669430	12310530	12319373
LOC125669431	glucose-induced degradation protein 4 homolog	12244230	12253123
LOC125669437	sushi%2C von Willebrand factor type A%2C EGF and pentraxin domain-containing protein 1-like	20196761	20255015
LOC125669438	uncharacterized protein LOC125669438 isoform X1	19856473	19879004
LOC125669439	uncharacterized protein LOC125669439 isoform X2	19938791	19945710
LOC125669440	acid sphingomyelinase-like phosphodiesterase 3b	19980647	20019052
LOC125669441	prostaglandin E2 receptor EP4 subtype-like isoform X2	20046438	20085146
LOC125669442	uncharacterized protein LOC125669442	20495696	20499279
LOC125669443	cholesterol 25-hydroxylase-like	19900360	19907096
LOC125669444	putative nuclease HARBI1	20127087	20129256
LOC125669445	uncharacterized protein LOC125669445	20118902	20127595
LOC125669446	uncharacterized protein LOC125669446 isoform X2	19922770	19937236
LOC125669447	caspase-7-like	19823501	19856326
LOC125669448	uncharacterized protein LOC125669448	20499976	20503193
LOC125669481	nucleolar protein 4-like isoform X1	23547513	23600394
LOC125669485	zinc transporter 7-like	24565172	24592999
LOC125669510	DNA polymerase subunit gamma-2%2C mitochondrial-like isoform X1	5392209	5408632
LOC125669512	uncharacterized protein LOC125669512	5367022	5368957
LOC125669513	diacylglycerol lipase-beta-like	5369407	5394737

LOC125669574	probable ATP-dependent RNA helicase DDX43	8130271	8163059
LOC125669575	MRG/MORF4L-binding protein-like isoform X3	8119856	8130155
LOC125669608	LOW QUALITY PROTEIN: probable global transcription activator SNF2L2	21323900	21345065
LOC125669611	potassium voltage-gated channel subfamily B member 2-like isoform X4	1534734	1610005
LOC125669619	potassium voltage-gated channel subfamily B member 2-like isoform X3	8330083	8405351
LOC125669625	LOW QUALITY PROTEIN: ras-GEF domain-containing family member 1B-like	16128050	16179149
LOC125669656	transcription factor MafK-like	10586815	10594009
LOC125669659	fizzy-related protein homolog isoform X1	20912766	20939998
LOC125669662	Ig-like and fibronectin type-III domain-containing protein 2	7446508	7537276
LOC125669667	uncharacterized protein LOC125669667 isoform X3	8888341	8927290
LOC125669671	uncharacterized protein LOC125669671 isoform X1	2092915	2131854
LOC125669680	LOW QUALITY PROTEIN: ras-associating and dilute domain-containing protein-like	12939974	12949921
LOC125669681	hepatocyte growth factor-regulated tyrosine kinase substrate-like	12906968	12924524
LOC125669683	LOW QUALITY PROTEIN: clusterin-associated protein 1-like	12987319	13000630
LOC125669684	LOW QUALITY PROTEIN: thioredoxin domain-containing protein 15-like	12950019	12958130
LOC125669685	serine/threonine-protein phosphatase alpha-2 isoform-like	12823614	12850790
LOC125669686	testis-specific serine/threonine-protein kinase 1-like	12983246	12985002
LOC125669687	elongation of very long chain fatty acids protein 6-like	12976268	12979250
LOC125669688	methyltransferase-like 26	12924475	12928185
LOC125669689	MAPK regulated corepressor interacting protein 2-like	12927030	12933892
LOC125669690	ADP-ribosylation factor-like protein 16	12892684	12906724
LOC125669692	LOW QUALITY PROTEIN: mismatch repair endonuclease PMS2-like	12777521	12821510
LOC125669693	serine hydroxymethyltransferase-like	13007671	13027086
LOC125669701	von Willebrand factor A domain-containing protein 3A-like	3234994	3250921
LOC125669702	probable chitinase 10	3485503	3608911
LOC125669704	dynein axonemal assembly factor 5-like	3256278	3262725
LOC125669705	uncharacterized protein LOC125669705	3755108	3766556
LOC125669706	uncharacterized protein LOC125669706	3613845	3619210
LOC125669707	uncharacterized protein LOC125669707	3334847	3337211
LOC125669709	uncharacterized protein LOC125669709	3267879	3270094
LOC125669710	QRFP-like peptide receptor	3265676	3267756
LOC125669711	uncharacterized protein LOC125669711	3372455	3387822
LOC125669712	transmembrane protein 26-like	3717809	3724143
LOC125669713	uncharacterized protein LOC125669713	3271683	3302012
LOC125669714	uncharacterized protein LOC125669714	3208859	3219656
LOC125669715	eukaryotic translation initiation factor 4E-like isoform X1	3306324	3327129
LOC125669716	uncharacterized protein LOC125669716	3301943	3303573
LOC125669717	uncharacterized protein LOC125669717	3740589	3748710
LOC125669718	endochitinase-like isoform X1	3337846	3347870
LOC125669725	LOW QUALITY PROTEIN: transcription factor MafK-like	3791370	3798779
LOC125669730	uncharacterized protein LOC125669730 isoform X3	4619872	4652798
LOC125669733	probable ATP-dependent RNA helicase DDX43	1334940	1367725
LOC125669734	MRG/MORF4L-binding protein-like isoform X3	1324524	1334824
LOC125669739	protein flightless-1 homolog isoform X2	25688710	25720625
LOC125669740	HAUS augmin-like complex subunit 2	25720958	25731880
LOC125669743	FAD-dependent oxidoreductase domain-containing protein 2-like isoform X1	11415371	11448308
LOC125669755	transcription factor MafK-like	7374923	7382119
LOC125669757	ciliogenesis and planar polarity effector 1-like	23331401	23397705
LOC125669820	vasculin-like protein 1	24532026	24550339
LOC125669824	uncharacterized protein LOC125669824 isoform X1	790389	817611
LOC125669828	uncharacterized protein LOC125669828	1094276	1109448
LOC125669829	glucokinase regulatory protein-like isoform X1	997560	1027966
LOC125669830	LOW QUALITY PROTEIN: phosphatase and actin regulator 4B-like	860411	894393
LOC125669833	toll-like receptor Tollo	1017371	1031443
LOC125669834	RNA 3'-terminal phosphate cyclase-like	1084778	1094231
LOC125669835	uncharacterized protein DDB_G0283697-like	1062638	1071545
LOC125669842	LOW QUALITY PROTEIN: tuberin-like	14518301	14580440
LOC125669843	tolloid-like protein 1 isoform X1	14372407	14426325
LOC125669844	uncharacterized protein LOC125669844	14285366	14312441

LOC125669847	uncharacterized protein LOC125669847 isoform X2	14490189	14502052
LOC125669848	pancreatic triacylglycerol lipase-like	14587550	14642841
LOC125669849	stromal membrane-associated protein 1-like isoform X1	14733426	14749052
LOC125669850	beta-1%2C4-N-acetylgalactosaminyltransferase bre-4-like	14332049	14345938
LOC125669851	R3H domain-containing protein 4-like	14350183	14367031
LOC125669852	uncharacterized protein LOC125669852 isoform X2	14724176	14731789
LOC125669853	uncharacterized protein LOC125669853 isoform X2	14503147	14513444
LOC125669854	uncharacterized protein LOC125669854	14584150	14587459
LOC125669855	LOW QUALITY PROTEIN: 40S ribosomal protein S15Aa-like	14314666	14323459
LOC125669856	LOW QUALITY PROTEIN: DNA-directed RNA polymerase I subunit RPA1-like	14755148	14808547
LOC125669858	LOW QUALITY PROTEIN: phospholipid phosphatase-related protein type 5-like	14677435	14706833
LOC125669894	LOW QUALITY PROTEIN: DNA-directed RNA polymerase I subunit RPA1-like	17048936	17101221
LOC125669895	E3 ubiquitin-protein ligase TRIM71-like	17082418	17084565
LOC125669896	LOW QUALITY PROTEIN: piwi-like protein 1	13373337	13446647
LOC125669897	LOW QUALITY PROTEIN: polycystic kidney disease 2-like 1 protein	13346217	13357263
LOC125669898	sodium-coupled monocarboxylate transporter 1-like	13280669	13292142
LOC125669900	LOW QUALITY PROTEIN: alpha-2-macroglobulin receptor-associated protein-like	13253611	13275369
LOC125669901	FAS-associated death domain protein-like	13248089	13253561
LOC125669902	ADP-ribosylation factor 4-like	13318884	13320066
LOC125669903	uncharacterized protein LOC125669903	13300765	13301774
LOC125669904	uncharacterized protein LOC125669904	13292418	13294144
LOC125669905	uncharacterized protein LOC125669905	13412272	13414327
LOC125669906	LOW QUALITY PROTEIN: tyrosine-protein phosphatase non-receptor type 13-like	13673699	13784713
LOC125669925	ubiquitin carboxyl-terminal hydrolase 24-like	20739298	20794132
LOC125669942	cerebral cavernous malformations protein 2 homolog isoform X5	15427485	15442763
LOC125669946	calpain-9-like	13115656	13126695
LOC125669947	LOW QUALITY PROTEIN: cytochrome P450 4V2-like	13094210	13115601
LOC125669949	uncharacterized protein LOC125669949 isoform X2	26092148	26127024
LOC125669960	cyanocobalamin reductase / alkylcobalamin dealkylase-like	21396899	21402509
LOC125669961	uncharacterized protein LOC125669961	7889607	7904778
LOC125669962	RNA 3'-terminal phosphate cyclase-like	7880105	7889562
LOC125670034	40-kDa huntingtin-associated protein-like	5859197	5872602
LOC125670098	KH domain-containing%2C RNA-binding%2C signal transduction-associated protein 2-like isoform X2	20541817	20553549
LOC125670101	uncharacterized protein LOC125670101	8947737	8974236
LOC125670102	uncharacterized protein LOC125670102	8974460	8988384
LOC125670104	uncharacterized protein LOC125670104	1124102	1128099
LOC125670105	transmembrane protein 180-like isoform X1	7392281	7411561
LOC125670107	transmembrane protein 180-like isoform X1	10603702	10623456
LOC125670117	LOW QUALITY PROTEIN: leucine-rich repeat-containing protein 40-like	3968543	3988610
LOC125670118	cobalamin binding intrinsic factor-like	3988793	3995989
LOC125670121	uncharacterized protein LOC125670121	7919436	7923432
LOC125670131	uncharacterized protein LOC125670131	2152305	2178795
LOC125670132	uncharacterized protein LOC125670132	2179019	2192945
LOC125670150	glucokinase regulatory protein-like isoform X1	7792902	7823325
LOC125670151	toll-like receptor Tollo	7812690	7826795
LOC125670157	minor histocompatibility antigen H13-like	26340675	26356162
LOC125670161	leucine-rich repeat-containing protein 40-like	10764260	10784102
LOC125670162	cobalamin binding intrinsic factor-like	10784285	10791479
LOC125670164	UPF0728 protein-like	4662456	4663815
LOC125670165	L-threonine ammonia-lyase-like	21002703	21015754
LOC125670168	lysine-specific demethylase 4C-like	10843707	10860817
LOC125670173	UPF0728 protein-like	11457978	11459336
LOC125670180	lysine-specific demethylase 4C-like	4048182	4065288
LOC125670181	protein Wnt-8b-like isoform X4	16073189	16098937
LOC125670182	substance-P receptor-like isoform X1	16098515	16118648
LOC125670183	uncharacterized protein LOC125670183 isoform X2	16094912	16097015
LOC125670184	uncharacterized protein LOC125670184	5095561	5098717
LOC125670185	LOW QUALITY PROTEIN: ribosome biogenesis protein BMS1 homolog	5145801	5192481

LOC125670187	integrator complex subunit 1-like	25166578	25205787
LOC125670188	nuclear pore complex protein Nup155-like isoform X2	25051134	25082609
LOC125670189	LOW QUALITY PROTEIN: trimethylguanosine synthase-like	25011921	25032092
LOC125670190	atrial natriuretic peptide-converting enzyme-like	25412375	25452595
LOC125670191	very low-density lipoprotein receptor-like isoform X1	25258808	25291876
LOC125670192	palmitoyltransferase ZDHHC6-like	25391049	25401690
LOC125670193	gastrin/cholecystokinin type B receptor-like	25094118	25098332
LOC125670194	elastase-1-like	24951361	24957574
LOC125670195	protein aveugle-like	24976484	24988933
LOC125670196	low-density lipoprotein receptor-like	25209168	25211436
LOC125670197	anaphase-promoting complex subunit 16-like	25401931	25404813
LOC125670198	diencephalon/mesencephalon homeobox protein 1-A-like	25336498	25343506
LOC125670205	receptor-type tyrosine-protein phosphatase alpha-like	18874111	18898242
LOC125670206	voltage-dependent calcium channel subunit alpha-2/delta-2-like	18779272	18800598
LOC125670207	BRCA1-associated ATM activator 1-like isoform X2	18683816	18695917
LOC125670209	THO complex subunit 1-like	18951663	18975160
LOC125670210	E3 ubiquitin-protein ligase RNF14-like isoform X1	18924724	18940433
LOC125670211	histone acetyltransferase KAT6B-like isoform X2	18910348	18917774
LOC125670212	adenosine 3'-phospho 5'-phosphosulfate transporter 2-like isoform X1	18975367	18984194
LOC125670213	serine/threonine-protein phosphatase 6 regulatory ankyrin repeat subunit C-like	18732157	18734008
LOC125670214	serine/threonine-protein phosphatase 6 regulatory ankyrin repeat subunit C-like	18740008	18741615
LOC125670215	prostaglandin E2 receptor EP4 subtype-like	18867935	18875577
LOC125670216	CD82 antigen-like isoform X2	18702104	18717146
LOC125670217	palmitoyl-protein thioesterase 1-like	18801232	18817578
LOC125670218	exosome complex component RRP46-like	18675006	18678716
LOC125670219	transmembrane protein 65-like isoform X1	18821672	18833621
LOC125670223	trichohyalin-like isoform X2	25501528	25539675
LOC125670224	cilia- and flagella-associated protein 299-like	25495938	25501263
LOC125670225	uncharacterized protein LOC125670225 isoform X1	23622394	23625089
LOC125670251	diphosphoinositol polyphosphate phosphohydrolase 1-like	26375716	26395891
LOC125670253	uncharacterized protein LOC125670253	11901492	11904388
LOC125670261	rhodopsin%2C GQ-coupled-like	24010529	24013861
LOC125670263	serine/threonine-protein phosphatase 6 regulatory ankyrin repeat subunit A-like	20562801	20590318
LOC125670277	transcription elongation factor A protein 1-like	17697534	17720706
LOC125670278	integrin beta-1-binding protein 1-like isoform X2	17720891	17734041
LOC125670284	uncharacterized protein LOC125670284	13086247	13088607
LOC125670305	WASH complex subunit 5-like	1625412	1639432
LOC125670308	TATA-binding protein-associated factor 172-like	25639529	25684454
LOC125670312	WASH complex subunit 5-like	8420754	8434780
LOC125670314	UPF0489 protein C5orf22 homolog	5198951	5204552
LOC125670316	hydroxyacyl-coenzyme A dehydrogenase%2C mitochondrial-like	5204664	5215898
LOC125670319	guanine nucleotide exchange factor subunit RIC1-like	4173799	4212897
LOC125670321	uncharacterized protein LOC125670321	11899203	11900166
LOC125670322	uncharacterized protein LOC125670322	11897052	11899112
LOC125670323	tetratricopeptide repeat protein 39B-like	18989730	19019314
LOC125670324	hydroxymethylglutaryl-CoA synthase 1-like isoform X3	14960697	14984533
LOC125670328	nucleoprotein TPR-like isoform X2	1667471	1718217
LOC125670329	LOW QUALITY PROTEIN: uncharacterized protein LOC125670329	1981185	2090211
LOC125670330	inactive rhomboid protein 1-like	1726799	1752545
LOC125670331	transcription factor AP-2-epsilon-like isoform X3	1791354	1817913
LOC125670332	solute carrier family 17 member 9-like	1875189	1889577
LOC125670333	tektin-2-like	1719431	1722642
LOC125670334	substance-K receptor-like	1914861	1940660
LOC125670335	FMRFamide receptor-like	2070022	2072740
LOC125670336	ATP synthase mitochondrial F1 complex assembly factor 1-like	1897024	1905546
LOC125670337	uncharacterized protein LOC125670337 isoform X1	1905539	1909931
LOC125670338	uncharacterized protein LOC125670338	1865857	1869879
LOC125670339	uncharacterized protein LOC125670339	1873362	1875028
LOC125670345	Ig-like and fibronectin type-III domain-containing protein 2	10662276	10749187
LOC125670346	guanine nucleotide exchange factor subunit RIC1-like	10969341	11008452
LOC125670349	RE1-silencing transcription factor B-like	26326363	26327118

LOC125670350	nucleoprotein TPR-like isoform X2	8462803	8513552
LOC125670351	LOW QUALITY PROTEIN: uncharacterized protein LOC125670351	8776512	8885571
LOC125670352	inactive rhomboid protein 1-like	8522133	8547884
LOC125670353	transcription factor AP-2-epsilon-like isoform X1	8586694	8613259
LOC125670354	solute carrier family 17 member 9-like	8670537	8684927
LOC125670355	tektin-2-like	8514764	8517975
LOC125670356	substance-K receptor-like	8710211	8736006
LOC125670358	FMRFamide receptor-like	8865340	8868058
LOC125670359	ATP synthase mitochondrial F1 complex assembly factor 1-like	8692375	8700896
LOC125670360	uncharacterized protein LOC125670360 isoform X2	8700888	8705282
LOC125670361	uncharacterized protein LOC125670361	8661211	8665233
LOC125670362	uncharacterized protein LOC125670362	8668703	8670376
LOC125670365	transmembrane protein 26-like	12711931	12712980
LOC125670366	LOW QUALITY PROTEIN: 116 kDa U5 small nuclear ribonucleoprotein component-like	12720221	12739652
LOC125670369	alpha-(1%2C3)-fucosyltransferase 10-like	9052830	9060169
LOC125670370	alpha-(1%2C3)-fucosyltransferase 10-like	2257396	2264735
LOC125670375	profilin-2-like	21572188	21573119
LOC125670383	RYamide receptor-like	2360775	2392333
LOC125670398	N-acetyltransferase ESCO2-like	4473859	4495655
LOC125670399	opine dehydrogenase-like	4495652	4498853
LOC125670413	N-acetyltransferase ESCO2-like	11269341	11291135
LOC125670414	opine dehydrogenase-like	11291132	11294333
LOC125670417	eukaryotic translation initiation factor 3 subunit L-like	26564416	26582305
LOC125670418	uncharacterized protein LOC125670418 isoform X1	26556384	26558654
LOC125670423	LOW QUALITY PROTEIN: WD repeat-containing protein 90-like	18330610	18371878
LOC125670424	microsomal triglyceride transfer protein large subunit-like	18263093	18284304
LOC125670425	protein EFR3 homolog B-like isoform X1	18157368	18208205
LOC125670427	SEC14-like protein 1 isoform X6	18209152	18241229
LOC125670428	outer mitochondrial transmembrane helix translocase-like isoform X1	18308896	18330355
LOC125670429	tRNA methyltransferase 10 homolog A-like isoform X3	18260792	18297483
LOC125670431	zinc finger CCHC domain-containing protein 24-like isoform X2	18255617	18287472
LOC125670442	neurotrypsin-like	24021892	24029364
LOC125670443	trans-1%2C2-dihydrobenzene-1%2C2-diol dehydrogenase-like	25480376	25493055
LOC125670444	LOW QUALITY PROTEIN: otoferlin-like	17954322	18123286
LOC125670445	LOW QUALITY PROTEIN: regulator of G-protein signaling 22-like	17810714	17873606
LOC125670446	eyes absent homolog 2-like isoform X3	17876290	17945982
LOC125670447	uncharacterized protein LOC125670447	18093770	18099758
LOC125670448	cerebral cavernous malformations protein 2 homolog isoform X5	17744077	17759408
LOC125670449	U2 small nuclear ribonucleoprotein A'-like	17794947	17809959
LOC125670458	uncharacterized protein LOC125670458 isoform X2	10797685	10824921
LOC125670460	LOW QUALITY PROTEIN: glutathione S-transferase 1-1-like	13209474	13211047
LOC125670462	protocadherin Fat 4-like	26781880	27010309
LOC125670463	uncharacterized protein LOC125670463	27029034	27057867
LOC125670464	synaptotagmin-15-like	26772007	26781075
LOC125670465	uncharacterized protein LOC125670465	26729318	26746692
LOC125670466	F-box/LRR-repeat protein 15-like	26655570	26661947
LOC125670467	TNF receptor-associated factor 6-B-like isoform X2	26751493	26758495
LOC125670469	LOW QUALITY PROTEIN: glutathione S-transferase 1-1-like	6371671	6373244
LOC125670472	ras-GEF domain-containing family member 1B-like isoform X4	13841455	13890212
LOC125670474	neuropeptide FF receptor 2-like isoform X2	13814738	13831221
LOC125670475	protein Wnt-8b-like isoform X2	13791351	13815154
LOC125670476	LOW QUALITY PROTEIN: E3 ubiquitin-protein ligase PDZRN3-like	14032003	14038643
LOC125670478	oxidized purine nucleoside triphosphate hydrolase-like	14004487	14025041
LOC125670479	uncharacterized protein LOC125670479	13963147	13972061
LOC125670480	uncharacterized protein LOC125670480	13977715	13982759
LOC125670482	LOW QUALITY PROTEIN: dynein axonemal heavy chain 3-like	13895131	13961993
LOC125670515	opine dehydrogenase-like	4499660	4502009
LOC125670516	ZAR1-like protein	23421163	23425334
LOC125670520	ubiquitin conjugation factor E4 A-like isoform X2	25732231	25744894
LOC125670521	UPF0764 protein C16orf89 homolog	25745030	25778819
LOC125670525	disks large-associated protein 5-like	21583090	21625472
LOC125670532	LOW QUALITY PROTEIN: focal adhesion kinase 1-like	17526337	17556095
LOC125670533	membrane progestin receptor beta-like	17592028	17594762

LOC125670534	cytochrome c oxidase subunit 5B%2C mitochondrial-like	17512378	17520697
LOC125670535	LOW QUALITY PROTEIN: cytochrome c oxidase subunit 5B%2C mitochondrial-like	17491343	17501115
LOC125670536	uncharacterized protein LOC125670536	17397869	17399056
LOC125670544	oviduct-specific glycoprotein-like isoform X1	10475372	10490027
LOC125670545	uncharacterized protein LOC125670545	10550567	10565617
LOC125670546	uncharacterized protein LOC125670546	10409224	10414589
LOC125670547	uncharacterized protein LOC125670547	10130287	10132651
LOC125670548	chitotriosidase-1-like	10450124	10467753
LOC125670549	uncharacterized protein LOC125670549	10167906	10183280
LOC125670550	eukaryotic translation initiation factor 4E-like isoform X1	10101739	10122548
LOC125670551	uncharacterized protein LOC125670551 isoform X4	10133286	10143530
LOC125670552	transmembrane protein 26-like	10513260	10519601
LOC125670554	gastrin/cholecystokinin type B receptor-like	27539760	27542314
LOC125670556	ankyrin repeat domain-containing protein 29-like	21990965	22008809
LOC125670560	cytochrome c oxidase subunit 5B%2C mitochondrial-like	15184860	15194603
LOC125670567	opine dehydrogenase-like	11295140	11297489
LOC125670570	LOW QUALITY PROTEIN: uncharacterized protein LOC125670570	4002195	4029425
LOC125670584	beta-1%2C3-galactosyltransferase 4-like	17111880	17117385
LOC125670588	organic solute transporter subunit alpha-like	21878716	21894506
LOC125670589	uncharacterized protein LOC125670589	21894553	21899517
LOC125670632	mitogen-activated protein kinase kinase kinase 1-like	21215047	21240594
LOC125670633	uncharacterized protein LOC125670633 isoform X1	20983610	20990186
LOC125670634	L-threonine 3-dehydrogenase%2C mitochondrial-like	20973898	20982719
LOC125670637	dystrophin-like isoform X1	21109364	21135859
LOC125670638	RING finger protein 11-like	8940893	8947358
LOC125670642	sodium-dependent lysophosphatidylcholine symporter 1-like	21182825	21206391
LOC125670644	uncharacterized protein LOC125670644	23520100	23524319
LOC125670645	uncharacterized protein LOC125670645	23524316	23529335
LOC125670649	V-type proton ATPase 21 kDa proteolipid subunit c"-like	20727141	20736527
LOC125670651	RING finger protein 11-like	2145463	2151926
LOC125670656	sorting nexin-30-like isoform X1	4227089	4236029
LOC125670657	uncharacterized protein LOC125670657	20637022	20647234
LOC125670658	beta-1%2C3-galactosyltransferase 4-like	14819224	14824711
LOC125670659	rho GTPase-activating protein 44-like isoform X5	18627133	18665603
LOC125670662	NAD-dependent protein deacetylase sirtuin-1-like isoform X2	18561289	18577188
LOC125670663	isovaleryl-CoA dehydrogenase%2C mitochondrial-like isoform X1	18474791	18490117
LOC125670664	ribosome biogenesis regulatory protein homolog	18606312	18627041
LOC125670665	uncharacterized protein LOC125670665 isoform X3	18594908	18606109
LOC125670667	histone-arginine methyltransferase METTL23-like	18490252	18496508
LOC125670668	J domain-containing protein-like isoform X1	18549824	18561182
LOC125670669	DNA-binding transcriptional regulator BolA-like	18496527	18505356
LOC125670670	PHD finger-like domain-containing protein 5A	18536993	18546003
LOC125670671	probable ATP-dependent RNA helicase DDX27	18505353	18536897
LOC125670680	sorting nexin-30-like isoform X1	11018920	11031607
LOC125670681	uncharacterized protein LOC125670681 isoform X3	2703710	2711199
LOC125670682	uncharacterized protein LOC125670682	2865899	2868123
LOC125670683	myosin-G heavy chain-like isoform X1	2687162	2703479
LOC125670684	uncharacterized protein LOC125670684	2810887	2815864
LOC125670685	uncharacterized protein LOC125670685	2965988	2972060
LOC125670686	RYamide receptor-like isoform X1	2953907	3008628
LOC125670699	uncharacterized protein LOC125670699 isoform X1	9499187	9506655
LOC125670700	uncharacterized protein LOC125670700	9661362	9663586
LOC125670701	myosin-G heavy chain-like isoform X1	9482620	9498936
LOC125670702	uncharacterized protein LOC125670702	9606369	9611346
LOC125670703	uncharacterized protein LOC125670703	9663684	9668246
LOC125670704	uncharacterized protein LOC125670704	9761355	9767479
LOC125670705	RYamide receptor-like	9749354	9804040
LOC125670732	mediator of DNA damage checkpoint protein 1-like	24347547	24390624
LOC125670734	ubiquitin-protein ligase E3C-like	24449179	24467366
LOC125670735	uncharacterized protein LOC125670735	24486974	24497225
LOC125670736	uncharacterized protein LOC125670736	24301399	24347136
LOC125670737	neuronal acetylcholine receptor subunit alpha-9-like	24339571	24341882
LOC125670738	diphthine methyl ester synthase-like	24467431	24482875

LOC125670739	peptidyl-prolyl cis-trans isomerase FKBP1A-like	24411262	24415251
LOC125670740	peptidyl-prolyl cis-trans isomerase FKBP1B-like	24390623	24403882
LOC125670741	peptidyl-prolyl cis-trans isomerase FKBP1A-like	24436036	24446496
LOC125670742	uncharacterized protein LOC125670742	24415970	24422872
LOC125670745	bone morphogenetic protein 3-like	25547593	25557108
LOC125670749	uncharacterized protein LOC125670749	4586099	4588542
LOC125670767	U2 small nuclear ribonucleoprotein A'-like	15476395	15490553
LOC125670768	kelch-like ECH-associated protein 1	21156813	21175867
LOC125670772	uncharacterized protein LOC125670772	11381571	11384023
LOC125670799	LOW QUALITY PROTEIN: 116 kDa U5 small nuclear ribonucleoprotein component-like	5902284	5920536
LOC125670804	alpha-(1%2C3)-fucosyltransferase 10-like	2245692	2252963
LOC125670812	E3 ubiquitin-protein ligase TRIM71-like	22334393	22337502
LOC125670813	uncharacterized protein LOC125670813 isoform X1	22337581	22342738
LOC125670822	peroxisomal membrane protein PEX13-like isoform X2	8271003	8278713
LOC125670831	peroxisomal membrane protein PEX13-like isoform X2	1475663	1483369
LOC125670832	alpha-(1%2C3)-fucosyltransferase 10-like	9041134	9046082
LOC125670833	NFU1 iron-sulfur cluster scaffold homolog%2C mitochondrial-like	11459509	11478651
LOC125670839	NFU1 iron-sulfur cluster scaffold homolog%2C mitochondrial-like	4663988	4683129
LOC125670846	uncharacterized protein LOC125670846	16265898	16270935
LOC125670854	uncharacterized protein LOC125670854 isoform X2	23494590	23500185
LOC125670858	uncharacterized protein LOC125670858	1182576	1219837
LOC125670894	uncharacterized protein LOC125670894 isoform X1	21560664	21567795
LOC125670895	forkhead box protein E1-like	26411267	26412751
LOC125670913	LOW QUALITY PROTEIN: tachykinin-like peptides receptor 99D	5242455	5282803
LOC125670914	uncharacterized protein LOC125670914	5228688	5231017
LOC125670915	uncharacterized protein LOC125670915 isoform X1	16321053	16360720
LOC125670921	probable rRNA-processing protein EBP2	20950802	20957548
LOC125670922	protein FAM183B-like	20946753	20950804
LOC125670937	uncharacterized protein LOC125670937	5350687	5365485
LOC125670941	alpha-mannosidase 2-like	5939359	5945183
LOC125670943	ADP-ribosylation factor-related protein 1-like	26397157	26410186
LOC125670955	uncharacterized protein LOC125670955 isoform X7	22367983	22375417
LOC125670970	transmembrane protein 68-like	21931950	21947893
LOC125670979	BSD domain-containing protein 1-like isoform X2	24622220	24633601
LOC125670980	uncharacterized protein LOC125670980 isoform X1	5543162	5556967
LOC125670981	TOM1-like protein 2 isoform X1	5459579	5494915
LOC125670982	LOW QUALITY PROTEIN: dynein regulatory complex subunit 3-like	5453584	5458859
LOC125670983	LOW QUALITY PROTEIN: ATP synthase mitochondrial F1 complex assembly factor 2-like	5441510	5448361
LOC125670984	uncharacterized protein LOC125670984	5643612	5686193
LOC125670985	uncharacterized protein LOC125670985	5676464	5678656
LOC125670987	uncharacterized protein LOC125670987	5498850	5507715
LOC125670988	integumentary mucin A.1-like	5514855	5515740
LOC125670989	LOW QUALITY PROTEIN: glucose-induced degradation protein 4 homolog	5432297	5441451
LOC125670992	uncharacterized protein LOC125670992 isoform X2	22271678	22295603
LOC125670993	uncharacterized protein LOC125670993	22269382	22271667
LOC125671094	EF-hand calcium-binding domain-containing protein 6-like isoform X1	27165180	27176570
LOC125671116	exosome complex component RRP40-like isoform X1	21278772	21295457
LOC125671133	uncharacterized protein LOC125671133	21241010	21265687
LOC125671199	histone-arginine methyltransferase CARMER-like	21295890	21307693
LOC125671226	peroxiredoxin prdx-2-like	14838491	14851940
LOC125671232	sister chromatid cohesion protein DCC1-like	22044675	22065690
LOC125671251	uncharacterized protein LOC125671251 isoform X2	21648022	21655448
LOC125671260	RNA exonuclease 1 homolog	24284252	24293594
LOC125671263	unconventional myosin-VIIa-like isoform X1	18447523	18474751
LOC125671264	mitochondrial enolase superfamily member 1-like isoform X2	1654214	1667226
LOC125671265	prefoldin subunit 1-like	20531763	20539646
LOC125671267	sodium/calcium exchanger 3-like isoform X1	25842576	25878126
LOC125671270	mitochondrial enolase superfamily member 1-like isoform X2	8449543	8462558
LOC125671273	somatostatin receptor type 2-like	4996807	4999398
LOC125671274	uncharacterized protein LOC125671274 isoform X1	7585779	7613013
LOC125671275	leucine-rich repeat-containing protein 40-like	7552122	7572188

LOC125671276	phosphatase and actin regulator 4B-like isoform X2	7655810	7689768
LOC125671277	cobalamin binding intrinsic factor-like	7572371	7579569
LOC125671278	lysine-specific demethylase 4C-like	7631798	7648904
LOC125671282	transcription elongation factor A protein 1-like	15384138	15404967
LOC125671321	peroxiredoxin prdx-2-like	17131130	17144573
LOC125671332	histone H1-delta-like	10750265	10750937
LOC125671335	40S ribosomal protein S21-like	21987275	21990509
LOC125671338	E3 SUMO-protein ligase ZBED1-like	21736957	21741568
LOC125671339	uncharacterized protein LOC125671339 isoform X2	21735705	21736825
LOC125671340	histone H1-delta-like	7538353	7539025
LOC125671341	GRB2-associated and regulator of MAPK protein 1-like isoform X2	23602627	23609630
LOC125671342	uncharacterized protein LOC125671342	7981600	8015135
LOC125671344	histone H1-delta-like	3954781	3955453
LOC125671376	cilia- and flagella-associated protein 58-like isoform X1	12508356	12515791
LOC125671395	uncharacterized protein LOC125671395	22300744	22327644
LOC125671396	T-cell acute lymphocytic leukemia protein 1-like	20896888	20899987
LOC125671400	uncharacterized protein LOC125671400	26336729	26340380
LOC125671405	uncharacterized protein LOC125671405	26637067	26641342
LOC125671406	LOW QUALITY PROTEIN: PHD finger protein 24-like	22016928	22021381
LOC125671412	uncharacterized protein LOC125671412	24606408	24619605
LOC125671418	uncharacterized protein LOC125671418	22256226	22258117
LOC125671419	spindle and centriole-associated protein 1-like isoform X2	21310318	21323529
LOC125671420	cilia- and flagella-associated protein 58-like	5695509	5703220
LOC125671422	uncharacterized protein LOC125671422 isoform X3	16567594	16595432
LOC125671423	tolloid-like protein 1	16655437	16709785
LOC125671425	uncharacterized protein LOC125671425 isoform X1	16774535	16786723
LOC125671426	beta-1%2C4-N-acetylgalactosaminyltransferase bre-4-like	16614993	16628921
LOC125671427	R3H domain-containing protein 4-like	16633171	16650045
LOC125671428	uncharacterized protein LOC125671428 isoform X2	16787816	16798530
LOC125671429	40S ribosomal protein S15Aa-like	16597613	16606403
LOC125671434	U4/U6.U5 tri-snRNP-associated protein 2-like	27178302	27201189
LOC125671435	N6-adenosine-methyltransferase non-catalytic subunit-like	27383751	27393872
LOC125671436	neuromedin-K receptor-like isoform X2	27347973	27369941
LOC125671437	neuromedin-K receptor-like isoform X2	27306706	27347020
LOC125671438	carbohydrate sulfotransferase 1-like	27232213	27255060
LOC125671439	G patch domain and ankyrin repeat-containing protein 1-like	27396159	27414465
LOC125671440	testis-expressed protein 47-like	27393644	27401712
LOC125671441	uncharacterized protein LOC125671441	27255150	27256971
LOC125671442	UPF0561 protein C2orf68 homolog	27200323	27213206
LOC125671443	rhodopsin-like	27492231	27536691
LOC125671446	protein FAM166C A-like	21412339	21415973
LOC125671460	cytochrome c oxidase subunit 5B%2C mitochondrial-like	15205807	15214098
LOC125671462	octopine dehydrogenase-like	21919691	21924842
LOC125671468	iron-sulfur cluster assembly 1 homolog%2C mitochondrial-like isoform X2	21267795	21274621
LOC125671494	integrin beta-1-binding protein 1-like isoform X1	15405149	15417282
LOC125671552	uncharacterized protein LOC125671552	15792584	15798573
LOC125671553	LOW QUALITY PROTEIN: tyrosine-protein phosphatase non-receptor type 13-like	15950629	16067793
LOC125671554	LOW QUALITY PROTEIN: otoferlin-like	15652135	15822084
LOC125671559	SPRY domain-containing SOCS box protein 3-like	15465373	15467607
LOC125671566	uncharacterized protein LOC125671566	22384096	22389646
LOC125671570	uncharacterized protein LOC125671570	1128899	1130621
LOC125671573	terminal uridylyltransferase 7-like isoform X1	24251328	24284057
LOC125671574	cubilin-like	24031427	24045679
LOC125671575	cholecystokinin receptor-like	24236395	24239583
LOC125671576	probable thiopurine S-methyltransferase isoform X2	24054833	24071236
LOC125671577	plasminogen-like	24181164	24199104
LOC125671579	probable thiopurine S-methyltransferase	24082818	24092209
LOC125671580	dynein light chain Tctex-type 5-like	24246182	24247790
LOC125671581	acyl-coenzyme A thioesterase 13-like	24051805	24054844
LOC125671584	uncharacterized protein DDB_G0283697-like	7857966	7866873
LOC125671585	NAD kinase 2%2C mitochondrial-like	24554929	24564983
LOC125671635	salivary acidic proline-rich phosphoprotein 1/2-like	18374462	18377079
LOC125671639	uncharacterized protein LOC125671639	15358463	15377771

LOC125671641	LOW QUALITY PROTEIN: uncharacterized protein LOC125671641	17672105	17690161
LOC125671643	uncharacterized protein LOC125671643 isoform X3	4346861	4357599
LOC125671644	uncharacterized protein LOC125671644 isoform X1	4411084	4418867
LOC125671646	putative ferric-chelate reductase 1 isoform X2	4263924	4286138
LOC125671647	serine/threonine-protein kinase Sgk1-like isoform X5	4296501	4332127
LOC125671648	intraflagellar transport protein 52 homolog	4285779	4292613
LOC125671649	uncharacterized protein LOC125671649	4419625	4421723
LOC125671650	F-box only protein 25-like isoform X2	4372835	4379505
LOC125671651	very-long-chain 3-oxoacyl-CoA reductase-like isoform X1	4335289	4346179
LOC125671652	uncharacterized protein LOC125671652	4431099	4444232
LOC125671653	uncharacterized protein LOC125671653	4460942	4468232
LOC125671654	uncharacterized protein LOC125671654	4445563	4447553
LOC125671655	uncharacterized protein LOC125671655	4452297	4454232
LOC125671657	coiled-coil-helix-coiled-coil-helix domain-containing protein 7-like	4357559	4364381
LOC125671661	uncharacterized protein LOC125671661 isoform X3	11142388	11153113
LOC125671662	uncharacterized protein LOC125671662 isoform X1	11206580	11214363
LOC125671663	putative ferric-chelate reductase 1 isoform X2	11059463	11081681
LOC125671665	serine/threonine-protein kinase Sgk1-like isoform X2	11092042	11127634
LOC125671666	intraflagellar transport protein 52 homolog	11081322	11088154
LOC125671667	uncharacterized protein LOC125671667	11215121	11217219
LOC125671668	F-box only protein 32-like	11168351	11175015
LOC125671670	uncharacterized protein LOC125671670	11226589	11239722
LOC125671671	dehydrogenase/reductase SDR family member 11-like isoform X1	11130794	11141706
LOC125671672	uncharacterized protein LOC125671672	11256432	11263735
LOC125671673	uncharacterized protein LOC125671673	11241053	11243040
LOC125671674	uncharacterized protein LOC125671674	11247785	11249720
LOC125671675	coiled-coil-helix-coiled-coil-helix domain-containing protein 7-like	11153073	11159888
LOC125671678	uncharacterized protein LOC125671678	7924232	7925913
LOC125671692	FYN-binding protein 1-like isoform X5	21440535	21492295
LOC125671693	vacuolar protein sorting-associated protein 28 homolog isoform X2	21431087	21440550
LOC125671694	calcium and integrin-binding protein 1-like	21426834	21430882
LOC125671699	SOSS complex subunit C-like	11031702	11042067
LOC125671703	LOW QUALITY PROTEIN: uncharacterized protein LOC125671703	17226852	17251748
LOC125671704	hydroxymethylglutaryl-CoA synthase 1-like isoform X4	17253434	17278478
LOC125671706	N(6)-adenine-specific methyltransferase METTL4-like	17212058	17240326
LOC125671707	uncharacterized protein LOC125671707	17209168	17212050
LOC125671710	SOSS complex subunit C-like	4236124	4246538
LOC125671730	helicase with zinc finger domain 2-like isoform X1	23250356	23275427
LOC125671731	LOW QUALITY PROTEIN: helicase with zinc finger domain 2-like	23304051	23328358
LOC125671732	helicase with zinc finger domain 2-like isoform X2	23275188	23291989
LOC125671754	zinc finger protein 862-like isoform X1	21730961	21734998
LOC125671759	dynein light chain Tctex-type 5-B-like	11008579	11013524
LOC125671760	somatostatin receptor type 2-like	11797763	11799906
LOC125671761	DIS3-like exonuclease 1	24824321	24859862
LOC125671762	disabled homolog 1-like isoform X1	24774247	24799189
LOC125671763	calreticulin-like	24799017	24802492
LOC125671764	transmembrane protein 59-like isoform X2	24808742	24822991
LOC125671767	cysteine-rich protein 1-like	27568627	27572511
LOC125671768	protein sine oculis-like	21065737	21099338
LOC125671771	dynein light chain Tctex-type 5-B-like	4213024	4217968
LOC125671822	probable serine/threonine-protein kinase fhkB	7907638	7909819
LOC125671824	probable serine/threonine-protein kinase fhkB	1112308	1114489
LOC125671856	rhomboid-related protein 3-like isoform X1	25796695	25818385
LOC125671866	zinc metalloproteinase nas-6-like	25455188	25468346
LOC125671870	uncharacterized protein LOC125671870	26419946	26427996
LOC125671875	zinc finger protein Xfin-like	19404868	19426348
LOC125671876	LOW QUALITY PROTEIN: polycystic kidney disease protein 1-like 2	19458723	19479984
LOC125671877	conserved oligomeric Golgi complex subunit 3-like isoform X2	19359307	19391076
LOC125671878	uncharacterized protein LOC125671878	19431006	19436842
LOC125671879	mRNA export factor-like	19649334	19684655
LOC125671880	regucalcin-like	19689399	19704691
LOC125671881	regucalcin-like	19710411	19719388
LOC125671882	regucalcin-like	19736508	19763958
LOC125671883	uncharacterized protein LOC125671883 isoform X2	19504782	19507384

LOC125671885	uncharacterized protein LOC125671885	19726424	19727903
LOC125671887	histone H2B-like	19328757	19331707
LOC125671888	histone H2B-like	19491994	19494483
LOC125671889	histone H3	19333300	19498625
LOC125671892	histone H2A	19343460	19343894
LOC125671893	histone H4	19494567	19496330
LOC125671894	histone H4	19332705	19333236
LOC125671895	cytochrome b-c1 complex subunit 6%2C mitochondrial-like	19790973	19808846
LOC125671903	oxidized purine nucleoside triphosphate hydrolase-like	16292890	16315462
LOC125671906	LOW QUALITY PROTEIN: protocadherin Fat 3-like	7418200	7432995
LOC125671952	phosphatase and actin regulator 4B-like isoform X1	10867717	10917482
LOC125671953	tyrosine-protein kinase SRK2-like isoform X1	10928379	10958519
LOC125671955	syntenin-1-like	10917634	10926351
LOC125671958	tyrosine-protein kinase SRK2-like isoform X1	4132837	4162976
LOC125671959	syntenin-1-like	4122094	4130809
LOC125671972	protein transport protein Sec31A-like isoform X1	4788502	4811596
LOC125671973	MAM and LDL-receptor class A domain-containing protein 1-like	4696903	4720886
LOC125671974	uncharacterized protein LOC125671974	4778993	4788433
LOC125671975	uncharacterized protein LOC125671975	4723724	4774286
LOC125671980	serine-rich adhesin for platelets-like isoform X1	26291696	26311531
LOC125671987	sodium/calcium exchanger 3-like	25916109	25926239
LOC125671988	uncharacterized protein LOC125671988	23999384	24002924
LOC125671991	LOW QUALITY PROTEIN: protocadherin Fat 3-like	10630095	10644914
LOC125671993	transmembrane channel-like protein 7	12520574	12566537
LOC125671994	chitobiosyldiphosphodolichol beta-mannosyltransferase-like	12574404	12587296
LOC125671995	40-kDa huntingtin-associated protein-like	12676552	12690139
LOC125671996	5'(3')-deoxyribonucleotidase%2C mitochondrial-like isoform X2	12567378	12574254
LOC125671997	LOW QUALITY PROTEIN: unconventional myosin-XV-like	12592235	12652505
LOC125672029	protein transport protein Sec31A-like isoform X1	11584008	11607101
LOC125672030	MAM and LDL-receptor class A domain-containing protein 1-like	11492425	11516416
LOC125672032	uncharacterized protein LOC125672032	11574496	11583939
LOC125672033	uncharacterized protein LOC125672033	11519244	11569788
LOC125672035	pancreatic lipase-related protein 2-like	21544091	21548357
LOC125672083	protein rolling stone-like	23504296	23514351
LOC125672093	SCO-spondin-like	21520747	21543018
LOC125672097	uncharacterized protein LOC125672097	23484139	23487242
LOC125672104	toll-like receptor 4	24643391	24648014
LOC125672113	uncharacterized protein LOC125672113	19128396	19318594
LOC125672130	helicase with zinc finger domain 2-like isoform X2	23146007	23178788
LOC125672131	helicase with zinc finger domain 2-like isoform X2	23107346	23125988
LOC125672132	intraflagellar transport protein 172 homolog	23043853	23071748
LOC125672133	helicase with zinc finger domain 2-like isoform X1	23071809	23105076
LOC125672140	uncharacterized protein LOC125672140	7911560	7913868
LOC125672152	uncharacterized protein LOC125672152	1116230	1118532
LOC125672153	phospholipid phosphatase-related protein type 5-like	16971265	16999835
LOC125672154	uncharacterized protein LOC125672154	11336129	11338129
LOC125672155	uncharacterized protein LOC125672155	907865	996388
LOC125672158	uncharacterized protein LOC125672158	4540650	4542650
LOC125672161	LOW QUALITY PROTEIN: uncharacterized protein LOC125672161	14934175	14959043
LOC125672174	dimethyladenosine transferase 1%2C mitochondrial-like	24599223	24606312
LOC125672175	LOW QUALITY PROTEIN: uncharacterized protein LOC125672175	1220105	1267198
LOC125672209	transcription factor Sox-17-alpha-A-like	21914372	21918674
LOC125672212	uncharacterized protein LOC125672212	1490604	1492673
LOC125672223	G-protein coupled receptor 15-like	2266002	2267011
LOC125672225	carbohydrate sulfotransferase 12-like	2283245	2284375
LOC125672231	uncharacterized protein LOC125672231	2455023	2463501
LOC125672232	uncharacterized protein LOC125672232 isoform X1	21965502	21974068
LOC125672234	uncharacterized protein LOC125672234	20966109	20969046
LOC125672248	uncharacterized protein LOC125672248	2868221	2875625
LOC125672249	protein qui-1-like	8993854	9019516
LOC125672250	alpha-(1%2C3)-fucosyltransferase 10-like	9019516	9024354
LOC125672251	protein qui-1-like	2198415	2224067
LOC125672252	alpha-(1%2C3)-fucosyltransferase 10-like	2224067	2228904
LOC125672253	nucleosome-remodeling factor subunit BPTF-like	2895225	2896227

LOC125672268	uncharacterized protein LOC125672268	2896290	2898005
LOC125672276	cell division cycle protein 20 homolog	21974757	21980541
LOC125672303	uncharacterized protein LOC125672303	3144981	3148137
LOC125672306	uncharacterized protein LOC125672306	3201272	3201919
LOC125672307	probable chitinase 10	3455487	3642544
LOC125672310	uncharacterized protein LOC125672310	3679963	3684045
LOC125672312	chitotriosidase-1-like	3684048	3694606
LOC125672313	uncharacterized protein LOC125672313	3752855	3754108
LOC125672315	uncharacterized protein LOC125672315	3851423	3854745
LOC125672320	uncharacterized protein LOC125672320	4385658	4393535
LOC125672321	uncharacterized protein LOC125672321	4471977	4472804
LOC125672322	A disintegrin and metalloproteinase with thrombospondin motifs 3-like	9345729	9367170
LOC125672323	inactive rhomboid protein 1-like	9259027	9276202
LOC125672324	tetratricopeptide repeat protein 30A-like	9299082	9324306
LOC125672325	zinc finger CCHC domain-containing protein 7-like	9281211	9298914
LOC125672326	uncharacterized protein LOC125672326	9367221	9404048
LOC125672327	uncharacterized protein LOC125672327	9227745	9229811
LOC125672328	A disintegrin and metalloproteinase with thrombospondin motifs 3-like	2550279	2571729
LOC125672329	inactive rhomboid protein 1-like	2463603	2480780
LOC125672330	tetratricopeptide repeat protein 30A-like	2503634	2528864
LOC125672331	zinc finger CCHC domain-containing protein 7-like	2485514	2503466
LOC125672332	uncharacterized protein LOC125672332	2571780	2608601
LOC125672333	uncharacterized protein LOC125672333	2432336	2434400
LOC125672346	putative defense protein isoform X1	17017184	17025086
LOC125672371	nucleosome-remodeling factor subunit BPTF-like	4978896	4979735
LOC125672373	von Willebrand factor A domain-containing protein 3A-like	6818468	6834403
LOC125672375	LOW QUALITY PROTEIN: polycystic kidney disease 2-like 1 protein	6506838	6519321
LOC125672376	dynein axonemal assembly factor 5-like	6839763	6846208
LOC125672377	oviduct-specific glycoprotein-like isoform X2	7263438	7278109
LOC125672379	uncharacterized protein LOC125672379	7197292	7202659
LOC125672381	uncharacterized protein LOC125672381	6918333	6920697
LOC125672382	chitotriosidase-1-like	7238207	7255574
LOC125672384	uncharacterized protein LOC125672384	6851367	6853582
LOC125672385	chymotrypsinogen B-like	6670395	6682918
LOC125672386	QRFP-like peptide receptor	6849180	6851268
LOC125672387	uncharacterized protein LOC125672387	6955934	6971312
LOC125672388	transmembrane protein 26-like	7301346	7307679
LOC125672389	alpha-2-macroglobulin receptor-associated protein-like	6415902	6437440
LOC125672390	uncharacterized protein LOC125672390	6855416	6885497
LOC125672391	G-protein coupled receptor Mth2-like	6527578	6529133
LOC125672392	uncharacterized protein LOC125672392	6792320	6803130
LOC125672393	FAS-associated death domain protein-like	6410362	6415843
LOC125672395	eukaryotic translation initiation factor 4E-like isoform X2	6889813	6910611
LOC125672396	uncharacterized protein LOC125672396	6479712	6480961
LOC125672397	uncharacterized protein LOC125672397	6454515	6455683
LOC125672399	uncharacterized protein LOC125672399	6485028	6486603
LOC125672400	uncharacterized protein LOC125672400	6497130	6498809
LOC125672401	uncharacterized protein LOC125672401	6885428	6887750
LOC125672402	uncharacterized protein LOC125672402 isoform X1	6921331	6931486
LOC125672403	uncharacterized protein LOC125672403	7324124	7332242
LOC125672404	uncharacterized protein LOC125672404	6499882	6501078
LOC125672405	LOW QUALITY PROTEIN: piwi-like protein 1	6533931	6604942
LOC125672419	uncharacterized protein LOC125672419	5091359	5094548
LOC125672421	probable chitinase 10	5515839	5522759
LOC125672451	bifunctional arginine demethylase and lysyl-hydroxylase JMJD6-B-like	5844667	5855299
LOC125672452	transmembrane protein 26-like	5881650	5897146
LOC125672458	uncharacterized protein LOC125672458	6002977	6019639

B) Coding genes annotated within the inversions at C5

LOC125645885	33 kDa inner dynein arm light chain%2C axonemal-like	90527922	90532026
LOC125645926	39S ribosomal protein L45%2C mitochondrial-like	92033041	92051282
LOC125683265	5-hydroxytryptamine receptor 1D-like	91729228	91734048

LOC125683267	5-hydroxytryptamine receptor 1D-like	91752630	91754571
LOC125683268	5-hydroxytryptamine receptor 2B-like	91715120	91728162
LOC125683713	60S ribosomal protein L11-like	91541398	91553926
LOC125646373	alcohol dehydrogenase-like	93721388	93724479
LOC125647447	alpha-(1%2C3)-fucosyltransferase C-like	93212671	93213786
LOC125646234	alpha-glucosidase-like isoform X1	89459272	89469859
LOC125646496	ALX homeobox protein 1-like	89296587	89308402
LOC125647889	aromatic-L-amino-acid decarboxylase-like	92915055	92923704
LOC125647765	aspartate aminotransferase-like	91955642	91972071
LOC125647901	atrial natriuretic peptide receptor 1-like	90923810	90947485
LOC125683605	B-cell lymphoma 6 protein homolog isoform X3	88305527	88343413
LOC125683606	bombesin receptor subtype-3-like	88303200	88305252
LOC125647768	BTB and MATH domain-containing protein 38-like	91890051	91902808
LOC125647764	calcium-binding mitochondrial carrier protein Aralar2-like isoform X2	92005961	92028330
LOC125646069	calpain-1 catalytic subunit-like	93552475	93566850
LOC125645667	calumenin-B-like isoform X1	90541200	90553514
LOC125683608	cAMP-regulated phosphoprotein 21-like isoform X5	87297766	87367072
LOC125647983	carbohydrate sulfotransferase 1-like isoform X1	88126225	88136329
LOC125647568	CD81 antigen-like	90573438	90594615
LOC125646304	coatomer subunit alpha-like isoform X1	87375873	87393314
LOC125646463	complement C1q-like protein 4	88157714	88174729
LOC125647450	C-type lectin domain family 4 member E-like	93582299	93594545
LOC125646345	cyclic AMP-dependent transcription factor ATF-2-like isoform X3	89639796	89663303
LOC125683610	cyclin-dependent kinase 6-like	90306635	90329994
LOC125647948	cysteine--tRNA ligase%2C cytoplasmic-like isoform X1	88382284	88481952
LOC125683445	delta-like protein D isoform X1	87929904	87940855
LOC125647454	dentin sialophosphoprotein-like	93734162	93735250
LOC125683799	dermatopontin-like isoform X1	91125148	91134262
LOC125646780	DNA damage-regulated autophagy modulator protein 1-like	89258822	89270006
LOC125645840	DNA endonuclease RBBP8-like	87212793	87219013
LOC125648248	DNA repair protein XRCC4-like	90661051	90679933
LOC125646233	dolichyl-diphosphooligosaccharide--protein glycosyltransferase subunit STT3A	89323464	89346763
LOC125683711	dynein regulatory complex protein 1-like	91553935	91567302
LOC125647947	E3 ubiquitin-protein ligase DCST1-like	88447413	88454306
LOC125647430	eggshell protein-like	90816680	90817383
LOC125645884	ER membrane protein complex subunit 2-like	90509239	90527924
LOC125647427	ESX-1 secretion-associated protein EspK-like	90432201	90433600
LOC125645652	ETS homologous factor-like isoform X7	88627104	88671122
LOC125647950	eukaryotic translation initiation factor 3 subunit M-like	88367177	88382399
LOC125648130	fatty acid-binding protein Fh15-like	88145240	88147874
LOC125645922	F-box/LRR-repeat protein 7-like isoform X2	92288313	92313849
LOC125646667	gamma-aminobutyric acid type B receptor subunit 2-like	93437556	93524197
LOC125646662	gamma-tubulin complex component 6-like isoform X2	86624971	86653232
LOC125646335	gastrin-releasing peptide receptor-like	89588392	89595964
LOC125646241	GATA zinc finger domain-containing protein 1-like	89414065	89418475
LOC125647417	GATA zinc finger domain-containing protein 8-like	87689109	87690119
LOC125683449	general transcription factor IIH subunit 1-like	87854863	87872877
LOC125683442	glutamate receptor ionotropic%2C kainate 2-like	87466614	87487656
LOC125683441	glutamate receptor ionotropic%2C kainate 2-like	87487722	87514815
LOC125683444	glutathione hydrolase 1 proenzyme-like	87536561	87571380
LOC125646236	glycerol-3-phosphate dehydrogenase [NAD(+)]%2C cytoplasmic-like isoform X1	89369759	89388339
LOC125647900	growth hormone secretagogue receptor type 1-like	91356745	91359300
LOC125647460	growth hormone secretagogue receptor type 1-like	94256357	94257424
LOC125683611	hepatic lectin-like isoform X2	90351406	90366903
LOC125645929	hepatic leukemia factor-like	92428597	92458580
LOC125647766	histone acetyltransferase type B catalytic subunit-like	91973311	92005940
LOC125648268	histone-lysine N-trimethyltransferase SMYD5-like	88494290	88500326
LOC125683678	homeobox even-skipped homolog protein 1-like	90216644	90222163
LOC125683677	homeobox even-skipped homolog protein 2-like	90100350	90103405
LOC125683363	hydroxymethylglutaryl-CoA lyase%2C mitochondrial-like isoform X1	91486470	91505331
LOC125646237	immunoglobulin-binding protein 1-like	89392468	89407955
LOC125683438	intermembrane lipid transfer protein VPS13B-like	87396007	87461323

LOC125647458	killer cell lectin-like receptor subfamily F member 1	94049821	94056996
LOC125647440	kyphoscoliosis peptidase-like	92821842	92830266
LOC125647449	lectin BRA-3-like	93577714	93578204
LOC125645947	low molecular weight phosphotyrosine protein phosphatase 1-like	89089893	89116407
LOC125683667	LOW QUALITY PROTEIN: bromodomain adjacent to zinc finger domain protein 2B-like	89788337	89825052
LOC125683452	LOW QUALITY PROTEIN: cytosolic non-specific dipeptidase-like	87991578	88016502
LOC125645842	LOW QUALITY PROTEIN: dual specificity tyrosine-phosphorylation-regulated kinase 4-like	87233790	87288763
LOC125646108	LOW QUALITY PROTEIN: glutaminase kidney isoform%2C mitochondrial-like	90440704	90472171
LOC125647994	LOW QUALITY PROTEIN: glycosyl hydrolase YngK-like	86737961	86740014
LOC125645928	LOW QUALITY PROTEIN: kelch domain-containing protein 9-like	92503433	92516902
LOC125683000	LOW QUALITY PROTEIN: kinesin-like protein KIF13B	92595007	92726552
LOC125648277	LOW QUALITY PROTEIN: NADH-cytochrome b5 reductase 3-like	87004847	87018178
LOC125683456	LOW QUALITY PROTEIN: NFX1-type zinc finger-containing protein 1-like	87799244	87819569
LOC125683440	LOW QUALITY PROTEIN: PHD and RING finger domain-containing protein 1-like	87966726	87991549
LOC125647422	LOW QUALITY PROTEIN: protocadherin Fat 4-like	89506026	89547142
LOC125646369	LOW QUALITY PROTEIN: uncharacterized protein LOC125646369	93937773	93974499
LOC125646392	LOW QUALITY PROTEIN: uncharacterized protein LOC125646392	86683617	86692651
LOC125648249	LOW QUALITY PROTEIN: uncharacterized protein LOC125648249	90711897	90727413
LOC125683270	lysozyme 3-like	91708289	91713515
LOC125646242	mediator of RNA polymerase II transcription subunit 30-like	89346635	89363178
LOC125646029	metal cation symporter ZIP14-like isoform X2	88050098	88084795
LOC125683362	methenyltetrahydrofolate synthase domain-containing protein-like isoform X2	91508715	91523001
LOC125648247	microfibril-associated glycoprotein 4-like isoform X2	90649052	90653533
LOC125683451	MOXD1 homolog 1-like	87845521	87854675
LOC125647432	M-phase inducer phosphatase-like	90876551	90884138
LOC125647462	multiple epidermal growth factor-like domains protein 10	94376101	94389781
LOC125646752	myosin-M heavy chain-like	87142232	87159899
LOC125645563	nacrein-like protein	94352739	94358948
LOC125683269	neuropeptide S receptor-like	91760447	91761937
LOC125646318	nitric oxide synthase-interacting protein-like isoform X2	93378579	93408807
LOC125645432	oxysterol-binding protein-related protein 1-like	92524422	92583268
LOC125646757	peptidyl-prolyl cis-trans isomerase FKBP9-like	87190468	87195250
LOC125683453	peroxisome proliferator-activated receptor delta-like	87614860	87626727
LOC125646374	phospholipid scramblase 3-like isoform X1	93919692	93935848
LOC125683446	potassium voltage-gated channel protein Shaw-like isoform X1	87519538	87530693
LOC125648471	prestin-like	89236645	89239217
LOC125683670	programmed cell death 6-interacting protein-like isoform X2	90278323	90302358
LOC125647698	prostaglandin D2 receptor-like	88833442	88853133
LOC125645550	proteasome inhibitor PI31 subunit-like	90481303	90497305
LOC125646243	protein FMC1 homolog	89408140	89410107
LOC125683679	protein HEXIM1-like	90271768	90274000
LOC125645932	protein Hikeshi-like	92076689	92090741
LOC125645949	protein lin-9 homolog isoform X3	90841627	90873057
LOC125683455	protein pitchfork-like	87872909	87877545
LOC125645927	protein YIPF3-like isoform X1	92058369	92076594
LOC125647433	proteoglycan 4-like	90885660	90887249
LOC125648293	putative inhibitor of apoptosis	92989515	92993853
LOC125647694	putative nuclease HARBI1	88900966	88905881
LOC125645956	pyruvate dehydrogenase (acetyl-transferring) kinase isozyme 2%2C mitochondrial-like isoform X1	88193716	88214948
LOC125645848	RBPJ-interacting and tubulin-associated protein 1-like	91615046	91653743
LOC125647416	RE1-silencing transcription factor-like	87107837	87108514
LOC125645711	replication factor C subunit 1-like isoform X1	91769126	91827171
LOC125648294	retinal homeobox protein Rx-B-like	93299400	93311612
LOC125647453	RNA-binding protein 33-like	93669821	93708046
LOC125646235	serine hydroxymethyltransferase%2C mitochondrial-like	89431575	89450979
LOC125647468	signal peptide%2C CUB and EGF-like domain-containing protein 1 isoform X2	89053570	89085584

LOC125646372	sodium-coupled monocarboxylate transporter 1-like	94026064	94044181
LOC125648252	soluble guanylate cyclase 88E-like	90640679	90660949
LOC125645930	sorting nexin-10-like	92351848	92361766
LOC125646986	sulfate transporter-like	89185243	89190610
LOC125646599	sulfate transporter-like	89220968	89228998
LOC125647692	sulfotransferase 1B1-like isoform X1	88965680	88985988
LOC125647696	sulfotransferase 1B1-like isoform X3	88773605	88895280
LOC125647695	sulfotransferase 1C2-like	88934826	88964542
LOC125645847	SUMO-specific isopeptidase USPL1-like	91638147	91645927
LOC125647437	TBC1 domain family member 9-like	91225250	91299872
LOC125645931	tetraspanin-13-like isoform X1	92364350	92381600
LOC125646460	toll-like receptor 4	88164515	88167714
LOC125646461	toll-like receptor 4	88168261	88173077
LOC125645923	transcription factor CP2-like	92329020	92351677
LOC125683676	transmembrane and ubiquitin-like domain-containing protein 1	89830097	89835126
LOC125647853	transmembrane protein 18-like	86616436	86622289
LOC125645946	transmembrane protein 237-like	89116415	89122214
LOC125646665	transmembrane protein 241-like	91568880	91591338
LOC125645559	tripartite motif-containing protein 2-like isoform X1	94223302	94226138
LOC125645883	tRNA (guanine(10)-N2)-methyltransferase homolog isoform X2	90497492	90508661
LOC125645556	tubulin epsilon chain-like	94215123	94237418
LOC125647763	tudor domain-containing protein 7-like isoform X1	91836484	91940934
LOC125683814	tumor protein p53-inducible protein 11-like isoform X1	87020581	87102130
LOC125647992	U1 small nuclear ribonucleoprotein C-like isoform X1	92844063	92849514
LOC125647653	U5 small nuclear ribonucleoprotein 40 kDa protein-like	91591603	91606722
LOC125683735	UBX domain-containing protein 4-like isoform X3	88106396	88125283
LOC125647411	uncharacterized PE-PGRS family protein PE_PGRS46-like	86658574	86659254
LOC125646252	uncharacterized protein DDB_G0284459-like isoform X1	88239237	88252984
LOC125647410	uncharacterized protein F54H12.2-like	86551063	86552379
LOC125647438	uncharacterized protein K02A2.6-like	92212558	92216496
LOC125647457	uncharacterized protein K02A2.6-like	94017835	94021287
LOC125646537	uncharacterized protein K02A2.6-like	94137798	94139751
LOC125645549	uncharacterized protein LOC125645549	90473695	90481301
LOC125645564	uncharacterized protein LOC125645564	94446371	94449427
LOC125645565	uncharacterized protein LOC125645565	94335198	94336650
LOC125645567	uncharacterized protein LOC125645567	94320723	94328881
LOC125645568	uncharacterized protein LOC125645568	94364742	94372045
LOC125645841	uncharacterized protein LOC125645841	87202954	87212403
LOC125645924	uncharacterized protein LOC125645924	92123018	92132954
LOC125645933	uncharacterized protein LOC125645933	92061308	92062607
LOC125645950	uncharacterized protein LOC125645950	90830028	90840367
LOC125646238	uncharacterized protein LOC125646238	89479850	89491784
LOC125646239	uncharacterized protein LOC125646239	89493101	89504161
LOC125646240	uncharacterized protein LOC125646240	89553478	89558871
LOC125646327	uncharacterized protein LOC125646327	88277121	88279236
LOC125646330	uncharacterized protein LOC125646330	86554295	86559151
LOC125646331	uncharacterized protein LOC125646331 isoform X3	86559259	86565042
LOC125646357	uncharacterized protein LOC125646357	86546244	86548766
LOC125646370	uncharacterized protein LOC125646370	93895034	93902732
LOC125646371	uncharacterized protein LOC125646371	94057088	94086445
LOC125646375	uncharacterized protein LOC125646375	94044505	94050676
LOC125646507	uncharacterized protein LOC125646507	92835190	92841258
LOC125646606	uncharacterized protein LOC125646606	86746718	86767037
LOC125646661	uncharacterized protein LOC125646661	89133747	89142812
LOC125646663	uncharacterized protein LOC125646663	86633405	86635098
LOC125646717	uncharacterized protein LOC125646717	93321935	93324856
LOC125646845	uncharacterized protein LOC125646845	90909266	90920984
LOC125646909	uncharacterized protein LOC125646909	91304167	91314500
LOC125646930	uncharacterized protein LOC125646930	88582127	88604102
LOC125647409	uncharacterized protein LOC125647409	86548936	86550090
LOC125647413	uncharacterized protein LOC125647413	86784582	86790373
LOC125647415	uncharacterized protein LOC125647415	86909908	86916703
LOC125647418	uncharacterized protein LOC125647418	87739227	87744997
LOC125647419	uncharacterized protein LOC125647419	89454345	89457005

LOC125647420	uncharacterized protein LOC125647420	89457309	89459144
LOC125647425	uncharacterized protein LOC125647425	90255719	90257475
LOC125647426	uncharacterized protein LOC125647426	90377661	90381689
LOC125647428	uncharacterized protein LOC125647428	90610441	90622099
LOC125647429	uncharacterized protein LOC125647429	90815459	90815839
LOC125647435	uncharacterized protein LOC125647435	91083844	91086754
LOC125647442	uncharacterized protein LOC125647442	92858545	92880689
LOC125647443	uncharacterized protein LOC125647443	93011454	93014652
LOC125647444	uncharacterized protein LOC125647444	93075655	93080097
LOC125647445	uncharacterized protein LOC125647445	93083594	93084922
LOC125647448	uncharacterized protein LOC125647448	93274463	93276105
LOC125647455	uncharacterized protein LOC125647455	93877386	93893868
LOC125647459	uncharacterized protein LOC125647459	94117181	94120288
LOC125647461	uncharacterized protein LOC125647461	94328929	94332577
LOC125647471	uncharacterized protein LOC125647471	92744987	92750519
LOC125647553	uncharacterized protein LOC125647553	89022341	89024913
LOC125647585	uncharacterized protein LOC125647585	86565148	86567436
LOC125647597	uncharacterized protein LOC125647597	86584099	86593851
LOC125647654	uncharacterized protein LOC125647654 isoform X1	91603420	91604651
LOC125647689	uncharacterized protein LOC125647689	87196981	87202776
LOC125647699	uncharacterized protein LOC125647699	88896388	88900926
LOC125647769	uncharacterized protein LOC125647769	91941203	91943074
LOC125647898	uncharacterized protein LOC125647898 isoform X1	91532645	91536156
LOC125647951	uncharacterized protein LOC125647951	88391249	88443494
LOC125648054	uncharacterized protein LOC125648054	89017295	89021609
LOC125648055	uncharacterized protein LOC125648055	89014883	89017299
LOC125648095	uncharacterized protein LOC125648095 isoform X2	92786183	92799903
LOC125648241	uncharacterized protein LOC125648241 isoform X2	90951986	90983987
LOC125648250	uncharacterized protein LOC125648250 isoform X1	90738647	90748442
LOC125648251	uncharacterized protein LOC125648251	90753242	90761392
LOC125648276	uncharacterized protein LOC125648276	86851080	86862755
LOC125648278	uncharacterized protein LOC125648278	86992554	86996455
LOC125648279	uncharacterized protein LOC125648279	86926966	86930239
LOC125648280	uncharacterized protein LOC125648280	86990463	86992195
LOC125648281	uncharacterized protein LOC125648281	86955860	86988280
LOC125648295	uncharacterized protein LOC125648295 isoform X2	93237421	93274289
LOC125648296	uncharacterized protein LOC125648296	92970809	92973153
LOC125648297	uncharacterized protein LOC125648297	93027379	93071143
LOC125683191	uncharacterized protein LOC125683191	94141887	94178963
LOC125683192	uncharacterized protein LOC125683192 isoform X1	94179044	94205642
LOC125683422	uncharacterized protein LOC125683422 isoform X1	90415493	90423664
LOC125683423	uncharacterized protein LOC125683423	90384152	90412393
LOC125683443	uncharacterized protein LOC125683443 isoform X2	87880512	87895921
LOC125683592	uncharacterized protein LOC125683592	91244486	91248990
LOC125683669	uncharacterized protein LOC125683669	90235575	90243651
LOC125683672	uncharacterized protein LOC125683672	89925050	89927823
LOC125683673	uncharacterized protein LOC125683673 isoform X5	89666284	89734273
LOC125683681	uncharacterized protein LOC125683681 isoform X2	89934517	89947822
LOC125683682	uncharacterized protein LOC125683682	90048188	90061848
LOC125683683	uncharacterized protein LOC125683683	89882616	89885584
LOC125683685	uncharacterized protein LOC125683685	89969036	89973124
LOC125683688	uncharacterized protein LOC125683688	89986224	89998558
LOC125683798	uncharacterized protein LOC125683798	91058630	91072565
LOC125645921	vacuolar protein sorting-associated protein 16 homolog	92389488	92420509
LOC125683450	vesicular glutamate transporter 2-like	87825402	87840851
LOC125683686	V-type proton ATPase subunit F-like	89835329	89851220
LOC125683675	WD repeat%2C SAM and U-box domain-containing protein 1-like isoform X1	89734761	89754576
LOC125683736	zinc finger protein 271-like	88091590	88104212
LOC125647423	zinc finger protein 862-like	90035663	90037844
LOC125683780	zinc metalloproteinase nas-37-like	91364963	91415822
LOC125645560	zinc transporter 2-like	94408734	94429894
LOC125645558	zinc transporter 2-like isoform X4	94430908	94444797
LOC125647531	zinc transporter ZIP10-like	94086805	94114394

C) Coding genes annotated within the inversions at C8

LOC125659629	2-acylglycerol O-acyltransferase 2-A-like	57694664	57700133
LOC125658796	39S ribosomal protein L35%2C mitochondrial-like	66978495	66985670
LOC125658553	39S ribosomal protein L43%2C mitochondrial-like	48094713	48098563
LOC125657902	4-hydroxyphenylpyruvate dioxygenase-like protein	54096866	54115122
LOC125657881	5-hydroxytryptamine receptor 1D-like	64337437	64341762
LOC125658411	5-hydroxytryptamine receptor 1-like	45497248	45618895
LOC125657504	5-hydroxytryptamine receptor 2C-like	49487564	49499784
LOC125657681	5-hydroxytryptamine receptor 4-like	62170292	62222947
LOC125657691	5'-nucleotidase domain-containing protein 3-like	51065515	51083174
LOC125658303	A disintegrin and metalloproteinase with thrombospondin motifs adt-1-like	64716758	64728259
LOC125660215	A disintegrin and metalloproteinase with thrombospondin motifs adt-2-like	44743686	44744493
LOC125660216	A disintegrin and metalloproteinase with thrombospondin motifs adt-2-like	44745504	44749490
LOC125660217	A disintegrin and metalloproteinase with thrombospondin motifs adt-2-like	44751154	44751840
LOC125660219	A disintegrin and metalloproteinase with thrombospondin motifs adt-2-like	44762290	44763002
LOC125659162	acetylcholine receptor subunit beta-like	37600062	37601166
LOC125659149	acetylcholine receptor subunit beta-like	45791496	45793980
LOC125660230	acetylcholine receptor subunit delta-like	46309891	46310964
LOC125660231	acetylcholine receptor subunit delta-like	46337263	46338513
LOC125657800	acetylcholinesterase-like	50129773	50143744
LOC125658253	acid sphingomyelinase-like phosphodiesterase 3b	39996367	40001484
LOC125658904	actin-interacting protein 1-like	45664724	45679442
LOC125657630	ADAM 17-like protease	63524121	63589523
LOC125660152	adhesion G-protein coupled receptor D1-like	34896976	34899453
LOC125659411	adhesion G-protein coupled receptor D1-like	61246276	61265917
LOC125659680	ADP-ribosylation factor 5-like	50235753	50241116
LOC125658727	ADP-ribosylhydrolase ARH3-like isoform X1	39641715	39651185
LOC125658778	alkaline ceramidase 3-like	38892000	38913309
LOC125659208	allantoicase-like	45770618	45789647
LOC125659013	alpha-1%2C6-mannosyl-glycoprotein 2-beta-N-acetylglucosaminyltransferase-like	48278770	48335807
LOC125658804	alpha-1A adrenergic receptor-like	65268931	65316513
LOC125658208	alpha-2A adrenergic receptor-like	46034009	46035339
LOC125657875	alpha-centractin	53858272	53872817
LOC125659645	alpha-latrocrustotoxin-Lt1a-like	53163566	53189249
LOC125658410	amidophosphoribosyltransferase-like	45323664	45326451
LOC125657532	amiloride-sensitive amine oxidase [copper-containing]-like isoform X1	52589297	52595948
LOC125657531	amiloride-sensitive amine oxidase [copper-containing]-like isoform X2	52502457	52510598
LOC125658339	amine oxidase [flavin-containing]-like	34605094	34617745
LOC125658665	AMME syndrome candidate gene 1 protein homolog	36784572	36800974
LOC125657601	angiomotin-like protein 1 isoform X1	63838555	63847298
LOC125659967	ankycorbin-like isoform X2	40175227	40180732
LOC125659926	ankyrin repeat and SOCS box protein 8-like	51938522	51941570
LOC125660463	ankyrin repeat domain-containing protein 42-like	41211737	41224459
LOC125657610	ankyrin repeat domain-containing protein 50-like	63462167	63464392
LOC125658724	ankyrin repeat domain-containing protein 53-like	39731994	39739675
LOC125659112	anti-sigma-I factor RsgI2-like	61111015	61113150
LOC125659444	AP-5 complex subunit sigma-1-like	41167438	41169389
LOC125659807	APGW-amide-related neuropeptide-like	49718734	49735733
LOC125659175	aprataxin-like	49338699	49357420
LOC125658129	arf-GAP domain and FG repeat-containing protein 1-like isoform X1	39102463	39124449
LOC125659997	armadillo-like helical domain-containing protein 3	47513295	47549984
LOC125657483	arsenite methyltransferase-like	58840884	58857701
LOC125658752	arsenite methyltransferase-like	67263872	67296011
LOC125658504	arylacetamide deacetylase-like	34570018	34589409
LOC125658505	arylacetamide deacetylase-like	34593393	34600702
LOC125657698	arylacetamide deacetylase-like	51135922	51150364
LOC125657696	arylacetamide deacetylase-like isoform X1	51112636	51354665
LOC125658031	arylacetamide deacetylase-like isoform X2	54765807	54780120
LOC125657692	arylacetamide deacetylase-like isoform X3	51088317	51103213
LOC125658896	asparagine-rich protein-like isoform X2	51859066	51871624

LOC125657642	aspartate aminotransferase%2C cytoplasmic-like	60788481	60808225
LOC125658260	ATP-binding cassette sub-family C member 4-like isoform X2	43074200	43131442
LOC125659551	ATP-dependent DNA helicase RecQ-like	43313806	43318405
LOC125659805	ATP-dependent DNA helicase RecQ-like	49995823	49997965
LOC125660286	ATP-dependent DNA helicase RecQ-like	54904612	54906209
LOC125658775	ATP-dependent RNA helicase A-like isoform X2	46068891	46085197
LOC125659850	autophagy-related protein 16-1-like	48587489	48614126
LOC125657602	basic immunoglobulin-like variable motif-containing protein isoform X2	63685545	63713115
LOC125658495	beta-1%2C3-galactosyltransferase 1-like	37764178	37814785
LOC125658949	BRCA2-interacting transcriptional repressor EMSY-like	48137677	48160498
LOC125659730	bridging integrator 3-like	43977629	43985488
LOC125658872	BRISC complex subunit Abraxas 2-like	34629184	34637200
LOC125658599	BTB/POZ domain-containing protein 16-like isoform X2	52878908	52938981
LOC125659136	BTB/POZ domain-containing protein 6-like	57142695	57151657
LOC125659522	BTB/POZ domain-containing protein 6-like	64684735	64688107
LOC125659737	C1q-related factor-like	67350958	67352592
LOC125659566	caldesmon-like	34842174	34855958
LOC125658506	cAMP-dependent protein kinase catalytic subunit 3-like	43562752	43593388
LOC125660293	carbohydrate sulfotransferase 14-like	56309589	56327032
LOC125658007	carbohydrate sulfotransferase 15-like	64415699	64439440
LOC125658217	casein kinase I-like	67568985	67588131
LOC125659442	cell growth-regulating nucleolar protein-like isoform X1	50397739	50416206
LOC125659723	centrosomal protein of 19 kDa-like	48160663	48162737
LOC125658168	C-factor-like	33919477	33926687
LOC125658408	chaoptin-like	45219242	45234580
LOC125659315	charged multivesicular body protein 7-like	43720269	43740878
LOC125657613	chitinase domain-containing protein 1-like isoform X2	63589448	63609282
LOC125659358	chondroadherin-like	50755283	50759678
LOC125659529	cilia- and flagella-associated protein 300-like	57679710	57684012
LOC125659533	cilia- and flagella-associated protein 58-like	47971557	47978476
LOC125657684	ciliary-associated calcium-binding coiled-coil protein 1-like isoform X1	62136801	62156009
LOC125657833	clathrin interactor 1-like isoform X8	56433034	56458693
LOC125659914	coagulation factor XI-like	35232686	35237276
LOC125659476	coagulation factor XI-like isoform X1	35823075	35829373
LOC125659101	coiled-coil domain-containing protein 125-like	48098759	48109660
LOC125659667	coiled-coil domain-containing protein 1-like	37009390	37017041
LOC125657621	complement C1q tumor necrosis factor-related protein 6-like	63769495	63770465
LOC125659739	complement C1q-like protein 4	67349335	67350519
LOC125658059	complexin-like isoform X1	39808763	39879052
LOC125659603	condensin complex subunit 2-like	60462429	60491186
LOC125659404	COP9 signalosome complex subunit 6-like	64758152	64774710
LOC125657585	copper homeostasis protein cutC homolog isoform X2	58893589	58905577
LOC125659952	craniofacial development protein 2-like	53395253	53398840
LOC125659695	ctenidin-1-like	46104227	46105752
LOC125659668	cyclic nucleotide-gated channel rod photoreceptor subunit alpha-like	68357852	68421599
LOC125658899	cyclin-C-like isoform X2	56066333	56082747
LOC125658361	cysteine and tyrosine-rich protein 1-like	38746766	38755018
LOC125657616	cysteine-rich venom protein latisemin-like	63485423	63519970
LOC125659014	cytochrome c oxidase assembly protein COX15 homolog	48231482	48240663
LOC125659425	cytochrome P450 26A1-like	48024893	48029471
LOC125657818	cytochrome P450 26B1-like	60007751	60011571
LOC125657802	cytochrome P450 2B15-like isoform X1	40045830	40055688
LOC125657804	cytochrome P450 2B4-like	40090535	40107456
LOC125657803	cytochrome P450 2C15-like isoform X1	40063322	40126704
LOC125658252	cytochrome P450 2C8-like isoform X1	39974073	39978977
LOC125657726	cytochrome P450 2U1-like isoform X3	48977689	48998726
LOC125658894	cytochrome P450 3A24-like	40620887	40625926
LOC125658684	cytoplasmic dynein 2 intermediate chain 2-like isoform X2	47861521	47873118
LOC125658315	cytoplasmic protein NCK2-like	57735496	57745536
LOC125659114	cytosol aminopeptidase-like	46450856	46471104
LOC125659342	D-beta-hydroxybutyrate dehydrogenase-like isoform X1	57544619	57554206
LOC125657644	DCC-interacting protein 13-alpha-like isoform X1	58649267	58690791
LOC125659431	decreased expression in renal and prostate cancer protein-like	66506028	66527526
LOC125659552	dehydrogenase/reductase SDR family member 12-like	43347904	43361445

LOC125658995	dehydrogenase/reductase SDR family member 12-like	44269236	44283553
LOC125659681	dehydrogenase/reductase SDR family member 9-like isoform X1	61336853	61346281
LOC125659671	deleted in malignant brain tumors 1 protein-like	68286943	68304923
LOC125660366	deleted in malignant brain tumors 1 protein-like	68516029	68542207
LOC125658154	deleted in malignant brain tumors 1 protein-like isoform X1	33972069	34026968
LOC125657600	delta-1-pyrroline-5-carboxylate synthase-like	63610429	63630028
LOC125658184	demethylmenaquinone methyltransferase-like	55262757	55283768
LOC125658675	demethylmenaquinone methyltransferase-like	55296401	55300669
LOC125660440	dentin matrix acidic phosphoprotein 1-like	48730019	48732854
LOC125659698	dentin sialophosphoprotein-like	67030062	67032410
LOC125659550	deoxynucleoside triphosphate triphosphohydrolase SAMHD1-like isoform X3	43320835	43414698
LOC125659463	disks large homolog 1-like isoform X2	35543213	35617497
LOC125657901	divergent protein kinase domain 2A-like isoform X2	54118648	54130041
LOC125657587	DNA polymerase lambda-like isoform X4	66698090	66752495
LOC125657966	DNA polymerase nu-like	49295140	49325909
LOC125659725	DNA replication complex GINS protein SLD5-like	46781353	46803433
LOC125659606	DNA-directed DNA/RNA polymerase mu-like isoform X2	60445021	60464176
LOC125660260	DNA-directed RNA polymerase II subunit RPB1-like	51895437	51897791
LOC125658176	DNA-directed RNA polymerase II subunit RPB2	65836420	65862662
LOC125657788	docking protein 2-like	63275604	63290223
LOC125659180	dopamine receptor 1-like	52106423	52112263
LOC125657825	drebrin-like protein	60203380	60225206
LOC125658405	dual specificity protein phosphatase 4-like	68150804	68161765
LOC125658747	dynactin subunit 1-like isoform X5	67045211	67098342
LOC125660000	E3 SUMO-protein ligase KIAA1586-like	47579672	47583640
LOC125660362	E3 SUMO-protein ligase ZBED1-like	67880519	67882668
LOC125660238	E3 ubiquitin-protein ligase hrd-like protein 1	48062195	48071832
LOC125658989	E3 ubiquitin-protein ligase KCMF1-like isoform X2	41811270	41824369
LOC125658462	E3 ubiquitin-protein ligase MSL2-like	55600069	55603473
LOC125658336	E3 ubiquitin-protein ligase RMND5A-like	63234400	63255681
LOC125658963	E3 ubiquitin-protein ligase RNF168-like	59277076	59293234
LOC125659903	E3 ubiquitin-protein ligase RNF4-like	55337167	55352257
LOC125660241	E3 ubiquitin-protein ligase TRIM33-like	48640332	48642600
LOC125657817	E3 ubiquitin-protein ligase TRIM71-like	60258166	60262225
LOC125660027	E3 ubiquitin-protein ligase TRIM71-like	62643415	62654550
LOC125659996	E3 ubiquitin-protein ligase TRIM71-like	66257083	66268657
LOC125659836	early growth response protein 1-B-like	36660270	36663570
LOC125657899	EF-hand domain-containing family member C2-like	53985850	53991766
LOC125658406	elongation factor 1-alpha 1-like	45241138	45251511
LOC125657697	elongation factor 1-alpha-like	51108814	51112573
LOC125657832	elongation factor G%2C mitochondrial-like isoform X2	56576018	56594129
LOC125658990	enolase-phosphatase E1-like isoform X2	44327454	44349426
LOC125658749	equilibrative nucleoside transporter 1-like	67099666	67144741
LOC125659865	ER membrane protein complex subunit 5-like	59958264	59965781
LOC125659746	erythroid differentiation-related factor 1-like	40859702	40916103
LOC125658434	eukaryotic translation initiation factor 2-alpha kinase 3-like	42514132	42527508
LOC125657877	eukaryotic translation initiation factor 3 subunit A-like isoform X2	64168852	64192816
LOC125657993	exocyst complex component 4-like	54838806	54869251
LOC125658066	exocyst complex component 6B-like isoform X5	42852666	42878996
LOC125660196	exonuclease 3'-5' domain-containing protein 2-like	41771236	41808971
LOC125658908	exosome component 10-like isoform X2	62097244	62126379
LOC125658207	exportin-7-like	67604478	67640984
LOC125659499	fatty acid CoA ligase Acsl3-like isoform X2	42089357	42121545
LOC125658337	fatty acid desaturase 6-like	63237206	63239567
LOC125657925	F-box/SPRY domain-containing protein 1-like	38848016	38852970
LOC125657718	FERM%2C ARHGEF and pleckstrin domain-containing protein 2-like isoform X2	61440180	61520695
LOC125658556	fibroblast growth factor 18-like isoform X3	35375199	35395958
LOC125658793	fibronectin type 3 and ankyrin repeat domains protein 1-like isoform X1	37209955	37243348
LOC125657829	fibronectin type-III domain-containing protein 3A-like isoform X4	56203025	56268328
LOC125660009	FMRFamide receptor-like	52362953	52373223
LOC125658964	fragile X mental retardation syndrome-related protein 1-like isoform X2	59574780	59605189
LOC125659803	free fatty acid receptor 4-like	43224160	43235383

LOC125657892	fucose mutarotase-like	38258958	38265391
LOC125657891	fucose mutarotase-like isoform X1	38242908	38254397
LOC125657748	fumarylacetoacetate hydrolase domain-containing protein 2-like isoform X1	37678672	37685923
LOC125660388	G protein-coupled receptor kinase 5-like	55002002	55049807
LOC125658994	galactose mutarotase-like	44349658	44362150
LOC125659802	galactoside alpha-(1%2C2)-fucosyltransferase 2-like	43247510	43260349
LOC125659849	gamma-tubulin complex component 3-like isoform X1	48655280	48679592
LOC125660017	glucans biosynthesis glucosyltransferase H-like	39540662	39545933
LOC125658079	glutaredoxin 3-like isoform X1	48741967	48754521
LOC125659501	glutathione reductase%2C mitochondrial-like	42250658	42265769
LOC125660443	glycerol-3-phosphate acyltransferase 1%2C mitochondrial-like	34693545	34714251
LOC125659375	glycine N-acyltransferase-like	40529488	40536621
LOC125659851	glycogenin-1-like isoform X1	48692737	48724078
LOC125658973	glycoprotein-N-acetylgalactosamine 3-beta-galactosyltransferase 1-like isoform X1	59224314	59247429
LOC125657791	golgin subfamily A member 6-like protein 7	63293670	63312036
LOC125657882	GPALPP motifs-containing protein 1-like	64343160	64353015
LOC125657534	G-protein coupled estrogen receptor 1-like	52443791	52476569
LOC125660275	G-protein coupled receptor 183-A-like	52716285	52717349
LOC125660161	G-protein coupled receptor GRL101-like	36255916	36265352
LOC125659465	G-protein coupled receptor GRL101-like	36449830	36452309
LOC125660162	G-protein coupled receptor GRL101-like	36480492	36487178
LOC125660330	G-protein coupled receptor GRL101-like	62056939	62074115
LOC125658979	GRIP and coiled-coil domain-containing protein 2-like	59456064	59492942
LOC125660028	growth hormone secretagogue receptor type 1-like	41482829	41537823
LOC125658471	growth hormone-regulated TBC protein 1-A-like	62662904	62691121
LOC125659201	growth hormone-regulated TBC protein 1-A-like	66217671	66248548
LOC125659750	grpE protein homolog 1%2C mitochondrial-like isoform X1	40914725	40931734
LOC125659498	guanylate cyclase soluble subunit beta-2-like	42242399	42250537
LOC125657727	H/ACA ribonucleoprotein complex subunit 2-like protein	49005840	49066159
LOC125658312	H/ACA ribonucleoprotein complex subunit DKC1-like	56099959	56113526
LOC125658056	HAUS augmin-like complex subunit 8 isoform X1	53411910	53436616
LOC125658960	heavy metal-binding protein HIP-like	67356978	67357859
LOC125659915	helicase POLQ-like	61829476	61908203
LOC125659527	heme-binding protein 2-like	67537319	67540724
LOC125659733	hemicentin-1-like	37399833	37406624
LOC125658907	heparanase-like	45967797	45989630
LOC125659483	hephaestin-like	35692854	35710626
LOC125657870	hexokinase-1-like	35216925	35230859
LOC125659469	hexokinase-1-like	35855201	35873337
LOC125659467	hexokinase-2-like isoform X1	35496407	35530735
LOC125658413	hexokinase-2-like isoform X1	45054784	45073932
LOC125658818	homeobox protein EMX1-like	47368071	47374178
LOC125658743	homeobox protein EMX2-like	47472245	47477463
LOC125657542	homeobox protein Nkx-2.5-like	50247641	50258182
LOC125658167	homeobox protein Nkx-6.2-like	34383479	34398033
LOC125658881	homeobox protein slou-like	45729829	45734578
LOC125658073	huntingtin-like isoform X1	39895864	39966623
LOC125659929	hydroxylysine kinase-like	55936303	55948965
LOC125660218	IgGFc-binding protein-like	44754176	44759042
LOC125660221	IgGFc-binding protein-like	44814622	44820575
LOC125659452	inositol 2-dehydrogenase-like	44065113	44087596
LOC125657724	integrator complex subunit 4-like	48945535	49005590
LOC125657599	integrator complex subunit 6-like	63718355	63746329
LOC125659188	integrin beta-6-like	38770601	38785522
LOC125660173	involucrin-like	37480163	37480846
LOC125660018	ionotropic receptor 25a-like isoform X2	61623271	61648143
LOC125659608	kappa-type opioid receptor-like	60565324	60569826
LOC125659009	KAT8 regulatory NSL complex subunit 3-like isoform X1	48338651	48358528
LOC125657900	kelch-like protein diablo	53975734	53985633
LOC125659659	keratin%2C type I cytoskeletal 10-like	46094683	46095552
LOC125660184	keratin-associated protein 4-3-like	39084448	39085047
LOC125660496	kyphoscoliosis peptidase-like	35249591	35252534
LOC125659654	kyphoscoliosis peptidase-like	42426349	42437558

LOC125659965	kyphoscoliosis peptidase-like	64232726	64238630
LOC125658632	lactosylceramide 1%2C3-N-acetyl-beta-D-glucosaminyltransferase-like	34886601	34887929
LOC125659604	leucine zipper putative tumor suppressor 2 homolog	60520145	60548671
LOC125659213	leucine-rich repeat and immunoglobulin-like domain-containing nogo receptor-interacting protein 2	57308966	57311749
LOC125659947	leucine-rich repeat-containing protein 27-like isoform X4	53330163	53357940
LOC125657615	leukocyte elastase inhibitor-like	63436472	63445654
LOC125657622	leukocyte elastase inhibitor-like	63437137	63438095
LOC125657903	LIM domain-binding protein 2-like	54312679	54335361
LOC125658256	lipase maturation factor 1-like	52957730	52973351
LOC125658373	lipid droplet-regulating VLDL assembly factor AUP1-like	34538438	34560347
LOC125657502	LOW QUALITY PROTEIN: 26S proteasome non-ATPase regulatory subunit 1-like	49390039	49545541
LOC125660247	LOW QUALITY PROTEIN: acetylcholine receptor subunit beta-like	48936134	48938680
LOC125660444	LOW QUALITY PROTEIN: alpha-adducin-like	34653724	34692825
LOC125658692	LOW QUALITY PROTEIN: biotin--protein ligase-like	55713350	55763401
LOC125657744	LOW QUALITY PROTEIN: centromere protein F-like	66859445	66946902
LOC125658433	LOW QUALITY PROTEIN: condensin complex subunit 3-like	34799944	34833116
LOC125658313	LOW QUALITY PROTEIN: DNA excision repair protein ERCC-5 homolog	56113630	56123548
LOC125658489	LOW QUALITY PROTEIN: DNA polymerase alpha catalytic subunit-like	38167236	38226059
LOC125660169	LOW QUALITY PROTEIN: DNA-directed RNA polymerase II subunit RPB1-like	37100668	37169103
LOC125658491	LOW QUALITY PROTEIN: dynein axonemal assembly factor 9-like	38099238	38164088
LOC125659602	LOW QUALITY PROTEIN: E3 ubiquitin-protein ligase TRIP12-like	60608001	60669194
LOC125657835	LOW QUALITY PROTEIN: ecto-NOX disulfide-thiol exchanger 2-like	56272062	56291908
LOC125659271	LOW QUALITY PROTEIN: enolase 4-like	44642920	44656392
LOC125659308	LOW QUALITY PROTEIN: Fanconi anemia group I protein-like	34488241	34538369
LOC125659277	LOW QUALITY PROTEIN: filamin-A-like	57315593	57337409
LOC125659064	LOW QUALITY PROTEIN: filamin-A-like	57559926	57573375
LOC125659449	LOW QUALITY PROTEIN: filamin-C-like	43986569	44046599
LOC125658461	LOW QUALITY PROTEIN: GATOR complex protein WDR24-like	55603645	55626315
LOC125657592	LOW QUALITY PROTEIN: histone deacetylase complex subunit SAP130-like	57411016	57442425
LOC125658863	LOW QUALITY PROTEIN: homeobox protein EMX2-like	47261918	47294740
LOC125658285	LOW QUALITY PROTEIN: importin-5-like	43600136	43634864
LOC125658156	LOW QUALITY PROTEIN: inositol polyphosphate-5-phosphatase A-like	34284923	34349399
LOC125659462	LOW QUALITY PROTEIN: kinase non-catalytic C-lobe domain-containing protein 1-like	35634939	35676813
LOC125658514	LOW QUALITY PROTEIN: lateral signaling target protein 2 homolog	43695242	43716176
LOC125657798	LOW QUALITY PROTEIN: leucine-rich repeat and calponin homology domain-containing protein 2-like	36849151	36885857
LOC125658419	LOW QUALITY PROTEIN: loricrin-like	45042341	45054498
LOC125658750	LOW QUALITY PROTEIN: mannose-6-phosphate isomerase-like	67144706	67155640
LOC125657871	LOW QUALITY PROTEIN: MORN repeat-containing protein 4-like	35210451	35214409
LOC125660300	LOW QUALITY PROTEIN: mucin-2-like	56782101	56822004
LOC125659651	LOW QUALITY PROTEIN: multidrug resistance-associated protein 1-like	38924452	38938446
LOC125659526	LOW QUALITY PROTEIN: NACHT domain- and WD repeat-containing protein 1-like	64651223	64682559
LOC125657934	LOW QUALITY PROTEIN: NFX1-type zinc finger-containing protein 1-like	57500823	57509784
LOC125660020	LOW QUALITY PROTEIN: nitric oxide-associated protein 1-like	61569817	61588829
LOC125657920	LOW QUALITY PROTEIN: nucleotide exchange factor SIL1-like	35264610	35297677
LOC125658791	LOW QUALITY PROTEIN: peripheral plasma membrane protein CASK-like	37247954	37355001
LOC125659904	LOW QUALITY PROTEIN: phosphatidylinositide phosphatase SAC2-like	55352371	55486922
LOC125659618	LOW QUALITY PROTEIN: presenilins-associated rhomboid-like protein%2C mitochondrial	61292313	61303048
LOC125660261	LOW QUALITY PROTEIN: protein FAM204A-like	51943724	51950414
LOC125657815	LOW QUALITY PROTEIN: protein hunchback-like	60112256	60125797
LOC125657812	LOW QUALITY PROTEIN: protein mono-ADP-ribosyltransferase PARP14-like	60348837	60441657
LOC125660019	LOW QUALITY PROTEIN: protein O-mannosyl-transferase TMTC4-like	61647696	61676601
LOC125659196	LOW QUALITY PROTEIN: protoporphyrinogen oxidase-like	34860049	34878948
LOC125657745	LOW QUALITY PROTEIN: putative aminopeptidase W07G4.4	37686027	37698174

LOC125658009	LOW QUALITY PROTEIN: ras-related C3 botulinum toxin substrate 2-like	37498668	37525316
LOC125659065	LOW QUALITY PROTEIN: ras-related protein Rab-28-like	41200504	41209867
LOC125658150	LOW QUALITY PROTEIN: receptor for retinol uptake stra6-like	67668999	67688700
LOC125660350	LOW QUALITY PROTEIN: SCO-spondin-like	65692548	65759084
LOC125660351	LOW QUALITY PROTEIN: SCO-spondin-like	65769058	65823719
LOC125659324	LOW QUALITY PROTEIN: serine/arginine repetitive matrix protein 2-like	53607654	53633871
LOC125660359	LOW QUALITY PROTEIN: skin-specific protein 32-like	67723674	67729532
LOC125659900	LOW QUALITY PROTEIN: slit homolog 2 protein-like	55491332	55532631
LOC125659670	LOW QUALITY PROTEIN: splicing factor 3A subunit 1-like	68304221	68320030
LOC125658209	LOW QUALITY PROTEIN: titin-like	46000966	46027841
LOC125659697	LOW QUALITY PROTEIN: transcription factor IIIB 50 kDa subunit-like	50369873	50373758
LOC125659325	LOW QUALITY PROTEIN: UDP-glucose:glycoprotein glucosyltransferase 1-like	53726661	53769665
LOC125657590	LOW QUALITY PROTEIN: uncharacterized protein LOC125657590	34718530	34775481
LOC125657591	LOW QUALITY PROTEIN: uncharacterized protein LOC125657591	34772513	34791301
LOC125657593	LOW QUALITY PROTEIN: uncharacterized protein LOC125657593	57445553	57454663
LOC125657595	LOW QUALITY PROTEIN: uncharacterized protein LOC125657595	57380614	57401778
LOC125657801	LOW QUALITY PROTEIN: uncharacterized protein LOC125657801	53017557	53111304
LOC125657898	LOW QUALITY PROTEIN: uncharacterized protein LOC125657898	42732954	42751783
LOC125657917	LOW QUALITY PROTEIN: uncharacterized protein LOC125657917	44839883	44860549
LOC125658634	LOW QUALITY PROTEIN: uncharacterized protein LOC125658634	39027533	39030364
LOC125658798	LOW QUALITY PROTEIN: uncharacterized protein LOC125658798	64988774	65039975
LOC125659281	LOW QUALITY PROTEIN: uncharacterized protein LOC125659281	42893902	42909308
LOC125659318	LOW QUALITY PROTEIN: uncharacterized protein LOC125659318	43908687	43973649
LOC125659448	LOW QUALITY PROTEIN: uncharacterized protein LOC125659448	44088431	44150507
LOC125660324	LOW QUALITY PROTEIN: uncharacterized protein LOC125660324	61159947	61245651
LOC125660346	LOW QUALITY PROTEIN: uncharacterized protein LOC125660346	64933179	64955698
LOC125660497	LOW QUALITY PROTEIN: uncharacterized protein LOC125660497	42378215	42426183
LOC125658537	LOW QUALITY PROTEIN: WD repeat-containing protein 11-like	66787779	66838973
LOC125660262	LOW QUALITY PROTEIN: WD repeat-containing protein 6-like	51950472	51991070
LOC125657583	LOW QUALITY PROTEIN: zinc finger CCCH domain-containing protein 13-like	58902678	58937833
LOC125658224	low-density lipoprotein receptor-related protein 4-like	39488588	39520119
LOC125658731	lys-63-specific deubiquitinase BRCC36-like	39584743	39598079
LOC125660210	lysosome-associated membrane glycoprotein 1-like	44257087	44267345
LOC125658991	lysosome-associated membrane glycoprotein 1-like	44294695	44318915
LOC125659804	macrophage mannose receptor 1-like	49632771	49673192
LOC125657481	major facilitator superfamily domain-containing protein 10-like	58857699	58878216
LOC125659911	mannan endo-1%2C4-beta-mannosidase-like	50432010	50442293
LOC125659528	mannose-P-dolichol utilization defect 1 protein homolog	62737438	62750659
LOC125659202	mannose-P-dolichol utilization defect 1 protein homolog	66147839	66161159
LOC125659439	mannosyl-oligosaccharide glucosidase-like	48130413	48135790
LOC125658696	matrix metallopeptidase-21-like isoform X2	63085319	63111062
LOC125657807	max dimerization protein 1-like	60876157	60882526
LOC125659508	mediator of RNA polymerase II transcription subunit 11-like	42076845	42084924
LOC125659415	meiotic recombination protein REC8 homolog	51697046	51766535
LOC125658078	melanotransferrin-like	48757693	48771682
LOC125658860	methionine--tRNA ligase%2C mitochondrial-like	47155033	47170391
LOC125658855	methionine--tRNA ligase%2C mitochondrial-like isoform X1	47038793	47054415
LOC125658820	methyltransferase-like protein 27	43545667	43554564
LOC125659138	methyltransferase-like protein 27	56846150	56850878
LOC125659703	methyltransferase-like protein 27 isoform X2	54552782	54566849
LOC125658795	MICOS complex subunit MIC60-like isoform X1	66959465	66978455
LOC125659419	MIF-like protein mif-2	51691978	51696840
LOC125657922	mitochondrial intermediate peptidase-like	38853180	38882632
LOC125658430	mitochondrial proton/calcium exchanger protein-like	64006460	64027921
LOC125657510	mitogen-activated protein kinase kinase kinase kinase 4-like isoform X4	65899398	65974556
LOC125659109	mitotic apparatus protein p62-like isoform X6	35453712	35485124
LOC125657959	mitotic checkpoint protein BUB3-like isoform X2	62832983	62865825
LOC125658064	mitotic checkpoint serine/threonine-protein kinase BUB1-like isoform X1	62244572	62317900
LOC125658700	MMS19 nucleotide excision repair protein homolog	62964304	63007241
LOC125657816	monocarboxylate transporter 12-like isoform X1	59971902	60004135
LOC125659090	monocarboxylate transporter 12-like isoform X2	60994034	61000881
LOC125659169	monocarboxylate transporter 12-like isoform X3	50484687	50495785

LOC125659397	monocarboxylate transporter 12-like isoform X4	44956756	44962139
LOC125658414	monocarboxylate transporter 13-like	45028932	45042278
LOC125658028	monocarboxylate transporter 13-like	54787403	54798999
LOC125657941	monocarboxylate transporter 13-like isoform X7	61063416	61070462
LOC125658826	monocarboxylate transporter 14-like	38961131	38971587
LOC125658563	monocarboxylate transporter 14-like isoform X1	44968676	45000843
LOC125658603	monocarboxylate transporter 2-like isoform X3	55562697	55596650
LOC125657740	monocarboxylate transporter 5-like	60949385	60975981
LOC125657943	monocarboxylate transporter 5-like isoform X1	61039234	61061660
LOC125659089	monocarboxylate transporter 5-like isoform X2	61001467	61029427
LOC125659837	MORN repeat-containing protein 3-like	36718360	36719384
LOC125659481	MORN repeat-containing protein 4-like	35875231	35879664
LOC125658996	motile sperm domain-containing protein 1-like	44205226	44210075
LOC125660278	M-phase inducer phosphatase 2-like	52814794	52828769
LOC125659221	M-phase inducer phosphatase-like	42265996	42273199
LOC125660279	M-phase inducer phosphatase-like	52840618	52855852
LOC125660298	mucin-2-like	56678570	56681456
LOC125659933	mucin-2-like	56754968	56772606
LOC125659352	mucin-2-like	62467612	62478805
LOC125660302	mucin-5AC-like	56822527	56839781
LOC125660320	mucin-5AC-like	60142931	60161850
LOC125657884	mucin-5AC-like isoform X1	57178508	57193050
LOC125658761	muscleblind-like protein 2a	58974775	59095826
LOC125657869	mushroom body large-type Kenyon cell-specific protein 1-like	35195669	35208709
LOC125658993	myb-like protein U	44235028	44257250
LOC125659525	myosin essential light chain%2C striated adductor muscle-like	64562358	64568268
LOC125659178	myosin heavy chain%2C striated muscle-like isoform X1	52227527	52243666
LOC125658074	myosin regulatory light chain B%2C smooth adductor muscle-like	48079302	48087450
LOC125659554	myosin-VIIa-like isoform X2	39310432	39473707
LOC125659250	nacrein-like protein	43005365	43055901
LOC125659265	negative elongation factor A-like	64375800	64396655
LOC125659507	neurogenic protein mastermind-like	42037066	42054355
LOC125659005	neuroligin-4%2C X-linked-like isoform X3	40200633	40280955
LOC125659127	neuroligin-4%2C Y-linked-like isoform X2	40322206	40402660
LOC125660177	neuronal acetylcholine receptor subunit alpha-3-like	37626380	37633825
LOC125659333	neuropeptide F receptor-like	46689314	46690930
LOC125658730	neuropeptide Y receptor type 2-like	39727113	39731846
LOC125658415	neuropeptide Y receptor type 2-like	45331127	45366564
LOC125658905	neuropeptide Y receptor type 5-like	45931558	45940606
LOC125658057	NF-kappa-B inhibitor alpha-like isoform X2	39816602	39825473
LOC125658151	NF-kappa-B-activating protein-like isoform X1	67688959	67708852
LOC125657967	nicotinamide/nicotinic acid mononucleotide adenylyltransferase 1-like isoform X4	49273321	49295929
LOC125659684	NPC intracellular cholesterol transporter 2-like	50459185	50480194
LOC125660462	nuclear fragile X mental retardation-interacting protein 1-like	41224585	41243323
LOC125657607	nuclear hormone receptor HR96-like isoform X1	63968680	64004234
LOC125659748	nuclear hormone receptor HR96-like isoform X5	40985972	41089914
LOC125660248	nucleolar protein 14-like	49234883	49262466
LOC125657793	nucleolar protein 56-like	44484980	44497973
LOC125660336	octapeptide-repeat protein T2-like	63875887	63876255
LOC125659942	omega-amidase NIT2-like	34643685	34644703
LOC125659696	O-phosphoseryl-tRNA(Sec) selenium transferase-like isoform X1	43203020	43215606
LOC125659336	ornithine aminotransferase%2C mitochondrial-like	56000872	56013353
LOC125659521	P2R1A-PPP2R2A-interacting phosphatase regulator 1-like isoform X2	64691098	64703822
LOC125659479	P2X purinoceptor 7-like	36135620	36140016
LOC125659360	paired mesoderm homeobox protein 2-like	50667327	50676004
LOC125659216	palmitoyltransferase ZDHHC16B-like	64815119	64834631
LOC125659319	pancreatic triacylglycerol lipase-like	43891448	43895083
LOC125658180	pantothenate kinase 3-like	62501608	62520270
LOC125659558	PCI domain-containing protein 2-like	39132774	39151729
LOC125658707	pentatricopeptide repeat-containing protein 3%2C mitochondrial-like	68084030	68144714
LOC125658500	peptide methionine sulfoxide reductase MsrB-like	37741662	37745139
LOC125658169	peptidoglycan-recognition protein SC2-like	34434099	34436231
LOC125657883	peptidyl-prolyl cis-trans isomerase NIMA-interacting 4-like isoform X1	64346932	64359064

LOC125658499	perlucin-like	37870251	37899203
LOC125659130	perlucin-like	64362930	64368293
LOC125659675	perlucin-like	68600343	68610343
LOC125658714	perlucin-like protein	67813573	67817063
LOC125659355	peroxidase-like protein	50822341	50834315
LOC125659354	peroxidase-like protein isoform X1	50835239	50868965
LOC125659132	peroxisome biogenesis factor 1-like	57041696	57080057
LOC125658682	peroxisome proliferator-activated receptor gamma coactivator 1-alpha-like	47721624	47741270
LOC125658782	phosphatidylinositol 3%2C4%2C5-trisphosphate 3-phosphatase TPTE2-like isoform X1	65992516	66028133
LOC125657846	phosphatidylinositol 3%2C4%2C5-trisphosphate 5-phosphatase 2A-like isoform X3	48533162	48587314
LOC125658418	phospholipase DDHD2-like	45190158	45205777
LOC125659316	phospholipid scramblase 2-like	43789491	43802642
LOC125658383	poly [ADP-ribose] polymerase tankyrase-1-like	44564639	44588797
LOC125657933	poly(U)-binding-splicing factor PUF60-like isoform X1	41705629	41725932
LOC125657794	polycomb group RING finger protein 3-like	44498050	44511515
LOC125660363	polysialic acid O-acetyltransferase-like	67982893	67983246
LOC125660244	pre-mRNA-splicing factor ISY1 homolog	48865464	48869834
LOC125658754	probable 28S ribosomal protein S26%2C mitochondrial	67212546	67221064
LOC125660396	probable ATP-dependent DNA helicase RecQ	52785985	52787198
LOC125659218	probable ATP-dependent DNA helicase RecS	52734910	52738222
LOC125659131	probable ATP-dependent RNA helicase DDX56	49556076	49586320
LOC125659015	probable E3 ubiquitin-protein ligase DTX3	50320378	50327640
LOC125658819	probable E3 ubiquitin-protein ligase HECTD2 isoform X1	46412611	46450654
LOC125658567	probable glutamate receptor	41122782	41140913
LOC125659295	probable hydrolase PNKD	37643403	37657754
LOC125659329	probable tRNA(His) guanylyltransferase isoform X1	53552412	53571871
LOC125659128	probable Werner syndrome ATP-dependent helicase homolog 1	54905280	54907634
LOC125658047	programmed cell death protein 4-like	55122027	55130523
LOC125660303	prominin-1-A-like	57247715	57263107
LOC125659402	protease-associated domain-containing protein 1-like	41826936	41835795
LOC125659869	protein DPCD-like isoform X1	54586535	54598865
LOC125659470	protein draper-like isoform X2	35819662	36099039
LOC125659278	protein FAM124A-like isoform X2	61997041	62015339
LOC125658219	protein FAM193A-like isoform X1	55306398	55332860
LOC125658829	protein FAM53A-like	36816383	36841722
LOC125658779	protein farnesyltransferase/geranylgeranyltransferase type-1 subunit alpha-like	65880903	65893132
LOC125659369	protein fem-1 homolog C-like	48114366	48121359
LOC125658686	protein FRA10AC1 homolog	47689083	47706065
LOC125658766	protein glass-like	56028755	56036052
LOC125659461	protein mono-ADP-ribosyltransferase PARP14-like isoform X4	36492252	36545492
LOC125657889	protein neuralized-like isoform X2	48793329	48829751
LOC125659410	protein N-lysine methyltransferase METTL21D-like	57483425	57496620
LOC125660389	protein PBDC1-like	55068989	55085090
LOC125660468	protein PF3D7_1417600-like isoform X1	44419900	44453186
LOC125658125	protein phosphatase 1 regulatory subunit 3B-like isoform X3	46817914	46842719
LOC125659280	protein phosphatase 1L-like	66988024	66997356
LOC125659999	protein RFT1 homolog isoform X1	47553148	47575553
LOC125658789	protein RRP5 homolog	42909544	42950613
LOC125659726	protein shisa-5-like	42656606	42665392
LOC125660008	protein SSUH2 homolog	57701537	57718634
LOC125660345	protein toll-like	64913765	64917416
LOC125658225	protein unc-13 homolog C-like	39504147	39505266
LOC125659326	protein unc-93 homolog A-like	53657317	53673852
LOC125658723	protein wech-like	39561545	39564556
LOC125659396	protein Wnt-11b-2-like isoform X1	64453289	64500195
LOC125658870	pseudouridylate synthase 1 homolog isoform X1	45869029	45904478
LOC125657598	puromycin-sensitive aminopeptidase-like isoform X2	63635304	63676476
LOC125657836	putative ankyrin repeat protein RF_0381	56567235	56580005
LOC125659340	putative defense protein 2 isoform X2	41691681	41699741
LOC125659144	putative DENN domain-containing protein 10 B	64193012	64207324
LOC125659530	putative lipoyltransferase 2%2C mitochondrial	57675264	57679758

LOC125659451	putative nuclease HARBI1	44070308	44073246
LOC125660343	putative nuclease HARBI1	64862854	64863585
LOC125658509	putative pre-mRNA-splicing factor ATP-dependent RNA helicase PRP1	49590128	49607318
LOC125659612	putative transferase CAF17 homolog%2C mitochondrial	47979876	47987635
LOC125657837	putative tRNA (cytidine(32)/guanosine(34)-2'-O)-methyltransferase	56596469	56597682
LOC125657605	pyrin-like	63663923	63667717
LOC125658409	pyruvate kinase-like	45146378	45174075
LOC125658006	ras-related protein Rab-24-like isoform X1	46348676	46399320
LOC125658733	ras-related protein Rap-2c-like	39572131	39581805
LOC125660175	RE1-silencing transcription factor B-like	37544992	37545726
LOC125657834	regulator of nonsense transcripts 3B-like	56337983	56348794
LOC125658070	renin receptor-like	62701808	62719416
LOC125659200	renin receptor-like	66179314	66206376
LOC125659371	retinol dehydrogenase 11-like	48381616	48389751
LOC125660013	retinol dehydrogenase 11-like	48520479	48528751
LOC125657814	rho-related BTB domain-containing protein 1-like	60225179	60272032
LOC125657618	ribonuclease H2 subunit B-like	63790411	63831933
LOC125657612	ribonuclease P protein subunit p38-like	63775553	63790373
LOC125657824	RING finger protein 24-like isoform X2	60186024	60201904
LOC125657586	RING finger protein 37-like	66645741	66651367
LOC125659254	RING-box protein 2-like	59878754	59885689
LOC125658035	RNA/RNP complex-1-interacting phosphatase-like	46497018	46512851
LOC125659011	RNA/RNP complex-1-interacting phosphatase-like	48358722	48377791
LOC125658466	run domain Beclin-1-interacting and cysteine-rich domain-containing protein-like isoform X1	61303131	61332451
LOC125660168	RYamide receptor-like	37045134	37046326
LOC125659453	ryncolin-4-like	44154132	44164351
LOC125660182	sarcoplasmic calcium-binding protein-like	38553201	38556900
LOC125657960	sarcoplasmic calcium-binding protein-like	62865457	62881519
LOC125660220	SCO-spondin-like	44763321	44810474
LOC125659377	sepiapterin reductase-like	42840624	42847832
LOC125657589	serine protease HTRA2%2C mitochondrial-like isoform X4	66636326	66645678
LOC125659199	serine/threonine-protein kinase 26-like	66088532	66099215
LOC125659197	serine/threonine-protein kinase 26-like isoform X7	66102897	66141582
LOC125658024	serine/threonine-protein kinase 26-like isoform X8	62756117	62794970
LOC125659951	serine/threonine-protein kinase 32B-like isoform X2	53269966	53301873
LOC125659314	serine/threonine-protein kinase PAK 3-like isoform X1	43809497	43833631
LOC125660357	serine-enriched protein-like	67427401	67430638
LOC125660237	serine-rich adhesin for platelets-like	47997138	48000996
LOC125660296	serine-rich adhesin for platelets-like	56621012	56660371
LOC125657916	sex peptide receptor-like	63032206	63033540
LOC125657831	SH3 and PX domain-containing protein 2A-like isoform X2	56353358	56383677
LOC125659309	SH3 domain-binding protein 2-like	50303679	50319858
LOC125659644	SH3 domain-binding protein 2-like	53226303	53263268
LOC125660232	shematrin-like protein 2	46404910	46406529
LOC125657911	short stature homeobox protein 2-like	54260427	54279556
LOC125657658	short-chain collagen C4-like	57995658	58003754
LOC125657668	short-chain collagen C4-like	58144257	58151298
LOC125657669	short-chain collagen C4-like	58214857	58218063
LOC125657652	short-chain collagen C4-like	58239420	58244265
LOC125658318	sialin-like	44543847	44559990
LOC125658319	sialin-like isoform X2	44523949	44536555
LOC125658859	sideroflexin-5-like	47235336	47257346
LOC125658876	signal recognition particle subunit SRP72-like	41176162	41195520
LOC125658000	slit homolog 1 protein-like isoform X1	62554615	62635927
LOC125657657	slit homolog 2 protein-like	58441798	58459715
LOC125659185	small nuclear ribonucleoprotein G-like	52184039	52190730
LOC125658683	sodium- and chloride-dependent GABA transporter 2-like isoform X1	47748740	47768705
LOC125659264	sodium-coupled monocarboxylate transporter 1-like isoform X1	42671525	42691656
LOC125657689	sodium-dependent multivitamin transporter-like isoform X2	51549610	51565968
LOC125660457	solute carrier family 22 member 4-like	64800008	64809376
LOC125658801	solute carrier family 22 member 4-like	65607451	65636644
LOC125658802	solute carrier family 22 member 4-like	65644866	65662261
LOC125658840	solute carrier family 23 member 1-like	57771371	57805010

LOC125659356	solute carrier family 23 member 2-like isoform X1	50577937	50600798
LOC125659328	solute carrier family 49 member A3-like isoform X2	53572924	53589914
LOC125660465	soma ferritin-like	41284628	41291077
LOC125659372	spermatogenesis-associated protein 24-like	62520325	62540378
LOC125660021	sphingolipid delta(4)-desaturase DES1-like isoform X2	61607461	61614164
LOC125660235	spore coat protein G-like	47714106	47715267
LOC125659808	spore coat protein SP96-like	49913757	49961962
LOC125659378	stAR-related lipid transfer protein 7%2C mitochondrial-like	66615477	66629424
LOC125657550	STE20-like serine/threonine-protein kinase isoform X3	44665024	44711348
LOC125658356	steroid 17-alpha-hydroxylase/17%2C20 lyase-like	38362089	38399352
LOC125658354	steroid 17-alpha-hydroxylase/17%2C20 lyase-like	38430862	38442584
LOC125660181	steroid 17-alpha-hydroxylase/17%2C20 lyase-like	38474085	38476481
LOC125658352	steroid 17-alpha-hydroxylase/17%2C20 lyase-like	38504731	38525533
LOC125658355	steroid 17-alpha-hydroxylase/17%2C20 lyase-like	38528495	38550396
LOC125658353	steroid 17-alpha-hydroxylase/17%2C20 lyase-like isoform X1	38484730	38502709
LOC125658971	stimulator of interferon genes protein-like	59340648	59388631
LOC125659133	stimulator of interferon genes protein-like isoform X1	56868607	56908315
LOC125659007	structural maintenance of chromosomes protein 3-like isoform X1	48166457	48226155
LOC125660197	sulfotransferase 2B1-like	41985646	41988128
LOC125658874	suppressor of fused homolog isoform X1	37363649	37383402
LOC125660001	swi5-dependent recombination DNA repair protein 1 homolog isoform X1	47500821	47513086
LOC125659259	synaptic vesicular amine transporter-like	64108452	64156438
LOC125658897	synaptobrevin homolog YKT6-like	36765683	36780116
LOC125660176	syntaxin-18-like	37574968	37579240
LOC125660179	syntaxin-18-like	38265391	38314415
LOC125658722	TATA box-binding protein-associated factor RNA polymerase I subunit B-like	39656266	39680853
LOC125658792	TBC1 domain family member 12-like	37173139	37199050
LOC125657705	T-cell leukemia homeobox protein 3-like	51192366	51204910
LOC125659998	T-complex protein 1 subunit eta-like	47575726	47605293
LOC125658701	telomeric repeat-binding factor 2-interacting protein 1-like isoform X1	42614300	42651983
LOC125659361	terepressin/terephysin-like	50807750	50819599
LOC125657702	testicular haploid expressed gene protein-like isoform X1	51642535	51660679
LOC125658732	testis-expressed protein 36-like isoform X1	39601072	39611951
LOC125659478	tetraspanin-33-like	35682897	35692233
LOC125659253	tetraspanin-33-like	42273357	42299982
LOC125659477	tetraspanin-33-like isoform X2	35717386	35756004
LOC125659147	tetraspanin-7-like	38943409	38953640
LOC125658998	thialysine N-epsilon-acetyltransferase-like isoform X3	44359834	44364189
LOC125659004	thioredoxin reductase-like selenoprotein T	46131899	46141471
LOC125659245	THO complex subunit 3-like	66841286	66857924
LOC125657913	thrombospondin-2-like	54140348	54168637
LOC125659205	thymidylate kinase-like	66039078	66075223
LOC125657874	TM2 domain-containing protein 2-like	53849530	53857142
LOC125658510	TNFAIP3-interacting protein 2-like	67553657	67563989
LOC125658608	toll-like receptor 13	37556468	37558601
LOC125659847	toll-like receptor 13	37569824	37573329
LOC125659471	toll-like receptor 2	36381736	36382947
LOC125659464	toll-like receptor 8	36321146	36411005
LOC125658072	trans-1%2C2-dihydrobenzene-1%2C2-diol dehydrogenase-like isoform X1	44588875	44641497
LOC125658950	transcription factor AP-2-epsilon-like	48143582	48146666
LOC125658050	transcription factor Dp-1-like	59903742	59941323
LOC125657708	transcription factor LBX1b-like	51180359	51182689
LOC125658039	transcription factor LBX2-like	54483562	54485787
LOC125659137	transcription factor Sox-14-like	56949353	56951340
LOC125659146	transcription factor Sox-2-like	49123494	49125505
LOC125658304	transcription initiation factor TFIID subunit 9B-like	64734174	64746825
LOC125659135	transcriptional coactivator YAP1-A-like isoform X1	57090403	57107850
LOC125657953	transforming acidic coiled-coil-containing protein 2-like isoform X3	66559415	66606389
LOC125659418	transforming growth factor beta regulator 1-like isoform X1	51673930	51688519
LOC125658536	transient receptor potential cation channel subfamily M member-like 2 isoform X1	62902635	62956950
LOC125659648	translationally-controlled tumor protein homolog	53193449	53207360
LOC125658407	transmembrane anterior posterior transformation protein 1 homolog	45175500	45190128

DE SANTIAGO DE COMPOSTELA

LOC125658345	transmembrane emp24 domain-containing protein eca-like isoform X1	49614637	49629030
LOC125659718	transmembrane protein 254-like	61412666	61423442
LOC125658976	transmembrane protein 256 homolog	59647656	59659103
LOC125658975	transmembrane protein 256 homolog	59675335	59681124
LOC125658898	trimethyllysine dioxygenase%2C mitochondrial-like	49210984	49230422
LOC125659919	tripartite motif-containing protein 2-like	61816180	61817607
LOC125659920	tripartite motif-containing protein 2-like	61822781	61824411
LOC125659941	tripartite motif-containing protein 2-like isoform X4	53894785	53902231
LOC125659353	tripeptidyl-peptidase 2-like	50617901	50666579
LOC125657850	TSC22 domain family protein 1-like isoform X1	61355437	61404826
LOC125657931	tubulin beta chain	38230265	38232610
LOC125658178	tubulin beta chain-like isoform X2	58956713	58962196
LOC125659502	tumor necrosis factor ligand superfamily member 10-like	42025257	42031563
LOC125659170	type VI secretion system spike protein VgrG1b-like	50488740	50493387
LOC125659902	tyramine receptor tyra-2-like isoform X2	55408272	55419252
LOC125658053	tyrosine-protein kinase HTK16-like	46142573	46175965
LOC125658799	tyrosine-protein kinase receptor torso-like	65479220	65553884
LOC125660410	tyrosine-protein kinase SRK2-like isoform X2	60672097	60690912
LOC125658992	U2 small nuclear ribonucleoprotein auxiliary factor 35 kDa subunit-related protein 2-like	44194412	44203120
LOC125658734	U4/U6.U5 small nuclear ribonucleoprotein 27 kDa protein-like	39635150	39642067
LOC125657764	U5 small nuclear ribonucleoprotein 200 kDa helicase-like	63171227	63233997
LOC125659842	U6 snRNA-associated Sm-like protein LSm1	35083914	35091141
LOC125658719	ubiquitin domain-containing protein 2-like isoform X2	63007491	63015332
LOC125659010	ubiquitin thioesterase zranb1-B-like	48249539	48264452
LOC125659806	ubiquitin-like domain-containing CTD phosphatase 1 isoform X1	49827790	49867214
LOC125659495	uncharacterized protein 5-like	44920969	44927513
LOC125659541	uncharacterized protein C5orf34 homolog isoform X1	48773394	48793196
LOC125658685	uncharacterized protein C6orf163 homolog	47717234	47726738
LOC125657584	uncharacterized protein DDB_G0290685-like	58886930	58893010
LOC125660148	uncharacterized protein K02A2.6-like	34112205	34114883
LOC125660151	uncharacterized protein K02A2.6-like	34217288	34221235
LOC125659639	uncharacterized protein K02A2.6-like	37047338	37052020
LOC125660239	uncharacterized protein K02A2.6-like	48421509	48425250
LOC125660304	uncharacterized protein K02A2.6-like	57574337	57579408
LOC125660329	uncharacterized protein K02A2.6-like	61809497	61815043
LOC125660360	uncharacterized protein K02A2.6-like	67754509	67758603
LOC125659724	uncharacterized protein K02A2.6-like	68181538	68188737
LOC125657484	uncharacterized protein LOC125657484	58868028	58870948
LOC125657503	uncharacterized protein LOC125657503 isoform X2	49452382	49472359
LOC125657512	uncharacterized protein LOC125657512	50452196	50455128
LOC125657533	uncharacterized protein LOC125657533	52475714	52481505
LOC125657535	uncharacterized protein LOC125657535	52518445	52523066
LOC125657536	uncharacterized protein LOC125657536	52633927	52635748
LOC125657538	uncharacterized protein LOC125657538	52433546	52436344
LOC125657551	uncharacterized protein LOC125657551	44713799	44717305
LOC125657594	uncharacterized protein LOC125657594	57374031	57375523
LOC125657606	uncharacterized protein LOC125657606 isoform X2	63716299	63718287
LOC125657608	uncharacterized protein LOC125657608	63452191	63461339
LOC125657611	uncharacterized protein LOC125657611	63885140	63887775
LOC125657619	uncharacterized protein LOC125657619	63359021	63360931
LOC125657620	uncharacterized protein LOC125657620 isoform X2	63754096	63763417
LOC125657623	uncharacterized protein LOC125657623	63922212	63923393
LOC125657624	uncharacterized protein LOC125657624	63365729	63373793
LOC125657625	uncharacterized protein LOC125657625	63478155	63482529
LOC125657628	uncharacterized protein LOC125657628	63361045	63361679
LOC125657629	uncharacterized protein LOC125657629	63815348	63817367
LOC125657635	uncharacterized protein LOC125657635	41674547	41676695
LOC125657645	uncharacterized protein LOC125657645	58635198	58637311
LOC125657646	uncharacterized protein LOC125657646	58624798	58626964
LOC125657647	uncharacterized protein LOC125657647 isoform X2	58711097	58718913
LOC125657648	uncharacterized protein LOC125657648	58547581	58552659
LOC125657649	uncharacterized protein LOC125657649 isoform X2	58390041	58715702
LOC125657650	uncharacterized protein LOC125657650 isoform X2	57868147	57888634

LOC125657653	uncharacterized protein LOC125657653	58604190	58609690
LOC125657654	uncharacterized protein LOC125657654 isoform X2	58435605	58443688
LOC125657655	uncharacterized protein LOC125657655 isoform X2	58169072	58174339
LOC125657659	uncharacterized protein LOC125657659	57945431	57949464
LOC125657660	uncharacterized protein LOC125657660	58103495	58108858
LOC125657661	uncharacterized protein LOC125657661	58694105	58697785
LOC125657662	uncharacterized protein LOC125657662	58593176	58598119
LOC125657663	uncharacterized protein LOC125657663	58532994	58534771
LOC125657665	uncharacterized protein LOC125657665	58766811	58768522
LOC125657666	uncharacterized protein LOC125657666	58524060	58527278
LOC125657667	uncharacterized protein LOC125657667	58222694	58409702
LOC125657683	uncharacterized protein LOC125657683	62130635	62136713
LOC125657686	uncharacterized protein LOC125657686 isoform X1	50911979	51033869
LOC125657690	uncharacterized protein LOC125657690 isoform X1	51617243	51633075
LOC125657693	uncharacterized protein LOC125657693	51604591	51610475
LOC125657694	uncharacterized protein LOC125657694	51573586	51600591
LOC125657699	uncharacterized protein LOC125657699	51634190	51669551
LOC125657700	uncharacterized protein LOC125657700 isoform X4	51156647	51162845
LOC125657703	uncharacterized protein LOC125657703	51040321	51051822
LOC125657704	uncharacterized protein LOC125657704 isoform X1	50874256	50891589
LOC125657706	uncharacterized protein LOC125657706	51267994	51290937
LOC125657709	uncharacterized protein LOC125657709 isoform X2	51402147	51406257
LOC125657720	uncharacterized protein LOC125657720	61494227	61495562
LOC125657728	uncharacterized protein LOC125657728 isoform X4	43639699	43676404
LOC125657746	uncharacterized protein LOC125657746	37664933	37667059
LOC125657747	uncharacterized protein LOC125657747	37667455	37679374
LOC125657781	uncharacterized protein LOC125657781	46863942	46927642
LOC125657789	uncharacterized protein LOC125657789	63312229	63317155
LOC125657795	uncharacterized protein LOC125657795	44477369	44485517
LOC125657799	uncharacterized protein LOC125657799 isoform X1	50153045	50228983
LOC125657805	uncharacterized protein LOC125657805 isoform X1	60871702	60875137
LOC125657806	uncharacterized protein LOC125657806	60872527	60873417
LOC125657813	uncharacterized protein LOC125657813	60065387	60068344
LOC125657819	uncharacterized protein LOC125657819	60283341	60286440
LOC125657820	uncharacterized protein LOC125657820 isoform X1	60283229	60313305
LOC125657822	uncharacterized protein LOC125657822	60132183	60133933
LOC125657823	uncharacterized protein LOC125657823	60392798	60396893
LOC125657838	uncharacterized protein LOC125657838 isoform X2	56522735	56575047
LOC125657839	uncharacterized protein LOC125657839 isoform X1	56412085	56413693
LOC125657840	uncharacterized protein LOC125657840 isoform X2	56465329	56519606
LOC125657841	uncharacterized protein LOC125657841	56415559	56416746
LOC125657853	uncharacterized protein LOC125657853 isoform X3	54434007	54464916
LOC125657854	uncharacterized protein LOC125657854	54465052	54469998
LOC125657864	uncharacterized protein LOC125657864 isoform X4	46941402	46988755
LOC125657865	uncharacterized protein LOC125657865 isoform X2	46957861	46963890
LOC125657866	uncharacterized protein LOC125657866	46954624	46957857
LOC125657904	uncharacterized protein LOC125657904	53910598	53920339
LOC125657905	uncharacterized protein LOC125657905 isoform X1	53965094	53974283
LOC125657907	uncharacterized protein LOC125657907	53957990	53963210
LOC125657908	uncharacterized protein LOC125657908	53922540	53930167
LOC125657909	uncharacterized protein LOC125657909	54284620	54308688
LOC125657912	uncharacterized protein LOC125657912	53991699	54031944
LOC125657924	uncharacterized protein LOC125657924	38834637	38838361
LOC125657927	uncharacterized protein LOC125657927	59786632	59858298
LOC125657935	uncharacterized protein LOC125657935 isoform X1	57500544	57518181
LOC125657945	uncharacterized protein LOC125657945 isoform X2	45822699	45853905
LOC125657961	uncharacterized protein LOC125657961	48504660	48516731
LOC125657963	uncharacterized protein LOC125657963	48400205	48442238
LOC125657968	uncharacterized protein LOC125657968	55682738	55706662
LOC125657969	uncharacterized protein LOC125657969 isoform X1	55659415	55665399
LOC125658037	uncharacterized protein LOC125658037	46645008	46654190
LOC125658046	uncharacterized protein LOC125658046 isoform X1	55129969	55151254
LOC125658055	uncharacterized protein LOC125658055 isoform X2	53443092	53461054
LOC125658076	uncharacterized protein LOC125658076	57297129	57305502

LOC125658077	uncharacterized protein LOC125658077	57275362	57289939
LOC125658130	uncharacterized protein LOC125658130	50553375	50569811
LOC125658155	uncharacterized protein LOC125658155 isoform X1	33926921	33946331
LOC125658157	uncharacterized protein LOC125658157	34157279	34159945
LOC125658161	uncharacterized protein LOC125658161	34154455	34157162
LOC125658162	uncharacterized protein LOC125658162	34470263	34483173
LOC125658165	uncharacterized protein LOC125658165 isoform X1	34445777	34457736
LOC125658166	uncharacterized protein LOC125658166	34258459	34272878
LOC125658170	uncharacterized protein LOC125658170	34221577	34248252
LOC125658177	uncharacterized protein LOC125658177	58953867	58956474
LOC125658179	uncharacterized protein LOC125658179	62483066	62498830
LOC125658220	uncharacterized protein LOC125658220	42457022	42510032
LOC125658221	uncharacterized protein LOC125658221	42465486	42467306
LOC125658226	uncharacterized protein LOC125658226	39484446	39488595
LOC125658250	uncharacterized protein LOC125658250 isoform X4	39982588	39995233
LOC125658254	uncharacterized protein LOC125658254	39980150	39981958
LOC125658257	uncharacterized protein LOC125658257	52989434	52995086
LOC125658258	uncharacterized protein LOC125658258	52979827	52997949
LOC125658340	uncharacterized protein LOC125658340 isoform X3	34601847	34604502
LOC125658348	uncharacterized protein LOC125658348	38363952	38382723
LOC125658349	uncharacterized protein LOC125658349	38760874	38763340
LOC125658358	uncharacterized protein LOC125658358	38352186	38357942
LOC125658359	uncharacterized protein LOC125658359	38736647	38745238
LOC125658360	uncharacterized protein LOC125658360	38559715	38569342
LOC125658362	uncharacterized protein LOC125658362	38446621	38447556
LOC125658363	uncharacterized protein LOC125658363	38447108	38468816
LOC125658375	uncharacterized protein LOC125658375	35113437	35183849
LOC125658416	uncharacterized protein LOC125658416	45205299	45209311
LOC125658417	uncharacterized protein LOC125658417	45117058	45137563
LOC125658420	uncharacterized protein LOC125658420	45487584	45493903
LOC125658428	uncharacterized protein LOC125658428	67472104	67517258
LOC125658435	uncharacterized protein LOC125658435 isoform X2	42527567	42535592
LOC125658463	uncharacterized protein LOC125658463	51669763	51672699
LOC125658494	uncharacterized protein LOC125658494	38127104	38128777
LOC125658496	uncharacterized protein LOC125658496	37899536	37905487
LOC125658497	uncharacterized protein LOC125658497	37865885	37867275
LOC125658498	uncharacterized protein LOC125658498	38083776	38096001
LOC125658528	uncharacterized protein LOC125658528	66549979	66552204
LOC125658564	uncharacterized protein LOC125658564	44990731	44995875
LOC125658606	uncharacterized protein LOC125658606	51889593	51920745
LOC125658624	uncharacterized protein LOC125658624	62083487	62091198
LOC125658680	uncharacterized protein LOC125658680	61706978	61715089
LOC125658681	uncharacterized protein LOC125658681 isoform X3	47616048	47713600
LOC125658687	uncharacterized protein LOC125658687 isoform X4	47884265	47964861
LOC125658688	uncharacterized protein LOC125658688 isoform X1	47890113	47897254
LOC125658689	uncharacterized protein LOC125658689	47837933	47843873
LOC125658690	uncharacterized protein LOC125658690	47780950	47812973
LOC125658705	uncharacterized protein LOC125658705	68071406	68075687
LOC125658706	uncharacterized protein LOC125658706 isoform X1	68011807	68083866
LOC125658708	uncharacterized protein LOC125658708 isoform X10	67732938	67750140
LOC125658709	uncharacterized protein LOC125658709	67935580	67956112
LOC125658711	uncharacterized protein LOC125658711	67837090	67840301
LOC125658713	uncharacterized protein LOC125658713	67993250	68004445
LOC125658720	uncharacterized protein LOC125658720	39620144	39625450
LOC125658721	uncharacterized protein LOC125658721	39685419	39712491
LOC125658725	uncharacterized protein LOC125658725 isoform X1	39785276	39801624
LOC125658726	uncharacterized protein LOC125658726	39631316	39635005
LOC125658729	uncharacterized protein LOC125658729 isoform X1	39718064	39723163
LOC125658735	uncharacterized protein LOC125658735	39746382	39774337
LOC125658753	uncharacterized protein LOC125658753	67178947	67205499
LOC125658755	uncharacterized protein LOC125658755	67237351	67244159
LOC125658760	uncharacterized protein LOC125658760	59105947	59111316
LOC125658790	uncharacterized protein LOC125658790	37079643	37100149
LOC125658800	uncharacterized protein LOC125658800	65671229	65684260

LOC125658803	uncharacterized protein LOC125658803 isoform X2	65084855	65089446
LOC125658805	uncharacterized protein LOC125658805	65070555	65074957
LOC125658807	uncharacterized protein LOC125658807	65577974	65596457
LOC125658808	uncharacterized protein LOC125658808	65223957	65224949
LOC125658810	uncharacterized protein LOC125658810	65207542	65210201
LOC125658824	uncharacterized protein LOC125658824	61083437	61086454
LOC125658825	uncharacterized protein LOC125658825	44912090	44916464
LOC125658827	uncharacterized protein LOC125658827	61759000	61778947
LOC125658828	uncharacterized protein LOC125658828	61779413	61780112
LOC125658830	uncharacterized protein LOC125658830	57687494	57691153
LOC125658835	uncharacterized protein LOC125658835 isoform X3	61542483	61552851
LOC125658856	uncharacterized protein LOC125658856	47193811	47197549
LOC125658857	uncharacterized protein LOC125658857	47077317	47081057
LOC125658861	uncharacterized protein LOC125658861	47197759	47200205
LOC125658864	uncharacterized protein LOC125658864 isoform X1	47092076	47224108
LOC125658869	uncharacterized protein LOC125658869	37437873	37454958
LOC125658875	uncharacterized protein LOC125658875	41173102	41176046
LOC125658880	uncharacterized protein LOC125658880	62357153	62359970
LOC125658883	uncharacterized protein LOC125658883	61288334	61289406
LOC125658886	uncharacterized protein LOC125658886	39080751	39083663
LOC125658890	uncharacterized protein LOC125658890 isoform X4	42699545	42717415
LOC125658891	uncharacterized protein LOC125658891 isoform X2	53812316	53844267
LOC125658951	uncharacterized protein LOC125658951	44719486	44722426
LOC125658956	uncharacterized protein LOC125658956	38763686	38766372
LOC125658961	uncharacterized protein LOC125658961 isoform X3	59681184	59753942
LOC125658965	uncharacterized protein LOC125658965	59525598	59538102
LOC125658966	uncharacterized protein LOC125658966	59506922	59509940
LOC125658969	uncharacterized protein LOC125658969	59611051	59638171
LOC125658970	uncharacterized protein LOC125658970	59394808	59396306
LOC125658972	uncharacterized protein LOC125658972	59249414	59253395
LOC125658974	uncharacterized protein LOC125658974	59397664	59400336
LOC125658985	uncharacterized protein LOC125658985 isoform X1	45644268	45647228
LOC125658987	uncharacterized protein LOC125658987	61725866	61735279
LOC125659002	uncharacterized protein LOC125659002	37457382	37467199
LOC125659018	uncharacterized protein LOC125659018	57221898	57225989
LOC125659069	uncharacterized protein LOC125659069	44768801	44771547
LOC125659070	uncharacterized protein LOC125659070	52862030	52866332
LOC125659086	uncharacterized protein LOC125659086	62813880	62817319
LOC125659087	uncharacterized protein LOC125659087	62818622	62822464
LOC125659091	uncharacterized protein LOC125659091 isoform X1	61007706	61013689
LOC125659093	uncharacterized protein LOC125659093	43163075	43180110
LOC125659129	uncharacterized protein LOC125659129	57458294	57483195
LOC125659134	uncharacterized protein LOC125659134	57121462	57158365
LOC125659164	uncharacterized protein LOC125659164	56132649	56176936
LOC125659165	uncharacterized protein LOC125659165	56156342	56158298
LOC125659166	uncharacterized protein LOC125659166	57360616	57362142
LOC125659167	uncharacterized protein LOC125659167 isoform X1	45809982	45813191
LOC125659168	uncharacterized protein LOC125659168	57207823	57211410
LOC125659181	uncharacterized protein LOC125659181	52267338	52268970
LOC125659182	uncharacterized protein LOC125659182	52315046	52317655
LOC125659183	uncharacterized protein LOC125659183	52040829	52046813
LOC125659184	uncharacterized protein LOC125659184	52287887	52292314
LOC125659203	uncharacterized protein LOC125659203 isoform X1	66166951	66175696
LOC125659217	uncharacterized protein LOC125659217	61283093	61284188
LOC125659219	uncharacterized protein LOC125659219 isoform X4	52726364	52730186
LOC125659220	uncharacterized protein LOC125659220	41658650	41661106
LOC125659224	uncharacterized protein LOC125659224	39001465	39010498
LOC125659248	uncharacterized protein LOC125659248	54359412	54360758
LOC125659260	uncharacterized protein LOC125659260	64118382	64119420
LOC125659262	uncharacterized protein LOC125659262	65865324	65875094
LOC125659276	uncharacterized protein LOC125659276	54926963	54930093
LOC125659307	uncharacterized protein LOC125659307 isoform X1	44892695	44906239
LOC125659310	uncharacterized protein LOC125659310	41735322	41755287
LOC125659312	uncharacterized protein LOC125659312 isoform X1	43835368	43883296

LOC125659313	uncharacterized protein LOC125659313	43770457	43773331
LOC125659317	uncharacterized protein LOC125659317	43749365	43755838
LOC125659323	uncharacterized protein LOC125659323	35073729	35083694
LOC125659335	uncharacterized protein LOC125659335 isoform X1	64255800	64280541
LOC125659338	uncharacterized protein LOC125659338 isoform X1	50346468	50354682
LOC125659359	uncharacterized protein LOC125659359	50762927	50765847
LOC125659368	uncharacterized protein LOC125659368	67461741	67465595
LOC125659405	uncharacterized protein LOC125659405	36558654	36561138
LOC125659406	uncharacterized protein LOC125659406	36552079	36555031
LOC125659409	uncharacterized protein LOC125659409	57496026	57498771
LOC125659413	uncharacterized protein LOC125659413	35244298	35246442
LOC125659417	uncharacterized protein LOC125659417 isoform X3	51766472	51819918
LOC125659454	uncharacterized protein LOC125659454	44052975	44056079
LOC125659455	uncharacterized protein LOC125659455	44072215	44077445
LOC125659456	uncharacterized protein LOC125659456 isoform X5	67009441	67026011
LOC125659459	uncharacterized protein LOC125659459	57352815	57355169
LOC125659472	uncharacterized protein LOC125659472 isoform X3	36190756	36220455
LOC125659473	uncharacterized protein LOC125659473	36383021	36384112
LOC125659474	uncharacterized protein LOC125659474 isoform X1	35765045	35779191
LOC125659480	uncharacterized protein LOC125659480	35937438	36026703
LOC125659482	uncharacterized protein LOC125659482	36139370	36140964
LOC125659503	uncharacterized protein LOC125659503	41994113	42004880
LOC125659505	uncharacterized protein LOC125659505	42003221	42004728
LOC125659506	uncharacterized protein LOC125659506	42164423	42195805
LOC125659514	uncharacterized protein LOC125659514	39037449	39060350
LOC125659518	uncharacterized protein LOC125659518	64548288	64561972
LOC125659520	uncharacterized protein LOC125659520	64587729	64600345
LOC125659523	uncharacterized protein LOC125659523	64517576	64520117
LOC125659524	uncharacterized protein LOC125659524	64541598	64543600
LOC125659539	uncharacterized protein LOC125659539 isoform X2	68616860	68660267
LOC125659546	uncharacterized protein LOC125659546 isoform X2	43469713	43515691
LOC125659548	uncharacterized protein LOC125659548	43519256	43537562
LOC125659549	uncharacterized protein LOC125659549	43444396	43461773
LOC125659555	uncharacterized protein LOC125659555 isoform X1	39317669	39323045
LOC125659556	uncharacterized protein LOC125659556	39205137	39207386
LOC125659557	uncharacterized protein LOC125659557 isoform X2	39327311	39374458
LOC125659589	uncharacterized protein LOC125659589	50508948	50511831
LOC125659601	uncharacterized protein LOC125659601	46251391	46268217
LOC125659619	uncharacterized protein LOC125659619	57345938	57351751
LOC125659643	uncharacterized protein LOC125659643 isoform X2	53134627	53156022
LOC125659646	uncharacterized protein LOC125659646 isoform X3	53210061	53221692
LOC125659658	uncharacterized protein LOC125659658 isoform X2	37588981	37596235
LOC125659664	uncharacterized protein LOC125659664	64086134	64090722
LOC125659672	uncharacterized protein LOC125659672	68324246	68345842
LOC125659673	uncharacterized protein LOC125659673 isoform X1	68464887	68496888
LOC125659688	uncharacterized protein LOC125659688	39071189	39075904
LOC125659690	uncharacterized protein LOC125659690	42881618	42884656
LOC125659692	uncharacterized protein LOC125659692	62388653	62391548
LOC125659716	uncharacterized protein LOC125659716	59192402	59221012
LOC125659720	uncharacterized protein LOC125659720	62375155	62377881
LOC125659744	uncharacterized protein LOC125659744	60758011	60760953
LOC125659809	uncharacterized protein LOC125659809	50000986	50002851
LOC125659810	uncharacterized protein LOC125659810	49967627	49970859
LOC125659843	uncharacterized protein LOC125659843	62440677	62465286
LOC125659853	uncharacterized protein LOC125659853	48684547	48692722
LOC125659854	uncharacterized protein LOC125659854	48619379	48620976
LOC125659859	uncharacterized protein LOC125659859	40002317	40008053
LOC125659867	uncharacterized protein LOC125659867	54723014	54725311
LOC125659901	uncharacterized protein LOC125659901	55450465	55470495
LOC125659906	uncharacterized protein LOC125659906	41962398	41977154
LOC125659908	uncharacterized protein LOC125659908	68227609	68260475
LOC125659912	uncharacterized protein LOC125659912 isoform X1	35237608	35242156
LOC125659917	uncharacterized protein LOC125659917	61914307	61938329
LOC125659918	uncharacterized protein LOC125659918	61946579	61949308

LOC125659921	uncharacterized protein LOC125659921 isoform X2	61905407	61910895
LOC125659927	uncharacterized protein LOC125659927	53117200	53131539
LOC125659930	uncharacterized protein LOC125659930	62723115	62732335
LOC125659934	uncharacterized protein LOC125659934	56729717	56738001
LOC125659938	uncharacterized protein LOC125659938	53786939	53804653
LOC125659940	uncharacterized protein LOC125659940	54350878	54352296
LOC125659948	uncharacterized protein LOC125659948 isoform X1	53357593	53381797
LOC125659964	uncharacterized protein LOC125659964	60982056	60982794
LOC125659966	uncharacterized protein LOC125659966	48390687	48393644
LOC125659994	uncharacterized protein LOC125659994	55796464	55799625
LOC125659995	uncharacterized protein LOC125659995 isoform X1	57842607	57850538
LOC125660007	uncharacterized protein LOC125660007	50356745	50365176
LOC125660015	uncharacterized protein LOC125660015	57580577	57598158
LOC125660146	uncharacterized protein LOC125660146	34046031	34077025
LOC125660147	uncharacterized protein LOC125660147	34093037	34094305
LOC125660153	uncharacterized protein LOC125660153	34919227	34921793
LOC125660154	uncharacterized protein LOC125660154	34986178	35041485
LOC125660155	uncharacterized protein LOC125660155	35044797	35046861
LOC125660156	uncharacterized protein LOC125660156	35058334	35068981
LOC125660157	uncharacterized protein LOC125660157	36140922	36143503
LOC125660159	uncharacterized protein LOC125660159	36169037	36172275
LOC125660160	uncharacterized protein LOC125660160	36235880	36238991
LOC125660163	uncharacterized protein LOC125660163	36590617	36630239
LOC125660164	uncharacterized protein LOC125660164	36759958	36761190
LOC125660166	uncharacterized protein LOC125660166	37029931	37030611
LOC125660170	uncharacterized protein LOC125660170	37200133	37202336
LOC125660171	uncharacterized protein LOC125660171	37202450	37203098
LOC125660172	uncharacterized protein LOC125660172	37422894	37423511
LOC125660178	uncharacterized protein LOC125660178	37863330	37865876
LOC125660180	uncharacterized protein LOC125660180	38382719	38385119
LOC125660186	uncharacterized protein LOC125660186	39297529	39298491
LOC125660187	uncharacterized protein LOC125660187	40020376	40038601
LOC125660189	uncharacterized protein LOC125660189	40301541	40302107
LOC125660191	uncharacterized protein LOC125660191	40957491	40958249
LOC125660192	uncharacterized protein LOC125660192	41146029	41147931
LOC125660193	uncharacterized protein LOC125660193	41400551	41402602
LOC125660194	uncharacterized protein LOC125660194	41612009	41613813
LOC125660195	uncharacterized protein LOC125660195	41684213	41688396
LOC125660198	uncharacterized protein LOC125660198	42206560	42224929
LOC125660200	uncharacterized protein LOC125660200	42557254	42560328
LOC125660201	uncharacterized protein LOC125660201	42668343	42669629
LOC125660202	uncharacterized protein LOC125660202	42767763	42804803
LOC125660203	uncharacterized protein LOC125660203	42805761	42811411
LOC125660204	uncharacterized protein LOC125660204	42828753	42830076
LOC125660205	uncharacterized protein LOC125660205	42889610	42890536
LOC125660206	uncharacterized protein LOC125660206	43320425	43326471
LOC125660207	uncharacterized protein LOC125660207	43974765	43975535
LOC125660209	uncharacterized protein LOC125660209	44219920	44223506
LOC125660211	uncharacterized protein LOC125660211	44364269	44377405
LOC125660222	uncharacterized protein LOC125660222	45695945	45699179
LOC125660223	uncharacterized protein LOC125660223	45707618	45711934
LOC125660224	uncharacterized protein LOC125660224	45796296	45797066
LOC125660225	uncharacterized protein LOC125660225	45797964	45799604
LOC125660226	uncharacterized protein LOC125660226	45801103	45809584
LOC125660227	uncharacterized protein LOC125660227	45909639	45911018
LOC125660233	uncharacterized protein LOC125660233	46530814	46533127
LOC125660234	uncharacterized protein LOC125660234	46601090	46645049
LOC125660240	uncharacterized protein LOC125660240	48518982	48519329
LOC125660242	uncharacterized protein LOC125660242	48737443	48741461
LOC125660243	uncharacterized protein LOC125660243	48833587	48836164
LOC125660246	uncharacterized protein LOC125660246	48921448	48923076
LOC125660249	uncharacterized protein LOC125660249	50014206	50049645
LOC125660251	uncharacterized protein LOC125660251	50096597	50097841
LOC125660252	uncharacterized protein LOC125660252	50332241	50333008

LOC125660254	uncharacterized protein LOC125660254	50901700	50911301
LOC125660258	uncharacterized protein LOC125660258	51505343	51508306
LOC125660259	uncharacterized protein LOC125660259	51514368	51519258
LOC125660265	uncharacterized protein LOC125660265	52342602	52348673
LOC125660269	uncharacterized protein LOC125660269	52545660	52550465
LOC125660270	uncharacterized protein LOC125660270	52556746	52562850
LOC125660273	uncharacterized protein LOC125660273	52665826	52667932
LOC125660276	uncharacterized protein LOC125660276	52729304	52734762
LOC125660280	uncharacterized protein LOC125660280	53651689	53652498
LOC125660282	uncharacterized protein LOC125660282	54188147	54241986
LOC125660285	uncharacterized protein LOC125660285	54698213	54703794
LOC125660288	uncharacterized protein LOC125660288	54982460	54994205
LOC125660289	uncharacterized protein LOC125660289	55056126	55114428
LOC125660290	uncharacterized protein LOC125660290	55174193	55203638
LOC125660294	uncharacterized protein LOC125660294	56328789	56331489
LOC125660295	uncharacterized protein LOC125660295	56416746	56420300
LOC125660297	uncharacterized protein LOC125660297	56662769	56671827
LOC125660305	uncharacterized protein LOC125660305	57861168	57865483
LOC125660306	uncharacterized protein LOC125660306	57903168	57910642
LOC125660311	uncharacterized protein LOC125660311	58199708	58208131
LOC125660312	uncharacterized protein LOC125660312	58343804	58347981
LOC125660316	uncharacterized protein LOC125660316	58774963	58796254
LOC125660321	uncharacterized protein LOC125660321	60336343	60340411
LOC125660323	uncharacterized protein LOC125660323	60980073	60981904
LOC125660325	uncharacterized protein LOC125660325	61556497	61563087
LOC125660327	uncharacterized protein LOC125660327	61795984	61799368
LOC125660328	uncharacterized protein LOC125660328	61804742	61806722
LOC125660331	uncharacterized protein LOC125660331	62165635	62166468
LOC125660333	uncharacterized protein LOC125660333	63035988	63038954
LOC125660334	uncharacterized protein LOC125660334	63109125	63114523
LOC125660337	uncharacterized protein LOC125660337	64034122	64077784
LOC125660338	uncharacterized protein LOC125660338	64312707	64315894
LOC125660342	uncharacterized protein LOC125660342	64795752	64796486
LOC125660347	uncharacterized protein LOC125660347	65152290	65153756
LOC125660348	uncharacterized protein LOC125660348	65187159	65189975
LOC125660349	uncharacterized protein LOC125660349	65229483	65231459
LOC125660354	uncharacterized protein LOC125660354	66673119	66675308
LOC125660355	uncharacterized protein LOC125660355	66764276	66787567
LOC125660356	uncharacterized protein LOC125660356	67307466	67333065
LOC125660361	uncharacterized protein LOC125660361	67819818	67831338
LOC125660364	uncharacterized protein LOC125660364	68167018	68170437
LOC125660376	uncharacterized protein LOC125660376	54963116	54979650
LOC125660411	uncharacterized protein LOC125660411 isoform X2	60723195	60738263
LOC125660413	uncharacterized protein LOC125660413	60698729	60746228
LOC125660456	uncharacterized protein LOC125660456	46479905	46485514
LOC125660461	uncharacterized protein LOC125660461	41245299	41283098
LOC125660467	uncharacterized protein LOC125660467	44382072	44407639
LOC125660470	uncharacterized protein LOC125660470	44457102	44463933
LOC125660498	uncharacterized protein LOC125660498 isoform X4	42314598	42378115
LOC125659393	UPF0687 protein C20orf27 homolog	45991317	46000695
LOC125657821	uracil-DNA glycosylase-like isoform X2	60161914	60186410
LOC125657765	uroporphyrinogen-III synthase-like	63149890	63171065
LOC125659263	UV-stimulated scaffold protein A-like	55155545	55168819
LOC125658785	vacuolar protein sorting-associated protein 4-like	46041561	46050138
LOC125659500	very long-chain specific acyl-CoA dehydrogenase%2C mitochondrial-like	42058918	42076674
LOC125658962	WD repeat-containing protein 44-like isoform X2	59542637	59574796
LOC125660165	WD repeat-containing protein 53-like	36894078	36895638
LOC125657790	WD repeat-containing protein 54-like	63258521	63275462
LOC125658314	X-ray radiation resistance-associated protein 1-like	57747766	57762292
LOC125659430	xylulose kinase-like isoform X2	66467073	66510728
LOC125659870	zinc finger HIT domain-containing protein 1-like	54570485	54580381
LOC125660274	zinc finger MYM-type protein 1-like	52689875	52691077
LOC125659852	zinc finger protein 227-like	48624077	48632490
LOC125660167	zinc finger protein 407-like	37030790	37031428

LOC125659611	zinc finger protein 93-like	61430003	61431868
LOC125658492	zinc finger protein Gfi-1b-like	37846461	37851733
LOC125658967	zinc finger protein OZF-like	59441251	59456017
LOC125660284	zinc finger protein Pegasus-like	54612574	54613236
LOC125659100	zinc finger Y-chromosomal protein 2-like	50537639	50540139
LOC125658034	zinc metalloproteinase nas-36-like	46548741	46577684
LOC125657730	zinc transporter ZIP13-like	43668866	43693212
LOC125659876	zwei Ig domain protein zig-4-like	55867691	55870733

USC
UNIVERSIDADE DE SANTIAGO DE COMPOSTELA

Table S3A: GO enrichment terms associated with genes annotated at C2

ontology	node_id	node_name	raw_p_overrep	FDR
biological_process	GO:0007218	neuropeptide signaling pathway	3.76E-06	0.002
biological_process	GO:0009581	detection of external stimulus	2.76E-05	0.024
biological_process	GO:0009582	detection of abiotic stimulus	2.76E-05	0.024
biological_process	GO:0042058	regulation of epidermal growth factor receptor signaling pathway	4.07E-05	0.032
biological_process	GO:1901184	regulation of ERBB signaling pathway	4.07E-05	0.032
biological_process	GO:0051606	detection of stimulus	5.69E-05	0.045
cellular_component	GO:0030992	intraciliary transport particle B	2.83E-08	0
cellular_component	GO:0043226	organelle	3.91E-07	0
cellular_component	GO:0043227	membrane-bounded organelle	6.06E-07	0
cellular_component	GO:0043229	intracellular organelle	2.29E-06	0
cellular_component	GO:0030990	intraciliary transport particle	2.36E-06	0
cellular_component	GO:0005622	intracellular anatomical structure	5.67E-05	0.008
cellular_component	GO:0043231	intracellular membrane-bounded organelle	6.53E-05	0.016
cellular_component	GO:0000786	nucleosome	9.24E-05	0.024
molecular_function	GO:0008188	neuropeptide receptor activity	1.07E-09	0
molecular_function	GO:0046920	alpha-(1->3)-fucosyltransferase activity	1.81E-08	0
molecular_function	GO:0043139	5'-3' DNA helicase activity	3.59E-08	0
molecular_function	GO:0004806	triglyceride lipase activity	1.42E-06	0.001
molecular_function	GO:0004983	neuropeptide Y receptor activity	5.10E-06	0.001
molecular_function	GO:0008528	G protein-coupled peptide receptor activity	6.96E-06	0.002
molecular_function	GO:0003723	RNA binding	3.41E-05	0.01
molecular_function	GO:0030527	structural constituent of chromatin	5.12E-05	0.014
molecular_function	GO:0004341	gluconolactonase activity	5.21E-05	0.023
molecular_function	GO:0001653	peptide receptor activity	5.33E-05	0.023
molecular_function	GO:0004252	serine-type endopeptidase activity	6.03E-05	0.024
molecular_function	GO:0001216	DNA-binding transcription activator activity	6.59E-05	0.03
molecular_function	GO:0008236	serine-type peptidase activity	8.72E-05	0.033
molecular_function	GO:0032451	demethylase activity	0.000108677	0.036
molecular_function	GO:0140098	catalytic activity, acting on RNA	0.000129417	0.041
molecular_function	GO:0045505	dynein intermediate chain binding	0.000139362	0.042
molecular_function	GO:0000339	RNA cap binding	0.000158023	0.045
molecular_function	GO:0004568	chitinase activity	0.000158023	0.045

Table S3B: GO enrichment terms associated with genes annotated at C5

ontology	node_id	node_name	raw_p_overre	FDR
molecular_function	GO:0005385	zinc ion transmembrane transporter activity	0.000114374	0.03
biological_process	GO:0071577	zinc ion transmembrane transport	0.000100286	0.061

Table S3C: GO enrichment terms associated with genes annotated at C8

ontology	node_id	node_name	raw_p_overrep	FDR
biological_process	GO:0015718	monocarboxylic acid transport	4.45E-06	0.001
biological_process	GO:0071880	adenylate cyclase-activating adrenergic receptor signaling pathway	4.64E-05	0.035
cellular_component	GO:0005581	collagen trimer	0.000151108	0.043
molecular_function	GO:0008028	monocarboxylic acid transmembrane transporter activity	5.47E-07	0
molecular_function	GO:0004340	glucokinase activity	2.75E-06	0.003
molecular_function	GO:0004396	hexokinase activity	2.75E-06	0.003
molecular_function	GO:0005536	glucose binding	2.75E-06	0.003
molecular_function	GO:0008865	fructokinase activity	2.75E-06	0.003
molecular_function	GO:0005164	tumor necrosis factor receptor binding	4.29E-06	0.004
molecular_function	GO:0032813	tumor necrosis factor receptor superfamily binding	8.19E-06	0.006
molecular_function	GO:0005126	cytokine receptor binding	2.52E-05	0.009

Table S4: Frequencies of chromosome arrangements at C2, C5 and C8 inversions

	Crom_2		
Pop	**arrangements**		**Count**
	"green"	"red"	
BER	0.3	0.7	60
GVR	0.548	0.452	42
OS	0.5	0.5	56
LR	0.844	0.156	32
LW	0.766	0.234	64
TB	0.594	0.406	32
GAL	0.784	0.216	74
QUI	0.633	0.367	30
OR	0.75	0.25	32
NO	0.788	0.212	66
PON	0.803	0.197	66
ALI	0.933	0.067	60
MS	0.957	0.043	70
average	0.708	0.292	

USC UNIVERSIDADE DE SANTIAGO DE COMPOSTELA

Crom_5			
Pop	**arrangements**		**Count**
	"pink"	"dark blue"	
BER	0.267	0.733	60
GVR	0.143	0.857	42
OS	0.268	0.732	56
LR	0.469	0.531	32
LW	0.297	0.703	64
TB	0.375	0.625	32
GAL	0.23	0.77	74
QUI	0.6	0.4	30
OR	0.531	0.469	32
NO	0.485	0.515	66
PON	0.667	0.333	66
ALI	0.95	0.05	60
MS	1	0	70
average	0.483	0.517	

Crom_8			
Pop	**arrangements**		**Count**
	"blue"	"orange"	
BER	0.917	0.083	60
GVR	0.857	0.143	42
OS	0.821	0.179	56
LR	0.844	0.156	32
LW	0.734	0.266	64
TB	0.562	0.438	32
GAL	0.554	0.446	74
QUI	0.367	0.633	30
OR	0.25	0.75	32
NO	0.197	0.803	66
PON	0.348	0.652	66
ALI	0.05	0.95	60
MS	0.1	0.9	70
average	0.508	0.492	

USC UNIVERSIDADE DE SANTIAGO DE COMPOSTELA

Table S5: HWE exact tests for chromosome arrangements at C2, C5 and C8 inversions

C2		
	Fis	
POP	**P-val**	**W&C**
BER	0.2178	-0.2541
GVR	1	-0.0329
OS	0.7062	-0.125
LR	1	-0.1538
LW	0.1528	-0.2917
TB	0.2909	0.3802
GAL	0.657	0.0568
QUI	0.5785	-0.26
OR	0.1995	0.3617
NO	0.6079	0.1086
PON	1	-0.0383
ALI	1	-0.0545
MS	1	-0.0303
overall/average	0.9331	-0.0256

C5		
	Fis	
POP	**P-val**	**W&C**
BER	1	-0.0058
GVR	1	-0.1429
OS	1	0.0166
LR	1	-0.0976
LW	0.6842	-0.1071
TB	1	-0.0345
GAL	0.1566	-0.2857
QUI	0.5985	0.2
OR	0.3123	-0.3525
NO	0.307	-0.1985
PON	0.4282	0.1967
ALI	1	-0.0357
MS	-	-0.0706
overall/average	0.5086	-0.0706

C8		
	Fis	
POP	**P-val**	**W&C**
BER	1	-0.0741
GVR	0.3374	0.2453
OS	1	0.0442
LR	1	-0.1538
LW	1	-0.0254
TB	0.1204	-0.5
GAL	0.3191	0.1928
QUI	0.2943	0.3137
OR	0.5122	-0.3043
NO	1	-0.0383
PON	0.0511	-0.3884
ALI	1	-0.0357
MS	1	-0.0968
overall/average	0.859816	-0.0632

USC UNIVERSIDADE DE SANTIAGO DE COMPOSTELA

Table S6. Pairwise Fst for chromosome arrangements at C2, C5 and C8 inversions

Crom_2

pop	BER	GVR	OS	LR	LW	TB	GAL	QUI	OR	NO	PON	ALI
GVR	0.1044											
OS	0.0671	-0.0148										
LR	0.4371	0.1601	0.2053									
LW	0.3506	0.0883	0.1308	0.0009								
TB	0.1434	-0.0281	-0.0086	0.1103	0.047							
GAL	0.3757	0.1068	0.152	-0.0115	-0.0122	0.0619						
QUI	0.1888	-0.0103	0.0143	0.0863	0.0256	-0.0327	0.0358					
OR	0.3187	0.0557	0.0984	-0.0095	-0.0217	0.0115	-0.0232	-0.0018				
NO	0.3792	0.109	0.1544	-0.0145	-0.0127	0.0634	-0.0157	0.0375	-0.0243			
PON	0.4009	0.1283	0.174	-0.0164	-0.0087	0.0817	-0.0136	0.0538	-0.0178	-0.0153		
ALI	0.5903	0.3365	0.3708	0.0236	0.0916	0.2964	0.0698	0.2601	0.1119	0.067	0.0558	
MS	0.6403	0.4037	0.4302	0.0659	0.1363	0.3716	0.1102	0.3357	0.1754	0.1088	0.0954	-0.0094

Crom_5

pop	BER	GVR	OS	LR	LW	TB	GAL	QUI	OR	NO	PON	ALI
GVR	0.0255											
OS	-0.0177	0.0257										
LR	0.0658	0.2115	0.0636									
LW	-0.0131	0.0471	-0.014	0.0424								
TB	0.0039	0.1138	0.0023	-0.0116	-0.0078							
GAL	-0.0092	0.0095	-0.0096	0.1104	-0.0001	0.0343						
QUI	0.1876	0.3596	0.1846	0.0003	0.1533	0.0638	0.245					
OR	0.1228	0.2843	0.1203	-0.0169	0.0932	0.0236	0.1738	-0.0205				
NO	0.0832	0.2137	0.0812	-0.0192	0.0593	0.0044	0.1239	0.004	-0.0134			
PON	0.2634	0.4155	0.2608	0.0544	0.2283	0.1363	0.3155	-0.0199	0.0153	0.0512		
ALI	0.6519	0.8026	0.6552	0.4854	0.6144	0.5861	0.6819	0.3363	0.4174	0.4057	0.2095	
MS	0.7448	0.8872	0.7506	0.637	0.7087	0.7211	0.763	0.5137	0.5788	0.5169	0.3282	0.0396

USC UNIVERSIDADE DE SANTIAGO DE COMPOSTELA

Crom_8

pop	BER	GVR	OS	LR	LW	TB	GAL	QUI	OR	NO	PON	ALI
GVR	-0.004											
OS	0.0226	-0.0192										
LR	0.006	-0.0295	-0.0228									
LW	0.0936	0.0231	0.0048	0.0115								
TB	0.306	0.18	0.1387	0.1567	0.0476							
GAL	0.2655	0.1668	0.1337	0.1439	0.0527	-0.0224						
QUI	0.5282	0.395	0.3507	0.3634	0.2262	0.0469	0.0402					
OR	0.6527	0.5384	0.4919	0.5132	0.366	0.1686	0.148	-0.0018				
NO	0.6799	0.5935	0.5531	0.5745	0.4419	0.2505	0.2248	0.0484	-0.012			
PON	0.5042	0.4009	0.3623	0.3758	0.2516	0.0773	0.0692	-0.02	0.0075	0.0453		
ALI	0.8562	0.8016	0.7529	0.8	0.6489	0.523	0.4363	0.2944	0.1567	0.0788	0.2312	
MS	0.7965	0.7321	0.6883	0.7234	0.5835	0.4266	0.3666	0.1906	0.0686	0.0233	0.1561	0.0032

All loci

pop	BER	GVR	OS	LR	LW	TB	GAL	QUI	OR	NO	PON	ALI
GVR	0.0585											
OS	0.0283	-0.0034										
LR	0.2421	0.1398	0.1032									
LW	0.1787	0.0561	0.0485	0.021								
TB	0.1468	0.0831	0.0415	0.0823	0.029							
GAL	0.2414	0.1055	0.1006	0.0933	0.0172	0.0218						
QUI	0.3044	0.2603	0.1889	0.166	0.145	0.0278	0.1138					
OR	0.3905	0.3202	0.2584	0.2218	0.179	0.0716	0.1139	-0.0086				
NO	0.4225	0.3479	0.2973	0.2602	0.208	0.1092	0.1292	0.0277	-0.0162			
PON	0.3932	0.335	0.2719	0.182	0.183	0.1002	0.1511	0.0021	0.0037	0.0318		
ALI	0.7127	0.705	0.6231	0.5994	0.5438	0.4895	0.492	0.2976	0.2649	0.2449	0.1796	
MS	0.7327	0.7297	0.6476	0.6215	0.5679	0.5287	0.5228	0.3414	0.3198	0.2948	0.2027	0.0046

USC UNIVERSIDADE DE SANTIAGO DE COMPOSTELA

Table S7. Genetic diversity (Ho and He) and intrapopulation fixation index in the 13 *O. edulis* populations using different SNP datasets considering the inversions detected at C2, C5 and C8

Whole panel:

Sample	Ho	He	Fis
Bergen	0.385	0.389	0.010
Grevelingen	0.394	0.401	0.016
Oosterschelde	0.406	0.403	-0.007
Loch Ryan	0.402	0.409	0.018
Lough Swilly	0.404	0.400	-0.010
Tralee Bay	0.414	0.417	0.007
Galway	0.397	0.402	0.012
Quiberon	0.411	0.411	0.000
Ortigueira	0.408	0.417	0.022
Noya	0.394	0.394	0.000
Pontevedra	0.401	0.399	-0.003
Alicante	0.377	0.360	-0.047
Mali Stone Bay	0.334	0.334	0.001
average	0.394	0.395	0.001

Without the inversions:

Sample	Ho	He	Fis
Bergen	0.384	0.391	0.018
Grevelingen	0.395	0.402	0.017
Oosterschelde	0.405	0.403	-0.005
Loch Ryan	0.405	0.414	0.022
Lough Swilly	0.403	0.401	-0.005
Tralee Bay	0.411	0.414	0.009
Galway	0.400	0.402	0.007
Quiberon	0.408	0.415	0.016
Ortigueira	0.411	0.414	0.007
Noya	0.399	0.398	-0.001
Pontevedra	0.398	0.400	0.006
Alicante	0.394	0.376	-0.047
Mali Stone Bay	0.347	0.348	0.002
average	0.397	0.398	0.003

Only the inversions:

Sample	Ho	He	Fis
Bergen	0.401	0.363	-0.105
Grevelingen	0.382	0.384	0.005
Oosterschelde	0.421	0.408	-0.033
Loch Ryan	0.376	0.366	-0.029
Lough Swilly	0.417	0.392	-0.062
Tralee Bay	0.452	0.445	-0.016
Galway	0.373	0.400	0.069
Quiberon	0.408	0.378	-0.079
Ortigueira	0.403	0.437	0.076
Noya	0.346	0.352	0.017
Pontevedra	0.428	0.389	-0.099
Alicante	0.207	0.198	-0.046
Mali Stone Bay	0.198	0.196	-0.009
average	0.370	0.362	-0.024

C2:

Sample	Ho	He	Fis
Bergen	0.452	0.378	-0.195
Grevelingen	0.474	0.461	-0.028
Oosterschelde	0.490	0.459	-0.068
Loch Ryan	0.356	0.337	-0.056
Lough Swilly	0.450	0.382	-0.178
Tralee Bay	0.332	0.452	0.265
Galway	0.350	0.369	0.050
Quiberon	0.474	0.457	-0.035
Ortigueira	0.358	0.372	0.039
Noya	0.319	0.350	0.089
Pontevedra	0.366	0.360	-0.019
Alicante	0.237	0.226	-0.050
Mali Stone Bay	0.172	0.180	0.045
average	0.372	0.368	-0.011

USC UNIVERSIDADE DE SANTIAGO DE COMPOSTELA

C5:

Sample	Ho	He	Fis
Bergen	0.392	0.388	-0.011
Grevelingen	0.304	0.282	-0.078
Oosterschelde	0.393	0.395	0.004
Loch Ryan	0.519	0.483	-0.075
Lough Swilly	0.430	0.440	0.022
Tralee Bay	0.520	0.448	-0.160
Galway	0.409	0.378	-0.082
Quiberon	0.389	0.487	0.200
Ortigueira	0.625	0.468	-0.336
Noya	0.508	0.470	-0.080
Pontevedra	0.395	0.426	0.074
Alicante	0.141	0.140	-0.008
Mali Stone Bay	0.097	0.104	0.068
average	0.394	0.377	-0.036

C8:

Sample	Ho	He	Fis
Bergen	0.335	0.328	-0.024
Grevelingen	0.301	0.339	0.112
Oosterschelde	0.342	0.344	0.005
Loch Ryan	0.355	0.351	-0.012
Lough Swilly	0.402	0.389	-0.033
Tralee Bay	0.522	0.441	-0.183
Galway	0.392	0.433	0.095
Quiberon	0.366	0.412	0.112
Ortigueira	0.377	0.355	-0.063
Noya	0.323	0.319	-0.011
Pontevedra	0.490	0.402	-0.219
Alicante	0.201	0.189	-0.064
Mali Stone Bay	0.233	0.227	-0.026
average	0.357	0.348	-0.024

USC
UNIVERSIDADE DE SANTIAGO DE COMPOSTELA

Table S8. Pairwise F_{ST} in the 13 *O edulis* populations using different SNP datasets considering the inversions detected at C2, C5 and C8

Whole panel:

	BER	GVR	OS	LR	LW	TB	GAL	QUI	OR	NO	PON	ALI	MS	correlation
BER														
GVR	0.018													
OS	0.018	0.000												
LR	0.051	0.027	0.028											
LW	0.058	0.033	0.035	0.024										
TB	0.056	0.033	0.033	0.016	0.024									
GAL	0.062	0.035	0.038	0.026	0.008	0.023								
QUI	0.071	0.048	0.046	0.036	0.046	0.027	0.038							
OR	0.059	0.037	0.034	0.025	0.040	0.014	0.032	0.010						
NO	0.073	0.050	0.049	0.050	0.031	0.042	0.022	0.018	0.025					
PON	0.074	0.053	0.051	0.043	0.027	0.038	0.020	0.018	0.026	0.001				
ALI	0.117	0.099	0.094	0.094	0.078	0.088	0.068	0.047	0.064	0.028	0.026			
MS	0.149	0.136	0.130	0.126	0.112	0.126	0.103	0.079	0.097	0.059	0.055	0.022		0.050

Without inversions:

	BER	GVR	OS	LR	LW	TB	GAL	QUI	OR	NO	PON	ALI	MS	correlation
BER														
GVR	0.016													
OS	0.017	0.000												
LR	0.036	0.021	0.022											
LW	0.048	0.030	0.032	0.024										
TB	0.050	0.032	0.032	0.012	0.023									
GAL	0.051	0.032	0.034	0.023	0.007	0.023								
QUI	0.051	0.031	0.030	0.012	0.033	0.013	0.027							
OR	0.053	0.036	0.036	0.019	0.035	0.021	0.032	0.009						
NO	0.054	0.039	0.039	0.032	0.018	0.035	0.015	0.023	0.019					
PON	0.056	0.041	0.041	0.032	0.019	0.034	0.015	0.025	0.019	0.000				
ALI	0.079	0.069	0.068	0.061	0.048	0.064	0.045	0.052	0.042	0.021	0.019			
MS	0.112	0.106	0.104	0.098	0.088	0.105	0.084	0.086	0.074	0.053	0.050	0.022		0.0399

Only inversions:

	BER	GVR	OS	LR	LW	TB	GAL	QUI	OR	NO	PON	ALI	MS	correlation
BER														
GVR	0.047													
OS	0.027	-0.003												
LR	0.216	0.100	0.098											
LW	0.175	0.069	0.072	0.023										
TB	0.124	0.047	0.039	0.052	0.035									
GAL	0.197	0.078	0.086	0.056	0.014	0.019								
QUI	0.267	0.180	0.156	0.193	0.157	0.082	0.097							
OR	0.155	0.108	0.075	0.143	0.110	0.023	0.071	0.013						
NO	0.275	0.180	0.162	0.213	0.152	0.110	0.089	0.008	0.043					
PON	0.268	0.192	0.165	0.141	0.104	0.077	0.071	0.018	0.028	0.017				
ALI	0.481	0.424	0.378	0.410	0.346	0.324	0.289	0.121	0.205	0.113	0.108			
MS	0.513	0.459	0.412	0.399	0.340	0.336	0.293	0.154	0.227	0.136	0.115	0.025		0.158

C2:

	BER	GVR	OS	LR	LW	TB	GAL	QUI	OR	NO	PON	ALI	MS	
BER														
GVR	0.08													
OS	0.05	-0.011												
LR	0.36	0.117	0.158											
LW	0.29	0.080	0.116	0.021										
TB	0.17	-0.001	0.028	0.030	0.025									
GAL	0.31	0.090	0.128	0.009	-0.006	0.025								
QUI	0.13	-0.009	0.009	0.073	0.051	-0.023	0.056							
OR	0.3	0.075	0.117	-0.009	0.016	0.003	0.004	0.035						
NO	0.33	0.104	0.144	0.011	0.001	0.040	-0.005	0.071	0.003					
PON	0.31	0.091	0.131	0.014	-0.002	0.031	-0.006	0.060	0.002	-0.010				
ALI	0.48	0.242	0.283	0.054	0.069	0.157	0.054	0.209	0.069	0.038	0.048			
MS	0.53	0.306	0.342	0.110	0.120	0.223	0.105	0.276	0.132	0.089	0.094	0.017		0.106

C5:

	BER	GVR	OS	LR	LW	TB	GAL	QUI	OR	NO	PON	ALI	MS	
BER														
GVR	0.017													
OS	-0.012	0.017												
LR	0.068	0.176	0.056											
LW	0.009	0.072	0.007	0.022										
TB	0.003	0.075	-0.002	0.006	- 0.010									
GAL	0.010	0.035	0.005	0.078	0.008	0.010								
QUI	0.117	0.245	0.108	- 0.018	0.054	0.035	0.129	-						
OR	0.136	0.267	0.126	- 0.002	0.070	0.057	0.150	- 0.025						
NO	0.084	0.185	0.077	- 0.002	0.023	0.020	0.082	- 0.005	0.004					
PON	0.238	0.365	0.229	0.057	0.150	0.145	0.243	0.010	0.010	0.047				
ALI	0.579	0.717	0.576	0.406	0.487	0.527	0.580	0.325	0.315	0.352	0.169			
MS	0.625	0.759	0.623	0.473	0.537	0.589	0.625	0.395	0.382	0.404	0.223	0.028		0.189

C8:

	BER	GVR	OS	LR	LW	TB	GAL	QUI	OR	NO	PON	ALI	MS	
BER														
GVR	0.001													
OS	0.010	0.000												
LR	0.022	0.015	0.016											
LW	0.064	0.052	0.041	0.025										
TB	0.117	0.106	0.086	0.082	0.054									
GAL	0.107	0.087	0.069	0.079	0.027	0.015								
QUI	0.216	0.189	0.156	0.229	0.160	0.050	0.056							
OR	0.292	0.266	0.235	0.339	0.258	0.138	0.131	0.010						
NO	0.308	0.283	0.249	0.371	0.273	0.188	0.146	0.038	0.014					
PON	0.221	0.200	0.169	0.230	0.147	0.082	0.051	0.006	0.031	0.024				
ALI	0.412	0.395	0.355	0.550	0.432	0.356	0.292	0.160	0.084	0.045	0.132			
MS	0.394	0.376	0.338	0.491	0.378	0.312	0.246	0.131	0.087	0.030	0.099	0.029		0.166

USC UNIVERSIDADE DE SANTIAGO DE COMPOSTELA

SUPPLEMENTARY FIGURES CHAPTER III:

Table S1. Classification of the oyster samples genotyped with the chip. In the IDD column, the color also represents the C8 orientation

IID	Population	Sampling Month	Resistance	Bonamia in gill	Bonamia in heart	Level of infection
GO1.1	Galway	May				
GO1.11	Galway	May	X	X		
GO1.13	Galway	May		X		
GO1.14	Galway	May		X		
GO1.15	Galway	May				
GO1.16	Galway	May				
GO1.17	Galway	May	X			
GO1.19	Galway	May				
GO1.2	Galway	May				
GO1.20	Galway	May				
GO1.21	Galway	May				
GO1.22	Galway	May				
GO1.3	Galway	May				
GO1.31	Galway	May			X	Level 1
GO1.39	Galway	May	X	X		
GO1.4	Galway	May	X			
GO1.44	Galway	May			X	Level 2
GO1.45	Galway	May				
GO1.46	Galway	May				
GO1.47	Galway	May				
GO1.48	Galway	May	X			
GO1.49	Galway	May				
GO1.5	Galway	May		X		
GO1.50	Galway	May				
GO1.51	Galway	May				
GO1.52	Galway	May	X			
GO1.53	Galway	May				
GO1.54	Galway	May	X			
GO1.7	Galway	May	X	X		
GO5_1	Galway	May	X			
GO5_2	Galway	May				
GO5_3	Galway	May	X			
GO5_34	Galway	May			X	Level 2
GO5_35	Galway	May		X	X	Level 1
GO5_4	Galway	May				
GO5_40	Galway	May			X	Level 1
GO5_5	Galway	May				
GO5_53	Galway	May				
GO5_55	Galway	May			X	Level 1
GO5_6	Galway	May				
GO6_1	Galway	July	X			
GO6_2	Galway	July				
GO6_27	Galway	July	X			
GO6_3	Galway	July				
GO6_31	Galway	July	X			
GO6_32	Galway	July				
GO6_33	Galway	July				
GO6_37	Galway	July		X	X	Level 2
GO6_38	Galway	July		X	X	Level 1
GO6_4	Galway	July				
GO6_41	Galway	July				
GO6_42	Galway	July				
GO6_43	Galway	July				
GO6_48	Galway	July				
GO6_50	Galway	July				

GO6_51	Galway	July					
GO6_57	Galway	July				X	Level 1
GO6_58	Galway	July				X	Level 1
GO6_59	Galway	July			X	X	Level 1
GO6_60	Galway	July			X	X	Level 1
GO2.11	Galway	July				X	Level 1
GO2.12	Galway	July				X	Level 2
GO2.18	Galway	July				X	Level 2
GO2.24	Galway	July				X	Level 2
GO2.25	Galway	July			X	X	Level 4
GO2.26	Galway	July				X	Level 2
GO2.27	Galway	July				X	Level 1
GO2.29	Galway	July			X	X	Level 1
GO2.30	Galway	July				X	Level 1
GO2.31	Galway	July				X	Level 2
GO2.32	Galway	July				X	Level 1
GO2.33	Galway	July				X	Level 2
GO2.34	Galway	July				X	Level 1
GO2.36	Galway	July				X	Level 3
GO2.38	Galway	July				X	Level 1
GO2.41	Galway	July				X	Level 2
GO2.42	Galway	July				X	Level 1
GO2.43	Galway	July	X				
GO2.44	Galway	July				X	Level 3
GO2.45	Galway	July				X	Level 2
GO2.47	Galway	July				X	Level 3
GO2.48	Galway	July				X	Level 2
GO2.6	Galway	July				X	Level 2
GO3.1	Galway	August					
GO3.10	Galway	August	X				
GO3.11	Galway	August	X				
GO3.12	Galway	August	X				
GO3.13	Galway	August					
GO3.14	Galway	August	X				
GO3.15	Galway	August					
GO3.16	Galway	August	X				
GO3.17	Galway	August					
GO3.18	Galway	August					
GO3.19	Galway	August					
GO3.2	Galway	August					
GO3.20	Galway	August					
GO3.21	Galway	August					
GO3.22	Galway	August					
GO3.23	Galway	August	X				
GO3.24	Galway	August	X				
GO3.25	Galway	August					
GO3.26	Galway	August					
GO3.3	Galway	August	X				
GO3.31	Galway	August				X	Level 2
GO3.32	Galway	August					
GO3.4	Galway	August	X				
GO3.43	Galway	August				X	Level 2
GO3.45	Galway	August				X	Level 1
GO3.49	Galway	August				X	Level 2
GO3.5	Galway	August					
GO3.6	Galway	August	X				
GO3.7	Galway	August				X	Level 2
GO3.9	Galway	August	X				
GO4.1	Galway	September					
GO4.10	Galway	September	X				
GO4.11	Galway	September	X				
GO4.12	Galway	September					
GO4.13	Galway	September					
GO4.14	Galway	September					

GO4.15	Galway	September	X			
GO4.16	Galway	September				
GO4.17	Galway	September				
GO4.18	Galway	September	X			
GO4.19	Galway	September				
GO4.2	Galway	September				
GO4.20	Galway	September				
GO4.23	Galway	September				
GO4.3	Galway	September				
GO4.4	Galway	September	X			
GO4.5	Galway	September				
GO4.6	Galway	September				
GO4.7	Galway	September	X			
GO4.8	Galway	September				
GO4.9	Galway	September				
LO1.1	Lough Swilly	May				
LO1.10	Lough Swilly	May				
LO1.11	Lough Swilly	May				
LO1.12	Lough Swilly	May	X			
LO1.15	Lough Swilly	May		X	Level 1	
LO1.2	Lough Swilly	May				
LO1.20	Lough Swilly	May		X	Level 3	
LO1.28	Lough Swilly	May		X	Level 2	
LO1.3	Lough Swilly	May	X			
LO1.33	Lough Swilly	May		X	Level 2	
LO1.30	Lough Swilly	May		X	Level 1	
LO1.4	Lough Swilly	May				
LO1.41	Lough Swilly	May				
LO1.42	Lough Swilly	May				
LO1.43	Lough Swilly	May				
LO1.44	Lough Swilly	May				
LO1.45	Lough Swilly	May	X			
LO1.5	Lough Swilly	May		X	Level 1	
LO1.7	Lough Swilly	May	X			
LO1.8	Lough Swilly	May				
LO1.9	Lough Swilly	May				
LO6_1	Lough Swilly	May				
LO6_2	Lough Swilly	May				
LO6_3	Lough Swilly	May				
LO6_4	Lough Swilly	May				
LO6_5	Lough Swilly	May	X			
LO6_6	Lough Swilly	May				
LO2.1	Lough Swilly	June				
LO2.10	Lough Swilly	June				
LO2.11	Lough Swilly	June				
LO2.12	Lough Swilly	June				
LO2.13	Lough Swilly	June				
LO2.14	Lough Swilly	June				
LO2.15	Lough Swilly	June	X			
LO2.16	Lough Swilly	June				
LO2.17	Lough Swilly	June				
LO2.18	Lough Swilly	June				
LO2.19	Lough Swilly	June				
LO2.2	Lough Swilly	June				
LO2.20	Lough Swilly	June				
LO2.21	Lough Swilly	June				
LO2.22	Lough Swilly	June				
LO2.23	Lough Swilly	June				
LO2.24	Lough Swilly	June				
LO2.25	Lough Swilly	June				
LO2.26	Lough Swilly	June				
LO2.27	Lough Swilly	June				
LO2.29	Lough Swilly	June				
LO2.3	Lough Swilly	June				

LO2.37	Lough Swilly	June			X		
LO2.4	Lough Swilly	June					
LO2.48	Lough Swilly	June			X		
LO2.5	Lough Swilly	June					
LO2.52	Lough Swilly	June					
LO2.58	Lough Swilly	June			X		
LO2.6	Lough Swilly	June					
LO2.7	Lough Swilly	June					
LO2.8	Lough Swilly	June					
LO2.9	Lough Swilly	June					
LO7_1	Lough Swilly	June	X				
LO7_2	Lough Swilly	June					
LO7_3	Lough Swilly	June					
LO7_4	Lough Swilly	June				X	Level 1
LO7_5	Lough Swilly	June					
LO7_56	Lough Swilly	June					
LO7_6	Lough Swilly	June					
LO7_7	Lough Swilly	June				X	Level 1
LO7_8	Lough Swilly	June					
LO3.1	Lough Swilly	July					
LO3.10	Lough Swilly	July	X				
LO3.11	Lough Swilly	July					
LO3.12	Lough Swilly	July					
LO3.13	Lough Swilly	July	X				
LO3.14	Lough Swilly	July					
LO3.15	Lough Swilly	July					
LO3.16	Lough Swilly	July					
LO3.17	Lough Swilly	July					
LO3.18	Lough Swilly	July					
LO3.19	Lough Swilly	July				X	Level 1
LO3.2	Lough Swilly	July					
LO3.3	Lough Swilly	July					
LO3.4	Lough Swilly	July					
LO3.5	Lough Swilly	July					
LO3.6	Lough Swilly	July					
LO3.7	Lough Swilly	July			X	X	Level 4
LO3.8	Lough Swilly	July			X	X	Level 4
LO3.9	Lough Swilly	July				X	Level 2
LO4.1	Lough Swilly	August			X	X	Level 2
LO4.10	Lough Swilly	August					
LO4.11	Lough Swilly	August					
LO4.12	Lough Swilly	August					
LO4.13	Lough Swilly	August					
LO4.14	Lough Swilly	August					
LO4.15	Lough Swilly	August	X				
LO4.16	Lough Swilly	August					
LO4.17	Lough Swilly	August					
LO4.18	Lough Swilly	August					
LO4.19	Lough Swilly	August					
LO4.2	Lough Swilly	August					
LO4.20	Lough Swilly	August					
LO4.21	Lough Swilly	August					
LO4.22	Lough Swilly	August	X				
LO4.23	Lough Swilly	August					
LO4.3	Lough Swilly	August			X	X	Level 3
LO4.38	Lough Swilly	August	X				
LO4.4	Lough Swilly	August			X	X	Level 1
LO4.6	Lough Swilly	August					
LO4.7	Lough Swilly	August					
LO4.8	Lough Swilly	August					
LO4.9	Lough Swilly	August					
LO5.1	Lough Swilly	September				X	Level 1
LO5.11	Lough Swilly	September	X				
LO5.12	Lough Swilly	September					

LO5.13	Lough Swilly	September					
LO5.14	Lough Swilly	September			X	Level 2	
LO5.15	Lough Swilly	September					
LO5.16	Lough Swilly	September					
LO5.17	Lough Swilly	September	X				
LO5.18	Lough Swilly	September					
LO5.19	Lough Swilly	September					
LO5.2	Lough Swilly	September					
LO5.20	Lough Swilly	September					
LO5.21	Lough Swilly	September					
LO5.22	Lough Swilly	September					
LO5.23	Lough Swilly	September	X				
LO5.24	Lough Swilly	September					
LO5.25	Lough Swilly	September	X				
LO5.26	Lough Swilly	September					
LO5.27	Lough Swilly	September					
LO5.28	Lough Swilly	September					
LO5.29	Lough Swilly	September					
LO5.3	Lough Swilly	September					
LO5.30	Lough Swilly	September					
LO5.31	Lough Swilly	September					
LO5.32	Lough Swilly	September					
LO5.33	Lough Swilly	September					
LO5.34	Lough Swilly	September			X	Level 2	
LO5.35	Lough Swilly	September					
LO5.4	Lough Swilly	September					
LO5.5	Lough Swilly	September					
LO5.55	Lough Swilly	September			X	Level 2	
LO5.6	Lough Swilly	September	X				
LO5.7	Lough Swilly	September					
LO5.8	Lough Swilly	September					
LO5.9	Lough Swilly	September					
RO1.1	Rossmore	May					
RO1.12	Rossmore	May		X			
RO1.14	Rossmore	May					
RO1.17	Rossmore	May					
RO1.2	Rossmore	May					
RO1.21	Rossmore	May			X	Level 2	
RO1.22	Rossmore	May					
RO1.24	Rossmore	May					
RO1.25	Rossmore	May					
RO1.26	Rossmore	May					
RO1.27	Rossmore	May	X				
RO1.28	Rossmore	May					
RO1.29	Rossmore	May					
RO1.3	Rossmore	May					
RO1.30	Rossmore	May					
RO1.31	Rossmore	May					
RO1.36	Rossmore	May					
RO1.37	Rossmore	May					
RO1.4	Rossmore	May					
RO1.43	Rossmore	May					
RO1.5	Rossmore	May					
RO1.54	Rossmore	May					
RO1.57	Rossmore	May	X				
RO1.6	Rossmore	May	X	X			
RO6_1	Rossmore	May					
RO6_2	Rossmore	May					
RO6_3	Rossmore	May	X				
RO6_4	Rossmore	May					
RO6_5	Rossmore	May					
RO6_6	Rossmore	May			X	Level 2	
RO2.1	Rossmore	June		X			
RO2.10	Rossmore	June		X			

RO2.11	Rossmore	June					
RO2.12	Rossmore	June					
RO2.13	Rossmore	June		X			
RO2.14	Rossmore	June					
RO2.15	Rossmore	June		X			
RO2.16	Rossmore	June		X			
RO2.17	Rossmore	June		X			
RO2.18	Rossmore	June		X			
RO2.19	Rossmore	June	X	X			
RO2.20	Rossmore	June		X			
RO2.21	Rossmore	June		X			
RO2.22	Rossmore	June		X			
RO2.23	Rossmore	June		X			
RO2.24	Rossmore	June		X			
RO2.25	Rossmore	June		X			
RO2.26	Rossmore	June					
RO2.27	Rossmore	June		X			
RO2.28	Rossmore	June		X			
RO2.29	Rossmore	June		X			
RO2.3	Rossmore	June					
RO2.31	Rossmore	June		X			
RO2.32	Rossmore	June					
RO2.33	Rossmore	June		X			
RO2.34	Rossmore	June	X	X			
RO2.35	Rossmore	June		X			
RO2.36	Rossmore	June		X			
RO2.37	Rossmore	June		X			
RO2.38	Rossmore	June	X	X			
RO2.39	Rossmore	June	X	X			
RO2.4	Rossmore	June		X			
RO2.41	Rossmore	June		X			
RO2.42	Rossmore	June		X			
RO2.43	Rossmore	June		X			
RO2.44	Rossmore	June		X			
RO2.45	Rossmore	June		X			
RO2.46	Rossmore	June	X	X			
RO2.47	Rossmore	June					
RO2.48	Rossmore	June		X			
RO2.49	Rossmore	June		X			
RO2.5	Rossmore	June		X			
RO2.50	Rossmore	June					
RO2.51	Rossmore	June	X	X			
RO2.52	Rossmore	June		X			
RO2.53	Rossmore	June		X			
RO2.54	Rossmore	June		X			
RO2.55	Rossmore	June		X			
RO2.56	Rossmore	June		X			
RO2.57	Rossmore	June					
RO2.58	Rossmore	June		X			
RO2.59	Rossmore	June	X	X			
RO2.6	Rossmore	June		X			
RO2.7	Rossmore	June	X	X			
RO2.8	Rossmore	June		X			
RO2.9	Rossmore	June					
RO3.1	Rossmore	July	X				
RO3.15	Rossmore	July		X			
RO3.16	Rossmore	July	X				
RO3.17	Rossmore	July	X				
RO3.18	Rossmore	July	X				
RO3.2	Rossmore	July	X				
RO3.20	Rossmore	July				X	Level 1
RO3.21	Rossmore	July				X	
RO3.22	Rossmore	July					
RO3.23	Rossmore	July				X	Level 1

RO3.24	Rossmore	July			X	Level 1
RO3.27	Rossmore	July			X	Level 1
RO3.29	Rossmore	July			X	Level 2
RO3.3	Rossmore	July	X			
RO3.34	Rossmore	July			X	Level 1
RO3.37	Rossmore	July				
RO3.4	Rossmore	July				
RO3.44	Rossmore	July			X	Level 1
RO3.47	Rossmore	July		X		
RO3.5	Rossmore	July				
RO3.53	Rossmore	July			X	Level 1
RO3.57	Rossmore	July			X	Level 1
RO3.58	Rossmore	July			X	Level 1
RO3.6	Rossmore	July				
RO3.9	Rossmore	July		X		
RO4.1	Rossmore	August				
RO4.10	Rossmore	August	X			
RO4.11	Rossmore	August				
RO4.12	Rossmore	August				
RO4.13	Rossmore	August	X			
RO4.14	Rossmore	August				
RO4.15	Rossmore	August				
RO4.16	Rossmore	August				
RO4.17	Rossmore	August				
RO4.18	Rossmore	August				
RO4.19	Rossmore	August				
RO4.2	Rossmore	August				
RO4.20	Rossmore	August	X			
RO4.3	Rossmore	August				
RO4.4	Rossmore	August				
RO4.5	Rossmore	August	X			
RO4.6	Rossmore	August				
RO4.7	Rossmore	August	X			
RO4.8	Rossmore	August				
RO4.9	Rossmore	August	X			
RO5.1	Rossmore	September				
RO5.10	Rossmore	September				
RO5.11	Rossmore	September				
RO5.12	Rossmore	September				
RO5.13	Rossmore	September				
RO5.14	Rossmore	September				
RO5.15	Rossmore	September				
RO5.16	Rossmore	September				
RO5.17	Rossmore	September				
RO5.18	Rossmore	September				
RO5.19	Rossmore	September	X			
RO5.2	Rossmore	September	X			
RO5.20	Rossmore	September	X			
RO5.21	Rossmore	September				
RO5.22	Rossmore	September	X			
RO5.23	Rossmore	September				
RO5.24	Rossmore	September				
RO5.25	Rossmore	September				
RO5.26	Rossmore	September				
RO5.3	Rossmore	September	X			
RO5.4	Rossmore	September				
RO5.5	Rossmore	September	X			
RO5.6	Rossmore	September				
RO5.7	Rossmore	September				
RO5.8	Rossmore	September				
RO5.9	Rossmore	September				

USC
DE SANTIAGO
DE COMPOSTELA

Table S2. Classification of individuals according to their orientation for each inversion (C8, C2 and C5)

IID	C8 orientation	C2 orientation	C5 orientation
GO1.1	blue	heterokaryon	pink
GO1.11	orange	green	heterokaryon
GO1.13	heterokaryon	red	heterokaryon
GO1.14	heterokaryon	green	pink
GO1.15	heterokaryon	green	heterokaryon
GO1.16	heterokaryon	green	pink
GO1.17	orange	red	pink
GO1.19	heterokaryon	green	pink
GO1.2	heterokaryon	green	pink
GO1.20	heterokaryon	green	pink
GO1.21	heterokaryon	green	pink
GO1.22	heterokaryon	heterokaryon	pink
GO1.3	heterokaryon	heterokaryon	pink
GO1.31	blue	heterokaryon	heterokaryon
GO1.39	orange	green	heterokaryon
GO1.4	orange	heterokaryon	heterokaryon
GO1.44	heterokaryon	green	pink
GO1.45	blue	green	heterokaryon
GO1.46	heterokaryon	green	heterokaryon
GO1.47	heterokaryon	heterokaryon	heterokaryon
GO1.48	orange	green	heterokaryon
GO1.49	blue	heterokaryon	pink
GO1.5	blue	green	heterokaryon
GO1.50	heterokaryon	green	heterokaryon
GO1.51	blue	heterokaryon	pink
GO1.52	orange	green	deep
GO1.53	heterokaryon	green	heterokaryon
GO1.54	orange	green	pink
GO1.7	orange	red	heterokaryon
GO2.11	heterokaryon	green	pink
GO2.12	blue	heterokaryon	pink
GO2.18	heterokaryon	green	deep
GO2.24	heterokaryon	green	heterokaryon
GO2.25	blue	heterokaryon	pink
GO2.26	blue	green	heterokaryon
GO2.27	blue	green	heterokaryon
GO2.29	blue	heterokaryon	heterokaryon
GO2.30	blue	green	pink
GO2.31	blue	green	heterokaryon
GO2.32	blue	green	heterokaryon
GO2.33	blue	green	heterokaryon
GO2.34	heterokaryon	green	pink
GO2.36	heterokaryon	green	deep
GO2.38	blue	red	heterokaryon
GO2.41	blue	green	pink
GO2.42	blue	green	pink
GO2.43	orange	heterokaryon	pink
GO2.44	heterokaryon	green	heterokaryon
GO2.45	blue	green	heterokaryon

USC UNIVERSIDADE DE SANTIAGO DE COMPOSTELA

GO2.47	blue	green	heterokaryon
GO2.48	heterokaryon	green	pink
GO2.6	blue	green	heterokaryon
GO3.1	heterokaryon	green	heterokaryon
GO3.10	orange	green	pink
GO3.11	orange	green	pink
GO3.12	orange	green	heterokaryon
GO3.13	heterokaryon	green	pink
GO3.14	orange	red	heterokaryon
GO3.15	heterokaryon	heterokaryon	pink
GO3.16	orange	green	heterokaryon
GO3.17	blue	red	pink
GO3.18	blue	green	pink
GO3.19	heterokaryon	red	heterokaryon
GO3.2	blue	green	heterokaryon
GO3.20	heterokaryon	green	pink
GO3.21	heterokaryon	heterokaryon	pink
GO3.22	blue	red	pink
GO3.23	orange	heterokaryon	heterokaryon
GO3.24	orange	heterokaryon	pink
GO3.25	blue	green	pink
GO3.26	heterokaryon	heterokaryon	pink
GO3.3	orange	green	pink
GO3.31	blue	green	heterokaryon
GO3.32	heterokaryon	heterokaryon	heterokaryon
GO3.4	orange	heterokaryon	pink
GO3.43	blue	green	heterokaryon
GO3.45	heterokaryon	heterokaryon	heterokaryon
GO3.49	blue	green	heterokaryon
GO3.5	blue	green	heterokaryon
GO3.6	orange	heterokaryon	pink
GO3.7	heterokaryon	green	pink
GO3.9	orange	green	pink
GO4.1	blue	green	pink
GO4.10	orange	heterokaryon	heterokaryon
GO4.11	orange	green	pink
GO4.12	blue	heterokaryon	pink
GO4.13	blue	heterokaryon	pink
GO4.14	heterokaryon	green	pink
GO4.15	orange	green	heterokaryon
GO4.16	blue	green	pink
GO4.17	blue	heterokaryon	pink
GO4.18	orange	green	pink
GO4.19	blue	green	heterokaryon
GO4.2	heterokaryon	green	heterokaryon
GO4.20	heterokaryon	heterokaryon	pink
GO4.23	heterokaryon	green	pink
GO4.3	heterokaryon	red	pink
GO4.4	orange	green	pink
GO4.5	heterokaryon	heterokaryon	heterokaryon
GO4.6	heterokaryon	green	pink

USC UNIVERSIDADE DE SANTIAGO DE COMPOSTELA

GO4.7	orange	green	deep
GO4.8	blue	green	pink
GO4.9	blue	heterokaryon	deep
GO5_1	orange	green	pink
GO5_2	blue	heterokaryon	pink
GO5_3	orange	green	pink
GO5_34	blue	green	pink
GO5_35	heterokaryon	green	heterokaryon
GO5_4	blue	green	pink
GO5_40	heterokaryon	heterokaryon	pink
GO5_5	heterokaryon	heterokaryon	pink
GO5_53	heterokaryon	green	heterokaryon
GO5_55	blue	green	pink
GO5_6	blue	green	heterokaryon
GO6_1	orange	green	pink
GO6_2	heterokaryon	green	pink
GO6_27	orange	heterokaryon	heterokaryon
GO6_3	heterokaryon	green	heterokaryon
GO6_31	orange	green	pink
GO6_32	blue	green	pink
GO6_33	heterokaryon	green	heterokaryon
GO6_37	blue	green	pink
GO6_38	heterokaryon	green	pink
GO6_4	heterokaryon	green	pink
GO6_41	blue	green	heterokaryon
GO6_42	heterokaryon	heterokaryon	heterokaryon
GO6_43	blue	green	heterokaryon
GO6_48	blue	green	pink
GO6_50	heterokaryon	heterokaryon	pink
GO6_51	heterokaryon	green	heterokaryon
GO6_57	heterokaryon	green	heterokaryon
GO6_58	heterokaryon	heterokaryon	pink
GO6_59	heterokaryon	heterokaryon	heterokaryon
GO6_60	heterokaryon	green	pink
LO1.1	heterokaryon	heterokaryon	pink
LO1.10	blue	heterokaryon	heterokaryon
LO1.11	heterokaryon	green	heterokaryon
LO1.12	orange	heterokaryon	pink
LO1.15	heterokaryon	green	pink
LO1.2	blue	heterokaryon	heterokaryon
LO1.20	blue	heterokaryon	pink
LO1.28	blue	heterokaryon	heterokaryon
LO1.3	orange	heterokaryon	heterokaryon
LO1.33	heterokaryon	green	pink
LO1.30	heterokaryon	heterokaryon	pink
LO1.4	blue	green	heterokaryon
LO1.41	heterokaryon	heterokaryon	pink
LO1.42	blue	green	heterokaryon
LO1.43	blue	green	heterokaryon
LO1.44	blue	green	pink
LO1.45	orange	green	pink

USC UNIVERSIDADE DE SANTIAGO DE COMPOSTELA

LO1.5	heterokaryon	heterokaryon	pink
LO1.7	orange	heterokaryon	pink
LO1.8	heterokaryon	green	pink
LO1.9	heterokaryon	heterokaryon	heterokaryon
LO2.1	heterokaryon	green	pink
LO2.10	blue	green	deep
LO2.11	blue	green	heterokaryon
LO2.12	heterokaryon	green	pink
LO2.13	blue	green	deep
LO2.14	blue	heterokaryon	heterokaryon
LO2.15	orange	heterokaryon	heterokaryon
LO2.16	blue	heterokaryon	heterokaryon
LO2.17	heterokaryon	green	pink
LO2.18	blue	heterokaryon	heterokaryon
LO2.19	heterokaryon	heterokaryon	pink
LO2.2	blue	green	pink
LO2.20	heterokaryon	heterokaryon	heterokaryon
LO2.21	heterokaryon	green	pink
LO2.22	blue	heterokaryon	pink
LO2.23	heterokaryon	heterokaryon	pink
LO2.24	blue	green	pink
LO2.25	blue	heterokaryon	pink
LO2.26	heterokaryon	green	heterokaryon
LO2.27	blue	heterokaryon	pink
LO2.29	blue	heterokaryon	heterokaryon
LO2.3	blue	green	pink
LO2.37	blue	heterokaryon	pink
LO2.4	heterokaryon	green	pink
LO2.48	blue	green	pink
LO2.5	heterokaryon	green	pink
LO2.52	blue	green	pink
LO2.58	blue	heterokaryon	pink
LO2.6	blue	heterokaryon	heterokaryon
LO2.7	heterokaryon	heterokaryon	pink
LO2.8	heterokaryon	green	heterokaryon
LO2.9	blue	green	pink
LO3.1	heterokaryon	heterokaryon	pink
LO3.10	orange	heterokaryon	heterokaryon
LO3.11	blue	green	heterokaryon
LO3.12	blue	green	pink
LO3.13	orange	heterokaryon	heterokaryon
LO3.14	heterokaryon	green	heterokaryon
LO3.15	heterokaryon	heterokaryon	pink
LO3.16	heterokaryon	green	pink
LO3.17	heterokaryon	heterokaryon	heterokaryon
LO3.18	blue	green	pink
LO3.19	blue	green	pink
LO3.2	heterokaryon	heterokaryon	pink
LO3.3	blue	green	pink
LO3.4	blue	heterokaryon	pink
LO3.5	heterokaryon	heterokaryon	pink

USC UNIVERSIDADE DE SANTIAGO DE COMPOSTELA

LO3.6	heterokaryon	heterokaryon	heterokaryon
LO3.7	blue	heterokaryon	pink
LO3.8	blue	green	deep
LO3.9	blue	green	pink
LO4.1	blue	green	pink
LO4.10	blue	heterokaryon	heterokaryon
LO4.11	heterokaryon	heterokaryon	deep
LO4.15	heterokaryon	green	pink
LO4.13	blue	heterokaryon	pink
LO4.14	blue	green	pink
LO4.12	orange	green	heterokaryon
LO4.16	heterokaryon	green	heterokaryon
LO4.17	heterokaryon	green	pink
LO4.18	heterokaryon	heterokaryon	heterokaryon
LO4.19	blue	heterokaryon	pink
LO4.2	blue	green	pink
LO4.20	blue	green	heterokaryon
LO4.21	heterokaryon	green	heterokaryon
LO4.22	orange	heterokaryon	heterokaryon
LO4.23	blue	green	heterokaryon
LO4.3	heterokaryon	green	heterokaryon
LO4.38	orange	green	heterokaryon
LO4.4	heterokaryon	heterokaryon	heterokaryon
LO4.6	blue	heterokaryon	deep
LO4.7	blue	green	heterokaryon
LO4.8	heterokaryon	heterokaryon	pink
LO4.9	heterokaryon	heterokaryon	pink
LO5.1	blue	heterokaryon	pink
LO5.11	orange	green	pink
LO5.12	blue	green	heterokaryon
LO5.13	blue	green	heterokaryon
LO5.14	blue	heterokaryon	heterokaryon
LO5.15	heterokaryon	green	heterokaryon
LO5.16	heterokaryon	green	heterokaryon
LO5.17	orange	heterokaryon	heterokaryon
LO5.18	blue	green	pink
LO5.19	blue	heterokaryon	deep
LO5.2	blue	red	heterokaryon
LO5.20	heterokaryon	green	pink
LO5.21	heterokaryon	green	pink
LO5.22	blue	green	pink
LO5.23	orange	green	heterokaryon
LO5.24	heterokaryon	heterokaryon	pink
LO5.25	orange	green	pink
LO5.26	heterokaryon	green	heterokaryon
LO5.27	blue	heterokaryon	heterokaryon
LO5.28	heterokaryon	heterokaryon	heterokaryon
LO5.29	heterokaryon	heterokaryon	heterokaryon
LO5.3	blue	green	heterokaryon
LO5.30	blue	heterokaryon	heterokaryon
LO5.31	blue	green	heterokaryon

USC UNIVERSIDADE DE SANTIAGO DE COMPOSTELA

LO5.32	heterokaryon	heterokaryon	pink
LO5.33	heterokaryon	green	pink
LO5.34	heterokaryon	green	pink
LO5.35	heterokaryon	heterokaryon	deep
LO5.4	blue	heterokaryon	heterokaryon
LO5.5	heterokaryon	red	pink
LO5.55	blue	green	pink
LO5.6	orange	green	heterokaryon
LO5.7	heterokaryon	heterokaryon	deep
LO5.8	heterokaryon	red	deep
LO5.9	heterokaryon	heterokaryon	pink
LO6_1	blue	green	heterokaryon
LO6_2	blue	heterokaryon	pink
LO6_3	blue	green	heterokaryon
LO6_4	heterokaryon	green	pink
LO6_5	orange	green	pink
LO6_6	heterokaryon	red	pink
LO7_1	orange	green	heterokaryon
LO7_2	blue	green	heterokaryon
LO7_3	blue	green	pink
LO7_4	blue	green	deep
LO7_5	heterokaryon	heterokaryon	pink
LO7_56	blue	green	pink
LO7_6	heterokaryon	heterokaryon	deep
LO7_7	heterokaryon	green	heterokaryon
LO7_8	blue	heterokaryon	heterokaryon
RO1.1	heterokaryon	green	heterokaryon
RO1.12	heterokaryon	heterokaryon	heterokaryon
RO1.14	orange	green	heterokaryon
RO1.17	heterokaryon	red	pink
RO1.2	heterokaryon	green	heterokaryon
RO1.21	heterokaryon	heterokaryon	heterokaryon
RO1.22	blue	heterokaryon	heterokaryon
RO1.24	heterokaryon	heterokaryon	heterokaryon
RO1.25	heterokaryon	green	pink
RO1.26	heterokaryon	red	heterokaryon
RO1.27	orange	heterokaryon	heterokaryon
RO1.28	blue	green	pink
RO1.29	heterokaryon	heterokaryon	pink
RO1.3	heterokaryon	red	pink
RO1.30	heterokaryon	green	heterokaryon
RO1.31	blue	green	heterokaryon
RO1.36	heterokaryon	heterokaryon	heterokaryon
RO1.37	blue	green	heterokaryon
RO1.4	heterokaryon	red	pink
RO1.43	blue	green	pink
RO1.5	blue	green	heterokaryon
RO1.54	blue	green	pink
RO1.57	orange	green	heterokaryon
RO1.6	orange	green	heterokaryon
RO2.1	heterokaryon	green	heterokaryon

USC UNIVERSIDADE DE SANTIAGO DE COMPOSTELA

RO2.10	blue	green	deep
RO2.11	blue	heterokaryon	pink
RO2.12	heterokaryon	heterokaryon	heterokaryon
RO2.13	heterokaryon	green	pink
RO2.14	heterokaryon	green	pink
RO2.15	heterokaryon	green	pink
RO2.16	heterokaryon	heterokaryon	heterokaryon
RO2.17	heterokaryon	green	pink
RO2.18	heterokaryon	green	pink
RO2.19	orange	heterokaryon	pink
RO2.20	blue	red	pink
RO2.21	blue	green	heterokaryon
RO2.22	heterokaryon	green	heterokaryon
RO2.23	heterokaryon	heterokaryon	heterokaryon
RO2.24	blue	heterokaryon	pink
RO2.25	heterokaryon	green	heterokaryon
RO2.26	blue	heterokaryon	heterokaryon
RO2.27	blue	green	heterokaryon
RO2.28	heterokaryon	green	pink
RO2.29	heterokaryon	green	pink
RO2.3	heterokaryon	heterokaryon	pink
RO2.31	heterokaryon	heterokaryon	heterokaryon
RO2.32	heterokaryon	green	heterokaryon
RO2.33	heterokaryon	green	pink
RO2.34	orange	green	pink
RO2.35	heterokaryon	green	heterokaryon
RO2.36	heterokaryon	green	heterokaryon
RO2.37	heterokaryon	green	pink
RO2.38	orange	green	heterokaryon
RO2.39	orange	green	heterokaryon
RO2.4	heterokaryon	heterokaryon	pink
RO2.41	heterokaryon	heterokaryon	pink
RO2.42	blue	heterokaryon	heterokaryon
RO2.43	blue	green	pink
RO2.44	heterokaryon	green	pink
RO2.45	blue	red	heterokaryon
RO2.46	orange	green	pink
RO2.47	blue	green	heterokaryon
RO2.48	heterokaryon	green	pink
RO2.49	heterokaryon	heterokaryon	heterokaryon
RO2.5	blue	heterokaryon	pink
RO2.50	blue	heterokaryon	pink
RO2.51	orange	heterokaryon	pink
RO2.52	heterokaryon	green	heterokaryon
RO2.53	blue	green	deep
RO2.54	blue	heterokaryon	pink
RO2.55	heterokaryon	heterokaryon	heterokaryon
RO2.56	blue	heterokaryon	pink
RO2.57	heterokaryon	heterokaryon	heterokaryon
RO2.58	blue	heterokaryon	heterokaryon
RO2.59	orange	green	deep

USC UNIVERSIDADE DE SANTIAGO DE COMPOSTELA

RO2.6	heterokaryon	heterokaryon	heterokaryon
RO2.7	orange	green	pink
RO2.8	blue	heterokaryon	pink
RO2.9	blue	heterokaryon	heterokaryon
RO3.1	orange	heterokaryon	heterokaryon
RO3.15	heterokaryon	green	heterokaryon
RO3.16	orange	heterokaryon	heterokaryon
RO3.17	orange	green	heterokaryon
RO3.18	orange	green	pink
RO3.2	orange	heterokaryon	pink
RO3.20	heterokaryon	heterokaryon	pink
RO3.21	heterokaryon	heterokaryon	pink
RO3.22	heterokaryon	heterokaryon	pink
RO3.23	heterokaryon	heterokaryon	pink
RO3.24	heterokaryon	green	pink
RO3.27	heterokaryon	heterokaryon	heterokaryon
RO3.29	heterokaryon	green	deep
RO3.3	orange	green	pink
RO3.34	heterokaryon	heterokaryon	pink
RO3.37	blue	green	pink
RO3.4	heterokaryon	heterokaryon	deep
RO3.44	blue	heterokaryon	heterokaryon
RO3.47	blue	green	pink
RO3.5	heterokaryon	green	pink
RO3.53	blue	green	pink
RO3.57	blue	heterokaryon	heterokaryon
RO3.58	blue	heterokaryon	heterokaryon
RO3.6	heterokaryon	green	heterokaryon
RO3.9	heterokaryon	green	pink
RO4.1	blue	heterokaryon	heterokaryon
RO4.10	orange	heterokaryon	heterokaryon
RO4.11	heterokaryon	heterokaryon	heterokaryon
RO4.12	blue	green	heterokaryon
RO4.13	orange	green	pink
RO4.14	blue	heterokaryon	pink
RO4.15	heterokaryon	green	pink
RO4.16	heterokaryon	green	pink
RO4.17	blue	heterokaryon	pink
RO4.18	heterokaryon	red	pink
RO4.19	blue	heterokaryon	heterokaryon
RO4.2	blue	heterokaryon	heterokaryon
RO4.20	orange	green	heterokaryon
RO4.3	blue	green	heterokaryon
RO4.4	blue	green	heterokaryon
RO4.5	orange	green	pink
RO4.6	blue	green	pink
RO4.7	orange	green	heterokaryon
RO4.8	blue	green	pink
RO4.9	orange	heterokaryon	heterokaryon
RO5.1	heterokaryon	heterokaryon	pink
RO5.10	blue	heterokaryon	heterokaryon

USC UNIVERSIDADE DE SANTIAGO DE COMPOSTELA

RO5.11	heterokaryon	green	heterokaryon
RO5.12	heterokaryon	green	pink
RO5.13	heterokaryon	heterokaryon	heterokaryon
RO5.14	heterokaryon	green	heterokaryon
RO5.15	blue	green	heterokaryon
RO5.16	blue	green	heterokaryon
RO5.17	heterokaryon	green	heterokaryon
RO5.18	heterokaryon	green	heterokaryon
RO5.19	orange	green	pink
RO5.2	orange	heterokaryon	pink
RO5.20	orange	heterokaryon	pink
RO5.21	heterokaryon	green	pink
RO5.22	orange	green	pink
RO5.23	heterokaryon	red	heterokaryon
RO5.24	heterokaryon	heterokaryon	pink
RO5.25	heterokaryon	heterokaryon	pink
RO5.26	heterokaryon	green	pink
RO5.3	orange	heterokaryon	heterokaryon
RO5.4	blue	heterokaryon	heterokaryon
RO5.5	orange	heterokaryon	heterokaryon
RO5.6	heterokaryon	heterokaryon	deep
RO5.7	heterokaryon	heterokaryon	heterokaryon
RO5.8	blue	green	deep
RO5.9	blue	heterokaryon	heterokaryon
RO6_1	heterokaryon	green	pink
RO6_2	heterokaryon	heterokaryon	heterokaryon
RO6_3	orange	red	heterokaryon
RO6_4	heterokaryon	green	heterokaryon
RO6_5	heterokaryon	red	heterokaryon
RO6_6	blue	red	heterokaryon

USC
UNIVERSIDADE DE SANTIAGO DE COMPOSTELA

Table S3. Differentially expressed genes (DEGs) across infection levels in *Ostrea edulis* exposed to *Bonamia ostreae* (A) Control vs Level 1 (B) Control vs Level 2 (C) Control vs Level 3. Negative log2FoldChange = higher expression in controls

A) Control vs Level 1

Gene	log2FoldChange	pvalue	Anotation
LOC125665579	-28.17778903	5.49E-13	EF-hand calcium-binding domain-containing protein 1-like
LOC125675579	-26.39539617	1.42E-11	caveolin-1-like
LOC125673466	-15.96544508	5.90E-07	--
LOC125676136	-13.88017993	1.54E-15	cytochrome c oxidase subunit 6A2%2C mitochondrial-like
LOC125678492	-13.66893217	0.000467431	protein lev-9-like isoform X2
LOC125679804	-12.9635005	1.09E-09	--
LOC125669385	-12.8232414	2.16E-08	grainyhead-like protein 1 homolog isoform X4
LOC125663585	-12.7748755	1.53E-09	uncharacterized protein LOC125663585
LOC125654081	-12.5882948	3.71E-09	A disintegrin and metalloproteinase with thrombospondin motifs adt-1-like isoform X7
LOC125683864	-12.51131883	5.23E-08	cerebellin-3-like
LOC125678347	-12.47159576	3.18E-09	receptor-type tyrosine-protein phosphatase F-like isoform X2
LOC125674238	-12.406748	0.001495028	uncharacterized protein LOC125674238
LOC125654813	-12.30886675	3.71E-08	myosin heavy chain%2C skeletal muscle-like
LOC125675283	-12.30424827	0.001636033	caveolin-3-like
LOC125665218	-12.25851687	4.37E-08	uncharacterized protein LOC125665218 isoform X1
LOC125675855	-11.97949877	0.00057026	uncharacterized protein LOC125675855 isoform X1
LOC125662017	-11.9582662	1.52E-05	uncharacterized protein LOC125662017 isoform X1
LOC125659142	-11.95757166	5.72E-10	malignant fibrous histiocytoma-amplified sequence 1 homolog isoform X1
LOC125646641	-11.72674704	5.90E-07	cadherin EGF LAG seven-pass G-type receptor 2-like isoform X1
LOC125673449	-11.66129016	1.42E-06	cerebellin-1-like
LOC125647472	-11.52721852	4.93E-09	--
LOC125654854	-11.4746866	2.90E-05	caveolin-1-like
LOC125653797	-11.45220245	4.76E-08	LOW QUALITY PROTEIN: glutathione S-transferase-like
LOC125665948	-11.43512999	2.44E-08	tripartite motif-containing protein 59-like
LOC125683865	-11.36031174	3.26E-05	complement C1q-like protein 4
LOC125680895	-11.35901995	1.97E-07	--
LOC125646759	-11.34241436	9.62E-08	uncharacterized protein LOC125646759
LOC125674083	-11.31136011	5.57E-08	uncharacterized protein LOC125674083 isoform X2
LOC125682006	-11.27247853	5.13E-08	sphingomyelin synthase-related protein 1-like
LOC125683044	-11.23740009	7.43E-07	uncharacterized protein LOC125683044
LOC125667767	-11.21749242	6.70E-05	uncharacterized protein LOC125667767
LOC125678107	-11.20389913	2.21E-07	ankyrin-1-like
LOC125678350	-11.20116289	3.54E-08	deleted in malignant brain tumors 1 protein-like
LOC125667682	-11.18581763	4.22E-05	uncharacterized protein LOC125667682
LOC125679528	-11.17875464	2.01E-09	collagen alpha-1(I) chain-like
LOC125646997	-11.17246279	1.43E-07	--
LOC125659107	-11.16211849	1.99E-09	--
LOC125654886	-11.15965795	1.09E-08	metalloproteinase inhibitor 2-like
LOC125670325	-11.13719033	7.71E-09	uncharacterized protein LOC125670325
LOC125678077	-11.0451803	6.55E-07	ficolin-1-A-like isoform X2
LOC125650184	-11.04112351	2.87E-09	uncharacterized protein LOC125650184 isoform X1
LOC125682720	-11.01929384	6.61E-05	uncharacterized protein LOC125682720
LOC125672096	-11.0134439	1.63E-07	uncharacterized protein LOC125672096 isoform X1
LOC125650712	-11.00140203	8.22E-05	paired box protein Pax-1-like
LOC125678298	-10.94791134	2.68E-11	tubulin beta chain-like

USC UNIVERSIDADE DE SANTIAGO DE COMPOSTELA

LOC125682475	-10.94791134	2.68E-11	tubulin beta chain-like
LOC125658890	-10.91285988	7.65E-05	uncharacterized protein LOC125658890 isoform X4
LOC125646019	-10.80097622	9.23E-05	perlucin-like protein
LOC125681872	-10.78431228	3.97E-07	tetraspanin-9-like
LOC125654748	-10.74270637	9.52E-05	--
LOC125659528	-10.67185219	1.02E-09	mannose-P-dolichol utilization defect 1 protein homolog
LOC125665863	-10.6483965	2.94E-07	uncharacterized protein LOC125665863 isoform X2
LOC125663783	-10.61776965	0.000155703	uncharacterized protein LOC125663783 isoform X1
LOC125677362	-10.61340905	1.60E-06	uncharacterized protein LOC125677362 isoform X2
LOC125661913	-10.60137479	6.32E-06	tenascin-like isoform X3
LOC125681441	-10.56938934	5.00E-07	serine/arginine repetitive matrix protein 1-like isoform X2
LOC125671604	-10.55655009	8.22E-06	doublesex- and mab-3-related transcription factor A2-like
LOC125661450	-10.54198126	8.13E-06	complement C1q-like protein 4
LOC125661875	-10.52586442	9.49E-07	uncharacterized protein LOC125661875
LOC125665557	-10.47175304	1.52E-06	uncharacterized protein LOC125665557 isoform X2
LOC125683197	-10.4495643	9.53E-06	nmrA-like family domain-containing protein 1 isoform X5
LOC125654909	-10.41038262	0.000222843	caveolin-1-like isoform X2
LOC125681633	-10.3177615	4.02E-06	ficolin-2-like
LOC125677027	-10.31507971	0.000265289	--
LOC125673331	-10.31463052	4.22E-07	tripartite motif-containing protein 2-like isoform X1
LOC125678075	-10.25163548	3.94E-06	C1q-related factor-like isoform X4
LOC125647945	-10.22609314	4.80E-07	filamin A-interacting protein 1-like
LOC125646407	-10.22336117	6.88E-08	uncharacterized protein LOC125646407
LOC125679096	-10.22336117	6.88E-08	uncharacterized protein LOC125679096
LOC125646798	-10.21036346	6.06E-07	putative ankyrin repeat protein RF_0381 isoform X1
LOC125669752	-10.17821426	2.00E-08	--
LOC125666579	-10.12663087	9.28E-07	uncharacterized protein LOC125666579 isoform X2
LOC125672258	-10.10232426	2.96E-11	uncharacterized protein LOC125672258
LOC125681847	-10.09916359	2.45E-06	dehydrogenase/reductase SDR family member 9-like
LOC125681393	-10.08186537	0.00048921	C-type lectin domain family 4 member E-like
LOC125661698	-9.93514111	3.78E-05	--
LOC125646785	-9.911644146	0.000664213	LOW QUALITY PROTEIN: myomodulin neuropeptides 2-like
LOC125658807	-9.906449963	0.000688901	uncharacterized protein LOC125658807
LOC125677066	-9.903787889	1.70E-05	heavy metal-binding protein HIP-like isoform X7
LOC125659934	-9.894411503	0.00072803	uncharacterized protein LOC125659934
LOC125656087	-9.869838941	2.27E-05	uncharacterized protein LOC125656087
LOC125658469	-9.86615149	4.55E-05	--
LOC125675914	-9.838624632	7.39E-07	uncharacterized protein LOC125675914
LOC125662599	-9.837377608	2.28E-05	uncharacterized protein LOC125662599
LOC125655603	-9.832465924	8.99E-06	uncharacterized protein LOC125655603
LOC125646071	-9.823002049	9.76E-06	MORN repeat-containing protein 1-like isoform X1
LOC125671919	-9.809918168	4.98E-06	uncharacterized protein LOC125671919
LOC125652777	-9.756101268	6.73E-05	uncharacterized protein LOC125652777
LOC125668219	-9.727915249	2.63E-08	uncharacterized protein LOC125668219
LOC125665752	-9.695957302	5.54E-05	acid-sensing ion channel 5-like isoform X3
LOC125665726	-9.659658175	1.09E-05	uncharacterized protein LOC125665726
LOC125666899	-9.657177301	3.33E-06	uncharacterized protein LOC125666899
LOC125670204	-9.651724223	3.38E-05	uncharacterized protein LOC125670204
LOC125645482	-9.633842701	2.57E-06	uncharacterized protein LOC125645482 isoform X2
LOC125679882	-9.613323493	2.64E-07	uncharacterized protein LOC125679882
LOC125675507	-9.602707969	2.02E-06	microsomal glutathione S-transferase 3-like

USC UNIVERSIDADE DE SANTIAGO DE COMPOSTELA

LOC125650883	-9.588179346	0.001329965	rho-related GTP-binding protein RhoQ-like
LOC125679568	-9.555560895	7.00E-06	Golgi-associated plant pathogenesis-related protein 1-like
LOC125659920	-9.551580344	2.94E-08	tripartite motif-containing protein 2-like
LOC125680672	-9.540403443	8.73E-05	allatotropins-like
LOC125653464	-9.521331702	9.57E-07	fibropellin-3-like isoform X2
LOC125646956	-9.501809182	0.000120355	--
LOC125663587	-9.469273109	1.53E-08	metabotropic glutamate receptor 3-like
LOC125662552	-9.466732442	7.29E-09	uncharacterized protein LOC125662552
LOC125655472	-9.452973123	0.001873177	A disintegrin and metalloproteinase with thrombospondin motifs 4-like isoform X5
LOC125681429	-9.402232078	0.001990184	uncharacterized protein LOC125681429
LOC125651650	-9.398693575	5.28E-05	uncharacterized protein CXorf65 homolog
LOC125646253	-9.393981104	2.12E-05	FMRF-amide neuropeptides-like
LOC125681465	-9.379290946	0.000189828	tetraspanin-18-like
LOC125670160	-9.355673146	0.002280228	uncharacterized protein LOC125670160
LOC125659954	-9.328239428	0.000171525	zinc finger and BTB domain-containing protein 49-like
LOC125658627	-9.320895857	9.07E-05	zinc finger protein 667-like
LOC125669885	-9.302388032	0.000100883	uncharacterized protein LOC125669885
LOC125651862	-9.267422349	8.95E-06	uncharacterized protein LOC125651862 isoform X1
LOC125670321	-9.24081498	0.00265138	uncharacterized protein LOC125670321
LOC125680553	-9.224318167	0.002689154	twitchin-like
LOC125677266	-9.214734073	4.10E-06	transmembrane protein 45B-like isoform X1
LOC125649555	-9.212835214	7.71E-05	uncharacterized protein LOC125649555
LOC125675941	-9.211388753	0.000278002	uncharacterized protein LOC125675941
LOC125668356	-9.191736795	4.88E-06	coiled-coil domain-containing protein 33-like isoform X2
LOC125682512	-9.184702267	0.002897909	uncharacterized protein LOC125682512 isoform X1
LOC125646811	-9.174704184	3.03E-07	homeobox protein Dlx6a-like
LOC125667714	-9.160612344	0.000106451	ryncolin-1-like
LOC125659209	-9.154361119	3.01E-07	--
LOC125673467	-9.122772231	0.003901742	--
LOC125656219	-9.104267398	0.000205498	uncharacterized protein LOC125656219 isoform X1
LOC125663750	-9.08689498	0.00383215	uncharacterized protein LOC125663750
LOC125680341	-9.042529065	1.10E-05	uncharacterized protein LOC125680341
LOC125681876	-8.956661987	0.004542827	complement C1q-like protein 3 isoform X1
LOC125655003	-8.956537396	0.00043279	uncharacterized protein LOC125655003 isoform X3
LOC125680754	-8.942996244	5.64E-05	UPF0686 protein C11orf1 homolog
LOC125648022	-8.921745445	1.31E-06	uncharacterized protein LOC125648022 isoform X2
LOC125671701	-8.884569267	0.005327969	uncharacterized protein LOC125671701
LOC125659427	-8.817309033	5.77E-08	LOW QUALITY PROTEIN: cell surface hyaluronidase-like
LOC125671525	-8.794730632	2.04E-05	protein CFAP95-like
LOC125668997	-8.794660273	2.47E-05	collagen alpha-1(I) chain-like
LOC125677041	-8.793159363	0.000769779	otolin-1-like
LOC125676256	-8.782826563	2.82E-08	--
LOC125661197	-8.769553461	2.84E-07	calpain-5-like isoform X3
LOC125676046	-8.749527572	4.75E-06	--
LOC125653443	-8.747377554	7.78E-05	complement C1q subcomponent subunit A-like
LOC125661560	-8.737342606	0.005969895	DBH-like monooxygenase protein 1
LOC125668796	-8.716028473	3.34E-08	NAD-dependent protein deacetylase Sirt6-like isoform X1
LOC125671580	-8.71371277	1.13E-05	dynein light chain Tctex-type 5-like
LOC125648084	-8.691748395	1.78E-05	--
LOC125655683	-8.658743312	0.00035406	cysteine and tyrosine-rich protein 1-like isoform X1
LOC125679636	-8.615892721	1.74E-05	nicotinamidase-like

USC UNIVERSIDADE DE SANTIAGO DE COMPOSTELA

LOC125645866	-8.608826907	3.00E-07	mucin-4-like isoform X6
LOC125655410	-8.587713237	7.91E-06	von Willebrand factor D and EGF domain-containing protein-like isoform X1
LOC125679886	-8.585913338	1.02E-05	--
LOC125673455	-8.561046483	0.00228659	uncharacterized protein LOC125673455
LOC125649865	-8.534180438	4.35E-05	arrestin domain-containing protein 3-like
LOC125683873	-8.514152729	1.03E-07	contactin-like isoform X2
LOC125683223	-8.494269779	9.43E-06	uncharacterized protein LOC125683223 isoform X2
LOC125660998	-8.483380408	3.99E-05	--
LOC125657103	-8.475877959	0.001268324	heavy metal-binding protein HIP-like
LOC125669927	-8.472262907	8.58E-09	equilibrative nucleobase transporter 1-like
LOC125681914	-8.452021321	9.75E-08	octopamine receptor-like
LOC125647859	-8.43793343	4.95E-08	EF-hand domain-containing protein 1-like
LOC125664304	-8.425014224	8.73E-06	uncharacterized protein LOC125664304 isoform X12
LOC125649506	-8.424114568	2.98E-09	radial spoke head protein 4 homolog A-like
LOC125654912	-8.395411676	7.49E-05	uncharacterized protein LOC125654912
LOC125646484	-8.389868033	3.76E-07	--
LOC125671411	-8.370279492	5.28E-09	cilia- and flagella-associated protein 52-like
LOC125650749	-8.365438797	2.83E-06	uncharacterized protein LOC125650749
LOC125669918	-8.349299477	1.19E-06	spermatogenesis-associated protein 6-like isoform X2
LOC125647728	-8.33705265	8.10E-05	uncharacterized protein LOC125647728 isoform X1
LOC125671830	-8.336821886	5.26E-06	zinc metalloproteinase dpy-31-like
LOC125680779	-8.297007584	7.06E-05	uncharacterized protein LOC125680779
LOC125645567	-8.295985986	0.000135001	uncharacterized protein LOC125645567
LOC125656192	-8.256618759	1.74E-05	pre-mRNA-splicing factor CWC22 homolog
LOC125647970	-8.236279518	1.63E-05	uncharacterized protein C17orf98-like
LOC125665905	-8.232817575	1.14E-05	interferon alpha-inducible protein 27-like protein 2B isoform X3
LOC125645735	-8.226955735	1.26E-05	uncharacterized protein LOC125645735
LOC125675951	-8.212027706	1.13E-05	uncharacterized protein LOC125675951
LOC125670629	-8.204987155	0.000106054	cyclin-dependent kinase 12-like isoform X6
LOC125674088	-8.198827012	2.14E-05	neurogenic locus Notch protein-like
LOC125674305	-8.183343447	3.18E-06	uncharacterized protein LOC125674305 isoform X3
LOC125648317	-8.176108632	9.16E-05	calmodulin-beta-like
LOC125682365	-8.167383241	0.001600132	lithostathine-1-alpha-like
LOC125645876	-8.164479884	0.001184949	uncharacterized protein LOC125645876
LOC125669881	-8.151246908	5.94E-05	ras-related protein Rap-1b-like
LOC125655331	-8.143200309	0.000880749	uncharacterized protein LOC125655331
LOC125668779	-8.132642819	0.001241528	uncharacterized protein LOC125668779
LOC125654847	-8.128029117	1.84E-05	protein CFAP276-like isoform X2
LOC125681850	-8.061167689	3.32E-05	uncharacterized protein LOC125681850
LOC125667054	-8.047125415	0.001223948	uncharacterized protein LOC125667054 isoform X3
LOC125663040	-8.045693905	0.00020591	transmembrane protein 272-like
LOC125664326	-8.038702411	4.76E-05	uncharacterized protein LOC125664326
LOC125671570	-8.029456853	4.64E-06	uncharacterized protein LOC125671570
LOC125649577	-8.027953235	9.82E-08	neuroendocrine convertase 2-like
LOC125655847	-8.003931645	0.001150941	uncharacterized protein LOC125655847
LOC125653627	-7.972102184	0.001346219	uncharacterized protein LOC125653627
LOC125668606	-7.969632697	3.10E-06	--
LOC125646172	-7.96350457	0.000160923	--
LOC125683027	-7.958609573	6.52E-05	paired box protein Pax-6-like isoform X1
LOC125672154	-7.944821835	0.000192115	uncharacterized protein LOC125672154
LOC125672158	-7.944821835	0.000192115	uncharacterized protein LOC125672158

USC UNIVERSIDADE DE SANTIAGO DE COMPOSTELA

LOC125683927	-7.904175078	7.03E-06	LOW QUALITY PROTEIN: myeloid differentiation primary response protein MyD88-like
LOC125652363	-7.901962531	5.29E-05	golgin subfamily A member 6-like protein 22
LOC125673093	-7.884103086	7.54E-05	--
LOC125659807	-7.850565007	0.0028414	APGW-amide-related neuropeptide-like
LOC125657652	-7.849553528	0.00191091	short-chain collagen C4-like
LOC125650665	-7.841399581	1.45E-06	stabilizer of axonemal microtubules 2-like
LOC125645608	-7.819998699	0.000115489	alpha-(1%2C3)-fucosyltransferase fut-5-like isoform X1
LOC125680336	-7.816117609	2.13E-06	uncharacterized protein LOC125680336
LOC125679238	-7.801905506	7.67E-05	prestin-like isoform X2
LOC125681718	-7.792766393	5.54E-05	uncharacterized protein LOC125681718 isoform X13
LOC125649717	-7.754901441	1.52E-05	sodium/calcium exchanger 3-like
LOC125671987	-7.754901441	1.52E-05	sodium/calcium exchanger 3-like
LOC125683627	-7.743812182	2.14E-08	MAM and LDL-receptor class A domain-containing protein 1-like isoform X3
LOC125654684	-7.728069034	1.33E-06	uncharacterized protein LOC125654684
LOC125659146	-7.726679778	0.00017204	transcription factor Sox-2-like
LOC125673456	-7.686419164	0.000276422	uncharacterized protein LOC125673456 isoform X2
LOC125646697	-7.685392602	3.39E-05	uncharacterized protein LOC125646697
LOC125670881	-7.641538154	1.90E-05	LITAF domain-containing protein-like
LOC125662157	-7.63947871	0.000185146	uncharacterized protein LOC125662157
LOC125650546	-7.618332084	0.002218034	ras-related C3 botulinum toxin substrate 3-like
LOC125660999	-7.586072131	0.006888637	tyramine beta-hydroxylase-like
LOC125661562	-7.586072131	0.006888637	tyramine beta-hydroxylase-like
LOC125658452	-7.568351168	0.005055363	--
LOC125669911	-7.54071819	7.66E-07	cilia- and flagella-associated protein 57-like
LOC125654173	-7.524404297	7.88E-05	34 kDa antigenic protein-like isoform X6
LOC125664426	-7.523252522	2.74E-05	uncharacterized protein LOC125664426 isoform X2
LOC125680852	-7.517875102	2.42E-06	E3 ubiquitin-protein ligase TRIM71-like
LOC125675445	-7.505557563	1.20E-05	uncharacterized protein LOC125675445
LOC125649071	-7.492427383	1.21E-05	testis%2C prostate and placenta-expressed protein-like
LOC125658223	-7.482258047	0.002930112	uncharacterized protein LOC125658223 isoform X3
LOC125645999	-7.425864063	1.86E-06	D-beta-hydroxybutyrate dehydrogenase-like isoform X1
LOC125653936	-7.40674437	0.000155129	uncharacterized protein LOC125653936
LOC125672140	-7.400666502	0.003980349	uncharacterized protein LOC125672140
LOC125672152	-7.400666502	0.003980349	uncharacterized protein LOC125672152
LOC125680424	-7.385329528	2.62E-05	tetraspanin-9-like isoform X3
LOC125681164	-7.385164627	3.59E-05	uncharacterized protein LOC125681164
LOC125668705	-7.374755734	0.004574444	LOW QUALITY PROTEIN: hematopoietic prostaglandin D synthase-like
LOC125649497	-7.354475634	0.00057516	protein doublesex-like
LOC125673112	-7.333939993	0.000857597	adhesion G protein-coupled receptor B1-like isoform X2
LOC125646422	-7.332211174	1.13E-05	VWFA and cache domain-containing protein 1-like
LOC125662595	-7.290530014	6.45E-06	--
LOC125679357	-7.288643309	0.000748207	centrosome-associated protein CEP250-like isoform X3
LOC125674301	-7.277026649	0.000569273	uromodulin-like
LOC125670809	-7.271533796	0.00025926	collagen alpha-4(VI) chain-like
LOC125675289	-7.212371872	2.49E-05	outer dense fiber protein 3-like
LOC125670035	-7.172306962	1.25E-07	transmembrane channel-like protein 7 isoform X4
LOC125655260	-7.164227786	7.81E-05	uncharacterized protein LOC125655260 isoform X1
LOC125671469	-7.163063713	2.59E-05	tektin-3-like isoform X2
LOC125669459	-7.144952989	0.000170288	probable 3'%2C5'-cyclic phosphodiesterase pde-5 isoform X10
LOC125654853	-7.137562675	5.31E-08	uncharacterized protein LOC125654853
LOC125656147	-7.135523364	0.001445891	cysteine and tyrosine-rich protein 1-like

USC UNIVERSIDADE DE SANTIAGO DE COMPOSTELA

LOC125662692	-7.132110591	3.88E-05	uncharacterized protein LOC125662692
LOC125661935	-7.106053889	0.000183237	BPTI/Kunitz domain-containing protein-like
LOC125662861	-7.100023539	1.59E-05	tektin-1-like
LOC125677149	-7.095832522	0.000164658	semaphorin-5A-like isoform X2
LOC125670333	-7.093269803	1.00E-05	tektin-2-like
LOC125670355	-7.093269803	1.00E-05	tektin-2-like
LOC125679700	-7.077949303	0.00056024	epidermal growth factor receptor-like
LOC125666577	-7.023318486	2.33E-05	--
LOC125656100	-7.022908563	0.000924298	LHFPL tetraspan subfamily member 3 protein-like
LOC125671509	-7.018890178	8.91E-08	excitatory amino acid transporter 1-like isoform X2
LOC125666126	-7.013894015	0.001062592	uncharacterized protein LOC125666126
LOC125677109	-7.010066819	0.000763303	uncharacterized protein LOC125677109
LOC125675775	-7.008127229	1.61E-07	uncharacterized protein LOC125675775
LOC125645791	-7.006217035	0.00092299	testis-expressed protein 52-like
LOC125682745	-6.995697713	8.67E-07	uncharacterized protein LOC125682745
LOC125670863	-6.99336255	0.001643379	paired box protein Pax-8-like isoform X1
LOC125664338	-6.95195409	0.00721694	--
LOC125651301	-6.932684498	0.006775158	uncharacterized protein LOC125651301
LOC125651536	-6.931698121	0.001216096	C-type lectin domain family 4 member K-like isoform X1
LOC125668795	-6.888493218	8.00E-05	NAD-dependent protein deacetylase Sirt6-like
LOC125670408	-6.874066051	0.000178881	neurensin-1-like
LOC125659880	-6.85092881	3.55E-05	leucine-rich repeat protein soc-2-like
LOC125654008	-6.849809071	0.000453616	protein SSUH2 homolog isoform X1
LOC125677265	-6.825492656	8.00E-05	uncharacterized protein LOC125677265
LOC125675832	-6.798011853	0.000138066	uncharacterized protein LOC125675832 isoform X3
LOC125674306	-6.790070927	0.000812936	oncoprotein-induced transcript 3 protein-like
LOC125668947	-6.775294978	1.41E-05	uncharacterized protein LOC125668947
LOC125670666	-6.772178968	4.39E-05	uncharacterized protein LOC125670666 isoform X2
LOC125665618	-6.77215059	0.000377601	uncharacterized protein LOC125665618 isoform X2
LOC125657872	-6.765196854	0.000797601	cilia- and flagella-associated protein 119-like
LOC125682965	-6.762102749	8.78E-05	uncharacterized protein LOC125682965
LOC125677388	-6.761465188	7.57E-05	uncharacterized protein LOC125677388 isoform X2
LOC125652070	-6.756607254	0.000741423	uncharacterized protein LOC125652070 isoform X3
LOC125667337	-6.753998631	7.51E-05	glutathione S-transferase theta-1-like
LOC125647771	-6.743847426	1.59E-05	uncharacterized protein LOC125647771
LOC125683043	-6.724433395	5.74E-05	--
LOC125675925	-6.723664956	0.001396118	--
LOC125649923	-6.717651851	9.60E-05	uncharacterized protein LOC125649923
LOC125681419	-6.712573313	4.59E-06	fibrocystin-L-like isoform X1
LOC125650796	-6.671389749	0.002238646	uncharacterized protein LOC125650796
LOC125659601	-6.654701421	0.001078311	uncharacterized protein LOC125659601
LOC125681971	-6.653556906	2.91E-05	uncharacterized protein LOC125681971 isoform X40
LOC125680840	-6.652118364	1.84E-05	uncharacterized protein LOC125680840
LOC125683060	-6.646109755	0.001909453	uncharacterized protein LOC125683060 isoform X1
LOC125655708	-6.645630427	0.001036731	phospholipid-transporting ATPase ABCA3-like
LOC125665818	-6.638741828	4.97E-05	sperm-associated antigen 6
LOC125671321	-6.63342036	3.34E-05	peroxiredoxin prdx-2-like
LOC125679600	-6.630503083	1.55E-06	coiled-coil domain-containing protein 105-like isoform X1
LOC125676997	-6.614037798	0.000159884	uncharacterized protein LOC125676997
LOC125666029	-6.607437451	0.000561875	uncharacterized protein LOC125666029
LOC125652760	-6.559459657	0.001371187	cdc42 homolog

USC UNIVERSIDADE DE SANTIAGO DE COMPOSTELA

LOC125671402	-6.550640134	1.10E-05	LOW QUALITY PROTEIN: uncharacterized protein LOC125671402
LOC125681732	-6.513728292	0.000194489	uncharacterized protein LOC125681732
LOC125656954	-6.501696257	0.000420813	uncharacterized protein LOC125656954
LOC125680312	-6.499291095	0.000728693	uncharacterized protein LOC125680312
LOC125645609	-6.492742991	0.00279867	glycoprotein 3-alpha-L-fucosyltransferase A-like
LOC125677098	-6.492398097	0.000116615	--
LOC125660793	-6.483941655	7.59E-05	ceramide-1-phosphate transfer protein-like
LOC125673460	-6.453067745	0.000757853	uncharacterized protein LOC125673460 isoform X2
LOC125663775	-6.433994107	6.08E-06	uncharacterized protein LOC125663775
LOC125673558	-6.431730595	9.37E-05	uncharacterized protein LOC125673558
LOC125681343	-6.422358504	7.00E-06	uncharacterized protein LOC125681343 isoform X1
LOC125665341	-6.384057369	0.000193304	mucin-17-like
LOC125653934	-6.3823011	0.000263632	uncharacterized protein LOC125653934
LOC125671742	-6.366796318	1.10E-08	uncharacterized protein LOC125671742
LOC125657899	-6.35748966	0.000455614	EF-hand domain-containing family member C2-like
LOC125655578	-6.356682807	9.69E-07	uncharacterized protein LOC125655578 isoform X1
LOC125675825	-6.346094718	0.000101965	uncharacterized protein LOC125675825
LOC125673349	-6.34295881	0.001798227	hemagglutinin/amebocyte aggregation factor-like isoform X5
LOC125654330	-6.341388801	0.000152576	--
LOC125672343	-6.325311705	7.10E-06	--
LOC125654787	-6.310239829	0.001913453	protein PRQFV-amide-like
LOC125648180	-6.302097221	0.004856783	uncharacterized protein LOC125648180
LOC125679934	-6.298832398	0.000403511	uncharacterized protein LOC125679934 isoform X1
LOC125654207	-6.294556142	1.73E-06	uncharacterized protein LOC125654207
LOC125651796	-6.279659147	3.14E-08	piRNA biogenesis protein EXD1-like isoform X2
LOC125663827	-6.254575957	4.55E-10	PH domain leucine-rich repeat-containing protein phosphatase 2-like isoform X2
LOC125652465	-6.237315344	4.17E-05	DBH-like monooxygenase protein 2 homolog isoform X2
LOC125659227	-6.233855873	3.02E-07	--
LOC125676103	-6.218124607	3.74E-06	radial spoke head protein 3 homolog B-like
LOC125681931	-6.213549988	0.001545921	uncharacterized protein LOC125681931
LOC125680688	-6.209392293	0.000152361	mitochondria-eating protein-like isoform X3
LOC125666828	-6.203731141	2.80E-07	cilia- and flagella-associated protein 69-like
LOC125652517	-6.184949672	0.006176311	uncharacterized protein LOC125652517
LOC125653701	-6.184949672	0.006176311	uncharacterized protein LOC125653701
LOC125654741	-6.177015508	0.00029497	uncharacterized protein LOC125654741
LOC125667146	-6.155510825	0.006067324	uncharacterized protein LOC125667146
LOC125675071	-6.136223352	0.001032531	enteropeptidase-like
LOC125654269	-6.106008563	0.000264062	IQ and ubiquitin-like domain-containing protein
LOC125670652	-6.084196736	0.000171795	uncharacterized protein LOC125670652 isoform X4
LOC125670922	-6.052649538	0.000167913	protein FAM183B-like
LOC125650938	-6.041222753	0.005101932	--
LOC125654310	-6.03970682	0.000585496	sodium-dependent proline transporter-like
LOC125648216	-6.02425441	0.006151437	arrestin domain-containing protein 1-like isoform X1
LOC125680700	-6.019282388	0.000107133	uncharacterized protein LOC125680700
LOC125682298	-6.017694962	0.003111942	uncharacterized protein LOC125682298
LOC125678757	-6.007531863	0.000438875	cilia- and flagella-associated protein 45-like isoform X1
LOC125655489	-5.981072231	0.000750139	globin-like
LOC125657629	-5.978934333	0.000217869	uncharacterized protein LOC125657629
LOC125677332	-5.968349115	0.000374557	dnaJ homolog subfamily B member 13-like
LOC125673201	-5.943037204	9.63E-05	phenylalanine-4-hydroxylase-like isoform X1
LOC125650137	-5.940672517	9.37E-05	uncharacterized protein LOC125650137 isoform X6

USC UNIVERSIDADE DE SANTIAGO DE COMPOSTELA

LOC125665835	-5.938767658	4.41E-06	protein CFAP210-like
LOC125653345	-5.934174262	5.40E-05	metalloproteinase inhibitor 2-like isoform X1
LOC125659693	-5.928762768	0.00090233	uncharacterized protein LOC125659693
LOC125650791	-5.927945388	4.01E-08	uncharacterized protein LOC125650791
LOC125659544	-5.908703319	0.00012562	sperm axonemal maintenance protein CFAP97D1-like
LOC125645800	-5.890580906	0.002307599	uncharacterized protein LOC125645800
LOC125655888	-5.869764159	0.000789263	uncharacterized protein LOC125655888
LOC125671016	-5.869746635	0.000534635	protein TBATA-like isoform X2
LOC125645448	-5.857325955	0.000528566	uncharacterized protein LOC125645448 isoform X4
LOC125671286	-5.856074396	0.000379382	hillarin-like
LOC125658375	-5.855962599	0.003916442	uncharacterized protein LOC125658375
LOC125656218	-5.849028529	0.000499876	RIB43A-like with coiled-coils protein 2
LOC125649908	-5.845827207	0.002443814	uncharacterized protein LOC125649908
LOC125654907	-5.840643769	0.006149944	low affinity immunoglobulin epsilon Fc receptor-like
LOC125664212	-5.8301346	1.29E-05	coiled-coil domain-containing protein 63-like
LOC125652782	-5.821429254	0.003535	neuropeptide Y receptor type 6-like
LOC125668354	-5.810746137	0.000250992	uncharacterized protein LOC125668354 isoform X7
LOC125672113	-5.80842415	8.87E-07	uncharacterized protein LOC125672113
LOC125652000	-5.80176024	0.00535669	uncharacterized protein LOC125652000
LOC125670854	-5.789246194	0.000113308	uncharacterized protein LOC125670854 isoform X2
LOC125673372	-5.780062008	1.10E-06	pancreatic triacylglycerol lipase-like isoform X3
LOC125671772	-5.779357104	0.000252539	tektin-4-like
LOC125664454	-5.7648464	2.54E-05	fatty acid-binding protein%2C heart-like
LOC125656191	-5.76427395	0.003817599	pre-mRNA-splicing factor CWC22 homolog
LOC125645564	-5.758690967	2.36E-06	uncharacterized protein LOC125645564
LOC125654075	-5.757152405	0.00670146	protein ATP6V1FNB-like
LOC125682191	-5.757094904	0.001335966	tetraspanin-9-like isoform X1
LOC125675252	-5.739042321	0.001296566	--
LOC125681261	-5.738770973	0.000749171	sodium- and chloride-dependent taurine transporter-like isoform X1
LOC125678844	-5.708085228	4.68E-05	uncharacterized protein LOC125678844
LOC125660487	-5.685535698	0.000592264	E3 ubiquitin-protein ligase TRIM56-like
LOC125679123	-5.683752499	0.00070536	complement C1q tumor necrosis factor-related protein 2-like
LOC125671726	-5.667584205	0.004296142	cell migration-inducing and hyaluronan-binding protein-like
LOC125658990	-5.656903098	2.79E-06	enolase-phosphatase E1-like isoform X2
LOC125673407	-5.648583195	0.006683797	uncharacterized protein LOC125673407 isoform X1
LOC125680371	-5.647396036	7.17E-06	choline transporter-like protein 2
LOC125670167	-5.639934841	0.001703336	cytoplasmic dynein 2 heavy chain 1-like
LOC125645600	-5.635050453	0.00121934	uncharacterized protein LOC125645600 isoform X2
LOC125648923	-5.627986065	0.001435519	LOW QUALITY PROTEIN: sodium-dependent phosphate transport protein 2B-like
LOC125653264	-5.617643076	0.000214021	uncharacterized protein LOC125653264
LOC125669600	-5.611140992	0.002906659	prostaglandin E2 receptor EP4 subtype-like
LOC125677659	-5.609920244	0.003651	uncharacterized protein LOC125677659
LOC125668352	-5.605247543	0.001795178	uncharacterized protein LOC125668352 isoform X3
LOC125648138	-5.595729997	1.61E-06	--
LOC125682995	-5.585561674	0.000949812	uncharacterized protein LOC125682995
LOC125679178	-5.565270239	0.001044173	protein FAM166B-like
LOC125668843	-5.564215835	1.82E-06	LOW QUALITY PROTEIN: fatty acid synthase-like
LOC125666781	-5.551612596	0.000169202	--
LOC125681879	-5.539561056	0.000659534	protein unc-93 homolog A-like
LOC125681507	-5.522945846	0.001977021	uncharacterized protein LOC125681507
LOC125681186	-5.518731784	9.66E-06	uncharacterized protein LOC125681186

USC UNIVERSIDADE DE SANTIAGO DE COMPOSTELA

LOC125649115	-5.515522554	0.001131381	neuroendocrine convertase 1-like isoform X1
LOC125677370	-5.501911536	0.000132336	protein phosphatase 1 regulatory subunit 32-like
LOC125679759	-5.479483449	0.001216618	beta-1%2C3-galactosyltransferase 1-like
LOC125657479	-5.478997605	0.00097547	uncharacterized protein LOC125657479 isoform X1
LOC125670712	-5.462266754	0.000398441	protein FAM234B-like isoform X2
LOC125659726	-5.450237218	0.00087682	protein shisa-5-like
LOC125645747	-5.437150638	0.002376335	uncharacterized protein LOC125645747
LOC125649496	-5.434049337	3.00E-06	--
LOC125672973	-5.421262558	7.12E-06	uncharacterized protein LOC125672973 isoform X2
LOC125681060	-5.404078601	1.68E-05	uncharacterized protein LOC125681060
LOC125679510	-5.395351239	0.002127646	low-density lipoprotein receptor-related protein 4-like isoform X2
LOC125665991	-5.390499435	0.002000378	uncharacterized protein LOC125665991
LOC125671804	-5.379211688	0.000184182	--
LOC125679074	-5.376459085	0.000596404	annexin A5-like
LOC125655976	-5.369296722	9.82E-05	piercer of microtubule wall 1 protein-like
LOC125649994	-5.366994604	2.00E-05	sodium- and chloride-dependent neutral and basic amino acid transporter B(0+)-like isoform X1
LOC125680315	-5.354824896	0.002246678	uncharacterized protein LOC125680315
LOC125655876	-5.345555133	7.98E-05	--
LOC125672280	-5.338465755	0.003332917	spermatogenesis-associated protein 6-like
LOC125671978	-5.326907648	0.006990825	cytoplasmic dynein 2 heavy chain 1-like
LOC125649958	-5.314453525	0.000251979	spermatogenesis-associated protein 17-like isoform X2
LOC125682968	-5.311376688	4.67E-05	twisted gastrulation protein homolog 1-A-like
LOC125645789	-5.294203649	0.000595693	uncharacterized protein LOC125645789
LOC125667693	-5.26165904	0.003679693	A disintegrin and metalloproteinase with thrombospondin motifs adt-1-like
LOC125654171	-5.260665302	0.001656901	uncharacterized protein LOC125654171 isoform X3
LOC125669540	-5.253512638	7.08E-06	beta-1%2C3-galactosyl-O-glycosyl-glycoprotein beta-1%2C6-N-acetylglucosaminyltransferase-like
LOC125649563	-5.236226319	0.000370022	uncharacterized protein LOC125649563
LOC125681468	-5.232165359	0.004287599	radial spoke head 1 homolog isoform X1
LOC125668497	-5.227679769	0.005306354	nucleoside diphosphate kinase homolog 5-like
LOC125650639	-5.220620839	0.001767689	coiled-coil domain-containing protein 170-like
LOC125650674	-5.220620839	0.001767689	coiled-coil domain-containing protein 170-like
LOC125673328	-5.21496393	2.98E-10	four-jointed box protein 1-like
LOC125666040	-5.214338791	0.00521992	uncharacterized protein LOC125666040 isoform X2
LOC125674960	-5.20757084	0.003886013	EF-hand calcium-binding domain-containing protein 6-like isoform X5
LOC125649024	-5.20313245	0.001411094	adenylate kinase 7-like
LOC125683834	-5.190535721	0.000169565	tetraspanin-9-like
LOC125645434	-5.186140989	6.19E-05	uncharacterized protein LOC125645434 isoform X4
LOC125645461	-5.181814201	0.001834446	glutamate-rich protein 3-like isoform X2
LOC125683021	-5.147045329	8.59E-06	LOW QUALITY PROTEIN: protein unc-93 homolog A-like
LOC125654399	-5.138127626	0.001444852	LIM domain and actin-binding protein 1-like
LOC125668622	-5.131309432	0.002426419	uncharacterized protein LOC125668622
LOC125649474	-5.106919546	0.001679866	mitochondrial uncoupling protein 2-like isoform X2
LOC125680298	-5.086212547	0.000119213	ankyrin repeat and SOCS box protein 13-like
LOC125662347	-5.073657332	0.006994668	sodium- and chloride-dependent taurine transporter-like isoform X2
LOC125664158	-5.059669049	2.85E-05	atrial natriuretic peptide receptor 2-like isoform X2
LOC125664451	-5.05300139	0.003623661	dynein regulatory complex protein 10-like
LOC125668736	-5.052805989	0.002087647	calcyphosin-like protein isoform X1
LOC125645485	-5.035516584	0.001645362	thyroxine 5-deiodinase-like
LOC125650681	-5.020457388	0.002188415	uncharacterized protein LOC125650681
LOC125683830	-5.017362214	0.001498686	uncharacterized protein LOC125683830 isoform X1
LOC125668623	-5.001066527	0.006636172	LOW QUALITY PROTEIN: uncharacterized protein LOC125668623

USC UNIVERSIDADE DE SANTIAGO DE COMPOSTELA

LOC125665628	-5.00078005	0.003663838	sorcin-like
LOC125660021	-4.983964303	0.000239684	sphingolipid delta(4)-desaturase DES1-like isoform X2
LOC125646778	-4.981199646	0.005962142	tektin-3-like isoform X1
LOC125653821	-4.972119128	4.52E-05	uncharacterized protein LOC125653821
LOC125680304	-4.967811567	0.000104095	tetraspanin-1-like
LOC125654780	-4.953775398	0.003820217	meiosis expressed gene 1 protein homolog isoform X2
LOC125663323	-4.946278801	1.91E-05	matrilysin-like isoform X1
LOC125679426	-4.943525268	0.004231386	sushi domain-containing protein 2-like
LOC125677748	-4.908662494	0.000252564	uncharacterized protein LOC125677748
LOC125668435	-4.872523472	7.06E-06	uncharacterized protein LOC125668435
LOC125670754	-4.850976704	0.000223399	purine nucleoside phosphorylase-like isoform X1
LOC125671094	-4.842065061	0.000179933	EF-hand calcium-binding domain-containing protein 6-like isoform X1
LOC125663921	-4.836080543	0.000123603	--
LOC125651816	-4.833765766	0.000462765	FMRFamide receptor-like
LOC125671615	-4.795070457	0.004710979	uncharacterized protein LOC125671615
LOC125671281	-4.791075088	8.31E-06	uncharacterized protein LOC125671281 isoform X2
LOC125679523	-4.776072682	0.003897613	uncharacterized protein LOC125679523
LOC125665592	-4.772480834	0.005895222	uncharacterized protein LOC125665592
LOC125651313	-4.767984099	0.005491055	uncharacterized protein LOC125651313
LOC125669562	-4.750694372	0.00453709	uncharacterized protein LOC125669562 isoform X1
LOC125678353	-4.750054873	1.97E-05	EF-hand domain-containing family member B-like
LOC125674793	-4.733721894	0.000391105	microtubule-associated protein futsch-like isoform X4
LOC125658245	-4.729299731	0.004740434	postacrosomal sheath WW domain-binding protein-like isoform X2
LOC125669783	-4.725664204	5.75E-05	cadherin-87A-like isoform X1
LOC125683455	-4.716499116	0.002566602	protein pitchfork-like
LOC125665860	-4.700198302	0.000184726	uncharacterized protein LOC125665860 isoform X2
LOC125679737	-4.684618899	0.002722006	arrestin domain-containing protein 2-like
LOC125674780	-4.677728134	5.43E-05	putative inhibitor of apoptosis
LOC125652471	-4.672710884	0.000108374	uncharacterized protein LOC125652471
LOC125650855	-4.656363634	2.71E-05	advillin-like isoform X1
LOC125654309	-4.652497028	6.90E-06	sodium-dependent proline transporter-like isoform X2
LOC125650637	-4.652461272	0.000661682	uncharacterized protein LOC125650637 isoform X2
LOC125681020	-4.650023388	0.002487652	short-chain collagen C4-like
LOC125658680	-4.632724445	4.15E-05	uncharacterized protein LOC125658680
LOC125657931	-4.630932167	0.000199242	tubulin beta chain
LOC125678958	-4.627410753	0.00176033	LOW QUALITY PROTEIN: tryptophan 2%2C3-dioxygenase-like
LOC125666193	-4.606475083	0.000160573	uncharacterized protein LOC125666193
LOC125683094	-4.586553553	0.006604464	uncharacterized protein LOC125683094
LOC125671290	-4.585594735	2.84E-08	uncharacterized protein LOC125671290
LOC125658329	-4.585427059	0.000490808	XK-related protein 9-like
LOC125663672	-4.584289296	0.000441109	A disintegrin and metalloproteinase with thrombospondin motifs 7-like isoform X1
LOC125663732	-4.575947063	0.000124921	uncharacterized protein LOC125663732
LOC125647565	-4.572376344	3.92E-05	zinc finger MYND domain-containing protein 12-like
LOC125647979	-4.561846244	0.005618594	LOW QUALITY PROTEIN: sperm-associated antigen 16 protein-like
LOC125647987	-4.551501721	0.002136584	ropporin-1-like protein
LOC125647995	-4.551501721	0.002136584	ropporin-1-like protein
LOC125680466	-4.546158445	2.18E-05	uncharacterized protein LOC125680466
LOC125654578	-4.535221126	0.00258592	kinesin-like protein KIF28P
LOC125682074	-4.534298494	0.001253571	glutamine synthetase 2 cytoplasmic-like
LOC125659972	-4.531632013	0.006908982	LOW QUALITY PROTEIN: matrix metalloproteinase-16-like
LOC125651637	-4.527688473	0.004448396	protein dead ringer homolog

USC UNIVERSIDADE DE SANTIAGO DE COMPOSTELA

LOC125659971	-4.526539206	0.000116061	matrix metalloproteinase-16-like isoform X2
LOC125683685	-4.511096163	0.000401112	uncharacterized protein LOC125683685
LOC125673659	-4.497923388	0.001258318	snake venom 5'-nucleotidase-like isoform X1
LOC125650509	-4.481837053	9.56E-05	--
LOC125669700	-4.474792472	0.000239644	cadherin-87A-like
LOC125654740	-4.469557361	6.84E-08	gelsolin-like protein 2
LOC125652738	-4.438131729	0.000362185	radial spoke head protein 9 homolog isoform X2
LOC125658822	-4.424666035	3.99E-05	VPS10 domain-containing receptor SorCS1-like isoform X2
LOC125674237	-4.40797437	5.41E-05	threonylcarbamoyl-AMP synthase-like
LOC125675354	-4.40797437	5.41E-05	threonylcarbamoyl-AMP synthase-like
LOC125678751	-4.377266115	0.000484683	tetraspanin-9-like
LOC125659453	-4.359443748	0.00028486	ryncolin-4-like
LOC125671219	-4.357567846	0.000560558	dynein intermediate chain 3%2C ciliary-like isoform X2
LOC125669794	-4.349318371	0.000367226	uncharacterized protein LOC125669794
LOC125678666	-4.337458219	9.18E-06	tumor necrosis factor receptor superfamily member 10B-like
LOC125674188	-4.290302051	3.89E-05	uncharacterized protein LOC125674188 isoform X1
LOC125650172	-4.286590616	0.000166563	ceramide glucosyltransferase-like isoform X1
LOC125648850	-4.283104245	0.001767965	potassium channel subfamily K member 2-like
LOC125669397	-4.282309193	0.007350942	--
LOC125683616	-4.267096429	1.96E-11	buccalin-like
LOC125673014	-4.263912421	0.000832195	uncharacterized protein LOC125673014 isoform X2
LOC125665221	-4.262079404	0.000422356	D-3-phosphoglycerate dehydrogenase-like
LOC125673995	-4.241018168	0.000685599	uncharacterized protein LOC125673995
LOC125656190	-4.21754712	1.19E-07	protein sll1483-like
LOC125679884	-4.208434535	0.004289723	uncharacterized protein LOC125679884
LOC125649530	-4.203910131	0.000207397	uncharacterized protein LOC125649530 isoform X1
LOC125650768	-4.203704904	0.000576003	uncharacterized protein LOC125650768
LOC125680549	-4.202989826	5.29E-05	ankyrin repeat domain-containing protein 50-like
LOC125672007	-4.200770955	0.003352477	uncharacterized protein LOC125672007
LOC125681628	-4.200353793	3.63E-05	uncharacterized protein LOC125681628
LOC125663912	-4.200078901	2.90E-05	large neutral amino acids transporter small subunit 1-like
LOC125658736	-4.193786293	0.001776873	--
LOC125671901	-4.193375626	0.004837135	uncharacterized protein LOC125671901
LOC125682586	-4.176378357	0.001901748	inositol-trisphosphate 3-kinase homolog
LOC125654732	-4.173205255	0.001683419	uncharacterized protein LOC125654732
LOC125653613	-4.169148121	1.24E-05	dynein regulatory complex protein 11-like isoform X2
LOC125675870	-4.16304911	0.001293729	uncharacterized protein LOC125675870
LOC125658158	-4.158300379	0.002360644	uncharacterized protein C5orf49 homolog isoform X2
LOC125674714	-4.151772192	0.002825228	WW domain-containing oxidoreductase-like
LOC125658777	-4.151357111	0.000533057	uncharacterized protein LOC125658777 isoform X1
LOC125661370	-4.148447603	0.005802915	uncharacterized protein LOC125661370
LOC125675903	-4.139520609	0.002596317	--
LOC125649910	-4.133030007	0.000208396	cilia- and flagella-associated protein 36-like
LOC125660019	-4.131700267	7.10E-05	LOW QUALITY PROTEIN: protein O-mannosyl-transferase TMTC4-like
LOC125659763	-4.121554146	0.001923051	tripartite motif-containing protein 2-like
LOC125649607	-4.119965606	0.00721756	uncharacterized protein LOC125649607 isoform X3
LOC125683110	-4.096517338	0.002188199	uncharacterized protein LOC125683110
LOC125682231	-4.096088657	0.000838857	protein Flattop homolog
LOC125647661	-4.08686049	3.08E-05	pyridoxal 5'-phosphate synthase subunit PdxS-like
LOC125659762	-4.083352737	0.000835339	E3 ubiquitin-protein ligase TRIM71-like
LOC125663611	-4.080087858	5.51E-05	uncharacterized protein LOC125663611 isoform X2

USC UNIVERSIDADE DE SANTIAGO DE COMPOSTELA

LOC125656130	-4.029820026	0.000312353	uncharacterized protein LOC125656130 isoform X2
LOC125658432	-4.020125238	0.001517447	--
LOC125670713	-4.006896719	0.001115917	uncharacterized protein LOC125670713
LOC125668621	-3.98969974	0.000332915	uncharacterized protein LOC125668621
LOC125655217	-3.983488468	0.004797657	uncharacterized protein LOC125655217
LOC125666705	-3.970025751	7.28E-05	tubulin alpha-1A chain
LOC125645774	-3.96461075	0.00083652	uncharacterized protein LOC125645774 isoform X1
LOC125677957	-3.961952315	0.002915656	uncharacterized protein LOC125677957
LOC125680306	-3.93717999	0.000279718	transmembrane protein 145-like
LOC125657496	-3.916144385	0.001159928	sperm flagellar protein 1-like isoform X8
LOC125645895	-3.89871562	0.000110896	uncharacterized protein LOC125645895
LOC125666792	-3.887816108	0.000742251	cytochrome P450 3A4-like isoform X1
LOC125679668	-3.887531101	0.000685853	fibroblast growth factor receptor 2-like isoform X4
LOC125668518	-3.885083947	0.000622038	uncharacterized protein LOC125668518
LOC125669870	-3.879470756	0.000348385	dynein axonemal intermediate chain 4-like isoform X3
LOC125671784	-3.879343147	0.001055226	transmembrane protein 178B-like
LOC125673758	-3.877597994	0.003088554	androglobin-like isoform X5
LOC125670244	-3.876846235	0.000209483	uncharacterized protein LOC125670244 isoform X4
LOC125670593	-3.855970889	0.000299984	guanine nucleotide-binding protein G(o) subunit alpha-like
LOC125646264	-3.855537455	0.000382984	ETS-related transcription factor Elf-3-like isoform X3
LOC125674304	-3.848795002	0.005501824	oncoprotein-induced transcript 3 protein-like
LOC125654085	-3.846191738	0.003392145	calcium-activated chloride channel regulator 1-like isoform X1
LOC125668324	-3.842456302	0.002319934	sodium-coupled monocarboxylate transporter 1-like
LOC125654789	-3.829074862	0.000337929	uncharacterized protein C12orf56-like isoform X1
LOC125675636	-3.827549036	0.000303251	steroid 17-alpha-hydroxylase/17%2C20 lyase-like
LOC125655067	-3.822990625	0.000705802	uncharacterized protein LOC125655067
LOC125645885	-3.810942456	0.006258965	33 kDa inner dynein arm light chain%2C axonemal-like
LOC125650750	-3.803544176	0.000723585	basic leucine zipper transcriptional factor ATF-like 3
LOC125676659	-3.789814473	0.000220215	OTU domain-containing protein 3-like
LOC125675019	-3.783833544	0.00024363	protein MFI-like isoform X2
LOC125650288	-3.782523362	1.61E-07	methionine synthase-like isoform X2
LOC125671272	-3.772492844	0.00084606	uncharacterized protein LOC125671272
LOC125654161	-3.772270928	0.002525788	uncharacterized protein LOC125654161
LOC125672893	-3.767158189	0.001917128	--
LOC125674963	-3.757930818	1.04E-05	uncharacterized protein LOC125674963 isoform X5
LOC125665556	-3.743072717	0.001747	parathyroid hormone/parathyroid hormone-related peptide receptor-like isoform X1
LOC125680913	-3.736582659	0.000445703	uncharacterized protein LOC125680913 isoform X1
LOC125671791	-3.728986361	0.005351885	uncharacterized protein LOC125671791
LOC125679349	-3.707717438	0.004016322	cilia- and flagella-associated protein 157-like
LOC125677043	-3.705605908	0.006722067	complement C1q tumor necrosis factor-related protein 2-like
LOC125674691	-3.695385348	0.000729765	coiled-coil domain-containing protein 81-like isoform X2
LOC125679265	-3.673448302	0.002272623	innexin unc-9-like isoform X2
LOC125670249	-3.663539616	0.003118871	sperm-tail PG-rich repeat-containing protein 2-like
LOC125655701	-3.643428979	0.005864853	--
LOC125668023	-3.619402847	0.000100704	--
LOC125648739	-3.615743883	0.002388176	uncharacterized protein C20orf85-like
LOC125661653	-3.59845793	0.006763274	filamin-C-like
LOC125675772	-3.596980327	0.006373398	uncharacterized WD repeat-containing protein alr3466-like
LOC125680627	-3.590404047	0.00229847	abnormal spindle-like microcephaly-associated protein homolog isoform X4
LOC125651893	-3.572134808	0.003652427	uncharacterized protein LOC125651893
LOC125672132	-3.572099671	0.000131127	intraflagellar transport protein 172 homolog

USC UNIVERSIDADE DE SANTIAGO DE COMPOSTELA

LOC125659535	-3.561355127	0.00084861	cilia- and flagella-associated protein 206-like
LOC125655023	-3.550849679	0.000104629	acetoacetyl-CoA synthetase-like
LOC125670882	-3.537229919	7.34E-05	LITAF domain-containing protein-like
LOC125678257	-3.519023548	0.00037083	TNF receptor-associated factor 2-like
LOC125650697	-3.499501402	0.003887978	protein FAM227B-like isoform X2
LOC125668701	-3.499070103	0.001982464	LOW QUALITY PROTEIN: acyl-CoA desaturase-like
LOC125654303	-3.485910961	0.001617794	neuroglian-like isoform X1
LOC125650564	-3.48218284	0.003104844	limbic system-associated membrane protein-like
LOC125646086	-3.464359647	0.004647571	MAM and LDL-receptor class A domain-containing protein 1-like
LOC125660974	-3.462662823	0.001206297	core-binding factor subunit beta-like isoform X1
LOC125654181	-3.451066193	0.002885853	uncharacterized protein LOC125654181
LOC125650701	-3.441966471	0.00059566	uncharacterized protein LOC125650701
LOC125659199	-3.440941094	0.000645455	serine/threonine-protein kinase 26-like
LOC125675210	-3.43672556	1.03E-09	parkin coregulated gene protein homolog
LOC125659519	-3.435893566	0.000311886	--
LOC125663803	-3.434916757	2.43E-05	uncharacterized protein LOC125663803
LOC125678677	-3.426499198	0.002600835	prostaglandin G/H synthase 2-like
LOC125658175	-3.420231999	7.80E-05	telomerase protein component 1-like
LOC125673209	-3.402515446	0.001109532	ras-related and estrogen-regulated growth inhibitor-like protein
LOC125679018	-3.401980726	0.004465513	LIM and calponin homology domains-containing protein 1-like isoform X3
LOC125648777	-3.396293449	0.000486381	inositol hexakisphosphate kinase 3-like isoform X3
LOC125681167	-3.385004888	0.003773915	CD109 antigen-like isoform X3
LOC125646072	-3.384255288	2.72E-05	rootletin-like isoform X3
LOC125654995	-3.382374944	0.002493213	--
LOC125678695	-3.374884782	0.000282907	protocadherin Fat 1-like isoform X4
LOC125666032	-3.373420862	0.005374453	cilia- and flagella-associated protein 221-like
LOC125663914	-3.36331644	0.000813004	orexin receptor type 2-like
LOC125673814	-3.349317177	9.38E-05	uncharacterized protein LOC125673814 isoform X1
LOC125670747	-3.345243591	0.000556293	coiled-coil domain-containing protein 40-like
LOC125650532	-3.317546514	0.001197558	follistatin-A-like
LOC125676979	-3.316820323	0.001106277	runt-related transcription factor 1-like isoform X3
LOC125667735	-3.315095257	5.70E-06	phosphatidate phosphatase LPIN2-like isoform X1
LOC125675165	-3.311012048	0.000354896	uncharacterized protein LOC125675165 isoform X1
LOC125661887	-3.301130761	1.83E-05	ATP-dependent translocase ABCB1-like isoform X3
LOC125653316	-3.294790686	0.003143639	uncharacterized protein LOC125653316
LOC125650553	-3.293233288	0.001307671	uncharacterized protein LOC125650553 isoform X3
LOC125649218	-3.292878665	0.005338256	uncharacterized protein LOC125649218
LOC125670262	-3.285390682	7.73E-06	protein sidekick-2-like isoform X2
LOC125658848	-3.283516285	0.004791486	--
LOC125664249	-3.282655709	0.007783173	fatty acid-binding protein%2C heart-like
LOC125671205	-3.274742616	0.000170447	serine/threonine-protein kinase PLK1-like
LOC125674120	-3.25882023	0.000989404	LOW QUALITY PROTEIN: tyrosine--tRNA ligase%2C cytoplasmic-like
LOC125645439	-3.254720443	0.004397031	uncharacterized protein LOC125645439 isoform X2
LOC125669289	-3.244136714	0.00149998	F-box only protein 4-like
LOC125672055	-3.243838752	0.007381576	chondroitin sulfate N-acetylgalactosaminyltransferase 1-like
LOC125659703	-3.242578382	0.000256229	methyltransferase-like protein 27 isoform X2
LOC125667898	-3.228449328	9.93E-05	zinc finger protein GLIS3-like
LOC125662405	-3.226885904	0.00223267	uncharacterized protein LOC125662405
LOC125682062	-3.226567422	0.007826909	ATP-dependent RNA helicase DDX39A-like isoform X1
LOC125670679	-3.223042617	0.00311202	ras-related protein Rap-2a-like
LOC125671480	-3.210312212	0.006448979	uncharacterized protein LOC125671480

USC UNIVERSIDADE DE SANTIAGO DE COMPOSTELA

LOC125650792	-3.20325326	0.003351	--
LOC125648881	-3.197277508	0.000795498	--
LOC125667751	-3.196792422	9.92E-06	phosphatidate phosphatase LPIN2-like isoform X1
LOC125658518	-3.194857876	0.005815853	uncharacterized protein CXorf58-like isoform X1
LOC125683673	-3.194715145	0.006630216	uncharacterized protein LOC125683673 isoform X5
LOC125674128	-3.194322257	0.000432939	tubby protein-like isoform X4
LOC125670771	-3.175987347	6.88E-05	CD151 antigen-like
LOC125649775	-3.162946518	0.000525408	serine palmitoyltransferase 2-like
LOC125678813	-3.150196765	0.005799744	retrograde protein of 51 kDa-like isoform X2
LOC125646017	-3.146361394	0.000287228	uncharacterized protein LOC125646017
LOC125679471	-3.12050111	0.000912798	endonuclease V-like
LOC125679472	-3.114892556	0.001452823	cilia- and flagella-associated protein 77-like isoform X2
LOC125653965	-3.110425479	0.000220712	uncharacterized protein LOC125653965 isoform X1
LOC125667425	-3.108550491	0.004993184	E3 ubiquitin-protein ligase MYCBP2-like
LOC125647058	-3.107691495	0.002121858	uncharacterized protein LOC125647058
LOC125677735	-3.105222002	0.003589285	PC3-like endoprotease variant B isoform X1
LOC125668577	-3.100121484	5.68E-05	phospholipid-transporting ATPase ABCA1-like isoform X2
LOC125651838	-3.096014458	0.000838779	bone morphogenetic protein 2-like
LOC125668198	-3.077017312	0.003887286	uncharacterized protein LOC125668198
LOC125647309	-3.062231212	0.003683109	uncharacterized protein LOC125647309
LOC125672352	-3.058773623	0.000890865	uncharacterized protein LOC125672352
LOC125672065	-3.053208079	0.000482342	uncharacterized protein LOC125672065
LOC125649969	-3.043602698	0.000377101	LOW QUALITY PROTEIN: uncharacterized protein LOC125649969
LOC125663650	-3.035033183	0.002099492	uncharacterized protein LOC125663650
LOC125663949	-3.034306324	0.004502465	dynein regulatory complex subunit 2-like
LOC125683598	-3.01215165	2.58E-06	uncharacterized protein LOC125683598 isoform X1
LOC125659747	-3.007424183	0.00780379	sodium/calcium exchanger regulatory protein 1-like isoform X2
LOC125661479	-3.004689431	0.000985564	LOW QUALITY PROTEIN: testis-expressed protein 9-like
LOC125668133	-2.999071469	0.00072146	GTP-binding protein 1-like
LOC125681745	-2.997468213	0.001883234	LOW QUALITY PROTEIN: phosphatidylinositol 4%2C5-bisphosphate 3-kinase catalytic subunit alp like
LOC125682214	-2.986029618	0.003905761	calcium channel flower homolog
LOC125671607	-2.98480421	0.006718627	uncharacterized protein LOC125671607
LOC125652423	-2.974168807	0.000104527	--
LOC125650378	-2.966851092	0.006224434	clathrin heavy chain linker domain-containing protein 1-like
LOC125660390	-2.966563969	0.003989813	coiled-coil domain-containing protein 92-like
LOC125672119	-2.965522259	0.003341007	NAD-dependent protein deacetylase Sirt6-like isoform X2
LOC125680718	-2.964880631	0.005771883	dynein regulatory complex subunit 4-like
LOC125661074	-2.961962686	0.006708572	--
LOC125653750	-2.956472759	0.000120996	protein DD3-3-like isoform X1
LOC125666710	-2.901562231	0.000537494	LOW QUALITY PROTEIN: ATP-dependent translocase ABCB1-like
LOC125678428	-2.897857237	0.000617712	transmembrane protein 79-like
LOC125649470	-2.894357864	0.007202146	katanin p60 ATPase-containing subunit A-like 2 isoform X8
LOC125670216	-2.890082784	0.000760429	CD82 antigen-like isoform X2
LOC125658354	-2.889440022	0.001828347	steroid 17-alpha-hydroxylase/17%2C20 lyase-like
LOC125676996	-2.884944632	0.001194956	UDP-glucuronic acid decarboxylase 1-like isoform X2
LOC125656135	-2.877166398	2.86E-05	uncharacterized protein LOC125656135
LOC125674611	-2.859462499	4.19E-05	hillarin-like isoform X2
LOC125658978	-2.851621874	5.46E-05	cartilage matrix protein-like
LOC125649903	-2.839454309	0.006327424	circularly permutated Ras protein 1-like isoform X1
LOC125665605	-2.839055898	0.00475072	uncharacterized protein LOC125665605
LOC125680760	-2.83789182	0.003852435	proteolipid protein DM beta-like

LOC125679154	-2.837627536	0.002284188	testis-expressed protein 26-like isoform X2
LOC125675777	-2.835064622	0.00205009	uncharacterized protein LOC125675777 isoform X2
LOC125671283	-2.827327113	0.004641103	ADP-ribosylation factor-like protein 4C
LOC125678357	-2.823549604	0.000146721	innexin unc-9-like isoform X2
LOC125673668	-2.822965115	0.001170872	--
LOC125676114	-2.812442925	0.002852574	exportin-4-like
LOC125678056	-2.8103376	0.005950278	tripartite motif-containing protein 45-like
LOC125657220	-2.802905119	0.001129851	cell division cycle protein 123 homolog
LOC125669411	-2.800910554	0.004937627	LOW QUALITY PROTEIN: unconventional myosin-XV-like
LOC125662600	-2.779851661	0.006259297	uncharacterized protein LOC125662600 isoform X1
LOC125667290	-2.778230311	0.00436944	ETS translocation variant 4-like isoform X1
LOC125651557	-2.775943893	0.004154956	neuropilin and tolloid-like protein 1 isoform X2
LOC125678485	-2.773075534	0.001879592	uncharacterized protein LOC125678485 isoform X1
LOC125650244	-2.767539309	0.005088966	LOW QUALITY PROTEIN: 1%2C25-dihydroxyvitamin D(3) 24-hydroxylase%2C mitochondrial-like
LOC125646239	-2.766647452	0.000466581	uncharacterized protein LOC125646239
LOC125656241	-2.760442454	0.004082575	--
LOC125650398	-2.756577405	0.001835804	transmembrane protein 62-like isoform X1
LOC125658454	-2.75420152	0.006282427	--
LOC125650600	-2.733020234	0.003845941	serine/arginine repetitive matrix protein 2-like isoform X3
LOC125667894	-2.732019193	0.000751693	adhesion G protein-coupled receptor L3-like isoform X1
LOC125671559	-2.721680919	0.004856389	SPRY domain-containing SOCS box protein 3-like
LOC125646999	-2.713776573	0.00333413	vesicle-associated membrane protein 8-like
LOC125652204	-2.71000335	0.004347572	--
LOC125658263	-2.70273255	0.000941366	myosin-VIIa-like
LOC125670464	-2.695759395	0.004232268	synaptotagmin-15-like
LOC125678739	-2.693444548	0.002790948	WD repeat-containing protein 19-like
LOC125658638	-2.692152317	0.007144895	--
LOC125659358	-2.691955808	0.006850291	chondroadherin-like
LOC125659481	-2.68422239	2.20E-06	MORN repeat-containing protein 4-like
LOC125682946	-2.676130028	0.000824204	uncharacterized protein LOC125682946
LOC125666711	-2.676112457	0.001833661	tubulin alpha-1A chain-like
LOC125670920	-2.675585464	0.003031927	mpv17-like protein 2
LOC125658759	-2.667609743	0.007307223	protein FAM43A-like
LOC125669817	-2.661361297	0.000815212	AN1-type zinc finger protein 4-like
LOC125663581	-2.659664686	0.000866854	ribosomal protein S6 kinase beta-1-like
LOC125658101	-2.658348981	0.002012812	mid1-interacting protein 1A-like
LOC125675771	-2.646439061	0.00270162	uncharacterized protein LOC125675771 isoform X2
LOC125653312	-2.641443254	0.002990673	uncharacterized protein LOC125653312 isoform X1
LOC125683518	-2.634119707	2.80E-05	armadillo repeat protein deleted in velo-cardio-facial syndrome homolog isoform X4
LOC125645839	-2.631924534	0.000481755	contactin-5-like isoform X3
LOC125665621	-2.613098536	0.005110772	ciliogenesis-associated TTC17-interacting protein-like
LOC125668582	-2.606768004	0.000575851	repetitive organellar protein-like isoform X2
LOC125670040	-2.606203935	0.000607475	PDZ domain-containing protein GIPC1-like
LOC125647744	-2.595245206	0.003244447	--
LOC125662005	-2.591588011	0.007070435	--
LOC125659973	-2.587379348	0.001813975	uncharacterized protein LOC125659973
LOC125658405	-2.575501713	0.003968521	dual specificity protein phosphatase 4-like
LOC125676377	-2.560849639	0.002531684	major vault protein-like
LOC125665783	-2.548972643	0.001359827	secretin receptor-like isoform X4
LOC125677005	-2.532375668	0.002662975	LOW QUALITY PROTEIN: ATP-citrate synthase-like
LOC125645916	-2.511573747	0.001138921	phosphatidate phosphatase LPIN2-like isoform X2

USC UNIVERSIDADE DE SANTIAGO DE COMPOSTELA

LOC125680484	-2.506143821	0.000500137	mitogen-activated protein kinase kinase kinase 13-A-like isoform X1
LOC125674912	-2.502081952	0.001596969	glutamate receptor ionotropic%2C kainate 2-like isoform X1
LOC125657109	-2.500066536	0.000497754	haloacid dehalogenase-like hydrolase domain-containing 5
LOC125664669	-2.486466834	0.000585221	cilia- and flagella-associated protein 299-like
LOC125665220	-2.483008646	0.00061708	--
LOC125673040	-2.474348555	0.002187591	mucin-17-like isoform X2
LOC125674462	-2.46767153	4.23E-05	afadin-like isoform X1
LOC125683863	-2.463187777	0.002470396	glutathione S-transferase omega-1-like
LOC125648950	-2.455717367	0.001378166	selenoprotein N-like isoform X2
LOC125670728	-2.433999233	0.005376151	--
LOC125648977	-2.43036987	0.000532653	phospholipid-transporting ATPase ID-like isoform X1
LOC125682018	-2.424971414	0.005028481	transmembrane protein 41A-like
LOC125671119	-2.420225404	0.004939856	transcription factor SOX-11-like
LOC125669760	-2.409098771	0.004869947	MDS1 and EVI1 complex locus protein EVI1-A-like isoform X2
LOC125661036	-2.408960181	0.003527125	--
LOC125648190	-2.406306449	0.002489636	alanine--tRNA ligase%2C cytoplasmic-like
LOC125668209	-2.405268391	0.005666344	uncharacterized protein LOC125668209
LOC125678206	-2.39999698	0.003007145	advillin-like isoform X1
LOC125647837	-2.397732878	0.005407952	uncharacterized protein LOC125647837
LOC125647011	-2.377312009	1.41E-05	LOW QUALITY PROTEIN: neurexin-4-like
LOC125654720	-2.375341772	1.24E-05	glutathione S-transferase 1-like
LOC125645629	-2.373162619	0.002292706	LOW QUALITY PROTEIN: neural cell adhesion molecule L1-like
LOC125669542	-2.36261675	0.000181201	ATP-binding cassette sub-family A member 9-like isoform X1
LOC125680278	-2.347863291	0.00020616	folylpolyglutamate synthase%2C mitochondrial-like isoform X6
LOC125668463	-2.339928096	0.003117039	protein ecdysoneless homolog
LOC125668612	-2.331751254	0.003595777	--
LOC125656982	-2.314862097	0.001348738	LOW QUALITY PROTEIN: protein prickle-like
LOC125679695	-2.312577098	0.005643017	valine--tRNA ligase-like
LOC125681798	-2.311798803	0.002152895	tubulin-specific chaperone cofactor E-like protein
LOC125667260	-2.30713545	0.005863985	spartin-like
LOC125657999	-2.306661411	0.006170059	lipoma-preferred partner homolog isoform X2
LOC125670436	-2.301440399	0.001968523	uncharacterized protein LOC125670436 isoform X1
LOC125665955	-2.301072302	0.005433316	rho-related GTP-binding protein RhoE-like
LOC125678908	-2.297260969	0.004262229	metallophosphoesterase MPPED2-like
LOC125660093	-2.291893873	0.000765068	kelch-like protein 26 isoform X3
LOC125650425	-2.281399949	0.006435732	ubiquitin-associated protein 1-like isoform X2
LOC125656334	-2.279710606	0.000850952	neural-cadherin-like isoform X4
LOC125660879	-2.277741537	0.004949543	sodium-coupled monocarboxylate transporter 2-like isoform X3
LOC125658816	-2.263590032	0.005433172	--
LOC125670954	-2.251448582	0.003876204	tRNA-dihydrouridine(16/17) synthase [NAD(P)(+)]-like isoform X1
LOC125668291	-2.248948958	0.001370006	--
LOC125666707	-2.240723579	0.004369855	ATP-dependent translocase ABCB1-like isoform X5
LOC125656632	-2.227331713	3.23E-05	serine/threonine-protein kinase TBK1-like
LOC125669515	-2.219304713	0.000680609	tubulin polymerization-promoting protein family member 3-like
LOC125645539	-2.215827678	0.001144388	pyrroline-5-carboxylate reductase 2-like
LOC125651836	-2.200439746	0.002506225	phospholipid scramblase 2-like isoform X2
LOC125665172	-2.199607312	0.005610201	integral membrane protein GPR155-like isoform X5
LOC125670864	-2.199084114	0.002510711	MTOR-associated protein MEAK7-like
LOC125674087	-2.193389748	0.006701552	unconventional myosin-VI-like isoform X1
LOC125671648	-2.185140566	0.007254125	intraflagellar transport protein 52 homolog
LOC125671666	-2.185140566	0.007254125	intraflagellar transport protein 52 homolog

USC UNIVERSIDADE DE SANTIAGO DE COMPOSTELA

LOC125657106	-2.184757845	0.003504662	isoleucine--tRNA ligase%2C cytoplasmic-like isoform X1
LOC125647642	-2.183683578	0.003480314	WD repeat-containing protein 35-like isoform X2
LOC125667916	-2.17622464	0.00343716	prominin-1-like
LOC125665234	-2.173948851	0.001720856	solute carrier family 28 member 3-like isoform X2
LOC125683076	-2.155941476	0.000376395	uncharacterized protein LOC125683076 isoform X4
LOC125679519	-2.15031728	0.003570027	nose resistant to fluoxetine protein 6-like isoform X1
LOC125663721	-2.149053366	0.006180111	uncharacterized protein LOC125663721 isoform X1
LOC125647678	-2.145089354	0.002481736	DAZ-associated protein 2-like
LOC125645447	-2.144294606	0.003240226	uncharacterized protein LOC125645447
LOC125658517	-2.127009983	0.004058816	intraflagellar transport protein 80 homolog
LOC125683065	-2.115802959	0.005637214	nuclear receptor subfamily 1 group D member 2-like
LOC125657499	-2.110038684	0.000290236	uncharacterized protein LOC125657499
LOC125653749	-2.105994722	0.000841842	protein DD3-3-like
LOC125678234	-2.098317342	0.002404971	ETS translocation variant 4-like isoform X3
LOC125673545	-2.083883924	0.001053246	adenosylhomocysteinase A-like
LOC125682767	-2.080202582	0.002045183	serine/threonine-protein kinase H1 homolog
LOC125651484	-2.074688172	2.12E-06	cytochrome P450 2J4-like
LOC125683287	-2.07186991	0.000935777	uncharacterized protein LOC125683287
LOC125659917	-2.07001378	0.002297626	uncharacterized protein LOC125659917
LOC125678632	-2.067582675	0.001071503	advanced glycosylation end product-specific receptor-like isoform X1
LOC125675094	-2.062116113	0.001643005	innexin-11-like
LOC125678128	-2.058687583	0.003024776	poly [ADP-ribose] polymerase tankyrase-1-like
LOC125677553	-2.055925297	0.000850325	death-associated inhibitor of apoptosis 2-like
LOC125657971	-2.045772347	0.005149136	catenin alpha-2-like isoform X1
LOC125656514	-2.043143891	0.003690974	metallothionein-like
LOC125660494	-2.036739364	0.000913789	probable JmjC domain-containing histone demethylation protein 2C isoform X4
LOC125672122	-2.023146575	0.005605916	enkurin domain-containing protein 1-like
LOC125664286	-2.022384626	0.002140083	ADP-ribose pyrophosphatase%2C mitochondrial-like isoform X1
LOC125678360	-2.019924	6.60E-07	innexin unc-9-like
LOC125683670	-2.014583443	0.004793073	programmed cell death 6-interacting protein-like isoform X2
LOC125647936	-2.012870794	0.001428184	protein LKAAEAR1-like
LOC125663964	-1.995483176	0.005313112	uncharacterized protein LOC125663964
LOC125646279	-1.986302162	0.005580372	centriolar satellite-associated tubulin polyglutamylase complex regulator 1-like isoform X1
LOC125671635	-1.981133199	0.003780449	salivary acidic proline-rich phosphoprotein 1/2-like
LOC125650290	-1.977235374	0.005198715	neuronal PAS domain-containing protein 4-like isoform X2
LOC125680770	-1.971454906	0.003532775	transmembrane protein 165-like
LOC125666778	-1.969109641	0.001996906	sterol O-acyltransferase 1-like
LOC125682528	-1.964879743	0.002129003	protein crumbs-like isoform X3
LOC125668535	-1.959840461	0.003727267	elongation of very long chain fatty acids protein 6-like
LOC125680555	-1.948099554	0.000524006	LOW QUALITY PROTEIN: dynein axonemal heavy chain 5-like
LOC125674126	-1.935157134	0.004836288	LOW QUALITY PROTEIN: acetyl-CoA carboxylase-like
LOC125675886	-1.927886465	0.001277157	--
LOC125649846	-1.923440084	0.004552679	band 4.1-like protein 1 isoform X2
LOC125675697	-1.90904062	0.005290082	--
LOC125678371	-1.903828826	0.000199836	choline transporter-like protein 2 isoform X3
LOC125648951	-1.903325253	0.005645245	GTP-binding protein 2-like
LOC125680402	-1.890373868	0.005631888	dolichyl-phosphate beta-glucosyltransferase-like isoform X3
LOC125677980	-1.888135356	0.002191626	serine/threonine-protein kinase NLK-like isoform X2
LOC125649952	-1.886778499	0.006582906	uncharacterized protein LOC125649952 isoform X2
LOC125660883	-1.884212471	0.004181621	uncharacterized protein LOC125660883 isoform X2
LOC125669594	-1.874292704	0.001634425	inositol hexakisphosphate kinase 1-like

USC UNIVERSIDADE DE SANTIAGO DE COMPOSTELA

LOC125654836	-1.867947356	0.007230113	LHFPL tetraspan subfamily member 3 protein-like isoform X2
LOC125667164	-1.864554957	0.000191365	uncharacterized protein LOC125667164
LOC125673287	-1.854197971	6.44E-10	uncharacterized protein LOC125673287
LOC125660924	-1.838033426	0.001491176	ras-responsive element-binding protein 1-like isoform X1
LOC125676497	-1.835591294	0.005062071	prolyl 4-hydroxylase subunit alpha-1-like
LOC125658682	-1.833027667	0.000980576	peroxisome proliferator-activated receptor gamma coactivator 1-alpha-like
LOC125670435	-1.809023134	0.006881746	uncharacterized protein LOC125670435
LOC125647727	-1.789844208	0.005887967	uncharacterized protein LOC125647727
LOC125669693	-1.783379468	5.54E-06	serine hydroxymethyltransferase-like
LOC125663648	-1.782131248	0.000161265	uncharacterized protein LOC125663648
LOC125658506	-1.771438071	0.002115442	cAMP-dependent protein kinase catalytic subunit 3-like
LOC125649177	-1.763374518	0.001670704	perilipin-2-like isoform X2
LOC125678207	-1.76114958	0.003440769	dnaJ homolog subfamily C member 7-like
LOC125663620	-1.756578762	0.003814379	serine/threonine-protein kinase ULK2-like isoform X1
LOC125654313	-1.746829988	0.006452284	sulfate transporter-like isoform X3
LOC125662772	-1.742685337	0.005339762	ras-related protein Rab-11A isoform X2
LOC125678474	-1.736801041	0.006333285	LOW QUALITY PROTEIN: cyclin-dependent kinase 9-like
LOC125653655	-1.736468889	0.004128257	testin-like isoform X2
LOC125645849	-1.704456979	0.004841418	LITAF domain-containing protein-like
LOC125661177	-1.700678639	0.007589538	AN1-type zinc finger protein 6-like
LOC125680282	-1.69397743	0.003128054	--
LOC125650346	-1.69235814	0.005076419	LOW QUALITY PROTEIN: bifunctional glutamate/proline--tRNA ligase-like
LOC125683245	-1.687767884	0.002934986	ras-related protein Rab-20-like
LOC125669664	-1.683462882	0.000286212	uncharacterized protein LOC125669664
LOC125673981	-1.674069366	0.000162629	LOW QUALITY PROTEIN: serine/threonine-protein kinase LATS1-like
LOC125683004	-1.672403508	0.003043057	uncharacterized protein LOC125683004 isoform X1
LOC125658078	-1.669524551	0.003059245	melanotransferrin-like
LOC125646853	-1.656332398	0.007733281	--
LOC125671319	-1.647918584	0.006539616	testican-1-like
LOC125646119	-1.647257143	0.007573112	multidrug resistance-associated protein 1-like
LOC125668247	-1.636927143	2.22E-08	uncharacterized protein LOC125668247 isoform X1
LOC125658062	-1.636770656	0.003300275	spermine oxidase-like
LOC125659347	-1.633720071	5.59E-05	--
LOC125668691	-1.632177083	0.000248363	titin-like
LOC125652091	-1.626982649	0.000490553	glutathionyl-hydroquinone reductase YqjG-like isoform X1
LOC125669872	-1.620799864	0.000194392	mesoderm induction early response protein 1-like isoform X3
LOC125646695	-1.617467654	0.001850606	sodium/potassium-transporting ATPase subunit beta-1-interacting protein 3-like isoform X2
LOC125645893	-1.615363497	0.002848267	nuclear factor erythroid 2-related factor 2-like isoform X2
LOC125679009	-1.612237706	0.00186714	protocadherin beta-15-like
LOC125657118	-1.610739611	0.002417993	MAP kinase-activated protein kinase 2-like isoform X2
LOC125648926	-1.610107691	0.000301772	uncharacterized protein LOC125648926
LOC125669268	-1.597898954	0.001638933	S-adenosylmethionine synthase-like
LOC125678905	-1.581223724	0.006413181	leucine-rich repeat-containing protein 58-like
LOC125675880	-1.571936625	0.006365403	uncharacterized protein LOC125675880 isoform X4
LOC125653402	-1.570770475	0.004006947	OTU domain-containing protein 5-B-like
LOC125671665	-1.562289031	0.002884171	serine/threonine-protein kinase Sgk1-like isoform X2
LOC125669698	-1.557541819	0.005344454	receptor-type tyrosine-protein phosphatase kappa-like
LOC125664020	-1.555140562	0.000252829	uncharacterized protein C1orf50 homolog
LOC125681829	-1.550243942	0.001546854	calsyntenin-1-like
LOC125683593	-1.534233195	0.001203605	uncharacterized protein LOC125683593
LOC125657253	-1.52949878	0.004874395	protein kinase C delta type-like isoform X3

USC UNIVERSIDADE DE SANTIAGO DE COMPOSTELA

LOC125649281	-1.526785788	0.002243565	estrogen receptor beta-like
LOC125668355	-1.518549197	0.003311923	glutamine--fructose-6-phosphate aminotransferase [isomerizing] 1-like isoform X11
LOC125662386	-1.513366035	0.007304586	dymeclin-like
LOC125680401	-1.511957466	0.00700173	PGAP2-interacting protein-like isoform X1
LOC125669973	-1.510520268	0.002822725	transmembrane protein 184B-like
LOC125677729	-1.508141575	0.001635089	carnitine O-palmitoyltransferase 1%2C liver isoform-like isoform X4
LOC125658418	-1.503080361	0.003684245	phospholipase DDHD2-like
LOC125681929	-1.500041129	0.007675304	upstream stimulatory factor 2-like isoform X1
LOC125652289	-1.498777796	0.000202441	uncharacterized protein LOC125652289
LOC125669790	-1.49445604	0.005061234	histone H3.3A
LOC125678358	-1.489449351	1.32E-05	innexin unc-9-like
LOC125670024	-1.484555768	0.005423303	TNF receptor-associated factor 4-like isoform X3
LOC125683306	-1.479809456	0.002278112	SWI/SNF complex subunit SMARCC2-like isoform X2
LOC125654582	-1.472829077	0.005384968	helicase ARIP4-like
LOC125679204	-1.40368077	0.00492796	next to BRCA1 gene 1 protein-like isoform X2
LOC125678271	-1.38775618	0.000330538	copper-transporting ATPase 1-like isoform X3
LOC125649343	-1.382579746	0.001043947	carnitine O-palmitoyltransferase 1%2C liver isoform-like isoform X3
LOC125658927	-1.37130535	0.002934352	LOW QUALITY PROTEIN: tetraspanin-33-like
LOC125650286	-1.360626634	0.000619826	serine-rich adhesin for platelets-like isoform X6
LOC125673484	-1.35998027	0.000666405	uncharacterized protein DDB_G0284459-like isoform X1
LOC125652825	-1.353779916	0.003865754	TOG array regulator of axonemal microtubules protein 1-like isoform X4
LOC125666892	-1.349843527	0.00276675	caspase-3-like isoform X2
LOC125665804	-1.344204402	0.007690816	interferon alpha-inducible protein 27-like protein 2B
LOC125669663	-1.343190874	0.001202754	uncharacterized protein LOC125669663
LOC125651659	-1.33784537	0.002583562	E3 ubiquitin-protein ligase synoviolin-like
LOC125660869	-1.31527276	0.004206777	uncharacterized protein LOC125660869 isoform X4
LOC125648040	-1.309697761	0.001128949	heme transporter hrg1-B-like isoform X2
LOC125668529	-1.301105243	0.002971327	LOW QUALITY PROTEIN: serine hydroxymethyltransferase-like
LOC125682331	-1.28907368	0.003487579	band 7 protein AGAP004871-like isoform X2
LOC125668033	-1.283039787	0.003904542	serine/threonine-protein kinase/endoribonuclease IRE1-like
LOC125653521	-1.254149947	0.00187991	E3 ubiquitin-protein ligase HUWE1-like isoform X5
LOC125650522	-1.252443806	0.005670464	serine incorporator 5-like
LOC125683095	-1.217762346	0.002173158	V-type proton ATPase 116 kDa subunit a 1-like isoform X2
LOC125647677	-1.191889719	0.00178893	uncharacterized protein LOC125647677
LOC125683089	-1.177640608	0.001903779	myelin regulatory factor-like protein isoform X9
LOC125681974	-1.160623501	0.002939497	E3 ubiquitin-protein ligase AMFR-like
LOC125679136	-1.154455065	0.000287109	high affinity copper uptake protein 1-like isoform X5
LOC125678525	-1.152665045	0.000316162	disco-interacting protein 2 homolog C-like isoform X11
LOC125683479	-1.146367765	0.006700041	oxysterol-binding protein-related protein 11-like isoform X2
LOC125654580	-1.120917995	0.001147407	host cell factor 2-like isoform X3
LOC125657052	-1.117951406	0.007289765	tripartite motif-containing protein 45-like
LOC125664421	-1.090227188	0.006465673	vigilin-like
LOC125653661	-1.071446914	0.005031218	--
LOC125670981	-1.057282521	0.006003374	TOM1-like protein 2 isoform X1
LOC125671472	-1.044421724	0.003947989	store-operated calcium entry-associated regulatory factor-like
LOC125656827	-1.029667539	0.001529507	phosphatidylinositol transfer protein alpha isoform-like
LOC125649467	-0.999602997	0.007403263	ras guanyl-releasing protein 3-like isoform X4
LOC125662530	-0.962567549	0.003659442	--
LOC125682360	-0.917935686	0.004576498	Krueppel-like factor 8 isoform X1
LOC125659657	-0.906036067	0.004295899	ceramide glucosyltransferase-like
LOC125683707	-0.901709594	0.002815848	glutathione S-transferase A-like

USC UNIVERSIDADE DE SANTIAGO DE COMPOSTELA

LOC125646712	-0.898493103	0.00769638	chromodomain-helicase-DNA-binding protein Mi-2 homolog isoform X8
LOC125679459	-0.771451606	0.00378824	cyclin-I-like
LOC125663580	-0.738393805	0.00760078	eIF-2-alpha kinase activator GCN1-like
LOC125670560	0.797114513	0.002182898	cytochrome c oxidase subunit 5B%2C mitochondrial-like
LOC125655615	0.847271834	0.004507568	dihydrolipoyl dehydrogenase%2C mitochondrial-like isoform X1
LOC125668312	0.869300022	0.007309545	putative ATP synthase subunit f%2C mitochondrial
LOC125657875	0.879997738	0.006237979	alpha-centractin
LOC125647476	0.957400552	0.002195028	LOW QUALITY PROTEIN: signal transducer and activator of transcription 5B-like
LOC125664142	0.974132165	0.004667927	39S ribosomal protein L51%2C mitochondrial-like
LOC125645672	1.045235969	0.003924463	multiple epidermal growth factor-like domains protein 11
LOC125672062	1.094836809	0.000722779	glyceraldehyde-3-phosphate dehydrogenase-like
LOC125646216	1.099483903	0.000102512	NADH dehydrogenase [ubiquinone] 1 alpha subcomplex subunit 9%2C mitochondrial-like
LOC125683238	1.099971607	0.003710773	uncharacterized protein LOC125683238
LOC125661097	1.11810656	0.001251733	techylectin-5B-like
LOC125657651	1.138866437	0.00114301	--
LOC125652710	1.139504093	0.007751164	alpha-actinin-like isoform X1
LOC125681577	1.140631891	0.002310184	uncharacterized protein LOC125681577
LOC125657566	1.143645947	0.001073619	probable phosphoglycerate mutase
LOC125654419	1.16886868	0.004218086	macrophage-expressed gene 1 protein-like
LOC125664181	1.2147623	0.001797608	uncharacterized protein LOC125664181
LOC125682100	1.231568451	0.006392988	aquaporin AQPAn.G-like
LOC125657219	1.264016842	0.000651638	mitogen-activated protein kinase 14-like isoform X2
LOC125683084	1.277768719	0.005094702	uncharacterized protein LOC125683084
LOC125659158	1.28173102	0.000361495	succinate--CoA ligase [ADP-forming] subunit beta%2C mitochondrial-like
LOC125674341	1.286507578	0.001818664	toxin CfTX-A-like
LOC125677451	1.296265896	0.001618789	2-oxoisovalerate dehydrogenase subunit beta%2C mitochondrial-like
LOC125683606	1.31034006	0.000454468	bombesin receptor subtype-3-like
LOC125678221	1.32868673	0.000101598	EF-hand domain-containing protein D2-like
LOC125660464	1.328718934	0.000504735	--
LOC125669567	1.334052344	0.004149497	39S ribosomal protein L13%2C mitochondrial-like
LOC125673387	1.337295124	0.004063858	major egg antigen-like
LOC125653261	1.353423905	0.004267333	universal stress protein YxiE-like isoform X1
LOC125657735	1.384474286	0.003644035	uncharacterized protein LOC125657735
LOC125681684	1.396002029	0.006285155	glycosaminoglycan xylosylkinase-like
LOC125676170	1.40181678	0.007358701	uncharacterized protein LOC125676170 isoform X2
LOC125671497	1.405031073	0.005635094	inactive pancreatic lipase-related protein 1-like isoform X1
LOC125659568	1.415841552	0.002763862	emopamil-binding protein-like
LOC125682916	1.416738629	0.00604403	microtubule-associated protein futsch-like
LOC125658758	1.425240402	0.000230365	antiviral innate immune response receptor RIG-I-like isoform X1
LOC125675631	1.430291725	0.00712723	glutamate receptor ionotropic%2C kainate 2-like
LOC125672339	1.457808609	0.007048387	prostaglandin E2 receptor EP4 subtype-like
LOC125657114	1.477056065	0.007365786	isocitrate dehydrogenase [NAD] subunit gamma%2C mitochondrial-like isoform X2
LOC125671561	1.480130286	0.002509687	inactive tyrosine-protein kinase transmembrane receptor ROR1-like isoform X3
LOC125667022	1.496400253	0.001126337	aspartate aminotransferase%2C mitochondrial-like
LOC125669625	1.515593655	0.00030811	LOW QUALITY PROTEIN: ras-GEF domain-containing family member 1B-like
LOC125651999	1.517423092	0.005762696	peptidyl-prolyl cis-trans isomerase B-like
LOC125647595	1.518169179	0.003177855	uncharacterized protein LOC125647595
LOC125679602	1.518170874	0.006403349	uncharacterized protein LOC125679602
LOC125663675	1.518626947	0.000147262	tripartite motif-containing protein 5-like
LOC125649806	1.525734369	9.31E-05	probable methylmalonate-semialdehyde dehydrogenase [acylating]%2C mitochondrial
LOC125664174	1.529791846	0.000487931	--

USC UNIVERSIDADE DE SANTIAGO DE COMPOSTELA

LOC125680107	1.54011843	0.001738547	plancitoxin-1-like
LOC125672605	1.544472746	0.002250103	cytochrome c oxidase subunit 6A2%2C mitochondrial-like
LOC125674388	1.54851794	0.004479078	mitochondrial 2-oxoglutarate/malate carrier protein-like
LOC125674955	1.554282683	0.002873684	allograft inflammatory factor 1-like
LOC125674823	1.558561492	0.000108633	fructose-bisphosphate aldolase-like
LOC125655836	1.573418549	0.000746663	insulin-like growth factor-binding protein 2-B
LOC125649210	1.583076077	0.000883339	tropomyosin isoform X16
LOC125681016	1.591480829	0.002739225	--
LOC125672191	1.593500769	0.000257614	C3a anaphylatoxin chemotactic receptor-like
LOC125650843	1.595420992	0.000296979	uncharacterized protein LOC125650843
LOC125682999	1.598881464	0.001046168	glucose-6-phosphate isomerase-like
LOC125674964	1.634586797	0.000727706	coactosin-like protein
LOC125646125	1.634996989	0.004625323	complement component 1 Q subcomponent-binding protein%2C mitochondrial-like
LOC125683199	1.639477977	0.000498597	deoxyribonuclease-1-like isoform X2
LOC125657542	1.641202249	0.001493717	homeobox protein Nkx-2.5-like
LOC125652728	1.664494822	0.001143748	ribonuclease Oy-like
LOC125679399	1.693189145	0.005512697	vacuolar protein-sorting-associated protein 25-like
LOC125649412	1.696311933	3.51E-05	uncharacterized protein LOC125649412
LOC125654420	1.749603669	0.006055666	--
LOC125677070	1.767513252	0.000497081	interferon alpha-inducible protein 27-like protein 2B isoform X1
LOC125650387	1.781277016	0.002665962	zwei Ig domain protein zig-8-like
LOC125661365	1.800208393	3.43E-05	multiple epidermal growth factor-like domains protein 10 isoform X3
LOC125653770	1.817394134	0.000990811	LOW QUALITY PROTEIN: hepatocyte growth factor receptor-like
LOC125675550	1.827742905	0.004475522	uncharacterized protein LOC125675550 isoform X2
LOC125672363	1.843009083	0.007821254	uncharacterized protein LOC125672363 isoform X1
LOC125669744	1.85551685	0.000552196	uncharacterized protein LOC125669744
LOC125678595	1.863469824	0.00253169	actin%2C adductor muscle
LOC125679372	1.864141338	0.003439193	paramyosin-like isoform X1
LOC125681570	1.871262996	0.000331304	glycerophosphocholine cholinephosphodiesterase ENPP6-like isoform X1
LOC125678926	1.872077893	0.000887685	pantetheinase-like
LOC125669719	1.889657125	8.34E-05	uncharacterized protein LOC125669719
LOC125667559	1.909626433	0.007658568	uncharacterized protein LOC125667559
LOC125647196	1.933283576	0.007050661	low-density lipoprotein receptor-related protein 6-like
LOC125669291	1.941190553	0.000548736	endonuclease G%2C mitochondrial-like
LOC125682061	1.950955196	0.001895569	zinc finger protein 345-like
LOC125652053	1.954924309	0.006492062	DNA replication licensing factor mcm5-A-like
LOC125654839	1.972239665	0.000477039	protein NipSnap-like isoform X1
LOC125650004	1.980144232	5.75E-05	uncharacterized protein LOC125650004
LOC125670619	1.982991369	0.003154935	proliferating cell nuclear antigen-like
LOC125678559	1.988386608	0.001824066	LOW QUALITY PROTEIN: low-density lipoprotein receptor-related protein 4-like
LOC125650529	2.001621635	0.004254187	uncharacterized protein LOC125650529 isoform X3
LOC125652127	2.007282707	0.000417426	uncharacterized protein LOC125652127 isoform X5
LOC125663577	2.022802456	0.000892992	triosephosphate isomerase-like
LOC125665155	2.031797025	0.005061152	uncharacterized protein LOC125665155
LOC125658976	2.041363098	0.00028422	transmembrane protein 256 homolog
LOC125679365	2.047229305	0.000125269	phosphoglycerate kinase-like isoform X1
LOC125678163	2.051219498	0.002346733	matrilin-2-like isoform X1
LOC125667513	2.061808694	0.000885162	corepressor interacting with RBPJ 1-like
LOC125655262	2.062786316	0.001452537	uncharacterized protein LOC125655262
LOC125677498	2.077094682	0.004059833	E3 ubiquitin-protein ligase TRIM36-like isoform X1
LOC125683106	2.077733686	0.000809114	myosin regulatory light chain 12A-like

USC UNIVERSIDADE DE SANTIAGO DE COMPOSTELA

LOC125645440	2.09374939	0.003262652	uncharacterized protein LOC125645440
LOC125655997	2.094499766	0.003483896	calcium-transporting ATPase sarcoplasmic/endoplasmic reticulum type-like isoform X3
LOC125665828	2.104741804	0.000960147	RING finger protein nhl-1-like
LOC125678925	2.135599536	0.002232664	uncharacterized protein LOC125678925 isoform X2
LOC125650773	2.146614599	3.66E-05	uncharacterized protein LOC125650773 isoform X2
LOC125678231	2.147037133	0.002760623	innexin unc-9-like isoform X1
LOC125680249	2.151282524	0.002085796	14 kDa phosphohistidine phosphatase-like
LOC125648412	2.15212427	0.000135917	glycogen-binding subunit 76A-like
LOC125657692	2.156239511	0.001343125	arylacetamide deacetylase-like isoform X3
LOC125671873	2.159740433	0.007186754	chromatin assembly factor 1 subunit A-like
LOC125653992	2.171707782	0.006138432	uncharacterized protein LOC125653992 isoform X1
LOC125659712	2.192021101	6.56E-06	dual oxidase maturation factor 1-like
LOC125682010	2.200283726	0.001813982	16 kDa calcium-binding protein-like
LOC125646877	2.204375331	0.003383791	uncharacterized protein LOC125646877 isoform X2
LOC125667602	2.235295466	0.000789798	frizzled-5-like
LOC125655229	2.236529534	8.49E-05	uncharacterized protein LOC125655229 isoform X1
LOC125663985	2.243338595	0.000161212	uncharacterized protein LOC125663985 isoform X4
LOC125674025	2.266981645	0.007303855	uncharacterized protein LOC125674025
LOC125671396	2.285167854	0.005582206	T-cell acute lymphocytic leukemia protein 1-like
LOC125649465	2.293149724	0.005504902	inactive tyrosine-protein kinase 7-like
LOC125674478	2.299990683	0.001205547	allograft inflammatory factor 1-like
LOC125677612	2.302843867	0.001846081	multiple epidermal growth factor-like domains protein 11 isoform X4
LOC125668589	2.315625771	0.003698874	sarcoplasmic calcium-binding protein-like
LOC125663018	2.324996335	0.005026094	uncharacterized protein LOC125663018
LOC125652101	2.327356587	8.07E-06	uncharacterized protein LOC125652101
LOC125666260	2.346700343	0.001332289	kinetochore protein Spc25-like
LOC125683059	2.35494018	0.000448916	fatty acid-binding protein Fh15-like isoform X1
LOC125678504	2.357276914	1.02E-06	--
LOC125658767	2.365454052	0.001065158	propionyl-CoA carboxylase alpha chain%2C mitochondrial-like isoform X3
LOC125664510	2.366061175	0.000189053	carbonic anhydrase 7-like isoform X1
LOC125675565	2.390053418	0.000119807	secretin receptor-like
LOC125670955	2.390794006	0.004105517	uncharacterized protein LOC125670955 isoform X7
LOC125650876	2.396034658	0.002285674	uncharacterized protein LOC125650876
LOC125658044	2.405441035	0.001950609	ankyrin-1-like isoform X1
LOC125678437	2.410522121	0.005482424	serine/threonine-protein kinase Chk1-like isoform X2
LOC125646886	2.430259216	0.000749933	rac guanine nucleotide exchange factor B-like isoform X2
LOC125683373	2.438899108	0.001346793	uncharacterized protein LOC125683373 isoform X7
LOC125652524	2.440087576	0.000612078	uncharacterized protein LOC125652524 isoform X1
LOC125670258	2.446420843	0.000399569	angiopoietin-1 receptor-like
LOC125676515	2.463452725	9.02E-05	uncharacterized protein LOC125676515
LOC125665930	2.468780809	4.87E-06	glycine cleavage system H protein-like
LOC125673350	2.480017887	0.005877947	GTP-binding protein REM 1-like
LOC125668663	2.482818814	0.002684744	voltage-dependent T-type calcium channel subunit alpha-1H-like isoform X4
LOC125671566	2.493530361	0.000104023	uncharacterized protein LOC125671566
LOC125680686	2.522089984	3.81E-05	tetraspanin-18-like
LOC125648496	2.54873954	0.003776807	myosin-9-like
LOC125647490	2.549860913	0.002385533	uncharacterized protein LOC125647490
LOC125650437	2.557376133	0.000220413	placenta-specific gene 8 protein-like
LOC125679404	2.557861021	7.17E-05	uncharacterized protein LOC125679404
LOC125666012	2.558874443	0.000314151	uncharacterized protein LOC125666012
LOC125673174	2.585594854	1.61E-05	inhibitor of apoptosis protein-like

USC UNIVERSIDADE DE SANTIAGO DE COMPOSTELA

LOC125654421	2.608766109	0.000440705	dopamine beta-hydroxylase-like
LOC125645804	2.608920292	0.002337328	kinetochore protein NDC80 homolog
LOC125657728	2.616324918	0.002559532	uncharacterized protein LOC125657728 isoform X4
LOC125682001	2.617953839	0.000471334	poly [ADP-ribose] polymerase tankyrase-2-like
LOC125664042	2.620616836	0.002814647	isatin hydrolase-like isoform X1
LOC125668300	2.622057435	0.001089977	troponin C-like isoform X1
LOC125656680	2.627766815	0.003493544	galactose-specific lectin nattectin-like
LOC125650370	2.630163427	8.65E-13	homeobox protein SIX4-like
LOC125646732	2.630879933	0.000354804	3-hydroxyisobutyrate dehydrogenase%2C mitochondrial-like
LOC125645746	2.633998278	0.001873622	alpha-2A adrenergic receptor-like
LOC125659625	2.676162137	0.00091345	2'-deoxynucleoside 5'-phosphate N-hydrolase 1-like
LOC125649271	2.678157495	0.00042608	GTPase IMAP family member 9-like
LOC125658028	2.690810472	5.82E-06	monocarboxylate transporter 13-like
LOC125658074	2.717059972	3.95E-05	myosin regulatory light chain B%2C smooth adductor muscle-like
LOC125664320	2.7330861	9.45E-05	sushi%2C von Willebrand factor type A%2C EGF and pentraxin domain-containing protein 1-like
LOC125653801	2.761451714	0.000325213	ADP-sugar pyrophosphatase-like isoform X1
LOC125646127	2.796430734	0.003146432	uncharacterized protein LOC125646127
LOC125663824	2.814327232	1.62E-06	protein-glutamine gamma-glutamyltransferase K-like isoform X1
LOC125649174	2.823739594	0.000570639	uncharacterized protein LOC125649174 isoform X1
LOC125679812	2.827452348	0.002266698	uncharacterized protein LOC125679812 isoform X1
LOC125666744	2.848377124	0.007632289	--
LOC125670191	2.850191156	0.00121585	very low-density lipoprotein receptor-like isoform X1
LOC125656148	2.893718883	0.005329074	uncharacterized protein LOC125656148
LOC125654961	2.921892642	0.003961656	--
LOC125672003	2.925767094	0.002762482	bone morphogenetic protein 10-like
LOC125678168	2.952763596	0.000116109	uncharacterized protein LOC125678168 isoform X5
LOC125646249	2.955419041	0.000992434	--
LOC125672255	2.974389686	0.000156497	uncharacterized protein LOC125672255 isoform X3
LOC125664524	3.023236311	0.002769976	--
LOC125649398	3.034521874	0.002105989	mucin-5AC-like isoform X1
LOC125658353	3.0401496	0.007000175	steroid 17-alpha-hydroxylase/17%2C20 lyase-like isoform X1
LOC125679696	3.068646671	0.004247292	complement C1q tumor necrosis factor-related protein 7-like
LOC125658184	3.06880722	0.00147416	demethylmenaquinone methyltransferase-like
LOC125646719	3.107819832	0.000639817	uncharacterized protein LOC125646719
LOC125659525	3.112883887	0.000483559	myosin essential light chain%2C striated adductor muscle-like
LOC125666895	3.114043946	0.002399556	uncharacterized protein LOC125666895 isoform X2
LOC125649361	3.152113577	4.97E-05	putative amine oxidase [copper-containing] isoform X2
LOC125674204	3.187923149	0.00501276	43 kDa receptor-associated protein of the synapse-like
LOC125650318	3.195617502	8.95E-05	uncharacterized protein LOC125650318 isoform X1
LOC125661583	3.214938283	4.62E-05	aminopeptidase Ey-like isoform X4
LOC125669769	3.236298419	4.39E-05	pyrethroid hydrolase Ces2e-like
LOC125673562	3.241350401	0.001228881	uncharacterized protein LOC125673562
LOC125666115	3.276308766	0.000465864	--
LOC125647737	3.285446419	0.000707381	PDZ and LIM domain protein 1-like
LOC125665521	3.292493271	0.002181273	homologous-pairing protein 2 homolog
LOC125669283	3.310682596	6.47E-05	uncharacterized protein LOC125669283
LOC125676882	3.346185057	0.000686373	ras-related and estrogen-regulated growth inhibitor-like
LOC125671765	3.383033856	0.007067114	noggin-2-like isoform X2
LOC125659403	3.460568937	3.65E-09	LOW QUALITY PROTEIN: LHFPL tetraspan subfamily member 6 protein-like
LOC125657800	3.475018178	1.81E-05	acetylcholinesterase-like
LOC125666117	3.485198803	7.48E-06	fibroblast growth factor receptor 3-like isoform X1

USC UNIVERSIDADE DE SANTIAGO DE COMPOSTELA

LOC125662355	3.49103479	0.001393892	multiple epidermal growth factor-like domains protein 10 isoform X3
LOC125668286	3.512467408	0.000297702	uncharacterized protein LOC125668286 isoform X1
LOC125657676	3.514617949	8.22E-06	uncharacterized protein LOC125657676 isoform X2
LOC125646974	3.515192501	2.27E-06	major egg antigen-like
LOC125648015	3.591877309	0.000731015	alpha-crystallin A chain-like
LOC125651934	3.604588561	6.95E-07	universal stress protein in QAH/OAS sulfhydrylase 3'region-like
LOC125673817	3.674093729	0.000188004	complement C1q-like protein 2
LOC125671374	3.708910084	0.002985536	uncharacterized protein LOC125671374
LOC125672422	3.714967922	6.74E-07	myosin heavy chain%2C striated muscle-like isoform X5
LOC125647473	3.722553475	3.42E-07	uncharacterized protein LOC125647473
LOC125674758	3.73050524	1.04E-06	uncharacterized protein LOC125674758
LOC125664359	3.736746887	0.000147003	LOW QUALITY PROTEIN: LHFPL tetraspan subfamily member 7 protein-like
LOC125665829	3.744584559	6.80E-11	uncharacterized protein LOC125665829 isoform X1
LOC125650739	3.764199015	0.000389349	arginase%2C hepatic-like isoform X4
LOC125668397	3.83012994	1.65E-08	cysteine-rich venom protein latisemin-like
LOC125668398	3.836019012	9.91E-07	testis-specific serine/threonine-protein kinase 1-like
LOC125652056	3.838535387	0.000953903	protein nemuri-like isoform X1
LOC125676974	3.91615859	0.006851857	toll-like receptor 4
LOC125666154	3.921923361	5.41E-06	uncharacterized protein LOC125666154
LOC125645867	3.966625962	0.000253147	uncharacterized protein LOC125645867 isoform X1
LOC125655312	3.980509573	0.000823512	uncharacterized protein LOC125655312 isoform X2
LOC125683189	3.994072666	6.17E-06	protein-glutamine gamma-glutamyltransferase K-like isoform X2
LOC125649164	4.012100174	2.48E-10	cytochrome P450 2U1-like
LOC125659646	4.12793505	0.002305702	uncharacterized protein LOC125659646 isoform X3
LOC125656179	4.181410418	0.005148989	--
LOC125668742	4.234809411	3.84E-05	--
LOC125670650	4.338446996	4.39E-06	uncharacterized protein LOC125670650
LOC125678402	4.364689871	1.25E-16	uncharacterized protein LOC125678402
LOC125677074	4.383184353	0.000835071	--
LOC125671361	4.402008861	1.51E-06	carbohydrate sulfotransferase 15-like isoform X2
LOC125654030	4.446509705	3.27E-08	cadherin-like and PC-esterase domain-containing protein 1
LOC125679340	4.502507188	7.56E-08	uncharacterized protein LOC125679340 isoform X3
LOC125664873	4.505943106	7.87E-09	uncharacterized protein LOC125664873
LOC125669386	4.51136443	0.00024427	fibrinogen-like protein A isoform X1
LOC125646403	4.516801425	0.00065152	uncharacterized protein LOC125646403
LOC125683882	4.600611245	1.11E-05	neutral amino acid transporter A-like
LOC125682713	4.648214368	0.002034429	uncharacterized protein LOC125682713 isoform X1
LOC125652039	4.714624487	3.93E-09	uncharacterized protein LOC125652039
LOC125653842	4.714920239	0.000876855	DNA topoisomerase 1-like
LOC125653347	4.828375651	1.36E-08	uncharacterized protein LOC125653347
LOC125675603	4.831135217	4.76E-10	orexin receptor type 2-like
LOC125665731	4.879798382	1.72E-05	uncharacterized protein LOC125665731 isoform X2
LOC125664143	4.929742566	0.000116301	--
LOC125672586	5.321788352	7.67E-17	uncharacterized protein LOC125672586 isoform X2
LOC125683064	5.433608744	0.007734899	--
LOC125661361	5.791097814	2.85E-05	procathepsin L-like
LOC125654584	6.048867636	0.000417983	retinoid-inducible serine carboxypeptidase-like isoform X3
LOC125659941	6.261517355	1.90E-13	tripartite motif-containing protein 2-like isoform X4
LOC125651938	6.67216632	1.19E-05	uncharacterized protein LOC125651938
LOC125659279	6.999652643	1.31E-53	retinol dehydrogenase 12-like isoform X2
LOC125669079	7.083796826	1.38E-06	acetylcholine receptor subunit delta-like

USC UNIVERSIDADE DE SANTIAGO DE COMPOSTELA

LOC125656245	7.29907288	2.27E-10	uncharacterized protein LOC125656245
LOC125654795	7.758781607	2.09E-06	uncharacterized protein LOC125654795
LOC125654239	8.191911669	0.001357855	apolipoprotein D-like
LOC125679080	8.369762503	0.00037062	--
LOC125682220	8.579957517	1.30E-18	nose resistant to fluoxetine protein 6-like
LOC125657467	9.553310165	5.70E-07	--
LOC125667219	10.08753812	2.03E-09	--

B) Control vs Level 2

Gene	log2FoldChange	pvalue	Anotation
LOC125672817	-29.03717715	1.07E-13	--
LOC125665579	-28.06583571	6.78E-13	EF-hand calcium-binding domain-containing protein 1-like
LOC125673466	-15.88225626	6.44E-07	--
LOC125660998	-15.34627109	2.39E-14	--
LOC125661560	-14.96825457	2.95E-06	DBH-like monooxygenase protein 1
LOC125650772	-14.22187251	9.45E-12	uncharacterized protein LOC125650772
LOC125678492	-13.63184251	0.000484353	protein lev-9-like isoform X2
LOC125659209	-13.22041796	9.35E-12	--
LOC125648317	-13.19633635	2.15E-10	calmodulin-beta-like
LOC125666029	-13.02357326	1.32E-11	uncharacterized protein LOC125666029
LOC125654886	-12.99476845	2.19E-10	metalloproteinase inhibitor 2-like
LOC125663040	-12.95077235	3.17E-09	transmembrane protein 272-like
LOC125663587	-12.83027851	1.49E-11	metabotropic glutamate receptor 3-like
LOC125646407	-12.59754927	9.70E-09	uncharacterized protein LOC125646407
LOC125679096	-12.59754927	9.70E-09	uncharacterized protein LOC125679096
LOC125659146	-12.5729171	8.33E-10	transcription factor Sox-2-like
LOC125681850	-12.45832091	2.39E-10	uncharacterized protein LOC125681850
LOC125678071	-12.4245052	0.001471863	cerebellin-3-like isoform X4
LOC125682006	-12.26469092	6.85E-09	sphingomyelin synthase-related protein 1-like
LOC125675283	-12.24124244	0.001728662	caveolin-3-like
LOC125665218	-12.22180649	1.60E-08	uncharacterized protein LOC125665218 isoform X1
LOC125683160	-12.12814086	1.54E-10	uncharacterized protein LOC125683160 isoform X2
LOC125659107	-11.97024711	1.70E-10	--
LOC125658375	-11.92611043	3.05E-08	uncharacterized protein LOC125658375
LOC125662017	-11.91115229	0.002298083	uncharacterized protein LOC125662017 isoform X1
LOC125655683	-11.90659616	0.002306735	cysteine and tyrosine-rich protein 1-like isoform X1
LOC125658223	-11.80302909	0.002518686	uncharacterized protein LOC125658223 isoform X3
LOC125664304	-11.77330664	3.55E-09	uncharacterized protein LOC125664304 isoform X12
LOC125669385	-11.71795948	2.52E-08	grainyhead-like protein 1 homolog isoform X4
LOC125671726	-11.69780535	6.55E-10	cell migration-inducing and hyaluronan-binding protein-like
LOC125673449	-11.59741445	6.30E-07	cerebellin-1-like
LOC125654912	-11.51856646	0.003195692	uncharacterized protein LOC125654912
LOC125653627	-11.47553843	0.003311447	uncharacterized protein LOC125653627
LOC125645608	-11.43632865	5.70E-08	alpha-(1%2C3)-fucosyltransferase fut-5-like isoform X1
LOC125654854	-11.41747231	0.003473722	caveolin-1-like
LOC125669927	-11.38847528	9.52E-11	equilibrative nucleobase transporter 1-like
LOC125661875	-11.38815352	8.65E-08	uncharacterized protein LOC125661875
LOC125675855	-11.34352142	0.001259616	uncharacterized protein LOC125675855 isoform X1
LOC125679528	-11.317469	5.92E-10	collagen alpha-1(I) chain-like
LOC125646759	-11.29508678	3.92E-08	uncharacterized protein LOC125646759

USC UNIVERSIDADE DE SANTIAGO DE COMPOSTELA

LOC125683865	-11.29470175	1.24E-05	complement C1q-like protein 4
LOC125680365	-11.27244891	1.93E-08	neuroendocrine convertase 2-like
LOC125656147	-11.25357691	9.16E-08	cysteine and tyrosine-rich protein 1-like
LOC125655260	-11.21844215	1.42E-08	uncharacterized protein LOC125655260 isoform X1
LOC125667767	-11.16919137	2.60E-05	uncharacterized protein LOC125667767
LOC125683044	-11.16891795	3.37E-07	uncharacterized protein LOC125683044
LOC125674301	-11.0164283	4.60E-07	uromodulin-like
LOC125681750	-10.99889848	2.07E-05	CD63 antigen-like
LOC125645791	-10.93778989	4.63E-07	testis-expressed protein 52-like
LOC125663585	-10.91652799	1.37E-09	uncharacterized protein LOC125663585
LOC125657178	-10.90121291	0.000110423	uncharacterized protein LOC125657178 isoform X1
LOC125658890	-10.87570598	2.85E-05	uncharacterized protein LOC125658890 isoform X4
LOC125651301	-10.79335868	3.93E-06	uncharacterized protein LOC125651301
LOC125660999	-10.76501634	6.00E-12	tyramine beta-hydroxylase-like
LOC125661562	-10.76501634	6.00E-12	tyramine beta-hydroxylase-like
LOC125672258	-10.75525385	6.43E-11	uncharacterized protein LOC125672258
LOC125646019	-10.7339878	3.75E-05	perlucin-like protein
LOC125679886	-10.73323949	1.40E-08	--
LOC125682057	-10.73130007	4.02E-05	serine-rich adhesin for platelets-like
LOC125655847	-10.71126251	3.96E-05	uncharacterized protein LOC125655847
LOC125668997	-10.70933646	1.68E-10	collagen alpha-1(I) chain-like
LOC125655708	-10.69988248	1.04E-10	phospholipid-transporting ATPase ABCA3-like
LOC125655331	-10.64184258	5.32E-06	uncharacterized protein LOC125655331
LOC125648084	-10.5812808	7.12E-07	--
LOC125663783	-10.57939999	6.21E-05	uncharacterized protein LOC125663783 isoform X1
LOC125676997	-10.57470328	1.08E-08	uncharacterized protein LOC125676997
LOC125661913	-10.56394637	2.88E-06	tenascin-like isoform X3
LOC125668356	-10.53004281	1.51E-07	coiled-coil domain-containing protein 33-like isoform X2
LOC125671604	-10.51509579	3.85E-06	doublesex- and mab-3-related transcription factor A2-like
LOC125659920	-10.51406385	6.98E-09	tripartite motif-containing protein 2-like
LOC125661450	-10.47403585	4.18E-06	complement C1q-like protein 4
LOC125649497	-10.46323548	2.76E-09	protein doublesex-like
LOC125654909	-10.35293352	9.61E-05	caveolin-1-like isoform X2
LOC125674083	-10.31698161	6.58E-08	uncharacterized protein LOC125674083 isoform X2
LOC125673456	-10.2919504	0.000625184	uncharacterized protein LOC125673456 isoform X2
LOC125677027	-10.25592283	0.000115845	--
LOC125649865	-10.22266579	3.55E-06	arrestin domain-containing protein 3-like
LOC125680672	-10.22158061	1.51E-05	allatotropins-like
LOC125657179	-10.21446628	0.000561896	uncharacterized protein LOC125657179
LOC125645567	-10.19403482	8.72E-06	uncharacterized protein LOC125645567
LOC125647945	-10.18548712	2.22E-07	filamin A-interacting protein 1-like
LOC125651291	-10.17324007	0.000146625	--
LOC125645800	-10.16790577	6.55E-09	uncharacterized protein LOC125645800
LOC125646997	-10.14020383	2.06E-07	--
LOC125656191	-10.12919781	1.05E-05	pre-mRNA-splicing factor CWC22 homolog
LOC125652363	-10.09598042	0.00019643	golgin subfamily A member 6-like protein 22
LOC125677109	-10.0939552	5.58E-07	uncharacterized protein LOC125677109
LOC125673455	-10.08478007	0.000141077	uncharacterized protein LOC125673455
LOC125657652	-10.0836621	0.000197486	short-chain collagen C4-like
LOC125659601	-10.0806028	4.09E-08	uncharacterized protein LOC125659601
LOC125683043	-10.01228584	3.37E-10	--

USC UNIVERSIDADE DE SANTIAGO DE COMPOSTELA

LOC125674088	-9.983565245	8.49E-10	neurogenic locus Notch protein-like
LOC125682720	-9.978232942	3.14E-05	uncharacterized protein LOC125682720
LOC125652430	-9.972812643	7.22E-06	uncharacterized protein LOC125652430
LOC125672096	-9.97134503	2.49E-07	uncharacterized protein LOC125672096 isoform X1
LOC125652517	-9.883468303	0.000292921	uncharacterized protein LOC125652517
LOC125653701	-9.883468303	0.000292921	uncharacterized protein LOC125653701
LOC125646785	-9.867582862	0.000308136	LOW QUALITY PROTEIN: myomodulin neuropeptides 2-like
LOC125659934	-9.847616248	0.000344042	uncharacterized protein LOC125659934
LOC125677066	-9.840676072	9.41E-06	heavy metal-binding protein HIP-like isoform X7
LOC125680779	-9.810331775	0.000110099	uncharacterized protein LOC125680779
LOC125683530	-9.782753433	1.23E-05	uncharacterized protein LOC125683530
LOC125647472	-9.699755588	6.70E-09	--
LOC125677041	-9.693432021	0.000533437	otolin-1-like
LOC125661197	-9.693159866	5.25E-07	calpain-5-like isoform X3
LOC125679636	-9.674695751	2.10E-07	nicotinamidase-like
LOC125645735	-9.645136656	2.31E-08	uncharacterized protein LOC125645735
LOC125678298	-9.633318039	2.40E-09	tubulin beta chain-like
LOC125682475	-9.633318039	2.40E-09	tubulin beta chain-like
LOC125670204	-9.599237528	1.89E-05	uncharacterized protein LOC125670204
LOC125674306	-9.572202333	4.90E-08	oncoprotein-induced transcript 3 protein-like
LOC125652614	-9.543222285	3.28E-10	uncharacterized protein LOC125652614
LOC125646641	-9.53238969	5.46E-06	cadherin EGF LAG seven-pass G-type receptor 2-like isoform X1
LOC125662692	-9.53093747	2.31E-07	uncharacterized protein LOC125662692
LOC125682357	-9.526964849	7.00E-05	uncharacterized protein LOC125682357 isoform X2
LOC125664149	-9.517555439	1.07E-06	--
LOC125659807	-9.514718044	0.000794242	APGW-amide-related neuropeptide-like
LOC125652429	-9.497305911	6.08E-05	--
LOC125670863	-9.429566406	7.38E-07	paired box protein Pax-8-like isoform X1
LOC125675952	-9.401205823	7.29E-05	uncharacterized protein LOC125675952
LOC125655472	-9.400532905	0.000984087	A disintegrin and metalloproteinase with thrombospondin motifs 4-like isoform X5
LOC125666577	-9.368518238	3.42E-08	--
LOC125679568	-9.349918612	3.67E-07	Golgi-associated plant pathogenesis-related protein 1-like
LOC125646253	-9.343781463	1.22E-05	FMRF-amide neuropeptides-like
LOC125681429	-9.338322913	0.001075701	uncharacterized protein LOC125681429
LOC125681465	-9.30571077	0.000120754	tetraspanin-18-like
LOC125646761	-9.294917182	1.26E-06	uncharacterized protein LOC125646761
LOC125673331	-9.283540104	6.88E-07	tripartite motif-containing protein 2-like isoform X1
LOC125656100	-9.282662943	1.42E-09	LHFPL tetraspan subfamily member 3 protein-like
LOC125667054	-9.27837313	0.008830101	uncharacterized protein LOC125667054 isoform X3
LOC125658627	-9.277313592	5.27E-05	zinc finger protein 667-like
LOC125654008	-9.259479957	1.20E-11	protein SSUH2 homolog isoform X1
LOC125681718	-9.214022647	0.001258553	uncharacterized protein LOC125681718 isoform X13
LOC125683864	-9.208102375	5.41E-06	cerebellin-3-like
LOC125675951	-9.145079851	9.06E-07	uncharacterized protein LOC125675951
LOC125682512	-9.135328781	0.00158736	uncharacterized protein LOC125682512 isoform X1
LOC125649717	-9.134392606	1.49E-07	sodium/calcium exchanger 3-like
LOC125671987	-9.134392606	1.49E-07	sodium/calcium exchanger 3-like
LOC125667714	-9.097161129	6.76E-05	ryncolin-1-like
LOC125669881	-9.062061164	2.63E-05	ras-related protein Rap-1b-like
LOC125680312	-9.058980518	2.65E-06	uncharacterized protein LOC125680312
LOC125663775	-9.046947081	1.77E-07	uncharacterized protein LOC125663775

USC UNIVERSIDADE DE SANTIAGO DE COMPOSTELA

LOC125663750	-9.027733386	0.002205451	uncharacterized protein LOC125663750
LOC125679700	-9.002509132	1.02E-05	epidermal growth factor receptor-like
LOC125670325	-8.999402798	9.58E-10	uncharacterized protein LOC125670325
LOC125670809	-8.974411436	1.85E-07	collagen alpha-4(VI) chain-like
LOC125658987	-8.937132148	3.03E-07	uncharacterized protein LOC125658987
LOC125648836	-8.901106545	5.00E-11	uncharacterized protein LOC125648836
LOC125655003	-8.898867438	0.000282746	uncharacterized protein LOC125655003 isoform X3
LOC125654173	-8.891747162	8.42E-08	34 kDa antigenic protein-like isoform X6
LOC125666126	-8.885827941	0.000190245	uncharacterized protein LOC125666126
LOC125680671	-8.875235604	0.002916403	collectin-12-like
LOC125679238	-8.83515524	1.72E-08	prestin-like isoform X2
LOC125671701	-8.82918978	0.003160706	uncharacterized protein LOC125671701
LOC125659142	-8.828375594	1.57E-09	malignant fibrous histiocytoma-amplified sequence 1 homolog isoform X1
LOC125654081	-8.811023604	5.20E-06	A disintegrin and metalloproteinase with thrombospondin motifs adt-1-like isoform X7
LOC125678107	-8.772129248	1.08E-05	ankyrin-1-like
LOC125681875	-8.702801894	0.004074333	--
LOC125678757	-8.667160397	2.07E-09	cilia- and flagella-associated protein 45-like isoform X1
LOC125671580	-8.651866716	8.96E-06	dynein light chain Tctex-type 5-like
LOC125656772	-8.64052985	0.004542044	caveolin-1-like
LOC125673460	-8.62978087	6.83E-06	uncharacterized protein LOC125673460 isoform X2
LOC125656753	-8.624004297	7.98E-05	uncharacterized protein LOC125656753 isoform X2
LOC125683627	-8.617715346	2.01E-10	MAM and LDL-receptor class A domain-containing protein 1-like isoform X3
LOC125645609	-8.60954578	2.21E-05	glycoprotein 3-alpha-L-fucosyltransferase A-like
LOC125674960	-8.599719177	4.80E-08	EF-hand calcium-binding domain-containing protein 6-like isoform X5
LOC125670629	-8.58821329	6.98E-09	cyclin-dependent kinase 12-like isoform X6
LOC125679357	-8.577265459	1.70E-05	centrosome-associated protein CEP250-like isoform X3
LOC125655578	-8.574163647	4.36E-10	uncharacterized protein LOC125655578 isoform X1
LOC125655410	-8.561728472	2.06E-06	von Willebrand factor D and EGF domain-containing protein-like isoform X1
LOC125653441	-8.536974287	6.10E-05	complement C1q-like protein 2 isoform X4
LOC125657629	-8.530985395	3.80E-08	uncharacterized protein LOC125657629
LOC125655332	-8.501556887	2.48E-05	uncharacterized protein LOC125655332
LOC125665341	-8.466434875	1.85E-10	mucin-17-like
LOC125655214	-8.454537737	0.00504141	caveolin-3-like
LOC125648205	-8.447061057	0.006600591	uncharacterized protein LOC125648205
LOC125681931	-8.428938399	1.79E-06	uncharacterized protein LOC125681931
LOC125679882	-8.425693054	1.36E-06	uncharacterized protein LOC125679882
LOC125657103	-8.413431843	0.000918688	heavy metal-binding protein HIP-like
LOC125668219	-8.391977812	1.77E-07	uncharacterized protein LOC125668219
LOC125672140	-8.385558319	0.000575384	uncharacterized protein LOC125672140
LOC125672152	-8.385558319	0.000575384	uncharacterized protein LOC125672152
LOC125683197	-8.368459341	6.52E-05	nmrA-like family domain-containing protein 1 isoform X5
LOC125668795	-8.302764501	1.01E-07	NAD-dependent protein deacetylase Sirt6-like
LOC125659954	-8.296776954	0.00015294	zinc finger and BTB domain-containing protein 49-like
LOC125677659	-8.294751425	5.29E-10	uncharacterized protein LOC125677659
LOC125683027	-8.284244875	2.73E-09	paired box protein Pax-6-like isoform X1
LOC125665948	-8.278276318	2.62E-07	tripartite motif-containing protein 59-like
LOC125650184	-8.275582926	1.32E-07	uncharacterized protein LOC125650184 isoform X1
LOC125669885	-8.262059513	0.000108405	uncharacterized protein LOC125669885
LOC125679702	-8.244121402	1.36E-07	uncharacterized protein LOC125679702
LOC125651536	-8.19838326	2.25E-05	C-type lectin domain family 4 member K-like isoform X1
LOC125681847	-8.177233229	5.95E-05	dehydrogenase/reductase SDR family member 9-like

USC UNIVERSIDADE DE SANTIAGO DE COMPOSTELA

LOC125645482	-8.153397746	6.44E-05	uncharacterized protein LOC125645482 isoform X2
LOC125653797	-8.139736086	1.48E-05	LOW QUALITY PROTEIN: glutathione S-transferase-like
LOC125670712	-8.124167636	1.38E-09	protein FAM234B-like isoform X2
LOC125675507	-8.123395506	2.07E-06	microsomal glutathione S-transferase 3-like
LOC125650712	-8.084276643	0.000816559	paired box protein Pax-1-like
LOC125647779	-8.07650538	0.006527789	uncharacterized protein LOC125647779
LOC125673467	-8.057630944	0.002207606	--
LOC125665841	-8.033344771	0.001866525	uncharacterized protein LOC125665841
LOC125680424	-8.032599671	5.76E-07	tetraspanin-9-like isoform X3
LOC125667526	-8.019044084	1.46E-06	uncharacterized protein LOC125667526 isoform X2
LOC125680700	-8.015848875	1.01E-08	uncharacterized protein LOC125680700
LOC125654853	-8.015845242	2.99E-08	uncharacterized protein LOC125654853
LOC125667266	-7.967561686	3.87E-06	arginine/serine-rich protein 1-like
LOC125678075	-7.949056984	3.26E-05	C1q-related factor-like isoform X4
LOC125681020	-7.942041186	5.43E-08	short-chain collagen C4-like
LOC125648216	-7.941887116	9.48E-08	arrestin domain-containing protein 1-like isoform X1
LOC125670035	-7.930125803	4.26E-10	transmembrane channel-like protein 7 isoform X4
LOC125653345	-7.905226243	2.66E-12	metalloproteinase inhibitor 2-like isoform X1
LOC125670881	-7.858081219	7.44E-08	LITAF domain-containing protein-like
LOC125679074	-7.818226246	3.50E-10	annexin A5-like
LOC125683927	-7.80798622	3.47E-06	LOW QUALITY PROTEIN: myeloid differentiation primary response protein MyD88-like
LOC125683223	-7.806184024	1.20E-06	uncharacterized protein LOC125683223 isoform X2
LOC125666579	-7.79844546	4.02E-07	uncharacterized protein LOC125666579 isoform X2
LOC125649077	-7.797371942	0.000117209	dynein light chain Tctex-type protein 2B-like
LOC125656954	-7.786801035	0.000176387	uncharacterized protein LOC125656954
LOC125646798	-7.742276249	1.22E-06	putative ankyrin repeat protein RF_0381 isoform X1
LOC125673093	-7.72913429	1.72E-06	--
LOC125681853	-7.685169214	0.000193102	uncharacterized protein LOC125681853
LOC125675071	-7.664515361	2.86E-06	enteropeptidase-like
LOC125650796	-7.659582504	6.34E-08	uncharacterized protein LOC125650796
LOC125671469	-7.650244796	8.02E-10	tektin-3-like isoform X2
LOC125682351	-7.642114692	0.000121657	myeloperoxidase-like
LOC125666899	-7.615398378	8.10E-06	uncharacterized protein LOC125666899
LOC125675445	-7.595685047	8.66E-06	uncharacterized protein LOC125675445
LOC125678077	-7.569311205	0.00015555	ficolin-1-A-like isoform X2
LOC125647728	-7.529493981	3.14E-05	uncharacterized protein LOC125647728 isoform X1
LOC125651975	-7.476290232	0.000315058	type-2 ice-structuring protein-like isoform X2
LOC125650749	-7.459515261	1.04E-07	uncharacterized protein LOC125650749
LOC125668796	-7.456279301	5.95E-07	NAD-dependent protein deacetylase Sirt6-like isoform X1
LOC125681872	-7.454197672	8.37E-07	tetraspanin-9-like
LOC125675775	-7.444771564	1.05E-09	uncharacterized protein LOC125675775
LOC125677266	-7.442997564	1.21E-06	transmembrane protein 45B-like isoform X1
LOC125648180	-7.414648554	1.88E-05	uncharacterized protein LOC125648180
LOC125668352	-7.413701454	0.000171047	uncharacterized protein LOC125668352 isoform X3
LOC125650665	-7.405156429	9.20E-06	stabilizer of axonemal microtubules 2-like
LOC125669918	-7.391815198	3.30E-07	spermatogenesis-associated protein 6-like isoform X2
LOC125658452	-7.380805937	0.00546656	--
LOC125651313	-7.380452186	3.35E-10	uncharacterized protein LOC125651313
LOC125675825	-7.372992777	1.26E-08	uncharacterized protein LOC125675825
LOC125673407	-7.37045207	2.54E-06	uncharacterized protein LOC125673407 isoform X1
LOC125653934	-7.36484184	6.33E-07	uncharacterized protein LOC125653934

USC UNIVERSIDADE DE SANTIAGO DE COMPOSTELA

LOC125678350	-7.362243562	1.49E-05	deleted in malignant brain tumors 1 protein-like
LOC125653936	-7.358473263	5.07E-07	uncharacterized protein LOC125653936
LOC125675805	-7.346122322	6.16E-16	CCAAT/enhancer-binding protein beta-like
LOC125681419	-7.338840792	1.08E-07	fibrocystin-L-like isoform X1
LOC125647970	-7.32976431	2.14E-06	uncharacterized protein C17orf98-like
LOC125662595	-7.302804366	9.18E-08	--
LOC125678347	-7.296090643	2.91E-07	receptor-type tyrosine-protein phosphatase F-like isoform X2
LOC125675289	-7.260608077	1.09E-07	outer dense fiber protein 3-like
LOC125653531	-7.248859845	0.00052049	uncharacterized protein LOC125653531
LOC125655489	-7.239341309	3.23E-09	globin-like
LOC125654813	-7.21009622	1.83E-06	myosin heavy chain%2C skeletal muscle-like
LOC125648923	-7.187947925	9.77E-08	LOW QUALITY PROTEIN: sodium-dependent phosphate transport protein 2B-like
LOC125681243	-7.166263958	3.12E-06	cholesterol 7-desaturase nvd-like
LOC125675832	-7.156397017	1.16E-06	uncharacterized protein LOC125675832 isoform X3
LOC125679934	-7.141265391	0.000171421	uncharacterized protein LOC125679934 isoform X1
LOC125656192	-7.139837144	0.000159973	pre-mRNA-splicing factor CWC22 homolog
LOC125649506	-7.131412709	7.47E-07	radial spoke head protein 4 homolog A-like
LOC125670321	-7.117756959	0.001766861	uncharacterized protein LOC125670321
LOC125674013	-7.109721797	9.86E-09	--
LOC125667337	-7.090655103	2.86E-06	glutathione S-transferase theta-1-like
LOC125679523	-7.08651124	7.71E-08	uncharacterized protein LOC125679523
LOC125681186	-7.067503693	1.37E-08	uncharacterized protein LOC125681186
LOC125679123	-7.058927401	0.000154187	complement C1q tumor necrosis factor-related protein 2-like
LOC125663776	-7.056492502	5.83E-08	uncharacterized protein LOC125663776
LOC125654748	-7.052274751	0.003461091	--
LOC125670160	-7.04798247	0.006344022	uncharacterized protein LOC125670160
LOC125649607	-7.044905579	7.27E-07	uncharacterized protein LOC125649607 isoform X3
LOC125650883	-7.030623406	0.004913664	rho-related GTP-binding protein RhoQ-like
LOC125681441	-7.019648698	4.45E-05	serine/arginine repetitive matrix protein 1-like isoform X2
LOC125646071	-7.00997695	4.05E-05	MORN repeat-containing protein 1-like isoform X1
LOC125654360	-7.009844819	6.56E-08	uncharacterized protein LOC125654360 isoform X2
LOC125671411	-6.988136327	2.47E-08	cilia- and flagella-associated protein 52-like
LOC125680895	-6.97376147	3.21E-06	--
LOC125668947	-6.972001327	5.17E-06	uncharacterized protein LOC125668947
LOC125671094	-6.970235227	1.33E-07	EF-hand calcium-binding domain-containing protein 6-like isoform X1
LOC125656219	-6.955829801	0.00124027	uncharacterized protein LOC125656219 isoform X1
LOC125662599	-6.951833638	0.000765967	uncharacterized protein LOC125662599
LOC125672154	-6.94166754	4.07E-05	uncharacterized protein LOC125672154
LOC125672158	-6.94166754	4.07E-05	uncharacterized protein LOC125672158
LOC125666781	-6.939703856	2.20E-09	--
LOC125680754	-6.930796412	0.001054308	UPF0686 protein C11orf1 homolog
LOC125679804	-6.870651211	0.000300727	--
LOC125649577	-6.863944921	4.61E-07	neuroendocrine convertase 2-like
LOC125674305	-6.847656444	2.11E-05	uncharacterized protein LOC125674305 isoform X3
LOC125676286	-6.84481517	0.006906702	uncharacterized protein LOC125676286
LOC125670408	-6.834990404	9.01E-07	neurensin-1-like
LOC125683110	-6.805807513	4.85E-08	uncharacterized protein LOC125683110
LOC125680852	-6.797843928	3.95E-05	E3 ubiquitin-protein ligase TRIM71-like
LOC125671570	-6.797622165	0.0002936	uncharacterized protein LOC125671570
LOC125666331	-6.793069422	7.51E-05	MAM and LDL-receptor class A domain-containing protein 1-like
LOC125677748	-6.791620704	9.10E-06	uncharacterized protein LOC125677748

USC UNIVERSIDADE DE SANTIAGO DE COMPOSTELA

LOC125655888	-6.778177214	5.98E-05	uncharacterized protein LOC125655888
LOC125663323	-6.738318455	7.14E-09	matrilysin-like isoform X1
LOC125664212	-6.727879868	1.48E-06	coiled-coil domain-containing protein 63-like
LOC125675941	-6.727784538	0.000275432	uncharacterized protein LOC125675941
LOC125648022	-6.724733486	1.22E-06	uncharacterized protein LOC125648022 isoform X2
LOC125670879	-6.723508701	3.70E-05	cell death-inducing p53-target protein 1 homolog isoform X1
LOC125649071	-6.716073435	4.65E-06	testis%2C prostate and placenta-expressed protein-like
LOC125656840	-6.709603496	0.000573414	uncharacterized protein LOC125656840 isoform X2
LOC125652000	-6.695876427	0.00011528	uncharacterized protein LOC125652000
LOC125677332	-6.690408257	6.61E-06	dnaJ homolog subfamily B member 13-like
LOC125646484	-6.675567673	3.23E-08	--
LOC125680371	-6.675018286	1.45E-07	choline transporter-like protein 2
LOC125658469	-6.673493688	0.000375221	--
LOC125680304	-6.671083303	1.21E-06	tetraspanin-1-like
LOC125679510	-6.650243814	0.000877667	low-density lipoprotein receptor-related protein 4-like isoform X2
LOC125673112	-6.647935844	3.65E-05	adhesion G protein-coupled receptor B1-like isoform X2
LOC125668606	-6.637027383	5.56E-06	--
LOC125647943	-6.634619349	0.000977745	prothoracicostatic peptide-like
LOC125675252	-6.634080762	3.15E-05	--
LOC125659427	-6.628548117	2.77E-05	LOW QUALITY PROTEIN: cell surface hyaluronidase-like
LOC125681633	-6.614665162	0.000177033	ficolin-2-like
LOC125661935	-6.613973604	6.14E-06	BPTI/Kunitz domain-containing protein-like
LOC125670167	-6.599903456	0.00031591	cytoplasmic dynein 2 heavy chain 1-like
LOC125682965	-6.597637972	2.49E-05	uncharacterized protein LOC125682965
LOC125683834	-6.584681732	2.30E-07	tetraspanin-9-like
LOC125681261	-6.569493413	3.77E-08	sodium- and chloride-dependent taurine transporter-like isoform X1
LOC125654269	-6.569181882	6.94E-05	IQ and ubiquitin-like domain-containing protein
LOC125660487	-6.546225525	3.84E-07	E3 ubiquitin-protein ligase TRIM56-like
LOC125680336	-6.517652458	8.83E-05	uncharacterized protein LOC125680336
LOC125682191	-6.517451505	2.91E-05	tetraspanin-9-like isoform X1
LOC125683093	-6.500447842	2.45E-05	actin-5-like
LOC125676256	-6.499221979	3.35E-07	--
LOC125658807	-6.494933894	0.001738389	uncharacterized protein LOC125658807
LOC125681393	-6.485710111	0.001690402	C-type lectin domain family 4 member E-like
LOC125656104	-6.452321437	0.000219581	CD209 antigen-like protein B
LOC125645461	-6.41778672	1.59E-07	glutamate-rich protein 3-like isoform X2
LOC125649908	-6.399919475	5.05E-06	uncharacterized protein LOC125649908
LOC125669911	-6.379888408	5.66E-05	cilia- and flagella-associated protein 57-like
LOC125664426	-6.355401473	3.15E-05	uncharacterized protein LOC125664426 isoform X2
LOC125646778	-6.342382667	3.15E-07	tektin-3-like isoform X1
LOC125650639	-6.335879325	6.49E-07	coiled-coil domain-containing protein 170-like
LOC125650674	-6.335879325	6.49E-07	coiled-coil domain-containing protein 170-like
LOC125675925	-6.334380868	0.001794995	--
LOC125659880	-6.327401179	5.39E-06	leucine-rich repeat protein soc-2-like
LOC125666728	-6.325478272	3.73E-07	asparagine synthetase [glutamine-hydrolyzing]-like
LOC125679178	-6.282953492	2.08E-05	protein FAM166B-like
LOC125662157	-6.282473	0.000742506	uncharacterized protein LOC125662157
LOC125651816	-6.281127527	8.08E-05	FMRFamide receptor-like
LOC125664386	-6.267554866	9.06E-06	protein CFAP107-like
LOC125672092	-6.258907145	0.000429914	noggin-like
LOC125670333	-6.248249192	2.96E-06	tektin-2-like

USC UNIVERSIDADE DE SANTIAGO DE COMPOSTELA

LOC125670355	-6.248249192	2.96E-06	tektin-2-like
LOC125665818	-6.231508286	9.82E-07	sperm-associated antigen 6
LOC125680840	-6.229978616	1.52E-05	uncharacterized protein LOC125680840
LOC125681433	-6.228066782	2.26E-06	serine/threonine-protein kinase DCLK1-like isoform X2
LOC125671016	-6.226853833	9.65E-06	protein TBATA-like isoform X2
LOC125671830	-6.208347889	7.46E-06	zinc metalloproteinase dpy-31-like
LOC125647859	-6.176290256	4.71E-05	EF-hand domain-containing protein 1-like
LOC125649262	-6.160468808	2.38E-05	--
LOC125681876	-6.158708089	0.006802757	complement C1q-like protein 3 isoform X1
LOC125657899	-6.13716132	2.64E-05	EF-hand domain-containing family member C2-like
LOC125677265	-6.125408884	1.35E-05	uncharacterized protein LOC125677265
LOC125681507	-6.121640693	2.46E-06	uncharacterized protein LOC125681507
LOC125683873	-6.121048578	6.72E-06	contactin-like isoform X2
LOC125654207	-6.10989927	9.57E-07	uncharacterized protein LOC125654207
LOC125662347	-6.10484428	6.33E-05	sodium- and chloride-dependent taurine transporter-like isoform X2
LOC125680341	-6.092782329	7.51E-05	uncharacterized protein LOC125680341
LOC125659105	-6.087176678	0.000562028	complement C1q-like protein 4
LOC125652760	-6.083758634	0.000706388	cdc42 homolog
LOC125681732	-6.07186068	0.004010374	uncharacterized protein LOC125681732
LOC125677098	-6.064611155	1.72E-05	--
LOC125665835	-6.058105644	2.13E-05	protein CFAP210-like
LOC125659693	-6.057918663	2.06E-05	uncharacterized protein LOC125659693
LOC125682298	-6.045741679	0.0005612	uncharacterized protein LOC125682298
LOC125683830	-6.04507892	2.56E-07	uncharacterized protein LOC125683830 isoform X1
LOC125682365	-6.037679034	0.005948604	lithostathine-1-alpha-like
LOC125649994	-6.034464216	4.01E-07	sodium- and chloride-dependent neutral and basic amino acid transporter B(0+)-like isoform X1
LOC125653443	-6.032526002	0.005621059	complement C1q subcomponent subunit A-like
LOC125647771	-6.026868767	1.95E-05	uncharacterized protein LOC125647771
LOC125665557	-6.023478871	0.000294172	uncharacterized protein LOC125665557 isoform X2
LOC125649923	-6.020209956	7.48E-05	uncharacterized protein LOC125649923
LOC125651862	-5.988909983	0.000935935	uncharacterized protein LOC125651862 isoform X1
LOC125681468	-5.961998279	1.25E-06	radial spoke head 1 homolog isoform X1
LOC125645600	-5.958884203	1.83E-06	uncharacterized protein LOC125645600 isoform X2
LOC125675448	-5.958659939	0.006624063	--
LOC125659227	-5.951037428	3.22E-07	--
LOC125660463	-5.949261432	1.88E-07	ankyrin repeat domain-containing protein 42-like
LOC125670854	-5.946680275	1.81E-05	uncharacterized protein LOC125670854 isoform X2
LOC125651637	-5.945278515	3.03E-05	protein dead ringer homolog
LOC125667682	-5.939971826	0.004326887	uncharacterized protein LOC125667682
LOC125654085	-5.923983416	0.000421657	calcium-activated chloride channel regulator 1-like isoform X1
LOC125668623	-5.92149121	0.000626181	LOW QUALITY PROTEIN: uncharacterized protein LOC125668623
LOC125676103	-5.921324049	1.50E-05	radial spoke head protein 3 homolog B-like
LOC125676138	-5.897687859	1.45E-07	15-hydroxyprostaglandin dehydrogenase [NAD(+)]-like
LOC125665863	-5.890816742	0.000287889	uncharacterized protein LOC125665863 isoform X2
LOC125662861	-5.886338818	9.09E-06	tektin-1-like
LOC125668050	-5.885246304	0.000670719	dynein axonemal assembly factor 5-like
LOC125680688	-5.876308688	1.55E-06	mitochondria-eating protein-like isoform X3
LOC125645434	-5.871091121	1.62E-06	uncharacterized protein LOC125645434 isoform X4
LOC125665905	-5.869882552	1.26E-05	interferon alpha-inducible protein 27-like protein 2B isoform X3
LOC125654684	-5.86730366	5.53E-05	uncharacterized protein LOC125654684
LOC125681914	-5.866880566	8.80E-05	octopamine receptor-like

USC UNIVERSIDADE DE SANTIAGO DE COMPOSTELA

LOC125646811	-5.85932592	0.000105721	homeobox protein Dlx6a-like
LOC125682074	-5.859038392	1.01E-08	glutamine synthetase 2 cytoplasmic-like
LOC125672280	-5.848450335	0.000888562	spermatogenesis-associated protein 6-like
LOC125668620	-5.84509507	1.45E-07	uncharacterized protein LOC125668620 isoform X2
LOC125678751	-5.830892822	2.17E-06	tetraspanin-9-like
LOC125665726	-5.825073953	0.000816379	uncharacterized protein LOC125665726
LOC125654075	-5.812275524	0.000536759	protein ATP6V1FNB-like
LOC125665860	-5.79427846	9.58E-05	uncharacterized protein LOC125665860 isoform X2
LOC125654391	-5.781035312	0.000222283	uncharacterized protein LOC125654391
LOC125669459	-5.778426711	0.000154225	probable 3'%2C5'-cyclic phosphodiesterase pde-5 isoform X10
LOC125671978	-5.769391559	0.001827433	cytoplasmic dynein 2 heavy chain 1-like
LOC125665618	-5.764726618	1.84E-05	uncharacterized protein LOC125665618 isoform X2
LOC125670754	-5.753308414	5.48E-06	purine nucleoside phosphorylase-like isoform X1
LOC125668622	-5.748738272	0.000344867	uncharacterized protein LOC125668622
LOC125668843	-5.747850592	2.74E-06	LOW QUALITY PROTEIN: fatty acid synthase-like
LOC125652465	-5.734367842	0.00021937	DBH-like monooxygenase protein 2 homolog isoform X2
LOC125671402	-5.731026296	8.65E-06	LOW QUALITY PROTEIN: uncharacterized protein LOC125671402
LOC125671804	-5.730608716	2.54E-05	--
LOC125679884	-5.726956606	4.24E-06	uncharacterized protein LOC125679884
LOC125649496	-5.722659605	3.73E-07	--
LOC125654399	-5.720642056	2.64E-05	LIM domain and actin-binding protein 1-like
LOC125681343	-5.71763478	4.87E-06	uncharacterized protein LOC125681343 isoform X1
LOC125654204	-5.713594412	1.23E-05	uncharacterized protein LOC125654204 isoform X1
LOC125659972	-5.697338061	1.04E-08	LOW QUALITY PROTEIN: matrix metalloproteinase-16-like
LOC125656184	-5.696670649	0.000997672	calcium and integrin-binding protein 1-like
LOC125669752	-5.696251874	9.33E-06	--
LOC125673265	-5.671718073	0.00066263	uncharacterized protein LOC125673265
LOC125662552	-5.659291444	3.24E-05	uncharacterized protein LOC125662552
LOC125662633	-5.65321023	0.002989441	uncharacterized protein LOC125662633
LOC125670666	-5.632281574	5.60E-05	uncharacterized protein LOC125670666 isoform X2
LOC125655677	-5.630453026	0.000184596	uncharacterized protein LOC125655677
LOC125665628	-5.603732722	0.000104279	sorcin-like
LOC125670652	-5.603660156	2.66E-05	uncharacterized protein LOC125670652 isoform X4
LOC125652789	-5.598412708	0.001378903	uncharacterized protein LOC125652789 isoform X1
LOC125653999	-5.598412708	0.001378903	uncharacterized protein LOC125653999 isoform X1
LOC125650546	-5.594798257	0.001295636	ras-related C3 botulinum toxin substrate 3-like
LOC125659544	-5.592348643	4.49E-06	sperm axonemal maintenance protein CFAP97D1-like
LOC125671615	-5.591088623	0.000640627	uncharacterized protein LOC125671615
LOC125646422	-5.568357384	0.000429014	VWFA and cache domain-containing protein 1-like
LOC125647979	-5.545240079	0.001346063	LOW QUALITY PROTEIN: sperm-associated antigen 16 protein-like
LOC125656218	-5.542010184	2.00E-05	RIB43A-like with coiled-coils protein 2
LOC125667146	-5.535051914	0.003441692	uncharacterized protein LOC125667146
LOC125671742	-5.519598269	9.45E-07	uncharacterized protein LOC125671742
LOC125671919	-5.506898033	0.003361502	uncharacterized protein LOC125671919
LOC125646086	-5.506896186	2.51E-07	MAM and LDL-receptor class A domain-containing protein 1-like
LOC125671240	-5.500966065	2.93E-06	extracellular signal-regulated kinase 2-like isoform X1
LOC125674006	-5.480658114	0.003304634	--
LOC125664338	-5.475343792	0.007928162	--
LOC125645789	-5.469295333	0.001351499	uncharacterized protein LOC125645789
LOC125655876	-5.455012567	1.16E-13	--
LOC125654310	-5.444507492	4.54E-05	sodium-dependent proline transporter-like

USC UNIVERSIDADE DE SANTIAGO DE COMPOSTELA

LOC125645564	-5.417619953	5.66E-06	uncharacterized protein LOC125645564
LOC125650697	-5.402620718	1.11E-05	protein FAM227B-like isoform X2
LOC125679737	-5.390361303	0.001675635	arrestin domain-containing protein 2-like
LOC125673558	-5.388963752	7.42E-05	uncharacterized protein LOC125673558
LOC125682995	-5.374104169	0.001420337	uncharacterized protein LOC125682995
LOC125669700	-5.357767557	1.07E-06	cadherin-87A-like
LOC125645866	-5.353881526	0.00612531	mucin-4-like isoform X6
LOC125665991	-5.353719863	2.07E-05	uncharacterized protein LOC125665991
LOC125683060	-5.34100433	0.004001166	uncharacterized protein LOC125683060 isoform X1
LOC125664527	-5.335065732	0.001847833	uncharacterized protein LOC125664527 isoform X1
LOC125674188	-5.324167568	4.39E-07	uncharacterized protein LOC125674188 isoform X1
LOC125657479	-5.314753863	2.16E-05	uncharacterized protein LOC125657479 isoform X1
LOC125678353	-5.313621488	2.57E-07	EF-hand domain-containing family member B-like
LOC125654732	-5.27187049	7.33E-05	uncharacterized protein LOC125654732
LOC125652782	-5.263237619	8.11E-05	neuropeptide Y receptor type 6-like
LOC125668402	-5.261683416	0.000221539	uncharacterized protein LOC125668402 isoform X1
LOC125683673	-5.258263127	3.57E-05	uncharacterized protein LOC125683673 isoform X5
LOC125672343	-5.251224137	0.000113363	--
LOC125659971	-5.245404394	3.31E-06	matrix metalloproteinase-16-like isoform X2
LOC125681019	-5.243838782	9.75E-06	short-chain collagen C4-like
LOC125649732	-5.221999381	1.95E-05	opioid-binding protein/cell adhesion molecule-like isoform X1
LOC125669794	-5.21517989	2.03E-06	uncharacterized protein LOC125669794
LOC125658990	-5.212754398	0.000361104	enolase-phosphatase E1-like isoform X2
LOC125645885	-5.208583413	0.000160709	33 kDa inner dynein arm light chain%2C axonemal-like
LOC125681167	-5.189093577	6.83E-06	CD109 antigen-like isoform X3
LOC125682968	-5.18328574	4.42E-05	twisted gastrulation protein homolog 1-A-like
LOC125653464	-5.182857818	0.001309305	fibropellin-3-like isoform X2
LOC125654577	-5.180166862	0.003370211	--
LOC125645747	-5.164902169	0.001017705	uncharacterized protein LOC125645747
LOC125656197	-5.162259543	5.22E-05	--
LOC125654847	-5.159318264	0.000294246	protein CFAP276-like isoform X2
LOC125655947	-5.14066103	0.003837315	uncharacterized protein LOC125655947
LOC125673372	-5.134004251	8.59E-06	pancreatic triacylglycerol lipase-like isoform X3
LOC125671525	-5.111803717	0.005251348	protein CFAP95-like
LOC125655603	-5.107704307	0.002954042	uncharacterized protein LOC125655603
LOC125664158	-5.098246324	2.00E-05	atrial natriuretic peptide receptor 2-like isoform X2
LOC125666040	-5.076811634	5.77E-06	uncharacterized protein LOC125666040 isoform X2
LOC125658777	-5.046311087	1.26E-05	uncharacterized protein LOC125658777 isoform X1
LOC125675914	-5.044736043	0.005625147	uncharacterized protein LOC125675914
LOC125668621	-5.040430777	1.89E-05	uncharacterized protein LOC125668621
LOC125658822	-5.036548191	1.36E-05	VPS10 domain-containing receptor SorCS1-like isoform X2
LOC125678844	-5.035075297	5.02E-05	uncharacterized protein LOC125678844
LOC125681060	-5.028179173	9.40E-05	uncharacterized protein LOC125681060
LOC125656130	-5.023798928	1.06E-05	uncharacterized protein LOC125656130 isoform X2
LOC125663912	-5.017729056	2.56E-07	large neutral amino acids transporter small subunit 1-like
LOC125672973	-5.015513929	1.23E-05	uncharacterized protein LOC125672973 isoform X2
LOC125657392	-5.014267959	0.003598526	methyltransferase-like protein 27 isoform X1
LOC125669783	-5.003670533	1.34E-05	cadherin-87A-like isoform X1
LOC125658245	-4.989243582	0.000160636	postacrosomal sheath WW domain-binding protein-like isoform X2
LOC125645448	-4.974338093	4.27E-05	uncharacterized protein LOC125645448 isoform X4
LOC125671772	-4.972896489	2.73E-05	tektin-4-like

USC UNIVERSIDADE DE SANTIAGO DE COMPOSTELA

LOC125653821	-4.958149766	8.27E-05	uncharacterized protein LOC125653821
LOC125673201	-4.942608076	5.81E-05	phenylalanine-4-hydroxylase-like isoform X1
LOC125655976	-4.912754659	0.000217337	piercer of microtubule wall 1 protein-like
LOC125650137	-4.900807041	2.85E-05	uncharacterized protein LOC125650137 isoform X6
LOC125668354	-4.892700881	8.89E-05	uncharacterized protein LOC125668354 isoform X7
LOC125679600	-4.874729587	3.90E-05	coiled-coil domain-containing protein 105-like isoform X1
LOC125652292	-4.858130898	0.000492402	cdc42 homolog
LOC125681971	-4.854880129	6.11E-05	uncharacterized protein LOC125681971 isoform X40
LOC125649178	-4.851748583	0.005499287	fibroleukin-like isoform X1
LOC125650768	-4.834278745	0.000415024	uncharacterized protein LOC125650768
LOC125660021	-4.831483387	0.000114004	sphingolipid delta(4)-desaturase DES1-like isoform X2
LOC125677370	-4.795284328	0.000391564	protein phosphatase 1 regulatory subunit 32-like
LOC125651602	-4.792810991	0.001276412	furin-like protease kpc-1
LOC125669600	-4.782924122	0.001324046	prostaglandin E2 receptor EP4 subtype-like
LOC125652018	-4.765598487	2.66E-05	uncharacterized protein LOC125652018 isoform X2
LOC125645774	-4.741924025	3.54E-05	uncharacterized protein LOC125645774 isoform X1
LOC125676046	-4.735006005	0.000338345	--
LOC125652738	-4.733882799	0.00012772	radial spoke head protein 9 homolog isoform X2
LOC125672997	-4.702980983	0.000885732	dehydrogenase/reductase SDR family member on chromosome X-like isoform X3
LOC125645895	-4.683268205	1.32E-05	uncharacterized protein LOC125645895
LOC125653613	-4.674860697	5.82E-06	dynein regulatory complex protein 11-like isoform X2
LOC125669562	-4.669758406	6.10E-05	uncharacterized protein LOC125669562 isoform X1
LOC125683094	-4.66597888	0.000275748	uncharacterized protein LOC125683094
LOC125651650	-4.655731739	0.002070064	uncharacterized protein CXorf65 homolog
LOC125660019	-4.654959316	1.21E-06	LOW QUALITY PROTEIN: protein O-mannosyl-transferase TMTC4-like
LOC125682231	-4.654034853	1.81E-05	protein Flattop homolog
LOC125680298	-4.653017349	0.000457498	ankyrin repeat and SOCS box protein 13-like
LOC125669998	-4.646545039	0.000162976	beta-1%2C3-galactosyltransferase brn-like
LOC125683574	-4.643013483	0.001723872	uncharacterized protein LOC125683574
LOC125654907	-4.631328304	0.000659655	low affinity immunoglobulin epsilon Fc receptor-like
LOC125667484	-4.566110391	0.001741397	uncharacterized protein LOC125667484
LOC125673995	-4.55027198	0.000279391	uncharacterized protein LOC125673995
LOC125673014	-4.536357002	0.000218836	uncharacterized protein LOC125673014 isoform X2
LOC125660793	-4.530507002	0.001096472	ceramide-1-phosphate transfer protein-like
LOC125681271	-4.500450618	0.000501023	cytochrome P450 2J3-like
LOC125663672	-4.469925486	0.001635639	A disintegrin and metalloproteinase with thrombospondin motifs 7-like isoform X1
LOC125652471	-4.466756497	0.000194555	uncharacterized protein LOC125652471
LOC125674691	-4.463745454	3.78E-05	coiled-coil domain-containing protein 81-like isoform X2
LOC125664454	-4.458447688	0.000854024	fatty acid-binding protein%2C heart-like
LOC125664249	-4.457922808	0.000667682	fatty acid-binding protein%2C heart-like
LOC125663136	-4.44014124	0.00138261	uncharacterized protein LOC125663136
LOC125674793	-4.419087037	0.000349459	microtubule-associated protein futsch-like isoform X4
LOC125668506	-4.411653455	0.001045385	spermatogenesis-associated protein 1-like isoform X9
LOC125673170	-4.37256676	0.005413445	pancreatic triacylglycerol lipase-like
LOC125658680	-4.368572254	5.87E-05	uncharacterized protein LOC125658680
LOC125649024	-4.366227517	0.001653542	adenylate kinase 7-like
LOC125679759	-4.341802537	0.003711689	beta-1%2C3-galactosyltransferase 1-like
LOC125658248	-4.338695032	0.001994378	uncharacterized protein LOC125658248
LOC125663921	-4.328542331	0.00117166	--
LOC125654789	-4.31239277	1.38E-05	uncharacterized protein C12orf56-like isoform X1

USC UNIVERSIDADE DE SANTIAGO DE COMPOSTELA

LOC125681983	-4.307779972	0.00108742	--
LOC125664326	-4.307336287	0.00758216	uncharacterized protein LOC125664326
LOC125650637	-4.306537331	0.001254499	uncharacterized protein LOC125650637 isoform X2
LOC125656087	-4.300628738	0.003575068	uncharacterized protein LOC125656087
LOC125657931	-4.294236705	0.000241389	tubulin beta chain
LOC125671901	-4.277349411	0.00089212	uncharacterized protein LOC125671901
LOC125649530	-4.272701802	9.01E-05	uncharacterized protein LOC125649530 isoform X1
LOC125666792	-4.252793767	0.000769815	cytochrome P450 3A4-like isoform X1
LOC125670713	-4.252610502	0.000356947	uncharacterized protein LOC125670713
LOC125662642	-4.249236964	1.63E-06	tricarboxylate transport protein%2C mitochondrial-like
LOC125650509	-4.242808087	0.000191569	--
LOC125662405	-4.234136999	2.61E-05	uncharacterized protein LOC125662405
LOC125672893	-4.224987115	0.000479356	--
LOC125672113	-4.217300783	0.001222788	uncharacterized protein LOC125672113
LOC125650701	-4.206310375	5.25E-05	uncharacterized protein LOC125650701
LOC125650855	-4.206217775	1.71E-06	advillin-like isoform X1
LOC125645439	-4.201515733	0.000181521	uncharacterized protein LOC125645439 isoform X2
LOC125678705	-4.185219738	0.000867572	von Willebrand factor A domain-containing protein 5A-like isoform X2
LOC125674310	-4.177844147	7.97E-07	oncoprotein-induced transcript 3 protein-like
LOC125649910	-4.174848694	1.09E-05	cilia- and flagella-associated protein 36-like
LOC125665752	-4.161088631	0.007949532	acid-sensing ion channel 5-like isoform X3
LOC125658518	-4.160754093	0.000591144	uncharacterized protein CXorf58-like isoform X1
LOC125654578	-4.16034299	0.001005856	kinesin-like protein KIF28P
LOC125678108	-4.158460249	0.000687472	manganese-dependent ADP-ribose/CDP-alcohol diphosphatase-like isoform X1
LOC125680315	-4.148212947	0.001710259	uncharacterized protein LOC125680315
LOC125681703	-4.144922186	0.000554569	WD repeat-containing protein 38-like isoform X2
LOC125676659	-4.132436065	1.55E-05	OTU domain-containing protein 3-like
LOC125669289	-4.125026724	9.24E-05	F-box only protein 4-like
LOC125664358	-4.123706358	0.003333354	LHFPL tetraspan subfamily member 2a protein-like
LOC125669870	-4.118346282	7.51E-05	dynein axonemal intermediate chain 4-like isoform X3
LOC125677388	-4.096630986	0.005650495	uncharacterized protein LOC125677388 isoform X2
LOC125679668	-4.092936676	0.000709174	fibroblast growth factor receptor 2-like isoform X4
LOC125650997	-4.092201372	0.000940225	cilia- and flagella-associated protein 161-like
LOC125671219	-4.092184926	0.001297915	dynein intermediate chain 3%2C ciliary-like isoform X2
LOC125658158	-4.090653999	0.000236522	uncharacterized protein C5orf49 homolog isoform X2
LOC125682538	-4.087873944	0.000896182	ammonium transporter Rh type A-like
LOC125674780	-4.06518113	0.000413419	putative inhibitor of apoptosis
LOC125673866	-4.040375352	0.002080514	uncharacterized protein LOC125673866 isoform X4
LOC125671286	-4.027629124	0.000599637	hillarin-like
LOC125679265	-4.027426613	0.000438955	innexin unc-9-like isoform X2
LOC125655217	-4.024648692	0.000130663	uncharacterized protein LOC125655217
LOC125654780	-4.002210346	0.00407836	meiosis expressed gene 1 protein homolog isoform X2
LOC125680549	-3.980535292	4.25E-05	ankyrin repeat domain-containing protein 50-like
LOC125671509	-3.972775729	0.002744733	excitatory amino acid transporter 1-like isoform X2
LOC125660974	-3.972211901	0.000581349	core-binding factor subunit beta-like isoform X1
LOC125645922	-3.965033263	0.003511349	F-box/LRR-repeat protein 7-like isoform X2
LOC125673814	-3.958254239	5.26E-06	uncharacterized protein LOC125673814 isoform X1
LOC125647240	-3.949837937	0.004268959	uncharacterized protein LOC125647240
LOC125651893	-3.945165836	0.000908779	uncharacterized protein LOC125651893
LOC125669540	-3.913919093	0.009244624	beta-1%2C3-galactosyl-O-glycosyl-glycoprotein beta-1%2C6-N-acetylglucosaminyltransferase-like
LOC125650564	-3.91192342	0.000860924	limbic system-associated membrane protein-like

USC UNIVERSIDADE DE SANTIAGO DE COMPOSTELA

LOC125654161	-3.898452832	0.000118071	uncharacterized protein LOC125654161
LOC125682586	-3.894357562	0.000353558	inositol-trisphosphate 3-kinase homolog
LOC125650791	-3.890683012	0.000395065	uncharacterized protein LOC125650791
LOC125669397	-3.883535499	0.002774623	--
LOC125654309	-3.880726804	0.000115045	sodium-dependent proline transporter-like isoform X2
LOC125682062	-3.880671486	0.001125599	ATP-dependent RNA helicase DDX39A-like isoform X1
LOC125665556	-3.879906612	0.000335654	parathyroid hormone/parathyroid hormone-related peptide receptor-like isoform X1
LOC125670593	-3.874198702	0.000182122	guanine nucleotide-binding protein G(o) subunit alpha-like
LOC125666032	-3.870127585	0.00072217	cilia- and flagella-associated protein 221-like
LOC125649775	-3.859297681	8.96E-06	serine palmitoyltransferase 2-like
LOC125674128	-3.849619738	2.08E-05	tubby protein-like isoform X4
LOC125655023	-3.838420624	1.31E-05	acetoacetyl-CoA synthetase-like
LOC125650224	-3.836991561	0.000574442	dynein axonemal light chain 1-like
LOC125683014	-3.830054202	2.71E-05	transcription factor SOX-13-like isoform X2
LOC125682438	-3.824583884	0.005316871	uncharacterized protein LOC125682438
LOC125675772	-3.818338392	0.001546548	uncharacterized WD repeat-containing protein alr3466-like
LOC125671784	-3.81438233	0.000909008	transmembrane protein 178B-like
LOC125670922	-3.813311457	0.002994086	protein FAM183B-like
LOC125672007	-3.811409143	0.005557797	uncharacterized protein LOC125672007
LOC125650966	-3.800569883	0.000170516	uncharacterized protein LOC125650966 isoform X3
LOC125665221	-3.79712149	0.000968431	D-3-phosphoglycerate dehydrogenase-like
LOC125671290	-3.792987625	8.18E-07	uncharacterized protein LOC125671290
LOC125649474	-3.781646222	0.001685099	mitochondrial uncoupling protein 2-like isoform X2
LOC125680466	-3.779540889	0.000466121	uncharacterized protein LOC125680466
LOC125673758	-3.771540883	0.000120651	androglobin-like isoform X5
LOC125668736	-3.768183516	0.006230275	calcyphosin-like protein isoform X1
LOC125659762	-3.744496148	0.001873025	E3 ubiquitin-protein ligase TRIM71-like
LOC125650992	-3.742284751	0.000145108	uncharacterized protein LOC125650992 isoform X1
LOC125658175	-3.731537124	8.18E-05	telomerase protein component 1-like
LOC125659763	-3.718116567	0.003638316	tripartite motif-containing protein 2-like
LOC125648850	-3.714757268	0.003774336	potassium channel subfamily K member 2-like
LOC125650172	-3.714284677	0.000425218	ceramide glucosyltransferase-like isoform X1
LOC125664822	-3.702745773	0.006165926	cytochrome b5 domain-containing protein 1-like
LOC125673659	-3.698728827	0.005931822	snake venom 5'-nucleotidase-like isoform X1
LOC125670262	-3.687952901	8.73E-07	protein sidekick-2-like isoform X2
LOC125674237	-3.687174274	0.000408912	threonylcarbamoyl-AMP synthase-like
LOC125675354	-3.687174274	0.000408912	threonylcarbamoyl-AMP synthase-like
LOC125683616	-3.686699478	2.11E-06	buccalin-like
LOC125669882	-3.679615179	0.004313286	ras-related protein Rap-1b-like
LOC125649489	-3.674788314	0.00207037	L-rhamnose-binding lectin CSL3-like isoform X3
LOC125677004	-3.674786559	0.001962219	uncharacterized protein LOC125677004
LOC125648354	-3.674693313	0.007210411	acireductone dioxygenase-like
LOC125658432	-3.663702669	0.000861917	--
LOC125677957	-3.660198079	0.004422081	uncharacterized protein LOC125677957
LOC125658561	-3.658891972	0.002740479	uncharacterized protein LOC125658561
LOC125649263	-3.65113609	0.003202015	calmodulin-A-like
LOC125683829	-3.646687678	0.000827366	phosphatidylserine synthase 2-like
LOC125681579	-3.645553967	0.000280526	tumor necrosis factor receptor superfamily member 16-like isoform X2
LOC125648550	-3.643015546	0.002260721	LOW QUALITY PROTEIN: inositol-3-phosphate synthase 1-A-like
LOC125654303	-3.642244876	0.001921991	neuroglian-like isoform X1
LOC125670771	-3.641074521	4.52E-06	CD151 antigen-like

USC UNIVERSIDADE DE SANTIAGO DE COMPOSTELA

LOC125678666	-3.615687505	0.000209141	tumor necrosis factor receptor superfamily member 10B-like
LOC125683685	-3.609812112	0.003623503	uncharacterized protein LOC125683685
LOC125674963	-3.60776352	0.000778393	uncharacterized protein LOC125674963 isoform X5
LOC125650553	-3.607033005	0.00060153	uncharacterized protein LOC125650553 isoform X3
LOC125671272	-3.573253418	0.001452673	uncharacterized protein LOC125671272
LOC125666740	-3.571183477	0.001588818	enkurin-like
LOC125676979	-3.568326063	0.000369217	runt-related transcription factor 1-like isoform X3
LOC125646810	-3.568054031	0.008910706	calmodulin-A-like isoform X1
LOC125648130	-3.555412023	0.00046262	fatty acid-binding protein Fh15-like
LOC125668435	-3.55420919	0.000680317	uncharacterized protein LOC125668435
LOC125666705	-3.54995979	0.000155019	tubulin alpha-1A chain
LOC125654740	-3.547128664	7.76E-06	gelsolin-like protein 2
LOC125659199	-3.544468311	0.000367562	serine/threonine-protein kinase 26-like
LOC125652204	-3.541631584	0.000191054	--
LOC125657684	-3.540993039	0.002812524	ciliary-associated calcium-binding coiled-coil protein 1-like isoform X1
LOC125657496	-3.538885729	0.000984559	sperm flagellar protein 1-like isoform X8
LOC125649132	-3.529430632	0.000194249	basal body-orientation factor 1-like
LOC125666193	-3.521254793	0.002714319	uncharacterized protein LOC125666193
LOC125675903	-3.515120248	0.006258341	--
LOC125650681	-3.512648586	0.002062454	uncharacterized protein LOC125650681
LOC125663732	-3.507390563	0.000852391	uncharacterized protein LOC125663732
LOC125679018	-3.505164196	0.002932928	LIM and calponin homology domains-containing protein 1-like isoform X3
LOC125646072	-3.505159233	7.86E-05	rootletin-like isoform X3
LOC125650288	-3.499541527	6.19E-08	methionine synthase-like isoform X2
LOC125648777	-3.498814039	0.00048605	inositol hexakisphosphate kinase 3-like isoform X3
LOC125666710	-3.483342674	4.76E-05	LOW QUALITY PROTEIN: ATP-dependent translocase ABCB1-like
LOC125668023	-3.480262657	6.79E-05	--
LOC125671283	-3.473466409	0.000255791	ADP-ribosylation factor-like protein 4C
LOC125678957	-3.470459441	0.007591704	tryptophan--tRNA ligase%2C cytoplasmic-like
LOC125666828	-3.466745724	0.00157138	cilia- and flagella-associated protein 69-like
LOC125658848	-3.465629854	0.001205269	--
LOC125681427	-3.451501695	0.00341125	tetraspanin-9-like
LOC125668324	-3.45105117	0.005697125	sodium-coupled monocarboxylate transporter 1-like
LOC125678695	-3.450027737	0.000438462	protocadherin Fat 1-like isoform X4
LOC125657066	-3.446967515	0.001907042	amine sulfotransferase-like isoform X1
LOC125678677	-3.437426081	0.004355935	prostaglandin G/H synthase 2-like
LOC125647853	-3.434781271	0.002015988	transmembrane protein 18-like
LOC125673328	-3.43227847	2.53E-11	four-jointed box protein 1-like
LOC125671281	-3.431832576	0.000569867	uncharacterized protein LOC125671281 isoform X2
LOC125683021	-3.427635314	0.007077795	LOW QUALITY PROTEIN: protein unc-93 homolog A-like
LOC125646239	-3.406210924	9.07E-06	uncharacterized protein LOC125646239
LOC125668497	-3.39872697	0.006573593	nucleoside diphosphate kinase homolog 5-like
LOC125653316	-3.388887022	0.001782403	uncharacterized protein LOC125653316
LOC125658405	-3.366827873	0.000222584	dual specificity protein phosphatase 4-like
LOC125665605	-3.36624319	0.001173148	uncharacterized protein LOC125665605
LOC125670249	-3.35583547	0.004063588	sperm-tail PG-rich repeat-containing protein 2-like
LOC125668577	-3.347972582	2.71E-05	phospholipid-transporting ATPase ABCA1-like isoform X2
LOC125659449	-3.335284334	0.006102235	LOW QUALITY PROTEIN: filamin-C-like
LOC125650750	-3.332094794	0.007387596	basic leucine zipper transcriptional factor ATF-like 3
LOC125654995	-3.331920448	4.10E-06	--
LOC125670244	-3.324963185	0.002679679	uncharacterized protein LOC125670244 isoform X4

USC UNIVERSIDADE DE SANTIAGO DE COMPOSTELA

LOC125663611	-3.314725266	0.000208529	uncharacterized protein LOC125663611 isoform X2
LOC125649969	-3.304007358	0.000172161	LOW QUALITY PROTEIN: uncharacterized protein LOC125649969
LOC125648881	-3.300744555	1.15E-05	--
LOC125664451	-3.292001709	0.003938569	dynein regulatory complex protein 10-like
LOC125654171	-3.288114921	0.00864346	uncharacterized protein LOC125654171 isoform X3
LOC125672055	-3.28159766	0.006186274	chondroitin sulfate N-acetylgalactosaminyltransferase 1-like
LOC125676019	-3.273857613	0.008760558	uncharacterized protein LOC125676019
LOC125667735	-3.27091378	2.75E-05	phosphatidate phosphatase LPIN2-like isoform X1
LOC125647422	-3.254798983	0.001225545	LOW QUALITY PROTEIN: protocadherin Fat 4-like
LOC125648295	-3.251731781	0.001763246	uncharacterized protein LOC125648295 isoform X2
LOC125649958	-3.236980722	0.004390375	spermatogenesis-associated protein 17-like isoform X2
LOC125650690	-3.23610055	0.004989076	cell division control protein 42 homolog
LOC125650378	-3.228978816	0.002019054	clathrin heavy chain linker domain-containing protein 1-like
LOC125664214	-3.224349163	0.004597456	--
LOC125678257	-3.216553026	0.001799231	TNF receptor-associated factor 2-like
LOC125658076	-3.213837428	0.003321395	uncharacterized protein LOC125658076
LOC125658318	-3.209419111	0.002652744	sialin-like
LOC125680627	-3.201207617	0.00067172	abnormal spindle-like microcephaly-associated protein homolog isoform X4
LOC125658638	-3.200328099	0.000365025	--
LOC125663581	-3.199474944	3.10E-05	ribosomal protein S6 kinase beta-1-like
LOC125680306	-3.185046184	0.002171307	transmembrane protein 145-like
LOC125665782	-3.18238783	0.000644643	LOW QUALITY PROTEIN: inositol hexakisphosphate kinase 2-like
LOC125653307	-3.180296337	0.003327307	neuroglian-like isoform X1
LOC125655560	-3.174107843	0.003111048	heme-binding protein 2-like isoform X1
LOC125675019	-3.170145118	0.001159422	protein MFI-like isoform X2
LOC125671205	-3.168283253	0.000368229	serine/threonine-protein kinase PLK1-like
LOC125668133	-3.165692331	0.00028364	GTP-binding protein 1-like
LOC125670747	-3.157806107	0.000529869	coiled-coil domain-containing protein 40-like
LOC125681745	-3.149952438	0.000750098	LOW QUALITY PROTEIN: phosphatidylinositol 4%2C5-bisphosphate 3-kinase catalytic subunit alpha isoform-like
LOC125683047	-3.149504361	0.002152233	uncharacterized protein LOC125683047
LOC125658759	-3.144503836	0.00031874	protein FAM43A-like
LOC125662819	-3.140144689	0.002679367	cysteine dioxygenase-like
LOC125663949	-3.139698569	0.003521923	dynein regulatory complex subunit 2-like
LOC125651796	-3.13528944	0.001136403	piRNA biogenesis protein EXD1-like isoform X2
LOC125682519	-3.116268808	0.00415492	uncharacterized protein LOC125682519 isoform X3
LOC125667898	-3.101476958	3.74E-05	zinc finger protein GLIS3-like
LOC125650363	-3.096984854	4.52E-05	cyclin-dependent kinase-like 1 isoform X2
LOC125679948	-3.094287104	0.00869257	spermatogenesis-associated protein 4-like isoform X2
LOC125679471	-3.08893311	0.001275266	endonuclease V-like
LOC125667751	-3.088159168	6.81E-05	phosphatidate phosphatase LPIN2-like isoform X1
LOC125651560	-3.085729201	0.006089615	uncharacterized protein LOC125651560 isoform X1
LOC125679349	-3.081188422	0.000197985	cilia- and flagella-associated protein 157-like
LOC125670224	-3.078508107	0.004507969	cilia- and flagella-associated protein 299-like
LOC125646503	-3.07626193	0.000447983	zinc finger C2HC domain-containing protein 1A-like isoform X3
LOC125668209	-3.054500752	0.000377415	uncharacterized protein LOC125668209
LOC125648977	-3.049110401	5.98E-05	phospholipid-transporting ATPase ID-like isoform X1
LOC125682214	-3.046502233	0.002478125	calcium channel flower homolog
LOC125677198	-3.039507776	0.003614568	ryncolin-1-like isoform X1
LOC125675771	-3.018420607	0.001433173	uncharacterized protein LOC125675771 isoform X2
LOC125678206	-3.006286932	0.000667553	advillin-like isoform X1
LOC125659453	-2.996137848	0.006035203	ryncolin-4-like

USC UNIVERSIDADE DE SANTIAGO DE COMPOSTELA

LOC125657452	-2.990568832	0.007064143	tripartite motif-containing protein 45-like
LOC125656967	-2.962080377	0.002831843	complement C1q subcomponent subunit B-like isoform X2
LOC125661479	-2.956529751	0.000361718	LOW QUALITY PROTEIN: testis-expressed protein 9-like
LOC125663651	-2.95502004	0.000590236	secretin receptor-like isoform X2
LOC125669787	-2.954342653	0.001137396	protein phosphatase 1 regulatory subunit 42-like isoform X7
LOC125669817	-2.95011694	0.000222263	AN1-type zinc finger protein 4-like
LOC125648950	-2.948657523	0.000110785	selenoprotein N-like isoform X2
LOC125656687	-2.942316152	0.003326636	kelch-like protein 15
LOC125678675	-2.941258295	0.000107655	cytosolic phospholipase A2-like
LOC125678056	-2.938340541	0.002598352	tripartite motif-containing protein 45-like
LOC125650398	-2.935566445	0.000449412	transmembrane protein 62-like isoform X1
LOC125669542	-2.93492016	3.62E-06	ATP-binding cassette sub-family A member 9-like isoform X1
LOC125646098	-2.914746162	0.006559736	oxidoreductase HTATIP2-like
LOC125659519	-2.911661974	0.001350355	--
LOC125676114	-2.907651675	0.001483401	exportin-4-like
LOC125655918	-2.900324741	8.60E-05	dual specificity tyrosine-phosphorylation-regulated kinase 2-like
LOC125680718	-2.896982302	0.002663716	dynein regulatory complex subunit 4-like
LOC125670517	-2.894813432	0.008453864	uncharacterized protein LOC125670517
LOC125676377	-2.891050154	0.000378315	major vault protein-like
LOC125678739	-2.882838882	0.000948389	WD repeat-containing protein 19-like
LOC125649470	-2.882796778	0.001482264	katanin p60 ATPase-containing subunit A-like 2 isoform X8
LOC125658329	-2.880686646	0.006963401	XK-related protein 9-like
LOC125667894	-2.87770952	0.000938658	adhesion G protein-coupled receptor L3-like isoform X1
LOC125645839	-2.868315384	0.000334151	contactin-5-like isoform X3
LOC125672132	-2.866653418	0.001323881	intraflagellar transport protein 172 homolog
LOC125679472	-2.861009276	0.002836724	cilia- and flagella-associated protein 77-like isoform X2
LOC125680760	-2.86014102	0.001681197	proteolipid protein DM beta-like
LOC125646741	-2.856671174	0.00167509	uncharacterized protein LOC125646741
LOC125660390	-2.854119561	0.005474976	coiled-coil domain-containing protein 92-like
LOC125679328	-2.853414443	0.006836493	uncharacterized protein LOC125679328 isoform X6
LOC125658007	-2.852327932	0.000723237	carbohydrate sulfotransferase 15-like
LOC125672776	-2.841984416	0.008909702	gelsolin-like protein 1
LOC125680913	-2.822940793	0.004472959	uncharacterized protein LOC125680913 isoform X1
LOC125648979	-2.822746461	0.001862702	cilia- and flagella-associated protein 53-like
LOC125678836	-2.819424755	0.001972002	outer dynein arm-docking complex subunit 3-like
LOC125650600	-2.816461516	0.006498648	serine/arginine repetitive matrix protein 2-like isoform X3
LOC125646999	-2.810367472	0.001067051	vesicle-associated membrane protein 8-like
LOC125668582	-2.790584257	0.000206525	repetitive organellar protein-like isoform X2
LOC125681628	-2.785145173	0.005110247	uncharacterized protein LOC125681628
LOC125662600	-2.784633037	0.001892319	uncharacterized protein LOC125662600 isoform X1
LOC125668463	-2.780290629	0.000433134	protein ecdysoneless homolog
LOC125660422	-2.772072037	0.00197885	histone demethylase UTY-like isoform X4
LOC125674120	-2.766327229	0.004951842	LOW QUALITY PROTEIN: tyrosine--tRNA ligase%2C cytoplasmic-like
LOC125651622	-2.76501121	0.00357938	uncharacterized protein LOC125651622
LOC125669902	-2.760755452	0.006589014	ADP-ribosylation factor 4-like
LOC125675210	-2.756446406	4.35E-07	parkin coregulated gene protein homolog
LOC125663803	-2.751586351	0.000693706	uncharacterized protein LOC125663803
LOC125658263	-2.749022969	0.001607516	myosin-VIIa-like
LOC125650352	-2.74538762	0.006122737	leucine-rich repeat-containing protein 23-like isoform X2
LOC125646017	-2.744921613	0.000353151	uncharacterized protein LOC125646017
LOC125668800	-2.733308431	0.000541424	uncharacterized protein LOC125668800

USC UNIVERSIDADE DE SANTIAGO DE COMPOSTELA

LOC125677005	-2.731206326	0.001730487	LOW QUALITY PROTEIN: ATP-citrate synthase-like
LOC125647642	-2.730847103	0.000422172	WD repeat-containing protein 35-like isoform X2
LOC125663648	-2.729709821	3.90E-09	uncharacterized protein LOC125663648
LOC125660879	-2.719271773	0.000844289	sodium-coupled monocarboxylate transporter 2-like isoform X3
LOC125647058	-2.710850602	0.005618788	uncharacterized protein LOC125647058
LOC125670040	-2.707443127	0.000243157	PDZ domain-containing protein GIPC1-like
LOC125665621	-2.70424805	0.003314675	ciliogenesis-associated TTC17-interacting protein-like
LOC125670216	-2.702336766	0.001654412	CD82 antigen-like isoform X2
LOC125679154	-2.697715191	0.000285784	testis-expressed protein 26-like isoform X2
LOC125659692	-2.689290218	0.004124772	uncharacterized protein LOC125659692
LOC125670728	-2.688449957	0.004263456	--
LOC125645539	-2.688044476	4.89E-05	pyrroline-5-carboxylate reductase 2-like
LOC125678554	-2.686275892	0.003407268	glutaredoxin domain-containing cysteine-rich protein CG31559-like
LOC125649232	-2.684139059	0.003469563	uncharacterized protein LOC125649232 isoform X1
LOC125664669	-2.670599426	0.001187306	cilia- and flagella-associated protein 299-like
LOC125675777	-2.66465841	0.003659663	uncharacterized protein LOC125675777 isoform X2
LOC125679199	-2.662846928	0.005159195	acyl-CoA 6-desaturase-like isoform X1
LOC125658514	-2.650721077	0.000988886	LOW QUALITY PROTEIN: lateral signaling target protein 2 homolog
LOC125645629	-2.646064468	0.000676552	LOW QUALITY PROTEIN: neural cell adhesion molecule L1-like
LOC125647856	-2.637517017	0.00278952	cytochrome P450 302a1%2C mitochondrial-like
LOC125672324	-2.637305981	0.004997267	tetratricopeptide repeat protein 30A-like
LOC125672330	-2.637305981	0.004997267	tetratricopeptide repeat protein 30A-like
LOC125657109	-2.634428407	0.000243084	haloacid dehalogenase-like hydrolase domain-containing 5
LOC125667433	-2.632213721	0.001795936	uncharacterized protein LOC125667433 isoform X1
LOC125648190	-2.626004897	0.000813182	alanine--tRNA ligase%2C cytoplasmic-like
LOC125663827	-2.609184615	0.00145814	PH domain leucine-rich repeat-containing protein phosphatase 2-like isoform X2
LOC125663779	-2.60376105	0.002677862	uncharacterized protein LOC125663779
LOC125666711	-2.603340039	0.001021817	tubulin alpha-1A chain-like
LOC125678234	-2.603110746	0.000331445	ETS translocation variant 4-like isoform X3
LOC125650335	-2.592341197	0.008156905	uncharacterized protein LOC125650335 isoform X3
LOC125670464	-2.590212363	0.005368443	synaptotagmin-15-like
LOC125673040	-2.587408683	0.001797575	mucin-17-like isoform X2
LOC125674087	-2.580745054	0.000798377	unconventional myosin-VI-like isoform X1
LOC125683372	-2.567177697	0.000700479	methylenetetrahydrofolate reductase-like
LOC125682960	-2.56403948	0.003190385	serine-rich adhesin for platelets-like
LOC125683076	-2.553767123	9.11E-05	uncharacterized protein LOC125683076 isoform X4
LOC125683384	-2.550306332	0.001053272	uncharacterized protein LOC125683384
LOC125666741	-2.543311587	0.003000331	calaxin-like
LOC125657499	-2.5424043	0.00170735	uncharacterized protein LOC125657499
LOC125655067	-2.536410756	0.004643662	uncharacterized protein LOC125655067
LOC125670882	-2.534344225	0.004010906	LITAF domain-containing protein-like
LOC125670753	-2.532658798	0.004920367	uncharacterized protein LOC125670753 isoform X5
LOC125675094	-2.530359652	0.000223663	innexin-11-like
LOC125653750	-2.5258162	0.001186008	protein DD3-3-like isoform X1
LOC125656632	-2.525424431	0.000116436	serine/threonine-protein kinase TBK1-like
LOC125657220	-2.523932736	0.002591367	cell division cycle protein 123 homolog
LOC125661887	-2.511427254	0.00096996	ATP-dependent translocase ABCB1-like isoform X3
LOC125658217	-2.509318199	0.003024337	casein kinase I-like
LOC125683598	-2.504011134	0.001248853	uncharacterized protein LOC125683598 isoform X1
LOC125650711	-2.503482186	0.008892329	ryncolin-1-like
LOC125682436	-2.502898032	0.007202727	spartin-like

USC UNIVERSIDADE DE SANTIAGO DE COMPOSTELA

LOC125659376	-2.501547441	0.001115932	F-box only protein 36-like
LOC125679695	-2.501414795	0.002180732	valine--tRNA ligase-like
LOC125656334	-2.498342969	0.002047235	neural-cadherin-like isoform X4
LOC125678959	-2.494712663	0.003085278	serine/threonine-protein kinase Nek7-like
LOC125647011	-2.484989963	0.000149636	LOW QUALITY PROTEIN: neurexin-4-like
LOC125676996	-2.47604056	0.003948356	UDP-glucuronic acid decarboxylase 1-like isoform X2
LOC125683670	-2.474209768	0.000418357	programmed cell death 6-interacting protein-like isoform X2
LOC125656190	-2.469944497	0.009223821	protein sll1483-like
LOC125670050	-2.466828469	0.005000724	LOW QUALITY PROTEIN: IQ domain-containing protein K-like
LOC125670589	-2.463287448	0.004162232	uncharacterized protein LOC125670589
LOC125659770	-2.450928437	0.007326601	dynein regulatory complex protein 9-like isoform X2
LOC125667260	-2.442088242	0.000701863	spartin-like
LOC125653965	-2.432025073	0.002038343	uncharacterized protein LOC125653965 isoform X1
LOC125651874	-2.424737314	0.003484633	G2/mitotic-specific cyclin-B-like
LOC125674611	-2.421622565	0.001816325	hillarin-like isoform X2
LOC125675165	-2.408852995	0.004268377	uncharacterized protein LOC125675165 isoform X1
LOC125671194	-2.405583002	0.008341398	afadin- and alpha-actinin-binding protein-like
LOC125679944	-2.401226941	0.004054681	histidine--tRNA ligase-like isoform X1
LOC125645916	-2.394399797	0.000827986	phosphatidate phosphatase LPIN2-like isoform X2
LOC125657888	-2.386725581	0.005793996	dynein light chain Tctex-type protein 2B-like
LOC125661373	-2.375716122	0.00510164	uncharacterized protein LOC125661373
LOC125658101	-2.372012113	0.008397456	mid1-interacting protein 1A-like
LOC125657106	-2.360391251	0.000376	isoleucine--tRNA ligase%2C cytoplasmic-like isoform X1
LOC125666707	-2.360332767	0.003751621	ATP-dependent translocase ABCB1-like isoform X5
LOC125645632	-2.359189601	0.006973936	NPC intracellular cholesterol transporter 1-like
LOC125651836	-2.357721533	0.001055515	phospholipid scramblase 2-like isoform X2
LOC125678632	-2.354974058	0.001074479	advanced glycosylation end product-specific receptor-like isoform X1
LOC125678371	-2.341946409	5.82E-06	choline transporter-like protein 2 isoform X3
LOC125672122	-2.341922716	0.001491757	enkurin domain-containing protein 1-like
LOC125677980	-2.336550243	0.000290858	serine/threonine-protein kinase NLK-like isoform X2
LOC125680624	-2.331173806	0.004214022	leucine--tRNA ligase%2C cytoplasmic-like
LOC125683065	-2.328642613	0.001709652	nuclear receptor subfamily 1 group D member 2-like
LOC125683518	-2.326616478	0.0007401	armadillo repeat protein deleted in velo-cardio-facial syndrome homolog isoform X4
LOC125667585	-2.3264353	0.004145053	Krueppel-like factor 6 isoform X2
LOC125667604	-2.3264353	0.004145053	Krueppel-like factor 6 isoform X1
LOC125671119	-2.326364416	0.005624605	transcription factor SOX-11-like
LOC125666768	-2.324980878	0.001453304	insulin-induced gene 2 protein-like isoform X2
LOC125675220	-2.322044142	0.007983931	arrestin domain-containing protein 17-like
LOC125660494	-2.314050493	0.00083135	probable JmjC domain-containing histone demethylation protein 2C isoform X4
LOC125648076	-2.313991793	0.002649305	serine/threonine-protein kinase RIO3-like isoform X1
LOC125667916	-2.309870247	0.002525749	prominin-1-like
LOC125674462	-2.306174011	0.000442108	afadin-like isoform X1
LOC125668799	-2.302219079	0.005852353	E3 ubiquitin-protein ligase RNF170-like
LOC125653959	-2.300768318	0.003030527	inosine-5'-monophosphate dehydrogenase 1b-like isoform X1
LOC125680484	-2.30034742	0.001392125	mitogen-activated protein kinase kinase kinase 13-A-like isoform X1
LOC125672954	-2.295384545	0.001155606	SIN3-HDAC complex-associated factor-like
LOC125663721	-2.294493721	0.004636926	uncharacterized protein LOC125663721 isoform X1
LOC125653749	-2.275939219	0.000450269	protein DD3-3-like
LOC125663265	-2.270423951	0.005631428	cellular tumor antigen p53-like isoform X3
LOC125656982	-2.270180084	0.001943216	LOW QUALITY PROTEIN: protein prickle-like
LOC125678357	-2.268728273	0.004141987	innexin unc-9-like isoform X2

USC UNIVERSIDADE DE SANTIAGO DE COMPOSTELA

LOC125651575	-2.266208646	0.004221229	UDP-galactose transporter senju-like
LOC125657971	-2.264548515	0.001805414	catenin alpha-2-like isoform X1
LOC125668414	-2.260317057	0.000759722	midnolin-A-like
LOC125659973	-2.257318604	0.001305844	uncharacterized protein LOC125659973
LOC125672065	-2.25720403	0.007202694	uncharacterized protein LOC125672065
LOC125674020	-2.2423104	0.001388216	synaptotagmin-1-like isoform X1
LOC125669252	-2.238248823	0.005588882	uncharacterized protein LOC125669252
LOC125667290	-2.230077634	0.009177446	ETS translocation variant 4-like isoform X1
LOC125665955	-2.228793413	0.004865586	rho-related GTP-binding protein RhoE-like
LOC125670436	-2.2210451	0.001516883	uncharacterized protein LOC125670436 isoform X1
LOC125659917	-2.220975601	0.004764622	uncharacterized protein LOC125659917
LOC125650425	-2.215419773	0.007403419	ubiquitin-associated protein 1-like isoform X2
LOC125667422	-2.212790475	0.004647164	F-box only protein 8-like
LOC125673287	-2.201529522	1.80E-09	uncharacterized protein LOC125673287
LOC125665257	-2.197744755	0.006092038	arylsulfatase B-like isoform X5
LOC125665753	-2.195335113	0.002539122	transmembrane protein 198-like
LOC125658078	-2.192846665	0.000875822	melanotransferrin-like
LOC125658816	-2.191845895	0.008003032	--
LOC125674859	-2.185166748	0.006660046	tumor necrosis factor alpha-induced protein 3-like isoform X6
LOC125671011	-2.184939986	0.008686579	zinc finger protein 37-like
LOC125669634	-2.158950504	0.005641239	multiple epidermal growth factor-like domains protein 6
LOC125682528	-2.157107027	0.005396083	protein crumbs-like isoform X3
LOC125668535	-2.146437928	0.002368184	elongation of very long chain fatty acids protein 6-like
LOC125680770	-2.144131037	0.001110354	transmembrane protein 165-like
LOC125663964	-2.139127556	0.002915782	uncharacterized protein LOC125663964
LOC125657189	-2.133134645	0.00541293	ras-related protein Rab-34-like
LOC125681929	-2.128553249	0.000369396	upstream stimulatory factor 2-like isoform X1
LOC125649846	-2.124032394	0.002683976	band 4.1-like protein 1 isoform X2
LOC125678128	-2.122397419	0.00320495	poly [ADP-ribose] polymerase tankyrase-1-like
LOC125648951	-2.120610602	0.001626125	GTP-binding protein 2-like
LOC125683619	-2.112908369	0.00132983	MOB kinase activator 2-like isoform X3
LOC125646246	-2.101845205	0.003127881	rabphilin-3A-like isoform X2
LOC125665532	-2.090216901	0.003213855	nucleolar protein dao-5-like isoform X9
LOC125672828	-2.088449101	0.004590502	intraflagellar transport protein 74 homolog
LOC125674017	-2.084138687	0.00681222	major vault protein-like
LOC125674126	-2.08340418	0.00307348	LOW QUALITY PROTEIN: acetyl-CoA carboxylase-like
LOC125658062	-2.080019438	0.000448829	spermine oxidase-like
LOC125670463	-2.07892797	0.00618708	uncharacterized protein LOC125670463
LOC125665982	-2.076717972	0.003707221	fatty acid 2-hydroxylase-like isoform X3
LOC125682295	-2.070524272	0.00665925	sodium bicarbonate cotransporter 3-like isoform X4
LOC125659022	-2.069612737	0.006415682	fibroblast growth factor receptor 4-like isoform X1
LOC125646218	-2.05607317	0.005308429	elongation of very long chain fatty acids protein 4-like isoform X1
LOC125658897	-2.052936289	0.004631011	synaptobrevin homolog YKT6-like
LOC125649755	-2.047070498	0.000593384	sprouty-related%2C EVH1 domain-containing protein 2-like isoform X1
LOC125670093	-2.039575659	0.003282227	synaptogyrin-3-like
LOC125681697	-2.031395674	0.001716805	--
LOC125670864	-2.025339496	0.005986436	MTOR-associated protein MEAK7-like
LOC125659703	-2.01874273	0.006354581	methyltransferase-like protein 27 isoform X2
LOC125683287	-2.010685315	0.000123397	uncharacterized protein LOC125683287
LOC125676497	-2.009127172	0.000221002	prolyl 4-hydroxylase subunit alpha-1-like
LOC125649064	-2.003154153	0.00865254	spermatogenesis-associated protein 7-like isoform X2

USC UNIVERSIDADE DE SANTIAGO DE COMPOSTELA

LOC125668043	-2.001235115	0.000150791	maltase-glucoamylase-like
LOC125672196	-1.992652308	0.004070011	dynein axonemal light chain 4-like
LOC125661177	-1.983009044	0.002862489	AN1-type zinc finger protein 6-like
LOC125650547	-1.978938106	0.00113121	ERO1-like protein beta isoform X1
LOC125683839	-1.978136889	0.006801531	--
LOC125681203	-1.977583339	0.004240201	LOW QUALITY PROTEIN: calsyntenin-1-like
LOC125670055	-1.977352202	0.005852261	very low-density lipoprotein receptor-like isoform X1
LOC125682767	-1.969435106	0.003319305	serine/threonine-protein kinase H1 homolog
LOC125674900	-1.962247744	0.007165366	circularly permutated Ras protein 1-like
LOC125671319	-1.960952641	0.000459566	testican-1-like
LOC125683702	-1.943357358	0.008834007	uncharacterized protein LOC125683702
LOC125679009	-1.94255841	0.001245402	protocadherin beta-15-like
LOC125660924	-1.93879147	0.00372487	ras-responsive element-binding protein 1-like isoform X1
LOC125653511	-1.937853347	0.004970712	putative ankyrin repeat protein RF_0381
LOC125666671	-1.935378724	0.002925067	--
LOC125646279	-1.934633979	0.003279156	centriolar satellite-associated tubulin polyglutamylase complex regulator 1-like isoform X1
LOC125649550	-1.932783349	0.007948193	uncharacterized protein LOC125649550
LOC125665783	-1.930423151	0.006815333	secretin receptor-like isoform X4
LOC125654836	-1.92867956	0.005125633	LHFPL tetraspan subfamily member 3 protein-like isoform X2
LOC125683083	-1.926378192	0.006860813	LOW QUALITY PROTEIN: aspartate--tRNA ligase%2C cytoplasmic-like
LOC125669698	-1.912419321	0.000709505	receptor-type tyrosine-protein phosphatase kappa-like
LOC125673874	-1.907478816	0.008935047	TBC1 domain family member 15-like isoform X2
LOC125670805	-1.900731508	0.008673291	uncharacterized protein LOC125670805
LOC125662772	-1.895627329	0.002460178	ras-related protein Rab-11A isoform X2
LOC125647936	-1.894798824	0.008469089	protein LKAAEAR1-like
LOC125669594	-1.877774669	0.003084776	inositol hexakisphosphate kinase 1-like
LOC125657253	-1.8738829	0.003888932	protein kinase C delta type-like isoform X3
LOC125659638	-1.854191294	0.00520759	myosin%2C essential light chain%2C adductor muscle-like isoform X1
LOC125673545	-1.853318978	0.005107486	adenosylhomocysteinase A-like
LOC125677553	-1.850813512	0.001197813	death-associated inhibitor of apoptosis 2-like
LOC125657118	-1.849879489	0.001224768	MAP kinase-activated protein kinase 2-like isoform X2
LOC125668153	-1.843079686	0.002572767	uncharacterized protein LOC125668153
LOC125678207	-1.842836872	0.002167854	dnaJ homolog subfamily C member 7-like
LOC125656324	-1.842595934	0.007549381	tumor protein p63-regulated gene 1-like protein
LOC125645714	-1.837639172	0.003880501	ligand of Numb protein X 2-like isoform X2
LOC125646951	-1.831597006	0.004456813	--
LOC125680278	-1.8312514	0.000388277	folylpolyglutamate synthase%2C mitochondrial-like isoform X6
LOC125663686	-1.830768943	0.001823165	--
LOC125660497	-1.829955313	0.001647858	LOW QUALITY PROTEIN: uncharacterized protein LOC125660497
LOC125646608	-1.824630082	0.003027409	zinc finger protein 271-like
LOC125645893	-1.812313335	0.002866369	nuclear factor erythroid 2-related factor 2-like isoform X2
LOC125671665	-1.808849934	0.001306887	serine/threonine-protein kinase Sgk1-like isoform X2
LOC125675811	-1.808026784	0.006708714	transcription factor ces-2-like
LOC125667907	-1.807299663	0.007301399	tax1-binding protein 3 homolog
LOC125658927	-1.80048489	0.003460152	LOW QUALITY PROTEIN: tetraspanin-33-like
LOC125665234	-1.786277114	0.009233277	solute carrier family 28 member 3-like isoform X2
LOC125670153	-1.78195418	0.00315649	DCN1-like protein 3
LOC125646132	-1.781142764	0.000956736	uncharacterized protein LOC125646132
LOC125680555	-1.778649365	0.008175612	LOW QUALITY PROTEIN: dynein axonemal heavy chain 5-like
LOC125660862	-1.778340148	0.000244969	malectin-A-like
LOC125675880	-1.774183531	0.000763208	uncharacterized protein LOC125675880 isoform X4

USC UNIVERSIDADE DE SANTIAGO DE COMPOSTELA

LOC125666778	-1.773791515	0.009031251	sterol O-acyltransferase 1-like
LOC125645447	-1.771259652	0.002369764	uncharacterized protein LOC125645447
LOC125651766	-1.762933562	0.006191643	cyclic AMP-dependent transcription factor ATF-4-like
LOC125660093	-1.759850551	0.00723248	kelch-like protein 26 isoform X3
LOC125669515	-1.758854803	0.003260099	tubulin polymerization-promoting protein family member 3-like
LOC125658506	-1.756385351	0.000372137	cAMP-dependent protein kinase catalytic subunit 3-like
LOC125674133	-1.753386746	0.006861095	GDP-L-fucose synthase-like
LOC125669622	-1.751791854	0.007168794	uncharacterized protein LOC125669622 isoform X1
LOC125682018	-1.751731674	0.006524595	transmembrane protein 41A-like
LOC125653355	-1.751439525	0.001725131	--
LOC125672110	-1.749369265	0.00786572	MAP kinase-interacting serine/threonine-protein kinase 1-like isoform X1
LOC125666021	-1.74265897	0.007173103	tyrosine-protein phosphatase non-receptor type 4-like isoform X9
LOC125681420	-1.741004214	0.005573637	NF-kappa-B inhibitor zeta-like isoform X2
LOC125649472	-1.731645272	0.005603086	LOW QUALITY PROTEIN: la-related protein 6-like
LOC125669664	-1.731007743	0.001825605	uncharacterized protein LOC125669664
LOC125647727	-1.730416118	0.003843156	uncharacterized protein LOC125647727
LOC125679688	-1.728526206	0.000700247	NADPH--cytochrome P450 reductase-like isoform X2
LOC125674744	-1.727323898	0.00181321	staphylococcal nuclease domain-containing protein 1-like
LOC125658418	-1.721958267	0.000963523	phospholipase DDHD2-like
LOC125681829	-1.711478624	0.000613067	calsyntenin-1-like
LOC125659481	-1.706928987	0.004760637	MORN repeat-containing protein 4-like
LOC125672923	-1.703874292	0.008615774	coiled-coil domain-containing protein 102A-like
LOC125652060	-1.703529106	0.000160026	--
LOC125666795	-1.697604344	0.004622816	galectin-4-like
LOC125652825	-1.697425102	0.002555224	TOG array regulator of axonemal microtubules protein 1-like isoform X4
LOC125648922	-1.692521404	0.003613455	sodium-dependent phosphate transport protein 2B-like isoform X1
LOC125676109	-1.680943353	0.007277636	uncharacterized protein LOC125676109
LOC125659347	-1.67854233	0.000137204	--
LOC125669940	-1.648399916	0.004825253	E3 ubiquitin-protein ligase SMURF2-like
LOC125647590	-1.648117624	0.000112486	uncharacterized protein LOC125647590
LOC125648043	-1.640524319	0.008003996	uncharacterized protein LOC125648043
LOC125683004	-1.636804382	0.003191262	uncharacterized protein LOC125683004 isoform X1
LOC125673981	-1.631809458	0.003221235	LOW QUALITY PROTEIN: serine/threonine-protein kinase LATS1-like
LOC125649862	-1.629639798	0.00089458	3'(2')%2C5'-bisphosphate nucleotidase 1-like
LOC125678643	-1.626855777	0.006746623	uncharacterized protein LOC125678643 isoform X6
LOC125649343	-1.609645297	0.000496644	carnitine O-palmitoyltransferase 1%2C liver isoform-like isoform X3
LOC125645522	-1.601621292	0.004268384	uncharacterized protein LOC125645522
LOC125668691	-1.591213323	0.006440613	titin-like
LOC125660929	-1.591193943	0.005836412	disintegrin and metalloproteinase domain-containing protein 10-like isoform X1
LOC125669973	-1.586594575	0.001421556	transmembrane protein 184B-like
LOC125668355	-1.574725008	0.002185209	glutamine--fructose-6-phosphate aminotransferase [isomerizing] 1-like isoform X11
LOC125646356	-1.570827902	0.000778056	PHD finger protein 13-like isoform X2
LOC125670243	-1.567958603	0.005986771	uncharacterized protein LOC125670243 isoform X2
LOC125675748	-1.56495694	0.005355078	transmembrane protein 50B-like
LOC125680401	-1.561035305	0.001803794	PGAP2-interacting protein-like isoform X1
LOC125675415	-1.560927933	0.001567802	CUGBP Elav-like family member 2 isoform X7
LOC125655049	-1.558426262	0.004320798	adiponectin receptor protein-like
LOC125649281	-1.554847822	0.004363022	estrogen receptor beta-like
LOC125646695	-1.549064042	0.004234176	sodium/potassium-transporting ATPase subunit beta-1-interacting protein 3-like isoform X2
LOC125667164	-1.547485692	0.006793127	uncharacterized protein LOC125667164

USC UNIVERSIDADE DE SANTIAGO DE COMPOSTELA

LOC125670271	-1.547472886	0.004736448	carboxypeptidase E-like
LOC125678980	-1.539138421	0.007402173	phospholipid-transporting ATPase VB-like
LOC125673946	-1.538827289	0.008166598	solute carrier family 35 member E2A-like
LOC125645518	-1.535973626	0.004768607	one cut domain family member 2-like isoform X3
LOC125678525	-1.529058135	0.000508931	disco-interacting protein 2 homolog C-like isoform X11
LOC125678271	-1.523436025	0.000216997	copper-transporting ATPase 1-like isoform X3
LOC125651530	-1.519337515	0.003481892	--
LOC125669872	-1.504023193	0.000218985	mesoderm induction early response protein 1-like isoform X3
LOC125649140	-1.493559421	0.00052434	inositol-trisphosphate 3-kinase B-like isoform X3
LOC125678360	-1.475869277	0.002131936	innexin unc-9-like
LOC125680755	-1.467980201	0.003590629	serine/threonine-protein phosphatase 1 regulatory subunit 10-like isoform X3
LOC125647173	-1.467768973	0.004291204	LOW QUALITY PROTEIN: zinc finger protein 704-like
LOC125651466	-1.459753411	0.004639683	peptide-N(4)-(N-acetyl-beta-glucosaminyl)asparagine amidase-like
LOC125666077	-1.44601471	0.007365401	LOW QUALITY PROTEIN: rho GTPase-activating protein 21-like
LOC125669693	-1.445537377	0.001606422	serine hydroxymethyltransferase-like
LOC125655593	-1.438434506	0.008266616	ubiquitin-like modifier-activating enzyme 1 isoform X10
LOC125657901	-1.427969204	0.00201927	divergent protein kinase domain 2A-like isoform X2
LOC125659151	-1.425756984	0.000368889	nuclear hormone receptor HR96-like isoform X9
LOC125671020	-1.415052644	0.007253584	thymocyte selection-associated high mobility group box protein TOX-like isoform X1
LOC125679204	-1.413884279	0.007870086	next to BRCA1 gene 1 protein-like isoform X2
LOC125654580	-1.411021563	0.001492204	host cell factor 2-like isoform X3
LOC125657163	-1.407238793	0.005511235	serine/threonine-protein phosphatase 4 regulatory subunit 2-like isoform X3
LOC125683306	-1.404571993	0.004070961	SWI/SNF complex subunit SMARCC2-like isoform X2
LOC125680572	-1.403507649	0.003337914	N(G)%2CN(G)-dimethylarginine dimethylaminohydrolase 1-like
LOC125668792	-1.401107234	0.007957095	LOW QUALITY PROTEIN: ankyrin repeat and KH domain-containing protein 1-like
LOC125682545	-1.398354447	0.000661341	CCR4-NOT transcription complex subunit 7-like
LOC125669268	-1.395770376	0.003649485	S-adenosylmethionine synthase-like
LOC125669663	-1.393269987	0.000149688	uncharacterized protein LOC125669663
LOC125678735	-1.385439079	0.004897086	ubiquitin-conjugating enzyme E2 G1-like
LOC125674336	-1.37811662	0.003317068	carboxypeptidase D-like
LOC125646044	-1.37165939	0.005924614	uncharacterized protein LOC125646044 isoform X2
LOC125648862	-1.364357998	0.006016623	transcriptional repressor protein YY1-like isoform X7
LOC125668429	-1.363532016	0.005898636	multiple epidermal growth factor-like domains protein 10 isoform X1
LOC125653521	-1.36030246	0.006875868	E3 ubiquitin-protein ligase HUWE1-like isoform X5
LOC125678304	-1.357174789	0.005606656	ADP-ribosylation factor-like protein 3
LOC125678879	-1.354800794	0.005931604	la-related protein 4-like isoform X4
LOC125650522	-1.351633108	0.006016133	serine incorporator 5-like
LOC125662530	-1.349064683	0.000712157	--
LOC125670446	-1.347356987	0.006170998	eyes absent homolog 2-like isoform X3
LOC125676408	-1.345201562	0.001149455	zinc finger protein AEBP2-like
LOC125648809	-1.34380248	0.003280478	CKLF-like MARVEL transmembrane domain-containing protein 4
LOC125663981	-1.333229898	0.003293497	centrosomal protein of 76 kDa-like
LOC125670874	-1.330669993	0.008368314	ras-related protein Rab-23-like
LOC125674512	-1.32435465	0.005931458	sialomucin core protein 24-like
LOC125649467	-1.31483796	0.001947597	ras guanyl-releasing protein 3-like isoform X4
LOC125657526	-1.299541019	0.004563961	--
LOC125683095	-1.288464357	0.008468965	V-type proton ATPase 116 kDa subunit a 1-like isoform X2
LOC125649027	-1.279682079	0.008331404	REST corepressor 1-like isoform X2
LOC125654857	-1.275979982	0.003210127	constitutive coactivator of PPAR-gamma-like protein 1 homolog
LOC125677742	-1.275816928	0.000776418	bcl-2 homologous antagonist/killer-like

USC UNIVERSIDADE DE SANTIAGO DE COMPOSTELA

LOC125678358	-1.271500632	0.000802382	innexin unc-9-like
LOC125653661	-1.26940721	0.005037966	--
LOC125652938	-1.269305381	0.00652384	--
LOC125682515	-1.268817151	0.001824709	far upstream element-binding protein 1-like isoform X4
LOC125678913	-1.266686622	0.007084652	tyrosine-protein kinase ABL1-like isoform X2
LOC125664421	-1.264300582	0.008204123	vigilin-like
LOC125668310	-1.259221552	0.000199553	THO complex subunit 4-like isoform X1
LOC125664020	-1.252860638	0.000660725	uncharacterized protein C1orf50 homolog
LOC125657525	-1.238311207	0.005013311	receptor expression-enhancing protein 1-like isoform X1
LOC125672054	-1.214326166	0.002124878	protein tweety homolog 1-A-like isoform X2
LOC125648345	-1.207144676	0.002842293	Na(+)/H(+) exchange regulatory cofactor NHE-RF1-like
LOC125646355	-1.185417843	0.007881098	LOW QUALITY PROTEIN: BET1 homolog
LOC125651702	-1.185247723	0.00849242	--
LOC125683077	-1.174836091	0.004705547	N-chimaerin-like isoform X1
LOC125646712	-1.16730067	0.007805215	chromodomain-helicase-DNA-binding protein Mi-2 homolog isoform X8
LOC125649176	-1.15407901	0.007497077	LOW QUALITY PROTEIN: vasodilator-stimulated phosphoprotein-like
LOC125679361	-1.148753458	0.008291635	importin subunit beta-1-like isoform X3
LOC125663601	-1.142669548	0.008247132	NEDD4-like E3 ubiquitin-protein ligase WWP1 isoform X1
LOC125666617	-1.14216639	0.000914739	cytoplasmic dynein 1 light intermediate chain 2-like isoform X2
LOC125651792	-1.131401885	0.004674222	SH2 domain-containing adapter protein D-like isoform X5
LOC125673292	-1.117151357	0.003501025	uncharacterized protein LOC125673292
LOC125646047	-1.093580269	0.003682487	gamma-aminobutyric acid receptor-associated protein-like 2
LOC125665856	-1.091920925	0.002584149	bcl-2-like protein 1 isoform X2
LOC125679136	-1.088939315	0.001067131	high affinity copper uptake protein 1-like isoform X5
LOC125656827	-1.077088456	0.002891645	phosphatidylinositol transfer protein alpha isoform-like
LOC125668301	-1.063722057	0.005113172	epsin-2-like isoform X1
LOC125671472	-1.061637387	0.001050262	store-operated calcium entry-associated regulatory factor-like
LOC125680676	-1.031591067	0.009277137	protein GPR107-like
LOC125645935	-1.025789164	0.003061058	--
LOC125667675	-1.022147388	0.007353204	DNA-directed RNA polymerase II subunit RPB2
LOC125682360	-1.022122112	0.003446024	Krueppel-like factor 8 isoform X1
LOC125659657	-0.988712198	0.001152372	ceramide glucosyltransferase-like
LOC125650266	-0.98148179	0.008426952	ceramide transfer protein-like
LOC125645882	-0.977624493	0.007816125	LOW QUALITY PROTEIN: NGFI-A-binding protein 1-like
LOC125651968	-0.971428166	0.002099002	guanine nucleotide-binding protein G(s) subunit alpha-like
GeneID_11341132	0.91634722	0.008979042	--
LOC125671447	1.011845904	0.00531823	receptor-type tyrosine-protein phosphatase kappa-like isoform X6
LOC125680744	1.092689344	0.004892975	golgin subfamily A member 6-like protein 22
LOC125655615	1.112497267	0.006189198	dihydrolipoyl dehydrogenase%2C mitochondrial-like isoform X1
LOC125682916	1.128259402	0.009078637	microtubule-associated protein futsch-like
LOC125654881	1.129834312	0.004506689	steroid 17-alpha-hydroxylase/17%2C20 lyase-like
LOC125672535	1.140423681	0.00928807	uncharacterized protein LOC125672535
LOC125658690	1.201912633	0.009107856	uncharacterized protein LOC125658690
LOC125652345	1.204785691	0.003402079	uncharacterized protein LOC125652345
LOC125679741	1.210286364	0.006923171	uncharacterized protein LOC125679741
LOC125658264	1.21402546	0.009324335	serine/threonine-protein phosphatase 2A regulatory subunit B" subunit beta-like isoform X2
LOC125646888	1.228562404	0.00712212	peptidyl-prolyl cis-trans isomerase-like
LOC125669879	1.23420251	0.000919454	mitochondrial glycine transporter-like
LOC125649220	1.266489118	0.00821694	--
LOC125664142	1.270227277	0.008812949	39S ribosomal protein L51%2C mitochondrial-like
LOC125674217	1.282154299	0.007396254	uncharacterized protein LOC125674217

USC UNIVERSIDADE DE SANTIAGO DE COMPOSTELA

LOC125682601	1.282580745	0.004411367	uncharacterized protein LOC125682601
LOC125651824	1.284406868	0.008034424	uncharacterized protein LOC125651824
LOC125651999	1.288768777	0.005843242	peptidyl-prolyl cis-trans isomerase B-like
LOC125671524	1.292128527	0.003595244	S-methyl-5'-thioadenosine phosphorylase-like isoform X2
LOC125668312	1.297853913	0.007108569	putative ATP synthase subunit f%2C mitochondrial
LOC125670645	1.301546593	0.00252684	uncharacterized protein LOC125670645
LOC125671625	1.30591049	0.008293008	uncharacterized protein LOC125671625
LOC125658333	1.319154142	0.006914212	uncharacterized protein LOC125658333 isoform X2
LOC125671179	1.330383671	0.002976342	ATP synthase subunit d%2C mitochondrial-like
LOC125650545	1.34534037	0.000992818	--
LOC125671226	1.34688571	0.004582422	peroxiredoxin prdx-2-like
LOC125672089	1.348867182	0.005925685	NADH-ubiquinone oxidoreductase subunit 8-like isoform X1
LOC125670564	1.35489352	0.00646133	ATP synthase subunit delta%2C mitochondrial-like
LOC125682949	1.37357628	0.006012628	17-beta-hydroxysteroid dehydrogenase 14-like
LOC125666722	1.383858788	0.009228118	cytochrome c oxidase subunit 4 isoform 1%2C mitochondrial-like
LOC125673754	1.399223329	0.005436581	LOW QUALITY PROTEIN: xaa-Pro aminopeptidase 1-like
LOC125655977	1.408032592	0.002258731	NADH dehydrogenase [ubiquinone] 1 beta subcomplex subunit 11%2C mitochondrial-like
LOC125659158	1.412240258	0.005334611	succinate--CoA ligase [ADP-forming] subunit beta%2C mitochondrial-like
LOC125670560	1.418712392	0.000369168	cytochrome c oxidase subunit 5B%2C mitochondrial-like
LOC125645860	1.431445647	7.89E-05	RNA-binding protein 24-A-like isoform X1
LOC125677681	1.433919932	0.006249798	protein BCCIP homolog
LOC125652521	1.437515973	0.003360549	NADH dehydrogenase [ubiquinone] iron-sulfur protein 4%2C mitochondrial-like
LOC125663888	1.444503208	0.000910624	MICOS complex subunit Mic10-like
LOC125673856	1.455508256	0.001727831	uncharacterized protein LOC125673856 isoform X1
LOC125652336	1.473694381	0.007670156	uncharacterized protein LOC125652336
LOC125674369	1.482032319	0.004917476	malate dehydrogenase%2C mitochondrial-like isoform X1
LOC125667976	1.490730897	0.002661567	acyl carrier protein%2C mitochondrial-like
LOC125653790	1.495323158	0.002639433	uncharacterized protein LOC125653790 isoform X1
LOC125674388	1.51896593	0.009088511	mitochondrial 2-oxoglutarate/malate carrier protein-like
LOC125648682	1.538344716	0.006695548	trafficking protein particle complex subunit 2-like
LOC125672062	1.549641546	0.003791502	glyceraldehyde-3-phosphate dehydrogenase-like
LOC125659980	1.554771063	0.005299504	tumor necrosis factor ligand superfamily member 15-like
LOC125659346	1.566559909	0.002906035	monocarboxylate transporter 12-like isoform X2
LOC125662013	1.57481301	9.71E-05	adenosine 5'-monophosphoramidase HINT1-like
GeneID_11341123	1.575247062	0.004585382	--
LOC125681684	1.592999428	0.001873405	glycosaminoglycan xylosylkinase-like
LOC125649806	1.59312122	0.000167772	probable methylmalonate-semialdehyde dehydrogenase [acylating]%2C mitochondrial
LOC125666091	1.597343629	0.00089864	uncharacterized protein LOC125666091
LOC125674823	1.600479152	0.000242858	fructose-bisphosphate aldolase-like
LOC125649547	1.602893722	0.000605342	E3 ubiquitin-protein ligase TRIM71-like
LOC125663687	1.608294313	0.002379525	tripartite motif-containing protein 45-like isoform X1
LOC125674341	1.608446182	0.004046878	toxin CfTX-A-like
LOC125664152	1.610748474	0.008601632	39S ribosomal protein L16%2C mitochondrial-like
LOC125670619	1.620586341	0.002494178	proliferating cell nuclear antigen-like
LOC125659966	1.628106944	0.001345589	uncharacterized protein LOC125659966
LOC125679365	1.629465576	0.006250614	phosphoglycerate kinase-like isoform X1
LOC125669257	1.630533158	0.004237367	NADH dehydrogenase [ubiquinone] 1 beta subcomplex subunit 10-like isoform X1
LOC125649412	1.63330172	0.000426458	uncharacterized protein LOC125649412
LOC125654822	1.635294986	7.52E-06	universal stress protein Slr1101-like
LOC125669744	1.64704462	0.003929538	uncharacterized protein LOC125669744

USC UNIVERSIDADE DE SANTIAGO DE COMPOSTELA

LOC125671767	1.655082517	0.000279056	cysteine-rich protein 1-like
LOC125657542	1.668411342	0.001041155	homeobox protein Nkx-2.5-like
LOC125659799	1.669338356	0.002189763	--
LOC125673107	1.676534587	0.000501166	uncharacterized protein LOC125673107
LOC125678231	1.68417354	0.002183864	innexin unc-9-like isoform X1
LOC125671497	1.688017215	0.001451304	inactive pancreatic lipase-related protein 1-like isoform X1
LOC125680107	1.700604017	0.000767294	plancitoxin-1-like
LOC125667022	1.700901156	0.003145404	aspartate aminotransferase%2C mitochondrial-like
LOC125653946	1.718153109	0.006553474	--
LOC125682999	1.722638766	0.00104569	glucose-6-phosphate isomerase-like
LOC125664174	1.725040868	2.25E-05	--
LOC125658356	1.737099681	0.007277877	steroid 17-alpha-hydroxylase/17%2C20 lyase-like
LOC125659212	1.74390031	0.000915453	LOW QUALITY PROTEIN: insulin-like growth factor-binding protein-related protein 1
LOC125671120	1.749277264	0.00875872	uncharacterized protein LOC125671120
LOC125674955	1.752856859	0.003168261	allograft inflammatory factor 1-like
LOC125646454	1.754588108	0.007372036	pyruvate dehydrogenase protein X component%2C mitochondrial-like
LOC125653995	1.760257822	0.003565354	tubulin alpha-8 chain-like isoform X1
LOC125663682	1.764815005	0.004251047	macrophage migration inhibitory factor homolog
LOC125655144	1.78524699	0.005924569	39S ribosomal protein L42%2C mitochondrial-like
LOC125653468	1.794426041	0.006456267	uncharacterized protein LOC125653468
LOC125671864	1.811688075	0.006250619	uncharacterized protein LOC125671864
LOC125657114	1.813673867	0.002890714	isocitrate dehydrogenase [NAD] subunit gamma%2C mitochondrial-like isoform X2
LOC125657651	1.83941232	0.000262173	--
LOC125659043	1.840636724	0.004372203	glutamine amidotransferase-like class 1 domain-containing protein 3%2C mitochondrial
LOC125674964	1.841294645	0.000456717	coactosin-like protein
LOC125669567	1.849644726	0.000453723	39S ribosomal protein L13%2C mitochondrial-like
LOC125677612	1.865096135	0.005838334	multiple epidermal growth factor-like domains protein 11 isoform X4
LOC125650387	1.87142574	9.66E-05	zwei Ig domain protein zig-8-like
LOC125650529	1.87848646	3.12E-05	uncharacterized protein LOC125650529 isoform X3
LOC125650843	1.890496279	0.000104051	uncharacterized protein LOC125650843
LOC125683059	1.903773037	0.002343301	fatty acid-binding protein Fh15-like isoform X1
LOC125649210	1.922627117	5.86E-06	tropomyosin isoform X16
LOC125670790	1.94199977	0.004759089	tubulin alpha-1A chain-like isoform X3
LOC125667601	1.947872185	0.000391433	probable nuclear hormone receptor HR38
LOC125645440	1.948070703	0.0024868	uncharacterized protein LOC125645440
LOC125663577	1.950992632	0.003332535	triosephosphate isomerase-like
LOC125650004	1.965606239	0.002691455	uncharacterized protein LOC125650004
LOC125647739	1.966321359	0.00221301	uncharacterized protein LOC125647739
LOC125652125	1.96717562	0.001667033	uncharacterized protein LOC125652125 isoform X2
LOC125674770	1.96786903	0.00010599	ATP synthase F(0) complex subunit B1%2C mitochondrial-like
LOC125668663	1.978902587	1.27E-05	voltage-dependent T-type calcium channel subunit alpha-1H-like isoform X4
LOC125668299	1.985771826	0.001336474	calmodulin-A-like isoform X1
LOC125654839	1.98715121	6.31E-06	protein NipSnap-like isoform X1
LOC125679372	1.99856647	0.001151709	paramyosin-like isoform X1
LOC125675631	2.005787059	8.64E-06	glutamate receptor ionotropic%2C kainate 2-like
LOC125657099	2.007657272	0.000950734	uncharacterized protein LOC125657099
LOC125664181	2.010887279	2.56E-05	uncharacterized protein LOC125664181
LOC125660465	2.013740589	0.001873079	soma ferritin-like
LOC125652127	2.014414174	0.004968177	uncharacterized protein LOC125652127 isoform X5
LOC125674210	2.020362391	0.000256369	melanocortin receptor 5-like

USC UNIVERSIDADE DE SANTIAGO DE COMPOSTELA

LOC125682535	2.044093091	0.005523263	protein CutA homolog
LOC125672339	2.048592905	0.006871152	prostaglandin E2 receptor EP4 subtype-like
LOC125657960	2.051322315	0.007268245	sarcoplasmic calcium-binding protein-like
LOC125665828	2.05311817	0.001538606	RING finger protein nhl-1-like
LOC125669805	2.065604507	0.007528009	armadillo repeat-containing protein 7-like
LOC125678595	2.081832656	0.000544289	actin%2C adductor muscle
LOC125672605	2.082428375	0.000351398	cytochrome c oxidase subunit 6A2%2C mitochondrial-like
LOC125650095	2.08452289	0.000121815	uncharacterized protein LOC125650095
LOC125664510	2.089288697	0.008028716	carbonic anhydrase 7-like isoform X1
LOC125680249	2.090785326	4.92E-05	14 kDa phosphohistidine phosphatase-like
LOC125648343	2.094863149	0.000364252	uncharacterized protein LOC125648343 isoform X3
LOC125655997	2.095798748	0.000593416	calcium-transporting ATPase sarcoplasmic/endoplasmic reticulum type-like isoform X3
LOC125658767	2.096727618	0.006263497	propionyl-CoA carboxylase alpha chain%2C mitochondrial-like isoform X3
LOC125647828	2.111999839	0.005471122	troponin T%2C skeletal muscle-like isoform X1
LOC125652602	2.114981827	0.004021098	--
LOC125652101	2.162322551	0.000154339	uncharacterized protein LOC125652101
LOC125665757	2.166540293	0.002389632	uncharacterized protein LOC125665757
LOC125660464	2.168364721	0.000168363	--
LOC125678926	2.175591871	0.001609316	pantetheinase-like
LOC125649465	2.183917704	0.001180131	inactive tyrosine-protein kinase 7-like
LOC125656599	2.192724723	0.006118988	cholecystokinin receptor type A-like
LOC125677070	2.228541877	0.000209062	interferon alpha-inducible protein 27-like protein 2B isoform X1
LOC125668589	2.241413968	0.000811112	sarcoplasmic calcium-binding protein-like
LOC125665930	2.248519963	0.002581053	glycine cleavage system H protein-like
LOC125674478	2.249553727	0.003764011	allograft inflammatory factor 1-like
LOC125652524	2.257967906	0.002665056	uncharacterized protein LOC125652524 isoform X1
LOC125667602	2.292065318	0.007326871	frizzled-5-like
LOC125679404	2.30569858	0.000457729	uncharacterized protein LOC125679404
LOC125663824	2.322809926	3.13E-08	protein-glutamine gamma-glutamyltransferase K-like isoform X1
LOC125681503	2.325150509	0.003331461	uncharacterized protein LOC125681503
LOC125674725	2.330523143	0.004689529	--
LOC125683726	2.334627926	0.00275705	uncharacterized protein LOC125683726
LOC125673894	2.335324333	0.007131521	leucine-rich repeat-containing protein 15-like isoform X1
LOC125671608	2.342899953	0.002393795	calcyphosin-like protein isoform X1
LOC125677072	2.347239332	0.007085309	--
LOC125650370	2.357085043	4.77E-09	homeobox protein SIX4-like
LOC125674434	2.397444192	0.002815222	SH3 domain-binding glutamic acid-rich-like protein 3
LOC125663985	2.397758822	6.71E-05	uncharacterized protein LOC125663985 isoform X4
LOC125661583	2.401686255	0.001857986	aminopeptidase Ey-like isoform X4
LOC125655836	2.40388097	1.12E-05	insulin-like growth factor-binding protein 2-B
LOC125664424	2.404727832	5.74E-06	WAP four-disulfide core domain protein 1-like isoform X1
LOC125646186	2.413103281	3.09E-05	myosin light chain kinase%2C smooth muscle-like isoform X3
LOC125670411	2.42149579	0.006374757	glyoxalase domain-containing protein 5-like
LOC125676515	2.422762748	2.90E-05	uncharacterized protein LOC125676515
LOC125681570	2.452262113	0.000104937	glycerophosphocholine cholinephosphodiesterase ENPP6-like isoform X1
LOC125671873	2.461578923	0.007971729	chromatin assembly factor 1 subunit A-like
LOC125665326	2.487017859	0.007978778	uncharacterized protein LOC125665326
LOC125646886	2.489929774	2.11E-05	rac guanine nucleotide exchange factor B-like isoform X2
LOC125678504	2.496626691	1.84E-05	--
LOC125682581	2.496835054	0.001560947	putative ankyrin repeat protein RF_0381
LOC125659712	2.517454441	8.49E-07	dual oxidase maturation factor 1-like

USC UNIVERSIDADE DE SANTIAGO DE COMPOSTELA

LOC125655899	2.533360335	0.001195893	glutathione S-transferase 1-like
LOC125681803	2.54372995	0.006911256	lachesin-like
LOC125664871	2.549471206	0.002645756	uncharacterized protein LOC125664871
LOC125668467	2.554964461	0.007120322	uncharacterized protein LOC125668467 isoform X3
LOC125647490	2.563291056	0.002229428	uncharacterized protein LOC125647490
LOC125683439	2.565234318	1.67E-05	glyoxylate reductase/hydroxypyruvate reductase-like
LOC125650773	2.568003269	2.92E-06	uncharacterized protein LOC125650773 isoform X2
LOC125656097	2.571839339	0.005299278	uncharacterized protein LOC125656097 isoform X1
LOC125654864	2.577151087	0.001980704	heavy metal-binding protein HIP-like
LOC125655800	2.583939824	0.005543349	caveolin-3-like
LOC125665910	2.585850807	0.001203944	uncharacterized protein LOC125665910
LOC125656680	2.591528987	0.005037546	galactose-specific lectin nattectin-like
LOC125646877	2.602076706	0.000280003	uncharacterized protein LOC125646877 isoform X2
LOC125657800	2.628151872	0.000230081	acetylcholinesterase-like
LOC125682010	2.656988184	0.000146288	16 kDa calcium-binding protein-like
LOC125655229	2.679350352	0.000494923	uncharacterized protein LOC125655229 isoform X1
LOC125673562	2.695904617	0.008150813	uncharacterized protein LOC125673562
LOC125649639	2.710678359	1.30E-05	--
LOC125678168	2.713375374	0.000533729	uncharacterized protein LOC125678168 isoform X5
LOC125646732	2.727610612	0.000346035	3-hydroxyisobutyrate dehydrogenase%2C mitochondrial-like
LOC125675565	2.750772546	1.96E-07	secretin receptor-like
LOC125658074	2.768350545	7.76E-06	myosin regulatory light chain B%2C smooth adductor muscle-like
LOC125683106	2.803608107	3.37E-06	myosin regulatory light chain 12A-like
LOC125656148	2.816412208	0.005069225	uncharacterized protein LOC125656148
LOC125651596	2.823166289	0.00213879	uncharacterized protein LOC125651596
LOC125649813	2.833601005	0.006972582	uncharacterized protein LOC125649813
LOC125652368	2.8420132	0.001418726	rho-related protein racL-like
LOC125673350	2.84590939	0.00042572	GTP-binding protein REM 1-like
LOC125655262	2.850796344	0.000219892	uncharacterized protein LOC125655262
LOC125649271	2.867430494	0.000656572	GTPase IMAP family member 9-like
LOC125645746	2.877757935	0.000153106	alpha-2A adrenergic receptor-like
LOC125682061	2.900456455	5.33E-06	zinc finger protein 345-like
LOC125668300	2.948830889	5.11E-05	troponin C-like isoform X1
LOC125670955	2.950897746	0.00013977	uncharacterized protein LOC125670955 isoform X7
LOC125664042	2.951373518	8.69E-07	isatin hydrolase-like isoform X1
LOC125649174	2.959702752	0.003127647	uncharacterized protein LOC125649174 isoform X1
LOC125679194	2.969802286	0.00025664	protein mab-21-like 2
LOC125658028	2.972737094	2.02E-05	monocarboxylate transporter 13-like
LOC125646719	2.973795303	0.005920377	uncharacterized protein LOC125646719
LOC125669769	2.995432352	2.09E-05	pyrethroid hydrolase Ces2e-like
LOC125649534	3.005198039	0.003039266	calcitonin gene-related peptide type 1 receptor-like isoform X2
LOC125681717	3.051788427	0.005075501	heart- and neural crest derivatives-expressed protein 2-like
LOC125658951	3.059348744	0.003999731	uncharacterized protein LOC125658951
LOC125664320	3.065656264	0.001140701	sushi%2C von Willebrand factor type A%2C EGF and pentraxin domain-containing protein 1-like
LOC125658353	3.0780956	0.008503912	steroid 17-alpha-hydroxylase/17%2C20 lyase-like isoform X1
LOC125659403	3.108283177	1.09E-11	LOW QUALITY PROTEIN: LHFPL tetraspan subfamily member 6 protein-like
LOC125653992	3.144073421	0.0001102	uncharacterized protein LOC125653992 isoform X1
LOC125682001	3.149031333	2.06E-05	poly [ADP-ribose] polymerase tankyrase-2-like
LOC125674592	3.180358243	0.006487298	caveolin-1-like
LOC125649398	3.191915801	0.004852686	mucin-5AC-like isoform X1
LOC125678589	3.211990487	0.001962161	ankyrin repeat domain-containing protein 7-like

USC UNIVERSIDADE DE SANTIAGO DE COMPOSTELA

LOC125665743	3.212652434	0.004800274	pancreatic lipase-related protein 2-like
LOC125672003	3.228090689	0.000245073	bone morphogenetic protein 10-like
LOC125669283	3.233185935	0.001408205	uncharacterized protein LOC125669283
LOC125675135	3.233608093	0.002109057	uncharacterized protein LOC125675135
LOC125671566	3.241506698	0.000475051	uncharacterized protein LOC125671566
LOC125654365	3.25805556	0.000131799	angiopoietin-1-like
LOC125675608	3.281488205	0.000538833	kappa-type opioid receptor-like
LOC125682079	3.290216612	0.001404144	uncharacterized protein LOC125682079
LOC125670407	3.291528506	0.004171539	phytanoyl-CoA dioxygenase%2C peroxisomal-like
LOC125671765	3.318068582	0.006292487	noggin-2-like isoform X2
LOC125672255	3.328263651	1.93E-05	uncharacterized protein LOC125672255 isoform X3
LOC125672422	3.356339986	5.48E-08	myosin heavy chain%2C striated muscle-like isoform X5
LOC125651460	3.372826936	0.002661174	uncharacterized protein LOC125651460
LOC125665829	3.383797047	6.68E-14	uncharacterized protein LOC125665829 isoform X1
LOC125670191	3.414381925	4.22E-05	very low-density lipoprotein receptor-like isoform X1
LOC125649714	3.439942014	0.002449028	protein SPEC3-like
LOC125680686	3.440570815	0.001207725	tetraspanin-18-like
LOC125664524	3.467268189	9.17E-06	--
LOC125655369	3.485338349	0.00210637	apolipoprotein D-like
LOC125679696	3.525000465	0.001224247	complement C1q tumor necrosis factor-related protein 7-like
LOC125650318	3.529663893	2.22E-05	uncharacterized protein LOC125650318 isoform X1
LOC125654030	3.535778736	2.73E-08	cadherin-like and PC-esterase domain-containing protein 1
LOC125658044	3.542635078	8.43E-07	ankyrin-1-like isoform X1
LOC125646974	3.560612866	1.48E-06	major egg antigen-like
LOC125650876	3.569964757	3.47E-05	uncharacterized protein LOC125650876
LOC125666154	3.578448893	0.001136779	uncharacterized protein LOC125666154
LOC125655312	3.629017703	0.005753291	uncharacterized protein LOC125655312 isoform X2
LOC125657676	3.689594318	5.17E-09	uncharacterized protein LOC125657676 isoform X2
LOC125647776	3.701391875	2.22E-05	uncharacterized protein LOC125647776
LOC125647737	3.725133024	8.69E-05	PDZ and LIM domain protein 1-like
LOC125676882	3.840959153	9.42E-05	ras-related and estrogen-regulated growth inhibitor-like
LOC125674758	3.849389333	0.000405677	uncharacterized protein LOC125674758
LOC125645867	3.899257876	0.00328443	uncharacterized protein LOC125645867 isoform X1
LOC125659525	3.93170024	1.85E-05	myosin essential light chain%2C striated adductor muscle-like
LOC125679812	3.942424118	0.000274402	uncharacterized protein LOC125679812 isoform X1
LOC125650739	3.945898447	0.000948575	arginase%2C hepatic-like isoform X4
LOC125673817	3.965343586	0.00085141	complement C1q-like protein 2
LOC125664143	3.971110007	0.000104114	--
LOC125647473	4.145652033	4.35E-07	uncharacterized protein LOC125647473
LOC125652056	4.150975058	5.60E-05	protein nemuri-like isoform X1
LOC125648015	4.233830904	8.17E-05	alpha-crystallin A chain-like
LOC125664359	4.298402933	1.73E-05	LOW QUALITY PROTEIN: LHFPL tetraspan subfamily member 7 protein-like
LOC125649164	4.400641383	2.17E-11	cytochrome P450 2U1-like
LOC125669386	4.404022199	0.009070881	fibrinogen-like protein A isoform X1
LOC125683882	4.405522463	5.91E-06	neutral amino acid transporter A-like
LOC125677046	4.416684498	0.008896661	natterin-3-like
LOC125681949	4.432386303	0.001733131	--
LOC125671361	4.433908023	9.95E-07	carbohydrate sulfotransferase 15-like isoform X2
LOC125683189	4.505093035	2.26E-07	protein-glutamine gamma-glutamyltransferase K-like isoform X2
LOC125668397	4.513496127	7.46E-07	cysteine-rich venom protein latisemin-like
LOC125651934	4.520681897	4.58E-10	universal stress protein in QAH/OAS sulfhydrylase 3'region-like

USC UNIVERSIDADE DE SANTIAGO DE COMPOSTELA

LOC125650031	4.552595611	0.001734784	--
LOC125668742	4.555222194	4.79E-06	--
LOC125664873	4.570083972	1.28E-12	uncharacterized protein LOC125664873
LOC125666117	4.576125252	5.09E-08	fibroblast growth factor receptor 3-like isoform X1
LOC125656179	4.576762231	0.00035793	--
LOC125682713	4.578766899	0.001354032	uncharacterized protein LOC125682713 isoform X1
LOC125654884	4.674160672	0.003210731	prostaglandin reductase 1-like
LOC125678402	4.67585417	1.28E-11	uncharacterized protein LOC125678402
LOC125680866	4.698400289	0.001094265	uncharacterized protein LOC125680866
LOC125671374	4.722465031	0.000209128	uncharacterized protein LOC125671374
LOC125655456	4.730256222	0.000197924	uncharacterized protein LOC125655456
LOC125677074	4.875916105	2.14E-05	--
LOC125670650	5.003972631	5.73E-08	uncharacterized protein LOC125670650
LOC125675603	5.080252673	1.44E-09	orexin receptor type 2-like
LOC125664525	5.097895744	6.89E-05	uncharacterized protein LOC125664525
LOC125659646	5.141569493	8.11E-05	uncharacterized protein LOC125659646 isoform X3
LOC125668398	5.212661479	4.66E-11	testis-specific serine/threonine-protein kinase 1-like
LOC125676096	5.348422507	0.001998515	--
LOC125653347	5.421968961	2.43E-11	uncharacterized protein LOC125653347
LOC125651938	5.67426019	0.000211907	uncharacterized protein LOC125651938
LOC125672586	5.697251077	1.35E-19	uncharacterized protein LOC125672586 isoform X2
LOC125646735	5.732812479	0.00089676	low affinity immunoglobulin epsilon Fc receptor-like isoform X3
LOC125681172	5.941197224	0.001105134	prion-like-(Q/N-rich) domain-bearing protein 25
LOC125665731	5.95054142	5.03E-10	uncharacterized protein LOC125665731 isoform X2
LOC125674003	5.955101189	0.000391283	ganglioside GM2 activator-like
LOC125674991	6.092231662	2.61E-09	uncharacterized protein LOC125674991
LOC125669079	6.210747649	0.000143508	acetylcholine receptor subunit delta-like
LOC125659941	6.214736321	1.54E-20	tripartite motif-containing protein 2-like isoform X4
LOC125683333	6.528256506	0.001151585	uncharacterized protein LOC125683333 isoform X3
LOC125656245	6.52895464	7.77E-09	uncharacterized protein LOC125656245
LOC125661361	6.883805558	4.16E-07	procathepsin L-like
LOC125676014	7.035508199	4.22E-06	organic cation transporter protein-like isoform X2
LOC125652039	7.209583312	2.63E-32	uncharacterized protein LOC125652039
LOC125669901	7.304249185	0.000278965	FAS-associated death domain protein-like
LOC125659279	7.511009194	2.71E-44	retinol dehydrogenase 12-like isoform X2
LOC125682220	7.817978411	4.90E-11	nose resistant to fluoxetine protein 6-like
LOC125654239	8.351459103	0.000287739	apolipoprotein D-like
LOC125654795	8.39541932	3.41E-11	uncharacterized protein LOC125654795
LOC125662247	8.421316397	0.000475518	--
LOC125657467	8.718355382	0.000632801	--
LOC125679080	8.851841239	1.26E-05	--

C) Control vs Level 3

Genes	log2FoldChange	pvalue	Anotation
LOC125675579	-26.15308873	2.17E-11	caveolin-1-like
LOC125673466	-15.73655064	8.37E-07	--
LOC125657179	-14.57869851	7.50E-13	uncharacterized protein LOC125657179
LOC125673456	-14.15684509	1.92E-14	uncharacterized protein LOC125673456 isoform X2
LOC125679528	-13.88987476	5.63E-11	collagen alpha-1(I) chain-like
LOC125680779	-13.72062422	4.83E-15	uncharacterized protein LOC125680779

USC UNIVERSIDADE DE SANTIAGO DE COMPOSTELA

LOC125676136	-13.66630067	3.31E-15	cytochrome c oxidase subunit 6A2%2C mitochondrial-like
LOC125681718	-13.43433949	8.10E-10	uncharacterized protein LOC125681718 isoform X13
LOC125657178	-13.33147989	8.28E-13	uncharacterized protein LOC125657178 isoform X1
LOC125667266	-12.97006168	4.26E-11	arginine/serine-rich protein 1-like
LOC125655214	-12.93755072	2.31E-08	caveolin-3-like
LOC125663040	-12.72487918	1.23E-08	transmembrane protein 272-like
LOC125673455	-12.60096289	1.28E-12	uncharacterized protein LOC125673455
LOC125659146	-12.33739497	3.40E-09	transcription factor Sox-2-like
LOC125672258	-12.32150963	1.83E-11	uncharacterized protein LOC125672258
LOC125667146	-12.31959202	2.29E-10	uncharacterized protein LOC125667146
LOC125654081	-12.31109245	5.16E-09	A disintegrin and metalloproteinase with thrombospondin motifs adt-1-like isoform X7
LOC125657036	-12.26862597	0.001687775	peritrophin-1-like
LOC125683864	-12.25554408	6.34E-08	cerebellin-3-like
LOC125674006	-12.2408683	2.62E-09	--
LOC125678071	-12.21582754	0.00176743	cerebellin-3-like isoform X4
LOC125659209	-12.11636801	1.59E-11	--
LOC125679886	-12.08859018	5.03E-09	--
LOC125675283	-12.05340386	0.002034167	caveolin-3-like
LOC125650665	-12.02805886	3.94E-10	stabilizer of axonemal microtubules 2-like
LOC125672817	-11.94055003	5.45E-05	--
LOC125655260	-11.92727149	1.88E-08	uncharacterized protein LOC125655260 isoform X1
LOC125659660	-11.87629888	0.002366884	--
LOC125668997	-11.86538108	7.21E-12	collagen alpha-1(I) chain-like
LOC125679568	-11.82731176	2.70E-07	Golgi-associated plant pathogenesis-related protein 1-like
LOC125661560	-11.81856623	8.57E-09	DBH-like monooxygenase protein 1
LOC125655173	-11.80225233	0.002520225	uncharacterized protein LOC125655173
LOC125652363	-11.74121915	3.86E-10	golgin subfamily A member 6-like protein 22
LOC125667054	-11.71554407	0.002711313	uncharacterized protein LOC125667054 isoform X3
LOC125661197	-11.70274315	3.08E-08	calpain-5-like isoform X3
LOC125655683	-11.68147139	0.00278994	cysteine and tyrosine-rich protein 1-like isoform X1
LOC125655332	-11.58354562	1.86E-07	uncharacterized protein LOC125655332
LOC125656100	-11.576688	3.66E-09	LHFPL tetraspan subfamily member 3 protein-like
LOC125658223	-11.56104177	0.003084898	uncharacterized protein LOC125658223 isoform X3
LOC125683043	-11.49390307	7.81E-09	--
LOC125649497	-11.4923604	1.34E-08	protein doublesex-like
LOC125646641	-11.45303393	6.90E-07	cadherin EGF LAG seven-pass G-type receptor 2-like isoform X1
LOC125673449	-11.41292796	1.53E-06	cerebellin-1-like
LOC125654912	-11.32328937	1.93E-05	uncharacterized protein LOC125654912
LOC125681931	-11.31008979	2.43E-07	uncharacterized protein LOC125681931
LOC125665579	-11.30152089	0.002873696	EF-hand calcium-binding domain-containing protein 1-like
LOC125660999	-11.27142194	3.36E-14	tyramine beta-hydroxylase-like
LOC125661562	-11.27142194	3.36E-14	tyramine beta-hydroxylase-like
LOC125653627	-11.26384184	1.99E-05	uncharacterized protein LOC125653627
LOC125654854	-11.21907228	2.67E-05	caveolin-1-like
LOC125666331	-11.2140503	3.22E-07	MAM and LDL-receptor class A domain-containing protein 1-like
LOC125645608	-11.20215955	1.68E-07	alpha-(1%2C3)-fucosyltransferase fut-5-like isoform X1
LOC125660998	-11.18505962	5.07E-10	--
LOC125683865	-11.11338704	2.92E-05	complement C1q-like protein 4
LOC125665218	-11.01810565	1.30E-07	uncharacterized protein LOC125665218 isoform X1
LOC125680365	-11.01681486	6.94E-08	neuroendocrine convertase 2-like
LOC125683044	-10.99352996	7.64E-07	uncharacterized protein LOC125683044

USC UNIVERSIDADE DE SANTIAGO DE COMPOSTELA

LOC125680672	-10.98440325	3.06E-05	allatotropins-like
LOC125668356	-10.92865928	1.48E-07	coiled-coil domain-containing protein 33-like isoform X2
LOC125646997	-10.91094277	1.58E-07	--
LOC125679804	-10.8441825	3.61E-09	--
LOC125679547	-10.82770813	5.20E-05	uncharacterized protein LOC125679547 isoform X3
LOC125664386	-10.82375777	3.66E-07	protein CFAP107-like
LOC125679934	-10.8084225	9.40E-08	uncharacterized protein LOC125679934 isoform X1
LOC125678077	-10.79525751	6.87E-07	ficolin-1-A-like isoform X2
LOC125681750	-10.77468517	5.00E-05	CD63 antigen-like
LOC125682720	-10.75880239	5.91E-05	uncharacterized protein LOC125682720
LOC125672096	-10.74886985	1.78E-07	uncharacterized protein LOC125672096 isoform X1
LOC125654173	-10.69848975	4.28E-09	34 kDa antigenic protein-like isoform X6
LOC125657102	-10.6758445	6.42E-05	uncharacterized protein LOC125657102 isoform X2
LOC125659107	-10.67312779	1.05E-08	--
LOC125676256	-10.67311849	1.58E-08	--
LOC125646407	-10.66401149	2.89E-07	uncharacterized protein LOC125646407
LOC125679096	-10.66401149	2.89E-07	uncharacterized protein LOC125679096
LOC125658890	-10.6357789	6.90E-05	uncharacterized protein LOC125658890 isoform X4
LOC125664304	-10.60937491	3.58E-08	uncharacterized protein LOC125664304 isoform X12
LOC125654748	-10.56280464	6.89E-05	--
LOC125646019	-10.55516367	7.74E-05	perlucin-like protein
LOC125669385	-10.52735087	4.85E-07	grainyhead-like protein 1 homolog isoform X4
LOC125682057	-10.49727711	9.34E-05	serine-rich adhesin for platelets-like
LOC125649071	-10.47148115	1.69E-07	testis%2C prostate and placenta-expressed protein-like
LOC125647779	-10.42194611	2.32E-10	uncharacterized protein LOC125647779
LOC125679357	-10.35659926	2.34E-07	centrosome-associated protein CEP250-like isoform X3
LOC125668050	-10.35102382	5.04E-09	dynein axonemal assembly factor 5-like
LOC125683160	-10.33466694	6.52E-10	uncharacterized protein LOC125683160 isoform X2
LOC125661913	-10.32455144	6.39E-06	tenascin-like isoform X3
LOC125661450	-10.29783002	7.93E-06	complement C1q-like protein 4
LOC125671604	-10.28375043	8.51E-06	doublesex- and mab-3-related transcription factor A2-like
LOC125675855	-10.28322891	1.31E-06	uncharacterized protein LOC125675855 isoform X1
LOC125654008	-10.23705123	2.77E-12	protein SSUH2 homolog isoform X1
LOC125649908	-10.1843302	1.78E-09	uncharacterized protein LOC125649908
LOC125683197	-10.1771756	9.68E-06	nmrA-like family domain-containing protein 1 isoform X5
LOC125656104	-10.1443593	3.38E-06	CD209 antigen-like protein B
LOC125654909	-10.13358537	0.000197403	caveolin-1-like isoform X2
LOC125656147	-10.11374752	1.32E-06	cysteine and tyrosine-rich protein 1-like
LOC125672140	-10.1060648	0.000257746	uncharacterized protein LOC125672140
LOC125672152	-10.1060648	0.000257746	uncharacterized protein LOC125672152
LOC125647472	-10.08813461	3.44E-09	--
LOC125681465	-10.07175273	0.00021892	tetraspanin-18-like
LOC125677027	-10.06093423	0.000221725	--
LOC125646761	-10.04453442	9.04E-07	uncharacterized protein LOC125646761
LOC125649865	-9.994550855	7.41E-06	arrestin domain-containing protein 3-like
LOC125653531	-9.992878438	0.00026369	uncharacterized protein LOC125653531
LOC125645567	-9.96550392	1.77E-05	uncharacterized protein LOC125645567
LOC125662157	-9.961892237	1.06E-06	uncharacterized protein LOC125662157
LOC125651291	-9.942139341	0.00029515	--
LOC125656191	-9.900733288	2.09E-05	pre-mRNA-splicing factor CWC22 homolog
LOC125679882	-9.878693011	2.37E-11	uncharacterized protein LOC125679882

USC UNIVERSIDADE DE SANTIAGO DE COMPOSTELA

LOC125675951	-9.872587576	7.42E-07	uncharacterized protein LOC125675951
LOC125657652	-9.871465507	0.000372958	short-chain collagen C4-like
LOC125675831	-9.855578077	7.22E-08	uncharacterized protein LOC125675831
LOC125669927	-9.826883256	1.43E-10	equilibrative nucleobase transporter 1-like
LOC125666029	-9.804393476	1.39E-09	uncharacterized protein LOC125666029
LOC125656184	-9.796089299	1.23E-05	calcium and integrin-binding protein 1-like
LOC125650712	-9.76766593	7.12E-05	paired box protein Pax-1-like
LOC125680341	-9.742632082	6.43E-06	uncharacterized protein LOC125680341
LOC125681850	-9.741380579	4.52E-09	uncharacterized protein LOC125681850
LOC125656192	-9.733931601	2.16E-06	pre-mRNA-splicing factor CWC22 homolog
LOC125655708	-9.727922505	7.63E-10	phospholipid-transporting ATPase ABCA3-like
LOC125682351	-9.727904983	1.95E-06	myeloperoxidase-like
LOC125679884	-9.721952734	2.53E-10	uncharacterized protein LOC125679884
LOC125648180	-9.72044168	1.66E-06	uncharacterized protein LOC125648180
LOC125648216	-9.702912147	6.97E-07	arrestin domain-containing protein 1-like isoform X1
LOC125654684	-9.672921783	3.38E-07	uncharacterized protein LOC125654684
LOC125677066	-9.654835805	1.59E-05	heavy metal-binding protein HIP-like isoform X7
LOC125646785	-9.64156838	0.00056814	LOW QUALITY PROTEIN: myomodulin neuropeptides 2-like
LOC125650184	-9.637111576	1.65E-09	uncharacterized protein LOC125650184 isoform X1
LOC125659934	-9.627799597	0.000621004	uncharacterized protein LOC125659934
LOC125645609	-9.619615411	3.83E-06	glycoprotein 3-alpha-L-fucosyltransferase A-like
LOC125683530	-9.570241379	2.20E-05	uncharacterized protein LOC125683530
LOC125653759	-9.550317201	4.15E-10	uncharacterized protein LOC125653759
LOC125649506	-9.548795492	1.87E-10	radial spoke head protein 4 homolog A-like
LOC125673879	-9.546080941	0.000710177	uncharacterized protein LOC125673879 isoform X2
LOC125676286	-9.527451678	0.000821873	uncharacterized protein LOC125676286
LOC125667526	-9.498331331	8.67E-07	uncharacterized protein LOC125667526 isoform X2
LOC125648836	-9.490288374	1.10E-11	uncharacterized protein LOC125648836
LOC125663783	-9.462952574	0.000103915	uncharacterized protein LOC125663783 isoform X1
LOC125671580	-9.403571081	6.51E-06	dynein light chain Tctex-type 5-like
LOC125653441	-9.391271158	4.19E-05	complement C1q-like protein 2 isoform X4
LOC125666899	-9.384436693	3.20E-06	uncharacterized protein LOC125666899
LOC125666577	-9.37008902	4.10E-08	--
LOC125671919	-9.36397442	9.07E-06	uncharacterized protein LOC125671919
LOC125663587	-9.342259035	9.00E-07	metabotropic glutamate receptor 3-like
LOC125665948	-9.322687	5.21E-07	tripartite motif-containing protein 59-like
LOC125657244	-9.320606649	9.16E-06	uncharacterized protein LOC125657244
LOC125665341	-9.299784095	1.99E-11	mucin-17-like
LOC125653797	-9.294360941	9.73E-07	LOW QUALITY PROTEIN: glutathione S-transferase-like
LOC125659807	-9.293791125	0.001326958	APGW-amide-related neuropeptide-like
LOC125671469	-9.287302434	6.14E-11	tektin-3-like isoform X2
LOC125668352	-9.266717135	3.08E-05	uncharacterized protein LOC125668352 isoform X3
LOC125655410	-9.219577328	4.52E-07	von Willebrand factor D and EGF domain-containing protein-like isoform X1
LOC125670985	-9.218221799	0.001373346	uncharacterized protein LOC125670985
LOC125662692	-9.21053505	6.06E-07	uncharacterized protein LOC125662692
LOC125655472	-9.192247902	0.001565664	A disintegrin and metalloproteinase with thrombospondin motifs 4-like isoform X5
LOC125675952	-9.186476541	0.0001185	uncharacterized protein LOC125675952
LOC125667767	-9.18060929	0.00019902	uncharacterized protein LOC125667767
LOC125674083	-9.167229038	2.12E-07	uncharacterized protein LOC125674083 isoform X2
LOC125678075	-9.162016181	1.98E-05	C1q-related factor-like isoform X4
LOC125681429	-9.153469304	0.001630591	uncharacterized protein LOC125681429

USC UNIVERSIDADE DE SANTIAGO DE COMPOSTELA

LOC125646253	-9.132214051	1.95E-05	FMRF-amide neuropeptides-like
LOC125678757	-9.10643499	2.55E-10	cilia- and flagella-associated protein 45-like isoform X1
LOC125679636	-9.087963112	3.99E-08	nicotinamidase-like
LOC125681633	-9.083615668	8.47E-06	ficolin-2-like
LOC125659954	-9.059286194	0.000162916	zinc finger and BTB domain-containing protein 49-like
LOC125670809	-9.047550473	1.24E-10	collagen alpha-4(VI) chain-like
LOC125683027	-9.046485943	5.29E-10	paired box protein Pax-6-like isoform X1
LOC125646484	-9.030026617	7.74E-08	--
LOC125682965	-9.023777134	9.29E-08	uncharacterized protein LOC125682965
LOC125661935	-9.014168015	1.28E-05	BPTI/Kunitz domain-containing protein-like
LOC125681019	-9.013366697	3.96E-07	short-chain collagen C4-like
LOC125659601	-9.001583137	5.50E-08	uncharacterized protein LOC125659601
LOC125678347	-8.99420577	6.05E-08	receptor-type tyrosine-protein phosphatase F-like isoform X2
LOC125680553	-8.956730513	0.002274725	twitchin-like
LOC125682006	-8.951550149	5.34E-06	sphingomyelin synthase-related protein 1-like
LOC125649555	-8.946902471	7.20E-05	uncharacterized protein LOC125649555
LOC125678298	-8.922522091	5.46E-11	tubulin beta chain-like
LOC125682475	-8.922522091	5.46E-11	tubulin beta chain-like
LOC125682512	-8.920294499	0.00243994	uncharacterized protein LOC125682512 isoform X1
LOC125667714	-8.912275032	9.54E-05	ryncolin-1-like
LOC125670879	-8.910317913	6.26E-06	cell death-inducing p53-target protein 1 homolog isoform X1
LOC125659105	-8.900303848	1.13E-08	complement C1q-like protein 4
LOC125674301	-8.891153249	1.35E-05	uromodulin-like
LOC125646778	-8.869192051	1.98E-11	tektin-3-like isoform X1
LOC125669881	-8.851995079	3.92E-05	ras-related protein Rap-1b-like
LOC125656219	-8.839229028	0.000181732	uncharacterized protein LOC125656219 isoform X1
LOC125663750	-8.833347007	0.003191589	uncharacterized protein LOC125663750
LOC125651313	-8.817540956	3.74E-08	uncharacterized protein LOC125651313
LOC125645791	-8.806236783	1.38E-05	testis-expressed protein 52-like
LOC125658375	-8.779105946	7.91E-07	uncharacterized protein LOC125658375
LOC125663585	-8.778755248	1.23E-07	uncharacterized protein LOC125663585
LOC125650796	-8.74609064	2.35E-08	uncharacterized protein LOC125650796
LOC125674088	-8.737558537	3.97E-10	neurogenic locus Notch protein-like
LOC125681876	-8.70408376	0.003760964	complement C1q-like protein 3 isoform X1
LOC125655003	-8.701616654	0.000397402	uncharacterized protein LOC125655003 isoform X3
LOC125661698	-8.70052862	6.05E-05	--
LOC125652517	-8.689541722	0.000476465	uncharacterized protein LOC125652517
LOC125653701	-8.689541722	0.000476465	uncharacterized protein LOC125653701
LOC125680671	-8.685170078	0.004076567	collectin-12-like
LOC125680754	-8.681489135	6.43E-05	UPF0686 protein C11orf1 homolog
LOC125659142	-8.665020638	4.60E-07	malignant fibrous histiocytoma-amplified sequence 1 homolog isoform X1
LOC125650749	-8.643714382	9.19E-07	uncharacterized protein LOC125650749
LOC125648317	-8.637666281	4.16E-07	calmodulin-beta-like
LOC125671701	-8.626941302	0.004467219	uncharacterized protein LOC125671701
LOC125659920	-8.618395927	6.51E-07	tripartite motif-containing protein 2-like
LOC125662599	-8.604286243	3.95E-05	uncharacterized protein LOC125662599
LOC125670881	-8.57978814	1.90E-08	LITAF domain-containing protein-like
LOC125683627	-8.555938518	1.50E-09	MAM and LDL-receptor class A domain-containing protein 1-like isoform X3
LOC125677041	-8.542000026	0.000753201	otolin-1-like
LOC125649717	-8.54126575	5.24E-07	sodium/calcium exchanger 3-like
LOC125671987	-8.54126575	5.24E-07	sodium/calcium exchanger 3-like

USC UNIVERSIDADE DE SANTIAGO DE COMPOSTELA

LOC125671525	-8.538096194	2.38E-05	protein CFAP95-like
LOC125681875	-8.505951349	0.005572931	--
LOC125665863	-8.46801229	5.53E-06	uncharacterized protein LOC125665863 isoform X2
LOC125652789	-8.458559611	5.21E-05	uncharacterized protein LOC125652789 isoform X1
LOC125653999	-8.458559611	5.21E-05	uncharacterized protein LOC125653999 isoform X1
LOC125648084	-8.458206265	2.01E-05	--
LOC125670863	-8.453039303	3.19E-05	paired box protein Pax-8-like isoform X1
LOC125656772	-8.452118622	0.006071344	caveolin-1-like
LOC125678107	-8.426004607	6.13E-06	ankyrin-1-like
LOC125671726	-8.35576115	1.61E-07	cell migration-inducing and hyaluronan-binding protein-like
LOC125681441	-8.327614521	5.72E-07	serine/arginine repetitive matrix protein 1-like isoform X2
LOC125647771	-8.323805317	6.06E-09	uncharacterized protein LOC125647771
LOC125670712	-8.321446851	1.69E-08	protein FAM234B-like isoform X2
LOC125646759	-8.307700944	9.27E-06	uncharacterized protein LOC125646759
LOC125666126	-8.296351966	0.000644487	uncharacterized protein LOC125666126
LOC125668795	-8.249081819	1.17E-08	NAD-dependent protein deacetylase Sirt6-like
LOC125657103	-8.22553425	0.001148331	heavy metal-binding protein HIP-like
LOC125677149	-8.222732116	5.00E-05	semaphorin-5A-like isoform X2
LOC125654085	-8.215329634	1.68E-10	calcium-activated chloride channel regulator 1-like isoform X1
LOC125677332	-8.204446007	1.53E-06	dnaJ homolog subfamily B member 13-like
LOC125649077	-8.202726804	6.74E-05	dynein light chain Tctex-type protein 2B-like
LOC125651536	-8.188354226	2.43E-05	C-type lectin domain family 4 member K-like isoform X1
LOC125647728	-8.183333578	7.39E-06	uncharacterized protein LOC125647728 isoform X1
LOC125681433	-8.172709872	4.18E-07	serine/threonine-protein kinase DCLK1-like isoform X2
LOC125674238	-8.157796757	7.71E-05	uncharacterized protein LOC125674238
LOC125675071	-8.15611273	5.25E-08	enteropeptidase-like
LOC125673331	-8.138058068	1.59E-06	tripartite motif-containing protein 2-like isoform X1
LOC125670325	-8.135097207	5.07E-08	uncharacterized protein LOC125670325
LOC125646422	-8.132665035	3.23E-07	VWFA and cache domain-containing protein 1-like
LOC125679123	-8.095628573	9.53E-05	complement C1q tumor necrosis factor-related protein 2-like
LOC125675289	-8.081726227	2.02E-09	outer dense fiber protein 3-like
LOC125681020	-8.075378496	3.11E-08	short-chain collagen C4-like
LOC125680424	-8.051829447	1.11E-07	tetraspanin-9-like isoform X3
LOC125651301	-8.046812327	8.73E-05	uncharacterized protein LOC125651301
LOC125661875	-8.007744586	0.000174773	uncharacterized protein LOC125661875
LOC125673460	-8.006493394	5.87E-05	uncharacterized protein LOC125673460 isoform X2
LOC125655847	-7.97011296	0.000171143	uncharacterized protein LOC125655847
LOC125654075	-7.956767652	1.68E-06	protein ATP6V1FNB-like
LOC125681847	-7.955176832	1.02E-05	dehydrogenase/reductase SDR family member 9-like
LOC125655331	-7.937476883	0.000870363	uncharacterized protein LOC125655331
LOC125681393	-7.936967862	0.001338199	C-type lectin domain family 4 member E-like
LOC125673467	-7.931165686	0.002562167	--
LOC125683093	-7.930746122	2.03E-07	actin-5-like
LOC125677659	-7.912436421	2.98E-06	uncharacterized protein LOC125677659
LOC125652430	-7.849882218	0.000128515	uncharacterized protein LOC125652430
LOC125682357	-7.830831004	0.000246115	uncharacterized protein LOC125682357 isoform X2
LOC125665841	-7.824502907	0.002624784	uncharacterized protein LOC125665841
LOC125659427	-7.804017733	1.34E-08	LOW QUALITY PROTEIN: cell surface hyaluronidase-like
LOC125662595	-7.789758801	1.80E-07	--
LOC125651975	-7.73480328	0.000315018	type-2 ice-structuring protein-like isoform X2
LOC125671016	-7.730499618	1.07E-06	protein TBATA-like isoform X2

USC UNIVERSIDADE DE SANTIAGO DE COMPOSTELA

LOC125666579	-7.718089661	7.33E-07	uncharacterized protein LOC125666579 isoform X2
LOC125683223	-7.704383098	2.86E-07	uncharacterized protein LOC125683223 isoform X2
LOC125658469	-7.692937381	0.000328581	--
LOC125670629	-7.688746566	6.34E-08	cyclin-dependent kinase 12-like isoform X6
LOC125669752	-7.686911525	1.82E-08	--
LOC125654780	-7.682648046	2.36E-07	meiosis expressed gene 1 protein homolog isoform X2
LOC125653443	-7.680163904	0.000311888	complement C1q subcomponent subunit A-like
LOC125674960	-7.672871404	8.32E-07	EF-hand calcium-binding domain-containing protein 6-like isoform X5
LOC125656840	-7.657384951	1.36E-06	uncharacterized protein LOC125656840 isoform X2
LOC125677266	-7.657130177	1.03E-06	transmembrane protein 45B-like isoform X1
LOC125662769	-7.636951081	5.40E-08	uncharacterized protein LOC125662769
LOC125650772	-7.586412316	5.74E-05	uncharacterized protein LOC125650772
LOC125669911	-7.526225411	9.39E-07	cilia- and flagella-associated protein 57-like
LOC125665628	-7.518056302	5.82E-05	sorcin-like
LOC125655578	-7.49586044	4.35E-05	uncharacterized protein LOC125655578 isoform X1
LOC125654847	-7.495085899	6.78E-06	protein CFAP276-like isoform X2
LOC125681468	-7.492593023	4.76E-07	radial spoke head 1 homolog isoform X1
LOC125645800	-7.462226498	4.64E-07	uncharacterized protein LOC125645800
LOC125649563	-7.411654244	2.98E-09	uncharacterized protein LOC125649563
LOC125658452	-7.411435572	0.003774108	--
LOC125681732	-7.408299652	0.00018839	uncharacterized protein LOC125681732
LOC125656753	-7.403075284	0.000182295	uncharacterized protein LOC125656753 isoform X2
LOC125678350	-7.39861873	1.70E-06	deleted in malignant brain tumors 1 protein-like
LOC125673112	-7.392076838	9.92E-05	adhesion G protein-coupled receptor B1-like isoform X2
LOC125658627	-7.267965709	0.000499018	zinc finger protein 667-like
LOC125673407	-7.266080097	6.30E-06	uncharacterized protein LOC125673407 isoform X1
LOC125662017	-7.243419555	0.004793967	uncharacterized protein LOC125662017 isoform X1
LOC125671830	-7.242841071	7.91E-08	zinc metalloproteinase dpy-31-like
LOC125676997	-7.211164078	9.10E-06	uncharacterized protein LOC125676997
LOC125649923	-7.197126108	1.87E-05	uncharacterized protein LOC125649923
LOC125672092	-7.195671071	0.000735998	noggin-like
LOC125665818	-7.192022125	3.85E-08	sperm-associated antigen 6
LOC125674306	-7.172036457	0.000179794	oncoprotein-induced transcript 3 protein-like
LOC125673093	-7.117203951	3.50E-06	--
LOC125672280	-7.088844651	0.000444379	spermatogenesis-associated protein 6-like
LOC125657899	-7.067495001	5.34E-06	EF-hand domain-containing family member C2-like
LOC125654813	-7.033285697	5.72E-06	myosin heavy chain%2C skeletal muscle-like
LOC125664326	-7.004786127	3.57E-05	uncharacterized protein LOC125664326
LOC125653936	-6.982182867	9.46E-07	uncharacterized protein LOC125653936
LOC125675252	-6.974782322	1.70E-05	--
LOC125670333	-6.955310347	8.76E-07	tektin-2-like
LOC125670355	-6.955310347	8.76E-07	tektin-2-like
LOC125677109	-6.948728206	8.80E-05	uncharacterized protein LOC125677109
LOC125683927	-6.946493057	3.43E-05	LOW QUALITY PROTEIN: myeloid differentiation primary response protein MyD88-like
LOC125669918	-6.942700929	5.87E-06	spermatogenesis-associated protein 6-like isoform X2
LOC125671772	-6.925064964	7.98E-10	tektin-4-like
LOC125664426	-6.919304697	1.80E-05	uncharacterized protein LOC125664426 isoform X2
LOC125681853	-6.847889105	0.001575036	uncharacterized protein LOC125681853
LOC125649577	-6.8383722	2.12E-07	neuroendocrine convertase 2-like
LOC125647859	-6.83490719	2.72E-07	EF-hand domain-containing protein 1-like
LOC125668402	-6.82841219	1.54E-06	uncharacterized protein LOC125668402 isoform X1

USC UNIVERSIDADE DE SANTIAGO DE COMPOSTELA

LOC125670408	-6.828282846	1.56E-06	neurensin-1-like
LOC125668606	-6.821633179	3.07E-06	--
LOC125673265	-6.809324385	7.10E-06	uncharacterized protein LOC125673265
LOC125668947	-6.730414932	1.31E-05	uncharacterized protein LOC125668947
LOC125656218	-6.721362104	3.34E-06	RIB43A-like with coiled-coils protein 2
LOC125672154	-6.721041295	0.00025277	uncharacterized protein LOC125672154
LOC125672158	-6.721041295	0.00025277	uncharacterized protein LOC125672158
LOC125677265	-6.708905015	6.10E-05	uncharacterized protein LOC125677265
LOC125653821	-6.695250852	1.60E-07	uncharacterized protein LOC125653821
LOC125670035	-6.693635195	1.80E-07	transmembrane channel-like protein 7 isoform X4
LOC125659880	-6.653257095	7.24E-06	leucine-rich repeat protein soc-2-like
LOC125679702	-6.651300128	2.22E-05	uncharacterized protein LOC125679702
LOC125680371	-6.633584929	4.19E-06	choline transporter-like protein 2
LOC125658777	-6.623904626	1.04E-07	uncharacterized protein LOC125658777 isoform X1
LOC125671411	-6.612635258	4.17E-06	cilia- and flagella-associated protein 52-like
LOC125664149	-6.592705536	0.000152884	--
LOC125666740	-6.589141067	7.57E-08	enkurin-like
LOC125676103	-6.517573789	2.33E-07	radial spoke head protein 3 homolog B-like
LOC125665835	-6.513189328	2.15E-07	protein CFAP210-like
LOC125675914	-6.467389921	0.000166502	uncharacterized protein LOC125675914
LOC125679074	-6.462330576	7.74E-08	annexin A5-like
LOC125664358	-6.459748015	0.000149083	LHFPL tetraspan subfamily member 2a protein-like
LOC125665618	-6.439453098	3.63E-05	uncharacterized protein LOC125665618 isoform X2
LOC125678958	-6.421538626	4.78E-05	LOW QUALITY PROTEIN: tryptophan 2%2C3-dioxygenase-like
LOC125647970	-6.417101035	8.78E-05	uncharacterized protein C17orf98-like
LOC125664212	-6.39775144	3.40E-06	coiled-coil domain-containing protein 63-like
LOC125683110	-6.371983072	6.90E-07	uncharacterized protein LOC125683110
LOC125649115	-6.292899841	9.20E-07	neuroendocrine convertase 1-like isoform X1
LOC125649262	-6.28502743	0.000171456	--
LOC125647945	-6.276046483	4.46E-05	filamin A-interacting protein 1-like
LOC125671402	-6.257482971	4.65E-07	LOW QUALITY PROTEIN: uncharacterized protein LOC125671402
LOC125668736	-6.236891412	0.001115095	calcyphosin-like protein isoform X1
LOC125668796	-6.223190638	9.39E-06	NAD-dependent protein deacetylase Sirt6-like isoform X1
LOC125675507	-6.201204168	8.87E-05	microsomal glutathione S-transferase 3-like
LOC125645600	-6.193638259	6.44E-07	uncharacterized protein LOC125645600 isoform X2
LOC125679238	-6.18626328	0.000169044	prestin-like isoform X2
LOC125650637	-6.155348975	0.00210368	uncharacterized protein LOC125650637 isoform X2
LOC125681872	-6.155299104	3.09E-05	tetraspanin-9-like
LOC125655976	-6.120054598	3.26E-06	piercer of microtubule wall 1 protein-like
LOC125656087	-6.118849176	0.000814882	uncharacterized protein LOC125656087
LOC125654886	-6.117433497	6.16E-05	metalloproteinase inhibitor 2-like
LOC125673558	-6.087031381	3.48E-05	uncharacterized protein LOC125673558
LOC125654269	-6.073335357	0.000171543	IQ and ubiquitin-like domain-containing protein
LOC125655677	-6.069168407	0.000265039	uncharacterized protein LOC125655677
LOC125675825	-6.061064946	4.64E-06	uncharacterized protein LOC125675825
LOC125652429	-6.053951803	0.005444464	--
LOC125654207	-6.051303212	1.72E-06	uncharacterized protein LOC125654207
LOC125683834	-6.042945717	2.41E-06	tetraspanin-9-like
LOC125668705	-6.039338786	0.006068465	LOW QUALITY PROTEIN: hematopoietic prostaglandin D synthase-like
LOC125646071	-6.026132992	0.000493315	MORN repeat-containing protein 1-like isoform X1
LOC125652465	-6.01898511	0.000117436	DBH-like monooxygenase protein 2 homolog isoform X2

USC UNIVERSIDADE DE SANTIAGO DE COMPOSTELA

LOC125670167	-5.993722565	0.000995017	cytoplasmic dynein 2 heavy chain 1-like
LOC125654787	-5.989579196	5.83E-06	protein PRQFV-amide-like
LOC125673014	-5.972646242	9.90E-05	uncharacterized protein LOC125673014 isoform X2
LOC125660021	-5.963692982	8.22E-06	sphingolipid delta(4)-desaturase DES1-like isoform X2
LOC125679737	-5.962727488	0.000124366	arrestin domain-containing protein 2-like
LOC125679178	-5.961814345	2.20E-05	protein FAM166B-like
LOC125662861	-5.941688914	4.77E-06	tektin-1-like
LOC125679600	-5.926388736	1.75E-06	coiled-coil domain-containing protein 105-like isoform X1
LOC125671570	-5.921277936	0.001418381	uncharacterized protein LOC125671570
LOC125645774	-5.908369689	1.50E-06	uncharacterized protein LOC125645774 isoform X1
LOC125673170	-5.899884981	0.000867513	pancreatic triacylglycerol lipase-like
LOC125682191	-5.847946111	0.004301637	tetraspanin-9-like isoform X1
LOC125681186	-5.84128016	2.12E-06	uncharacterized protein LOC125681186
LOC125670652	-5.839079744	0.000189637	uncharacterized protein LOC125670652 isoform X4
LOC125652738	-5.838078409	3.68E-06	radial spoke head protein 9 homolog isoform X2
LOC125663775	-5.83052851	7.95E-05	uncharacterized protein LOC125663775
LOC125683094	-5.814797257	3.67E-05	uncharacterized protein LOC125683094
LOC125677388	-5.808247288	0.000189004	uncharacterized protein LOC125677388 isoform X2
LOC125645434	-5.798706301	7.94E-07	uncharacterized protein LOC125645434 isoform X4
LOC125678448	-5.771181147	0.000553806	uncharacterized protein LOC125678448
LOC125650681	-5.744072997	7.18E-06	uncharacterized protein LOC125650681
LOC125645747	-5.732751159	0.000933826	uncharacterized protein LOC125645747
LOC125654310	-5.732664118	3.45E-05	sodium-dependent proline transporter-like
LOC125679523	-5.726367645	1.79E-05	uncharacterized protein LOC125679523
LOC125680895	-5.706484507	0.000225776	--
LOC125679759	-5.693465479	3.87E-05	beta-1%2C3-galactosyltransferase 1-like
LOC125645461	-5.682798454	5.28E-07	glutamate-rich protein 3-like isoform X2
LOC125655489	-5.673631971	3.29E-06	globin-like
LOC125650639	-5.652387293	7.77E-06	coiled-coil domain-containing protein 170-like
LOC125650674	-5.652387293	7.77E-06	coiled-coil domain-containing protein 170-like
LOC125652777	-5.649006371	0.002432507	uncharacterized protein LOC125652777
LOC125646798	-5.646332165	8.87E-05	putative ankyrin repeat protein RF_0381 isoform X1
LOC125672997	-5.640687234	0.001065469	dehydrogenase/reductase SDR family member on chromosome X-like isoform X3
LOC125669794	-5.635660209	1.70E-06	uncharacterized protein LOC125669794
LOC125674310	-5.628782702	0.000355886	oncoprotein-induced transcript 3 protein-like
LOC125670666	-5.606792844	0.000696707	uncharacterized protein LOC125670666 isoform X2
LOC125653934	-5.60296881	0.000102597	uncharacterized protein LOC125653934
LOC125682995	-5.592883049	0.001440511	uncharacterized protein LOC125682995
LOC125679668	-5.575234013	1.68E-06	fibroblast growth factor receptor 2-like isoform X4
LOC125658248	-5.567449595	0.000285712	uncharacterized protein LOC125658248
LOC125674305	-5.538332526	5.31E-05	uncharacterized protein LOC125674305 isoform X3
LOC125681261	-5.526706292	4.50E-06	sodium- and chloride-dependent taurine transporter-like isoform X1
LOC125673372	-5.524917497	4.37E-07	pancreatic triacylglycerol lipase-like isoform X3
LOC125681983	-5.50430285	0.00041251	--
LOC125648739	-5.466115466	4.30E-06	uncharacterized protein C20orf85-like
LOC125654740	-5.442663464	1.09E-12	gelsolin-like protein 2
LOC125652000	-5.425910611	0.001033682	uncharacterized protein LOC125652000
LOC125650546	-5.424294681	0.003546852	ras-related C3 botulinum toxin substrate 3-like
LOC125658450	-5.409174465	0.00442997	--
LOC125660487	-5.391316051	0.002288278	E3 ubiquitin-protein ligase TRIM56-like
LOC125650137	-5.380271631	2.66E-05	uncharacterized protein LOC125650137 isoform X6

USC UNIVERSIDADE DE SANTIAGO DE COMPOSTELA

LOC125673172	-5.365105452	0.001553983	pancreatic triacylglycerol lipase-like
LOC125681419	-5.35911492	0.000217826	fibrocystin-L-like isoform X1
LOC125649263	-5.359111648	0.000128462	calmodulin-A-like
LOC125678957	-5.343081089	3.66E-05	tryptophan--tRNA ligase%2C cytoplasmic-like
LOC125667682	-5.339090901	0.004348038	uncharacterized protein LOC125667682
LOC125659544	-5.306067072	8.20E-06	sperm axonemal maintenance protein CFAP97D1-like
LOC125668622	-5.305329146	0.000200998	uncharacterized protein LOC125668622
LOC125646086	-5.292919619	6.88E-06	MAM and LDL-receptor class A domain-containing protein 1-like
LOC125651602	-5.283293782	0.000739149	furin-like protease kpc-1
LOC125671286	-5.270941751	3.24E-05	hillarin-like
LOC125651862	-5.265873054	0.000240187	uncharacterized protein LOC125651862 isoform X1
LOC125651637	-5.26334014	0.00017342	protein dead ringer homolog
LOC125680290	-5.261449599	2.23E-05	uncharacterized protein LOC125680290 isoform X2
LOC125680312	-5.24589601	0.000168931	uncharacterized protein LOC125680312
LOC125658245	-5.241171366	0.000253412	postacrosomal sheath WW domain-binding protein-like isoform X2
LOC125665905	-5.23092221	0.000168476	interferon alpha-inducible protein 27-like protein 2B isoform X3
LOC125657872	-5.228852302	0.003369407	cilia- and flagella-associated protein 119-like
LOC125650938	-5.223580082	0.005274731	--
LOC125665726	-5.207245675	0.000167612	uncharacterized protein LOC125665726
LOC125658990	-5.201218866	4.06E-05	enolase-phosphatase E1-like isoform X2
LOC125682074	-5.182611514	1.53E-06	glutamine synthetase 2 cytoplasmic-like
LOC125651182	-5.175623852	0.004407731	uncharacterized protein LOC125651182
LOC125680852	-5.170649473	7.67E-05	E3 ubiquitin-protein ligase TRIM71-like
LOC125675925	-5.143924562	0.003353404	--
LOC125683428	-5.143067149	1.30E-05	uncharacterized protein LOC125683428
LOC125673513	-5.142511664	0.000930493	uncharacterized protein LOC125673513
LOC125680688	-5.123948551	4.36E-06	mitochondria-eating protein-like isoform X3
LOC125649496	-5.117817736	3.55E-06	--
LOC125648138	-5.108924986	0.000119943	--
LOC125647979	-5.100012134	3.77E-05	LOW QUALITY PROTEIN: sperm-associated antigen 16 protein-like
LOC125655701	-5.091324209	4.49E-05	--
LOC125664158	-5.089605018	4.22E-06	atrial natriuretic peptide receptor 2-like isoform X2
LOC125664454	-5.081099201	0.000111071	fatty acid-binding protein%2C heart-like
LOC125659693	-5.079554142	0.003218803	uncharacterized protein LOC125659693
LOC125654853	-5.07035976	0.000208291	uncharacterized protein LOC125654853
LOC125654360	-5.069297666	0.001051401	uncharacterized protein LOC125654360 isoform X2
LOC125669397	-5.05887616	3.08E-05	--
LOC125667484	-5.036764865	0.005402472	uncharacterized protein LOC125667484
LOC125680336	-5.031173583	0.000471851	uncharacterized protein LOC125680336
LOC125677370	-5.021537701	0.000101559	protein phosphatase 1 regulatory subunit 32-like
LOC125663672	-5.014534462	0.000190545	A disintegrin and metalloproteinase with thrombospondin motifs 7-like isoform X1
LOC125658680	-5.01060649	5.70E-05	uncharacterized protein LOC125658680
LOC125647987	-4.981283116	0.000167819	ropporin-1-like protein
LOC125647995	-4.981283116	0.000167819	ropporin-1-like protein
LOC125663776	-4.980565933	3.29E-05	uncharacterized protein LOC125663776
LOC125681914	-4.978697336	0.00296573	octopamine receptor-like
LOC125664822	-4.974818095	0.000384387	cytochrome b5 domain-containing protein 1-like
LOC125670854	-4.967624614	0.00042289	uncharacterized protein LOC125670854 isoform X2
LOC125649994	-4.919856757	0.000649118	sodium- and chloride-dependent neutral and basic amino acid transporter B(0+)-like isoform X1
LOC125649489	-4.909506103	0.000210889	L-rhamnose-binding lectin CSL3-like isoform X3
LOC125650224	-4.876315408	1.19E-05	dynein axonemal light chain 1-like

USC UNIVERSIDADE DE SANTIAGO DE COMPOSTELA

LOC125659763	-4.875568126	0.000271709	tripartite motif-containing protein 2-like
LOC125671094	-4.866003478	3.10E-05	EF-hand calcium-binding domain-containing protein 6-like isoform X1
LOC125669885	-4.865721707	0.002130847	uncharacterized protein LOC125669885
LOC125648923	-4.856572283	0.000129276	LOW QUALITY PROTEIN: sodium-dependent phosphate transport protein 2B-like
LOC125671290	-4.855098699	4.99E-13	uncharacterized protein LOC125671290
LOC125671219	-4.851309229	0.000205304	dynein intermediate chain 3%2C ciliary-like isoform X2
LOC125670922	-4.850882464	0.000245019	protein FAM183B-like
LOC125652760	-4.84904081	0.00108499	cdc42 homolog
LOC125648022	-4.847749997	0.001087655	uncharacterized protein LOC125648022 isoform X2
LOC125669998	-4.81678705	8.34E-05	beta-1%2C3-galactosyltransferase brn-like
LOC125660019	-4.810864139	2.38E-06	LOW QUALITY PROTEIN: protein O-mannosyl-transferase TMTC4-like
LOC125648130	-4.784045824	0.003222547	fatty acid-binding protein Fh15-like
LOC125672343	-4.779075302	0.000220767	--
LOC125645885	-4.777059413	0.000509524	33 kDa inner dynein arm light chain%2C axonemal-like
LOC125678353	-4.767073522	3.38E-06	EF-hand domain-containing family member B-like
LOC125654578	-4.746657694	3.65E-05	kinesin-like protein KIF28P
LOC125668354	-4.739136548	9.19E-05	uncharacterized protein LOC125668354 isoform X7
LOC125669783	-4.733784359	4.10E-05	cadherin-87A-like isoform X1
LOC125672113	-4.707359063	0.000320262	uncharacterized protein LOC125672113
LOC125645866	-4.699576576	0.001142258	mucin-4-like isoform X6
LOC125656847	-4.693498761	0.002444392	uncharacterized protein LOC125656847 isoform X1
LOC125665556	-4.670263197	1.20E-05	parathyroid hormone/parathyroid hormone-related peptide receptor-like isoform X1
LOC125683673	-4.664747182	3.44E-05	uncharacterized protein LOC125683673 isoform X5
LOC125680298	-4.656506636	0.000352917	ankyrin repeat and SOCS box protein 13-like
LOC125660463	-4.647615933	8.26E-06	ankyrin repeat domain-containing protein 42-like
LOC125681691	-4.634652601	0.000344143	galectin-5-like isoform X2
LOC125672007	-4.626375338	0.001037279	uncharacterized protein LOC125672007
LOC125652242	-4.617048943	0.005258185	uncharacterized protein LOC125652242
LOC125670713	-4.579162233	0.00099821	uncharacterized protein LOC125670713
LOC125654309	-4.572514509	1.49E-05	sodium-dependent proline transporter-like isoform X2
LOC125676138	-4.560131144	0.000120302	15-hydroxyprostaglandin dehydrogenase [NAD(+)]-like
LOC125645895	-4.549233907	3.96E-06	uncharacterized protein LOC125645895
LOC125673659	-4.542761267	0.001023371	snake venom 5'-nucleotidase-like isoform X1
LOC125649530	-4.541335885	6.20E-05	uncharacterized protein LOC125649530 isoform X1
LOC125665860	-4.530752669	0.002913889	uncharacterized protein LOC125665860 isoform X2
LOC125674013	-4.530341844	0.002332024	--
LOC125656130	-4.529752109	0.000365027	uncharacterized protein LOC125656130 isoform X2
LOC125657629	-4.525330055	0.000414893	uncharacterized protein LOC125657629
LOC125673201	-4.523328946	5.45E-05	phenylalanine-4-hydroxylase-like isoform X1
LOC125645482	-4.515875132	0.003591358	uncharacterized protein LOC125645482 isoform X2
LOC125669700	-4.496714685	9.62E-05	cadherin-87A-like
LOC125676019	-4.495384716	0.000364958	uncharacterized protein LOC125676019
LOC125648850	-4.493245217	0.000845647	potassium channel subfamily K member 2-like
LOC125680700	-4.492673834	0.00081488	uncharacterized protein LOC125680700
LOC125671327	-4.474100551	1.57E-07	hairy and enhancer of split-related protein helt-like
LOC125663136	-4.466275688	0.001468686	uncharacterized protein LOC125663136
LOC125658518	-4.439855128	8.06E-05	uncharacterized protein CXorf58-like isoform X1
LOC125669562	-4.392685708	0.000144765	uncharacterized protein LOC125669562 isoform X1
LOC125666828	-4.38070202	5.81E-05	cilia- and flagella-associated protein 69-like
LOC125648436	-4.379897046	0.000643515	uncharacterized protein LOC125648436
LOC125657007	-4.370727048	4.59E-05	uncharacterized protein LOC125657007

USC UNIVERSIDADE DE SANTIAGO DE COMPOSTELA

LOC125681271	-4.361132909	0.001219466	cytochrome P450 2J3-like
LOC125650564	-4.35325443	0.000614372	limbic system-associated membrane protein-like
LOC125650027	-4.294010383	3.80E-05	uncharacterized protein LOC125650027
LOC125682298	-4.2747314	0.00180121	uncharacterized protein LOC125682298
LOC125651816	-4.268681032	0.002288492	FMRFamide receptor-like
LOC125654789	-4.265590135	2.23E-05	uncharacterized protein C12orf56-like isoform X1
LOC125673328	-4.25783281	2.15E-16	four-jointed box protein 1-like
LOC125655876	-4.256509029	9.17E-07	--
LOC125668324	-4.253186942	0.001513021	sodium-coupled monocarboxylate transporter 1-like
LOC125683830	-4.251119564	0.000265108	uncharacterized protein LOC125683830 isoform X1
LOC125650791	-4.231234952	6.41E-05	uncharacterized protein LOC125650791
LOC125671784	-4.21901171	0.000344394	transmembrane protein 178B-like
LOC125646332	-4.215272073	0.000151154	uncharacterized protein LOC125646332 isoform X2
LOC125657931	-4.209504207	0.000528737	tubulin beta chain
LOC125647943	-4.203121989	0.005298137	prothoracicostatic peptide-like
LOC125675832	-4.190048793	0.002737497	uncharacterized protein LOC125675832 isoform X3
LOC125654399	-4.188362482	0.000534662	LIM domain and actin-binding protein 1-like
LOC125670754	-4.186584867	0.001424367	purine nucleoside phosphorylase-like isoform X1
LOC125653307	-4.182155028	0.001005474	neuroglian-like isoform X1
LOC125680306	-4.15727006	8.97E-05	transmembrane protein 145-like
LOC125652471	-4.154082464	0.003550495	uncharacterized protein LOC125652471
LOC125679700	-4.148319574	0.003691081	epidermal growth factor receptor-like
LOC125649607	-4.147312353	0.004602563	uncharacterized protein LOC125649607 isoform X3
LOC125677304	-4.143580275	0.001631618	uncharacterized protein LOC125677304
LOC125682231	-4.134805309	7.57E-05	protein Flattop homolog
LOC125671240	-4.132973012	0.001066626	extracellular signal-regulated kinase 2-like isoform X1
LOC125657568	-4.125985549	0.002918847	uncharacterized protein LOC125657568
LOC125674793	-4.115245348	0.000641138	microtubule-associated protein futsch-like isoform X4
LOC125667337	-4.103415188	0.002396491	glutathione S-transferase theta-1-like
LOC125653802	-4.101184804	1.55E-06	uncharacterized protein LOC125653802
LOC125666900	-4.09398768	1.30E-06	extracellular superoxide dismutase [Cu-Zn]-like
LOC125680549	-4.061896825	9.35E-05	ankyrin repeat domain-containing protein 50-like
LOC125646811	-4.045505294	0.002798258	homeobox protein Dlx6a-like
LOC125669459	-4.031669986	0.001173004	probable 3'%2C5'-cyclic phosphodiesterase pde-5 isoform X10
LOC125682968	-4.02760322	0.001568402	twisted gastrulation protein homolog 1-A-like
LOC125677098	-3.984840152	0.002278827	--
LOC125650997	-3.978593427	0.00137142	cilia- and flagella-associated protein 161-like
LOC125674691	-3.973457519	0.000213446	coiled-coil domain-containing protein 81-like isoform X2
LOC125663949	-3.972365584	3.33E-05	dynein regulatory complex subunit 2-like
LOC125659519	-3.962226469	1.50E-05	--
LOC125660793	-3.926081872	0.004162674	ceramide-1-phosphate transfer protein-like
LOC125645564	-3.917179235	0.000550188	uncharacterized protein LOC125645564
LOC125681703	-3.911791927	0.002419396	WD repeat-containing protein 38-like isoform X2
LOC125674963	-3.887369612	7.02E-05	uncharacterized protein LOC125674963 isoform X5
LOC125669870	-3.886681057	0.000246658	dynein axonemal intermediate chain 4-like isoform X3
LOC125647240	-3.880894149	0.000887963	uncharacterized protein LOC125647240
LOC125659762	-3.880321953	0.006340148	E3 ubiquitin-protein ligase TRIM71-like
LOC125651796	-3.879232819	6.03E-05	piRNA biogenesis protein EXD1-like isoform X2
LOC125666193	-3.845027784	0.002215451	uncharacterized protein LOC125666193
LOC125680304	-3.839788129	0.001225143	tetraspanin-1-like
LOC125679472	-3.833428283	4.75E-05	cilia- and flagella-associated protein 77-like isoform X2

USC UNIVERSIDADE DE SANTIAGO DE COMPOSTELA

LOC125658432	-3.829336621	0.000528759	--
LOC125668497	-3.826256086	0.002277782	nucleoside diphosphate kinase homolog 5-like
LOC125670753	-3.80995782	0.000661249	uncharacterized protein LOC125670753 isoform X5
LOC125673758	-3.796869825	0.000143078	androglobin-like isoform X5
LOC125654325	-3.77840028	0.003918898	uncharacterized protein LOC125654325
LOC125664451	-3.773503779	0.001751865	dynein regulatory complex protein 10-like
LOC125649132	-3.773453959	8.02E-05	basal body-orientation factor 1-like
LOC125668518	-3.764377348	0.000236225	uncharacterized protein LOC125668518
LOC125650601	-3.759769053	0.004125979	zonadhesin-like
LOC125657684	-3.756864199	0.001019185	ciliary-associated calcium-binding coiled-coil protein 1-like isoform X1
LOC125649958	-3.727084487	0.000599741	spermatogenesis-associated protein 17-like isoform X2
LOC125672973	-3.722110903	0.000852467	uncharacterized protein LOC125672973 isoform X2
LOC125653316	-3.717683404	0.001490142	uncharacterized protein LOC125653316
LOC125650509	-3.698705559	0.001600047	--
LOC125649910	-3.686244161	9.55E-05	cilia- and flagella-associated protein 36-like
LOC125654171	-3.672591139	0.003149982	uncharacterized protein LOC125654171 isoform X3
LOC125676046	-3.659927633	0.002253265	--
LOC125675772	-3.657393591	0.003164096	uncharacterized WD repeat-containing protein alr3466-like
LOC125650768	-3.636011653	0.000314822	uncharacterized protein LOC125650768
LOC125658561	-3.632725155	0.002427497	uncharacterized protein LOC125658561
LOC125663827	-3.62692364	0.000279697	PH domain leucine-rich repeat-containing protein phosphatase 2-like isoform X2
LOC125670244	-3.626473047	0.000770556	uncharacterized protein LOC125670244 isoform X4
LOC125663914	-3.621881155	0.000201564	orexin receptor type 2-like
LOC125647565	-3.614533565	0.000920085	zinc finger MYND domain-containing protein 12-like
LOC125671194	-3.613353298	4.10E-05	afadin- and alpha-actinin-binding protein-like
LOC125671509	-3.612086014	0.003030178	excitatory amino acid transporter 1-like isoform X2
LOC125648354	-3.584621103	0.005834058	acireductone dioxygenase-like
LOC125657496	-3.58058975	0.0009575	sperm flagellar protein 1-like isoform X8
LOC125679328	-3.574784992	0.001620294	uncharacterized protein LOC125679328 isoform X6
LOC125646072	-3.566295034	1.05E-05	rootletin-like isoform X3
LOC125666040	-3.560239945	0.002291111	uncharacterized protein LOC125666040 isoform X2
LOC125648979	-3.559810455	0.000161241	cilia- and flagella-associated protein 53-like
LOC125650172	-3.55761571	0.000683477	ceramide glucosyltransferase-like isoform X1
LOC125675697	-3.543205913	1.52E-05	--
LOC125683455	-3.533871102	0.001408818	protein pitchfork-like
LOC125652180	-3.513719043	0.002751793	uncharacterized protein LOC125652180 isoform X2
LOC125673995	-3.504186798	0.004697329	uncharacterized protein LOC125673995
LOC125666770	-3.503510383	0.000545863	protein nemuri-like isoform X2
LOC125650277	-3.500602202	0.003080432	ras-related protein Rab-1A-like isoform X1
LOC125650701	-3.493729537	0.000287304	uncharacterized protein LOC125650701
LOC125671480	-3.469337358	0.002929375	uncharacterized protein LOC125671480
LOC125670593	-3.467251604	0.001157805	guanine nucleotide-binding protein G(o) subunit alpha-like
LOC125678108	-3.464302656	0.004920774	manganese-dependent ADP-ribose/CDP-alcohol diphosphatase-like isoform X1
LOC125679599	-3.461781281	0.001191313	neurofilament light polypeptide-like isoform X1
LOC125650855	-3.454804311	3.11E-05	advillin-like isoform X1
LOC125659535	-3.451439578	0.000909052	cilia- and flagella-associated protein 206-like
LOC125671742	-3.44260502	0.002237997	uncharacterized protein LOC125671742
LOC125673814	-3.422917427	5.79E-05	uncharacterized protein LOC125673814 isoform X1
LOC125666902	-3.405168546	0.000168448	extracellular superoxide dismutase [Cu-Zn]-like
LOC125654303	-3.400628184	0.002617385	neuroglian-like isoform X1
LOC125658175	-3.391461969	0.000119211	telomerase protein component 1-like

USC UNIVERSIDADE DE SANTIAGO DE COMPOSTELA

LOC125682586	-3.388120814	0.000972283	inositol-trisphosphate 3-kinase homolog
LOC125676949	-3.352295364	0.003096358	uncharacterized protein LOC125676949 isoform X2
LOC125670224	-3.34286533	0.002976124	cilia- and flagella-associated protein 299-like
LOC125672776	-3.338053179	0.003413077	gelsolin-like protein 1
LOC125670747	-3.335468817	0.001044464	coiled-coil domain-containing protein 40-like
LOC125670679	-3.325643559	0.001483128	ras-related protein Rap-2a-like
LOC125658158	-3.320116351	0.003226767	uncharacterized protein C5orf49 homolog isoform X2
LOC125670517	-3.313680518	0.002704321	uncharacterized protein LOC125670517
LOC125671272	-3.28141704	0.006177417	uncharacterized protein LOC125671272
LOC125668620	-3.274135653	0.00213298	uncharacterized protein LOC125668620 isoform X2
LOC125668506	-3.266981468	0.005025381	spermatogenesis-associated protein 1-like isoform X9
LOC125647309	-3.264382334	0.003553624	uncharacterized protein LOC125647309
LOC125659453	-3.258111062	0.003084357	ryncolin-4-like
LOC125654995	-3.212535457	2.52E-05	--
LOC125680627	-3.206206879	0.001885026	abnormal spindle-like microcephaly-associated protein homolog isoform X4
LOC125653613	-3.198516318	0.000788021	dynein regulatory complex protein 11-like isoform X2
LOC125679948	-3.181215161	0.006419993	spermatogenesis-associated protein 4-like isoform X2
LOC125674128	-3.177432506	0.000225039	tubby protein-like isoform X4
LOC125671202	-3.171416274	0.004240823	probable thiopurine S-methyltransferase
LOC125670249	-3.155886787	0.004749162	sperm-tail PG-rich repeat-containing protein 2-like
LOC125656073	-3.14536195	0.001753474	LOW QUALITY PROTEIN: S-crystallin SL11-like
LOC125662405	-3.130570634	0.005136358	uncharacterized protein LOC125662405
LOC125676659	-3.127339327	0.001118826	OTU domain-containing protein 3-like
LOC125650600	-3.124281054	0.001589291	serine/arginine repetitive matrix protein 2-like isoform X3
LOC125666792	-3.122745256	0.005979409	cytochrome P450 3A4-like isoform X1
LOC125648881	-3.11163348	1.29E-05	--
LOC125679349	-3.108214875	9.00E-05	cilia- and flagella-associated protein 157-like
LOC125680718	-3.100451101	0.001413014	dynein regulatory complex subunit 4-like
LOC125651560	-3.091790516	0.000839603	uncharacterized protein LOC125651560 isoform X1
LOC125671283	-3.09027514	0.00072299	ADP-ribosylation factor-like protein 4C
LOC125660930	-3.087560975	0.005843149	disintegrin and metalloproteinase domain-containing protein 10-like isoform X2
LOC125671559	-3.072430239	0.001152035	SPRY domain-containing SOCS box protein 3-like
LOC125670771	-3.07102909	9.40E-05	CD151 antigen-like
LOC125676996	-3.06663847	0.000588719	UDP-glucuronic acid decarboxylase 1-like isoform X2
LOC125655217	-3.057104948	0.002911043	uncharacterized protein LOC125655217
LOC125676012	-3.051181892	0.005118657	uncharacterized protein LOC125676012
LOC125663732	-3.038973667	0.003561207	uncharacterized protein LOC125663732
LOC125654312	-3.03589343	0.002281951	gelsolin-like protein 1
LOC125649470	-3.033046372	0.000984775	katanin p60 ATPase-containing subunit A-like 2 isoform X8
LOC125650352	-3.032610783	0.00252953	leucine-rich repeat-containing protein 23-like isoform X2
LOC125671205	-3.011645604	0.001341218	serine/threonine-protein kinase PLK1-like
LOC125668800	-3.009672662	0.000579722	uncharacterized protein LOC125668800
LOC125650553	-3.006699671	0.003189454	uncharacterized protein LOC125650553 isoform X3
LOC125683616	-2.998298202	3.27E-05	buccalin-like
LOC125680466	-2.981840761	0.006122985	uncharacterized protein LOC125680466
LOC125668133	-2.979090423	0.000940621	GTP-binding protein 1-like
LOC125650378	-2.973329968	0.003336635	clathrin heavy chain linker domain-containing protein 1-like
LOC125675019	-2.965724132	0.001924059	protein MFI-like isoform X2
LOC125679154	-2.962726184	2.89E-05	testis-expressed protein 26-like isoform X2
LOC125670262	-2.955201878	2.91E-05	protein sidekick-2-like isoform X2
LOC125678257	-2.954527185	0.003385868	TNF receptor-associated factor 2-like

USC UNIVERSIDADE DE SANTIAGO DE COMPOSTELA

LOC125682214	-2.945774709	0.003789621	calcium channel flower homolog
LOC125654821	-2.944258929	0.001924753	uncharacterized protein LOC125654821
LOC125646503	-2.932528914	0.000658455	zinc finger C2HC domain-containing protein 1A-like isoform X3
LOC125675593	-2.929505307	0.004484192	protein AMN1 homolog
LOC125674188	-2.91094899	0.004730706	uncharacterized protein LOC125674188 isoform X1
LOC125658263	-2.89942634	0.001225063	myosin-VIIa-like
LOC125663803	-2.886508257	8.64E-05	uncharacterized protein LOC125663803
LOC125649775	-2.853652146	0.001083843	serine palmitoyltransferase 2-like
LOC125653965	-2.846819693	0.000422538	uncharacterized protein LOC125653965 isoform X1
LOC125678836	-2.844516119	0.003671896	outer dynein arm-docking complex subunit 3-like
LOC125672132	-2.836098754	0.002984233	intraflagellar transport protein 172 homolog
LOC125672138	-2.833050558	0.00057668	uncharacterized protein LOC125672138
LOC125649969	-2.815997697	0.001083017	LOW QUALITY PROTEIN: uncharacterized protein LOC125649969
LOC125675210	-2.801318555	9.43E-07	parkin coregulated gene protein homolog
LOC125678035	-2.797771116	0.002599494	--
LOC125678206	-2.778354955	0.000273773	advillin-like isoform X1
LOC125673189	-2.76211167	0.006008664	uncharacterized protein LOC125673189 isoform X1
LOC125674795	-2.761821889	0.002829536	--
LOC125659770	-2.752065009	0.001164704	dynein regulatory complex protein 9-like isoform X2
LOC125678695	-2.742231165	0.003663771	protocadherin Fat 1-like isoform X4
LOC125650335	-2.738789092	0.001943226	uncharacterized protein LOC125650335 isoform X3
LOC125653920	-2.728303916	0.003720014	tyrosine-protein phosphatase 99A-like isoform X4
LOC125677735	-2.72758523	0.001092551	PC3-like endoprotease variant B isoform X1
LOC125667898	-2.698369286	0.000130267	zinc finger protein GLIS3-like
LOC125663611	-2.694207708	0.001915013	uncharacterized protein LOC125663611 isoform X2
LOC125655023	-2.693313257	0.00316041	acetoacetyl-CoA synthetase-like
LOC125676114	-2.691621714	0.004136756	exportin-4-like
LOC125672122	-2.669078795	0.000209806	enkurin domain-containing protein 1-like
LOC125680760	-2.666702969	0.005376122	proteolipid protein DM beta-like
LOC125668577	-2.659853785	0.000941748	phospholipid-transporting ATPase ABCA1-like isoform X2
LOC125678739	-2.65757474	0.002280017	WD repeat-containing protein 19-like
LOC125655067	-2.650368724	0.003275246	uncharacterized protein LOC125655067
LOC125648777	-2.634566509	0.006278631	inositol hexakisphosphate kinase 3-like isoform X3
LOC125667894	-2.616229988	0.003967678	adhesion G protein-coupled receptor L3-like isoform X1
LOC125650363	-2.609149904	0.000356496	cyclin-dependent kinase-like 1 isoform X2
LOC125664669	-2.609133424	0.00192804	cilia- and flagella-associated protein 299-like
LOC125683829	-2.605438459	0.004997013	phosphatidylserine synthase 2-like
LOC125665621	-2.600460076	0.003624023	ciliogenesis-associated TTC17-interacting protein-like
LOC125667260	-2.596874759	0.001391624	spartin-like
LOC125654776	-2.566443328	0.005993209	E3 ubiquitin-protein ligase TRIM36-like
LOC125670040	-2.558776787	0.000372341	PDZ domain-containing protein GIPC1-like
LOC125668463	-2.550716771	0.001546771	protein ecdysoneless homolog
LOC125646017	-2.536980341	0.000120169	uncharacterized protein LOC125646017
LOC125650288	-2.530544747	8.87E-05	methionine synthase-like isoform X2
LOC125669787	-2.514700701	0.006020141	protein phosphatase 1 regulatory subunit 42-like isoform X7
LOC125668209	-2.514239453	0.004076756	uncharacterized protein LOC125668209
LOC125655918	-2.506898942	0.000675887	dual specificity tyrosine-phosphorylation-regulated kinase 2-like
LOC125659376	-2.485038174	0.005364694	F-box only protein 36-like
LOC125648076	-2.476407413	0.000966868	serine/threonine-protein kinase RIO3-like isoform X1
LOC125666707	-2.475997549	0.001733269	ATP-dependent translocase ABCB1-like isoform X5
LOC125656334	-2.457933724	0.001064879	neural-cadherin-like isoform X4

USC UNIVERSIDADE DE SANTIAGO DE COMPOSTELA

LOC125654400	-2.453499165	0.000126522	uncharacterized protein LOC125654400
LOC125648977	-2.451941612	0.001723968	phospholipid-transporting ATPase ID-like isoform X1
LOC125661479	-2.44022875	0.005835836	LOW QUALITY PROTEIN: testis-expressed protein 9-like
LOC125651603	-2.435933124	0.003498861	furin-like protease kpc-1 isoform X1
LOC125675771	-2.433547115	0.002297929	uncharacterized protein LOC125675771 isoform X2
LOC125661373	-2.416894085	0.005021214	uncharacterized protein LOC125661373
LOC125675165	-2.406831085	0.002698293	uncharacterized protein LOC125675165 isoform X1
LOC125664467	-2.389259383	0.002274959	trichoplein keratin filament-binding protein-like isoform X1
LOC125669487	-2.374959929	0.005705557	receptor-type tyrosine-protein phosphatase alpha-like isoform X1
LOC125679071	-2.370689053	0.000414143	lachesin-like isoform X2
LOC125663779	-2.360961137	0.006008954	uncharacterized protein LOC125663779
LOC125670145	-2.35338465	0.000106182	uncharacterized protein LOC125670145
LOC125676377	-2.322957657	0.004622858	major vault protein-like
LOC125666531	-2.316576982	0.005245839	E3 ubiquitin-protein ligase TRIM36-like
LOC125683384	-2.313820539	0.000785078	uncharacterized protein LOC125683384
LOC125645697	-2.307140332	0.000795323	uncharacterized protein LOC125645697
LOC125648950	-2.306456125	0.002784591	selenoprotein N-like isoform X2
LOC125677687	-2.281706684	0.003764734	diacylglycerol kinase zeta-like isoform X3
LOC125669817	-2.279685805	0.005529487	AN1-type zinc finger protein 4-like
LOC125647642	-2.263766554	0.00252919	WD repeat-containing protein 35-like isoform X2
LOC125658816	-2.257902826	0.006039978	--
LOC125649064	-2.241405224	0.003077778	spermatogenesis-associated protein 7-like isoform X2
LOC125678234	-2.230471132	0.004934899	ETS translocation variant 4-like isoform X3
LOC125683839	-2.229588563	0.000485156	--
LOC125674087	-2.199317948	0.001688506	unconventional myosin-VI-like isoform X1
LOC125664286	-2.159365092	0.002189276	ADP-ribose pyrophosphatase%2C mitochondrial-like isoform X1
LOC125672971	-2.145058769	1.91E-05	alpha-protein kinase vwkA-like isoform X1
LOC125659481	-2.143497927	0.001814001	MORN repeat-containing protein 4-like
LOC125657499	-2.129878994	0.004399807	uncharacterized protein LOC125657499
LOC125646246	-2.12642209	0.002378962	rabphilin-3A-like isoform X2
LOC125647936	-2.119624653	0.000305021	protein LKAAEAR1-like
LOC125665532	-2.116668312	0.003067742	nucleolar protein dao-5-like isoform X9
LOC125674020	-2.104227646	0.001929116	synaptotagmin-1-like isoform X1
LOC125680278	-2.089760944	0.00040785	folylpolyglutamate synthase%2C mitochondrial-like isoform X6
LOC125672022	-2.085989569	0.006617847	intraflagellar transport protein 22 homolog
LOC125678371	-2.080801804	0.000327346	choline transporter-like protein 2 isoform X3
LOC125659917	-2.077884545	0.00216167	uncharacterized protein LOC125659917
LOC125659344	-2.069210643	0.000157596	prominin-1-like isoform X2
LOC125682018	-2.046876608	0.001326773	transmembrane protein 41A-like
LOC125670864	-2.041324534	0.004522961	MTOR-associated protein MEAK7-like
LOC125645447	-2.01311227	0.00105523	uncharacterized protein LOC125645447
LOC125683076	-2.007740134	0.001153716	uncharacterized protein LOC125683076 isoform X4
LOC125656135	-2.007414575	0.006093137	uncharacterized protein LOC125656135
LOC125681929	-2.003092015	0.000564768	upstream stimulatory factor 2-like isoform X1
LOC125655690	-2.000268553	0.002008907	SH3 and PX domain-containing protein 2A-like
LOC125660924	-1.991331886	0.001310186	ras-responsive element-binding protein 1-like isoform X1
LOC125683065	-1.974163302	0.004408888	nuclear receptor subfamily 1 group D member 2-like
LOC125657189	-1.961665678	0.001229117	ras-related protein Rab-34-like
LOC125669526	-1.952948491	0.002812101	meiosis regulator and mRNA stability factor 1-like isoform X1
LOC125646279	-1.935380919	0.003194459	centriolar satellite-associated tubulin polyglutamylase complex regulator 1-like isoform X1
LOC125683125	-1.930425152	0.000619699	beta-1%2C3-galactosyltransferase 5-like

USC UNIVERSIDADE DE SANTIAGO DE COMPOSTELA

LOC125683574	-1.919213679	0.004524046	uncharacterized protein LOC125683574
LOC125656305	-1.915569059	6.24E-08	serine-rich adhesin for platelets-like
LOC125678632	-1.902594659	0.006190928	advanced glycosylation end product-specific receptor-like isoform X1
LOC125667916	-1.901248468	0.003672414	prominin-1-like
LOC125670463	-1.889599072	0.003933578	uncharacterized protein LOC125670463
LOC125658567	-1.883619746	0.005174112	probable glutamate receptor
LOC125674902	-1.87018202	0.004417935	tumor susceptibility gene 101 protein-like
LOC125669515	-1.863725827	0.006349258	tubulin polymerization-promoting protein family member 3-like
LOC125669542	-1.844990451	0.001570236	ATP-binding cassette sub-family A member 9-like isoform X1
LOC125678643	-1.814282252	0.001573979	uncharacterized protein LOC125678643 isoform X6
LOC125661521	-1.805725522	0.000360603	uncharacterized protein LOC125661521
LOC125668426	-1.791449774	0.003980604	ferric-chelate reductase 1-like isoform X1
LOC125645522	-1.772535273	0.002380644	uncharacterized protein LOC125645522
LOC125654637	-1.758142695	0.006601592	E3 ubiquitin-protein ligase TRIM71-like
LOC125675880	-1.752702482	0.000805016	uncharacterized protein LOC125675880 isoform X4
LOC125658078	-1.740167551	0.003879908	melanotransferrin-like
LOC125672923	-1.731964123	0.005435083	coiled-coil domain-containing protein 102A-like
LOC125669622	-1.680435428	0.006484959	uncharacterized protein LOC125669622 isoform X1
LOC125649685	-1.676267302	0.004975189	uncharacterized protein LOC125649685
LOC125655126	-1.665095203	0.000771102	--
LOC125657052	-1.640627658	0.000939664	tripartite motif-containing protein 45-like
LOC125651466	-1.62252482	0.000543858	peptide-N(4)-(N-acetyl-beta-glucosaminyl)asparagine amidase-like
LOC125666892	-1.575319549	0.000531243	caspase-3-like isoform X2
LOC125679009	-1.574828592	0.003459657	protocadherin beta-15-like
LOC125650769	-1.570307603	0.00103019	mirror-image polydactyly gene 1 protein-like isoform X3
LOC125651530	-1.565882645	0.002246675	--
LOC125667931	-1.541213016	0.000960468	uncharacterized protein LOC125667931
LOC125658506	-1.526022052	0.00624948	cAMP-dependent protein kinase catalytic subunit 3-like
LOC125673582	-1.506283912	0.005000588	baculoviral IAP repeat-containing protein 7-A-like
LOC125652289	-1.497934457	0.003436441	uncharacterized protein LOC125652289
LOC125681704	-1.49022496	0.003996109	--
LOC125669940	-1.468667055	0.004552526	E3 ubiquitin-protein ligase SMURF2-like
LOC125683287	-1.459831934	0.006492704	uncharacterized protein LOC125683287
LOC125671472	-1.445279422	0.002072222	store-operated calcium entry-associated regulatory factor-like
LOC125681203	-1.417374127	0.000413795	LOW QUALITY PROTEIN: calsyntenin-1-like
LOC125669497	-1.414590816	0.001978201	UDP-glucose 4-epimerase-like
LOC125669627	-1.385114134	0.003853287	WW domain-binding protein 2-like
LOC125645488	-1.382537229	0.005207459	tubulin-specific chaperone cofactor E-like protein
LOC125669268	-1.357303195	0.005482187	S-adenosylmethionine synthase-like
LOC125670172	-1.354455277	0.000352359	--
LOC125669698	-1.331021598	0.00571252	receptor-type tyrosine-protein phosphatase kappa-like
LOC125646047	-1.302934374	0.001255668	gamma-aminobutyric acid receptor-associated protein-like 2
LOC125649862	-1.287663657	0.006545068	3'(2')%2C5'-bisphosphate nucleotidase 1-like
LOC125670480	-1.268969663	3.07E-05	uncharacterized protein LOC125670480
LOC125646331	-1.246176498	0.00641639	uncharacterized protein LOC125646331 isoform X3
LOC125647677	-1.240397353	0.001878461	uncharacterized protein LOC125647677
LOC125669237	-1.239431391	0.002742726	DNA-binding protein RFX2-like
LOC125680572	-1.224938784	0.003736721	N(G)%2CN(G)-dimethylarginine dimethylaminohydrolase 1-like
LOC125667675	-1.189252958	0.002093666	DNA-directed RNA polymerase II subunit RPB2
LOC125657901	-1.168534397	0.00243853	divergent protein kinase domain 2A-like isoform X2
LOC125657877	-1.058251993	0.000733346	eukaryotic translation initiation factor 3 subunit A-like isoform X2

USC UNIVERSIDADE DE SANTIAGO DE COMPOSTELA

LOC125674512	-1.014236756	0.00593042	sialomucin core protein 24-like
LOC125672054	-0.996923655	0.005648368	protein tweety homolog 1-A-like isoform X2
LOC125664020	-0.97366195	0.002554914	uncharacterized protein C1orf50 homolog
LOC125646044	-0.933478811	0.001044788	uncharacterized protein LOC125646044 isoform X2
LOC125648345	-0.903848857	0.003365326	Na(+)/H(+) exchange regulatory cofactor NHE-RF1-like
LOC125668966	-0.890978479	0.004371866	uncharacterized protein LOC125668966
LOC125650051	0.769931019	0.003302628	polyubiquitin-C
LOC125681242	0.931378736	0.003246026	ATP synthase-coupling factor 6%2C mitochondrial-like
LOC125650046	0.963356568	0.004405346	uncharacterized protein LOC125650046
LOC125668312	0.972199235	0.002957267	putative ATP synthase subunit f%2C mitochondrial
LOC125655977	0.981529367	0.003403275	NADH dehydrogenase [ubiquinone] 1 beta subcomplex subunit 11%2C mitochondrial-like
LOC125646906	0.984213057	0.006618209	prefoldin subunit 5-like
LOC125654881	1.01517019	0.006278909	steroid 17-alpha-hydroxylase/17%2C20 lyase-like
LOC125647831	1.06721294	0.001432598	uncharacterized protein LOC125647831
LOC125670560	1.070117103	0.002702209	cytochrome c oxidase subunit 5B%2C mitochondrial-like
LOC125648824	1.096036986	0.006254722	hemicentin-2-like isoform X2
LOC125663888	1.105342699	0.003436946	MICOS complex subunit Mic10-like
LOC125652521	1.106807956	0.003377832	NADH dehydrogenase [ubiquinone] iron-sulfur protein 4%2C mitochondrial-like
LOC125682601	1.132579283	0.002728321	uncharacterized protein LOC125682601
LOC125670645	1.136884155	0.002534713	uncharacterized protein LOC125670645
LOC125669879	1.141968377	0.001459397	mitochondrial glycine transporter-like
LOC125659158	1.153712541	0.005144766	succinate--CoA ligase [ADP-forming] subunit beta%2C mitochondrial-like
LOC125671524	1.165146879	0.00404575	S-methyl-5'-thioadenosine phosphorylase-like isoform X2
LOC125668044	1.172534885	8.94E-05	heat shock protein Hsp-16.48/Hsp-16.49-like
LOC125671179	1.177797638	0.003050075	ATP synthase subunit d%2C mitochondrial-like
LOC125674823	1.181004987	0.002434195	fructose-bisphosphate aldolase-like
LOC125659799	1.229001543	0.006117887	--
LOC125681684	1.232946689	0.003743107	glycosaminoglycan xylosylkinase-like
LOC125673856	1.25120438	0.00125886	uncharacterized protein LOC125673856 isoform X1
LOC125650545	1.308637837	0.000325231	--
LOC125654839	1.320449197	0.006157877	protein NipSnap-like isoform X1
LOC125683238	1.33956322	0.000149778	uncharacterized protein LOC125683238
LOC125651496	1.35363818	0.000277839	serum response factor-like
LOC125653790	1.372840297	0.003810087	uncharacterized protein LOC125653790 isoform X1
LOC125649806	1.38345962	0.000105284	probable methylmalonate-semialdehyde dehydrogenase [acylating]%2C mitochondrial
LOC125652336	1.407238412	0.002398098	uncharacterized protein LOC125652336
LOC125659867	1.416049927	0.002869548	uncharacterized protein LOC125659867
LOC125657651	1.424794369	0.000568934	--
LOC125683084	1.450389864	0.002463242	uncharacterized protein LOC125683084
LOC125682949	1.457618353	0.000534753	17-beta-hydroxysteroid dehydrogenase 14-like
LOC125671767	1.468542751	0.001687074	cysteine-rich protein 1-like
LOC125672535	1.469701374	0.000241451	uncharacterized protein LOC125672535
LOC125669257	1.479276599	0.004491968	NADH dehydrogenase [ubiquinone] 1 beta subcomplex subunit 10-like isoform X1
LOC125676008	1.485601704	0.002990326	cubilin-like isoform X4
LOC125663945	1.492869062	0.001842276	matrix metalloproteinase-19-like
LOC125679227	1.506370588	0.001487434	epidermal growth factor-like protein 8
LOC125662013	1.530409082	0.000606919	adenosine 5'-monophosphoramidase HINT1-like
LOC125663947	1.540267612	0.004751614	cytochrome P450 1A2-like
LOC125666119	1.567981764	0.003717924	--
LOC125647783	1.579601715	0.001076408	uncharacterized protein LOC125647783 isoform X1
LOC125654822	1.593670003	0.000866814	universal stress protein Slr1101-like

USC UNIVERSIDADE DE SANTIAGO DE COMPOSTELA

LOC125659966	1.610675852	0.000235099	uncharacterized protein LOC125659966
LOC125675437	1.610745523	0.003829363	ubiquitin carboxyl-terminal hydrolase 2-like isoform X3
LOC125653261	1.644307682	0.000990432	universal stress protein YxiE-like isoform X1
LOC125664347	1.670821063	0.000105346	phosphoenolpyruvate carboxykinase%2C cytosolic [GTP]-like isoform X1
LOC125668589	1.673541836	0.005209901	sarcoplasmic calcium-binding protein-like
LOC125673563	1.674725111	0.005920001	uncharacterized protein LOC125673563
LOC125658543	1.689496724	0.004299816	uncharacterized protein LOC125658543
LOC125679399	1.706193588	0.004024656	vacuolar protein-sorting-associated protein 25-like
LOC125674770	1.732547581	0.000969916	ATP synthase F(0) complex subunit B1%2C mitochondrial-like
LOC125649210	1.755408183	0.00138873	tropomyosin isoform X16
LOC125679195	1.763401448	0.002044698	microsomal glutathione S-transferase 2-like
LOC125674210	1.775539254	0.000299185	melanocortin receptor 5-like
LOC125660417	1.779403901	0.003880198	replication factor C subunit 4-like
LOC125672195	1.784811388	0.005629433	p53 and DNA damage-regulated protein 1-like
LOC125666757	1.80603602	0.000154628	transcription intermediary factor 1-beta-like
LOC125657099	1.808726946	0.000127451	uncharacterized protein LOC125657099
LOC125650843	1.810457495	0.000108863	uncharacterized protein LOC125650843
LOC125659212	1.818761195	0.000160793	LOW QUALITY PROTEIN: insulin-like growth factor-binding protein-related protein 1
LOC125647864	1.839185876	0.001283487	cholecystokinin receptor-like isoform X2
LOC125672605	1.848424327	0.000353215	cytochrome c oxidase subunit 6A2%2C mitochondrial-like
LOC125650529	1.876303575	0.004447006	uncharacterized protein LOC125650529 isoform X3
LOC125658859	1.907617977	0.005510382	sideroflexin-5-like
LOC125650748	1.915184672	0.003124225	uncharacterized protein LOC125650748
LOC125666753	1.928294091	5.07E-07	melatonin-related receptor-like isoform X1
LOC125651999	1.92949174	0.001223019	peptidyl-prolyl cis-trans isomerase B-like
LOC125658356	1.932489292	0.003645486	steroid 17-alpha-hydroxylase/17%2C20 lyase-like
LOC125680249	1.934990498	8.55E-05	14 kDa phosphohistidine phosphatase-like
LOC125670258	1.954104852	0.000429359	angiopoietin-1 receptor-like
LOC125670619	1.961618917	0.003154786	proliferating cell nuclear antigen-like
LOC125658287	1.984949943	0.000387671	--
LOC125655267	1.990888537	0.00282143	putative universal stress protein SAUSA300_1656
LOC125658096	1.994352329	0.003299197	uncharacterized protein LOC125658096
LOC125682061	2.020238579	0.004899675	zinc finger protein 345-like
LOC125653995	2.039464176	0.001434327	tubulin alpha-8 chain-like isoform X1
LOC125645440	2.071714566	0.002483294	uncharacterized protein LOC125645440
LOC125673793	2.079896441	0.002810047	transmembrane protein 201-like
LOC125655442	2.086983871	0.006145424	protein arginine N-methyltransferase 6-like isoform X2
LOC125671497	2.092946147	0.000207589	inactive pancreatic lipase-related protein 1-like isoform X1
LOC125676732	2.103536711	0.003428679	LOW QUALITY PROTEIN: ubiquitin carboxyl-terminal hydrolase 16-like
LOC125650370	2.107395126	4.08E-05	homeobox protein SIX4-like
LOC125652332	2.113716415	2.60E-06	uncharacterized protein LOC125652332 isoform X2
LOC125647590	2.114238254	0.00056797	uncharacterized protein LOC125647590
LOC125649465	2.121541122	0.005631493	inactive tyrosine-protein kinase 7-like
LOC125674964	2.143335537	0.005350983	coactosin-like protein
LOC125663985	2.14385448	0.000426715	uncharacterized protein LOC125663985 isoform X4
LOC125679044	2.144829604	0.000798363	cytochrome P450 2J1-like isoform X2
LOC125653468	2.164561594	0.000927237	uncharacterized protein LOC125653468
LOC125669567	2.174652906	1.62E-05	39S ribosomal protein L13%2C mitochondrial-like
LOC125649271	2.183509455	0.002134486	GTPase IMAP family member 9-like
LOC125669283	2.190751414	0.000853286	uncharacterized protein LOC125669283
LOC125668299	2.225699663	0.005172619	calmodulin-A-like isoform X1

USC UNIVERSIDADE DE SANTIAGO DE COMPOSTELA

LOC125674434	2.229413136	0.004287597	SH3 domain-binding glutamic acid-rich-like protein 3
LOC125671396	2.272255286	0.002479067	T-cell acute lymphocytic leukemia protein 1-like
LOC125671608	2.280878896	0.000181715	calcyphosin-like protein isoform X1
LOC125675608	2.309950486	0.000862908	kappa-type opioid receptor-like
LOC125646732	2.316251625	0.00332023	3-hydroxyisobutyrate dehydrogenase%2C mitochondrial-like
LOC125663824	2.321850198	0.002006352	protein-glutamine gamma-glutamyltransferase K-like isoform X1
LOC125668663	2.338931837	0.001277304	voltage-dependent T-type calcium channel subunit alpha-1H-like isoform X4
LOC125678504	2.350849481	2.05E-05	--
LOC125646186	2.352955653	0.000500467	myosin light chain kinase%2C smooth muscle-like isoform X3
LOC125658044	2.385012514	0.006657612	ankyrin-1-like isoform X1
LOC125659712	2.402160236	0.000558326	dual oxidase maturation factor 1-like
LOC125669719	2.408915247	0.005958363	uncharacterized protein LOC125669719
LOC125668398	2.421771041	0.001133988	testis-specific serine/threonine-protein kinase 1-like
LOC125656209	2.433979449	0.000486278	metalloproteinase inhibitor 1-like
LOC125664510	2.440394844	0.000209013	carbonic anhydrase 7-like isoform X1
LOC125646886	2.456562259	0.000155369	rac guanine nucleotide exchange factor B-like isoform X2
LOC125678595	2.459139286	8.58E-06	actin%2C adductor muscle
LOC125681016	2.47694598	0.000362132	--
LOC125650437	2.50444064	0.00328309	placenta-specific gene 8 protein-like
LOC125661583	2.528622726	0.005015218	aminopeptidase Ey-like isoform X4
LOC125650773	2.560612215	1.95E-07	uncharacterized protein LOC125650773 isoform X2
LOC125665910	2.571126582	0.005452281	uncharacterized protein LOC125665910
LOC125675565	2.645397706	5.10E-05	secretin receptor-like
LOC125646816	2.653106505	0.004140247	uncharacterized protein LOC125646816
LOC125655836	2.661682084	1.79E-07	insulin-like growth factor-binding protein 2-B
LOC125668300	2.694311607	0.000169953	troponin C-like isoform X1
LOC125653801	2.695625825	0.000338673	ADP-sugar pyrophosphatase-like isoform X1
LOC125682010	2.711303207	7.05E-05	16 kDa calcium-binding protein-like
LOC125658074	2.788335138	3.78E-05	myosin regulatory light chain B%2C smooth adductor muscle-like
LOC125683106	2.837524446	5.51E-07	myosin regulatory light chain 12A-like
LOC125647737	2.843322629	0.006617413	PDZ and LIM domain protein 1-like
LOC125659403	2.845986425	2.08E-07	LOW QUALITY PROTEIN: LHFPL tetraspan subfamily member 6 protein-like
LOC125682100	2.909012725	1.33E-14	aquaporin AQPAn.G-like
LOC125672422	2.915599112	0.000758069	myosin heavy chain%2C striated muscle-like isoform X5
LOC125648301	2.947697823	0.000613213	uncharacterized protein LOC125648301 isoform X2
LOC125678083	2.956487709	0.006539194	--
LOC125649534	2.963091693	0.005472726	calcitonin gene-related peptide type 1 receptor-like isoform X2
LOC125670191	3.010870299	0.006061858	very low-density lipoprotein receptor-like isoform X1
LOC125676882	3.046624042	0.003546181	ras-related and estrogen-regulated growth inhibitor-like
LOC125654864	3.055498955	0.001055351	heavy metal-binding protein HIP-like
LOC125650876	3.056396816	0.000127758	uncharacterized protein LOC125650876
LOC125675603	3.05715762	0.001384501	orexin receptor type 2-like
LOC125679404	3.072362528	2.53E-06	uncharacterized protein LOC125679404
LOC125652602	3.086101606	3.14E-20	--
LOC125658353	3.09321808	0.003569777	steroid 17-alpha-hydroxylase/17%2C20 lyase-like isoform X1
LOC125646974	3.117283101	0.00037644	major egg antigen-like
LOC125664359	3.137509208	0.005559165	LOW QUALITY PROTEIN: LHFPL tetraspan subfamily member 7 protein-like
LOC125673817	3.209215701	0.000486924	complement C1q-like protein 2
LOC125668598	3.209524385	0.001608971	FMRFamide receptor-like
LOC125655369	3.213375205	5.05E-09	apolipoprotein D-like
LOC125659525	3.253750253	0.001410699	myosin essential light chain%2C striated adductor muscle-like

USC UNIVERSIDADE DE SANTIAGO DE COMPOSTELA

LOC125649174	3.338359503	0.000216651	uncharacterized protein LOC125649174 isoform X1
LOC125651934	3.363424248	0.000424932	universal stress protein in QAH/OAS sulfhydrylase 3'region-like
LOC125655252	3.397082351	0.006023402	sex peptide receptor-like
LOC125650318	3.413459796	4.04E-05	uncharacterized protein LOC125650318 isoform X1
LOC125658028	3.54605014	7.40E-05	monocarboxylate transporter 13-like
LOC125670739	3.553747946	2.88E-07	peptidyl-prolyl cis-trans isomerase FKBP1A-like
LOC125656241	3.572386955	2.23E-06	--
LOC125677442	3.614107408	0.000624225	uncharacterized protein LOC125677442
LOC125681167	3.622490241	0.005737331	CD109 antigen-like isoform X3
LOC125657676	3.634538251	3.21E-06	uncharacterized protein LOC125657676 isoform X2
LOC125654030	3.641308129	0.001058956	cadherin-like and PC-esterase domain-containing protein 1
LOC125682079	3.660366351	0.00030716	uncharacterized protein LOC125682079
LOC125671361	3.665901777	0.000674157	carbohydrate sulfotransferase 15-like isoform X2
LOC125679696	3.690731274	0.000215944	complement C1q tumor necrosis factor-related protein 7-like
LOC125653347	3.710060894	0.00104428	uncharacterized protein LOC125653347
LOC125648015	3.723795097	0.000639573	alpha-crystallin A chain-like
LOC125680928	3.811621341	0.00062162	neuronal acetylcholine receptor subunit alpha-2-like
LOC125683189	3.821500685	6.04E-05	protein-glutamine gamma-glutamyltransferase K-like isoform X2
LOC125664873	3.841037134	9.00E-06	uncharacterized protein LOC125664873
LOC125678926	3.901915271	5.75E-08	pantetheinase-like
LOC125670650	3.922726489	0.000134111	uncharacterized protein LOC125670650
LOC125659571	3.927730941	0.000260551	monocarboxylate transporter 12-like isoform X2
LOC125647473	3.961435732	7.04E-05	uncharacterized protein LOC125647473
LOC125659646	4.150698825	0.002755789	uncharacterized protein LOC125659646 isoform X3
LOC125666117	4.201996733	3.44E-06	fibroblast growth factor receptor 3-like isoform X1
LOC125647776	4.246885779	0.000319994	uncharacterized protein LOC125647776
LOC125677046	4.254210695	0.001209007	natterin-3-like
LOC125659941	4.254336654	3.90E-05	tripartite motif-containing protein 2-like isoform X4
LOC125674991	4.281403522	0.000222416	uncharacterized protein LOC125674991
LOC125650739	4.338681111	1.71E-05	arginase%2C hepatic-like isoform X4
LOC125649164	4.366672775	2.96E-10	cytochrome P450 2U1-like
LOC125652039	4.392064626	1.38E-06	uncharacterized protein LOC125652039
LOC125679025	4.412019093	2.32E-05	sodium- and chloride-dependent glycine transporter 1-like
LOC125665566	4.430613564	2.32E-06	--
LOC125678402	4.448090904	1.57E-10	uncharacterized protein LOC125678402
LOC125678589	4.465536156	8.54E-06	ankyrin repeat domain-containing protein 7-like
LOC125672003	4.541265522	9.56E-07	bone morphogenetic protein 10-like
LOC125680866	4.878009561	0.00021953	uncharacterized protein LOC125680866
LOC125681949	4.951334974	0.000564501	--
LOC125645867	5.143768091	5.44E-05	uncharacterized protein LOC125645867 isoform X1
LOC125646735	5.193191864	0.00461678	low affinity immunoglobulin epsilon Fc receptor-like isoform X3
LOC125672586	5.241644106	9.95E-12	uncharacterized protein LOC125672586 isoform X2
LOC125678187	5.375213469	0.004295295	--
LOC125681172	5.485228538	0.002411257	prion-like-(Q/N-rich) domain-bearing protein 25
LOC125683649	5.566865458	0.003901476	peptidase inhibitor R3HDML-like
LOC125651938	5.707718105	0.000226949	uncharacterized protein LOC125651938
LOC125661361	6.020575698	2.23E-05	procathepsin L-like
LOC125665731	6.089800614	8.84E-07	uncharacterized protein LOC125665731 isoform X2
LOC125653842	6.139975245	0.00039567	DNA topoisomerase 1-like
LOC125656245	6.444795547	9.22E-07	uncharacterized protein LOC125656245
LOC125660337	6.774638922	2.20E-06	uncharacterized protein LOC125660337

USC UNIVERSIDADE DE SANTIAGO DE COMPOSTELA

LOC125671374	6.782053443	1.43E-06	uncharacterized protein LOC125671374
LOC125659279	6.960712585	1.37E-11	retinol dehydrogenase 12-like isoform X2
LOC125646189	7.862786635	2.24E-08	uncharacterized protein LOC125646189
LOC125648197	7.862786635	2.24E-08	uncharacterized protein LOC125648197
LOC125654795	8.019067417	1.81E-06	uncharacterized protein LOC125654795
LOC125662247	8.021668975	6.19E-06	--
LOC125682220	8.454260239	1.24E-07	nose resistant to fluoxetine protein 6-like

USC
UNIVERSIDADE
DE SANTIAGO
DE COMPOSTELA

USC
UNIVERSIDADE
DE SANTIAGO
DE COMPOSTELA

ANNEX III:

PERMISSIONS FOR RE-USE OF JOURNAL CONTENT

USC
UNIVERSIDADE DE SANTIAGO DE COMPOSTELA

USC
UNIVERSIDADE
DE SANTIAGO
DE COMPOSTELA

Figure 2 (Introduction).

Modified from: Helmer, L., Hauton, C., Bean, T., Bass, D., Hendy, I., Harris-Scott, E., & Preston, J. (2020). **Ephemeral detection of *Bonamia exitiosa* (Haplosporida) in adult and larval European flat oysters *Ostrea edulis* in the Solent, United Kingdom**. *Journal of Invertebrate Pathology*, *174*, 107421. doi: 10.1016/j.jip.2020.107421.

This Agreement between Mrs. Inés Martínez Sambade ("You") and Elsevier ("Elsevier") consists of your license details and the terms and conditions provided by Elsevier and Copyright Clearance Center.

License Number 6124310590821

License Date Oct 08, 2025

License Content Publisher Elsevier

Licensed Content Publication Journal of Invertebrate Pathology

Licensed Content Title Ephemeral detection of *Bonamia exitiosa* (Haplosporida) in adult and larval European flat oysters *Ostrea edulis* in the Solent, United Kingdom.

Licensed Content Author Luke Helmer, Chris Hauton, Tim Bean, David Bass, Ian Hendy, Eric Harris-Scott, Joanne Preston.

Licensed Content Date Jul 1, 2020

Licensed Content Volume 174

Licensed Content Issue n/a

Licensed Content Pages 8

Type of Use reuse in a thesis/dissertation

Portion figures/tables/illustrations

Number of figures/tables/illustrations 1

Format both print and electronic

Are you the author of this Elsevier article? No

Will you be translating? No

Title of new work Genomics of resistance to the parasite *Bonamia ostreae* in the European flat oyster *Ostrea edulis*

Institution name University of Santiago de Compostela

Expected presentation date Dec 2025

USC UNIVERSIDADE DE SANTIAGO DE COMPOSTELA

Requestor Location Avenida Carvalho Calero s/n Facultade de veterinaria pabellón 4 Lugo 27002, Spain

Publisher Tax ID GB 494 6272 12

Total 0.00 EUR

Figure 4 (Introduction).

Modified from:

Hoff SNK, Sambade IM, Ezeta Balic D, Gornik SG, Martínez P, et al. (2024). **Chromosomal fusions and large-scale inversions are key drivers of adaptive divergence in the European flat oyster (*Ostrea edulis*).** *bioRxiv* preprint. https://doi.org/10.1101/2024.06.28.599280

This figure is licensed under a **Creative Commons Attribution-NonCommercial 4.0 International License (CC BY-NC 4.0)**. This license allows users to **share** (copy and redistribute the material in any medium or format) and **adapt** (remix, transform, and build upon the material) for **non-commercial purposes**, provided that **appropriate credit** is given, a **link to the license** is provided, and any **changes** made are indicated. The licensor cannot revoke these freedoms as long as these terms are respected. No additional restrictions or technological barriers may be applied. Full license text available at: https://creativecommons.org/licenses/by-nc/4.0/

USC UNIVERSIDADE DE SANTIAGO DE COMPOSTELA

Chapter I.

Content adapted from:

Sambade, I. M., Casanova, A., Blanco, A., Gundappa, M. K., Bean, T. P., Macqueen, D. J., Houston, R. D., Villalba, A., Vera, M., Kamermans, P., & Martínez, P. (2022). A single genomic region involving a putative chromosome rearrangement in flat oyster (*Ostrea edulis*) is associated with differential host resilience to the parasite *Bonamia ostreae*. *Evolutionary Applications*, *15*(9), 1408-1422. https://doi.org/10.1111/eva.13446

This is an open access article. The author of this thesis is one of the first co-authors of this article. See the corresponding annex for the co-author authorizations to reflect this work in this thesis

Copyright © 2022 Sambade, Blanco, Gundappa, Bean, Macqueen, Houston, Villalba, Vera, Kamermans and Martínez. This is an open-access article distributed under the terms of the Creative Commons Attribution License (CC BY). The use, distribution or reproduction in other forums is permitted, provided the original author(s) and the copyright owner(s) are credited and that the original publication in this journal is cited, in accordance with accepted academic practice. No use, distribution or reproduction is permitted which does not comply with these terms.

and

Kamermans, P., Blanco, A., Van Dalen, P., Engelsma, M., Bakker, N., Jacobs, P., Dubbeldam, M., Sambade, I. M., Vera, M., & Martinez, P. (2023). *Bonamia*-free flat oyster (*Ostrea edulis* L.) seed for restoration projects: non-destructive screening of broodstock, hatchery production and test for Bonamia-tolerance. *Aquatic Living Resources*, *36*, 11. https://doi.org/10.1051/alr/2023005

This is an open access article. The author of this thesis is one of the first co-authors of this article. See the corresponding annex for the co-author authorizations to reflect this work in this thesis

Copyright © 2022 Sambade, Blanco, Gundappa, Bean, Macqueen, Houston, Villalba, Vera, Kamermans and Martínez. This is an open-access article distributed under the terms of the Creative Commons Attribution License (CC BY). The use, distribution or reproduction in other forums is permitted, provided the original author(s) and the copyright owner(s) are credited and that the original publication in this journal is cited, in accordance with accepted academic practice. No use, distribution or reproduction is permitted which does not comply with these terms.

USC UNIVERSIDADE DE SANTIAGO DE COMPOSTELA

Chapter II.

Content adapted from:

Sambade, I. M., Hlordzi, V., Blanco, A., Hermida, M., Vera, M., Culloty, S., Bean, T., Lynch, S. A., & Martínez, P. (2025). Disentangling the role of chromosome inversions in the structure of flat oyster (*Ostrea edulis*): origin, adaptation and phylogeography. *bioRxiv (Cold Spring Harbor Laboratory)*. https://doi.org/10.1101/2025.06.12.659260

This is an open access preprint. The author of this thesis is one of the first co-authors of this preprint. See the corresponding annex for the co-author authorizations to reflect this work in this thesis.

This is a preprint made available under the terms of the Creative Commons Attribution-NonCommercial 4.0 International License (CC BY-NC 4.0), which allows copying, redistribution and adaptation for non-commercial purposes, provided that appropriate credit is given, a link to the license is included, and any changes are indicated.

USC UNIVERSIDADE DE SANTIAGO DE COMPOSTELA

USC
UNIVERSIDADE
DE SANTIAGO
DE COMPOSTELA

Ostrea edulis is an ecologically, economically, and culturally valuable species, acting as a key ecosystem engineer in European coastal habitats. However, natural populations have dramatically declined due to overexploitation, habitat loss, and the emergence of bonamiosis, caused by Bonamia ostreae. This thesis integrates population genomics, chromosomal structure analyses, and transcriptomics to elucidate the genetic basis of resistance to B. ostreae. The results reveal a large inversion on chromosome 8 (C8) strongly associated with parasite exposure and survival, together with two additional inversions on chromosomes 2 and 5 showing signatures of adaptive maintenance. These regions are enriched in genes related to immunity, metabolism, and stress response, suggesting their role in host–parasite adaptation.